SYNTHESIS AND CHARACTERIZATIONS OF POLY(LACTIC ACID) AND ITS NANOPARTICLES

A THESIS

Submitted in partial fulfilment of the requirements for the award of the degree of

DOCTOR OF PHILOSOPHY

in

PAPER TECHNOLOGY

by

TUNGABIDYA MAHARANA

DEPARTMENT OF PAPER TECHNOLOGY
INDIAN INSTITUTE OF TECHNOLOGY ROORKEE
ROORKEE-247 667 (INDIA)

JUNE, 2010

INDIAN INSTITUTE OF TECHNOLOGY ROORKEE
ROORKEE

CANDIDATE'S DECLARATION

I hereby certify that the work which is being presented in this thesis entitled **SYNTHESIS AND CHARACTERIZATIONS OF POLY(LACTIC ACID) AND ITS NANOPARTICLES**, in partial fulfilment of the requirements for the award of the Degree of Doctor of Philosophy and submitted in the Department of Paper Technology of Indian Institute of Technology Roorkee, Roorkee is an authentic record of my own work carried out during a period from October, 2005 to June, 2010 under the supervision of Dr. Yuvraj Singh Negi, Associate Professor, Polymer Science and Technology Programme, Department of Paper Technology, and Dr. Bikash Mohanty, Professor, Department of Chemical Engineering, Indian Institute of Technology Roorkee, Roorkee.

The matter presented in this thesis has not been submitted by me for the award of any other degree of this or any other Institute.

Tungabidya Maharana
(TUNGABIDYA MAHARANA)

This is to certify that the above statement made by the candidate is correct to the best of our knowledge.

Bikash Mohanty
(Bikash Mohanty)
Supervisor

9/6/2010
(Yuvraj Singh Negi)
Supervisor

Date: 9/6/2010

The Ph.D. Viva-Voce Examination of **Mrs Tungabidya Maharana**, Research Scholar, has been held on 29-10-10

Bikash Mohanty
Signature of Supervisors

D. K. Varma 29/10/10
Signature of External Examiner

ABSTRACT

Global demand, for environmentally sustainable products supplemented with increasing restrictions on the use of non-degradable polymers, has motivated researchers to explore for biodegradable and biocompatible polymers which can be produced from renewable resources. Polylactic acid (PLA) – a member of the biodegradable polyester family is an important biopolymer, which can address the above mentioned environmental threats. However, the high cost of production of PLA limits its application as a commodity plastic. Thus, a systematic investigation for the improvement of already established synthesis procedure for the cost effective production of PLA is still under evolution. Further, an innovative use of this biodegradable & biocompatible polymer has found its way in the drug delivery systems in the form of nanoparticles as evident from available published research work. Under the above backdrop, the present research has been planned to revolve around the above thoughts.

Commercially, PLA is synthesized via ring opening polymerization (ROP) of lactide as well as through solution/melt polycondensation of lactic acid. The ROP is suffered from high production cost due to the involvement of complicated purification process of the lactide and azeotropic distillation of solvent. The second alternate route, which is solution polycondensation, is also not free from limitations as removal of solvent completely from the end product is difficult leading to poor quality of product. The third alternate route, i.e. melt polycondensation (MPC), produces low molecular weight PLA due to competitive reaction of lactide formation and simultaneous degradation at high temperature. Therefore, these methods of synthesis due to their inherent weaknesses increase the production cost substantially and thereby restricting their competitive use. Thus, many investigators have suggested an improved route which includes melt polycondensation under very high vacuum followed by solid-state polycondensation, which has potential to offer high molecular weight PLA with high yield (wt. %) comparable to the ROP process but at a lower cost.

In the present experimental investigation, PLA is synthesized by a two step process, of which the first step is melt polycondensation (MPC) under very high vacuum and the second step is solid-state polycondensation (SSP) which follows the first. After synthesizing PLA, its nanoparticles (NPs) are also prepared and characterized.

An experimental setup is designed, fabricated and commissioned to execute the above discussed steps of synthesis. To carry out the experiments in a methodical way that will help to develop input-output correlation using statistical analysis, design of experiment (DOE) technique is applied for the design and analysis of both steps of the experiment. After executing the experiments, the data is analyzed by statistical softwares. Analysis of variance (ANOVA) is performed to establish the relative significance of the individual input parameters and their interaction effects.

For both the MPC and SSP steps, two different sets, having five input parameters of significance, are screened out from fifteen and ten input parameters, respectively, from published literature, and the effect of these parameters and their interaction effects on the yield (wt. %) and M_w are identified. An attempt is also made to establish relationships between the input parameters and yield (wt. %) as well as M_w. Response surface methodology (RSM) of DOE is applied for the optimization of yield (wt. %) as well as M_w simultaneously for both MPC and SSP steps.

After synthesizing PLA by both the methods, the structural and physico-thermal properties of samples are characterized by different analytical methods such as gel permeation chromatography (GPC), FTIR, NMR spectroscopy, X- ray diffraction, thermogravimetric analysis (TGA), differential thermal analysis (DTA), differential scanning calorimetry (DSC) analysis and field emission scanning electron microscopy (FESEM).

Regression analysis of the experimental data for the MPC step confirmed that quadratic model is the best for the prediction of yield (wt. %), whereas; quadratic model is best for prediction of M_w only when these data are allowed to undergo square root transformation. The order of significance of input parameters of MPC for prediction of yield (wt. %) is: MPC temperature > MPC time > catalyst (wt. %) > ES time > amount of LLA, whereas; that for prediction of M_w is: MPC temperature > MPC time > ES time > amount of LLA > catalyst (wt.%). It is found that M_w around 179 kDa could be obtained by MPC after 2h of ES time, 10 h of MPC time and at 180°C MPC temperature. In addition, the yield (wt. %) and M_w are found to decrease with the increase in MPC temperature and MPC time, whereas; the effect of ES time appears to be insignificant. GPC chromatograms of some PLA samples obtained after MPC are found to be bimodal in nature indicating that the polymers produced have high as well as low

molecular weight species. It is further confirmed that D-lactic and L-lactic acid units are present in PLA chains due to racemization. The TGA/DTA/DSC analysis of PLA samples with different M_w samples show that T_d and T_m increases with the increase in M_w of PLA. Further, it is observed that the sample having M_w of 179 kDa, is thermally stable up to a temperature of 250°C and the corresponding T_d and T_m are 352°C and 167°C, respectively and have % crystallinity around 43% calculated from DSC and 40% calculated from XRD analysis.

However, regression analysis of the yield (wt. %) and M_w data, with input parameters, for SSP process shows quadratic model is the best. A value of M_w around 300 kDa could be obtained by SSP at 110°C HT temperature, 145°C SSP temperature and after 13 h of SSP time. Further, most of the GPC chromatograms of PLA samples obtained after SSP are found to be bimodal in nature attributed to the heterogeneous nature of SSP. The order of significance of input parameters for prediction of yield (wt. %) is: SSP time > HT temperature > SSP temperature > amount of PLA > HT time, whereas; that for prediction of M_w is: SSP temperature > SSP time > amount of PLA > HT temperature > HT time. The presence of D-lactic acid unit along with the L-lactic acid units are confirmed from studies of FTIR, NMR and XRD pattern for PLA. It is also revealed that racemization has taken place during SSP. From the TGA/DTA/DSC analysis of PLA samples, it has been found that the sample having M_w of 300 kDa is thermally stable up to a temperature of 250°C and the corresponding T_d and T_m are 354°C and 176°C, respectively and have % crystallinity around 22% calculated from DSC and 21.6% calculated from XRD analysis.

Recently, PLA nanoparticles (NPs) have attracted attention of many researchers as these materials play a major role by releasing drug in a controlled manner. To synthesize PLA NPs, a variety of preparation techniques are adopted ranging from polymerization of monomers to different polymer deposition methods. However, nanoprecipitation method is one of the best suited methods for preparation of PLA NPs as it is simple, fast and economical and also, it employs non-toxic solvents.

In the present investigation, PLA NPs are produced by nanoprecipitation method. Among ten parameters affecting nanoprecipitation, as identified from literature, four significant parameters such as concentration of PLA, solvent-to-non solvent volume ratio, M_w of PLA and type of solvent are considered as factors for experimentation. Taguchi method of DOE is used

for design and analysis of experiments and ANOVA is performed on results. Taguchi orthogonal array design (TOAD) is applied to simultaneously optimize the operating conditions for yield (wt. %) and size of PLA NPs. The effects of various input parameters and their interactions on the yield (wt. %) and size of NPs are also studied. The PLA NPs are characterized by dynamic light scattering (DLS), transmission electron microscopy (TEM) and FESEM. Zeta potential, for PLA NPs, is also measured using DLS instrument.

The relative effects of each input parameter observed on both the yield (wt. %) and size of PLA NPs in descending order are: PLA concentration > S/NS volume ratio > M_w of PLA > solvent. The optimal condition for the preparation of smaller sized PLA NPs of 115 nm along with higher yield (wt. %) of 79 %, is found to be at polymer concentration (10 mg/ml), S/NS volume ratio (0.2), PLAL and acetone. Under the range of input parameters such as concentration of PLA, S/NS volume ratio, M_w of PLA selected and two different solvents DMSO & acetone investigated, the sizes of the PLA NPs are found to vary from around 70 to 500 nm. The size distribution, for most of the samples, is found to be monomodal in nature having variation of PDI from 0-0.3. The sizes of PLA NPs observed from TEM are almost same as those obtained from DLS measurement and are found to be smooth, spherical and non-crystalline in nature. The zeta potential of PLA NPs is found to be negative and varied from -11.4 to -33.9 mV, in the pH range 3.7 to 7.4, respectively.

Finally, it is concluded that sequential MPC and SSP is an efficient method for the production of high M_w PLA of around 300 kDa with a good yield (wt. %) of about 80. Further, at alkaline pH (7.4) of blood, the zeta potential of PLA NPs is higher than acidic pH (3.7 - 6.0) and therefore, it is stable in extracellular fluid - blood and thus can facilitate the encapsulation and slow release of polycationic drugs.

ACKNOWLEDGEMENT

I feel myself fortunate to get an opportunity to work under the supervision of Prof. Bikash Mohanty, former Head, Department of Chemical Engineering; and Dr. Yuvraj Singh Negi, Associate Professor, Department of Paper Technology, Polymer Science and Technology Programme. I am heartily thankful to my supervisor(s), whose encouragement, guidance and support from the initial to the final level enabled me to develop an understanding of the subject. As an outstanding Engineer/scientist and teacher, they have given me the benefit of their excellent guidance throughout the course of the present work. I cannot forget their kind help and cooperation in bringing me to this position. Their teachings and advices were indispensable for whatever I have been able to do today. In the beginning of my tenure here, much of my efforts were unsuccessful for a substantial period of time, during which both of them were patient with great trust in me. Their encouraging words has always been inspiration for me and given me courage and confidence. I am always grateful to them for their continuous encouragement and support. Much of the bench top skills I learnt from them. Sir always uses to say "There is a very fine line between success and failure. Thus, one should have strong will power to get success."

I take this opportunity to express my deep sense of gratitude to Prof. AK Ray, Prof. J.S. Upadhyay, former Heads, Department of Paper Technology, and Present Head, Prof. Satish Kumar, Prof. Shri Chand (Chemical Eng.), Prof. ID Mall (Chemical Eng.), Dr. R. Bhargava (Chemical Eng.), Prof. VP Singh, Prof. MC Bansal, Prof. AK Singh and Dr. Vivek Kumar for their kind help in departmental affairs. I am also highly grateful to Mr. Debabrata Mohanty, elder brother of Prof. Bikash Mohanty for giving me a lot of experimental knowledge. I am also thankful to Mrs. Pratima Mohanty and Debajyoti Mohanty for the love and affection and moral support they have provided, during my stay at IIT Roorkee. I am also thankful to Mrs. Mohini Negi for her kind words.

I also thank members of the NMR centre and I.I.C. I.I.T. Roorkee for providing help at various stages of my work and for carrying out analysis and characterization of samples. I am thankful to Prof. Veena Choudhary (CPSE IIT Delhi) for allowing me to carry out GPC and Prof. AK Ganguly (Department of Chemistry, IIT Delhi) for allowing to carry out DLS studies.

My thanks must go to my beloved husband Dr. Alekha Kumar Sutar for his inspirational words. I also express thanks to Dr. Shabina, Sumitra, Sunila, Subhasree, Mitali, Sandhya, Jhuna, Swarna, Nigam, Rashmi apa, Vasundhara, Ramakrishna, Dr. Upendar, Dr. KP Samal, Sujata, Kavita, Himani, Kamini didi, Sunita, Mrunalini, Gunjan, Anjali, and my labmates, Divya, Amit, Kumar, Achyut, Gaurav, Manohar, Gopal, Mihir, Srinivas and Sukalyan whose friendship has always given me a mental support and whose communications, though from near and far places, have been great sources of inspiration.

I also take this opportunity to thank all my friends, seniors and colleagues at DPT Saharanpur and Roorkee campus of IIT Roorkee, whose names would form a big list, for their unparalleled company and valuable and timely assistance. I would also like to mention here about Mr. AP Jakhmola and his family, Mr. Sushil, Mr. Roshan Lal and all other staff members of DPT Saharanpur and Mr. Satyapal and Mr. Bhatnagar of Chemical Engineering for their kind help. I am highly thankful to Mr. Suresh C Sharma and Mr. Vijay Singh for their help during my experimental work in the Heat Transfer Research Lab. of Chemical Engineering Department.

On this special occasion of my life, I also remember and express my gratitude to some of my earlier teachers, Prof. BC Singh, Mrs. Minakshi, Prof. Jayant Pradhan and Prof. MS Dash, who literally steered my vision of career, throughout my days in the undergraduate and postgraduate studies.

Finally, I am deeply and thoroughly indebted to my parents, parent-in-laws for all the freedom they have given to my choice of career and life style. I thank Baby nani, Bulu bhai, Ruby nani, Surendra bhai, Smruti nani, Tuna bhai, Bibhu bhai, bhauja, Bhakta, lata nani, Swapna bhai, Padma didi, Bapi, Lina, Mami, Runa, Jhuna, Sipi, Happy and other family members and relatives for their continuous love and moral support.

My most pertinent thanks and gratitude are due to the All India Council of Technical Education (AICTE) New Delhi, India for the award of National Doctoral Fellowship.

And last but not the least; I am always thankful to the omnipresent, **GOD**, without whose elegance even this world does not exist.

(TUNGABIDYA MAHARANA)

CONTENTS

LIST OF FIGURES

LIST OF TABLES

NOMENCLATURE

Abbreviations

ANOVA	Analysis of variance
Axial	Axial point
b.p.	Boiling point
BBB	Blood-brain barrier
Center	Center point
Da	Dalton
DC	Decompression
DCM	Dichloromethane
DE7	Design expert 7.1.5 software
df	Degrees of freedom
DH	Dehydration
DOE	Design of experiments
DP	Degree of polymerization
DSC	Differential scanning calorimetry
DTA	Differential thermal analysis
ED	Experimental design
ES	Esterification
Fact	Factorial point
FESEM	Field emission scanning electron microscopy
FTIR	Fourier transform infrared spectroscopy

GPC	Gel permeation chromatography
HPLC	High performance liquid chromatography
kDa	Kilo dalton
LA	Lactic acid
LLA	L-Lactic acid
m.p.	Melting point
mm Hg (abs)	Millimeter of mercury measured as absolute pressure
MPC	Melt polycondensation
MW	Molecular weight
MWD	Molecular weight distribution
NMR	Nuclear magnetic resonance spectroscopy
NP	Nanoparticle
NS	Non-solvent
OA	Orthogonal array
OFAT	One-factor-at-a-time
PCS	Photon correlation spectroscopy
PDI	Polydispersity index
PDLA	Poly(D-lactic acid)
PDLLA	Poly(D,L-lactic acid)
PE	Polyelectrolyte
PLA	Poly(lactic acid)
PLAH	PLA of MW ca. 178 kDa

PLAL	PLA of MW ca. 98 kDa
PLLA	Poly(L-lactic acid)
PRESS	Predicted residual sum of squares
Prob	Probability
PTSA	p-Toluene sulfonic acid
ROP	Ring opening polymerization
R-Squared	Multiple correlation coefficient $1-[SS_{residual}/(SS_{model} + SS_{residual})]$
S	Solvent
SEC	Size exclusion chromatography
SNR	Signal-to-noise ratio
SS	Sum of squares
SSP	Solid state polymerization
TEM	Transmission electron microscopy
TGA	Thermo gravimetric analysis
TMED	Taguchi method of experimental design
TOAD	Taguchi orthogonal array design
UV	Ultraviolet
Vertex	Vertex point
XRD	X-Ray diffraction

Symbols

$[\eta]$	Intrinsic viscosity (dL/g)
M_n	Number average molecular weight (kDa)

M_w	Weight average molecular weight (kDa)
T_c	Crystallization temperature (°C)
T_d	Decomposition temperature (°C)
T_g	Glass transition temperature (°C)
T_m	Melting temperature (°C)
ΔH_m	Melt enthalpy (J/g)

INTRODUCTION

Petroleum based disposable plastics have proliferated throughout the global market since their expediency was discovered in the 1930s. However, the use of plastics, in large quantities has created a momentous disposal problem, as the conventional plastics can take several decades to degrade in landfill. And also, it is worth mentioning here that, the feedstock for plastics have become more expensive, as the global demand for petroleum has grown up. In response to these two challenges, scientists are looking for renewable-resource-based biodegradable plastics. Researchers around the world have made significant technological advances in the production of biodegradable plastics, since the mid-1990s.

At present, there is a growing interest towards biodegradable polymer materials (Fambri *et al.,* 1997; Grijpma *et al.,* 1991; Nakagawa *et al.,* 2004; Mohanty *et al.,* 2000). Its demand has increased as a replacement to non-biodegradable thermoplastic polymers. Specialized applications include, controlled release of medicaments into the human and animal bodies, manufacture of bioabsorbable prostheses, or, controlled release of insecticides in the agricultural field (Gilding and Reed, 1979; Bodmeier *et al.,* 1989; Gorner *et al.,* 1999; Ikada and Tsuji, 2000; Vega *et al.,* 2006). All these applications require complete biodegradability of the polymers and the degradation of the polymers must result in nontoxic compounds.

Amongst a number of biodegradable polymers, polyesters play an important role. Poly(lactic acid), PLA, biodegradable and biocompatible polyester, is of immense importance these days in the field of biomedical engineering and packaging industry. But it could not be popularized because of its high cost. It is derived from renewable resources such as corn, potato, cane molasses and beet sugar. It has a bright future as an environmentally friendly thermoplastic. With the help of this green polymer, industries will be able to close the carbon cycle, and their dependence on non-renewable fossil resources will be reduced considerably. It has promising applications in packaging, consumer goods, fibers and also in biomedicine because of its excellent mechanical properties, transparency, compostability and bio-safety.

Commercially, PLA is synthesized using ring opening polymerization (ROP) of lactide monomer, obtained through dimerization of lactic acid (LA), and also through polycondensation (PC) of LA. In case of ROP, complicated purification process of the lactide and azeotropic distillation of solvent make the production cost higher, thereby preventing its commodity application. The alternate route, i.e., solution polycondensation is also not free from limitations; in this case it is difficult to remove solvent completely from the end product. In bulk or melt PC, competitive reaction of lactide formation and simultaneous degradation process occurs at high temperature, leading to production of low molecular weight PLA. Therefore, these methods of synthesis increase the production cost substantially due to their inherent weaknesses (Moon *et al.,* 2000, 2001; Ajioka *et al.,* 1995; Shyamroy, 2003; Sodergard and Stolt, 2002; Xu *et al.,* 2006). Some merits and demerits of these methods of synthesis are discussed by Maharana *et al.* (2009). To eliminate the above drawbacks, many investigators (Moon *et al.,* 2000, 2001; Shyamroy, 2003; Xu *et al.,* 2006) have suggested alternate synthesis routes such as melt polycondensation and sequential melt-solid polycondensation. Out of these routes, melt polycondensation (MPC) followed by solid-state polycondensation (SSP) with a suitable catalyst, offers high molecular weight PLA with high yield which is comparable to the ROP route and also appears to be a cost effective method. Many investigators (Moon *et al.,* 2001; Xu *et al.,* 2006; Nagasawa *et al.,* 2005) have synthesized high molecular weight PLA by adopting a post polycondensation method also. Among various post polycondensation methods, solid-state polycondensation (SSP) is preferred, as it does not require any external agent during polymerization and therefore, yields pure PLA. In addition, it provides higher molecular weight (MW) as well as higher yield in comparison to melt polycondensation. The above facts provide necessary motivation and momentum to adopt sequential melt-solid polycondensation as an alternate synthesis route for PLA.

Although, the melt-solid polycondensation of L-lactic acid (LLA) has been investigated earlier (Moon *et al.,* 2001; Shyamroy, 2003; Fukushima *et al.,* 2005), little information is available on the regulation of its molecular weight and yield. A review shows that insufficient information is available to quantify effects of various input parameters on yield and molecular weight. And also, when the data available in literature for synthesis of PLA, was analyzed through Minitab software, no interaction amongst input parameters could

be studied because of the lack of sufficient data. Thus, through the present work an attempt has been taken to bridge this gap by conducting necessary experiments for synthesis of PLA.

Recently, PLA nanoparticles have attracted attention of many researchers as these plays a major role in drug delivery systems, by releasing drug in a controlled manner. In drug delivery, nanoparticles could readily be made biocompatible and biodegradable. In terms of controlled release, nanoparticles provide protection against the body metabolism resulting in sustained release and maintenance of bioactivity before the drug reaches the target. To process PLA into nanoparticles, a variety of preparation techniques are adopted ranging from polymerization of monomers to different polymer deposition methods (Lassalle and Ferreira, 2007; Legrand *et al.*, 2007; Wei *et al.*, 2008). Nanoprecipitation method is one of the best suited methods for preparation of PLA nanoparticles as it is simple, fast and economical and also it employs non-toxic solvents.

Further, an updated literature review on nanoprecipitation method for the preparation of PLA nanoparticles shows that there is hardly any information available on the proper regulation of effect of various parameters towards the yield and size of the PLA nanoparticles. Based on the above backdrops, it appears that a holistic approach should be adopted for the preparation of PLA nanoparticles by integrating the knowledge base already available for this purpose. Thus, in the present work, Taguchi method of Design of Experiment (DOE) was employed to design the experiment for production of nanoparticles of PLA.

Therefore, in nutshell, the present work is devoted to the synthesis and characterizations of PLA and its nanoparticles to investigate the effect of various input parameters on the output parameters so as to control these in required levels to get an optimum product. Response surface method of DOE was used for the synthesis of PLA whereas; Taguchi method of DOE was used for the design of experiments for the production of PLA nanoparticles. The design and analysis of the experiments were carried out by using the Design expert and MINITAB software to obtain relationships amongst the various input parameters and output parameters. Characterizations, of the PLA and its nanoparticles, were carried out by various methods like gel permeation chromatography (GPC), Fourier transform infrared (FTIR) spectroscopy, nuclear magnetic resonance (NMR), thermal

(TGA/DTA/DSC), X-ray diffraction (XRD), field emission scanning electron microscopy (FESEM), transmission electron microscopy (TEM) and dynamic light scattering (DLS).

To bridge the gaps stated above, a systematic study has been planned and executed with the following objectives.

1. To identify pertinent parameters, from published literature, for the synthesis of PLA using melt polycondensation (MPC), and then to use Response Surface Method (RSM) of DOE to design the actual experiments and to conduct them with an aim to develop relationships between input parameters and output parameters such as yield and molecular weight of PLA.
2. To identify pertinent parameters, from published literature, for the synthesis of high molecular weight PLA using solid state polycondensation (SSP), and then to use RSM of DOE to design the actual experiments and to conduct them with an aim to develop relationships between input parameters and output parameters such as yield and molecular weight of PLA.
3. To characterize PLA, produced through MPC and SSP routes, by GPC, NMR, FTIR, XRD, FESEM and thermal analysis.
4. To identify pertinent parameters, from published literature, for the preparation of PLA nanoparticles by nanoprecipitation method, and then to use Taguchi orthogonal array method to design the experiments with an aim to determine the value of operating parameters which could optimize the yield of monodisperse nanosized particles and also minimize the size of the PLA nanoparticles.
5. To characterize PLA nanoparticles by FESEM, transmission electron microscopy (TEM) and dynamic light scattering (DLS).

LITERATURE REVIEW

A literature review was conducted based on the objectives of the present investigation formulated in Chapter 1. As the central objective of the present work is to synthesize PLA polymer, literature review was carried out related to the synthesis of PLA by various methods and associated kinetics and reaction mechanisms. The synthesis of a substance needs its subsequent characterization; thus, literature review on the characterization of PLA was also carried out. PLA is synthesized to meet various applications. Consequently, present literature review also includes review on the applications of PLA in various fields. Besides the above, the present review also includes reviews on different properties of PLA such as physical, thermophysical, electrical, mechanical and degradation properties. As one of the objectives was preparation of PLA nanoparticles as a part of application of PLA, this Chapter also includes a thorough literature review on different methods available for production of PLA nanoparticles, their characterizations and applications.

However, there is lack of published information on the regulation of various parameters, on the molecular weight (MW) and yield in the case of PLA synthesis as well as size of PLA nanoparticles and its yield. This impelled us to attempt for their proper regulation by following design of experiment (DOE) method to proceed for the experimentation and the analysis of the results. Thus, literature review on DOE was also included in this Chapter.

2.1 SYNTHESIS OF POLY(LACTIC ACID)

PLA can be synthesized, from lactic acid (LA) - a renewable resource, mainly by two established routes such as ring opening polymerization (ROP) of lactide monomers and polycondensation (PC) of LA as shown in Fig. 2.1. The existence of both, a hydroxyl and a carboxyl group in LA, enables it to be converted directly into polyester via PC. However, the conventional condensation polymerization of LA does not increase the molecular weight sufficiently unless organic solvents are used for azeotropic distillation of condensation water and the time of polymerization is maintained for very long period. Conventional PC of LA yields a brittle glassy polymer, which is unusable for most applications (Drumright *et al.*, 2000, Lunt 1998, Bendix 1998, Ajioka *et al.*, 1995, Enomoto *et al.*, 1994).

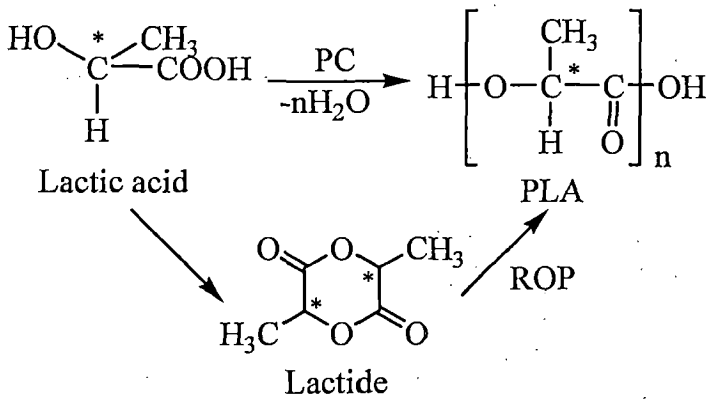

Fig. 2.1 Production scheme of PLA through PC and ROP

Thus, commercially the most preferred method is ROP, which provides high molecular weight PLA with better physical, thermal and mechanical properties. A further subdivision of above synthesis routes are illustrated in Fig. 2.2.

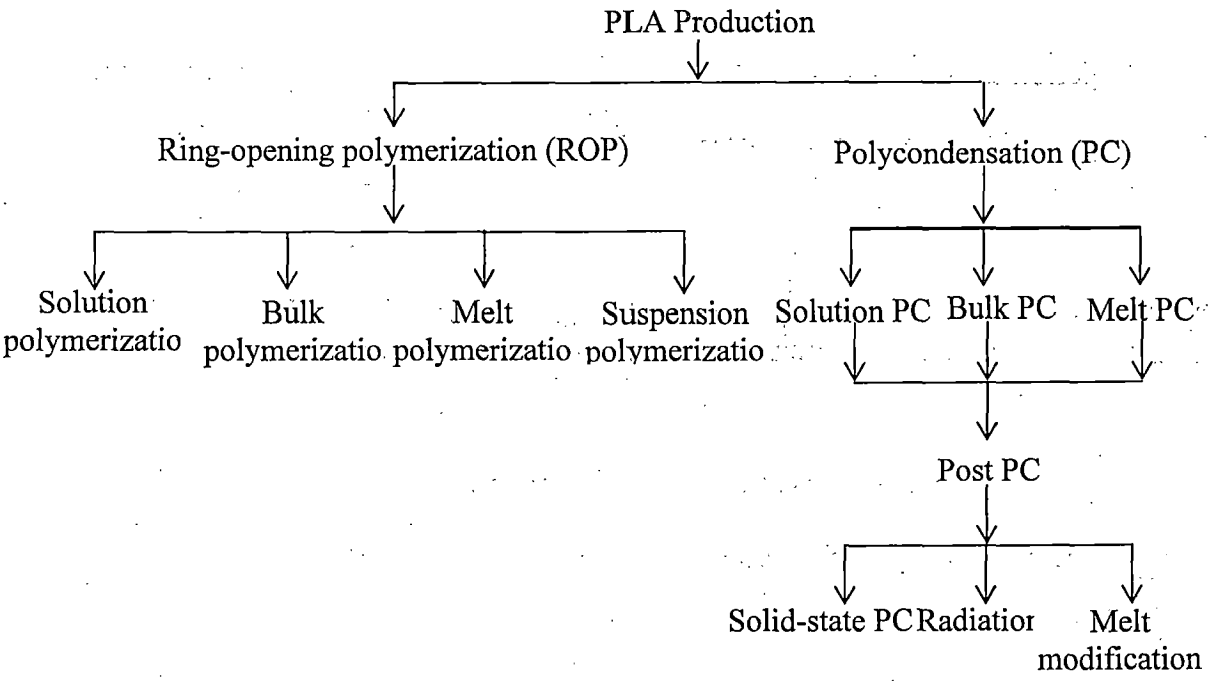

Fig. 2.2 Different methods for PLA production

2.1.1 Ring Opening Polymerization (ROP)

As suggested by Carothers's pioneering research (Carothers *et al.,* 1932), the most familiar way to obtain high-molecular-weight PLA is through ROP of lactide (Drumright *et al.,* 2000; Bendix 1998, Kricheldorf *et al.,* 1995, 2000). In this two-step method, the intermediate lactide - a cyclic lactic acid dimer, is formed in the first step when the condensation product water is removed by evaporation during oligomerization. L-lactic acid, D-lactic acid or mixtures thereof can be polymerized to corresponding low-molecular-weight

poly(lactic acid) oligomer, which is then catalytically depolymerized through an internal transesterification, i.e., by *back-biting* reaction to lactide. During depolymerization, three stereoforms of lactide are possible: L-lactide, D-lactide and *meso*-lactide. In the second step, purified L-lactide, D-lactide, DL-lactide (50:50 mixture of L and D isomers) / *meso*-lactide monomer is converted into the corresponding high-molecular weight PLA by catalytic ROP. It has been performed as melt, bulk, and solution or emulsion polymerization using a catalyst. Depending on the catalyst/co-catalyst combination, ROP can be carried out via a coordination/insertion, anionic, cationic, zwitter-ionic, active hydrogen, or free-radical mechanism (Spassky 1995; Albertsson and Varma 2003; Wu *et al.,* 2006). Through ROP it is possible to control properties such as molecular weight, molecular weight distribution and architecture of the polymer. The method also provides the possibility to achieve desired end groups and copolymerization of various monomers, depending upon the type of catalyst utilized (Albertsson and Varma 2003).

The ROP of lactide is catalyzed by compounds of transition and non-transition metals (Wu *et al.,* 2006) such as tin (Nijenhuis *et al.,*1992; Kricheldorf *et al.,* 1995; Kowalski *et al.,* 2000), lead (Kricheldorf and Serra 1985), zinc (Chabot *et al.,* 1983; Bero *et al.,* 1990), bismuth (Kricheldorf and Serra 1985), yttrium (Chamberlain *et al.,* 2000), iron (Stolt and Sodergard 1999), aluminum (Dubois *et al.,* 1991; Eguiburu *et al.,* 1995) and magnesium (Kricheldorf and Lee 1995). Of these, tin (II) compounds are frequently used and are considered to be the most efficient (Moon *et al.,* 2000, 2001). The mechanism, of tin (II) 2-ethylhexanoate, involves a pre-initiation step in which it is converted to a tin (II) alkoxide by reacting with an alcohol. Then the polymerization proceeds on the tin-oxygen bond of the alkoxide ligand (Kowalski *et al.,* 2000). Recent development on the use of main group metals as catalysts for lactide polymerization have been presented by Wu *et al.,* 2006.

2.1.2 Polycondensation (PC)

Polycondensation of LA in the presence of catalysts yields PLA along with water as a byproduct. In this method, raw LA is purified by removing its impurities, dehydrated, and then polymerized. PLA formed by PC of lactic acid mainly consists of lactyl units. Such polymer is either composed of one stereoisoform of both or a combination of both in various ratios (Mehta *et al.,* 2005). The presence of an asymmetric center in LA helps in the formation of different enantiomers such as poly(L-lactic acid) (PLLA), poly(D-lactic acid) (PDLA) or poly(D,L-lactic acid) (PDLLA) or a combination of these. Polymers derived from

LA by PC are referred to as polylactic acid whereas; those from lactide by ROP are termed polylactide. However, in common terminology, both of these products are called poly(lactic acid), PLA. Polycondensation can be carried out by different routes like solution, bulk or melt polycondensation.

2.1.2.1 Solution polycondensation

Until 1995, it was believed that a high molecular weight (MW) PLA could not be achieved by the direct PC owing to inherent difficulty in driving the dehydration equilibrium in the direction of esterification – which is a requirement for the formation of sufficiently high molecular weight PLA. To overcome this difficulty, equilibrium between LA, H_2O and PLA was manipulated by either using an organic solvent (Ajioka *et al.*, 1995) or a multifunctional branching agent (e.g. dipentaerythritol) (Sodergard and Stolt 2002; Hiltunen *et al.*, 1997).

Solution PC of LLA yields high molecular weight PLLA, as obtained by ROP, by using large volume of solvent compatible with PLLA (Buchholz, 1991). Solvents with high boiling point such as *p*-xylene and diphenyl ether, *o*-dichlorobenzene, *o*-chlorotoluene are used for the removal of the dissociated water by azeotropic distillation (Miyoshi *et al.*, 1996; Dutkiewicz *et al.*, 2003). The process is basically an acid-catalyzed intermolecular esterification of the hydroxyl and carboxylic acid groups of lactic acid, for which numerous Lewis acids such as $AlCl_3$, $CuCl_2$ etc., as well as protonic acids like H_3PO_4, Nafion-H, *p*-toluene sulfonic acid (PTSA) and methane sulfonic acid (MSA) have been used for trials as catalysts and co-catalysts, respectively (Ajioka *et al.*, 1995). Multiple reactors and complex facilities are needed for these synthesis routes and thus, invariably, increase the production cost of PLLA. Moreover, flammability and toxicity of the solvents make the solution process less attractive. Ajioka *et al.*, (1995) have carried out PC of LA with various catalysts and have compared the results. They have synthesized PLLA by PC of LLA in biphenyl ether solvent at different temperatures using various catalysts and compared M_w, and found that higher the reaction temperature higher is the molecular weight, when other parameters have been kept constant. The effect of normal boiling point of the solvent used and effect of negative pressure (to make the solvent reflux at a desired temperature) on the rate of PC have also been observed.

2.1.2.2 Melt polycondensation (MPC)

Polycondensation of LLA in bulk has been known to produce PLLA with molecular weight in order of 10^4 Da only due to the unfavorable reaction equilibrium constant (Miyoshi *et al.,* 1996). As the low molecular weight PLLA, thus produced, is too brittle to be used as a useful material, it is imperative to increase molecular weight.

The MPC of LA, like any other esterification reaction, is an equilibrium-controlled process. In this process, both esterification of the alcohol and carboxylic group and hydrolysis of the ester linkages by water - a byproduct of esterification, proceed simultaneously, thereby limiting the attainable molecular weight unless the byproduct water is removed from the system very efficiently. It involves two reaction equilibria, namely, dehydration equilibrium for esterification and ring-chain equilibrium for depolymerization of PLLA into L-lactide (Moon *et al.,* 2000).

A number of Lewis acids and different reaction conditions were investigated by Hiltunen *et al.,* (1997) for the MPC of LLA to make PLLA, and the polymers prepared thereof were characterized for molecular weight, conversion, cyclic dimer formation & racemization by ^{1}H NMR and for crystallinity by thermal analysis. 98 % H_2SO_4 was reported to be the best PC catalyst, which yielded PLA with number average molecular weight (M_n) of 31,000 Da, and minimum or no racemization. Sn $(Oct)_2$, which is a good Lewis acid and widely used in the coordination ROP of lactide, yielded a M_n of 30,000 Da when MPC was used, but racemization with this catalyst was found to be high (about 48 mol%) and consequently, the product polymer was found to be completely amorphous.

Sn (II) Lewis acid catalysts such as SnO, $SnCl_2.2H_2O$ etc., which are commonly used as catalysts for MPC of LA are found to be activated by various proton acids (Moon *et al.,* 2000). Such activated catalysts have been found to produce PLLA with high weight average molecular weight (M_w) of about 1,00,000 Da in relatively short reaction time (15 h), as compared to reactions catalyzed by non-activated catalysts mentioned above, which produced M_w of around 30,000 Da in 20 h. Such Lewis acid catalysts activated by proton acids are also reported to give less racemization.

A new type of tin-based Lewis acid catalyst, tetra butyl distannoxane, which can retard the hydrolysis, has been exploited for LA dehydro-polycondensation reaction by Ottera *et al.,* (1996), and thereby obtained a polymer with a maximum M_w of 75,000 Da. Although, a number of organometallic compounds have been tried as catalysts, it has been observed that binary catalysts, comprising of metal compounds activated with proton acids,

are more effective than single-metal-compound based catalysts (Moon *et al.,* 2000). Binary catalysts produce PLA of the order of ca. 10^5 Da with yield as high as ca. 98%. One of the disadvantages, for the direct PC, is that a low molar mass polymer showing substandard mechanical properties is usually obtained, owing to severe increase of melt viscosity and higher operating temperature. Since esterification is an equilibrium process, the efficiency of the process is dependent upon the removal of the water – a byproduct from the reaction. Normally, the byproduct water is sufficiently driven off by the reaction temperature itself, with the assistance of stirring. Higher degrees of polymerization normally require the use of azeotropic entrainment or reduced pressures to drive the reaction in the forward direction.

PLA with M_n of about 67,000 Da has been achieved by MPC of LA using dipentaerythritol as a chain branching agent (Kim and Kim 1999). MPC of LA using condensing agents such as 1,1-Carbonyldiimidazole (CDI), N,N,N',N'-tetramethylchloroformamidium chloride (TMCFAC) and N,N'-dicyclohexylcarbodiimide/4-dimethylaminopyridine (DCC/DMAP) has been carried out and their comparative effectiveness as condensing agents was studied (Akutsu *et al.,* 1998).

Mechanism of polycondensation

Though, the effect of PTSA on the PC mechanism is not yet well understood, a plausible mechanism has been proposed by Moon *et al.,* (2000). The hypothetical mechanistic aspects can be described as follows:

1. The hydroxyl and carboxyl terminal groups of PLLA form coordinate bonds with the catalyst center of Sn (II), present on tin (II)-oxide cluster, formed by hydrolysis of $SnCl_2.2H_2O$. Hydroxyl and carboxylate ligands present in PLLA are responsible for dehydration with the formation of Sn-OH.
2. The amounts of both terminal hydroxyl and carboxyl groups decrease with the increasing molecular weight of PLLA. When the molecular weight of the PLLA becomes high enough, the coordination sites of the catalyst center are not filled with the terminal groups. The catalyst site with this ligand vacancy induces side reactions, such as the decomposition of L-lactide, causing discoloration and racemization of PLLA. In fact, the reaction of L-lactide with the catalyst at high reaction temperature causes serious discoloration.
3. The proton acid added to the catalyst works as a ligand for the catalyst site. As the proton acid is not involved in the esterification, it fills the open coordination sites of

the catalyst to prevent side reactions. Addition of a strong proton acid like PTSA also stimulates the dehydration, and thereby increases the rate of reaction.

A detailed investigation is needed for confirmation of these mechanistic features of the MPC in which a high molecular weight PLLA (ca. 10^5 Da) with an average yield of 67% can be obtained by the catalysis of tin (II) chloride dihydrate with an equimolar amount of PTSA within 35 hours under 0.13-2.66 kPa pressure and within a temperature range of 180-200°C.

If the mole ratio of PTSA w.r.t. catalyst is too high, the catalyst activity is hindered. This may be attributed to the decrease in the number of vacant sites that are available for the coordination of the polymer tails. During the PC reaction, under rigorous reaction conditions, it appears that PTSA evaporates from the reaction mixture to induce side reactions such as racemization and discoloration. Discoloration of the product has been a serious problem in the PC of PLLA. During PC, the color of PLLA first changes to yellow, then to brown, and finally it becomes black. This discoloration may be due to various factors, such as, high reaction temperatures, long reaction times, catalyst used, solvents used and byproducts formed. It has been observed that with the addition of PTSA, the product discoloration is effectively prevented and the growth rate of the molecular weight is greatly enhanced (Moon *et al.,* 2000).

2.1.2.3 Solid-state polycondensation

To obtain high molecular weight PLA, the low molecular weight PLA obtained by PC or ROP can be processed further by various post-polycondensation methods, e.g. melt modification, radiation induced cross-linking and solid-state PC. Grafting and blending are two other post-processing methods for PLA that can produce heteropolymers (Sodergard and Stolt 2002). The PLA, obtained after PC or ROP, forms a homogeneous supercooled state with a monomer ratio more than 5 wt %. During the post polymerization process, crystallization of PLA occurs. In addition, the monomer consumption reaches 100% as the monomer and catalyst are concentrated in the amorphous part.

Melt modifications of polymers are often related to radical reactions, which can be generated by peroxides (Luft *et al.,* 1986) or by high-energy radiation (Boaler 1991). As this requires an external agent, this method is not appropriate for the synthesis of pure PLA. Radiation induced cross-linking also requires an external agent such as polyfunctional monomers (PFMs). PFMs such as triallyl isocyanurate (TAIC), trimethallyl isocyanurate

(TMAIC), trimethylolpropane triacrylate (TMPTA), trimethylolpropane trimethacrylate (TMPTMA), 1,6-hexanediol diacrylate (HDDA), ethylene glycol (EG), bis[pentakis(glycidyl allyl ether)]ether, and hydroxyl terminated EG, have been used as cross-linking agents (Nagasawa *et al.*, 2005).

Although Vouyiouka *et al.*, (2005) reviewed and discussed kinetics and simulation of SSP of polyamides and PET they did not discuss it for PLA. A limited amount of literature, including patents, is available on solid-state post-polycondensation of PLA (Fukushima *et al.*, 2005; Shinno *et al.*, 1997; Ren *et al.*, 2006; Zhou and Xu 2005; Xing and Yuan 2005; Zhang *et al.*, 2007; Kimura *et al.*, 2006; Ueda *et al.*, 2005; Wang *et al.*, 2004; Terado *et al.*, 1999, 2001; Okada *et al.*, 2000; Fukushima *et al.*, 2000; Sumihiro *et al.*, 1999; Obara *et al.*, 1996). However, a substantial amount of work is available on SSP of PBT, PET, polyamides and polycarbonates.

SSP appears to be an effective route for PLA synthesis when compared with ROP and simple PC. The process comes under Green Chemistry. It is simple, easy to handle, and because of the lower reaction temperature as compared to melt polymerization, does not promote undesirable side reactions. Further, high molecular weight PLA can be synthesized by MPC followed by SSP (Ren *et al.*, 2006). SSP involves both chemical and physical phenomena, since it is controlled by reaction kinetics, reactive chain-end mobility in the amorphous phase and condensate removal through diffusion. SSP increases the degree of polymerization considerably, and thus, can increase the molecular weight of a polycondensate up to 20 times (Ueda *et al.*, 2005).

In SSP, a semicrystalline solid polymer, of relatively low molecular weight, in powder, pellet, chip or fiber form, is heated to a temperature below T_m but above T_g (to improve mobility and subsequent reaction of the end groups) in the presence of a suitable catalyst. Simultaneous removal of the byproduct of condensation from the surface of the material is necessary, after it diffuses out from the bulk, either by evaporation under reduced pressure or by driving it away by a carrier gas. An optimum amount of crystallinity is required to prevent agglomeration of particles in the reactor (Gilding and Reed, 1979; Takahashi *et al.*, 2000). Use of crystal nucleating agents, such as magnesium stearate and titania, for bringing out a required amount of crystallinity to the PLA oligomer and making a solid solution of the PLA oligomer with biphenyl ether to effect more efficient removal of byproduct water are known to improve the progress of SSP reaction (Shyamroy, 2003; Okada *et al.*, 2000).

SSP essentially takes place in the amorphous region of the polymer, where all the reactive end groups reside. Since SSP actually starts at much lower temperatures, as compared to polymerization in the molten state or in solution (Pan *et al.,* 2005), the reaction temperature can range from a temperature sufficiently lower than T_m (Chen *et al.,* 1969) to a temperature just 5-15°C above T_m (Fortunato *et al.,* 1981). The T_m of PLLA is ca. 175°C and therefore, it is a high temperature reaction. Because of the restricted and slow mobility of end groups, the time needed to reach a particular molecular weight is generally much longer than that observed in the melt or solution (Chen *et al.,* 1969) polycondensation. SSP reduces discoloration and degradation associated with high temperature MPC, thereby, making it useful in polyester synthesis.

Although, SSP takes a considerably longer time, very high molecular weight PLA can be obtained, which cannot be accomplished in melt or solution polymerization, owing to viscosity restrictions and hydrolytic, thermal and oxidative degradation (Moon *et al.,* 2001). Almost all catalysts for melt and solution phase PC can be used as catalysts for SSP (Duh, 2002). Generally, the same Lewis acid catalysts, which are used for MPC of LLA, are used for SSP of PLA polymers, though some report of SSP of PLA without catalysts can also be found (Perego and Albizzati, 1994). SSP of PLLA using a binary catalyst system of tin dichloride hydrate and PTSA is reported to result in high molecular PLLA, generally not achievable by other condensation polymerization methods (Moon *et al.,* 2001).

Some progress has recently been achieved in obtaining high molar mass polymer by sequential melt-solid polycondensation (Moon *et al.,* 2001; Xu *et al.,* 2006; Chen *et al.,* 2006). The advantages and disadvantages of the different methods of synthesis are summarized by Maharana *et al.,* (2009).

2.1.3 Melt-Solid Polycondensation

Melt-solid polycondensation is an approach to increase the molecular weight of PLA by increasing the degree of polymerization (DP). A few investigators (Moon *et al.,* 2001; Shyamroy, 2003; Xu *et al.,* 2006; Fukushima *et al.,* 2005) have worked on sequential melt-solid polycondensation of LA. Xu *et al.,* (2006) studied the effect of crystallization time of PLLA pre-polymer on the molecular weight of PLLA. They first prepared PLLA pre-polymer with a molecular weight of 18,000 Da by the ordinary MPC process. The pre-polymer was then crystallized at 105°C for different time periods, and then heated at 135°C for 15–50 h for further SSP. Differential scanning calorimetry (DSC) and viscosity

measurements were used to characterize the crystalline properties and molecular weight of the resulting PLA polymers. The results showed that the molecular weight reached a maximum value for a crystallization period of 30 min and SSP of 35 h.

Moon *et al.,* (2001) obtained PLLA of M_w of 6×10^5 Da by melt-solid polycondensation of LLA using $SnCl_2.2H_2O$/PTSA binary system as a catalyst. They first prepared a polycondensate pre-polymer with M_w of 2×10^4 Da by MPC. This product was heat treated around 105°C to promote crystallization; and then it was heated at a temperature somewhere within 140-150°C for 10–30 h for further PC to produce PLLA of M_w of 6×10^5 Da. A high-quality PLLA, with high yield of about 90% having M_w exceeding 5×10^5 Da, was obtained within a relatively short reaction time of about 40 hrs. The M_w of PLLA thus achieved is comparable with that obtained by the lactide method using ROP. They further observed that, the polycondensate obtained after heat treatment does not show a crystallization exotherm in DSC, but does show a clear melting endotherm at 158°C. The heat-treated polycondensate did not melt up to 150°C, thus SSP was conducted at 150°C for different lengths of time (10-30 h) to obtain high M_w polymer without discoloration.

2.1.3.1 Key steps leading to poly(lactic acid) synthesis

The PC of LA takes place in several steps as discussed below. The associated mechanism for each step taking place in the sequential melt-solid polycondensation is discussed below:

Step 1: Dehydration

Commercial grade LA, used for PLA synthesis by PC reaction, contains about 80-95 wt. % LLA along with 10-15 % water, DLA and other impurities. During PC water is also produced and thus, for the forward reaction to proceed, the water molecules must be removed from the reaction product mixture as quickly as possible. This necessitates the removal of water from the raw material, LA, before the commencement of the reaction. This is also carried out during the dehydration step. The process includes heating LA under nitrogen atmosphere at a temperature from 100°C to 150°C under a pressure of 100-30 mm Hg to reduce the residual water content to 1-2 % (Chen *et al.,* 2006, Zhou and Xu 2005). Removal of water vapor will be comparatively more rapid, if the dehydration step is carried out under continuous flow of N_2 gas which helps in driving out water molecules. The complete dehydration process is carried out in a series of steps involving different

temperatures, pressures and dehydration time periods (Moon *et al.,* 2000, 2001; Chen *et al.,* 2006; Lee *et al.,* 2005). For example, LLA is first heated at constant temperature of ca. 150°C at atmospheric pressure for two hours; then the pressure is reduced to 100 mm Hg (abs) and heating is continued for another 2 hours at the same temperature; and finally the pressure is reduced to 30 mm Hg (abs) and the sample is heated again for another 4 hours without changing the temperature (Moon *et al.,* 2000, 2001; Lee *et al.,* 2005). Dehydration is done in stepwise manner to expel water in a controlled way. However, single-step dehydration is not uncommon. Chen *et al.,* (2006) carried out one-step dehydration at 100°C for 1 h at 760 mm Hg (abs). During dehydration, oligo(L-lactic acid) (OLLA) is obtained with a degree of polymerization (DP) varying from 8 to several hundred.

Step 2: Esterification

In this step, LA is converted into PLA along with the formation of water molecules as byproduct. As the reaction product contains water, it is imperative that the catalyst should be water–tolerant to achieve better yield and high molecular weight. Some investigators (Shyamroy 2003, Chen *et al.,* 2006, Shyamroy *et al.,* 2005) have employed water tolerant catalysts so that the DP is not affected. Appropriately substituted distannoxane catalysts are found to be hydrophobic due to the presence of bulky alkyl groups around the tin atoms and, therefore, can act as water-tolerant catalysts (Chen *et al.,* 2006). The esterification reaction is generally carried out at 180°C under a pressure of 30 mm Hg (abs). Higher temperature increases the vapor pressure of water and helps water molecules to escape from the polymer melt and thereby enhances the rate of the forward reaction. The reduction of pressure also helps the water removal process.

Step 3: Decompression

This step appears to be trivial but experiments shows that it helps in achieving high molecular weight PLLA. Little information is available on the suitability of this step. The decompression time may range from 3 to 7 hours in which pressure decreases from 30 to 1 mm Hg. It appears that the decompression step also removes water formed during PC and thereby enhances the rate of reaction. In fact, decompression can increase the molecular weight from 3×10^4 to 13×10^4 Da in the case of a titanium butoxide (TNBT) catalyzed PC reaction (Chen *et al.,* 2006).

Step 4: Melt polycondensation

The MPC of LA depends on two thermodynamic equilibria, one is the dehydration/hydration equilibrium for ester formation and the other is ring/chain equilibrium

for depolymerization to lactide formation. MPC is carried out above T_m of PLA, as at this temperature the lactide formed is evaporated to produce higher yield of polymer (Moon *et al.,* 2001). Racemization is also induced during PC (Moon and Kimura 2003) and is, most likely, due to the ester interchange reaction between the polymer chains (Shyamroy *et al.,* 2005). There are two ways, in which, the ester linkages between successive LA units can cleave and reform. One is acyl oxygen cleavage that does not involve the chiral carbon of the lactyl unit. The other is alkyl oxygen cleavage in which the covalent bond between the oxygen and the chiral carbon breaks and subsequently reforms resulting in an inversion of configuration. The change from the L-form to D,L-form in the presence of the TNBT catalyst is due to the racemization reaction, which has been confirmed from analysis of DSC and XRD results (Kim and Woo 2002). The strong proton acid co-catalyst promotes the breaking of the ester bond through the typical carbonyl-oxygen bond cleavage. As the reaction temperature increases, the probability of alkyl-oxygen cleavage increases and results in the formation of an inverted configuration (Cam *et al.,* 1995; Chen *et al.,* 2006). Chen *et al.,* (2006) proposed that the polymerization temperature should be as high as 180°C to produce high molecular weight PLA.

Step 5: Heat treatment

The PLA pre-polymer obtained from MPC is allowed to undergo heat treatment around its crystallization temperature (T_c). In this step the PLA, which is in the form of a white solid polycondensate, is crushed into granules and is put into a test tube which is then heated under vacuum at ca. 105°C for 1-2h. Since the crystallization exotherm is known to extend from 100 to 107°C, the melt polycondensate is heat treated at 105°C to crystallize the PLA. It has been reported that the extent of crystallinity is 29 and 30 % after 1 and 2 h, respectively (Moon *et al.,* 2001; Chen *et al.,* 2006). The product, after heat treatment, becomes resistant to fusion, even when heated at a higher temperature. Further, it did not reveal a crystallization exotherm in the DSC curve, which showed only a melting endotherm at 158°C. In the process of crystallization, both monomer and catalyst are segregated in the amorphous region of PLA. This helps the polymerization reaction to take place, even in the solid state, to allow the yield to reach 100%. Moon *et al.,* (2001) reported that during heat treatment, the M_w of PLLA increased from 1.3×10^4 Da to 1.5×10^4 Da.

Step 6: Solid-state polycondensation

Although the reaction rate is usually slow in solid-state reactions, increase in crystallinity does not hinder the dehydration reaction significantly. This is attributed not only

to the high activity of binary catalyst, even at low temperature, but also to the high mobility of the PLA chains in the amorphous phase (Moon *et al.,* 2001). SSP is generally carried out above T_g to enhance the molecular translational mobility within the amorphous regions of semicrystalline polymers, while the crystalline regions retain the geometrical shape of the polymer during polymerization (O'Keefe *et al.,* 2001). Although, the structure of the catalytic site is still unknown, the polymer terminals extended from the existing crystal surfaces can be brought sufficiently close to other crystal end groups present in the amorphous region to assist the process of esterification and thereby facilitate the growth of crystals. The polymer chains, thus elongated, can participate in the process of crystallization over the crystal surface available at crystal–amorphous borders (Moon *et al.,* 2001).

The polymer chains held inside the crystals experience difficulty in reacting with the neighboring chains and thus remain as relatively low molecular weight polymer, as can be verified from the bi-modal GPC chromatograms. The increase in crystallinity can continue until the crystallinity exceeds 43-45% (Kricheldorf and Lee 1995). The crystal growth during the post-polymerization is very large in the monomer-free products and the remaining monomer to polymer ratio decreases with increasing crystal growth (Shinno 1997). At this stage, the ester-forming rate among polymer terminals becomes too slow and the intramolecular ester exchange reaction may overcome the chain extension to form cyclics together with the linear fragments. The above hypothesis can be reasonably supported by the observed decrease in molecular weight and crystallinity of the polycondensate obtained after heating for more than 30 hrs. The bimodal GPC chromatograms obtained after SSP suggests that the chain elongation had proceeded in a heterogeneous manner during the crystallization of the polymer. If a high vacuum environment is created for an SSP process, subsequent return to atmospheric pressure may result in oxidation and discoloration of the polymer (Vouyiouka *et al.,* 2005). A number of patents (Ren *et al.,* 2006; Xing and Yuan, 2005) are available in which investigators have used molecular sieves to adsorb water during SSP. Molecular sieves can be represented by a chemical formula $[M(I),M(II)]O.Al_2O_3.nSiO_2.mH_2O$, where, M(I) and M(II), are monovalent (Na and K) and bivalent (Ca, Sr and Ba) ions; respectively and the range of values for n and m are 2-10 and 0-9, respectively.It is reported that while moving from the MPC step to the heat treatment step M_w increases by 1.5 times and again increases by 44.7 times in proceeding from the heat treatment step to the SSP step (Moon *et al.,* 2001). The experimental conditions employed by different investigators are summarized and analyzed in Table 2.1.

Table 2.1 In-depth analysis of different stages of melt/solid polymerization of lactic acid (LA) and their contribution towards MW

STATE (S)	Pressure (mm Hg)	Temperature (°C)	Steps of polymerization Reaction	Time Range (h)	Optimum Time(h)	Enhancement factor for MW	Remarks
Liquid	760	100/150	Dehydration (DH)	1-8	1		1. LA is dehydrated under N_2 atmosphere into Oligo(L-LA) (OLLA) whose degree of polymerization (DP) is 8 to few hundreds. 2. In this step excess water in LA gets evaporated.
Melt	760	180	Esterification (ES)	3-7	7	4 (Chen *et al.*, 2006)	1. In this step, water is produced and thus, water tolerant catalyst is required to enhance the reaction. 2. This step controls the MW. 3. Higher time period gives higher MW.
	1-760	180	Decompression (DC)	3-7	7	4.3 (Chen *et al.*, 2006)	1. Esterification time and decompression time are very important for enhancing MW. 2. High MW of PLLA can be obtained even in the absence of any additional reaction promoters, if the decompression step and/or the esterification step are well controlled. 3. Water gets evaporated in this step, thus, enhances reaction rate. 4. Higher decompression time gives higher MW.
	1-10	180	Melt polycondensation (MPC)	1-50	20, 40		1. The reaction is done at a temperature (T_r) where $T_g<T_r<T_m$. 2. Long time heating in melt state of PLLA induces lactide formation and causes polymer decomposition rather than polycondensation and hence this time period should be optimized. 3. Time period of polycondensation reaction is important for controlling MW and yield. 4. With time MW increases and then decreases. However, the time period provided for polycondensation step has less effect on MW than esterification and decompression time periods.

Table 2.1 Contd...

Table 2.1 Contd...

Solid	0.5	105	Heat Treatment (HT)	1-2	2	1.15 times (Moon *et al.*, 2001)	1. This step is done at T_c. 2. During HT the product crystallizes and becomes resistive to fusion even when heated at a higher temperature. 3. MW increases with increase in heat treatment time from 1 to 2 hr. 4. It increases yield
	0.5	150	Solid state polycondensation (SSP)	10-30	20	2.5 times after 2h heat treatment (Moon *et al.*, 2001)	1. SSP is conducted at ~ T_m for different lengths of time (10-30 h) to obtain high MW polymer. An optimum amount of crystallinity is required to prevent agglomeration of particles in the reactor. 2. SSP reaction essentially takes place in the amorphous region of the polymer, where all the reactive end groups reside. 3. SSP has to be performed at a temperature > T_g (to allow mobility of the end groups to react) and < T_m. 4. Since solid state reactions actually start at much lower temperatures, as compared to molten or solution state, the reaction temperature can range from sufficiently below T_m to just 5-15°C below T_m. 5. MW increases and then decreases with increase in SSP time period. 6. SSP reduces discoloration and degradation associated with high temperature melt polymerization in molten state. 7. Almost all catalysts for melt and solution phase polycondensation are suitable catalysts for SSP. 8. Plasticizers can be used with an aim to increase the mobility of the end groups in the amorphous region, which consequently increases the rate of the SSP.

2.1.3.2 Selection of catalyst

As PLA is primarily used for biomedical and food-packaging applications, the catalysts selected for its synthesis should be compatible with these applications. Many investigators (Moon *et al.,* 2000, 2001, 2003; Ajioka *et al.,* 1995; Shyamroy, 2003) have studied the effect of such catalysts for the synthesis of PLA. They have either used catalysts prepared from transition metal compounds or from a combination consisting of transition metal compounds along with protonic acid in the role of a co-catalyst. Tin compounds (Moon *et al.,* 2000; Ajioka *et al.,* 1995) are found to be effective catalysts for formation of high molecular weight polymers. Inorganic tin compounds are less toxic than organotins and tin (IV) compounds are less toxic than tin (II) compounds. Thus, inorganic tin will be a better choice as a catalyst in comparison to organotins. Toxicity grows with increasing tin concentrations. Tetraphenyltin (Shyamroy *et al.,* 2005) is a catalyst approved by FDA and therefore, can be used safely for the synthesis of polymers targeted for biomedical applications. Very few investigators have studied the effect of binary catalysts (Moon *et al.,* 2000; Kim and Kim, 1999; Terado *et al.,* 1999). Their investigations show that stannous octanoate is one of the most effective catalysts for the production of high molecular weight PLA with high yield.

However, like many other catalysts, it is difficult to remove this catalyst from the polymer, which can lead to cytotoxicity and thus limits its application. Although, some investigators have used Metal-Salen Schiff base complexes as initiator for ROP (O'Keefe *et al.,* 2001; Gregson *et al.,* 2006; Hung *et al.,* 2008; Chen *et al.,* 2005; Tang *et al.,* 2007; Wua *et al.,* 2005), no such investigation is reported so far on the use of these catalysts for PC reactions. Appropriately substituted distannoxane catalysts are themselves hydrophobic because of bulky alkyl groups around the tin atoms and, therefore, can act as water tolerant catalysts (Chen *et al.,* 2006). Tin atoms, which work as catalytic centers, retard hydrolysis of ester linkages to some extent (Keki *et al.,* 2001). From a study of variation of the substituents (R= n-Bu, X= Cl, OH, NCS) on the distannoxane ladder structure, Shyamroy (2003) concluded that the molecular weights of the synthesized PLA are relatively insensitive to the nature of the substituents.

2.1.3.3 Kinetics and reaction mechanism of sequential melt-solid polycondensation

Homopolycondensation of hydroxycarboxylic acids such as LA is a reversible process, and in order to prepare a high molar mass polymer the equilibrium constant for

condensation K_C has to be high enough. The polycondensation rate depends on both chemical (chemical reaction) and physical processes (heat treatment, crystallization). The possible rate-determining regimes are:

i. Chemical reaction control (a reversible chemical reaction);
ii. Interior diffusion control (diffusion of the volatile reaction products in the solid polymer);
iii. Surface diffusion control (diffusion of the volatile reaction product from the surface of the polymer to the surrounding inert gas).

Vouyiouka *et al.,* (2005) has also observed that there is no universal agreement on the relevant chemical kinetic expressions for SSP. The kinetic analysis of SSP shows that the rate of monomer consumption is inversely proportional to the square of the amorphous ratio of PLA, defined as the reciprocal of the crystal ratio (Shinno *et al.,* 1997). Crystal ratio is defined as the ratio of % crystallinity of the polymer and 100 % crystallinity. Shinno *et al.,* (1997), however, observed that the molecular weight did not increase with the monomer consumption as various oligomers are formed in the post-polymerization stage by the ester interchange reaction, in contrast to most observations (Moon *et al.,* 2001; Ueda *et al.,* 2005). The rate determining factor in SSP is the rate of removal of the condensate water. Greater surface area within the polymerizing solid favors faster evolution of small molecules. The condensate water can be removed from the solid by using static or dynamic vacuum or by exposure to a stream of inert gas (Zhang and Wang 2008).

2.2 DESIGN OF EXPERIMENT FOR POLY(LACTIC ACID) SYNTHESIS

Design of Experiment (DOE) is a structured, organized method that is used to determine the relationship between the different input parameters (Xs) affecting a process and the output parameters (Ys) of that process. This method was first developed in the 1920s and 1930, by Sir Ronald A. Fisher, the renowned mathematician and geneticist. Today, Fisher's methods of design and analysis are of international standards in business and applied science. DOE involves designing a set of experiments, in which all relevant factors are varied systematically (Montgomery, 2004). When the results of these experiments are analyzed, they help to identify optimal conditions, the factors that influence the results most, and those that do not, as well as the existence of interactions and synergies between factors. DOE methods implements well-structured data matrices. Analysis of variance (ANOVA) delivers accurate results, when applied to a well-structured matrix, even when the matrix is

quite small. An ANOVA is performed to establish the relative significance of the individual parameters and interaction parameters. DOE is a strategy to gather empirical knowledge, i.e. knowledge based on the analysis of experimental data and not on theoretical models. It can be applied to investigate a phenomenon in order to gain understanding or improve performance. Building a design means, carefully choosing a small number of experiments that are to be performed under controlled conditions. There are four interrelated steps in building a design:

1. Define an objective to the investigation, e.g. better understand or sort out important variables or find optimum.
2. Define the variables that will be controlled during the experiment (design variables), and their levels or ranges of variation.
3. Define the variables that will be measured to describe the outcome of the experimental runs (response variables), and examine their precision.
4. Amongst the available standard designs, choose the one that is compatible with the objective, number of design variables and precision of measurements, and which can be performed at a reasonable cost.

Standard designs are well-known classes of experimental designs. After deciding the objective, number and nature of design variables, nature of the responses and number of experimental runs one can afford, the experimental design can be generated using various softwares like Minitab, Design expert etc. Generating such a design will provide a list of experiments to be performed, to gather enough information on the experiment. DOE is widely used in research and development, where a large proportion of the resources go towards solving optimization problems. The key to minimize optimization costs is to conduct as few experiments as possible. DOE requires only a small set of experiments and thus helps to reduce costs. Designed experiments are often carried out in four phases: planning, screening (also called process characterization), optimization and verification.

DOE has been mainly classified into four categories viz., factorial design, mixture design, response surface method and Taguchi method. Among these, response surface method (RSM) is essentially a set of mathematical and statistical methods for experimental design, capable of evaluating the effects of variables and searching optimum conditions of variables required to predict targeted responses. Its greatest applications have been in industrial research, particularly in situations where a large number of variables influence the

production (Bajaj *et al.,* 2009). It is a well suited approach to study the main and interactive effects of distinct variables and also optimization of the process. Munguia *et al.,* (1992) have followed response surface method (RSM) for the optimization of molecular weight of dl-PLA using ROP method. But no literature is available on the use of DOE for melt polycondensation and solid state polycondensation.

Response surface methods are used to examine the relationship between one or more response variables and a set of quantitative experimental variables or factors. These methods are often employed after identifying a "vital few" controllable factors and to find the factor settings that optimize the response. RSM designs are usually chosen when curvature in the response surface is suspected. Many response surface applications are sequential in nature in that they require more than one stage of experimentation and analysis. One of the RSM designs is central composite design (CCD), which is often recommended when the design plans for sequential experimentation.

CCD consists of factorial or cube points, axial or star points and center points. There are 2^k cube points, where k is the number of factors/input parameters. The cube portion and center points may serve as a preliminary stage where first-order linear model can be fitted, but still providing evidence regarding the importance of a second-order contribution or curvature. CCD allows for efficient estimation of the quadratic terms in the second-order model. The inclusion of center points provides an estimate of experimental error and allows checking the adequacy of the model (lack of fit). Checking the adequacy of the fitted model is important as an incorrect or under-specified model can result in misleading conclusions. The positions of axial points in CCD are at a distance α from cube points. In case of face centered CCD, $\alpha = 1$ and the axial points are placed on the cube portion of the design. This is an appropriate choice when the cube points are at the operational limits.

2.3 CHARACTERIZATIONS OF POLY(LACTIC ACID)

The molecular weight of PLA is mainly determined by Gel Permeation Chromatography (GPC) although a number of secondary methods like viscometric method, NMR spectroscopy, vapor pressure osmometric (VPO) method etc. are available. Thermal properties like glass transition temperature (T_g), melting point (T_m), decomposition temperature (T_d), crystallization temperature (T_c) and % crystallinity etc. are determined by thermal methods of analysis (TGA/DTA/DSC). The crystalline nature and % crystallinity are obtained from X-ray diffraction (XRD) analysis. Structure of the polymer is obtained from

NMR and FTIR spectroscopy. The formation and removal of lactide during the process is also determined from NMR and FTIR spectroscopy. FESEM is carried out for the determination of surface structure. All these characterization processes have been described in the experimental section of the present investigation.

2.4 STRUCTURE-PROPERTY RELATIONSHIP OF POLY(LACTIC ACID)

Generally, physical, thermophysical, electrical, mechanical and degradation properties are studied for PLA. Out of these, physical, thermophysical and degradation properties are studied in the present investigation and thus, literature reviews of these are given in detail in this section. The thermal, mechanical and degradation properties of PLA are largely dependent on the ratio and distribution of the two stereoisomers of LA within the polymer chains (Garlotta, 2001). Polymers with high L-isomer produce crystalline products whereas; the higher D-levels (>15%) result in an amorphous product. Thus, commercial PLLA products are semicrystalline, with a high melting point (T_m) ca.180°C and a glass transition temperature (T_g) in the range of 55–60°C. It is desirable that PLA should have some crystalline content as it benefits the finished product (Lunt, 1998).

The degree of crystallinity depends on many factors, such as molecular weight, thermal and processing history, and the temperature and time of annealing treatments. The meso- and D,L-lactide form atactic PDLLA and are found to be amorphous in nature. The mechanical properties and degradation kinetics of the semicrystalline PLLA are quite different from those of completely amorphous PDLA. Mechanical and thermal properties of PLLA become almost constant when its molecular weight is above a threshold value of 70,000 Da (Moon and Kimura 2003). In general, for a particular use, the mechanical, physical and biodegradability properties of PLLA must be considered. The properties of PLA and its copolymers, synthesized by the PC, are not different from those of polymers obtained by the conventional lactide process (Ajioka *et al.*, 1995).

2.4.1 Physical Properties

Physical properties are very important as they reflect the highly ordered structure of the polymer and influence mechanical properties and their change during hydrolysis. Physical properties of polymeric materials depend on their molecular arrangement as well as ordered structures such as crystalline thickness, crystallinity, spherulite size, morphology and degree of chain orientation (Celli and Scandolat, 1992). For SSP of PLLA or PDLA

single polymer, molecular weight increases rapidly in comparison with block copolymer of PLLA and PDLA. Some significant properties of PLA are given in Table 2.2.

Table 2.2 Physical and mechanical properties of PLA produced by DURECT Corporation, Birmingham Polymers AL, USA

Property	L-PLA	DL-PLA
Glass Transition Temp. (T_g)	60-65°C	50-60°C
Melting Point (T_m)	184°C	Amorphous
Specfic Gravity	1.24	1.25
Tensile Strength (MPa)	55.2 – 82.7	27.6 – 41.4
Elongation (%)	5 - 10	3 – 10
Modulus (MPa)	2758-4137	1379-2758
Inherent Viscosity (dL/g)	0.90 - 1.2	0.55 - 0.75

The concept of solubility parameters was developed by Scatchard and Hildebrand (Siemann, 1992) on the basis of the theory of regular solutions. The Hildebrand solubility parameter, δ, at a given temperature can be expressed as the square root of the cohesive energy ΔE_v divided by the molecular volume V, i.e. the square root of the cohesive energy density as given by Eq. 2.1.

$$\delta = (\Delta E_v)/(V) \qquad (2.1)$$

The Hildebrand concept, in its most simplified form, is used in terms of a progression, attaching one solubility parameter to each solvent or solute. Substances with δ values of similar magnitude should be miscible or soluble. Solubility, of lactic acid based polymers, is highly dependent on the molar mass, degree of crystallinity and other comonomer units present in the polymer (Sodergard and Stolt, 2002). Chlorinated or fluorinated organic solvents, dioxane, dioxolane and furane are found to be good solvents for enantiomerically pure PLA. However, PDLLA is soluble in organic solvents such as acetone, pyridine, ethyl lactate, chloroform, tetrahydrofuran, xylene, ethyl acetate, dimethylsulfoxide, *N,N*-dimethylformamide and methylethyl ketone in addition to those listed above. Non-solvents for lactic acid based polymers are water, and unsubstituted hydrocarbons.

2.4.2 Thermophysical Properties

Thermophysical properties of PLA have been studied by various investigators using thermal analyzers such as TGA, DTA, DSC and TDMA. Enantiomerically pure PLA, is a

semicrystalline polymer with T_g of about 55°C and T_m of about 180°C, whereas; polymers prepared from meso- or rac-lactide are in general amorphous and do not have a sharp melting point. Polymers having regularity of structure have been obtained by using stereoselective catalysts (Sodergard and Stolt, 2002). The melt enthalpy estimated for enantiopure PLA of 100% crystallinity is 93 J/g (Tsuji *et al.,* 2004), the value most often referred to in the literature, although higher values (up to 135 J/g) have also been reported (Cohn *et al.,* 1987, Saha and Tsuji 2006). The T_m and degree of crystallinity are dependent on the molar mass, thermal history and purity of the polymer (Jamshidi *et al.,* 1988; Migliaresi *et al.,* 1991). Crystallization kinetics and melting behavior of PLAs of different optical purity have been investigated in several studies (Huang *et al.,* 1998; Vasanthakumari and Pennings, 1983; Kolstad, 1996; Barantian *et al.,* 2001). It has been observed by Tsuji and Ikada (1996) that an optical purity of at least 72-75 %, corresponding to about 30 isotactic lactyl units, is required for crystallization to take place. However, in contrast to above, Sarasua *et al.,* (1998) have been able to crystallize PLA having as low as 43% optical purity, obtained by using Salen-Al-OCH_3 (a complex resulting by using a Schiff based on $AlEt_2Cl$) as an initiator for polymerization. This is possible because of the formation of long isotactic sequences. They reported that a sample, of 47% optical purity, has T_m of 99°C (ΔH_m=18 J/g). Monodisperse oligomers of 22 isotactic lactyl units prepared by fractionation have also been reported to crystallize, exhibiting a melting temperature of 59°C (ΔH_m=39 J/g) (de Jong *et al.,* 1998). Enantiomeric oligomers of a few lactyl units show a molar mass dependent glass transition temperature. Values of T_m, T_g and ΔH_m are dependent mainly on the structure of PLA and its molecular weight (Radano *et al.,* 2000; Ikada *et al.,* 1987). Thermal properties of PLA can be changed by copolymerization of PLA with monomers such as glycolide, some lactone derivatives, trimethylene carbonate, etc.– and also by addition of cross-linkers (Grijpma *et al.,* 1991; Buchholz, 1993; Nijenhuis *et al.,* 1996) and plasticizers.

2.4.3 Electrical Properties

In order to apply PLA as an insulating material, for example, in electric wires and cables, it is necessary to study the basic electrical insulation properties such as volume resistivity, dielectric constant, dielectric loss tangent, impulse breakdown strength and storage of space charge, at room temperature. The basic electrical insulation properties of

biodegradable PLA have been measured by Nakagawa *et al.,* (2004). They have measured volume resistivity, dielectric constant and dielectric loss tangent at room temperature. These were found to be comparable to those of crosslinked polyethylene (XLPE), currently used as insulating material for cables and electric wires (Nakagawa *et al.,* 2004). The dielectric constant of PLA is higher than that of XLPE. One reason for this might be the existence of a carbonyl group in the polymer chain of PLA. The dielectric constant of PVC, currently used for insulating electric wires, is 3.4, and the dielectric constant of oil-immersed insulating paper used for insulating high-electrical-field cables, is about 3.5. The dielectric constant of PLA is lower at about 3.0. According to Nakagawa *et al.,* (2004) the mean impulse breakdown strength of PLA is about 1.3 times higher than that of XLPE. A more detailed analysis can be found in their paper.

2.4.4 Mechanical Properties

The mechanical properties of polymers of similar molar masses, but prepared by different polymerization processes, do not differ much. This is also true for PLAs prepared by both polycondensation and ROP (Sodergard and Stolt 2002). The mechanical properties of PLA can be varied to a large extent, ranging from soft and elastic plastics to stiff and high-strength materials. Semicrystalline PLA is preferred to amorphous polymer when better mechanical properties are desired. The molar mass of the polymer (Tsuji and Ikada, 1999; Engelberg and Kohn, 1991; Ikada and Tsuji, 2000) as well as the degree of crystallinity (Grijpma and Pennings, 1994; Grijpma *et al.,* 1993) have a significant influence on the mechanical properties (Perego *et al.,* 1996).

Grijpma and Pennings (1994) varied the crystallinity of PLA by preparing stereo-copolymers with small amounts of D-lactide and found maximum impact strength of 37kJ/m^2 when the copolymer had a ΔH_m of 60 J/g, corresponding to a crystallinity of 65%. In addition, a low degree of chain entanglements occurred in highly crystalline material (Bergsma *et al.,* 1994). When the crystallinity of the PLA was reduced, the density of chain entanglements increased, even though the crystallinity was high enough to give physical cross-linking and thus the material was not as brittle as amorphous or low-crystalline material (Fukushima *et al.,* 2000; Ueda *et al.,* 2005). Superior mechanical properties have been achieved by stereocomplexation of enantiomeric PLAs, which was ascribed to the formation of stereocomplex crystallites giving intermolecular cross-links (Tsuji and Ikada, 1999).

The viscometric molecular weight of PLA decreases when fibers are drawn from it by melt-spinning. Weight loss of 90 % occurred during extrusion and 10% during hot-drawing (Fambri *et al.,* 1997). PLLA of high molar mass has sufficient strength for use as load bearing material in medical applications, but it degrades slowly because of the reinforcing crystalline domains (Bergsma *et al.,* 1994). The crystallinity can be reduced by copolymerizing with D-lactide, leading to an amorphous DL-PLA with a faster degradation profile (Li *et al.,* 1990). Tensile strength of PLLA with 10% residual lactide was found to be 15% lower than that for a PLLA with 97% conversion (Jacobsen *et al.,* 2000). Gupta *et al.,* (2007) presented a more detailed critical review of PLA fiber. They have discussed the structure-property relationship of PLA fiber.

2.4.5 Degradation Properties

Thermal degradation

Degradation of PLA can be studied either by hydrolysis or by thermal methods. The degradation of polymers has been defined as the number of chain scissions produced during a known period and can be expressed by Eq. 2.2 (Reich and Stivala, 1971),

$$1/\overline{DP} = 1/\overline{DP}_0 + k_D t \qquad (2.2)$$

where, DP_0 and DP are, the initial and final values of the average degree of polymerization, respectively, k_D is the degradation rate constant and t is time. This equation is valid for condensation polymers when the amount of broken bonds is low, i.e., $k_D t \ll 1$. The degree of depolymerization can be monitored by the average molar mass as a function of the degradation time. As the viscosity of a polymer solution or a melt can be related to the average molar mass, the DP can be correlated with the viscosity changes as given by Eq. 2.3

$$1/(\eta_{0,t})^{\alpha} = 1/(\eta_0)^{\alpha} + k_D t \qquad (2.3)$$

where, the exponential factor α depends on molar mass and melt viscosity and is a constant equal to 0.294 for molar masses above the critical molar mass (Seo and Cloyd, 1991). Eq. 2.3 is valid for polymer melts for degradation by random main-chain scission (Sodergard and Nasman, 1996). For PLA, most of the degradation reactions were considered to involve highly concentrated ester bonds on the main chain. These reactions include thermohydrolysis, depolymerization, cyclic oligomerization and intermolecular and intramolecular transesterification. Low molecular weight compounds associated with the polymer and the hydroxyl end groups of the main chain seem to play an important role in

lowering the molecular weight at high temperatures. An increased amount of polymerization catalyst in the end product also catalyzes the degradation reactions (Jamshidi *et al.,* 1988). The degradation compounds include water, monomers, oligomers, and polymerization catalysts. Removal of the non-polymeric contents and blocking the hydroxyl end-groups enhanced the thermal stability of PLA. The thermal degradation was found to proceed by random main-chain scission.

The purity of the polymer affects the melt degradation of PLA significantly (Jamshidi *et al.,* 1988). Melt degradation is retarded when PLA dissolved in chloroform was precipitated in non-solvents such as methanol and *n*-hexane. This procedure removes the non-bonded tin (catalyst) and low-molar mass impurities. Acid extraction of the dissolved PLA was also found to remove a part of the bonded tin, which resulted in further reduction of the melt degradation (Sodergard and Nasman, 1996).

Degradation by radiation

The molecular weight decreases rapidly with increasing radiation dose but the molecular weight distribution of the irradiated copolymer does not change significantly for doses up to 250 kGy, perhaps because of the randomized distribution of the monomer units in the copolymer (Gupta and Deshmukh, 1983; Birkinshaw *et al.,* 1992; Nugroho *et al.,* 2001). A drastic decrease in the tensile strength and substantial embrittlement occur at higher dose levels above 250 kGy (Birkinshaw *et al.,* 1992). Radiation-induced reactions take place mainly in the amorphous phase of the polymer; and the degree of crystallinity of the polymer (Alariqi *et al.,* 2009), which in fact, decides the extent of amorphous phase in PLA, is, therefore, an important parameter. Gupta and Deshmukh, (1983) studied the effect of γ-irradiation on PLA, synthesized by the solution polymerization of lactic acid under air and N_2. The presence of air causes a decrease in both chain scission and cross-linking. The melting temperature decreases with γ-irradiation dose.

Biodegradation

Biodegradation is influenced by solid-state morphology, degree of crystallinity, primary chemical structure, such as the presence of functional groups and the hydrophilicity–hydrophobicity balance of PLA (Luciano *et al.,* 2003). The degree of crystallinity is the major rate-determining factor for biodegradation of solid polymers (Mochizuki and Hirami, 1997). In general, chain scission of the PLA main chain takes place where ester bonds are located, leading to formation of oligomers. Thus, the number of oligomers after chain scission will depend upon the number of ester bonds present in the

PLA main chain. The principal mode of degradation for lactic acid-based homopolymer and copolymer, is hydrolysis (Hyon *et al.,* 1997; Sodergard and Nasman, 1994; Singh *et al.,* 2003) which takes place in three important steps:

1. Degradation proceeding by diffusion of water into the material (initially into the more amorphous zones) followed by random hydrolysis.
2. Fragmentation of the material to OLLA.
3. Finally, through a more extensive hydrolysis accompanied by phagocytosis, diffusion and metabolism.

2.5 APPLICATIONS OF POLY(LACTIC ACID)

PLA is a versatile polymer which can be applied in a variety of fields including biomedical, packaging, electronics and electrical appliances like laptop, mobile, etc. Now days, companies like Ford Motors will be able one day to make auto interior parts out of bio-based and biodegradable plastics. NEC has developed a corn-based bioplastic which conducts heat faster than stainless steel (http://news.zdnet.com/2100-1035_22-6174371.html dated 12.04.07). The bioplastic could help make laptops and mobile phones thinner and lighter by eliminating the need for heat-releasing sheets or fans. NEC aims to replace 10 % of the plastic used in its products with bioplastic. The company began using plastic made from fermented corn (PLA) and kenaf fiber in its mobile phones. Although NEC's new plastic is cheaper than other fiber-reinforced plastics, as it requires less carbon fiber to conduct heat, but it is still more expensive than stainless steel. Air-cushions made of bio-film (PLA and its copolymers) will be made available in market by Storopack Hans Reichenecker GmbH. A novel bioabsorbable device for facial suspension and rejuvenation was developed by Knott *et al.,* (2009). Cattelan *et al.,* (2006) has invented PLA implants to correct facial lipoatrophy in Human Immunodeficiency Virus 1–Positive individuals receiving combination antiretroviral therapy. PLA can also be used as bioabsorbable polymer drug-eluting stents (BVS). Researchers from the UK has investigated that holes in brain tissue caused by stroke may be fixable using a scaffold for stem cells loaded with PLA particles. http://blogs.nature.com/news/thegreatbeyond/2009/03/stem_cells_scaffold_for_stroke.html.

2.6 PREPARATION OF POLY(LACTIC ACID) NANOPARTICLES

Controlled release of medicaments remains the most convenient way of drug delivery. In particular, the use of nanoparticle devices has received special attention during

the past two decades. Potential of polymer-based nanoparticles as drug delivery systems have been extensively investigated in recent years. PLA is the most preferred macromolecule in several biomedical applications since it is one of the most well-known bioabsorbable polymers. It is also non-toxic and has good biodegradability. Numerous methods for the manufacture of PLA nanoparticles have been described (Lassalle *et al.,* 2007, Legrand *et al.,* 2007, Wei *et al.,* 2008). Emulsification/solvent diffusion, emulsification/solvent evaporation, nanoprecipitation and salting-out methods are widely applied techniques and these have been discussed in several reviews (Lassalle *et al.,* 2007; Hans and Lowman, 2002; Soppimath *et al.,* 2001; Quintanar-Guerrero *et al.,* 1998) Polymeric nanoparticles are predominantly prepared by wet synthetic routes. A brief overview of suspension and dispersion-precipitation polymerization relevant to nanoparticles is included in this Chapter. Emulsion polymerization methods include reactive and non-reactive pathways to nanoparticle formation.

2.6.1 Nanoprecipitation

Nanoprecipitation is the most preferred method, amongst the different methods available for preparation of PLA nanoparticles. It is simple, fast, and economic, employs non toxic solvents and also has the advantage of using preformed polymers as starting materials rather than monomers (Fessi *et al.,* 1989; Jain, 2000). It can also be applied to materials other than synthetic polymers, including amphiphilic cyclodextrins, proteins (Duclairoir *et al.,* 1998), lipids (Trotta *et al.,* 2003) and drugs (Legrand *et al.,* 2007). For the above reasons, this method is widely used to prepare nanoparticles for the delivery of active compounds.

In nanoprecipitation, introduced by Fessi *et al.,* (1989), the particle formation is based on precipitation and subsequent solidification of the polymer at the interface of a solvent and a non-solvent. Thus, the process is often called solvent displacement or interfacial deposition. The polymer is dissolved in a water miscible organic solvent (or solvent mixture) and added to an aqueous solution, in which the organic solvent diffuses. Nanoparticles form instantaneously by precipitation of the polymer in a narrow window of composition, after which the organic solvent can be removed by evaporation (Stainmesse *et al.,* 1995). Under appropriate conditions, this technique leads to a dispersion of polymer particles that have a monomodal particle size distribution within the nanometer range, in a

reproducible manner (Stainmesse *et al.*, 1995; Molceperes *et al.*, 1996; Govender *et al.*, 1999; Lamprecht *et al.*, 2001).

According to the current opinion, the Marangoni effect is considered to explain the phenomena (Quintanar-Guerrero *et al.*, 1998). Solvent flow, diffusion and surface tensions at the interface of the organic solvent and the aqueous phase cause turbulences, which form small droplets containing the polymer. Subsequently, as the solvent diffuses out from the droplets, the polymer precipitates. Finally, the organic solvent is typically evaporated by applying vacuum. No emulsification step (which is usually part of a nanoparticle preparation process), labor intensive processing procedures or special laboratory ware is needed. The size of the nanoparticles prepared by nanoprecipitation varies typically from 100 to 500 nm.

Usually, surfactants or stabilizers are included in the process to modify the size and the surface properties, or to ensure the stability of the nanoparticle dispersion (especially during the early stages of the precipitation). However, presence of surfactants/stabilizers is not indispensable for the formation of the nanoparticles. The drug substance to be encapsulated, depending on its solubility, is dispersed as an aqueous solution or dissolved in the organic solvent before the fusion of the phases. The nanoprecipitation technique suffers from poor encapsulation efficacy of hydrophilic drugs, because the drug can diffuse to the aqueous outer phase during polymer precipitation (Barichello *et al.*, 1999).

The encapsulation has been increased by modifying the solubility of the drug by changing pH (Leo *et al.*, 2004; Govender *et al.*, 1999; Peltonen *et al.*, 2004). Encapsulation efficiency can also be improved by means of an accelerated precipitation rate of the polymer, modified solvent composition and increase in the molecular weight of the polymer. Overall, the challenge in nanoprecipitation is to find a drug/polymer/solvent/non-solvent combination, which allows successful nanoparticle production and drug encapsulation. However, scale-up of nanoprecipitation from laboratory-scale to pilot-scale has been recently reported (Galindo-Rodriguez *et al.*, 2005).

Nanoprecipitation has been extended using quite complex systems containing the three basic ingredients (polymer, solvent and non-solvent) plus a surfactant and, sometimes, even a binary mixture of solvents of the polymer or a drug to be encapsulated (Niwa *et al.*, 1993; Murakami *et al.*, 2000; Chorny *et al.*, 2002; Peltonen *et al.*, 2003). The choice of the ternary polymer/solvent/non-solvent system is critical for the success of the method. The nature of the polymer solvent interactions has been reported to affect the properties of the nanoparticle preparation (Thioune *et al.*, 1997; Murakami *et al.*, 2000; Galindo-Rodriguez *et*

al., 2005). However, apart from the requirements that the solvent of the polymer should be miscible with the non-solvent of the polymer and that the polymer concentration should be low (<2%), no clear guidelines about the influence of each of the three components of the system have yet emerged.

Some experimental work has attempted to investigate the effect of several parameters on the size and yield of nanoparticles, prepared with different polymers and solvents (Stainmesse *et al.,* 1995; Thioune *et al.,* 1997; Murakami *et al.,* 2000; Galindo-Rodriguez *et al.,* 2005). In general, by increasing the polarity of the polymer solvents and by decreasing concentration of the polymer in the solvent, the yield of nanoparticle production can be increased and the size of the nanoparticles be reduced (Sussman *et al.,* 2007). These studies have also pointed out the importance of the solvency properties of the solvent of the polymer in the control of nanoprecipitation process. In this context, Thioune *et al.,* (1997) suggested investigating the intrinsic viscosity of the polymer solution in the chosen solvent and determining the Huggin's interaction constant.

2.6.2 Emulsion Based Methods

In emulsion-based methods, the solvent in which the polymer is dissolved is being eliminated. This elimination can be achieved by evaporation or by extraction. The formation of an emulsion is a necessary prerequisite. Aqueous and oily phases can be present, according to the nature of the continuum phase of the formed emulsion. The polymer is contained in the organic phase and the emulsifier is present in the aqueous phase. The emulsified organic drops containing the polymer, form nanoparticles by the elimination of the organic solvent (Gorner *et al.,* 1999; Freitas *et al.,* 2005).

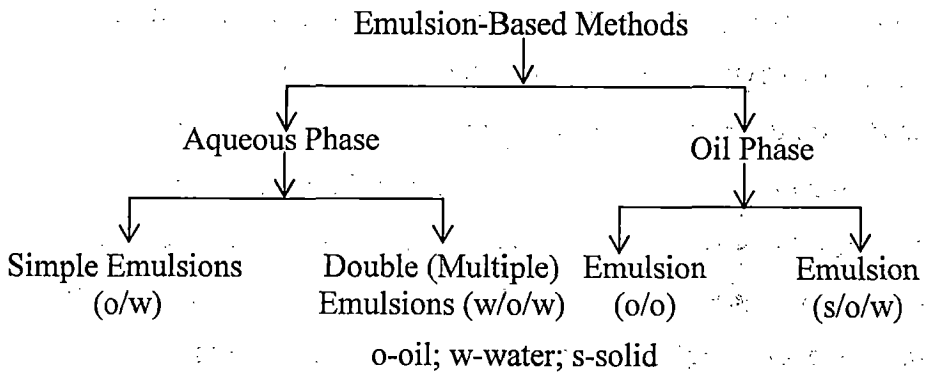

Fig. 2.3 Classification of emulsion-based method

In emulsification/solvent evaporation, the dissolved polymer is emulsified with aqueous phase with the help of a high-energy source such as ultrasound or homogenization followed

by solvent evaporation under reduced pressure. Similarly, in emulsification/solvent diffusion, nanoparticles are formed when the saturation limit of a partially water-miscible solvent (e.g. benzyl alcohol) is exceeded by addition of water. In both techniques, the phase separation is accompanied by vigorous stirring. The separated solvent is removed by cross-flow filtration. Emulsion based methods can be classified as shown in Fig. 2.3.

2.6.3 Salting-out

Salting-out method is one alternative to the widely applied emulsion and nanoprecipitation procedures. This method involves the use of a solution including the polymer and, eventually, the drug in a water-miscible solvent such as acetone or tetrahydrofuran (THF). The solution is emulsified under vigorous stirring in an aqueous gel containing the salting-out agent and, if required, a stabilizer. The compounds commonly employed as salting-out agents are electrolytes such as magnesium chloride, sodium chloride or magnesium acetate and non-electrolytes such as sucrose. This method involves polymer precipitation via phase separation (organic solvent - aqueous phase) by the addition of a salting-out agent, e.g. electrolytes in the case of acetone as a solvent for the polymer. The addition of high amount of water to the o/w emulsion allows the formation of nanoparticles that can be purified and recovered by cross-flow filtration. The needs for intensive purification of the resulted nanoparticles as well as the incompatibility of most of the salts employed with the bioactive compounds are the principal limitations associated with this technique (Quintanar-Guerrero *et al.,* 1998).

2.6.4 Spray Drying

Spray-drying method is another way to obtain nanoparticles, where the drug is solubilized or dispersed in an organic solution of the polymer which is then converted into a fine spray in a hot-air flow. The solvent is instantaneously evaporated and dried nanoparticles are finally recovered. From the point of view of solubility parameters of polymer and drug, this method seems to be more versatile, compared with the methods previously described (Vasir *et al.,* 2003). Contrary to the conventional methods (solvent evaporation/emulsion and nanoprecipitation), the spray-drying involves a very rapid procedure potentially useful at the industrial scale that can be carried out under mild conditions (Bishara and Domb, 2005).

In spite of the mentioned advantages related to the spray-drying method, non-uniform particle sizes are obtained, which represents an important limitation principally with regard to the administration way of the nanoparticles. As a consequence, novel preparative methods based on spray system have recently been emerged. Furthermore, Berkland *et al.,* (2001) established that extra benefits could be achieved by combining this methodology with some of the conventional techniques such as double emulsion or nanoprecipitation. Another limitation of spray-drying is that there may be very significant loss of product during the process due to the adhesion of the microparticles to the inside wall of the spray dryer apparatus and/or the agglomeration of the particles. A possible solution would be the double nozzle spray drying technique that employs an anti-adherent.

2.6.5 Miscellaneous Methods

Polymerization of monomers by various methods including emulsion, suspension, and dispersion techniques are currently employed in order to obtain nanoparticles (Soppimath *et al.,* 2001; Hans and Lowman, 2002). Recently, supercritical fluids have been used for nanoparticle synthesis. The benefits associated with the use of supercritical fluids have advocated the application of this kind of technology in the production of nanoparticles (Yeo and Kiran, 2005). The versatile operating conditions that are possible with supercritical fluids provide the flexibility in the control of the size of the particles that span from microns to nanometres. The possibility of fabrication of polymeric particles in a solvent-free system is the most attractive advantage provided by these techniques, especially with regard to the application of nanoparticles in the biomedical field. This method offers, low critical temperatures for processing (34°C) and the avoidance of oxygen exposure during atomization, both parameters of particular importance to encapsulate drugs like antigens and proteins (Reverchon and Antonacci, 2007). The use of PLA-based polymers to carry out these novel approaches have rapidly emerged. Cooper (2000) has reviewed the use of the supercritical techniques in the encapsulation of various pharmaceutically active compounds with PLA, PGA and PLGA polymers.

Tu *et al.,* (2002) have encapsulated *p*-hydroxybenzoic acid and lysozyme onto PLA using supercritical CO_2. They evaluated several parameters associated with the method such as pressure, temperature, solution concentration, polymer solvent system, etc. They obtained uniform PLA spheres of diameter of about < 2 μm. The increase in the temperature aroused agglomeration and slight plasticization on the obtained particles. The effect of spraying rate

was also demonstrated since a size reduction was noticed when the spray velocity increased. From the encapsulation efficiency point of view, lower values were reached compared with those obtained using conventional techniques. In spite of this, other valuable benefits offered by supercritical process are: requirement of small amounts of organic solvent, use of a non-toxic antisolvent, rapid processing time and moderate temperatures (Tu *et al.*, 2002).

2.7 DESIGN OF EXPERIMENT FOR POLY(LACTIC ACID) NANOPARTICLE PREPARATION

The application of PLA-based nanoparticles as the reservoir for different kinds of drugs to be released in a controlled way has been an object of study in the past years. In spite of this, to the best of our knowledge, there is not enough information available on the relationship between the properties of PLA nanoparticles and the methods used for their preparation. A better knowledge of the experimental parameters involved in the preparation process can be a valid tool to improve the drug-release efficiency and for the understanding of the mechanisms of the release system, especially considering the required particle size. There is no open literature available on the use of DOE for the preparation of PLA nanoparticles, although Angellier *et al.*, (2004) has prepared starch nanocrystals using response surface methodology and Jahanshahi *et al.*, (2008) have used Taguchi design for gelatin nanoparticles preparation.

Although the research on pharmaceutical nanoparticles has been extensive during recent years, advancement of products to the market has not yet occurred. Problems like poor drug encapsulation efficiency and difficulties in controlling and scaling up of the preparation process have inhibited progress. Thus, there is need for the proper regulation of effects of various parameters affecting the yield, particle size and different properties of the nanoparticles. Thus, DOE was applied for the preparation of PLA NPs. Full factorial design produces a very large number of experimental trials, whereas; fractional factorial design can produce different subsets of the full factorial design, of which a particular subset is designed by particular experimenter, which may or may not be identical as other experimenter. The combination of experimental trials may be different, when operated by different people at different places. Thus, to overcome this shortcoming, Taguchi Method of Experimental Design (TMED) - a typical fractional factorial design, developed orthogonal arrays. TMED produces same combination of experimental trials. These orthogonal arrays force all experimenters to design almost identical experiments.

TMED has proved to be the most powerful tool for process optimization (Antony *et al.*, 2006) as it focuses on minimizing variation and/or sensitivity to noise. Taguchi's parameter design or robust design methodology involves maximization of performance and quality at minimum cost. This is fundamentally achieved by determining the best settings of those design or process parameters which influence the product performance variation and by fine tuning those design or process parameters which influence the average performance. There are ten steps in a systematic approach to the use of Taguchi's parameter design methodology (Antony *et al.*, 2006).

1. *Problem recognition and formulation:* To establish a good understanding of the problem and the objective of the experiment.
2. *Select quality characteristic:* Select the appropriate quality characteristic(s) to measure the experimental results.
3. *Select design or process parameters:* Identify the design or process parameters which are believed to influence the quality characteristic of interest.
4. *Classify design parameters into control, noise and signal factors:* Control parameters are those which can be controlled easily under standard conditions, noise factors are those which cannot be controlled or are expensive to control during normal or standard conditions. Signal factors are those which are used for process tuning or adjustments.
5. *Determine levels of design or process parameters:* Determine the number of test levels for the design or process parameters (two or three levels are commonly used).
6. *Identify interactions:* Determine which, if any, design parameter interactions should be studied or analyzed.
7. *Choose appropriate orthogonal array (OA):* Select most suitable OA from standard OA designs.
8. *Conduct experiments:* Execute the experiment based on pre-prepared experimental layout showing all the experimental trial conditions.
9. *Perform statistical analysis:* Determine the best design parameter settings, predict the optimal condition, and establish confidence interval for the predicted response or quality characteristic.
10. *Perform a confirmatory experiment and implement results:* A confirmatory experiment is performed to verify the optimal settings of design parameters and to see whether or not the optimal condition derived by the experiment actually yields an improvement in product quality, yield or performance. If the results from the confirmatory experiment are

conclusive, a specific action on the product or process must be taken for improvement. On the other hand, if unsatisfactory results are obtained, further investigation of the problem may be required.

One common approach for analysis of experimental results, as suggested by Taguchi's method, involves graphing of the effects and visual identification of parameters, which appear to be significant. This technique uses a statistical measure of performance called signal-to-noise ratio (SNR). Taguchi stresses the importance of studying the response variation, using the SNR, resulting in the minimization of the quality characteristic variation, due to noise factors (Taguchi, 2005). SNR is the statistical quantity representing the power of a response signal divided by the power of the variation (noise) in the signal. It is derived from the loss function and assumes different forms depending on the optimization objective. The first step is to compute the SNR corresponding to each experimental condition. Secondly, the main effect plots and the interaction plots are analyzed.

SNR is a measure of robustness and it represents an index of data quality. The output parameter will possess one of the following three characteristics:

1. The bigger the better
2. The smaller the better
3. The nominal the best

The appropriate SNR must be chosen using previous knowledge, expertise, and understanding of the process. When the target is fixed and there is no signal factor, it is possible to choose the SNR depending on the goal of the design. When the goal is to maximize the response, SNR for larger the better is chosen, which is calculated using the Eq. 2.4. When the goal is to minimize the response, smaller the better SNR is chosen, which is calculated using Eq. 2.5. SNR for nominal-the-best quality characteristic is calculated using the Eq. 2.6.

$$S/N = -10[\log(\sum(1/Y^2)/n)] \quad \ldots (2.4)$$

$$S/N = -10[\log(\sum(Y^2/n)] \quad \ldots (2.5)$$

$$S/N = 10\log(\bar{Y}^2/s^2) \quad \ldots (2.6)$$

where, $\bar{Y} = \frac{1}{n}\sum_{i=1}^{n} y_i$ and $s^2 = \frac{1}{n-1}\sum_{i=1}^{n}(y_i - \bar{Y})^2$ and $(\bar{Y})$ is the average response, y_i represents the response obtained from n experiments of identical parameters, where i is equal to 1to n and s is the variance of the n experiments (MINITAB guide).

Based on our objective and the design parameters involved in this present investigation, Taguchi method of DOE is applied for determining the effects of various parameters on maximizing the yield and minimizing the particle size. When the factorial design was tried it produced 64 runs, which is very large. But when Taguchi method is used it produced only 16 runs, which is controllable. Taguchi orthogonal array design (TOAD) allows analyzing many factors with few runs. The details of the design are described under Section 3.3 of the Experimental part of this thesis.

2.8 CHARACTERIZATIONS OF POLY(LACTIC ACID) NANOPARTICLES

In nanoparticle characterizations, the measurement of particle size, bulk and surface chemical composition are of critical importance. Importantly, the internal structure of the particles can be measured by combinations of microscopy and thermal analysis. Colloidal systems like nanoparticles differ from macroscopic objects because of sub-micron properties such as high surface area and energy, and movement of the particles by diffusion (Brownian motion). The different behavior, of nanoparticles, leads to the use of different pattern of characterization methods. Extensive characterization of nanoparticles is essential for understanding and predicting its performance in the body. As the field of pharmaceutical nanoparticles is evolving constantly, the need for more thorough characterization and comprehensive understanding of the nanoparticles is essential. As in the present work, the main objective is to prepare PLA nanoparticles, characterization methods focus on the determination of size of the nanoparticles.

Size, morphology and physical state of the encapsulated drug as well as molecular weight and crystallinity of the polymer influence drug release and degradation of the nanoparticles. Meanwhile, size, surface charge and hydrophobicity / hydrophilicity are parameters that affect the body distribution and interactions with the biological environment. Stability of nanoparticles is also a general issue governing the above mentioned properties (Hirsjärvi *et al.*, 2008).

Conventional light microscopy is not suitable for nanoparticle characterization as its resolution is limited to about 1 μm. Instead, techniques for the characterization of nanoparticle size and morphology are field emission scanning electron microscopy (FESEM) and transmission electron microscopy (TEM). Now days, nanoparticles are usually studied with 5,000 – 30,000-fold magnifications. In FESEM setup, the nanoparticle sample is coated with gold to make it conductive and then is scanned in a high vacuum chamber with a

focused electron beam. Secondary electrons, emitted from the sample, are detected and the image formed. In TEM, electrons scattered by the sample are detected; the sample is kept between the electron gun and the detector. Another technique in pharmaceutical nanoparticle characterizations is atomic force microscopy (AFM) which is also called scanning probe microscopy technique.

Photon correlation spectroscopy (PCS), a technique based on dynamic (laser) light scattering, also called DLS technique, is widely used in size determinations of nanoparticles. PCS measures the intensity variation (because of the Brownian motion of nanoparticles) of scattered light, and relates it to the particle size with the help of an autocorrelation function. As a result, a hydrodynamic diameter is obtained (PCS presumes all the particles to be spherical). The theoretical hydrodynamic radius (R_{hyd}) arises in the study of the dynamic properties of polymers moving in a solvent. It is often similar in magnitude to the radius of gyration. However, the Malvern instrument, used in the present work, used the Stokes-Einstein equation, Eq. 2.7, to calculate the size of a particle from the translational diffusion coefficient.

$$d(H) = \frac{kT}{3\pi\eta D} \qquad \ldots. (2.7)$$

Where; $d(H)$ = hydrodynamic diameter; D = Translational diffusion coefficient;

k = Boltzmann's constant; T = absolute temperature; η = viscosity.

PCS is a fast technique, sensitive to nanoscale particles, and provides information about the whole particulate population. On the other hand, the dispersion has to be diluted and filtered. The results are based on mathematical calculations. The dispersant viscosity, temperature and refractive index should be known to proceed for PCS. Therefore, one should be vigilant when interpreting size information from PCS experiments. Instead, SEM/TEM provides visual and descriptive information, a real overview about the nanoparticle population. However, this information is not usually quantitative in terms of distributions. As a conclusion, initial size should be determined by considering together the information obtained from micrographic images obtained from Scanning/Transmission electron microscopy and light scattering.

The zeta (ζ) potential of nanoparticles is commonly used to characterize the surface charge property of nanoparticles. Surface charge of nanoparticles determines the performance of the nanoparticle system in the body, for e.g. interactions with cell membranes. It is important in determining whether the nanoparticles would cluster in blood

flow and how they would adhere to and interact with cells whose membranes are negatively charged. It reflects the electrical potential of particles and is influenced by the composition of the particle and the medium in which it is dispersed. Nanoparticles with a zeta potential above (+/-) 30 mV have been shown to be stable in suspension, as the surface charge prevents aggregation of the particles. The ζ-potential can also be used to determine whether a charged active material is encapsulated within the centre of the nanocapsule or adsorbed onto the surface (Hirsjärvi *et al.,* 2008).

2.9 APPLICATIONS OF POLY(LACTIC ACID) NANOPARTICLES

Polymer nanoparticles have been produced for decades for use in a variety of high performance materials such as high impact resistant polymers and specialty coatings long before it was fashionable to use the "nano" label. The extraordinarily large surface area of the nanoparticles presents diverse opportunities to place functional groups on the surface. Nanoparticles can expand/contract with change in pH, or interact with anti-bodies in special ways to provide rapid ex-vivo medical diagnostic tests. Important extensions have been made in combining inorganic materials with polymers and in combining different classes of polymers together in nanoparticle form. The most traditional field of application is waterborne paints, adhesives, and coatings. Of more recent emergence is the field of redispersible latices and pressure sensitive adhesives. A recent boom in the range of application of polymeric nanoparticles is in the sector of biotechnology, and more specifically biomedical products. These include the critical delivery of sensitive drugs and medical diagnostics. Last but not the least, polymeric nanoparticles have found their ways in EMO devices (Electronics, Magnetics, Optoelectronics).

While the research in the field on pharmaceutical nanoparticles is extensively reviewed, its commercialization has not yet occurred. Instead, research in the field of biodegradable nanoparticles has concentrated on the formulation of systems that takes advantage of their smaller size. The following paragraphs present examples of recent, in vivo tested nanoparticulate drug delivery applications based on PLA and PLGA polymers.

Recently, tumor targeting, independent of body distribution, has been reported: paclitaxel loaded poly(vinyl alcohol)-PLGA nanoparticles have been successfully targeted to prostate tumors of mice with the help of an RNA aptamer (binds to the tumors) on the particle surface (Cheng *et al.,* 2007). Another studied application of nanoparticles is drug delivery across the blood-brain barrier (BBB). Nanoparticles with mucoadhesive properties

can improve ocular drug delivery by prolonging the residence time of the drug in the tear film, controlling release and reducing irritation after topical administration. Because of these benefits, flurbiprofen (an anti-inflammatory drug) encapsulated in PLGA nanoparticles showed higher anti-inflammatory effect than the corresponding commercial eye-drops (Vega *et al.*, 2006).

2.10 SUMMARY

In the present investigation our main objective is to synthesize PLA homopolymer. Based on the review, melt polycondensation method followed by SSP was found to be one of the best methods to synthesize high molecular weight of PLA. Among the various post polycondensation methods, SSP was selected, as during post-polycondensation any external agent is not required and thereby pure PLA is produced. In the present investigation, response surface method (RSM) of DOE is used for the purpose of preparation of PLA and optimization of its yield and M_w. The number and levels of the selected operating parameters advocated for the use of CCD of RSM. Small face centered CCD of RSM was chosen to proceed for the MPC and SSP as this gives lower number of experiments with three levels to determine the non-linearity in the variation of effect of different operating parameters on the yield and M_w of PLA.

Another objective of this study is also to prepare nanoparticles from poly(lactic acid) polymer and to characterize physicochemical properties of the starting raw materials and the nanoparticles by different methods. Amongst the various processes for nanoparticle preparation, nanoprecipitation method was chosen for the preparation of PLA nanoparticles as it is economic and less labor intensive. Taguchi method was applied with an aim to evaluate and understand the effect of different operating parameters on the yield and size of the nanoparticles.

EXPERIMENTATION

To meet the objectives formulated in Chapter 1, experimental setups were designed, fabricated, tested and commissioned. The design considerations of experimental setups, selection of the range of operating parameters and their levels, experimental procedures and details of the characterization methods for raw materials and products are discussed in this Chapter.

In the present work, three different sets of experiments have been conducted to achieve the underlined objectives formulated in Chapter 1. In the first set of experiments, PLA was synthesized using melt polycondensation method and through second set of experiments, it was synthesized using solid-state polycondensation method. For these two cases, response surface methodology (RSM) was used for the design and analysis of the experiments. In the third set of experiments, PLA nanoparticles were prepared by nanoprecipitation method. For this method Taguchi design was used for the design and analysis of experiments.

3.1 DESIGN OF EXPERIMENT FOR MELT POLYCONDENSATION OF LACTIC ACID (LA)

It is a known fact that treatment of each factor at a time separately, is a tedious and time consuming task, especially when large numbers of variables are involved in an experiment. Furthermore, if several factors contribute towards an output parameter, their interactions could not be discernable even if they were dominated (Roy *et al.,* 2008). Thus, statistical experimental method (SEM), a powerful technique for quantifying the effect of multiple process variables on output parameters, is applied in the present investigation. In addition to it, interactions between variables can also be identified and quantified by such a technique (Shih *et al.,* 2002). Further, statistical design of experiment (DOE) techniques, which are based on statistical approaches, provide an efficient means to optimize a process (Anderson *et al.,* 1996).

Based on the objectives and experimental constraints, the RSM method of DOE was followed for melt polycondensation of L-lactic acid. The design and analysis of the response surface method (RSM) design was carried out using Design Expert Software.

Although, MPC of L-lactic acid (LLA) have been investigated earlier, little information is available on the regulation of its molecular weight. A review, as given in Section 2.1.2.2, shows that insufficient information is available to quantify effects of various parameters on yield and molecular weight. The present work is an attempt to bridge this gap. While screening the available data in the cited and related literature for MPC, it has been found that there exist no correlation which could establish the relationship between all the pertinent variables required for synthesis of PLA and output variables such as yield and molecular weight. Further, a scrutiny of available data using MINITAB software shows that, interaction parameters could not be studied due to insufficient data points. It has also been observed from the literature that fifteen parameters such as the amount of LLA, amount of catalyst, amount of co-catalyst, dehydration time, dehydration temperature, dehydration pressure, esterification time, esterification temperature, esterification pressure, decompression time, decompression temperature, decompression pressure, MPC time, MPC temperature and MPC pressure affect the process of melt polycondensation of LA directly or indirectly (Maharana *et al.,* 2009).

However, it is quite cumbersome to investigate such a large number of factors through experiments. Therefore, on the basis of information available in literature related to the synthesis of PLA by MPC (Moon *et al.,* 2000, 2001, 2003, Chen *et al.,* 2006, Lee *et al.,* 2005), five most significant parameters such as amount of LLA, amount of catalyst, esterification (ES) time, MPC temperature and MPC time have been selected keeping in view their extent of contribution towards yield and molecular weight, whereas; other remaining parameters have been kept at conducive fixed values. The fixed parameters are set as per the experimentations of Moon *et al.,* (2000, 2001), as they have achieved high molecular weight PLA at these values. The experimental conditions for MPC of LLA are given in Table 3.1 and the fixed operating parameters for MPC are given in Table 3.2.

The settings of the different parameters were determined for all of the predictors from published literature keeping in mind the two intuitive rules. Firstly, the optimal conditions could lie outside the region of interest if too narrow a variation range is selected. Secondly, the predictive power of the model becomes poor if too large a range is selected. The setting levels of different parameters are given in Table 3.1. Table 3.1 shows the minimal ($X_{i,\ min}$), the mid range ($X_{i,\ mid}$) and the maximal ($X_{i,\ max}$) values used for each parameter, which corresponds to -1, 0 and +1 levels, respectively, in terms of orthogonal variable X_i defined by Eq. 3.1.

$$X_{i,\text{coded}} = \frac{2(X_{actaul} - \overline{X})}{X_{i,\max} - X_{i,\min}} \quad \text{...Eq. 3.1}$$

Where, $\overline{X} = \frac{X_{i,\max} + X_{i,\min}}{2}$.

In spite of reduction of operating parameters from fifteen to five, the effect of these on yield and molecular weight of PLA could not be ascertained due to lack of data available in literature. Thus, it was thought to conduct experiments with the help of DOE to generate relationships between the five pertinent parameters, thus selected, with the yield and molecular weight and also to generate a response surface to find out optimum operating parameter which could generate maximum yield and weight average molecular weight (M_w) within the design space.

Table 3.1 Experimental conditions for MPC of LLA

Factor	Name	Units	Low level $X_{i,\min} = -1$	Mid level $X_{i,\text{mid}} = 0$	High level $X_{i,\max} = +1$
X_1	LLA	g	20	30	40
X_2	Catalyst	Wt. %	0.4	0.7	1.0
X_3	ES time	h	2	5	8
X_4	MPC temperature	°C	180	210	240
X_5	MPC time	h	10	20	30

Table 3.2 Fixed operating parameters for MPC

Operating parameter	Units	Fixed Value(s)		
Dehydration (DH) step				
DH temperature	°C	150	150	150
DH time	h	2	2	4
DH pressure	mm Hg (abs)	760	100	30
Esterification (ES) step				
ES pressure	mm Hg (abs)	30	ES time variable as given in Table 3.1	
ES temperature	°C	180		
Decompression (DC) step				
DC temperature	°C	180		
DC time	h	1		
DC pressure	mm Hg (abs)	30-10	Pressure was reduced from 30 to 10 mmHg (abs)	
Melt polycondensation (MPC) step				
MPC pressure	mm Hg (abs)	10	Variable MPC time & MPC temperature as given in Table 3.1	

The current research goal was to synthesize PLA by using MPC technique with the help of tin chloride dihydrate-PTSA as the binary catalyst and to optimize the yield as well as the weight average molecular weight (M_w) of synthesized PLA by using response surface methodology which is largely used and well adapted to process optimization in the macromolecular science area (Karlsson and Albertsson, 2002). Four sub-steps in MPC viz., dehydration, esterification, decompression and melt polycondensation were applied. The influence of five pertinent parameters such as amount of LLA, catalyst wt. %, esterification time, MPC time and MPC temperature on the molecular weight of PLA were studied with the help of RSM. Experiments, particularly those which seek to optimize a process or product, should proceed sequentially. RSM is one such sequential method of DOE. The most commonly used design, to estimate a model that has at least as many distinct treatment combinations as terms in the models and has at least three levels for each factor, is the central composite design of RSM. Response surface graphics, which can be produced with statistical software, makes it easy to find the optimum performance.

Central composite design (CCD) is the most popular of many classes of RSM designs as it can be run sequentially, and is very efficient and flexible. Among the different classes of CCDs such as rotatable, spherical, face centered etc., face centered design is simpler one as it requires operating the process at only three level settings of each variable in contrast to the other five level designs. And also a face-centered CCD can be used when the region of operability encompasses the region of interest as defined by the variable bounds. The region of interest has been screened from the previous literature. The increased number of reconfigurations in rotatable design provides a much greater opportunity for sources of experimental error associated with setup and operation to express themselves. Still then, the benefits of rotatable designs do not offset the added complexity and associated risk in most cases, making the face-centered CCD more than adequate for most experiments (Montgomery, 2004).

Keeping in view the objective along with number, nature and levels of parameters, a small face centered central composite design (SFCCCD) of RSM was applied to find out, input-output correlations, interaction amongst different screened parameters and optimization of process parameters for MPC experimentation and analysis. Experiments were conducted at set of parameters suggested by the design generated by Design-Expert 7.1.5 (henceforth will be called DE7) software, Stat-Ease statistical software, as given in Table 3.3. The coded values of different combination of parameters generated by DE7 are

reported in Table E.1 of the Appendix E. The results obtained after doing experiments at the set of parameters suggested by DE7 are reported in Table 4.2 of Section 4.2. Based on the response data of Table 4.2 an analysis to develop the model was carried out using DE7. The predictive models for yield and M_w were produced using DE7 and are given in Section 4.2.1.

A small face centered central composite design (SFCCCD) results in 26 different combinations of five different parameters instead of 50 and 32 combinations for full and half fraction, respectively. SFCCCD consists of 11 factorial points, 10 axial points and 5 center points. The combination of operating parameters corresponding to the central point of the design was replicated five times in order to confirm the validity of the model and to reduce the estimate variance of the values predicted by the model (Cochran and Cox, 1992).

Table 3.3 lists the values selected for the five independent variables studied, which clearly shows it is a 3-level experiment.

Table 3.3 Set of operating parameters obtained by CCD of RSM in terms of actual values

Run	Point Type	X_1: LLA(g)	X_2: Catalyst(Wt.%)	X_3: ES time(h)	X_4:MPC temperature(°C)	X_5:MPC time (h)
1	Factorial	40	1.0	2	240	10
2	Factorial	40	0.4	8	240	10
3	Factorial	20	1.0	8	180	30
4	Factorial	40	1.0	8	180	10
5	Factorial	40	1.0	2	180	30
6	Factorial	40	0.4	2	240	30
7	Factorial	20	0.4	8	240	30
8	Factorial	20	1.0	2	240	30
9	Factorial	40	0.4	8	180	30
10	Factorial	20	1.0	8	240	10
11	Factorial	20	0.4	2	180	10
12	Center	30	0.7	5	210	20
13	Center	30	0.7	5	210	20
14	Center	30	0.7	5	210	20
15	Center	30	0.7	5	210	20
16	Center	30	0.7	5	210	20
17	Axial	20	0.7	5	210	20
18	Axial	40	0.7	5	210	20
19	Axial	30	0.4	5	210	20
20	Axial	30	1.0	5	210	20
21	Axial	30	0.7	2	210	20
22	Axial	30	0.7	8	210	20
23	Axial	30	0.7	5	180	20
24	Axial	30	0.7	5	240	20
25	Axial	30	0.7	5	210	10
26	Axial	30	0.7	5	210	30

3.1.1 Design Considerations for Experimental Setup

In order to get accurate and reliable results from the experiments, the following important considerations have been taken into account for the design of the various components of the experimental setup.

1. The polycondensation reaction was carried out under nitrogen atmosphere to maintain inert atmosphere inside the reactor so as to prevent oxidation of the reactants and the products.
2. The commercially supplied nitrogen gas cylinder may contain trace amount of oxygen as impurity. Thus, nitrogen gas was purified using pyrogallol solution. After passing through pyrogallol solution, it was passed through $CaCl_2$ to absorb any traces of water vapors present and then passed through cotton to get purified nitrogen gas.
3. A 100 ml three neck round bottom flask was used as a reaction vessel (henceforth referred to as a reactor). This is selected keeping in view the fact that such reaction vessels can withstand lower pressure/vacuum better than flat bottom one. Further, to maintain minimum empty space inside the reactor, a 100 ml capacity flask was selected rather than that of higher volume flask. A still smaller vessel was not used as the condenser and stirrer may not fit properly into it. A minimum available space will prevent reactants and products from getting oxidized.
4. When the condenser was directly joined to the reactor through an adaptor, the water vapor generated due to reaction and the evaporated LA, used to condense at the mouth of the condenser and clog the path of vapor flow. Thus, a splash head was used instead of the adaptor, so that the light water vapors will pass easily and the lactide and lactic acid vapors cannot pass easily and condense back to the reactor, thereby enhancing yield and molecular weight.
5. When the reaction proceeds, the content inside the reactor becomes viscous. Thus, a mechanical stirrer should be used instead of magnetic stirrer which is not efficient for stirring the viscous substance. But when a mechanical stirrer with stuffing box was used the high vacuum inside the reactor could not be maintained even after adopting best sealing technique for the rotating shaft of the stirrer. Thus, to overcome this difficulty, a hermetically sealed magnetic stirrer was designed and fabricated for use. The schematic diagram and the photographic view of the stirrer are given in Figs. 3.1 and 3.2, respectively.

6. To maintain the accurate temperature of the silicone oil bath fluid which surrounds the reactor, the oil bath was kept over a temperature controlled hot plate having an accuracy of 0.1°C. The oil bath was stirred by a magnetic stirrer to homogenize oil temperature.
7. As MPC is carried out under very low pressure, a specialized vacuum pump (Part number 22 mentioned in Fig. 3.3) supplied by ILMVAC (Model No: 6 Dp 101 chemvac) with diaphragm pump was used to maintain high vacuum. This pump has a provision to program and control high vacuum.
8. As the condensate vapors which may pass to the vacuum pump can damage it, 3 traps were used between the condensate collector vessel and the vacuum pump. Cold traps provided between the condenser and the vacuum pump eliminates the possibility of vapors entering into the vacuum pump, and thus, protects it from its malfunctioning and increases the life of the vacuum pump.
9. Another design consideration of paramount importance was related to the water to be circulated inside the condenser. For this purpose, a chilled water (C.W.) circulator was connected with the condenser to condense maximum amount of vapor produced in the reactor.

Keeping in view the above mentioned design considerations, the present experimental setup was designed, fabricated and commissioned. The experimental setup employed in the present investigation is shown schematically and photographically in Figs. 3.3 and 3.4, respectively. The individual parts of the experimental setup have also been presented in Appendix D. It essentially consists of nitrogen cylinder (1), gas washing bottles (2-4, 18-20), temperature controlled hot plate with magnetic stirrer (5), silicone oil bath (6), 100 ml three neck round bottom flask (8), perforated metallic ring (10), magnetic needle (11), hermetically sealed magnetic stirrer (7,9) splash head (12), condenser (13), inlet and outlet pipe (14,15), cold trap (16), chilled water (C.W.) circulator (17), trap (21) and a vacuum pump (22).

The temperature of the oil bath (6) and stirring speed were controlled by using a SLR Model hot plate with stirrer (5), procured from SCHOTT Instruments GmbH, Germany. The temperature of hot plate can be controlled up to 350°C. In this all functions can be viewed and monitored on a large, clear LCD display. The stirrer speed ranges from 100 to 1000 rpm and can be set in steps of 10 rpm. The heating power can be set in 24 steps and reaches an average heating output of 0.9 kW at step 24. For external temperature control, a Pt 1000 temperature sensor was connected to the hot plate which offered a temperature control between 25°C to 200°C at an accuracy level of +/- 2° to 5°C.

The cryostat constant temperature circulating bath (17) (Metrex MCC 12) was supplied by Metrex Scientific Instruments (P) Ltd. New Delhi, India. The temperature is controlled by a digital temperature controller-cum-indicator. Fine tuning of the heating system ensure high accuracy within a limit of +/-0.1°C. The unit can be operated continuously and is equipped with bottom discharge. The unit is fitted with circulation pump, having stainless steel contact parts with capacity 10 liters per minute at zero head. This was used to circulate water in the condenser.

The vacuum pump (Part No. 22 of Figure 3.3) Model Number 6 Dp-101 chemvac was supplied by ILMVAC GmbH Germany. The chemvac Combination Pump System consists of a two-stage, oil-combined rotary vane pump and a chemical diaphragm pump. The two pumps are functionally connected to each other by suitable separators and a pressure control valve to form a compact unit. The rotary vane pump and diaphragm pump were driven by 0.37 and 0.06 kW motor, respectively. The pumping speed is 5.8-6.6 m^3/h and the ultimate pressure is $<3x10^{-3}$ mbar. It was supplied with a sensor and PIZA 1000 LCD display to sense and display the pressure of the reactor.

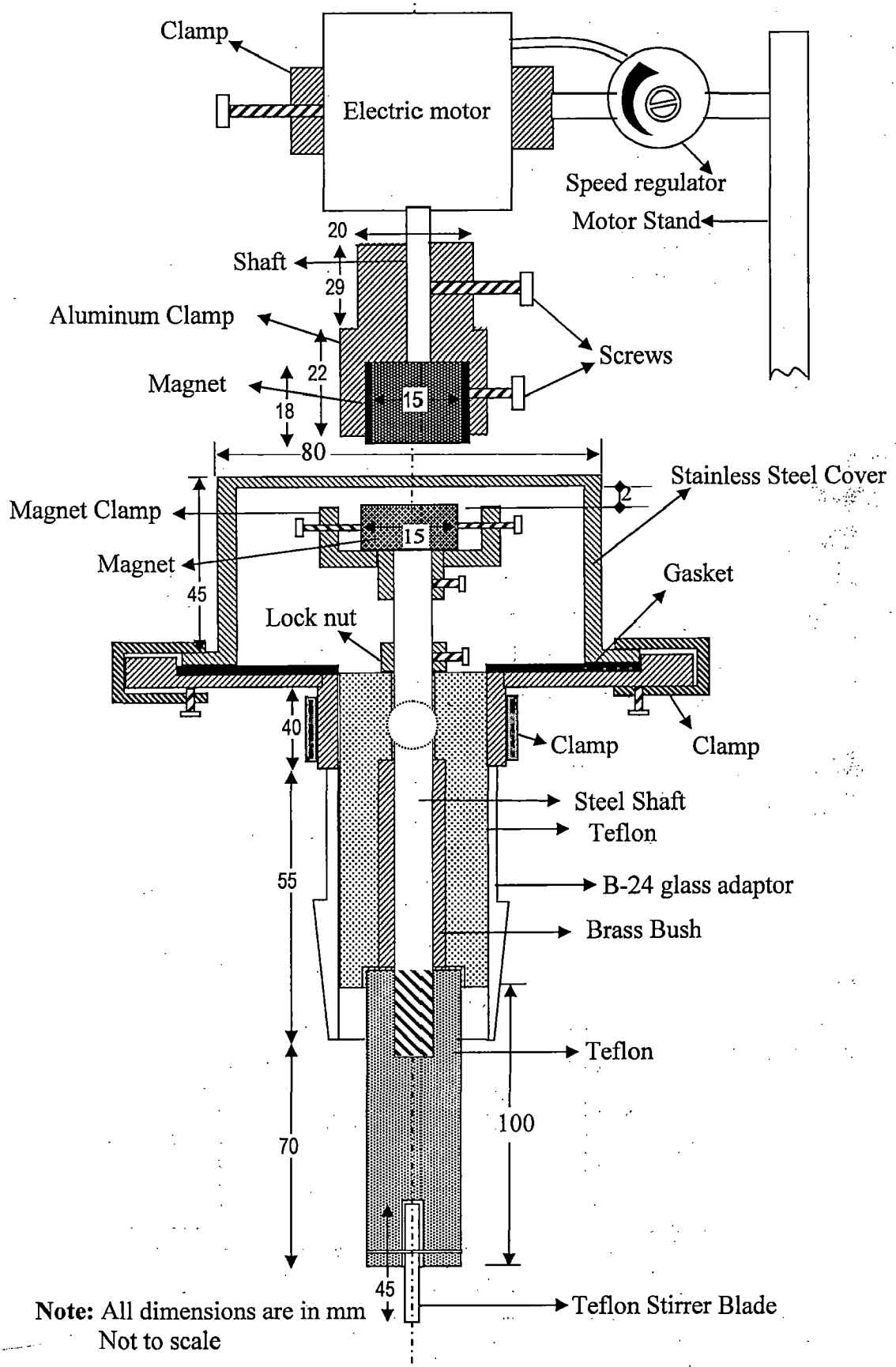

Fig. 3.1 Schematic diagram of the designed hermetically sealed magnetic stirrer

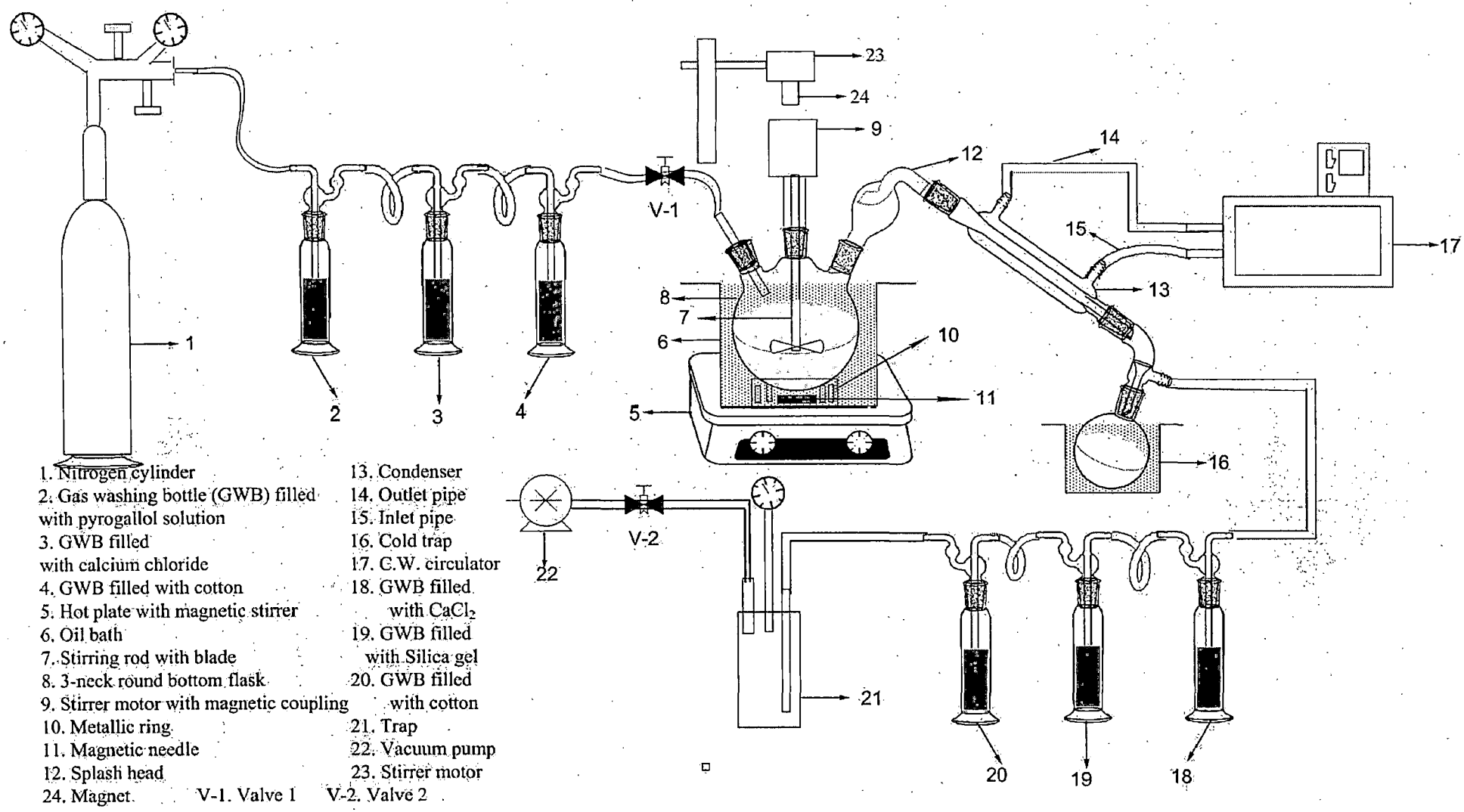

Fig. 3.3 Schematic diagram of experimental setup for MPC of LLA

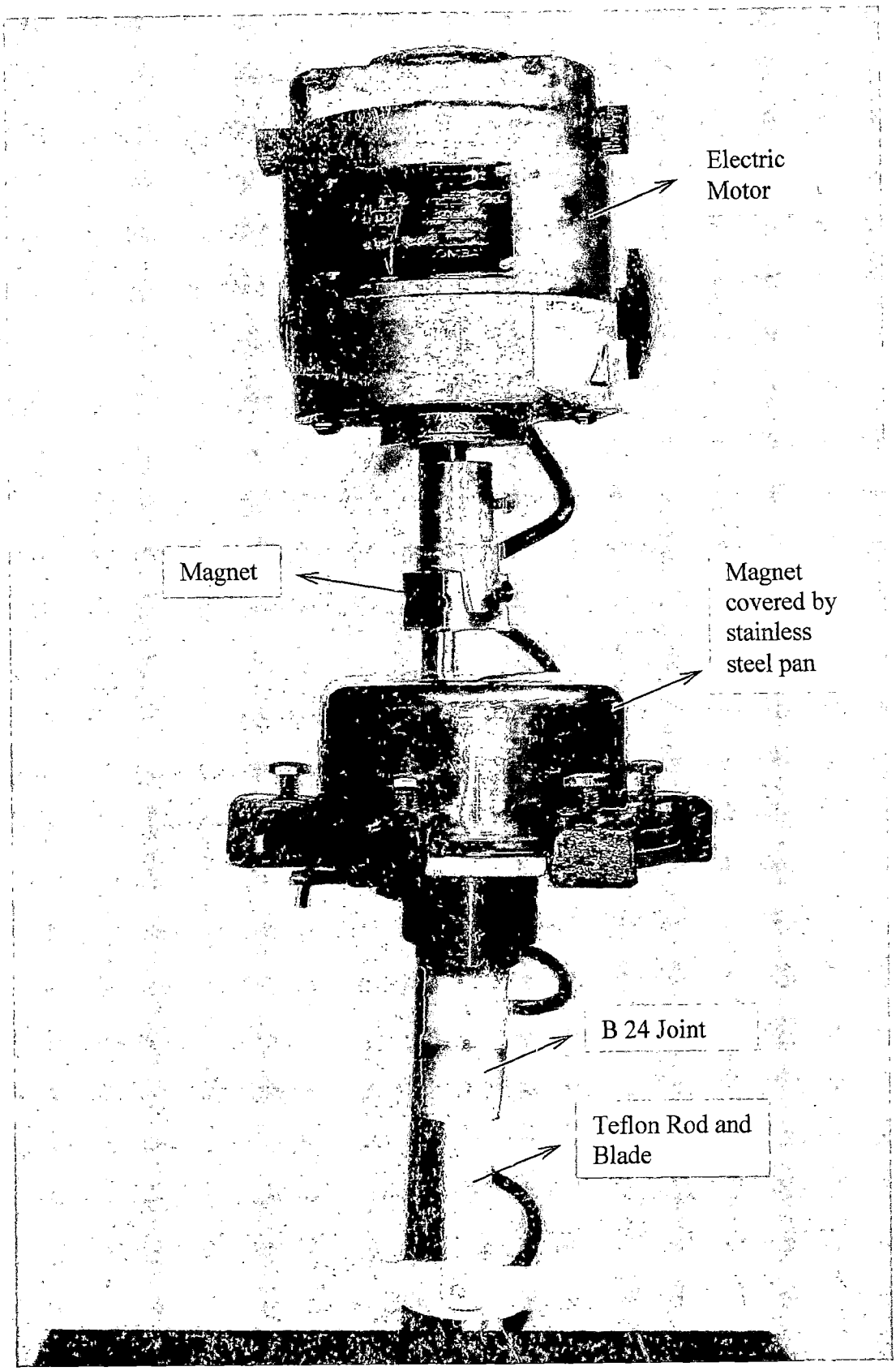

Fig. 3.2 Photographic view of the hermetically sealed magnetic stirrer

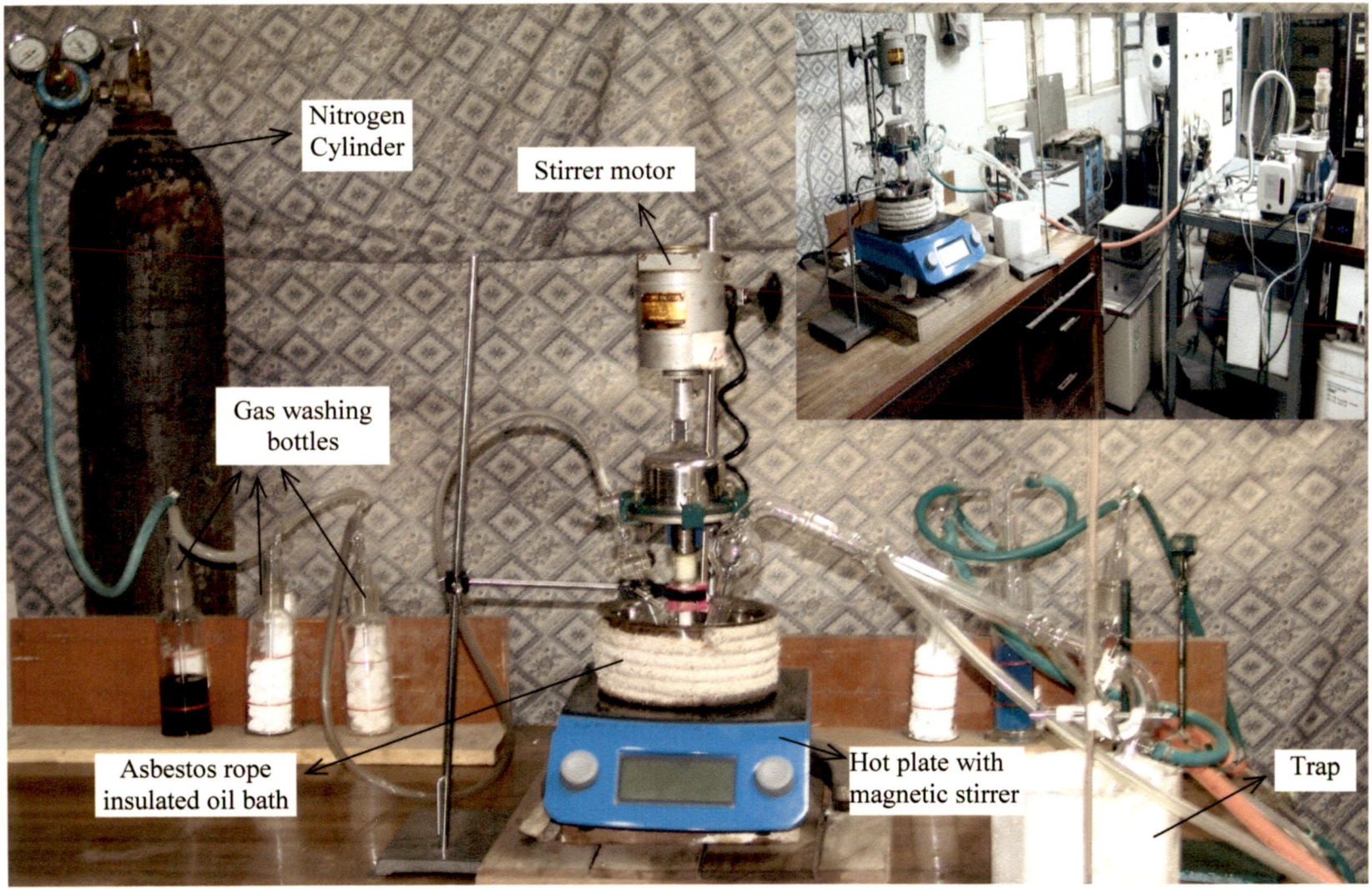

Fig. 3.4 Photographic view of experimental setup for MPC of LLA

3.1.2 Experimental Procedure for Melt polycondensation of Lactic Acid

Materials and Methods

L(+) Lactic acid with 88% assay and containing minimum 95% L(+) isomer supplied by Lactochem Limited, India, was used as received. Tin chloride dihydrate was procured from Ranbaxy Fine Chemicals Limited, India and PTSA was procured from Thomas Baker (Chemicals) Private Limited, India and both were used without purification. The numbers in the bracket in the Fig. 3.3 refers to the part number.

Step 1. **Preparation for purification of N_2 purge gas:** The crude N_2 gas available in the cylinder should be purified to make it free from oxygen impurities before it is used as a purged gas in the reactor to drive oxygen and humidity out from the connected vessels and pipe lines. For this purpose crude nitrogen gas should pass through a series of three gas washing bottles (2-4) each containing different materials. The first bottle contains pyrogallol solution, which removes trace amounts of oxygen by absorbing it. The second bottle contains $CaCl_2$ which absorbs water present in the oxygen free N_2 gas which might have been picked up from pyrogallol solution. The third bottle contains cotton to remove water droplets if any entrained by N_2 gas or any particulate material. The above three gas washing bottles were prepared. For preparing pyrogallol solution, 50 ml of water was degassed neatly by boiling it for 2 hrs in a conical flask. Six grams of potassium hydroxide was added to the hot water and immediately the stopper of conical flask was closed and the solution was cooled to room temperature. Two grams of pyrogallol was filled into the gas washing bottle (2) and the contents in the conical flask was then transferred to it and the bottle head was closed under purging of nitrogen.

Step 2. **Preparation of Traps (GWB 18-20):** Three gas washing bottles (18-20) were filled with silica gel, $CaCl_2$ and cotton, respectively and are connected in series as shown in the Fig. 3.3.

Step 3. **Cleaning of Glass surface:** Cleaning of the inner surface of glass reactor was done by washing with methanol and drying in 150°C in an oven. Before feeding, it was cooled to room temperature.

Step 4. **Experimental set-up:** The experimental setup was assembled as per the Fig. 3.3. LLA was charged into the three neck round bottom flask (8) by opening the neck of reactor used for nitrogen inlet. Cold water circulation through the condenser (13) was resumed using the C.W. circulator (17). The hot plate with magnetic stirrer (5)

was switched on to maintain the oil bath (6) at a temperature of 150°C. For maintaining uniform temperature of the oil bath (6), a magnetic needle (11) was placed inside a perforated metallic ring (10) to stir the oil, which was used to support the 3-neck round bottom flask (8).

Step 5. **Purification of Nitrogen Gas:** Pressure of the nitrogen gas in the nitrogen cylinder (1), was set to 5 kg/cm^2 (abs) through a pressure regulator. Once the nitrogen pressure was fixed, the valve V-1 was opened to start the purging of nitrogen gas into the reactor and the valve V-2 was kept closed.

Step 6. **Polymerization:** LLA was dehydrated at 150°C at atmospheric pressure, under purified nitrogen atmosphere, for 2 hours. After completion of 2 hrs, the valve V-1 was closed and vacuum pump (22) was switched on. Then dehydration was continued at the same temperature for 2 hours at 100 mm Hg (abs) pressure followed by 30 mm Hg (abs) pressure for 4 hour (Moon *et al.*, 2000, 2001) and a stirring speed of 200 rpm was maintained through out.

Step 7. A sample of the glassy white solid oligomer was obtained after dehydration and was characterized by gel permeation chromatography (GPC) for its molecular weight.

Step 8. Binary catalyst consisting of $SnCl_2.2H_2O$ and *p*-toluene sulphonic acid (PTSA) was added to the oligomer and then proceeded for esterification, decompression and melt polycondensation with a stirring speed of 100 rpm. The catalyst and co-catalyst were used in 1:1 equimolar ratio.

Step 9. Esterification was carried out at 180°C and at 30 mm Hg (abs) pressure for a range of time period, 2-8 hour. Time period was considered as a variable and was changed in different run numbers as per Table 3.3.

Step 10. Then the decompression process was carried out at 180°C, by reducing the pressure from 30-10 mm Hg (abs) in a stepwise manner within a time period of one hour.

Step 11. Melt polycondensation was done at 180-240°C at 10 mm Hg (abs) pressure for different time periods, which varied from 10-30 hour as per Table 3.3 for different runs.

Step 12. After completion of the reaction, the reactor was removed from the oil bath and was let to cool down to room temperature. Then valve V-2 was opened to make the vessel vacuum free and the product was dissolved in $CHCl_3$ and precipitated in excess methanol and then filtered using G4 Gooch crucible.

Step 13. The precipitate was washed well with methanol repeatedly, to wash out the residual lactide, lactic acid and catalyst and then dried in vacuum oven for about one hour at a temperature of 40°C. The photographs of the PLA samples are presented in Fig. 3.5.

Step 14. **Determination of Yield**: The yield (wt. %) of PLA was computed using Eq. 3.2.

$$\text{Yield}(\%) = \frac{\text{wt. of PLA obtained}}{\text{wt. of LA taken initially}} x100 \qquad \ldots \text{Eq. 3.2}$$

Step 15. PLA thus produced was characterized by GPC for obtaining its molecular weight. PLA was also characterized by FTIR, NMR, TGA/DTA/DSC, XRD and FESEM. Details of these processes are described under Section 3.4.

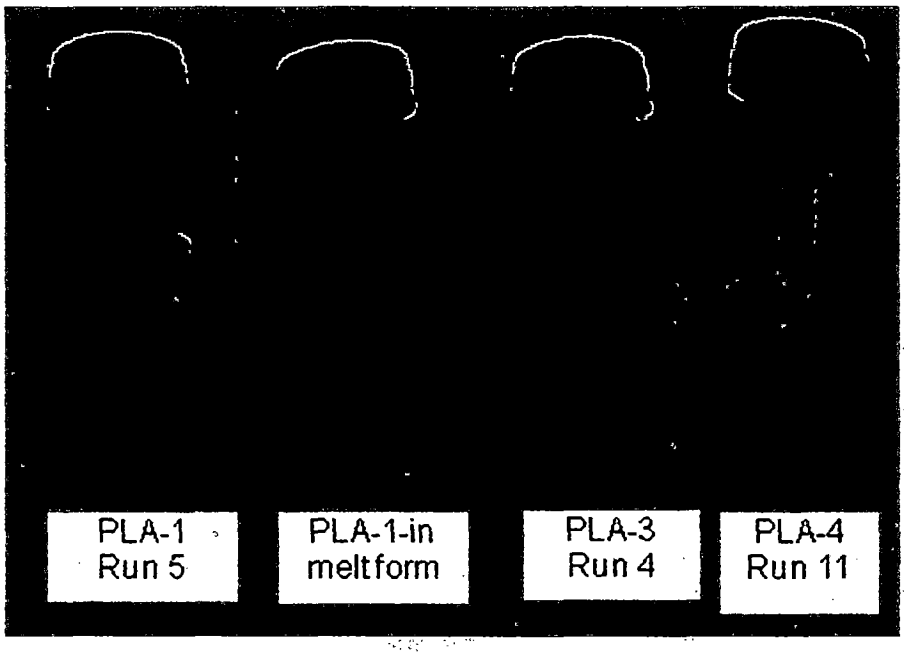

Fig. 3.5 Photographs of the PLA samples

3.2 DESIGN OF EXPERIMENT FOR SOLID-STATE POLYCONDENSATION OF POLY(LACTIC ACID)

Melt-solid polycondensation is an approach to increase the molecular weight of PLA by increasing the degree of polymerization (Fukushima and Kimura, 2008; Moon *et al.*, 2001). Thus, in the present investigation, sequential melt-solid polycondensation method was used to synthesize PLA. For this purpose, PLA sample synthesized using method prescribed under Section 3.1.2 have been used.

Solid-state polycondensation is mainly performed in two steps. The first step is heat treatment (HT) and the second is solid-state polycondensation (SSP). A review, as given in

Section 2.1.2.3, shows that insufficient information is available to quantify effects of various parameters on yield and molecular weight. Although, ten parameters of importance in this process are, particle size, amount of PLA, molecular weigh of PLA, % crystallinity of PLA, heat treatment time (crystallization time), HT temperature (crystallization temperature), HT pressure, SSP time, SSP temperature and SSP pressure, only five pertinent parameters are selected from these based on the published literature. The selected five parameters are shown in Table 3.4 and the remaining five parameters such as HT pressure, SSP pressure, particle size, molecular weight of PLA and % crystallinity (X_c) of PLA are fixed at predetermined values of 0.5 mm Hg, 0.5 mm Hg, 150-180 μm, 55 kDa and 14.73 %, respectively, as can be seen from Table 3.4.

Table 3.4 Operating parameters for heat treatment followed by SSP

Varying operating parameters		Fixed operating parameters	
Parameter	Range	Parameter	Value
Amount of PLA	3-5 g	HT pressure	0.5 mm Hg
HT temperature	100-120°C	SSP pressure	0.5 mm Hg
HT time	1-5 h	Particle size	150-180 μm
SSP time	10-30 h	M_w of PLA	55.634 kDa
SSP temperature	130-160°C	% X_c of PLA	14.73[a] %

[a] Based on enthalpy of fusion ; measured by DSC.

The setting levels of different parameters are given in Table 3.5. Table 3.5 shows the minimal ($X_{i,\ min}$), the mid range ($X_{i,\ mid}$) and the maximal ($X_{i,\ max}$) values used for each parameter, which corresponds to -1, 0 and +1 levels, respectively, in terms of orthogonal variable X_i defined by Eq. 3.1

Table 3.5 Experimental conditions for SSP of PLA

Factor	Name	Units	Low level $X_{i,\ min} = -1$	Mid level $X_{i,\ mid} = 0$	High level $X_{i,\ max} = +1$
X_1	Amount of PLLA	g	3	4	5
X_2	HT temperature	°C	100	110	120
X_3	HT time	h	1	3	5
X_4	SSP time	h	10	20	30
X_5	SSP temperature	°C	130	145	160

These parameters are fixed on the basis of the fact that at these values, Moon *et al.* have produced PLA of M_w ca. 600 kDa, a very high molecular weight. Again, it was studied

that SSP of low M_w PLA produced high M_w PLA because of the higher mobility of the end groups. Although hardly any investigation is reported on the SSP of PLA of M_w higher than 20 kDa, few patents (Terado *et al.,* 2001; Zhang *et al.,* 2007) have claimed that they have obtained 50 kDa$\leq M_w \leq$1,000 kDa from 2kDa$\leq M_w \leq$100 kDa PLA but no detailed information is available on the regulation of parameters on molecular weight. Zhang and Wang (2008) have studied the SSP of PLA of M_w in the range of 23 -59 kDa and obtained PLA of M_w in the range of 45 -162.1 kDa. PLA of M_w 52 kDa produced highest molecular weight. But no clear guideline is available on the effect of various parameters. And also very few literature, mostly Chinese and Japanese patents and publications are available on SSP of PLA.

Thus, in the present work, the M_w of PLA chosen for SSP was fixed to ca. 55 kDa. HT is carried out at the temperature range reported in Table 3.4, as the crystallization exotherm of the PLA sample produced in Section 4.2 was found to extend from 100-120°C as per the results obtained through DSC analysis. SSP reaction temperature can range from a temperature sufficiently below T_m to a temperature just 5-10°C below T_m. The PLA sample after heat treatment, becomes more stable to heat, and did not melt upto 160°C as the T_m was found to be ~165°C. Thus, in the present work, SSP was carried out in the range of 130-160°C. Moon *et al.,* (2001) has reported that increasing HT time from 1 to 2 hr increases the M_w. However, for other time periods (except 1 & 2 h) no study has been carried out. Thus, HT was carried out in the range of 1-5 hr time period. As SSP is a slow process it takes longer time duration to be completed and thus it was studied in a range of time period of 10-30 hrs. The PLA used for the SSP was linear with carboxylic acid and hydroxyl end groups, as discussed in Section 4.2.3. In spite of the fact that the number of operating parameters has been reduced to five, the effect of these on yield and molecular weight of PLA could not be ascertained due to lack of data available in literature. This is partly due to the fact that very few investigations are available in open literature on SSP of PLA, and these do not contain the effects of various operating parameters on yield and M_w. Thus, experiments are planned with the help of DOE to generate relationships between the above five selected parameters with the yield and molecular weight and also to generate a response surface to find out optimum set of operating parameters which could generate maximum yield and weight average molecular weight (M_w) within the design space. For the present work, predictive models, main effect and interaction plots for yield and molecular weight were produced using DE7 and Minitab.

Because of the facts discussed in Section 3.1, in this case also, a small face centered central composite design (SFCCCD) of RSM was applied to find out, input-output correlation, estimation of interaction amongst five screened parameters and optimization of process parameters. Experiments were conducted at the set of operating parameters suggested by the design generated by DE7 software as given in Table 3.6. The coded values of different combinations of operating parameters are presented in Table E.2 of the Appendix E.

Table 3.6 Set of operating parameters obtained by CCD of RSM in terms of actual values

Run	Type	Factor 1	Factor 2	Factor 3	Factor 4	Factor 5
		X_1: Amount of PLLA(g)	X_2: HT temperature(°C)	X_3: HT time (h)	X_4: SSP time (h)	X_5: SSP temperature(°C)
1	Factorial	5	120	1	30	130
2	Factorial	5	100	5	30	130
3	Factorial	3	120	5	10	160
4	Factorial	5	120	5	10	130
5	Factorial	5	120	1	10	160
6	Factorial	5	100	1	30	160
7	Factorial	3	100	5	30	160
8	Factorial	3	120	1	30	160
9	Factorial	5	100	5	10	160
10	Factorial	3	120	5	30	130
11	Factorial	3	100	1	10	130
12	Center	4	110	3	20	145
13	Center	4	110	3	20	145
14	Center	4	110	3	20	145
15	Center	4	110	3	20	145
16	Center	4	110	3	20	145
17	Axial	3	110	3	20	145
18	Axial	5	110	3	20	145
19	Axial	4	100	3	20	145
20	Axial	4	120	3	20	145
21	Axial	4	110	1	20	145
22	Axial	4	110	5	20	145
23	Axial	4	110	3	10	145
24	Axial	4	110	3	30	145
25	Axial	4	110	3	20	130
26	Axial	4	110	3	20	160

The experimental results obtained are presented in Table 4.38 under Section 4.3 of Chapter 4. Based on the response data of Table 4.38, an analysis to develop the model was undertaken using DE7. The models are shown in Section 4.3.1. Based on the above models, numerical optimizations have been carried out to know the values of parameters which will

produce highest yield and M_w. And thereafter, experiments have been conducted at the predicted optimum operating parameters to verify the predicted responses (yield and M_w) of the analysis. Table 3.6 lists the values selected for the five independent operating parameters studied, which clearly shows it is a 3-level experiment.

3.2.1 Design Considerations for Experimental Setup

The experimental setup for SSP is same as that of MPC (Sodergard and Stolt, 2009), except the fact that the reactor is a 50 mL test tube with B-24 glass joint, in place of the three-neck round bottom flask. The test tube is connected to a still head. To the side end of the still head, the condenser is attached and to the upper end, nitrogen inlet was connected. In this step magnetic stirrer was used instead of the mechanical stirrer. When the bath attains the required temperature, the reactor was placed inside the bath and the valve V-1, shown in Fig. 3.3, was opened and V-2 was kept closed to purge N_2 gas. After 15 min of passing of nitrogen, the valve V-1 shown in Fig. 3.3 is closed and the vacuum pump (22) was switched on and the pressure was reduced slowly to 0.5 mbar within a time period of 10-15 minutes. The samples obtained after SSP were cooled and dried under reduced pressure in a vacuum oven.

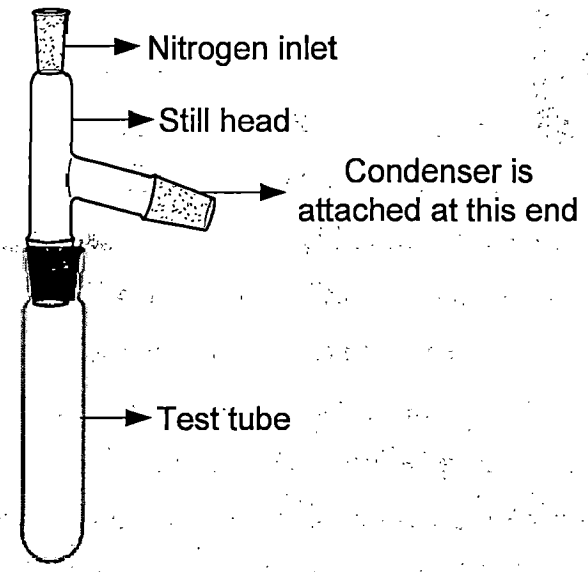

Fig. 3.6 Reactor for the SSP of PLA

3.2.2 Experimental Procedure for Solid-State Polycondensation of Poly(Lactic Acid)

Materials and Methods

PLA of M_w 55 kDa obtained by melt polycondensation, described in Section 3.1.2, has been used for the solid-state polycondensation of PLA. Its structure is linear with

carboxylic acid and hydroxyl end-groups. The PLA sample was crushed into powders. PLA powders were sieved using a mechanical sieving instrument (BEAUTEX Instruments, New Delhi, India) and two sieves of 100 and 80 mesh size, to separate particles of size in the range 150-180 μm and then these were vacuum dried prior to use. These particles were used for carrying out SSP of PLA without the presence of any catalyst.

Step 1. Step 1-3 of Section 3.1.2 were followed.

Step 2. **Experimental setup:** PLA was fed into the test tube as shown in Fig. 3.6. The experimental setup was assembled as per the Fig. 3.3, except the reactor was replaced by the reactor shown in Fig. 3.6. Chilled water circulation through the condenser (13) was started using the C.W. circulator (17). The hot plate (5) was switched on to maintain the oil bath (6) at the heat treatment temperature of the particular experiment as per the Table 3.6. Step 5 of Section 3.1.2 was repeated.

Step 3. The reactor was placed in an oil bath (6) of desired temperature and Nitrogen was passed for 15 minutes by opening the valve V-1. After 15 minutes, nitrogen supply was stopped by closing valve V-1 and immediately the vacuum pump (22) was started. A stirring speed of 200 rpm was maintained throughout the experiment.

Step 4. Heat treatment was carried out under a pressure of 0.5 mm Hg (abs) and at temperatures and time periods shown in Table 3.6.

Step 5. After the appropriate time period of heat treatment, the temperature of bath was increased to a SSP temperature shown in Table 3.6. SSP was conducted at 0.5 mm Hg (abs) for a time period as shown in Table 3.4.

Step 6. After conducting the SSP for a certain time period as defined in Table 3.6, the reactor was cooled down to produce PLA polymers. The PLA was dried under vacuum at ambient temperature prior to use.

Step 7. **Determination of Yield:** The yield (wt. %) of PLA was calculated using the following formula.

$$\text{Yield}(wt.\%) = \frac{\text{wt. of PLA obtained after SSP}}{\text{wt. of PLA taken initially}} x100 \qquad \ldots \text{Eq. 3.3}$$

Step 8. The produced polymer was analyzed without purification as no monomer, catalyst and co-catalyst are added during SSP. The PLA thus obtained was characterized by GPC, NMR, FTIR, XRD and FESEM for determining its molecular weight, structure, functional groups and crystalline properties etc. It was also characterized by TG/DTA/DSC for its thermal properties.

3.3 DESIGN OF EXPERIMENT FOR POLY(LACTIC ACID) NANOPARTICLE PREPARATION

Although, a number of methods are available for preparation of nanoparticles (NPs), nanoprecipitation is one of the best suited methods as discussed in Section 2.6. However, there is hardly any information available for studying proper regulation of effects of various parameters. Thus, DOE was applied to conduct experiments to obtain a proper relationship between input and output variables. The principal objective was to explore the influence of different parameters on the yield and size of nanoparticles. After going through the available literature, it was found that eight parameters play role in this process. But considering so many factors into consideration might lead to very large number of experiments. Thus, a few parameters of significance were considered by analyzing the published data in the literature.

For the preparation of nanoparticles (NPs) by nanoprecipitation method, eight parameters play important role. These are nature of solvent, nature of non-solvent, solvent/non-solvent (S/NS) volume ratio, polymer molecular weight, polymer concentration, surfactant type, surfactant volume and stirring speed. In addition to these, time of sonication may also play an important role. It appears that this effect has not been studied by any other investigator. It was seen practically that sonication for a time period of less than 20 minutes does not increase the temperature of the solution appreciably, whereas; further increase in sonication time increases the temperature of solution. Heating up of solution might damage the nanoparticles and thus sonication time may not be considered as an input variable. Thus, in the present case sonication time was fixed at 20 minutes.

Amongst the non-solvents; methanol, ethanol, propanol, isopropanol, butanol, and water, methanol was found to be the best. Further, size of nanoparticles were found to increase in the sequence, methanol<ethanol<propanol, when these are used as non-solvents (Bilati *et al.,* 2005). Thus, methanol was selected as the non-solvent and non-solvent was removed from the list of variables. Bilati *et al.,* (2005) have reported that surfactants were usually unnecessary for final suspension stabilization. A review of the cited and related literature shows that contributions of surfactants are not appreciable and thus these can be neglected.

A too high polymer concentration in the solvent, however, prevents nanoparticle formation (Bilati *et al.,* 2005). So polymer concentration should be optimized to get optimum results. However, it was studied that Legrand *et al.,* (2007) and Bilati *et al.* (2005) have studied in the range 5-20 mg/ml and got good yield with desirable size range of PLA

nanoparticles. Thus, in the present study the range of study of PLA concentration was fixed to be 5-20 mg/ml. The selected solvent and non-solvent should be non-toxic. Amongst the solvents such as acetone, chloroform, MeCN, DMSO, THF, MEK, MIBK, methyl propyl ketone and isopropyl acetate; DMSO and acetone were found to produce smaller nanoparticles when methanol was taken as the non-solvent. These were found to produce nanoparticles of almost similar size. The suitability of the above two solvents for the nanoprecipitation of PLA was based on the Hansen's two dimensional graph, Fig. 3.7, of the partial solubility parameters of the solvents w.r.t. the partial solubility parameters of PLA (Legrand *et al.,* 2007). A detailed theoretical consideration for the choice of solvents for PLA is given in Section 3.3.1. As their effect has not been quantified so far, the present investigation tries to quantify these effects and their interactions on the output response like yield (wt. %) and size of nanoparticles using DOE. As the requirement is to produce lower dimension nanoparticles with high yield, parameters for preparation of nanoparticles were selected as per Table 3.7 and 3.8. Two different PLA compounds, one having low M_w (PLAL, 98.470 kDa) and the other having high M_w (PLAH, 178.857 kDa) were selected to study the effect of molecular weight of PLA on the size of NPs produced.

Table 3.7 List of all design parameters along with their range, for nanoprecipitation of PLA

Parameter	Range	Factor type	Levels
X_1: Polymer concentration	5-20 mg/ml	Numerical	4
X_2: S/NS volume ratio	0.05-0.6	Numerical	4
X_3: Polymer molecular weight	PLAL; PLAH	Categorical	2
X_4: Solvent (S) type	Acetone, DMSO	Categorical	2

Table 3.8 Set of fixed operating parameters

Fix parameter	Value
Sonication time	20 min
Non-solvent (NS)	Methanol
Surfactant	Nil

After deciding the factors and their levels, Taguchi Orthogonal Array Design (TOAD) [L16(4**2 2**2)] was employed as it was found to be the best suited design, producing less number of runs in comparison to Factorial design. The general factorial design, for above described combinations of factors and their levels, produced 64 runs when DE7 was used for design of experiments. However, when TOAD was adopted using

MINITAB software it suggested only 16 runs. Table 3.9 reports of the combinations of the operating parameters obtained from MINITAB. The details of the values of factors for different experimental runs along with the output parameters (Yield (wt. %) and nanoparticle size) are given in the Section 4.4.

Table 3.9 Experimental design points obtained by Taguchi Orthogonalm Array Design in terms of actual values

Sl. No.	Polymer conc (mg/mL)	S/NS vol ratio	MW of PLA	Solvent
1	5	0.05	PLAL	Acetone
2	5	0.2	PLAL	Acetone
3	5	0.35	PLAH	DMSO
4	5	0.6	PLAH	DMSO
5	10	0.05	PLAL	DMSO
6	10	0.2	PLAL	DMSO
7	10	0.35	PLAH	Acetone
8	10	0.6	PLAH	Acetone
9	15	0.05	PLAH	Acetone
10	15	0.2	PLAH	Acetone
11	15	0.35	PLAL	DMSO
12	15	0.6	PLAL	DMSO
13	20	0.05	PLAH	DMSO
14	20	0.2	PLAH	DMSO
15	20	0.35	PLAL	Acetone
16	20	0.6	PLAL	Acetone

3.3.1 Design Considerations for Preparation of Poly(Lactic Acid) Nanoparticles

In order to get accurate and reliable results from the experiments, the following important design considerations have been taken into account for the preparation of PLA nanoparticles.

1. In the present investigation, methanol is the non-solvent and acetone and DMSO are the solvents for PLA. Because of the lower dielectric constant value of methanol than water, it is chosen as non-solvent in the present study. Lower the dielectric constant value, the less the non-solvent will dissolve hydrophilic compounds, thus, preventing drug leakage (Bilati *et al.*, 2005).
2. Methanol also produces smaller nanoparticles in comparison to other alcohols and water when they are taken as non-solvent.

3. The diffusing phase is not added drop-wise, but with the needle of the syringe kept directly in the non-solvent, in order to avoid an additional superfluous air–liquid interface (Fessi *et al.,* 1992).
4. The choice of the ternary polymer/solvent/non-solvent system is critical for the success of nanoprecipitation. The nature of the polymer-solvent interaction affects the properties of the nanoparticles. However, no clear guidelines are available on the influence of each of the three systems (polymer/solvent/non-solvent) on the nanoprecipitation.
5. In general, by increasing the polarity of the polymer solvents and by decreasing polymer concentration, yield of nanoparticle production was found to increase and size of nanoparticles was found to decrease (Thioune *et al.,* 1997, Stainmesse *et al.,* 1995).

3.3.1.1 Theoretical considerations for the choice of the solvents for poly(lactic acid)

The choice of two solvents suitable for the nanoprecipitation of PLA was based on the requirements of the method and on the physico-chemical characteristics of PLA. The physico-chemical characteristics of solvents, non-solvent and PLA are given in Table 3.10. The organic solvents must be able to dissolve PLA. They must also be miscible with non-solvent and water and have a low boiling point to facilitate their elimination by evaporation. Taking these criteria into account, solvents were selected to allow the effects of polymer–solvent interactions to be investigated. The main physico-chemical parameters which may influence such interactions are those defining the polarity of the solvent.
The details of the calculations necessary for the Table 3.10 are presented in Appendix G-I.

In the present study, two solvents were chosen whose physico-chemical properties are different. These are acetone and DMSO, which are widely used in nanoprecipitation of polyesters including PLA (Bilati *et al.,* 2005). Table 3.10 gives their main physico-chemical properties and shows that the main differences between the two solvents are found in their dielectric constant and dipole moment.
The solubility parameters of DMSO are around 1.4 times those of acetone. DMSO is more polar than acetone. The partial solubility parameters of PLA were calculated according to the Van Krevelen group contribution method based on the classical Hansen solubility parameter method (Van Krevelen and Hoftyzer, 1976) as described in Appendix I. The partial

solubility parameters of PLA were compared with those of methanol, acetone and DMSO on a Hansen's two-dimensional graph (Van Krevelen and Hoftyzer, 1976) (Fig. 3.7).

Table 3.10 Physico-chemical characteristics, of the solvents and PLA used in the preparation of nanoparticles, at 20°C

Parameter	Methanol	Acetone	DMSO	PLA[a]
Dielectric constant	33.62	20.70/21	46.68	
Dipole moment (μ) (debye)	1.7-1.71	2.86-2.9	3.9	
Solubility parameters $(J/cm^3)^{1/2}$				
$\delta_t=(\delta_d^2+\delta_p^2+\delta_h^2)^{1/2}$	29.2-29.7	20.0-20.5	26.5-26.7	20.85
$\delta_d = \Sigma F_{di}/V$	15.2	15.5	18.4-19.3	15.49
$\delta_p = (\Sigma F_{pi}^2)^{1/2}/V$	12.3	10.4	16.4	8.53
$\delta_h = (-\Sigma E_{hi}/V)^{1/2}$	22.3	7.0	10.2	11.04
$\delta_v =(\delta_d^2+\delta_p^2)^{1/2}$	19.5	18.7	24.7-25.3	17.68
Boiling point (°C)	65	57	189	
Density (g/cm^3)	0.792	0.792	1.102	
Viscosity (Cp)	0.59	0.32	2.14	
Surface tension (γ) $10^{-3}(J/m^2)$	22.61	23.70	43.54	
Molar volume (V) cc/mol	40.7	73.3	71.0	57.45

The values of different parameters of the solvents and non-solvent are taken from Van Krevelen and Hoftyzer, 1976; δ solubility parameter, subscripts t, total; d, contribution of the dispersion forces; p, polar contribution; h, hydrogen bonding contribution; v, dispersion and polar contribution. V, molar volume of the compound; F_{di}, molar attraction constant due to dispersion interactions; F_{pi}, molar attraction constant due to polar interactions; E_{hi}, hydrogen bound energy. [a]Calculations for the molar volume and partial solubility parameters of PLA by using the Van Krevelen group contribution method based on the classical method for Hansen solubility parameters (Van Krevelen and Hoftyzer, 1976).

This graph is useful for predicting whether a given solvent will be a solvent or a non-solvent for a polymer because solvents of a polymer are generally included in a circle of a radius of five δ-units around the polymer (Van Krevelen and Hoftyzer, 1976). As expected, methanol appeared far outside the solubility circle of PLA, in agreement with the fact that it is a non-solvent for PLA. DMSO and acetone are located inside the solubility circle (Fig. 3.7). This indicates that they should both be good solvents for PLA. Thus, in ternary systems consisting of either PLA/acetone/methanol or PLA/DMSO/methanol, the difference in the interactions between the organic solvent and methanol might be negligible. This would allow to study in more details, the influence of parameters related only to the polymer and to the polymer–solvent interactions on nanoprecipitation.

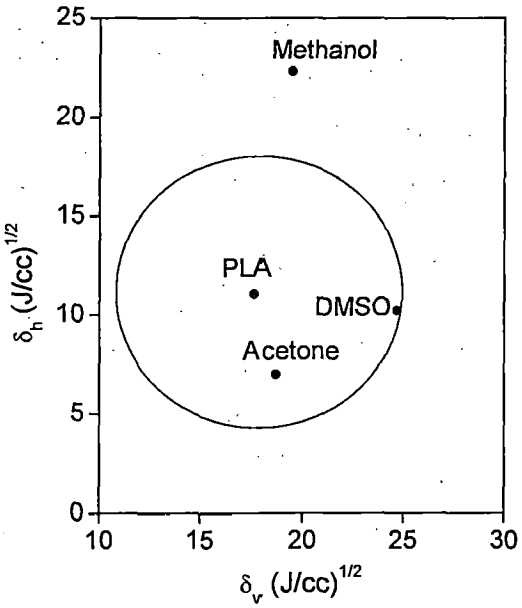

Fig. 3.7 Hansen's two-dimensional graph of partial solubility parameters of solvents w.r.t. those of PLA.

3.3.2 Experimental Setup

The schematic diagram of the nanoprecipitation method is depicted in Fig. 3.8.

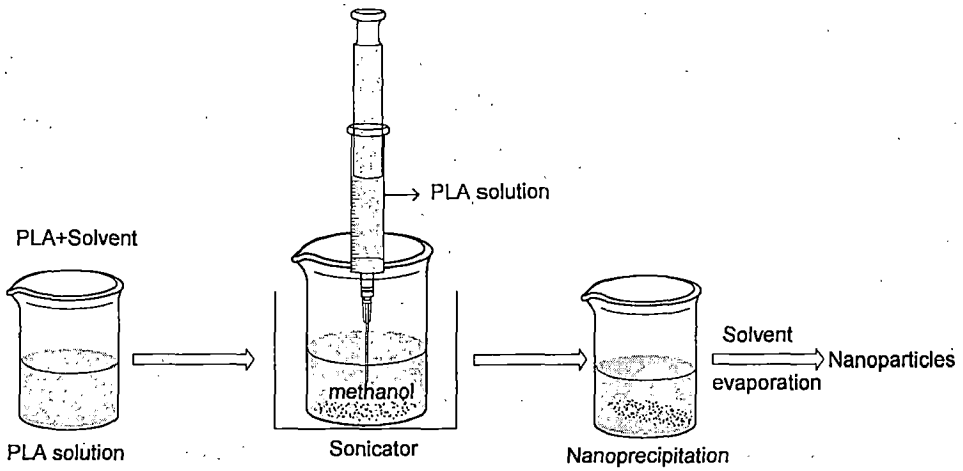

Fig. 3.8 Schematic diagram for nanoprecipitation

3.3.3 Experimental Procedure for Poly(Lactic Acid) Nanoparticle Preparation

Materials and Methods

The poly(lactic acid) (PLA) homopolymer synthesized by melt polycondensation and having M_w of 98 kDa (PLA-L) and 178 kDa (PLA-H) were used for this purpose. HPLC grade methanol was used as non-solvent and was obtained from MERCK Mumbai, India. HPLC grade acetone and extra pure DMSO were also purchased from MERCK Mumbai, India. HPLC grade or the highest available purity of solvents and non-solvents should

always be used for better results. The purity, of all these solvents, was higher than 99%. Doubly distilled deionized (DI) (18MΩcm^2/cm) water (Milli-Q system, Waters Corp., Milford, MA, USA) was used throughout the study.

Step 1. The PLA samples were dissolved in a suitable organic solvent (S) at concentrations from 5 to 20 mg/mL as per Table 3.9 to form the diffusing phase. The solvent chosen were acetone and DMSO.

Step 2. This phase (with volumes typically ranging from 1 to 7 mL) was then added to the 10-20 mL of dispersing phase by means of a syringe positioned with the needle directly in the dispersing phase under sonication to maintain the S/NS ratio as per the Table 3.9. The dispersing phase was basically a non-solvent (NS) in which PLA is insoluble. The NS used was methanol.

Step 3. The freshly formed nanoparticles with solvent and non-solvent, present in the supernatant fluid, were then centrifuged for 15-min at 15000×g and 4°C using a Heraeus Biofuge Stratos centrifuge, Henderson Biomedical Ltd. United Kingdom. It was then mixed with 2 ml of deionized Millipore water obtained using a Milli-Q system of Millipore (Bedford, MA, USA) and again centrifuged for 15 minutes. This step was repeated twice.

Step 4. The samples prepared were subsequently vacuum–dried for a period of 24 h to obtain a fine powder and then kept at 4°C till further use.

Step 5. **Determination of Yield:** The yield (wt. %) was calculated according to the formula given below in Eq.3.4.

$$\text{Yield}\,(wt.\%) = \frac{\text{wt. of PLA NP obtained}}{\text{wt. of PLA taken initially}} x100 \qquad \ldots \text{Eq. 3.4}$$

Step 6. The nanoparticles were characterized by different methods like FESEM, TEM and DLS for determination of their size, size distribution and zeta potential.

3.4 CHARACTERIZATION METHODS

It is a scientific practice that characterization of raw materials and products of an investigation should be done meticulously. Adhering to the above principle, in the present investigation, LA, tin chloride dihydrate, PTSA used and PLA and its nanoparticles produced were characterized using different instruments such as GPC, NMR, FTIR, XRD, Thermal, FESEM, TEM, DLS, CHNS analyzer, polarimeter and refractometer. PLA was characterized by GPC, NMR, FTIR, XRD, Thermal analysis and FESEM; whereas; PLA

nanoparticles were characterized by FESEM, TEM and DLS. For accurate size characterization of the PLA nanoparticles, they should be analyzed immediately after their purification. This is to avoid changes in the size distribution due to degradation reactions (such as hydrolysis) or Ostwald ripening (Contado *et al.,* 2007).

3.4.1 Gel Permeation Chromatography (GPC)

The molecular weights (M_n and M_w) and polydispersity index (M_w/M_n) were determined by using GPC instrument manufactured by Waters. Molecular weight was determined at 25°C by eluting PLA solutions of 1 mg/ml concentration in THF, with toluene as internal standard. The GPC instrument consists of a pump, columns and detector. Waters 1525 Binary HPLC pump was used for the purpose. Two columns, namely, Waters Styragel HR4 7.8×300 mm WAT10573", and "Waters Styragel HR3 7.8×300 mm WAT044223" were used in a series for separation using THF as solvents. THF was used as the mobile phase with flow rate 1.0 ml/min. The injection volume of PLA solution sample was 20 µL. An ELS detector, Waters 2420, was used for detection of different molecular weight fractions. The GPC chromatograms were analyzed through Breeze version 3.3 software. The calibration of molecular weight was done using monodisperse polystyrene as standard supplied by Waters and having M_n of 1060, 10700, 55100 and 197000 Da.

3.4.2 Nuclear Magnetic Resonance (NMR) Spectroscopy

The ^1H NMR and ^{13}C NMR spectra were recorded on Bruker Avance 500 spectrometer at room temperature. For NMR measurements, the samples were dissolved in $CDCl_3$-D (Chloroform-D) or DMSO-D6 (deuterated dimethyl sulphoxide) in eppendrof at room temperature and then transferred into 5 mm dia. NMR tubes using a micropipette. TMS was internal standard for all deuterated solvents used. 5mm PABBO BB probhead was used and the operating frequency was 500.13 MHz for the ^1H nucleus and 125.77 MHz for ^{13}C nucleus. The chemical shifts in parts per million (ppm) are reported up field with reference to internal standard chloroform-d at 7.25 ppm. The ^1H and ^{13}C chemical shifts were measured in δ (ppm) and referenced to TMS as internal standard. The sample concentration for ^1H NMR was 4 % w/v, whereas; for ^{13}C-NMR measurements, it was 10 % by weight. Proton decoupled ^{13}C-NMR spectra with NOE were recorded on a Bruker DRX 500 MHz NMR spectrometer working at 125.577 MHz for Carbon-13. A digital resolution of 32 K data points/ 18,000 Hz spectral width was used, a pulse angle of about 30° along

with a relaxation delay of 2s, and 10^{3} –10^{4} transients were accumulated. Relative peak areas were proportional to the number of hydrogen/carbon atoms. The NMR spectra processing and analysis was done using TOPSPIN software. Relative peak areas were proportional to the number of carbon atoms. 2D NMR experiments were also carried out using the same instrument. The structures of LA, PTSA and PLA were determined from NMR. Functional groups present, amount of residual monomer and lactide and M_n have also been determined from NMR.

3.4.3 Fourier Transform Infrared (FTIR) Spectroscopy

Dried samples were ground into powder, mixed and crushed with KBr for homogenization. The KBr to polymer ratio was between 1:20 and 1:50. A Nicolet economy sample press was used to obtain optically clear pellets. Pellets were analyzed using transmission FTIR using a Thermo Nicolet Avatar 370 FT-IR Spectrometer System. Dry air was used as the chamber purge stream for all samples. The scanning resolution was set to 1 nm with a total of 1024 scans per sample. The FTIR spectra were obtained at room temperature over a spectral frequency range of 400-4000 cm^{-1}. IR bands are expressed in terms of frequency (cm^{-1}). The background was obtained against a pure KBr pellet and the data was analyzed by Omnic software. Functional groups present and thus the structure of LA, PTSA and PLA can be determined from FTIR.

3.4.4 Thermal Analysis

TGA, DTG and DSC were carried out simultaneously by using a PYRIS Diamond TG/DTA thermal analyzer, supplied by Perkin Elmer and the data was processed and analyzed by PYRIS Muse Measure and standard analysis software (v. 3.3U;. #. 2002 Seiko Instruments Inc.). The sample was kept in alumina pan, the reference material was alumina powder and thermal study was carried out at heating rate 10°C/min under 200 ml/min flow rate of nitrogen atmosphere. Indium and gallium were used as standards for temperature calibration. The measurements were run from room temperature to 600°C. The glass transition temperature (T_g), T_m, T_d, T_c and the % crystallinity were recorded. % Crystallinity values for different samples were calculated from the heat of fusion. By integrating the normalized area of the melting endotherm, melt enthalpy and crystallization enthalpy were determined, and rating it to the reference 100 % crystalline polymer (93.6 J/ g), the relative

crystallinity of the polymer was assessed. In the present work, the relative degree of crystallinity is referred to as crystallinity, and T_m is the melting temperature.

3.4.5 X-Ray Diffraction (XRD) Studies

Powder X-ray diffraction of PLA was studied by using Bruker AXS D8 Advance (Germany) using Nickel filtered CuKα radiation and Copper as target at wavelength of 1.54 Å. Goniometer speed was kept at 2°/min. Wide angle X-ray scattering (WAXS) pattern of the samples were obtained using the DIFFRAC Plus XRD Commander software and analysis was done by DIFFRAC Plus (Version 8.0) software. The range of scanning angle for the sample was kept in the range 2θ=10–120°.

3.4.6 Field Emission Scanning Electron Microscopy (FESEM)/EDAX

The morphology of PLA samples was examined by FE scanning electron microscopy, FESEM QUANTA 200FEG model, (FEI NETHERLAND make) with operating voltage ranging from 200 V to 30 kV and with 2nm resolution and 1000 KX magnification. FESEM micrographs were taken after coating the surfaces of PLA samples with a thin layer of gold by using BAL-TEC-SCD-005 Sputter Coater, BAL-TEC AG, Balzers, Liechtenstein; Germany under argon atmosphere to make the sample conducting.

The surface appearance and shape of nanoparticles were also analyzed by FESEM. Samples were prepared by finely spreading concentrated nanoparticle dispersions over glass slabs and by drying them under vacuum. The samples were then coated in a cathodic evaporator with a fine gold layer. The FESEM micrographs are analyzed by xT Microscope Server software and for EDAX analysis EDAX Genesis software was used.

3.4.7 Transmission Electron Microscopy (TEM)

The morphology of PLA nanoparticle samples were examined by TEM (TECNAI 20 G2 S-TWIN, FEI NETHERLANDS) at high tension of 200 kV and ultra high vacuum of 26 mPa. The samples for TEM were prepared by sonicating the samples in methanol for 10 minutes using Ultrasoniccation (LOBA Life Ultrasonics, Model 3.5L100). A drop of sample was kept on the grey color side of the copper grid, allowed to dry in air and was inserted into the TEM instrument for taking its micrographs using CCD Camera. FEI software was used for Tecnai control and imaging.

3.4.8 Dynamic Light Scattering (DLS) Analysis

Particle size, polydispersity index (PDI) and Zeta potential were determined by DLS, alternatively known as photon correlation spectroscopy (PCS), by using a Zetasizer nano ZS-90 (Malvern Instruments Ltd., UK) using 12 μL quartz cuvette. The resulting data were analyzed by "DTS (Version 5.10)" software (Malvern Instruments Ltd., Malvern, UK). For size measurements, the NP suspension was diluted by a factor of 15 with Millipore water prior to analysis. Mean size and PDI were measured three times for each batch. Mean particle diameter was calculated according to a size distribution processor mode using the following conditions: fluid refractive index 1.33, temperature 25°C, viscosity 0.93 cp, angle of measurement 90° and measuring time 60 sec. The results of particle sizing were analyzed by CONTIN algorithm and the sizes presented based on the intensity distributions. For zeta potential measurements, the NP suspension was prepared as per Run No. 6 and was diluted 15 times with DI water and pH of the NP suspension was adjusted to the desired pH by using HCl or NaOH prior to analysis. The pH is measured by a digital pH meter and was put into a dip cell for zeta potential measurement. The mobility of charged particles is determined with the help of electric potential (electrophoretic mobility) and transferred to ζ-potential, e.g. with the help of Smoluchowski's equation.

3.4.9 Polarimeter

Polarimeter P-3002 (Kruss, Hamburg, Germany) was used for determining the DL content in LLA solution at 25°C using a cell of path length 10 cm.

3.4.10 Digital Refractometer

The automatic digital refractometer DR6000, Kruss Optronic GmbH Germany make, with a sapphire prism was used for measuring the refractive index of PTSA and LLA samples. It can be operated at working voltage of 100-250 V, 50/60 Hz, 60 W. Refractive index was measured at room temperature and at wavelength of 590 nm.

3.4.11 CHNS Analyzer

CHNS analysis was carried out using Vario EL III model CHNSO Elementar Analysen systeme GmbH to determine the % age of CHNS present in LLA and PTSA.

Table 3.11 shows the summary of instruments used along with their critical settings for the characterization of LA, Tin chloride dihydrate, PTSA, PLA and PLA nanoparticles.

Table 3.11 Summary of characterization methods used in present investigation

Name of Instrument	Purpose	Instrument make	Important parameter / setting under which the instrument was run
GPC	Determination of M_n, M_w and polydispersity index (PDI) Sample tested: PLA	HPLC GPC 1525 Make: Waters	- Temperature: 25°C - Solution: 0.1% concentration in THF. - Internal standard: toluene - Columns: Styragel HR4 and HR3 - Mobile phase: THF - Flow rate: 1.0 ml/min. - Injection volume: 20 µL. - ELS detector, Waters 2420 - Software: Breeze version 3.3. - Standard: polystyrene
NMR	Determination of M_n, end-group determination, functional group, structure, amount of residual monomer, optical purity, amount of lactide. Sample tested: LA; PTSA; PLA	Bruker Avance 500 spectrometer Make: Bruker Germany	- Solvents: $CDCl_3$-D (Chloroform-D), D_2O, DMSO-D6 - 5mm PABBO BB probe head - Operating frequency: 500.13 MHz for the ^1H nucleus and 125.77 MHz for ^{13}C nucleus - Internal standard: TMS - TOPSPIN software
FTIR	Functional group, structure Sample tested: LA; PTSA; PLA	Thermo Nicolet Avatar 370 FT-IR Spectrometer Make: Thermo Fisher Scientific Inc.	- Scanning resolution: 1 nm - 1024 scans per sample - Room temperature - Spectra frequency range: 400-4000 cm^{-1} - Omnic software
Thermal study	Thermal degradation behaviour, T_g, T_m, T_c, ΔH Sample tested: PLA.	Perkin Elmer (PYRIS Diamond TG/DTA) thermal analyzer Make: Perkin Elmer	- PYRIS Muse Measure and standard analysis software. - alumina pan

			- reference material: alumina powder - heating rate: 10, 20, 30, 40, 50°C/min - 200 ml/min flow rate of nitrogen atmosphere. - Standards: Indium and gallium - Temperature measurement range: RT to 600°C.
XRD	Crystalline nature, Percent crystallinity Sample tested: $SnCl_2.2H_2O$; PLA.	Bruker AXS D8 Advance Make: Bruker (Germany)	- Nickel filtered CuKα radiation - Copper as target - Wavelength: 1.54 Å - Goniometer speed: 2°/min - Software: DIFFRAC Plus XRD Commander - Scanning angle, 2θ=10–120°
FESEM	Morphology and nanoparticle size Sample tested: $SnCl_2.2H_2O$; PLA and its nanoparticles	FESEM QUANTA 200FEG model, Make: FEI NETHERLAND	- Operating voltage: 200 V to 30 kV - 2nm resolution - 1000 KX magnification - Gold coating the surfaces
TEM	Nanoparticle size Sample tested: PLA nanoparticles	TECNAI 20 G2 S-TWIN, Make: FEI NETHERLANDS	- High tension: 200 kV - Ultra high vacuum: 26 mbar - Copper grid - CCD Camera - Software: FEI software
DLS	NP size, size distribution and zeta potential Sample tested: PLA nanoparticles	Zetasizer nano ZS-90 Make: Malvern Instruments Ltd., UK	- Fluid refractive index: 1.33 - Temperature: 20°C - Viscosity: 0.93 cp - Angle of measurement: 90° - Measuring time: 60 sec.

Polarimeter	DL Content, Specific rotation, enantiomeric purity Sample tested: LLA	Polarimeter P-3002 Make: Kruss, Hamburg, Germany	- Measuring range: ±45° - Resolution: 0.001° - Accuracy: <0.004° - Measurement duration: 1°/sec - Light source: Sodium lamp (589 nm) - Power supply 230 or 110 V, AC, 50/60 Hz, 100 W
Refractometer	Refractive index Sample tested: PTSA and LLA	Automatic refractometer DR 6000 Make: Kruess Germany	- High range from 1.32000 up to 1.70000 nD; 0.00 - 95.00 %Brix - Resolution up to 0.00001 nD; 0.01 %Brix - Prism: Sapphire - Illumination :LED 590 nm - Working voltage: 100-250 V, 50/60 Hz, 60 W
CHNSO Analyzer	% age of carbon, hydrogen, nitrogen and sulfur Sample tested: PTSA	Vario EL III model CHNSO Make:Elementar Analysensysteme GmbH Germany	- Standard: Sulfanilic acid - Flow of oxygen: 199 ml/min - Temp. of Furnaces: 1150, 851, 209°C

RESULTS AND DISCUSSION

The objectives of the present study are mentioned in Chapter 1. A systematic literature review has been carried out based on these objectives and has been presented in Chapter 2. Based on these objectives, three sets of experiments are designed and carried out as described in Sections 3.1-3.3 of Chapter 3, for the synthesis of PLA through two different routes and then subsequent formation of its nanoparticles. As a standard research practice the input raw materials (L-lactic acid, catalyst tin chloride dihydrate, co-catalyst PTSA) and the output products, PLA and its nanoparticles, are characterized by using different instruments and methods as described under Section 3.4 of Chapter 3. Results obtained during characterization of the input raw material, L-lactic acid (LLA), are presented in Appendix A, whereas; those for tin chloride dihydrate and *p*-toluene sulfonic acid (PTSA) are given in Appendix B and C, respectively. In the present investigation, PLA is produced through two routes namely; melt polycondensation (MPC) and solid state polycondensation (SSP). The design of experiments for synthesis of PLA by MPC and SSP has been carried out by Design Expert software Ver.7 (hence forth is called DE7) developed by Stat-Ease Inc. Details of these designs are discussed exhaustively in Section 3.1 and 3.2 and are also reported in Appendix E.1 and E.2 of Appendix E. However, the design of experiments for the preparation of PLA nanoparticles is carried out using Minitab (v. 13.20) developed by Minitab Inc. USA, and is discussed in Section 3.3.

The values of yield (wt. %) and M_w obtained during production of PLA through MPC as per the operating conditions described in Table 3.3 are reported in Table 4.2 and are analyzed using statistical softwares such as DE7 and Minitab. And, the values of yield (wt. %) and M_w obtained during production of PLA through SSP, as per the operating conditions described in Table 3.6, are reported in Table 4.38 and are also analyzed using the statistical software DE7 and Minitab. The yield (wt. %) and size of PLA nanoparticles produced through experiments conducted as per the operating conditions given in Table 3.9, are reported in Table 4.65 and are analyzed using Minitab software. The details of the chemical shifts of the solvents employed for the characterization of LLA, PTSA and PLA through NMR are given in Appendix F. Computation of zeroth-order and first-order connectivity indices for the polymer repeat unit,

used for PLA nanoparticles preparation part, is given in Appendix G, whereas; computation of molar volume (V) of PLA is given in Appendix H. Determination method of Hansen solubility parameters (HSP) for PLA is given in Appendix I. The raw experimental data and the raw analysis results of MPC and SSP are given in Appendix J and K, respectively. The raw experimental data of PLA nanoparticle preparation are produced in Appendix L. The error analysis for the calculation of yield (wt. %) is given in Appendix M. The present Chapter embodies the salient results and their interpretations obtained from the analysis of the experimental results of the present investigation. For clarity, analysis reports obtained from different instruments during characterization of PLA and its nanoparticles are presented at appropriate places of this Chapter.

4.1 CHARACTERIZATIONS OF LACTIC ACID, TIN CHLORIDE DIHYDRATE AND *P*-TOLUENE SULFONIC ACID

In the present investigation the raw materials used for the production of PLA are characterized. The details of results of the characterizations of LLA, tin chloride dihydrate (catalyst) and *p*-toluene sulfonic acid (co-catalyst) are reported in the Appendix A, B and C, respectively. The details of the instruments used for characterization are discussed in Table 3.11 of Chapter 3. The salient results are discussed below:

1. FTIR spectrum of LLA is shown in Fig. A.1 of Appendix A, which shows its characteristic peaks as given in Table A.1. The spectral interpretation also showed that the compound contains aliphatic carboxylic acid group, primary aliphatic alcohol and aliphatic hydrocarbons. The peak at 1458.34 cm^{-1} may be due to CO stretching of lactide. Thus, it can be concluded that few amount of residual lactide is present in the crude LLA
2. ^{1}H and ^{13}C NMR spectra of LLA is shown in Figs. A.2 and A.4, respectively. And from Figs. A.2 and A.3, it can be concluded that the peak at ~1.3 is due to $-CH_3$ group and a doublet peak due to the methyl protons of LLA. And quartet peak is generated from the -CH peaks of LLA as can be predicted theoretically. A detail discussion is also given under Section A.2 of Appendix A. Thus, structure of LLA is confirmed.
3. The refractive index of the L-lactic acid is observed to be 1.4253 at 25°C when a sodium D-line light is used.

4. From the polarimetric study of LLA, given under Section A.3, it is also confirmed that the stereochemical purity of the L-lactic acid is > 95 %.
5. From Appendix B, the structure of tin chloride dihydrate and its high purity is confirmed.
6. The FTIR spectrum of PTSA is shown in Fig. C.1 of Appendix C. The spectral interpretation confirms the presence of para-substituted aromatic hydrocarbon and aromatic sulfonic acid.
7. The ^{1}H and ^{13}C NMR of PTSA is also in good agreement with the structure of the PTSA.
8. From the CHNS, FTIR, NMR and refractive index analysis data given in Appendix C, the structure of PTSA is confirmed.

4.2 SYNTHESIS OF POLY(LACTIC ACID) BY MELT POLYCONDENSATION AND ITS SUBSEQUENT CHARACTERIZATIONS

In the present work, PLA has been synthesized by melt polycondensation, as discussed in Section 3.1 of Chapter 3. The total numbers of operating parameters that influence the synthesis of PLA are about 15. Out of these, the pertinent parameters are five as concluded in Section 3.1. These parameters are termed as input parameters. The most significant output parameters for PLA synthesis are yield (wt. %) and wt. average molecular weight (M_w), as these regulate value addition and physical & mechanical properties of the polymer, respectively. The input parameters, with their ranges of variation for PLA synthesis are given in Tables 3.1 and 3.2. For brevity, a part of these tables is reproduced below in Table 4.1.

Table 4.1 Input and output parameters involved in MPC of PLA synthesis

Input Parameters		Low level	Mid level	High level	Output Parameters	
Name(s)	Unit	$X_{i,min} = -1$	$X_{i,mid} = 0$	$X_{i,max} = +1$	Name(s)	Unit
X_1: Amount of LLA	g	20	30	40	Yield	wt. %
X_2: Catalyst	wt. %	0.4	0.7	1.0	M_w	kDa
X_3: ES time	h	2	5	8		
X_4: MPC temperature	°C	180	210	240		
X_5: MPC time	h	10	20	30		

To develop statistically reliable correlations between input and output parameters with almost minimum number of experiments, the technique of design of experiment (DOE) has been used as discussed below.

4.2.1 Design and Analysis of Experiments

Small face centered central composite design (SFCCCD) of RSM consisting of a set of 26 experiments (Run No. 1-26), containing factorial, axial and center points, are developed as given in Table 3.3, for conduct of experiments. The results for the output parameters of experiments, namely yield (wt. %) and M_w, along with the input parameters are given in Table 4.2. The data available in the Table 4.2 are analyzed using statistical software DE7. The analysis indicated that *degrees of freedom* for the *lack of fit* is 1 and that for the *pure error* is 4, whereas; for valid results, the *degrees of freedom* for the *lack of fit* should be ≥ 3 and that for the *pure error* should be ≥ 4. To achieve the minimum value of *lack of fit* as well as *pure error* the design was augmented by adding 4 model points, which in turn added four vertex points to the design space. Thus, four additional experiments were conducted at above mentioned vertex points (Run No. 27-30) and the yield (wt. %) and M_w are also recorded in Table 4.2. After augmentation of the SFCCCD design, the design gets converted to D-optimal design which provides the most accurate estimates of the model coefficients. Again, the analysis has been repeated using DE7, for yield (wt. %) as well as M_w. The *degrees of freedom*, for the *lack of fit* and *pure error*, for the augmented design has been found to be 5 and 4, respectively, which is satisfactory and is an indication of a better fit to the proposed model.

Based on the experimental results presented in Table 4.2, input-output relationships, called regression models, for yield (wt. %) as well as M_w are developed. The different proposed models which are investigated for the relationships given by Eq. 4.1 – 4.3 are listed below in Table 4.3. The listed models are regressed using statistical software DE7, and based on the results of regression, the final model is selected which reproduces the experimental results best, with minimum error.

Table 4.2 Yield (wt. %) and M_w obtained at different experimental conditions proposed by DOE

Run No.	Point Type	X_1: Amount of LLA(g)	X_2: Catalyst (wt.%)	X_3: ES time(h)	X_4: MPC temperature(°C)	X_5: MPC time(h)	Yield (wt.%)	M_w (kDa)
1	Factorial	40	1.0	2	240	10	35.6	2.943
2	Factorial	40	0.4	8	240	10	39.2	0.951
3	Factorial	20	1.0	8	180	30	45.3	8.514
4	Factorial	40	1.0	8	180	10	68.9	51.729
5	Factorial	40	1.0	2	180	30	65.2	55.634
6	Factorial	40	0.4	2	240	30	30.3	1.572
7	Factorial	20	0.4	8	240	30	29.0	0.447
8	Factorial	20	1.0	2	240	30	40.3	2.266
9	Factorial	40	0.4	8	180	30	65.3	89.675
10	Factorial	20	1.0	8	240	10	37.6	4.072
11	Factorial	20	0.4	2	180	10	85.3	178.857
12	Center	30	0.7	5	210	20	55.6	45.871
13	Center	30	0.7	5	210	20	56.4	46.645
14	Center	30	0.7	5	210	20	52.6	44.352
15	Center	30	0.7	5	210	20	46.0	40.974
16	Center	30	0.7	5	210	20	46.3	39.046
17	Axial	20	0.7	5	210	20	53.3	35.874
18	Axial	40	0.7	5	210	20	46.2	48.579
19	Axial	30	0.4	5	210	20	49.7	34.265
20	Axial	30	1.0	5	210	20	57.4	23.465
21	Axial	30	0.7	2	210	20	45.2	32.606
22	Axial	30	0.7	8	210	20	52.4	45.301
23	Axial	30	0.7	5	180	20	66.2	75.929
24	Axial	30	0.7	5	240	20	21.3	6.923
25	Axial	30	0.7	5	210	10	59.4	68.896
26	Axial	30	0.7	5	210	30	46.6	40.123
27	Vertex	40	0.4	2	180	10	79.0	67.070
28	Vertex	20	1.0	2	180	10	69.9	67.234
29	Vertex	20	0.4	2	180	30	59.6	9.103
30	Vertex	20	0.4	2	240	10	30.7	2.079

The input parameters can also be referred to as variables. The generic forms of different regression models (Montgomery, 2004) are given below:

Linear model

Linear model of the independent variables, is a first-order model as shown in Eq. 4.1.

$$Y=\beta_0 + \beta_1 X_1 + \beta_2 X_2 +....+ \beta_5 X_5 \quad \ldots (4.1)$$

where, Y= Response; $\beta_0, \ldots \beta_5$ are regression coefficients; $X_1 \ldots X_5$ are regressor variables.

2-factor interaction model

The generic form of the 2-factor interaction is given by Eq. 4.2.

$$Y=\text{Linear model} + \beta_{12}X_1X_2 +....+ \beta_{15}X_1X_5+\beta_{23}X_2X_3+ \ldots+\beta_{25}X_2X_5+\ldots+\beta_{45}X_4X_5 \quad \ldots (4.2)$$

Quadratic model

The general form of the quadratic model is given by Eq. 4.3.

$$Y=\text{2-factor interaction model} +\beta_{11}X_1^2+ \beta_{22}X_2^2+\ldots+ \beta_{55}X_5^2 \quad \ldots (4.3)$$

Table 4.3 Regression models selected for development of input-output relationships

Output parameter	Input parameters	Model Type	General form	Remarks
Yield (wt. %)	Amount of LLA; Catalyst wt. %; esterification time; MPC time and MPC temperature	Linear	Eq. 4.1	- Main input parameters can be modeled.
		2-factor interaction	Eq. 4.2	- Interaction can be modeled along with main input parameters
		Quadratic	Eq. 4.3	- Curvature of the response can be detected
M_w	Amount of LLA; Catalyst wt. %; esterification time; MPC time and MPC temperature	Linear	Eq. 4.1	- Main input parameters can be modeled.
		2-factor interaction	Eq. 4.2	- Interaction can be modeled along with main input parameters
		Quadratic	Eq. 4.3	- Curvature of the response can be detected

The output parameters for Eq. 4.1– 4.3 can be either yield (wt. %) or M_w whereas; the input parameters are fixed and are amount of LLA (X_1), catalyst (X_2), ES time (X_3), MPC temperature (X_4) and MPC time (X_5) as depicted in Table 4.1. As all input parameters used for the development of correlations should be independent of each other, therefore, before proceeding for the regression analysis, it is felt necessary to know about the correlations between the input parameters. The correlation coefficients obtained through the analysis provided an indication of the extent of relation between one input parameter to the other. The correlation coefficients are reported in Table 4.4. The value of correlation coefficients ranges from –1 (a perfect inverse relationship) to +1 (a perfect direct relationship). A value of 0 indicates no linear relationship.

Table 4.4 Correlation analysis of the input parameters

	X_1: Amount of LLA	X_2: Catalyst	X_3: ES time	X_4: MPC temperature	X_5: MPC time
X_1	1	−0.061	0.053	−0.061	−0.061
X_2	−0.061	1	0.053	−0.061	−0.061
X_3	0.053	0.053	1	0.053	0.053
X_4	−0.061	−0.061	0.053	1	−0.061
X_5	−0.061	−0.061	0.053	−0.061	1

From the values of the correlation coefficients given in Table 4.4, it is clear that no correlation exists between the input parameters, as the values are almost close to zero. Thus, it can be safely concluded that no correlationship exists between the input parameters. And, thus, the regression analysis can be carried out to get the desired relationship between the input and output parameters.

Statistical testing of the models were performed with F-test to obtain the mathematical relationship between input and output parameters. To examine the goodness of fit of a model, the test for significance of regression model was performed and ANOVA is applied to the response data. The following points must be taken into consideration for determining the best fit of a model.

1. Significance analysis is performed based on the P-values. The terms with P-value ≤ 0.05 are significant.
2. P-value for the model should also be significant, i.e., $p \leq 0.05$.
3. P-value for *lack of fit* should be insignificant. The insignificant *lack of fit* (>0.05) is good for data fitness to the model.
4. The model maximizing the correlation coefficients, "R-Square" values such as "R-square", "adjusted R-square" and "predicted R-square", is the best model.
5. The "predicted R-square" value must be in reasonable aggreement with the values of "adjusted R-square" and "R-square".
6. A difference of < 0.2 between "R-square" and "predicted R-square" is an indication of a suitable model.
7. The predictive power of the model, as evidenced by "predicted R-square" value, must be greater than 0.5. Larger the "predicted R-square" value, better the model.

8. Moreover, a classical analysis of variance (ANOVA) using F-tests allows us to analyze the total response variation by identifying the parts corresponding to the sources of variation (regression model, pure experimental error) and to analyze the residuals in order to point out the possible *lack of fit* of the postulated model when replicates are available.
9. "Adequate Precision" – a measure of the signal to noise ratio, greater than 4 is desirable.

4.2.1.1 Regression analysis to develop correlation for the prediction of yield (wt. %)

Experimental results obtained for yield (wt. %), reported in Table 4.2, are analyzed to figureout the best correlation between yield (wt. %) and input parameters, out of the input-output correlations proposed in Table 4.3.

Case I: Development of linear model

First of all, the linear model is fitted considering all the five input parameters and the regressed linear model is given by Eq. 4.4. An ANOVA is performed to establish the relative significance of the individual factors. ANOVA results for linear model for yield (wt. %) are shown in Table 4.5. In Table 4.5, 'df' is the *degree of freedom*, F-value is the variance ratio and p-value is the probability. These nomenclatures are also used throughout this chapter. In ANOVA, the F-value and p-value determines whether an effect is significant or insignificant, so whether an effect is strong or weak cannot only be determined only from its Sum of Squares (SS). *Degrees of freedom* of an effect should also be considered. Mean square (MS) of an effect should also be used to determine whether an effect is weak—the smaller the MS, the weaker the effect. MS is the better criterion to pool the weak effects. The regression coefficients of regression analysis are given in Table 4.6.

$$YIELD = 186 + 0.043.X_1 - 3.52.X_2 - 0.576.X_3 - 0.578.X_4 - 0.53.X_5 \quad \ldots (4.4)$$

Now, from Table 4.5, it is clear that X_4 and X_5 are the significant parameters, whereas; X_1, X_2 and X_3 are insignificant. The correlation coefficients "R-square", "adjusted R–square" and "predicted R-square" values for Eq. 4.4 are 0.838929, 0.805373 and 0.709812, respectively. The "Predicted R-Square" of 0.7098 is in reasonable agreement with the "Adjusted R-Square" of 0.8054. To maintain hierarchy, the terms corresponding to the individual parameters cannot be removed from a model and thus, are kept in the model according to the hierarchy principle

(Montgomery, 2004). Adequate precision of 16.71 indicates an adequate signal. For the present model, the lack of fit is insignificant. Thus, taking all the above facts into consideration, it can be concluded that the linear model is a good model.

Table 4.5 ANOVA for RSM variables fitted to linear model

Source	Sum of Squares	df	Mean Square	F-value	p-value	Significance
Model	5505.087	5	1101.017	25.00054	< 0.0001	Significant
X_1:Amount of LLA	3.077001	1	3.077001	0.069869	0.7938	Insignificant
X_2:Catalyst	18.58307	1	18.58307	0.421961	0.5221	Insignificant
X_3:ES time	49.24188	1	49.24188	1.118124	0.3009	Insignificant
X_4:MPC temperature	5016.902	1	5016.902	113.9176	< 0.0001	Significant
X_5:MPC time	467.7514	1	467.7514	10.62112	0.0033	Significant
Residual	1056.954	24	44.03974			
Lack of fit	957.7438	20	47.88719	1.930743	0.2765	Insignificant
Pure Error	99.20988	4	24.80247			
Cor Total	6562.041	29				

Table 4.6 Regression analysis for linear model, Eq. 4.4

Predictor	Coefficients	
	Actual	Coded
(Constant)	186.2825	50.23593
X_1:Amount of LLA	0.04295	0.4295
X_2:Catalyst	–3.51833	–1.0555
X_3:ES time	–0.57643	–1.72929
X_4:MPC temperature	–0.57809	–17.3427
X_5:MPC time	–0.52955	–5.2955

Case II: Development of 2-factor interaction model

The 2-factor interaction (2FI) model is developed using the experimental yield (wt. %) values reported in Table 4.2. The regressed 2FI model is given by the Eq. 4.5. ANOVA results for 2FI model for yield (wt. %) are shown in Table 4.7. The regression coefficients of regression analysis are given in Table 4.8.

$$YIELD = 336 - 0.68.X_1 - 125.X_2 + 10.0.X_3 - 1.27.X_4 - 4.69.X_5 + 0.415.X_1X_2 - 0.0527.X_1X_3 + 0.00033.X_1X_4 + 0.0248.X_1X_5 - 4.9.X_2X_3 + 0.532.X_2X_4 + 0.861.X_2X_5 - 0.0098.X_3X_4 - 0.133.X_3X_5 + 0.016.X_4X_5 \quad \ldots (4.5)$$

Table 4.7 ANOVA for RSM variables fitted to 2FI model

Source	Sum of Squares	df	Mean Square	F-value	p-value	Significance
Model	6153.041	15	410.2027	14.04119	< 0.0001	Significant
X_1:Amount of LLA	4.587919	1	4.587919	0.157044	0.6979	Insignificant
X_2:Catalyst	33.40187	1	33.40187	1.143342	0.3030	Insignificant
X_3:ES time	8.99221	1	8.99221	0.307802	0.5878	Insignificant
X_4:MPC temperature	2086.189	1	2086.189	71.41001	< 0.0001	Significant
X_5:MPC time	261.316	1	261.316	8.944817	0.0097	Significant
X_1X_2	17.83291	1	17.83291	0.610418	0.4476	Insignificant
X_1X_3	12.50216	1	12.50216	0.427947	0.5236	Insignificant
X_1X_4	0.115722	1	0.115722	0.003961	0.9507	Insignificant
X_1X_5	70.9618	1	70.9618	2.429014	0.1414	Insignificant
X_2X_3	96.96815	1	96.96815	3.319209	0.0899	Insignificant
X_2X_4	263.7458	1	263.7458	9.027987	0.0095	Significant
X_2X_5	76.87079	1	76.87079	2.631279	0.1271	Insignificant
X_3X_4	3.907925	1	3.907925	0.133768	0.7200	Insignificant
X_3X_5	79.16226	1	79.16226	2.709715	0.1220	Insignificant
X_4X_5	264.0215	1	264.0215	9.037426	0.0094	Significant
Residual	408.9993	14	29.21424			
Lack of Fit	309.7894	10	30.97894	1.249027	0.4483	Insignificant
Pure Error	99.20988	4	24.80247			
Cor Total	6562.041	29				

Table 4.8 Regression analysis for 2-FI model, Eq. 4.5

Predictor	Coefficients	
	Actual	Coded
(Constant)	335.7931	51.22269
X_1:Amount of LLA	–0.68048	–0.87444
X_2:Catalyst	–124.672	–2.35944
X_3:ES time	10.03713	0.93303
X_4:MPC temperature	–1.27362	–18.6467
X_5:MPC time	–4.69408	–6.59944
X_1X_2	0.414653	1.243958
X_1X_3	–0.05273	–1.58195
X_1X_4	0.000334	0.100208
X_1X_5	0.024815	2.481458
X_2X_3	–4.89522	–4.4057
X_2X_4	0.531551	4.783958
X_2X_5	0.860903	2.582708
X_3X_4	–0.00983	–0.88445
X_3X_5	–0.13269	–3.9807
X_4X_5	0.015955	4.786458

Now, from Table 4.7, it is evident that the individual parameter terms such as X_4 and X_5, and second order interaction terms such as X_2X_4 and X_4X_5 are the only significant model terms, whereas; all the other terms are insignificant. The correlation coefficients "R-square", "adjusted R–square" and "predicted R-square" values for Eq. 4.5 are 0.937672, 0.870892 and –0.11849, respectively. Eq. 4.5 offers negative "predicted R-square", which implies that the overall mean is a better predictor of the response than the current model. The "Adequate precision" value of 14.33 indicates an adequate signal, whereas; the *lack of fit* is insignificant. Thus, taking all the above facts into consideration, it can be concluded that the 2FI model is not a good model. The model can be improved by removing the insignificant model terms. For this case, the removal of insignificant terms, in a step by step manner (starting from largest insignificant to smallest insignificant term), produced higher "predicted R-square" value. The ANOVA for reduced 2FI model is given in Table 4.9. The regression coefficients of regression analysis are given in Table 4.10. The regression equation for the reduced 2FI model is given by Eq. 4.6.

$$YIELD = 290.8+0.09.X_1-88.8.X_2-0.15.X_3-1.1.X_4-3.1.X_5+0.414.X_2X_4+0.012.X_4X_5 \quad \ldots. (4.6)$$

Table 4.9 ANOVA for RSM variables fitted to reduced 2FI model

Source	Sum of Squares	df	Mean Square	F-value	p-value	Significance
Model	5847.553	7	835.3648	25.72198	< 0.0001	Significant
X_1:Amount of LLA	13.40939	1	13.40939	0.412893	0.5271	Insignificant
X_2:Catalyst	5.618932	1	5.618932	0.173014	0.6815	Insignificant
X_3:ES time	3.066655	1	3.066655	0.094426	0.7615	Insignificant
X_4:MPC temperature	4696.606	1	4696.606	144.6147	< 0.0001	Significant
X_5:MPC time	383.9249	1	383.9249	11.82155	0.0023	Significant
X_2X_4	193.1947	1	193.1947	5.948718	0.0233	Significant
X_4X_5	193.4542	1	193.4542	5.956709	0.0232	Significant
Residual	714.4872	22	32.47669			
Lack of Fit	615.2773	18	34.18207	1.378172	0.4141	Insignificant
Pure Error	99.20988	4	24.80247			
Cor Total	6562.041	29				

Now, from Table 4.9, it is comprehensible that the individual parameters and second order interaction terms such as X_4, X_5, X_2X_4 and X_4X_5 are significant, whereas; all the other model terms are insignificant. The correlation coefficients "R-square", "adjusted R–square" and "predicted R-square" values for Eq. 4.6 are 0.891, 0.856 and 0.767, respectively. *Adequate*

precision of 18.19 indicates an adequate signal. For the present model, the *lack of fit* is also insignificant. Thus, taking all the above facts into consideration, it can be concluded that the 2FI model is a good model.

Table 4.10 Regression analysis for reduced 2-FI model, Eq. 4.6

Predictor	Coefficients	
	Actual	Coded
(Constant)	290.798	50.67527
X_1:Amount of LLA	0.090146	0.901462
X_2:Catalyst	–88.8228	–0.58354
X_3:ES time	–0.14942	–0.44826
X_4:MPC temperature	–1.10034	–16.8708
X_5:MPC time	–3.09044	–4.82354
X_2X_4	0.413703	3.72333
X_4X_5	0.012419	3.72583

Case III: Development of quadratic model

The quadratic model is developed using the experimental yield (wt. %) values reported in Table 4.2. The regressed quadratic model is given by the Eq. 4.7. ANOVA results for quadratic model for yield (wt. %) are shown in Table 4.11. The regression coefficients of regression analysis are given in Table 4.12.

$$\begin{aligned} YIELD = {} & 121 - 1.32.X_1 - 204.X_2 + 11.9.X_3 + 1.25.X_4 - 6.58.X_5 + 0.537.X_1X_2 - 0.0605.X_1X_3 \\ & + 0.00156.X_1X_4 + 0.0285.X_1X_5 - 5.15.X_2X_3 + 0.572.X_2X_4 + 0.983.X_2X_5 \\ & - 0.0124.X_3X_4 - 0.14.X_3X_5 + 0.0172.X_4X_5 + 0.0044.X_1^2 + 47.X_2^2 - 0.059.X_3^2 \\ & - 0.00618.X_4^2 + 0.0368.X_5^2 \end{aligned} \quad \ldots (4.7)$$

Now, from Table 4.11, it is clear that the individual parameters and second order interaction terms such as X_4, X_5, X_2X_4 and X_4X_5 are significant, whereas; all the others are insignificant. The correlation coefficients "R-square", "adjusted R–square" and "predicted R-square" values for Eq. 4.7 are 0.960274, 0.871994and –1.32993, respectively. Eq. 4.7 offers negative "predicted R-square", which implies that the overall mean is a better predictor of the response than the current model. However, *adequate precision* of 13.29 indicates an adequate signal and the *lack of fit* for the present model is insignificant. Thus, taking all the above facts into consideration, it can be concluded that the quadratic model is not a good model. Further, for

the model Eq. 4.7, the "R-square" value is higher but the model contains a number of insignificant terms and thus leading to an inferior model and hence negative "predicted R-square" value. Thus, the model, Eq. 4.7, can be improved by removing the insignificant model terms.

Table 4.11 ANOVA for RSM variables fitted to quadratic model

Source	Sum of Squares	df	Mean Square	F-value	p-value	Significance
Model	6301.357	20	315.0679	10.8776	0.0004	Significant
X_1:Amount of LLA	4.587919	1	4.587919	0.158396	0.6999	Insignificant
X_2:Catalyst	33.40187	1	33.40187	1.153187	0.3108	Insignificant
X_3:ES time	19.83059	1	19.83059	0.684644	0.4294	Insignificant
X_4:MPC temperature	2086.189	1	2086.189	72.02489	< 0.0001	Significant
X_5:MPC time	261.316	1	261.316	9.021837	0.0149	Significant
X_1X_2	28.11463	1	28.11463	0.970647	0.3503	Insignificant
X_1X_3	16.27906	1	16.27906	0.562029	0.4726	Insignificant
X_1X_4	2.360339	1	2.360339	0.08149	0.7817	Insignificant
X_1X_5	87.92801	1	87.92801	3.035681	0.1154	Insignificant
X_2X_3	106.3279	1	106.3279	3.670931	0.0876	Insignificant
X_2X_4	287.5856	1	287.5856	9.928786	0.0117	Significant
X_2X_5	94.29139	1	94.29139	3.255375	0.1047	Insignificant
X_3X_4	6.171672	1	6.171672	0.213075	0.6553	Insignificant
X_3X_5	87.73743	1	87.73743	3.029102	0.1158	Insignificant
X_4X_5	287.8649	1	287.8649	9.938427	0.0117	Significant
X_1^2	0.465464	1	0.465464	0.01607	0.9019	Insignificant
X_2^2	43.84851	1	43.84851	1.513853	0.2497	Insignificant
X_3^2	0.698732	1	0.698732	0.024123	0.8800	Insignificant
X_4^2	75.83583	1	75.83583	2.618204	0.1401	Insignificant
X_5^2	33.18927	1	33.18927	1.145847	0.3123	Insignificant
Residual	260.6835	9	28.96483			
Lack of Fit	161.4736	5	32.29472	1.302077	0.4107	Insignificant
Pure Error	99.20988	4	24.80247			
Cor Total	6562.041	29				

Table 4.12 Regression analysis for quadratic model, Eq. 4.7

Predictor	Coefficients	
	Actual	Coded
(Constant)	121.0567	50.10559
X_1:Amount of LLA	–1.31841	–0.87444
X_2:Catalyst	–203.846	–2.35944
X_3:ES time	11.92217	1.465956
X_4:MPC temperature	1.246343	–18.6467
X_5:MPC time	–6.57947	–6.59944
X_1X_2	0.536782	1.610345
X_1X_3	–0.0605	–1.81511
X_1X_4	0.001555	0.466595
X_1X_5	0.028478	2.847845
X_2X_3	–5.15428	–4.63886
X_2X_4	0.572261	5.150345
X_2X_5	0.983032	2.949095
X_3X_4	–0.01242	–1.11761
X_3X_5	–0.14046	–4.21386
X_4X_5	0.017176	5.152845
X_1^2	0.004359	0.435913
X_2^2	47.01014	4.230913
X_3^2	–0.05934	–0.53409
X_4^2	–0.00618	–5.56409
X_5^2	0.036809	3.680913

Due to this, the removal of insignificant terms one by one in a stepwise manner (starting from largest insignificant to smallest insignificant term) was carried out to improve the model which produced higher "R-square" or "predicted R-square". The regressed reduced quadratic model is given by the Eq. 4.8. ANOVA results for reduced quadratic model for yield (wt. %) are given in Table 4.13. The regression coefficients of regression analysis are given in Table 4.14.

$$YIELD = 143 - 0.45.X_1 - 191.9.X_2 + 4.8.X_3 + 0.79.X_4 - 4.5.X_5 + 0.02.X_1X_5 - 3.76.X_2X_3 + 0.5.X_2X_4 + 0.78.X_2X_5 - 0.099.X_3X_5 + 0.015.X_4X_5 + 60.34.X_2^2 - 0.005.X_4^2 \quad \ldots (4.8)$$

From Table 4.13, it is perceptible that the individual parameter terms and second order interaction terms such as X_4, X_5, X_2X_3, X_2X_4, X_3X_5, X_4X_5 and X_2^2 are significant. The correlation coefficients "R-square", "adjusted R–square" and "predicted R-square" values for Eq. 4.8 are 0.948883, 0.907351and 0.795662, respectively.

Table 4.13 ANOVA for RSM variables fitted to reduced quadratic model

Source	Sum of Squares	df	Mean Square	F-value	p-value	Significance
Model	6226.609	13	478.9699	22.84677	< 0.0001	Significant
X_1:Amount of LLA	0.014939	1	0.014939	0.000713	0.9790	Insignificant
X_2:Catalyst	31.96006	1	31.96006	1.524488	0.2348	Insignificant
X_3:ES time	5.28416	1	5.28416	0.252053	0.6225	Insignificant
X_4:MPC temperature	4398.003	1	4398.003	209.7838	< 0.0001	Significant
X_5:MPC time	459.9231	1	459.9231	21.93824	0.0002	Significant
X_1X_5	64.38228	1	64.38228	3.071021	0.0988	Insignificant
X_2X_3	130.2853	1	130.2853	6.21458	0.0240	Significant
X_2X_4	266.3546	1	266.3546	12.70506	0.0026	Significant
X_2X_5	70.37007	1	70.37007	3.356638	0.0856	Insignificant
X_3X_5	99.60571	1	99.60571	4.751172	0.0446	Significant
X_4X_5	266.6487	1	266.6487	12.71909	0.0026	Significant
X_2^2	101.0008	1	101.0008	4.817716	0.0433	Significant
X_4^2	65.23635	1	65.23635	3.11176	0.0968	Insignificant
Residual	335.4312	16	20.96445			
Lack of Fit	236.2213	12	19.68511	0.793675	0.6615	Insignificant
Pure Error	99.20988	4	24.80247			
Cor Total	6562.041	29				

Table 4.14 Regression analysis for reduced quadratic model, Eq. 4.8

Predictor	Coefficients	
	Actual	Coded
(Constant)	143.5417	50.47222
X_1:Amount of LLA	–0.44865	–0.03282
X_2:Catalyst	–191.946	–1.51782
X_3:ES time	4.816146	0.639173
X_4:MPC temperature	0.788831	–17.805
X_5:MPC time	–4.46635	–5.75782
X_1X_5	0.022268	2.22683
X_2X_3	–3.75879	–3.38291
X_2X_4	0.503259	4.52933
X_2X_5	0.776027	2.32808
X_3X_5	–0.0986	–2.95791
X_4X_5	0.015106	4.53183
X_2^2	60.33964	5.430568
X_4^2	–0.00485	–4.36443

Eq. 4.8 offers acceptable "predicted R-square". The "predicted R-Square" of 0.796 is in reasonable agreement with the "adjusted R-Square" of 0.907. Thus, it can be concluded that Eq. 4.8 offers 79.6 % [predicted R-Square] of the variability in predicting new observations in

comparision to approximately 94.9 % [R-square] variability in the original data. Adequate precision of 18.3 indicates an adequate signal and the *lack of fit* is insignificant. Insignificant *lack of fit* is good for data fitness to the model. Thus, this model can be used to navigate the design space. Thus, taking all the facts into consideration, it can be concluded that the reduced quadratic model is the best model.

The parity plot for the reduced quadratic model, given by Eq. 4.8 for the prediction of yield (wt. %), is shown in Fig. 4.1. The error band extends from –10.1 % to +15.6 %, and 96.7 % data points fall within this error band. Thus, the yield (wt. %) predicted by Eq. 4.8 lie within –10.1 % to +15.6 % of experimental values.

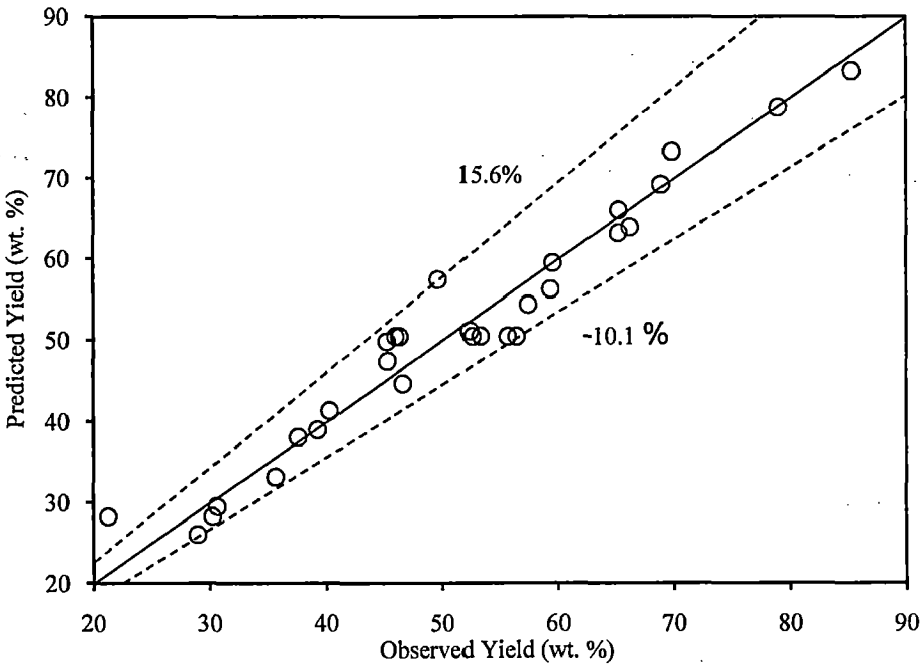

Fig. 4.1 Parity plot for the reduced quadratic model, Eq. 4.8, developed for prediction of yield (wt. %)

The error % is calculated using the formula:

$$Error\% = \frac{Y(P) - Y(E)}{Y(E)} x100 \qquad \ldots(4.9)$$

Where; *Y(P)* is the value of predicted output obtained using the model equation, Eq. 4.8, and *Y(E)* is the experimental output obtained from experiments.

Based on the above discussed criteria for individual models, it can be concluded that the reduced quadratic model described by Eq. 4.8 for yield (wt. %), best fits the experimental values

in comparision to other two models i.e. linear and 2-factor interaction models. This is because of the fact that the error band for this model is small and the "R-square", "adjusted R-Square" and "predicted R-Square" values are close to each other and also the error band contains 96.7 % data points. The main effects of different parameters and their interaction effects on yield (wt. %) are described in detail in Section 4.2.2.

4.2.1.2 Regression analysis to develop correlation for prediction of M_w

Experimental results obtained for M_w as reported in Table 4.2, are analyzed to determine the best correlation between M_w and input parameters, out of the input-output correlations proposed in Table 4.3.

Case I: Development of linear model

First of all, a linear model was fitted for M_w, considering all the five main input parameters. The regressed linear model is given by Eq. 4.10. ANOVA results for linear model for M_w are shown in Table 4.15. The regression coefficients of regression analysis are given in Table 4.16.

$$M_w = 330 - 0.05.X_1 - 34.6.X_2 - 0.98.X_3 - 1.11.X_4 - 1.42.X_5 \quad \ldots (4.10)$$

Table 4.15 ANOVA for RSM variables fitted to linear model

Source	Sum of Squares	df	Mean Square	F-value	p-value	Significance
Model	22566.85	5	4513.371	6.429532	0.0006	Significant
X_1:Amount of LLA	4.205963	1	4.205963	0.005992	0.9389	Insignificant
X_2:Catalyst	1798.5	1	1798.5	2.562057	0.1225	Insignificant
X_3:ES time	141.4958	1	141.4958	0.201568	0.6575	Insignificant
X_4:MPC temperature	18610.09	1	18610.09	26.51105	< 0.0001	Significant
X_5:MPC time	3353.997	1	3353.997	4.777944	0.0388	Significant
Residual	16847.4	24	701.975			
Lack of Fit	16805.02	20	840.2508	79.30177	0.0003	Significant
Pure Error	42.38245	4	10.59561			
Cor Total	39414.25	29				

From Table 4.15, it is evident that X_4 and X_5 are significant parameters. The correlation coefficients "R-square", "adjusted R–square" and "predicted R-square" values for Eq. 4.10 are 0.572556, 0.483505 and 0.113242, respectively. Thus, it can be said that Eq. 4.10 offers low "predicted R-square" and very small "R-square" values. The model can be improved by

removing the insignificant model terms. But to maintain hierarchy, these terms were kept in the model according to the hierarchy principle. The "Adequate precision" value of 9.78 indicates an adequate signal. For the present model, the *lack of fit* is also significant. Thus, taking all the above facts into consideration, it can be concluded that the linear model is a poor model.

Table 4.16 Regression analysis for linear model, Eq. 4.10

Predictor	Coefficients	
	Actual	Coded
(Constant)	329.5869	36.79109
X_1:Amount of LLA	-0.05021	-0.50215
X_2:Catalyst	-34.6125	-10.3838
X_3:ES time	-0.97713	-2.93139
X_4:MPC temperature	-1.1134	-33.4021
X_5:MPC time	-1.41801	-14.1801

Case II: Development of 2-factor interaction model

The 2FI model was developed using the experimental M_w values reported in Table 4.2. The regressed 2FI model is given by the Eq. 4.11. ANOVA results for 2FI model for M_w are shown in Table 4.17. The regression coefficients of regression analysis are given in Table 4.18.

$$M_w = 1431.61 - 16.58.X_1 - 742.98.X_2 + 32.62.X_3 - 5.22.X_4 - 30.22.X_5 + 5.18.X_1X_2 + 0.105.X_1X_3 + 0.039.X_1X_4 + 0.278.X_1X_5 - 14.45.X_2X_3 + 2.467.X_2X_4 + 5.792.X_2X_5 - 0.06.X_3X_4 - 0.043.X_3X_5 + 0.08.X_4X_5 \quad \ldots (4.11)$$

From Table 4.17, it is noticeable that the individual parameters and second order interaction terms such as X_3, X_4, X_5, X_1X_2, X_1X_4, X_1X_5, X_2X_3, X_2X_4, X_2X_5 and X_4X_5 are significant. The correlation coefficients "R-square", "adjusted R–square" and "predicted R-square" values for Eq. 4.11 are 0.965726, 0.929005 and -0.06938, respectively.

As the Eq. 4.11 offers negative "predicted R-square" value, the model can be improved by removing the insignificant model terms. The "Adequate precision" value of 24.5 indicates an adequate signal. For the present model, the *lack of fit* is significant. Thus, taking all the above facts into consideration, it can be concluded that the 2FI model is not an efficient model.

Table 4.17 ANOVA for RSM variables fitted to 2FI model

Source	Sum of Squares	df	Mean Square	F Value	p-value	Significance
Model	38063.38	15	2537.559	26.2985	< 0.0001	Significant
X_1:Amount of LLA	27.23773	1	27.23773	0.282284	0.6035	Insignificant
X_2:Catalyst	360.4654	1	360.4654	3.735756	0.0737	Insignificant
X_3:ES time	3090.343	1	3090.343	32.0274	< 0.0001	Significant
X_4:MPC temperature	5680.501	1	5680.501	58.87102	< 0.0001	Significant
X_5:MPC time	800.0493	1	800.0493	8.291472	0.0121	Significant
X_1X_2	2787.565	1	2787.565	28.88949	< 0.0001	Significant
X_1X_3	49.42233	1	49.42233	0.512198	0.4860	Insignificant
X_1X_4	1550.829	1	1550.829	16.07233	0.0013	Significant
X_1X_5	8934.657	1	8934.657	92.59612	< 0.0001	Significant
X_2X_3	845.2597	1	845.2597	8.760019	0.0103	Significant
X_2X_4	5680.609	1	5680.609	58.87214	< 0.0001	Significant
X_2X_5	3479.097	1	3479.097	36.05632	< 0.0001	Significant
X_3X_4	148.9881	1	148.9881	1.544068	0.2344	Insignificant
X_3X_5	8.180848	1	8.180848	0.084784	0.7752	Insignificant
X_4X_5	6693.717	1	6693.717	69.37168	< 0.0001	Significant
Residual	1350.869	14	96.49062			
Lack of Fit	1308.486	10	130.8486	12.34932	0.0136	Significant
Pure Error	42.38245	4	10.59561			
Cor Total	39414.25	29				

Table 4.18 Regression analysis for 2-FI model, Eq. 4.11

Predictor	Coefficients	
	Actual	Coded
(Constant)	1431.61	43.8839
X_1:Amount of LLA	-16.5809	2.130639
X_2:Catalyst	-742.981	-7.75097
X_3:ES time	32.62345	17.29679
X_4:MPC temperature	-5.21583	-30.7693
X_5:MPC time	-30.2193	-11.5474
X_1X_2	5.184249	15.55275
X_1X_3	-0.10484	-3.1453
X_1X_4	0.038668	11.6005
X_1X_5	0.278441	27.84412
X_2X_3	-14.4528	-13.0075
X_2X_4	2.466889	22.202
X_2X_5	5.791708	17.37512
X_3X_4	-0.06068	-5.46105
X_3X_5	-0.04266	-1.27967
X_4X_5	0.080335	24.10062

However, when the insignificant model terms of Eq. 4.11 were removed it did not produce better "predicted R-square". The modified regressed 2FI model is given by the Eq. 4.12. ANOVA results for the reduced 2FI model for M_w are shown in Table 4.19. The regression coefficients of regression analysis are given in Table 4.20.

$$M_w = 1467 - 16.48.X_1 - 737.37.X_2 + 13.58.X_3 - 5.35.X_4 - 29.78.X_5 + 5.08.X_1X_2 + 0.038.X_1X_4 + 0.275.X_1X_5 - 11.27.X_2X_3 + 2.43.X_2X_4 + 5.68.X_2X_5 + 0.079.X_4X_5 \quad \ldots(4.12)$$

Table 4.19 ANOVA for RSM variables fitted to reduced 2FI model

Source	Sum of Squares	df	Mean Square	F-value	p-value	Significance
Model	37854.46	12	3154.539	34.38098	< 0.0001	Significant
X_1:Amount of LLA	328.5035	1	328.5035	3.580325	0.0756	Insignificant
X_2:Catalyst	389.8595	1	389.8595	4.249038	0.0549	Insignificant
X_3:ES time	3032.768	1	3032.768	33.05383	< 0.0001	Significant
X_4:MPC temperature	11655.05	1	11655.05	127.0271	< 0.0001	Significant
X_5:MPC time	1176.068	1	1176.068	12.81784	0.0023	Significant
X_1X_2	2720.836	1	2720.836	29.6541	< 0.0001	Significant
X_1X_4	1492.036	1	1492.036	16.26155	0.0009	Significant
X_1X_5	8883.866	1	8883.866	96.82432	< 0.0001	Significant
X_2X_3	1277.099	1	1277.099	13.91897	0.0017	Significant
X_2X_4	5614.869	1	5614.869	61.19587	< 0.0001	Significant
X_2X_5	3410.849	1	3410.849	37.17449	< 0.0001	Significant
X_4X_5	6631.561	1	6631.561	72.27669	< 0.0001	Significant
Residual	1559.791	17	91.75242			
Lack of Fit	1517.409	13	116.7237	11.01623	0.0163	Significant
Pure Error	42.38245	4	10.59561			
Cor Total	39414.25	29				

From Table 4.19, it is apparent that the input parameter terms and second order interaction terms such as X_3, X_4, X_5, X_1X_2, X_1X_4, X_1X_5, X_2X_3, X_2X_4, X_2X_5 and X_4X_5 are significant. The correlation coefficients "R-square", "adjusted R–square" and "predicted R-square" values for Eq. 4.12 are 0.960426, 0.932491 and 0.687059, respectively. Thus, Eq. 4.12 offers 68.7 % "predicted R-square" values, which is not well acceptable. The "Predicted R-Square" of 0.687 is not as close to the "adjusted R-Square" of 0.9324 as one might normally expect. The "Adequate precision" value of 27.799 indicates an adequate signal. For the present

model, the lack of fit is significant. Thus, taking all the above facts into consideration, it can be safely concluded that the reduced 2FI model is a poor model.

Table 4.20 Regression analysis for reduced 2-FI model, Eq. 4.12

Predictor	Coefficients	
	Actual	Coded
(Constant)	1467.256	43.71815
X_1:Amount of LLA	-16.4812	4.72942
X_2:Catalyst	-737.373	-5.15219
X_3:ES time	13.57946	17.06592
X_4:MPC temperature	-5.35409	-28.1705
X_5:MPC time	-29.7766	-8.94858
X_1X_2	5.0772	15.2316
X_1X_4	0.037598	11.27935
X_1X_5	0.27523	27.52297
X_2X_3	-11.2726	-10.1453
X_2X_4	2.431206	21.88085
X_2X_5	5.684658	17.05397
X_4X_5	0.079265	23.77947

Case III: Development of quadratic model

The quadratic model was developed using the experimental M_w values reported in Table 4.2. The regressed quadratic model is given by the Eq. 4.13. ANOVA results for quadratic model for M_w are shown in Table 4.21. The regression coefficients of regression analysis are given in Table 4.22.

$$M_w = 1540.5 - 18.6.X_1 - 595.96.X_2 + 36.86.X_3 - 5.94.X_4 - 36.85.X_5 + 5.45.X_1X_2 - 0.122.X_1X_3 + 0.041.X_1X_4 + 0.286.X_1X_5 - 15.02.X_2X_3 + 2.56.X_2X_4 + 6.06.X_2X_5 - 0.066.X_3X_4 - 0.06.X_3X_5 + 0.083.X_4X_5 + 0.02.X_1^2 - 126.01.X_2^2 - 0.139.X_3^2 + 0.00136.X_4^2 + 0.143.X_5^2 \quad \ldots (4.13)$$

From Table 4.21, it is noticiable that the individual parameters and second order interaction terms such as X_2, X_3, X_4, X_5, X_1X_2, X_1X_4, X_1X_5, X_2X_3, X_2X_4, X_2X_5, X_4X_5, X_2^2 and X_5^2 are significant, whereas; all the other model terms are insignificant. The correlation coefficients "R-square", "adjusted R–square" and "predicted R-square" values for Eq. 4.13 are 0.985766, 0.954136 and -0.56573, respectively. An "Adequate precision" value of 26.92 indicates an adequate signal. For the present model, the *lack of fit* is significant. Thus, taking all the above facts into consideration, it can be concluded that the quadratic model is not a good

model. It appears that the above model can be further improved by removing the insignificant model terms.

Table 4.21 ANOVA for RSM variables fitted to quadratic model

Source	Sum of Squares	df	Mean Square	F-value	p-value	Significance
Model	38853.24	20	1942.662	31.16494	< 0.0001	Significant
X_1:Amount of LLA	27.23773	1	27.23773	0.436958	0.5252	Insignificant
X_2:Catalyst	360.4654	1	360.4654	5.782726	0.0396	Significant
X_3:ES time	3147.743	1	3147.743	50.49731	< 0.0001	Significant
X_4:MPC temperature	5680.501	1	5680.501	91.1288	< 0.0001	Significant
X_5:MPC time	800.0493	1	800.0493	12.8347	0.0059	Significant
X_1X_2	2901.373	1	2901.373	46.54495	< 0.0001	Significant
X_1X_3	66.12837	1	66.12837	1.060857	0.3299	Insignificant
X_1X_4	1668.802	1	1668.802	26.77156	0.0006	Significant
X_1X_5	8899.234	1	8899.234	142.765	< 0.0001	Significant
X_2X_3	903.2652	1	903.2652	14.49053	0.0042	Significant
X_2X_4	5739.295	1	5739.295	92.072	< 0.0001	Significant
X_2X_5	3583.802	1	3583.802	57.49274	< 0.0001	Significant
X_3X_4	176.3459	1	176.3459	2.82901	0.1269	Insignificant
X_3X_5	15.87947	1	15.87947	0.254745	0.6259	Insignificant
X_4X_5	6725.585	1	6725.585	107.8945	< 0.0001	Significant
X_1^2	9.998621	1	9.998621	0.160402	0.6981	Insignificant
X_2^2	315.0654	1	315.0654	5.054402	0.0512	Significant
X_3^2	3.843666	1	3.843666	0.061662	0.8095	Insignificant
X_4^2	3.64502	1	3.64502	0.058475	0.8143	Insignificant
X_5^2	501.1436	1	501.1436	8.039541	0.0195	Significant
Residual	561.0137	9	62.33486			
Lack of Fit	518.6313	5	103.7263	9.789547	0.0231	Significant
Pure Error	42.38245	4	10.59561			
Cor Total	39414.25	29				

Table 4.22 Regression analysis for quadratic model, Eq. 4.13

Predictor	Coefficients	
	Actual	Coded
(Constant)	1540.511	41.42594
X_1:Amount of LLA	-18.6212	2.130639
X_2:Catalyst	-595.959	-7.75097
X_3:ES time	36.85722	18.4694
X_4:MPC temperature	-5.95366	-30.7693
X_5:MPC time	-36.8494	-11.5474
X_1X_2	5.452972	16.35891
X_1X_3	-0.12194	-3.65832
X_1X_4	0.041356	12.40666
X_1X_5	0.286503	28.65029
X_2X_3	-15.0229	-13.5206
X_2X_4	2.556463	23.00816
X_2X_5	6.06043	18.18129
X_3X_4	-0.06638	-5.97407
X_3X_5	-0.05976	-1.79269
X_4X_5	0.083023	24.90679
X_1^2	0.020204	2.020351
X_2^2	-126.013	-11.3411
X_3^2	-0.13918	-1.25265
X_4^2	0.001355	1.219851
X_5^2	0.143034	14.30335

Thus, the removal of insignificant terms in a stepwise fashion (starting from largest insignificant to smallest insignificant term) was carried out to improve the model which produced higher "predicted R-square" value. The regressed "reduced quadratic model" is given by the Eq. 4.14. ANOVA results for "reduced quadratic model" for M_w are shown in Table 4.23. The regression coefficients of regression analysis are given in Table 4.24.

$$M_w = 1479.67 - 17.424.X_1 - 598.08.X_2 + 23.55.X_3 - 5.36.X_4 - 36.78.X_5 + 5.336.X_1X_2 + 0.04.X_1X_4 + 0.28.X_1X_5 - 12.54.X_2X_3 + 2.52.X_2X_4 + 5.94.X_2X_5 - 0.04.X_3X_4 + 0.08.X_4X_5 - 118.655.X_2^2 + 0.149656.X_5^2 \quad \ldots (4.14)$$

Table 4.23 ANOVA for RSM variables fitted to reduced quadratic model

Source	Sum of Squares	df	Mean Square	F-value	p-value	Significance
Model	38765.62	15	2584.375	55.78059	< 0.0001	Significant
X_1:Amount of LLA	223.0705	1	223.0705	4.814705	0.0456	Significant
X_2:Catalyst	444.8285	1	444.8285	9.601083	0.0079	Significant
X_3:ES time	3113.134	1	3113.134	67.19322	< 0.0001	Significant
X_4:MPC temperature	11027.41	1	11027.41	238.0133	< 0.0001	Significant
X_5:MPC time	1220.236	1	1220.236	26.33732	0.0002	Significant
X_1X_2	2859.205	1	2859.205	61.71247	< 0.0001	Significant
X_1X_4	1621.657	1	1621.657	35.00149	< 0.0001	Significant
X_1X_5	8935.64	1	8935.64	192.8649	< 0.0001	Significant
X_2X_3	1446.991	1	1446.991	31.23154	< 0.0001	Significant
X_2X_4	5727.777	1	5727.777	123.6271	< 0.0001	Significant
X_2X_5	3547.254	1	3547.254	76.56317	< 0.0001	Significant
X_3X_4	158.8911	1	158.8911	3.429473	0.0852	Insignificant
X_4X_5	6727.948	1	6727.948	145.2146	< 0.0001	Significant
X_2^2	386.1864	1	386.1864	8.335365	0.0119	Significant
X_5^2	758.4519	1	758.4519	16.37026	0.0012	Significant
Residual	648.635	14	46.33107			
Lack of Fit	606.2526	10	60.62526	5.721732	0.0537	Insignificant
Pure Error	42.38245	4	10.59561			
Cor Total	39414.25	29				

Table 4.24 Regression analysis for quadratic model, Eq. 4.14

Predictor	Coefficients	
	Actual	Coded
(Constant)	1479.67	41.62984
X_1:Amount of LLA	-17.4244	4.09663
X_2:Catalyst	-598.08	-5.78498
X_3:ES time	23.55113	18.13765
X_4:MPC temperature	-5.35718	-28.8033
X_5:MPC time	-36.7837	-9.58137
X_1X_2	5.335988	16.00796
X_1X_4	0.040186	12.05571
X_1X_5	0.282993	28.29934
X_2X_3	-12.5406	-11.2866
X_2X_4	2.517468	22.65721
X_2X_5	5.943446	17.83034
X_3X_4	-0.04156	-3.74006
X_4X_5	0.081853	24.55584
X_2^2	-118.655	-10.6789
X_5^2	0.149656	14.96557

However, from Table 4.23, it is observable that the individual parameters and second order interaction terms such as X_1, X_2, X_3, X_4, X_5, X_1X_2, X_1X_4, X_1X_5, X_2X_3, X_2X_4, X_2X_5, X_4X_5, X_2^2 and X_5^2 are significant. The correlation coefficients "R-square", "adjusted R–square" and "predicted R-square" values for Eq. 4.14 are 0.983543, 0.965911 and 0.56564, respectively. The "Predicted R-Square" of 0.566 is not in good agreement with the "Adjusted R-Square" of 0.966. Thus, it can be concluded that Eq. 4.14 offers 57 % [predicted R-Square] of the variability in predicting new observations in comparision to approximately 98.3% [R-square] variability in the original data. Adequate precision of 36.13 indicates an adequate signal. The *lack of fit* is insignificant. Insignificant lack of fit is good for data fitness in the model. However, taking all the facts into consideration, it can be concluded that the reduced quadratic model can be used to navigate the design space but one should still try to improve this model.

Thus, to improve the above model, the M_w data were transformed and then checked for correlation and it was observed that square root transformation of the response produced the desired model.

Case IV: Development of quadratic model after data transformation

As for the present case, the ratio of maximum to minimum M_w is around 400, a square root transformation best suits the data which converts the ratio to about 19. A square root transformation is often the best, when the distribution differs moderately from normality. Thus, the non-linear quadratic model was developed using the squareroot of experimental M_w values reported in Table 4.2. The regressed quadratic model is given by the Eq. 4.15. ANOVA results for transformed quadratic model for M_w are shown in Table 4.25. The regression coefficients of regression analysis are given in Table 4.26.

$$\begin{aligned}\text{Sqrt}\,(M_w) = {} & 45.4 - 0.73.X_1 - 23.6.X_2 + 2.62.X_3 + 0.063.X_4 - 2.21.X_5 + 0.265.X_1X_2 - 0.008.X_1X_3 \\ & + 0.001.X_1X_4 + 0.018.X_1X_5 - 1.066.X_2X_3 + 0.1496.X_2X_4 + 0.306.X_2X_5 - 0.004.X_3X_4 \\ & - 0.005.X_3X_5 + 0.005.X_4X_5 - 0.0001.X_1^2 - 12.7.X_2^2 - 0.03.X_3^2 - 0.0009.X_4^2 \\ & + 0.008.X_5^2 \qquad \ldots (4.15)\end{aligned}$$

Table 4.25 ANOVA for RSM variables fitted to quadratic model taking square root of M_w

Source	Sum of Squares	df	Mean Square	F-value	p-value	Significance
Model	269.373	20	13.46865	141.0531	< 0.0001	Significant
X_1:Amount of LLA	0.616254	1	0.616254	6.453839	0.0317	Significant
X_2:Catalyst	0.835358	1	0.835358	8.748453	0.0160	Significant
X_3:ES time	8.143327	1	8.143327	85.28257	< 0.0001	Significant
X_4:MPC temperature	55.30318	1	55.30318	579.1733	< 0.0001	Significant
X_5:MPC time	5.418314	1	5.418314	56.74434	< 0.0001	Significant
X_1X_2	6.834451	1	6.834451	71.57512	< 0.0001	Significant
X_1X_3	0.280176	1	0.280176	2.934202	0.1209	Insignificant
X_1X_4	1.460945	1	1.460945	15.30003	0.0036	Significant
X_1X_5	36.60226	1	36.60226	383.3243	< 0.0001	Significant
X_2X_3	4.548537	1	4.548537	47.63543	< 0.0001	Significant
X_2X_4	19.65934	1	19.65934	205.8862	< 0.0001	Significant
X_2X_5	9.142182	1	9.142182	95.74328	< 0.0001	Significant
X_3X_4	0.780344	1	0.780344	8.172301	0.0188	Significant
X_3X_5	0.093981	1	0.093981	0.984238	0.3471	Insignificant
X_4X_5	23.8552	1	23.8552	249.8282	< 0.0001	Significant
X_1^2	0.000368	1	0.000368	0.003851	0.9519	Insignificant
X_2^2	3.200657	1	3.200657	33.5195	0.0003	Significant
X_3^2	0.180622	1	0.180622	1.891596	0.2023	Insignificant
X_4^2	1.645018	1	1.645018	17.22777	0.0025	Significant
X_5^2	1.668793	1	1.668793	17.47676	0.0024	Significant
Residual	0.859378	9	0.095486			
Lack of Fit	0.611735	5	0.122347	1.976186	0.2645	Insignificant
Pure Error	0.247643	4	0.061911			
Cor Total	270.2324	29				

From Table 4.25, it is clear that the input parameters and their second order interaction terms such as X_1, X_2, X_3, X_4, X_5, X_1X_2, X_1X_4, X_1X_5, X_2X_3, X_2X_4, X_2X_5, X_3X_4, X_4X_5, X_2^2, X_4^2 and X_5^2 are significant, whereas; all the other model terms are insignificant. The correlation coefficients "R-square", "adjusted R–square" and "predicted R-square" values for Eq. 4.15 are 0.99682, 0.989753 and 0.723636, respectively. The "Adequate precision" value of 48.88 indicates an adequate signal. For the present model, the *lack of fit* is insignificant. Thus, taking all the above facts into consideration, it can be concluded that the square root transformed quadratic model needs further improvement. The model can be improved by removing the insignificant model terms.

Table 4.26 Regression analysis for quadratic model, Eq. 4.15

Predictor	Coefficients	
	Actual	Coded
(Constant)	45.40128	6.526728
X_1:Amount of LLA	-0.73062	0.320482
X_2:Catalyst	-23.6144	-0.37313
X_3:ES time	2.618431	0.939408
X_4:MPC temperature	0.062972	-3.03598
X_5:MPC time	-2.20604	-0.95029
X_1X_2	0.264657	0.793971
X_1X_3	-0.00794	-0.23812
X_1X_4	0.001224	0.367088
X_1X_5	0.018374	1.837412
X_2X_3	-1.06606	-0.95945
X_2X_4	0.149622	1.346595
X_2X_5	0.306095	0.918285
X_3X_4	-0.00442	-0.3974
X_3X_5	-0.0046	-0.13791
X_4X_5	0.004945	1.483352
X_1^2	-0.00012	-0.01225
X_2^2	-12.7009	-1.14308
X_3^2	-0.03017	-0.27154
X_4^2	-0.00091	-0.81949
X_5^2	0.008254	0.825388

Thus, the removal of insignificant terms in a stepwise manner was carried out to improve the model which produced higher "predicted R-square" value. The regressed reduced quadratic model is given by the Eq. 4.16. ANOVA results for reduced quadratic model for M_w are shown in Table 4.27. The regression coefficients of regression analysis are given in Table 4.28.

$$\text{Sqrt}(M_w) = 41.998 - 0.747.X_1 - 21.999.X_2 + 1.508.X_3 + 0.105.X_4 - 2.16.X_5 + 0.26.X_1X_2 + 0.001.X_1X_4 + 0.018.X_1X_5 - 0.896.X_2X_3 + 0.148.X_2X_4 + 0.301.X_2X_5 - 0.003.X_3X_4 + 0.005.X_4X_5 - 13.7.X_2^2 - 0.001.X_4^2 + 0.007.X_5^2 \quad \ldots (4.16)$$

Table 4.27 ANOVA for RSM variables fitted to reduced quadratic model taking $\sqrt{M_w}$

Source	Sum of Squares	df	Mean Square	F-value	p-value	Significance
Model	268.883	16	16.80519	161.8989	< 0.0001	Significant
X_1:Amount of LLA	2.81866	1	2.81866	27.1546	0.0002	Significant
X_2:Catalyst	0.720369	1	0.720369	6.939941	0.0206	Significant
X_3:ES time	8.142859	1	8.142859	78.44722	< 0.0001	Significant
X_4:MPC temperature	111.3572	1	111.3572	1072.8	< 0.0001	Significant
X_5:MPC time	8.714339	1	8.714339	83.95278	< 0.0001	Significant
X_1X_2	6.749615	1	6.749615	65.02489	< 0.0001	Significant
X_1X_4	1.378876	1	1.378876	13.28391	0.0030	Significant
X_1X_5	36.94333	1	36.94333	355.9071	< 0.0001	Significant
X_2X_3	7.38785	1	7.38785	71.17356	< 0.0001	Significant
X_2X_4	19.72358	1	19.72358	190.0143	< 0.0001	Significant
X_2X_5	9.075866	1	9.075866	87.43568	< 0.0001	Significant
X_3X_4	0.678677	1	0.678677	6.538288	0.0239	Significant
X_4X_5	23.98292	1	23.98292	231.0483	< 0.0001	Significant
X_2^2	4.284938	1	4.284938	41.28053	< 0.0001	Significant
X_4^2	2.330874	1	2.330874	22.45533	0.0004	Significant
X_5^2	1.52501	1	1.52501	14.69174	0.0021	Significant
Residual	1.349406	13	0.1038			
Lack of Fit	1.101764	9	0.122418	1.977336	0.2668	Insignificant
Pure Error	0.247643	4	0.061911			
Cor Total	270.2324	29				

From Table 4.27, it is apparent that the input parameters and second order interaction terms such as X_1, X_2, X_3, X_4, X_5, X_1X_2, X_1X_4, X_1X_5, X_2X_3, X_2X_4, X_2X_5, X_3X_4, X_4X_5, X_2^2, X_4^2 and X_5^2 are significant. The correlation coefficients "R-square", "adjusted R–square" and "predicted R-square" values for Eq. 4.16 are 0.995006, 0.988861 and 0.894553, respectively. Thus, it can be said that Eq. 4.16 offers good "predicted R-square" value. The "Predicted R-Square" of 0. 0.895 is in good agreement with the "Adjusted R-Square" of 0.966. Further, it can be concluded that Eq. 4.16 offers 89.5 % [predicted R-Square] of the variability in predicting new observations in comparision to approximately 99.5% [R-square] variability in the original data. Adequate precision of 52.599 indicates an adequate signal. This model can be used to navigate the design space. The lack of fit is insignificant. Insignificant lack of fit is good for data fitness in the model. Thus, taking all the above facts into consideration, it can be concluded that the reduced square root transformed quadratic model can be used to navigate the design space and is the best model.

Table 4.28 Regression analysis for quadratic model, Eq. 4.16

Predictor	Coefficients	
	Actual	Coded
(Constant)	41.99778	6.510714
X_1:Amount of LLA	-0.74662	0.460707
X_2:Catalyst	-21.9987	-0.23291
X_3:ES time	1.507735	0.930323
X_4:MPC temperature	0.104748	-2.89576
X_5:MPC time	-2.16055	-0.81007
X_1X_2	0.259654	0.778961
X_1X_4	0.001174	0.352078
X_1X_5	0.018224	1.822403
X_2X_3	-0.8961	-0.80649
X_2X_4	0.147954	1.331586
X_2X_5	0.301092	0.903276
X_3X_4	-0.00272	-0.24444
X_4X_5	0.004894	1.468343
X_2^2	-13.6992	-1.23293
X_4^2	-0.00101	-0.90934
X_5^2	0.007355	0.735535

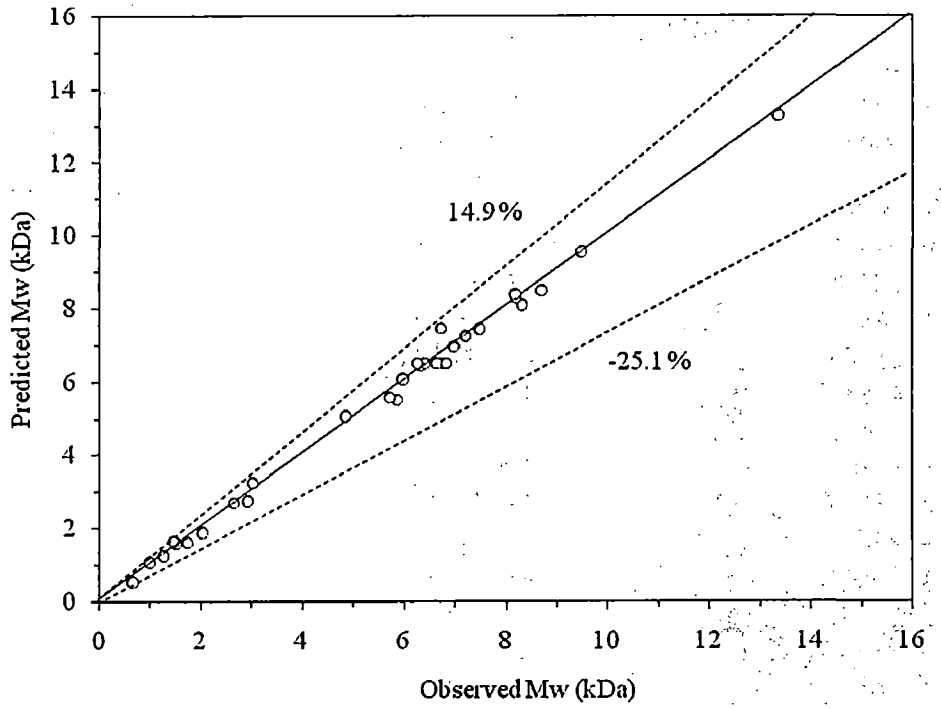

Fig. 4.2 Parity plot for the reduced quadratic model, Eq. 4.16, developed for prediction of M_w

The parity plot for the reduced quadratic model given by Eq. 4.16 for the prediction of M_w is shown in Fig. 4.2. The error band extends from –8.1 % to +14.9 %, and 96.7 % data points fall

within this error band. Thus, the M_w predicted by Eq. 4.16 lie within –8.1 % to +14.9 % of experimental values.

Based on the above discussed criteria for individual models, it can be concluded that the reduced quadratic model described by Eq. 4.16 for square root transformed M_w best fits the experimental values. This is because of the fact that the error band for this model is small and the "R-square", "adjusted R-Square" and "predicted R-Square" values are in reasonable aggrement with each other and also all the data points lie within the error band.

4.2.2 Effect of Various Parameters on Yield (wt. %) and M_w

To visualise how yield (wt. %) and M_w vary with input parameters, such as amount of LLA (X_1), wt. % of catalyst (X_2), ES time (X_3), MPC temperature (X_4) and MPC time (X_5), one factor plots has been plotted as given in Fig. 4.3 to Fig. 4.12,. These figures portray the complete picture of the variations in the whole range of the experimental domain studied, when the input parameters are varied from minimum to maximum of the range given in Table 4.2. These one factor main effect plots have been obtained by varying one of the factors and keeping all other factors at the central level as can be defined as base case in the Table 4.29. The full quadratic equations, Eq.4.7 and Eq.4.13, are used to generate the variation of yield (wt. %) and M_w, respectively, with input parameters as depicted through Fig. 4.3 to Fig. 4.12. LSD bars display Fisher's Least Significant Difference (LSD) bars (95% confidence interval) at the end points of line on the graph.

Table 4.29 Base case for determining the effects of parameters in MPC

Name of Input Parameters	Base case	Range	
		Lower	Upper
X_1: Amount of LLA (g)	30	20	40
X_2: Catalyst (wt. %)	0.7	0.4	1.0
X_3: ES time (h)	5	2	8
X_4: MPC temperature (°C)	210	180	240
X_5: MPC time (h)	20	10	30

4.2.2.1 Effect of amount of LLA on yield (wt. %) and M_w

The effects of amount of LLA on yield (wt. %) and M_w are shown in Figs. 4.3 and 4.4, respectively.

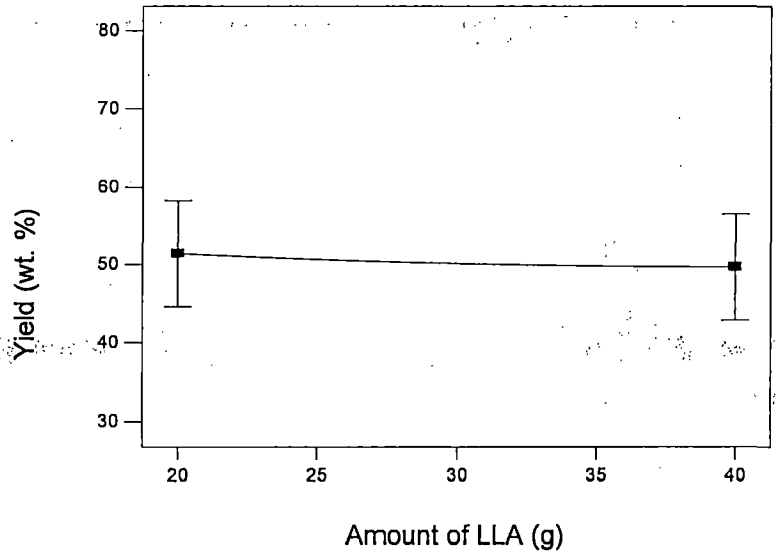

Fig. 4.3 Effect of amount of LLA on yield (wt. %) of PLA

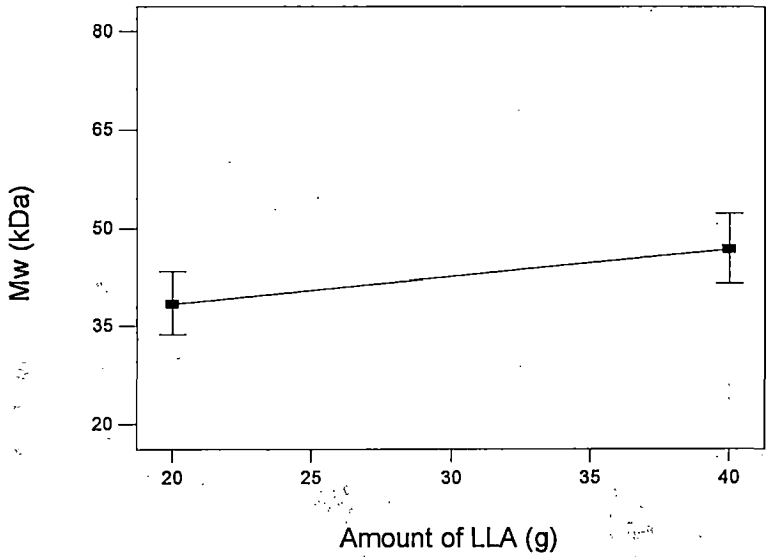

Fig. 4.4 Effect of amount of LLA on M_w of PLA

From the above figures following salient facts emerged out:

1. With the increase in the amount of LLA, the yield (wt. %) decreases very marginally and the observed variation is almost unnoticeable.
2. The M_w of PLA increases very slightly with the increase in amount of LLA.

The above facts can be explained as:

The effect of amount of LLA on yield (wt. %) is found to be insignificant which is also confirmed from the Section 4.2.1.1. The slight decrease in yield (wt. %) with the increase in

amount of LLA may be due to the increase in reaction mixture viscosity. The increased viscosity does not allow the reaction byproduct, water, to get out of the reaction mixture to shift the polymerization reaction in a forward direction. This in turn, activates the reverse reaction and thus leading to decreased yield (wt. %) (Proikakis *et al.*, 2002).

The minor increase in M_w with the increase in amount of LLA can be attributed to the increase in monomer to catalyst ratio. The monomer to catalyst ratio increases from 28.6 to 57, with the increase of amount of LLA from 20 to 40 g. This helps the polymerization reaction to shift in the forward direction. This in turn activates the forward reaction and enhances the chain propagation and thus forces the M_w to increase (Chen *et al.*, 2005).

4.2.2.2 Effect of wt. (%) of catalyst on yield (wt. %) and M_w

Figs. 4.5 and 4.6 demonstrates the effect of wt. % of catalysts on yield (wt. %) and M_w, respectively.

From the figures, following salient facts emerged out:

1. With the increase of the wt. % of catalyst, the yield (wt. %) decreases gradually and 0.4 wt % of catalyst leads to higher yield (wt. %).
2. With the increase in the wt. % of catalyst from 0.4 to 0.7, the M_w increases and with further increase from 0.7 to 1 wt. % of catalyst, the M_w decreases.

The above facts can be explained as:

Any increase in the wt. % of catalyst resulted in lower yield (wt. %) of the obtained PLA because of the formation of higher amount of lactide and oligomers of PLA. Formations of these side products consume lactic acid and are washed away when washed with methanol, and hence the yield (wt. %) decreases.

The variation of M_w with the increase in catalyst wt. % can be explained on the basis of monomer to catalyst ratio. The monomer to catalyst ratio varies from 75 to 42 when the catalyst wt. % varies from 0.4 to 0.7 % and further increase in catalyst wt. % from 0.7 to 1 %, decreases the monomer to catalyst ratio from 42 to 30. Thus, it can be concluded that the optimum of monomer to catalyst ratio lies in between 42 to 75. Further, with the increase in the wt. % of catalyst side reactions are favoured. As a side reaction, lactide formation and oligomeric PLA formation occurs which may seem prominent after 0.7 wt. % of catalysts and thus M_w decreases

with further increase in the wt. % of catalyst (Moon *et al.*, 2000; Zhang and Wang, 2008). The significant contribution of wt. % of catalysts has also been established in the discussion in Section 4.2.1.2.

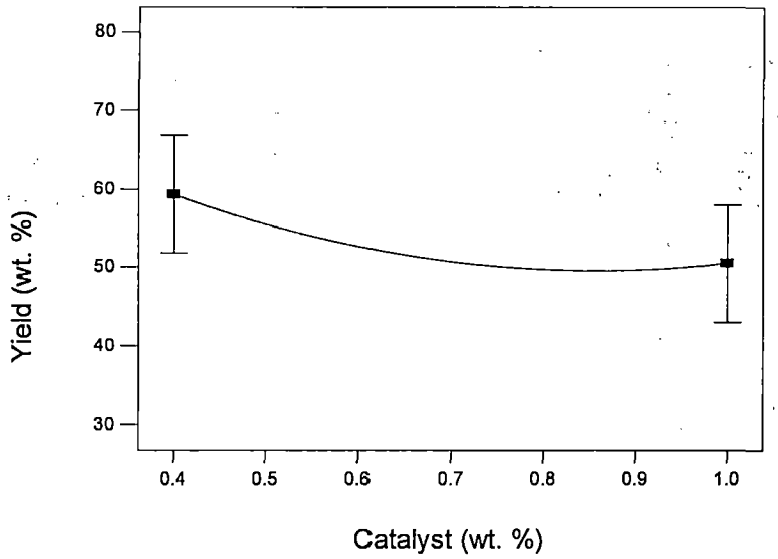

Fig. 4.5 Effect of wt. % of catalyst on yield (wt. %) of PLA

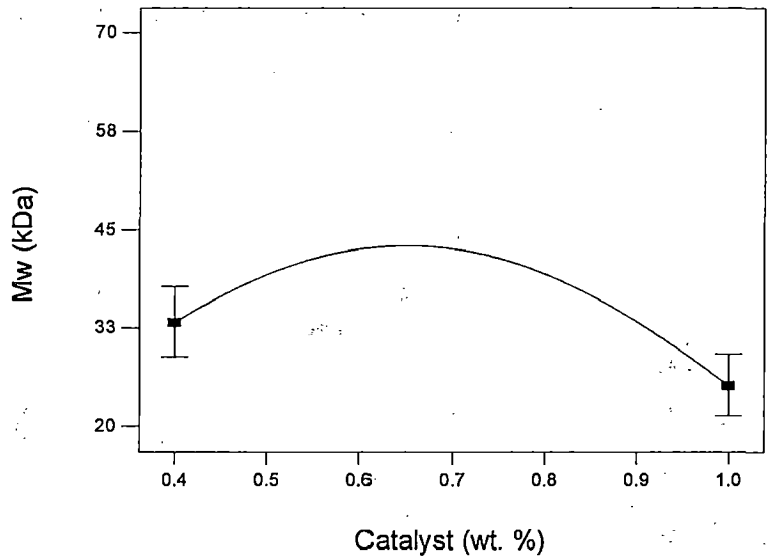

Fig. 4.6 Effect of wt. % of catalyst on M_w of PLA

4.2.2.3 Effect of esterification time on yield (wt. %) and M_w

Figs. 4.7 and 4.8 illustrates the effect of esterification time on yield (wt. %) and M_w of PLA, respectively.

From the figures, following relevant facts become apparent:

1. With the increase in esterification time from 2-8 h, the yield (wt. %) increases marginally and the variation is insignificant.
2. The M_w of PLA was observed to increase in a linear fashion with the increase in esterification time.

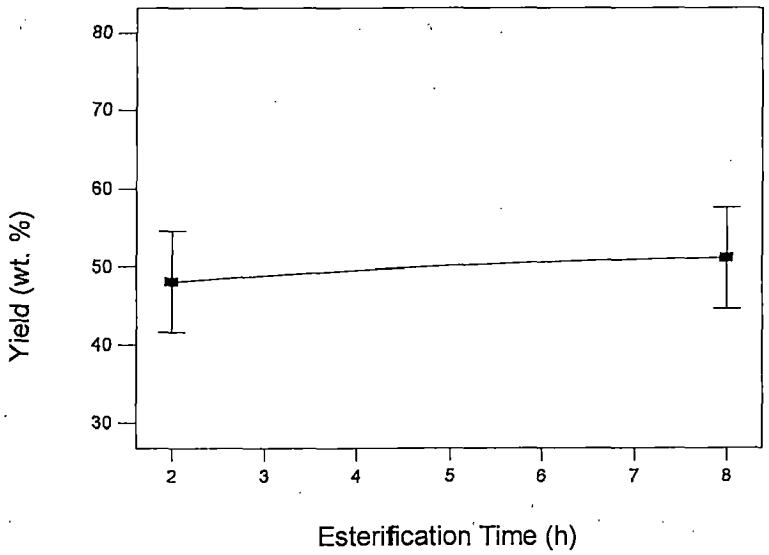

Fig. 4.7 Effect of esterification time on yield (wt. %) of PLA

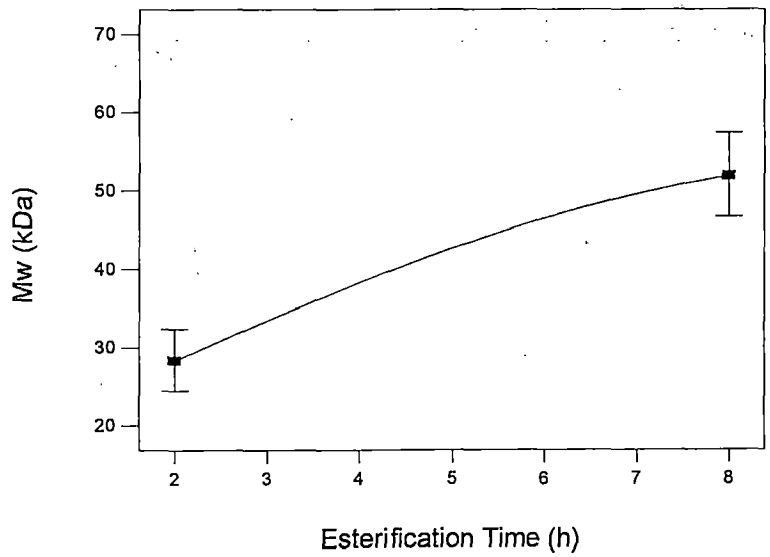

Fig. 4.8 Effect of esterification time on M_w of PLA

These facts can be justified as:

The effect of esterification time on yield (wt. %) is found to be insignificant which is also confirmed from the Section 4.2.1.1.

The increase in M_w with increase in esterification time may be attributed to the fact that with the controlled reduced pressure during the esterification step, water of condensation evaporates easily without any remarkable formation of lactide or macrocyclic oligomers, rather forming linear polymers. The same type of trend was also observed by Chen et al., 2006. They have reported that with the increase of ES time from 3 to 7 h, the M_w was found to increase by 4 times.

4.2.2.4 Effect of MPC temperature on yield (wt. %) and M_w

Figs. 4.9 and 4.10 elucidates the effect of MPC temperature on yield (wt. %) and M_w, respectively.

From the above figures, following significant facts become perceptible:

1. It was observed from Fig. 4.9 that the yield (wt. %) of PLA decreases significantly with the increase in MPC temperature.
2. From Fig. 4.10, it is clear that the M_w also decreases sharply with the increase in MPC temperature.

The above facts can be explained as:

Degradation of PLA occurs with the increase in MPC temperature of the polycondensation reaction (Moon *et al.,* 2001), along with the formation of large amount of lactide and oligomers. And these by-products are washed away with methanol and thereby decrease the yield (wt. %) (Jamshidi *et al.,* 1988).

With the increase in MPC temperature, the PLA degrades into smaller oligomer as well as lactide and hence the decrease in M_w is observed. Significant loss of lactic acid occurs during the polycondensation reaction at high MPC temperature. Cyclic and linear oligomers are found to be formed at very high temperature of 190°C and above (Shyamroy, 2003). Amorphous PLA is obtained at and above 210°C. It was also observed that discoloration of the PLA occurs on increasing the MPC temperature beyond 200°C which may be because of charring taking place at high temperature (Zhang and Wang, 2008). The significant contribution of MPC temperature has also been established in the discussion in Section 4.2.1.1 and 4.2.1.2. At higher polymerization temperature intramolecular transesterification of the polymer chains occurs, thus leading to lower yield (wt. %) and lower molecular weight (Achmad *et al.* 2009).

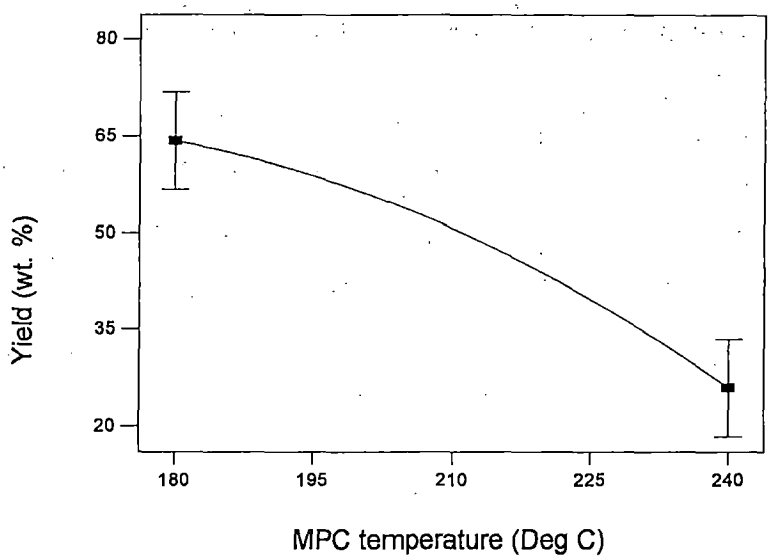

Fig. 4.9 Effect of MPC temperature on yield (wt. %) of PLA

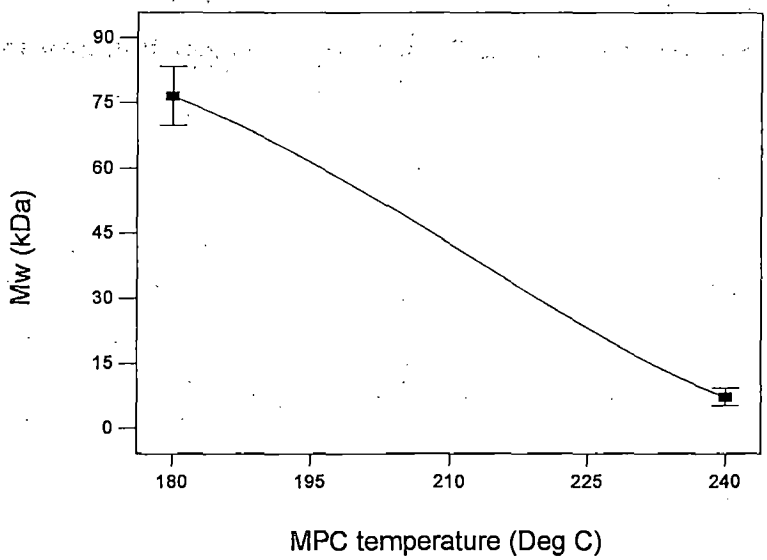

Fig. 4.10 Effect of MPC temperature on M_w of PLA

4.2.2.5 Effect of MPC time on yield (wt. %) and M_w

The effect of MPC time on yield (wt. %) and M_w of PLA are presented in Figs. 4.11 and 4.12, respectively.

From the above figures, following significant facts become noticeable:

1. Yield (wt. %) decreases remarkably with the increase in MPC time period.

2. The M_w of PLA is also observed to decrease significantly with the increase in MPC time.

The above facts may be explained as:

With the increase in the MPC time period of polycondensation reaction, beyond 10 hours, lactide formation and degradation of PLA process becomes prominent (Achmad *et al.*, 2009). It was also observed during experimentation that discoloration of the PLA occurs with prolonged MPC time period because of the carbonization of reactants (Zhang and Wang, 2008). The formation of oligomers also occurs on increasing the time period of MPC and thereby decreasing the yield (wt. %) (Jamshidi *et al.*, 1988). Because of the degradation of PLA molecule, M_w of PLA is also found to decrease (Moon et al., 2001). Further, polymerization for longer time period leads to intramolecular transesterification [back-biting transesterification] of the polymer chains, thus leading to lower yield (wt. %) and lower molecular weight (Achmad *et al.*, 2009). The significant contribution of MPC time has also been established in the discussion in Section 4.2.1.1 and 4.2.1.2.

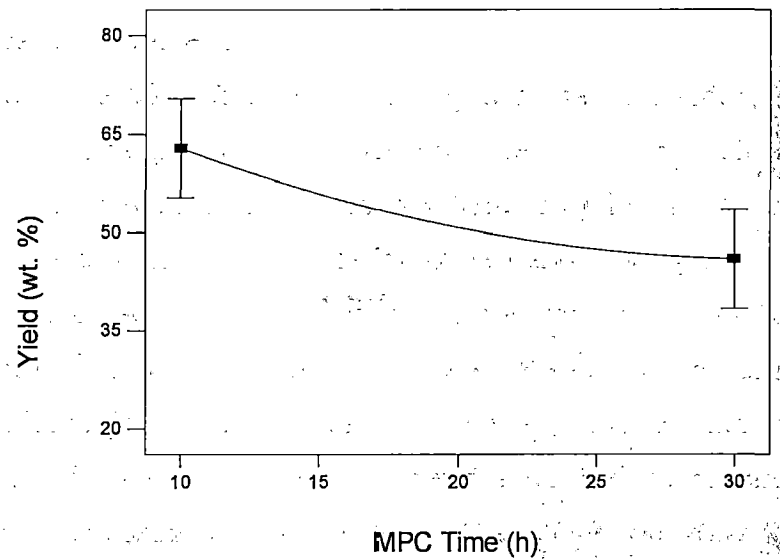

Fig. 4.11 Effect of MPC time on yield (wt. %) of PLA

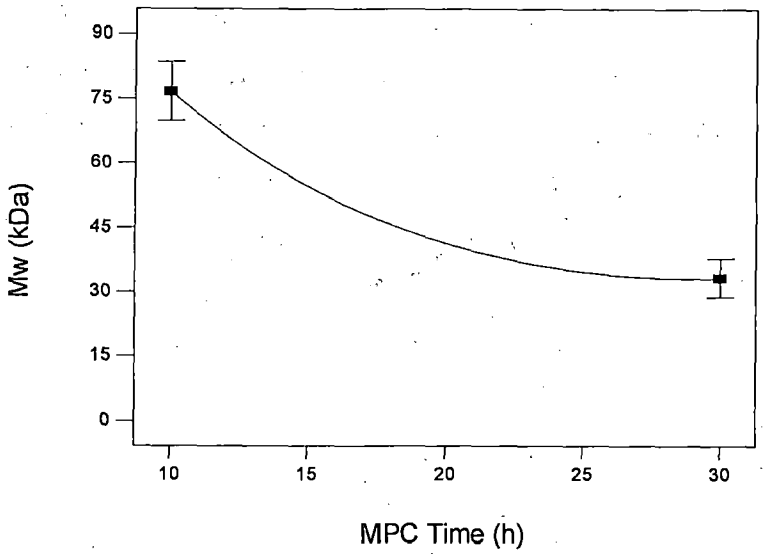

Fig. 4.12 Effect of MPC time on M_w of PLA

4.2.2.6 Effect of 2-parameter interactions on yield (wt. %)

Fig. 4.13 reports the 2-parameter interaction plots for yield (wt. %) of PLA, obtained from Minitab, for the different input parameters. Interaction is said to occur, when the effect of a particular parameter on the output parameter, behaves differently in the presence of another parameter. The 2-parameter interactions are shown inside the rectangular boxes numbered 1-10 in Fig. 4.13 and are given in Table 4.30. For example, the Box No.1, 2, 3 and 4 contains the effect of wt. % of catalyst, ES time, MPC temperature and MPC time, respectively, on yield (wt. %) at different levels of Amount of LLA. These rectangular boxes will be referred to as "Box No" in the discussion ahead.

Table 4.30 Two parameter interactions on yield (wt. %) and M_w of PLA

Box No.	2-parameter Interactions	Box No.	2-parameter Interactions
1	Amount of LLA and wt. % of catalyst	6	wt. % of catalyst and MPC temperature
2	Amount of LLA and ES time	7	wt. % of catalyst and MPC time
3	Amount of LLA and MPC temperature	8	ES time and MPC temperature
4	Amount of LLA and MPC time	9	ES time and MPC time
5	wt. % of catalyst and ES time	10	MPC temperature and MPC time

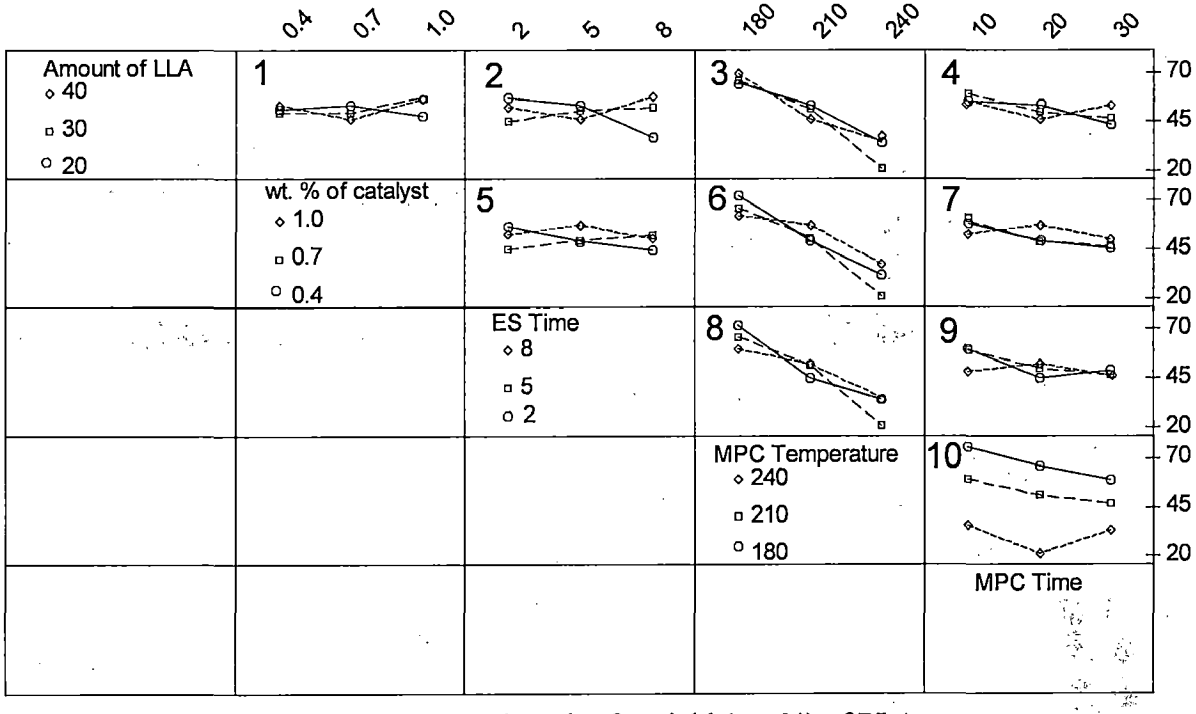

Fig. 4.13 Interaction plot for yield (wt. %) of PLA

From the above figure, the following fact emerged out:

1. All the input parameters were found to be involved in interactions within the range of parameters studied in the present investigation, though the extent of severity of interaction changes considerably.

The above fact can be explained as:

For the present case, interaction is said to occur between two parameters when one parameter affects the yield (wt. %) differently at different levels of the other parameter. This fact is obvious from the Fig. 4.13 as no two lines, in any of the Box. Nos., are parallel for two different levels of a parameter. From the discussion in Section 4.2.1.1, it can be stated that 2-parameter interaction between "wt. % of catalyst and MPC temperature" and "MPC temperature and MPC time", shown in box Nos.6 & 10, are almost equally significant. For example, if Box No. 10 is examined, it can be observed clearly that the change in yield (wt. %) is different when MPC time varies from 10 to 30 depending on the level of MPC temperature. The greater the lines depart from being parallel, the greater are the degrees of interaction. Thus, all the parameters should be considered for MPC reaction to study the proper regulation of various

parameters on the yield (wt. %). The order of magnitude of severity of 2-parameter interaction is calculated by using the formula given in Eq. 4.17, and is given in ascending order in Table 4.31.

$$Severity = \frac{F_i - F_{min}}{F_{max} - F_{min}} \quad \ldots (4.17)$$

Where, F_i = ith F-value; F_{min} = minimum F-value and F_{max} =maximum F-value.

Table 4.31 Order of severity of 2-parameter interactions for yield (wt. %) of PLA

2-parameter Interactions	Coefficient Actual	Coefficient Coded	p-value	F value	Order of severity (Ascending)
Amount of LLA and wt. % of catalyst	0.536782	1.610345	0.3503	0.970647	0.090
Amount of LLA and ES time	–0.0605	–1.81511	0.4726	0.562029	0.049
Amount of LLA and MPC temperature	0.001555	0.466595	0.7817	0.08149	0.00
Amount of LLA and MPC time	0.028478	2.847845	0.1154	3.035681	0.300
wt. % of catalyst and ES time	–5.15428	–4.63886	0.0876	3.670931	0.364
wt. % of catalyst and MPC temperature	0.572261	5.150345	0.0117	9.928786	0.999
wt. % of catalyst and MPC time	0.983032	2.949095	0.1047	3.255375	0.322
ES time and MPC temperature	–0.01242	–1.11761	0.6553	0.213075	0.013
ES time and MPC time	–0.14046	–4.21386	0.1158	3.029102	0.299
MPC temperature and MPC time	0.017176	5.152845	0.0117	9.938427	1.00

4.2.2.7 Effect of 2-parameter interactions on M_w

Fig. 4.14 presents the 2-parameter interaction plots, obtained from Minitab, for the different input parameters controlling M_w. The 2-parameter interactions are shown inside the rectangular boxes numbered 1-10 in Fig. 4.14 and are same as given in Table 4.30. For example, the Box No.1, 2, 3 and 4 contains the effect of wt. % of catalyst, ES time, MPC temperature and MPC time, respectively, on M_w at different levels of Amount of LLA. These rectangular boxes will be referred through "Box Nos." in the discussion ahead.

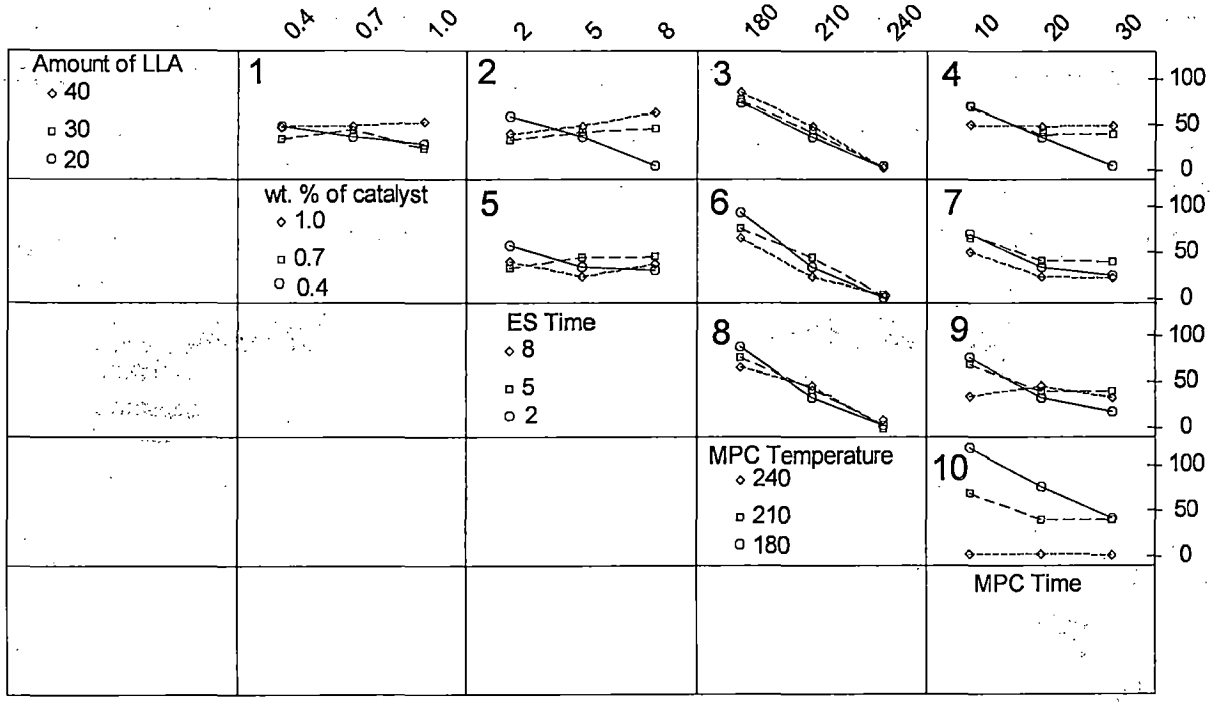

Fig. 4.14 Two-parameter interaction plot for M_w of PLA

From the above said figure, the following fact becomes apparent:

1. All the input parameters were found to be involved in interactions within the range of parameters studied in the present investigation, though the extent of severity of interaction changes considerably.

This fact can be described as:

In the present case, interaction is said to occur between two parameters when variation in M_w is found to be different w.r.t. a particular parameter, at different levels of the other parameter. This fact is obvious from the Fig. 4.14 as no two lines, in any of the Box. Nos., are parallel for two different levels of a parameter. For example, if Box No. 10 is examined, it can be observed that the recorded change in M_w is different, when MPC time varies from 10 to 30 h, for different levels of MPC temperature. From the Table 4.21, it is apparent that all the interactions are significant except the interactions between "Amount of LLA and ES time", "ES time and MPC temperature" and "ES time and MPC time". The significant interactions can also be visualized from the Box No. 1, 3, 4, 5, 6, 7 and 10 of the Fig. 4.14. Non-parallel plots in a given Box No. indicate higher degree of interaction. Among all these 2-parameter interactions, the order of interaction in ascending order is "ES time and MPC time"< "Amount of LLA and ES time"<

"ES time and MPC temperature"< "wt. % of catalyst and ES time"< "Amount of LLA and MPC temperature"< "Amount of LLA and wt. % of catalyst" <"wt. % of catalyst and MPC time" <"wt. % of catalyst and MPC temperature" <"MPC temperature and MPC time"< "Amount of LLA and MPC time". The order of magnitude of severity of 2-parameter interaction, calculated by using Eq. 4.17 of Section 4.2.2.6, in ascending order, is given in Table 4.32. Thus, all the five parameters, as given in Table 4.1, should be considered for MPC reaction to study the proper regulation of various parameters on the yield (wt. %) and M_w.

Table 4.32 Order of severity of 2-parameter interaction for M_w of PLA

2-parameter Interactions	Coefficient Actual	Coefficient Coded	p-value	F value	Order of severity (Ascending)
Amount of LLA and wt. % of catalyst	5.452972	16.35891	< 0.0001	46.54495	0.325
Amount of LLA and ES time	-0.12194	-3.65832	0.3299	1.060857	0.006
Amount of LLA and MPC temperature	0.041356	12.40666	0.0006	26.77156	0.186
Amount of LLA and MPC time	0.286503	28.65029	< 0.0001	142.765	1.00
wt. % of catalyst and ES time	-15.0229	-13.5206	0.0042	14.49053	0.100
wt. % of catalyst and MPC temperature	2.556463	23.00816	< 0.0001	92.072	0.644
wt. % of catalyst and MPC time	6.06043	18.18129	< 0.0001	57.49274	0.402
ES time and MPC temperature	-0.06638	-5.97407	0.1269	2.82901	0.018
ES time and MPC time	-0.05976	-1.79269	0.6259	0.254745	0.00
MPC temperature and MPC time	0.083023	24.90679	< 0.0001	107.8945	0.755

4.2.3 Characterization Studies of PLA Synthesized by MPC

In this section, the characterizations of PLA by different techniques such as GPC, FTIR, NMR, thermal study, XRD and FESEM are discussed. PLA samples of low M_w have low mechanical strength, and thus are of no use except their biomedical applications in drug formulation. Thus, in the present Section, complete characterizations of four PLA samples, PLA 1, PLA 2, PLA 3 and PLA 4, of higher M_w have been discussed in detail. The processing

conditions for these samples are given in Table 4.2. Among these four samples, the PLA sample taken as raw material for the SSP has also been considered. Characterizations of the two PLA samples taken for preparation of nanoparticles have also been included.

4.2.3.1 Molecular weight analysis

The weight average molecular weight (M_w), number average molecular weight (M_n) and molecular weight distribution (MWD) of PLA samples are determined from GPC analysis. MWD, also known as polydispersity index (PDI), is equal to the ratio of M_w and M_n. M_n can also be calculated from ^{13}C and ^{1}H NMR. But, the carboxylic acid end group could not be distinguished properly in ^{13}C NMR spectra. Thus, M_n could not be determined from it. The M_n is determined from the ^{1}H NMR spectra by computing the ratio of the area of peaks of methine/methyl hydrogen of the lactyl repeat unit to the methine/methyl peak of LA end group. But the M_n values obtained from GPC were found to be much higher than those obtained from NMR (Shyamroy *et al.*, 2005). Further, in case of present experiments, the degree of polymerization (DP) was found to be more than 200, whereas; the NMR spectrometer can be used to determine M_n for DP up to 100 only. This fact amply clears why better estimate of M_n could not be obtained even when a 500 MHz NMR spectrometer was used (Hatada *et al.*, 1990). Thus, NMR is not a powerful tool for high molecular weight determination when DP is more than 100. And hence, these data have not been discussed in the present thesis.

In GPC, the magnitude of the detector response is proportional to the amount of eluting sample. Thus, M_w and M_n can be calculated by calculating the area and molecular weight of each slice across the distribution. M_w and M_n can be calculated by using the Eq. 4.18:

$$\left.\begin{aligned} M_w &= \frac{\sum Area_i * MW_i}{\sum Area_i} \\ M_n &= \frac{\sum Area_i}{\sum Area_i / MW_i} \end{aligned}\right\} \quad \ldots. (4.18)$$

where: $Area(i)$ = Area of the ith slice.
$MW(i)$ = Molecular weight of the ith slice.

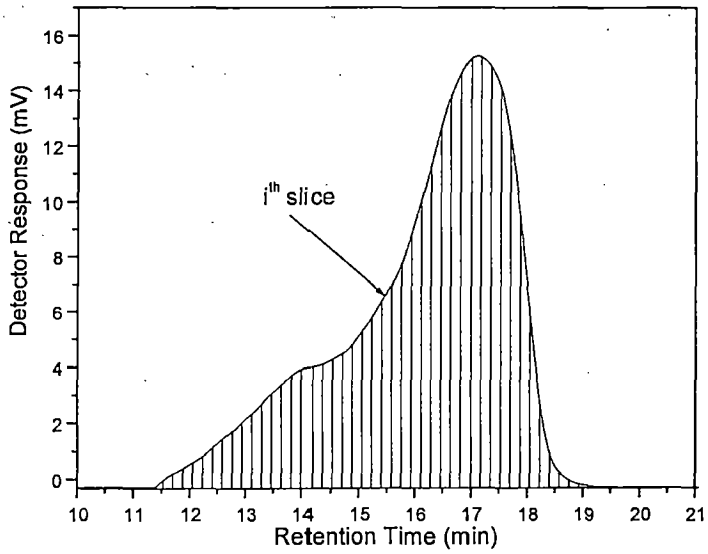

Fig. 4.15 Slices of PLA-2 sample for the calculation of M_w

The unimodal GPC chromatogram of the PLA oligomer, obtained after dehydration, is given in Fig. J.1 of Appendix J. The M_w of the oligomer was found to be ca. 13 kDa from GPC. And the GPC chromatograms of some of the PLA samples are also given in Appendix J. The bimodal GPC curve shown for the PLA sample obtained from Run No. 4, (Fig. J.2 of Appendix J) is due to the presence of low molecular weight oligomer in association with high molecular weight PLA (Chen *et al.*, 2006). This bimodal distribution of GPC is caused due to living polycondensation reaction occurring during the melt polycondensation process. In living polycondensation, first a small molecular weight fragment is formed and the small molecular weight fragments react further to give high molecular weight fragment. Bimodal GPC chromatograms might also be obtained due to transesterification reaction occurring during polycondensation which becomes prevalent at higher catalyst percent, leading to a range of different molecular weight product which further leads to a bimodal GPC chromatogram (McCleverty and Meyer; 2005). Transesterification reactions proceed via the attacking of oxygen of the hydroxyl end group of one chain at the carbons of the carbonyl group of another chain. The PDI values of the PLAs were found to vary from 1.2 to 2 as expected in case of the polymers synthesized by polycondensation method (Collins *et al.*, 1973). The molecular weight and PDI data of the four samples, to be discussed in this section, are presented in Table 4.33. The M_w, M_n and PDI of all PLA samples are given in Table J.1 of Appendix J.

Table 4.33 Molecular weight analysis using GPC

Polymer		Run No.	M_w kDa	M_n kDa	M_w/M_n	DP
PLA-1		5	55.634	26.759	2.079	372
PLA-2		23	75.929	50.096	1.516	696
PLA-3	(Peak 1)	4	98.470	82.295	1.197	1143
	(Peak 2)		24.438	21.373	1.143	297
	(Average)		51.729	29.262	1.768	406
PLA-4		11	178.857	90.531	1.976	1257

In case of bimodal GPC curves, the area under the peak corresponding to the low molecular weight fragment is higher than 10 %, and thus, the weighted average molecular weight of both the peaks is considered while proceeding for the analysis of experiments by DOE. Polymers having a bimodal molecular weight distribution have useful properties. The high molecular weight species in the bimodal distribution imparts higher melt strength properties to the polymer and the lower molecular weight species imparts improved processing and melt flow properties to the polymer (White, Donald A. (Keasbey, NJ); US Patent 5578682; 1996).

4.2.3.2 Structure and end-group analysis

The structure and end-group analysis of PLA has been carried out by using FTIR and NMR spectroscopy. However, although the presence of end group and residual lactide can be determined from FTIR, the quantification of end group and lactide is carried out by NMR technique. The residual lactide is formed by the unzipping of chain ends (Hiltunen *et al.,* 1997).

FTIR analysis

FTIR spectra of PLA samples, PLA 1 - PLA 4, are shown in Fig. 4.16. The FTIR spectrum of all PLA samples exhibits characteristic ester absorption peaks at ~1760 cm^{-1} for the stretching vibration of the –COO- and at ~1090, ~1131, and ~1185 cm^{-1} for the stretching vibration of the C-O-C of ester group. The other characteristic absorption peaks of PLA correspond to the C-H, CH_3 and the O-H at ~2997, ~1145, and ~3440 cm^{-1}, respectively (Teng *et al.,* 2004). The FTIR spectral interpretation for PLA is reported in Table 4.34.

Table 4.34 Characteristic FTIR bands of PLA

Wavelength (cm^{-1})	Assignment	Ref.
Primary Aliphatic Alcohol		
3900-3300	O-H stretching	Teng *et al.*, 2004; Zhang and Wang, 2008
1250-900	C-O stretching	Teng *et al.*, 2004; Zhang and Wang, 2008
Aliphatic Esters		
1800-1700	C=O of ester group	Zhang and Wang, 2008
~1090, ~1131, ~1185	C-O-C of ester	Zhang and Wang, 2008
Aliphatic Carboxylic Acids		
~1243	O-H bending	Teng *et al.*, 2004; Zhang and Wang, 2008
~1760	C=O	Achmad *et al.* 2009
Aliphatic Hydrocarbons		
~1145	$-CH_3$	Teng *et al.*, 2004
2850-3050	C-H stretching of $-CH_3$	Teng *et al.*, 2004
1445-1325	C-H bending and wagging	Teng *et al.*, 2004; Zhang and Wang, 2008

During polycondensation, the polymer may undergo thermal degradation via two routes. One of the routes is cyclization leading to formation of lactide, and the other is formation of vinyl end group (CH_2=C-) by random scission. Thus, FTIR spectrum of PLA should exhibit a peak at 1550 cm^{-1} indicating the presence of vinyl end group. But it is not observed in the FTIR spectrum of PLA samples as can be evidenced from the dotted vertical line at 1550 cm^{-1} in Fig. 4.16. Thus, it is confirmed that formation of vinyl end group did not occur during the polycondensation process. Further, it can be seen that the absorption at 935 cm^{-1} is observed due to the presence of lactide monomer. This band is assigned to the COO ring breathing mode (Braun *et al.* 2006).

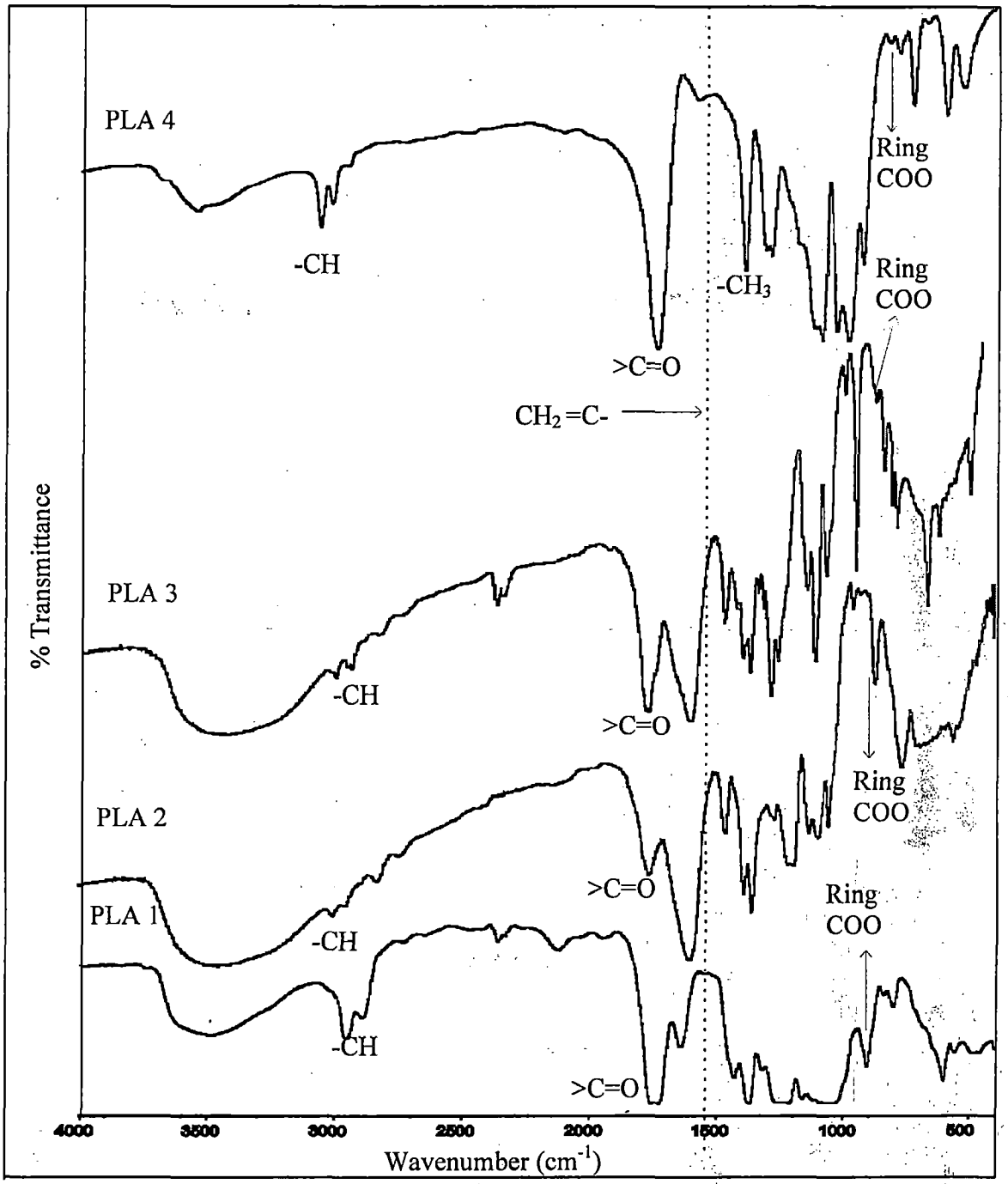

Fig. 4.16 FTIR spectra of PLA samples obtained by MPC

^{1}H NMR analysis

The ^{1}H NMR spectra of PLA 1 - 4 are visualized in Fig. 4.17 A-D. From these figures, it can be seen that all the PLAs produced almost same kind of spectral pattern consisting of mainly

three peaks corresponding to the presence of three different kinds of hydrogen atoms in the PLA solution.

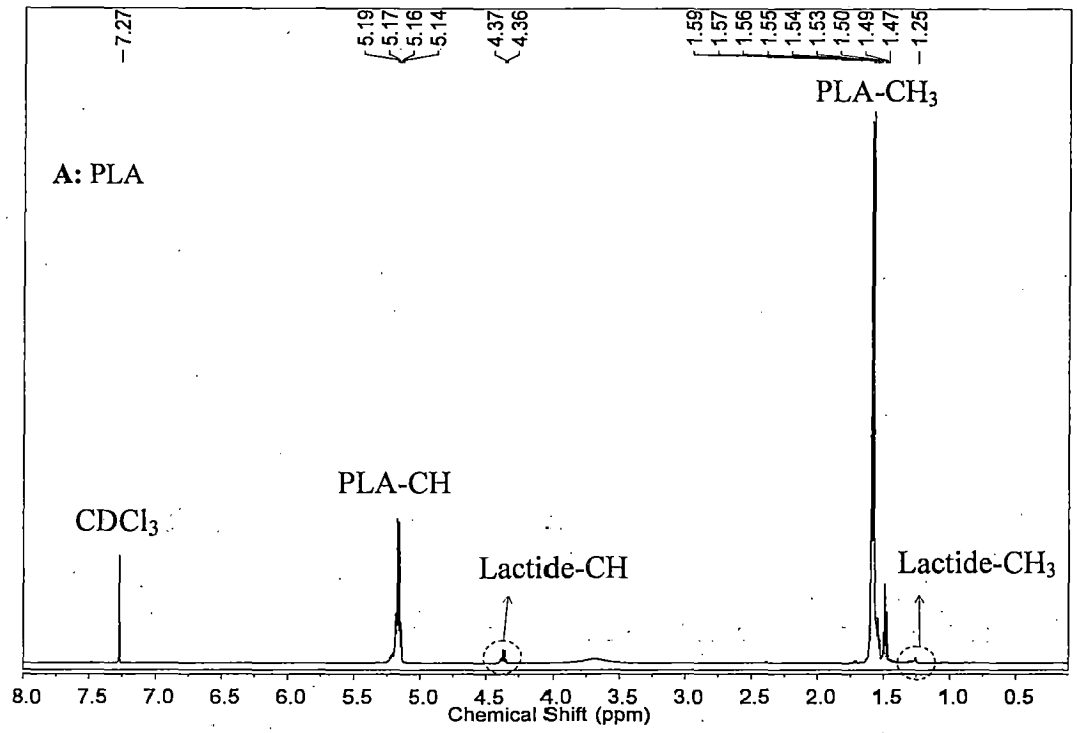

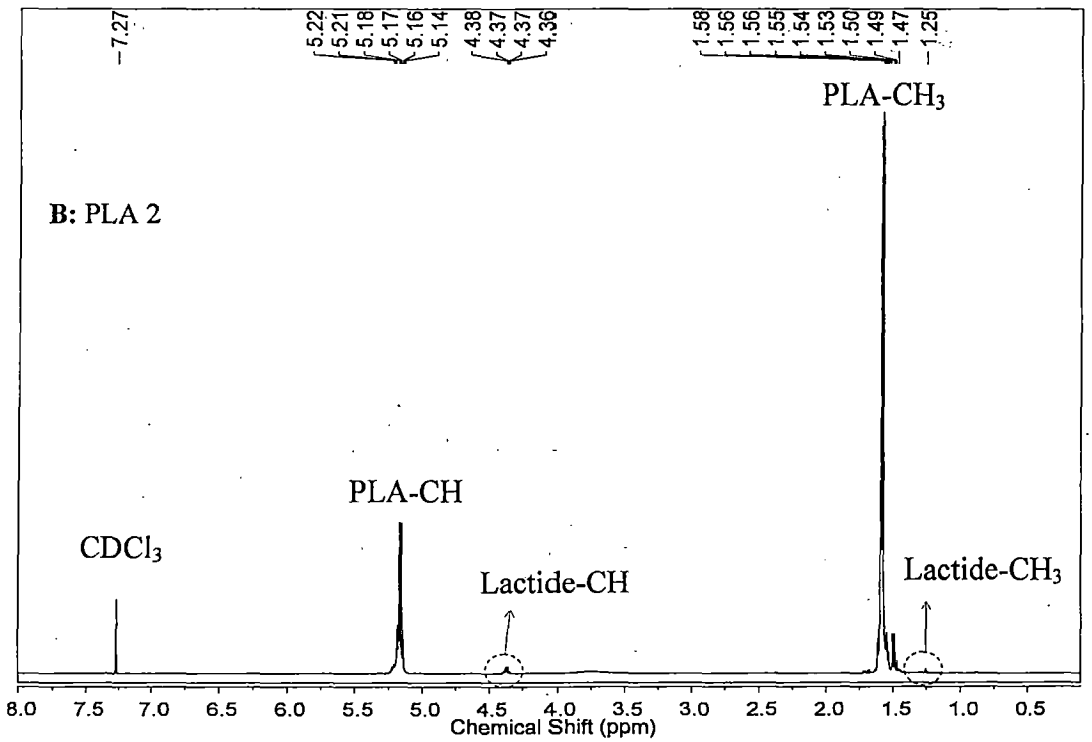

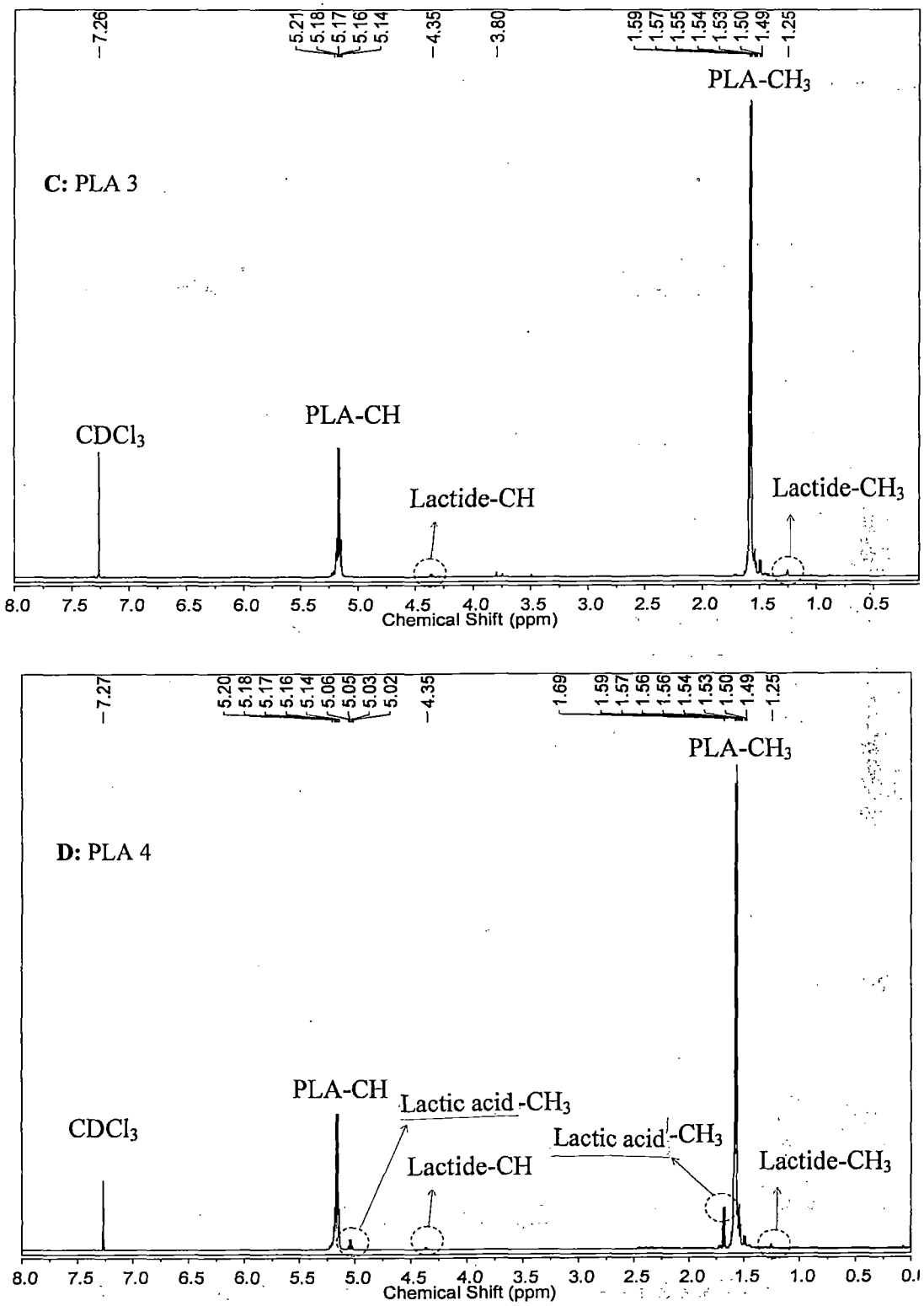

Fig. 4.17 ^{1}H NMR spectra of PLA

The three peaks are observed around chemical shift, δ (ppm, $CDCl_3$) 7.25 (s-singlet), 5.15-4.95 (q-quartet, 1H) and 1.60-1.45 (d-doublet, 3H), in the ^1H NMR spectrum of PLA. The peak at around 7.25 ppm is due to the solvent ($CDCl_3$) in which PLA was dissolved (Appendix F). The other two peaks around 5 ppm and 1.5 ppm are due to the methine (–CH) and methyl (–CH_3) groups of PLA, respectively (Ahmed *et al.,* 2009). The peaks corresponding to the acid and hydroxyl hydrogen atoms of –COOH and –OH of PLA are not observed. This is due to the fact that these hydrogen atoms produce very weak signals which are also not even observed for lactic acid (Appendix A). The peaks for hydrogen of methine or methyl group of lactide are also observed near the corresponding peak for PLA, but its intensity is very low to be perfectly noticeable, as can be seen from Fig. 4.17. This is due to presence of very small amount of lactide in PLA. The hydrogen of methine or methyl group for lactic acid produce very low intensity peaks (see Fig. 4.17 D) near the corresponding peak for PLA (Chisolm *et al.,* 2008) due to the presence of small amount of lactic acid in the PLA. In NMR, satellite peaks are also observed due to the presence of impurity in solvent and the sample, which should not be confused with the peaks originated from the main compound.

The resultant peaks obtained after applying resolution enhancement technique to the methyl and methine peaks are given in Fig. 4.18 (a-d) and Fig. 4.19 (a-d), respectively. From these figures, it can be seen that a doublet peak is observed for the methyl groups as these protons couple with the single methine proton, whereas; a quartet is observed for the methine groups as these protons couple with three equivalent protons of the methyl group of the lactic acid repeat unit. This is in agreement with the n+1 rule of peak splitting in NMR spectroscopy. From the ^1H NMR spectra shown in Fig. 4.18 (a-d) and Fig.4.19 (a-d), a number of very low intensity peaks to the left and right of the main quartet and doublet peak are observed. These peaks are due to stereodefect present in PLA polymer chain (Thakur *et al.,* 1997). The largest peak is due to pure L-isomer content and the small peaks are due to presence of D-units incorporated randomly in between the L-units and thereby creating stereodefects. Thus, it can be manifested that the PLA obtained is predominantly isotactic (Chabot *et al.,* 1983). From ^1H NMR spectra of PLA it is also seen that they do not show any significant peaks corresponding to the CH_3 and CH peak of LA. This is due to the fact that after dissolving, precipitating and

filtering, the un-reacted monomer gets removed from the PLA. However, in PLA 4, the small amount of LA is due to the fact that some amount of PLA gets trapped inside the pores of PLA.

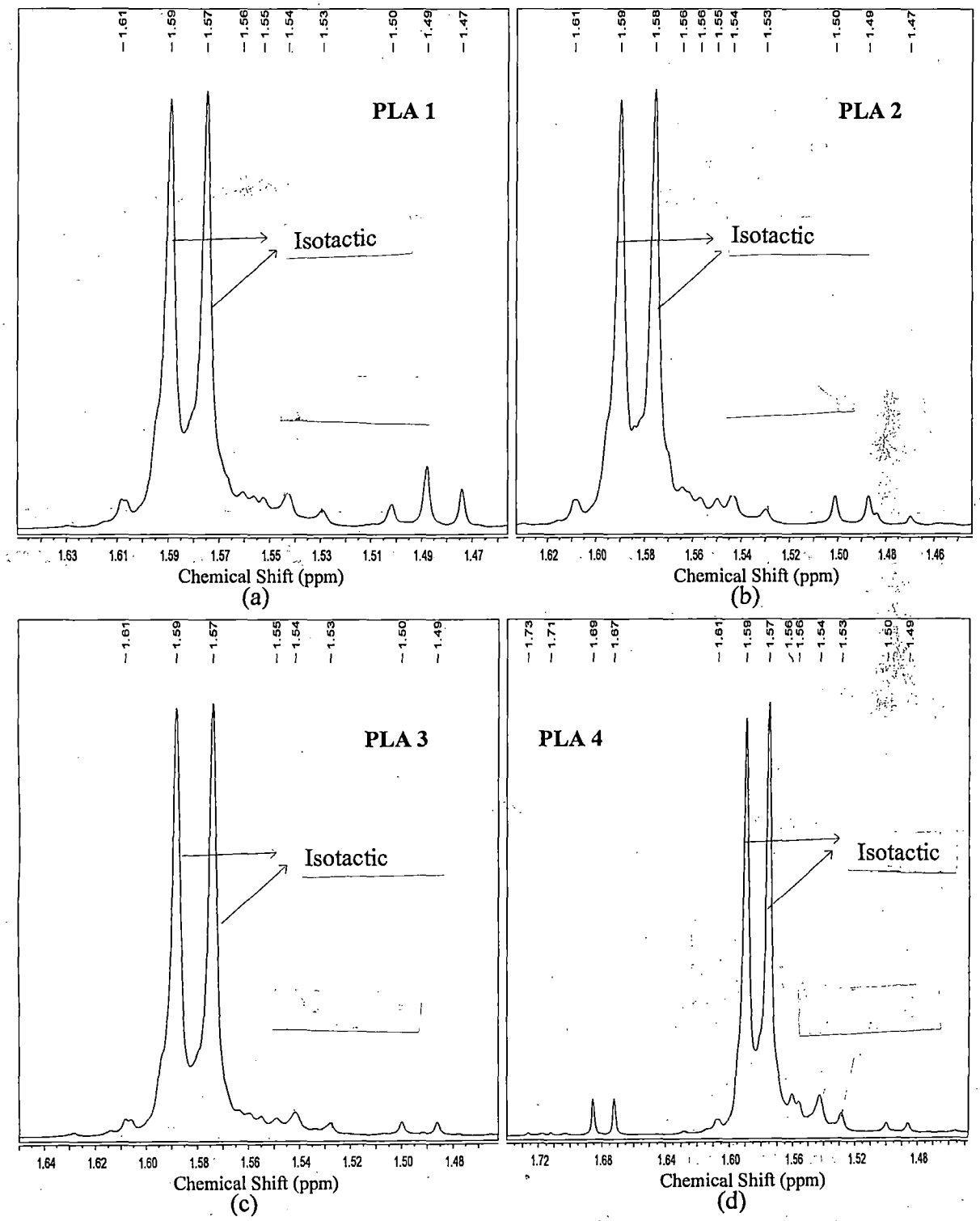

Fig. 4.18 Splitting pattern of methyl peak in ^{1}H NMR spectra of PLA

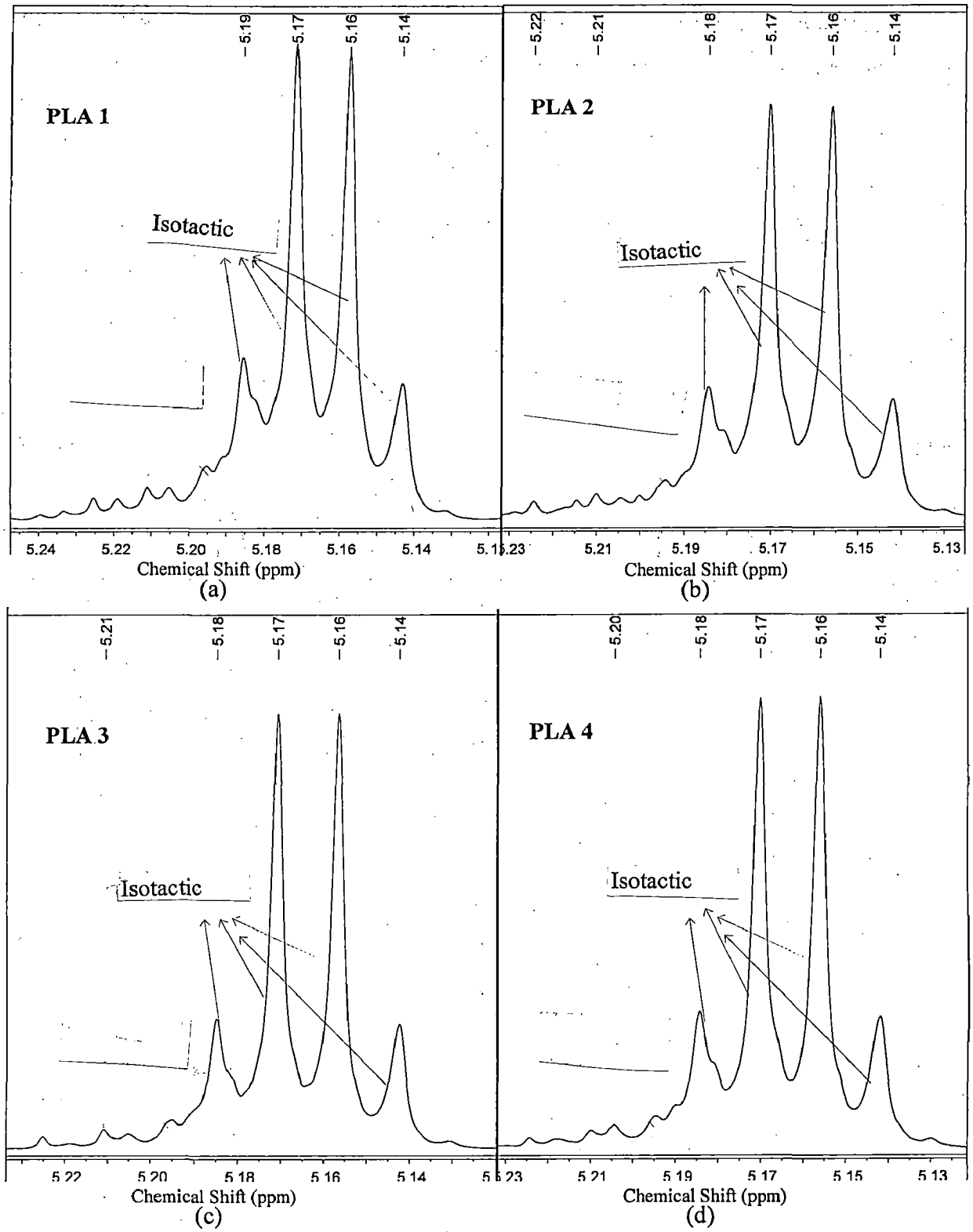

Fig. 4.19 Splitting pattern of methine peak in ^{1}H NMR spectra of PLA

Resolution enhancement technique was applied to the small peak around 4.3-4.4 ppm and is shown in Fig. 4.20 (a-d). This peak corresponds to the –CH proton of lactide, a doublet of quartet, which is due to coupling of one –CH proton first with adjacent $–CH_3$ and thus resulting in a quartet which in turn couples with the other –CH proton of the same lactide unit and thus, creating a doublet of quartet. Thus, from these figures, the presence of residual lactide in PLA is confirmed. The amount of residual lactide present in PLA is determined from the ratio of area under this peak and the area under the methine peak for lactyl repeat unit of PLA. The percentage of residual lactide of different PLA samples are calculated using the Eq. 4.19, and are given in Table 4.35.

$$\text{Wt \% of lactide} = [I_{lactide}/(I_{lactide}+I_{PLA})] * 100 \quad \ldots. (4.19)$$

Where, $I_{lactide}$ and I_{PLA} represent the integrals of the –CH signal due to lactide and PLA, respectively.

Table 4.35 Amount of lactide in PLA

Polymer	Residual lactide (%) (^{1}H NMR)
PLA 1	7.59
PLA 2	4.72
PLA 3	2.35
PLA 4	1.37

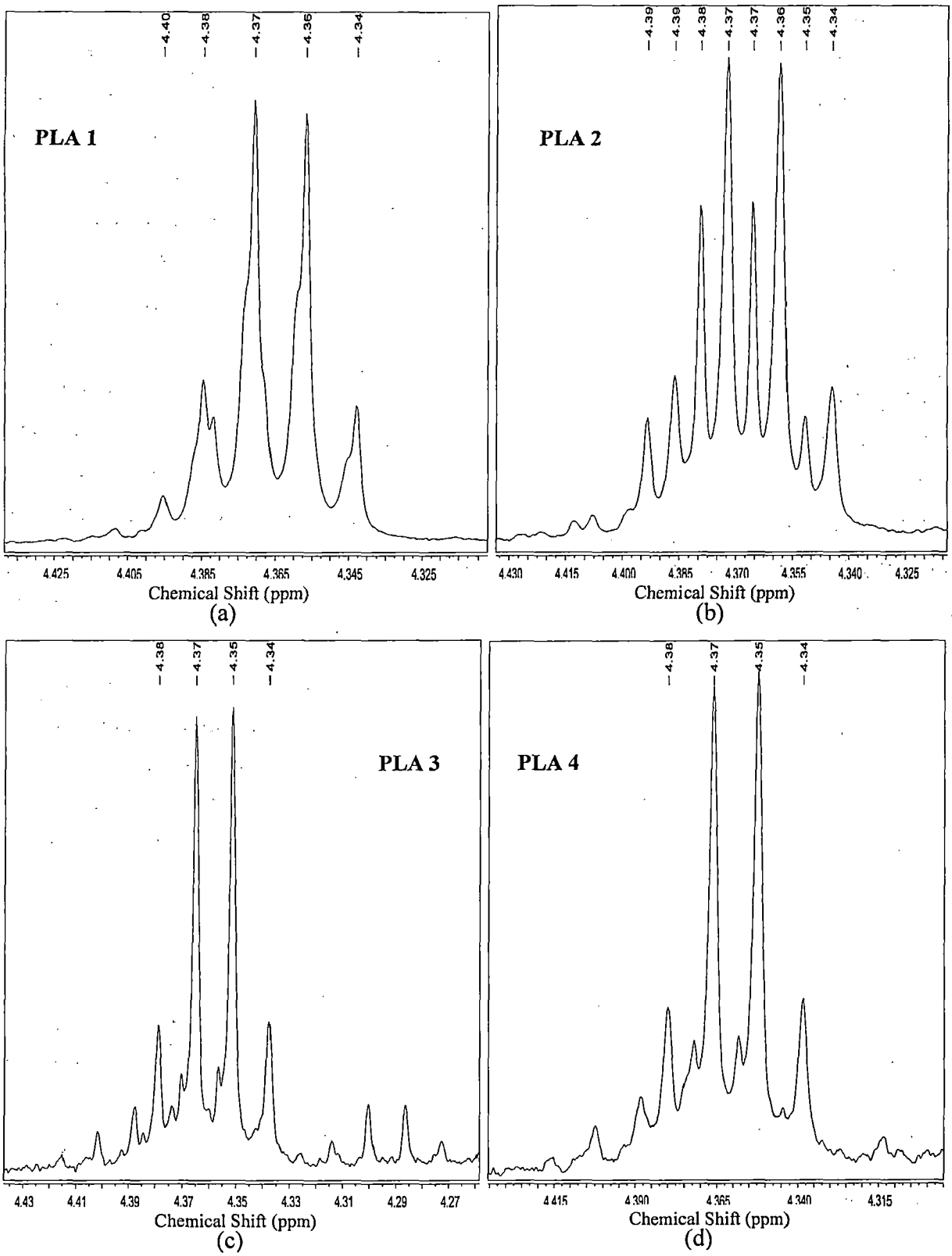

Fig. 4.20 Splitting pattern of eng group methine in ^{1}H NMR spectra of PLA

^{13}C NMR analysis

The ^{13}C NMR spectra of PLA 1 - 4 are visualized in Fig. 4.21 A-D. From these figures, it can be seen that all the PLAs produced almost same kind of spectral pattern consisting of mainly four peaks corresponding to the presence of four different kinds of carbon atoms in the PLA solution. The four peaks around chemical shift, δ (ppm, $CDCl_3$) 169, 76, 69 and 16 ppm are observed due to the ester, solvent, -CH and $-CH_3$ groups, respectively. These values match well with the reported values by many investigators (Moon *et al.,* 2000, 2001; Chen *et al.,* 2006). In the Fig. 4.21 A and B, the peaks around 66 and 20 ppm are due to the methine and methyl group, respectively, of residual lactide present in PLA. However, no residual lactide could be observed from the ^{13}C NMR for the PLA 3 and PLA 4. The peaks at downfield region to ester group corresponding to the acid end group do not appear in the ^{13}C NMR spectra. This may be due to the fact that the number of end groups present in the polymer is very small and is below the detectable limit. From ^{13}C NMR spectra of PLA it is also seen that they do not show any significant peaks corresponding to the CH_3 and CH peak of the monomer. This is due to the fact that after dissolving, precipitating and filtering the un-reacted monomer gets removed from the PLA.

The attempt to detect the fine structure arising from the stereosensitivity in the methyl and methine peaks could not be observed in ^{13}C NMR spectra even after the application of resolution enhancement technique. These peaks could not be well resolved because of high noise. However, application of resolution enhancement technique to the ester group, resolves the fine structure of the PLA as represented in Fig. 4.22 (a-d). The pattern of ester region is composed of several peaks whose respective intensities depended on the nature and enantiomeric composition of PLA (Thakur *et al.,* 1997). A number of very low intensity peaks to the right of the main peak are observed. These peaks are due to stereodefect present in PLA polymer chain. The unique largest peak in down field region is due to the presence of isotactic unit. The small peaks in the up field region are due to presence of D-units incorporated randomly in between the L-units and thereby creating stereodefects. These small peaks are due to heterotactic and syndiotactic triads. Thus, it can be manifested that the PLA obtained is predominantly isotactic (Chabot *et al.,* 1983).

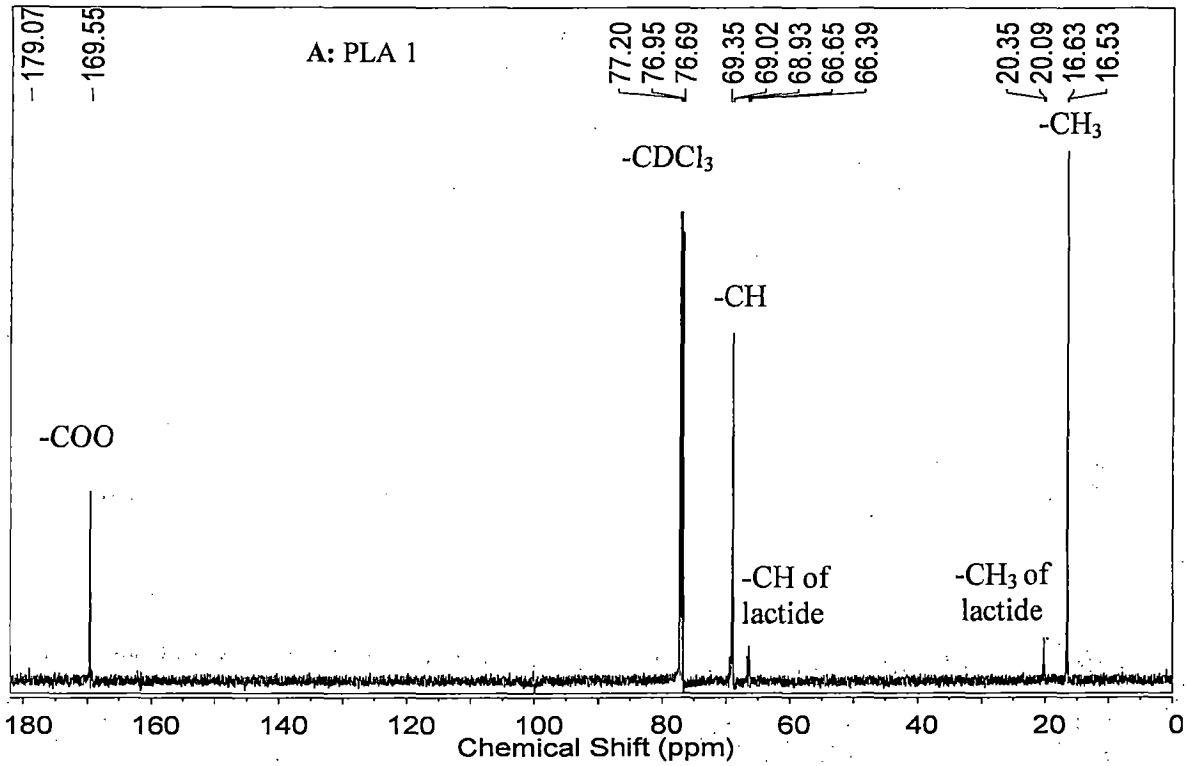
A: PLA 1
179.07
169.55
77.20
76.95
76.69
69.35
69.02
68.93
66.65
66.39
20.35
20.09
16.63
16.53
-CH3
-CDCl3
-CH
-COO
-CH of lactide
-CH3 of lactide
180
160
140
120
100
80
60
40
20
0
Chemical Shift (ppm)

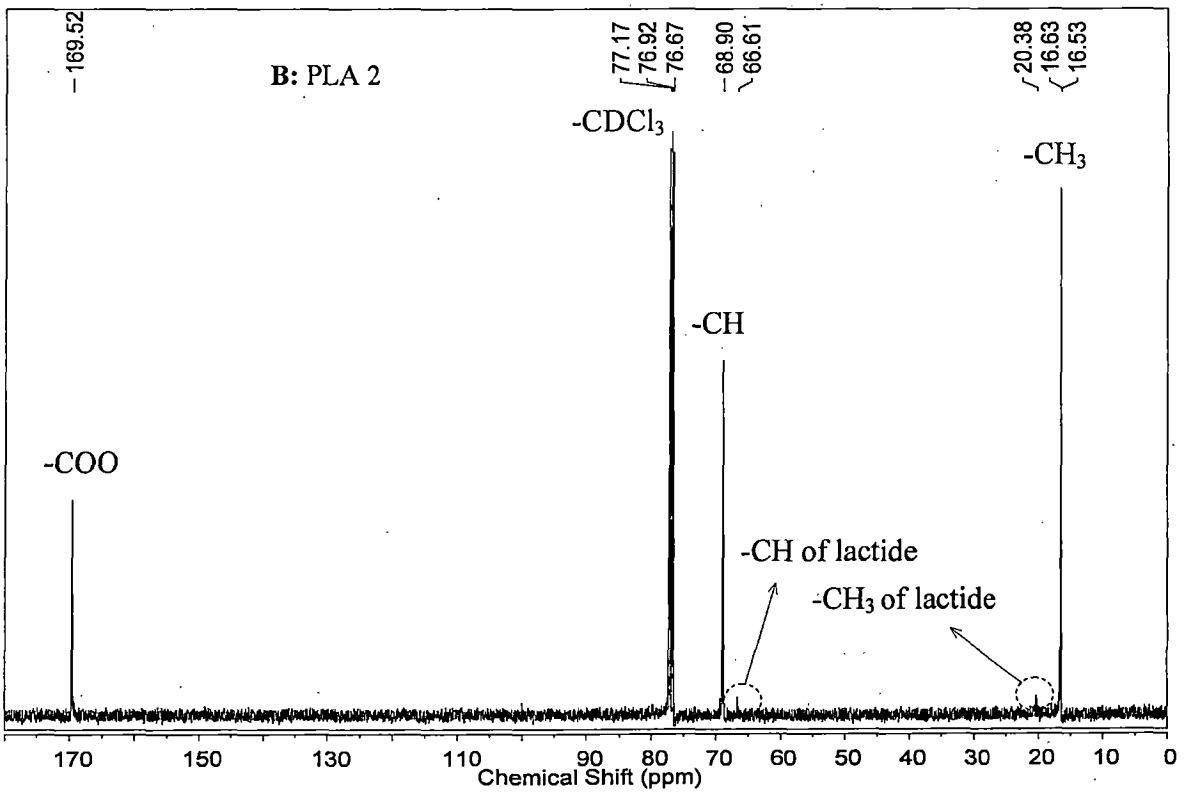
B: PLA 2
169.52
77.17
76.92
76.67
68.90
66.61
20.38
16.63
16.53
-CDCl3
-CH3
-CH
-COO
-CH of lactide
-CH3 of lactide
170
150
130
110
90
80
70
60
50
40
30
20
10
0
Chemical Shift (ppm)

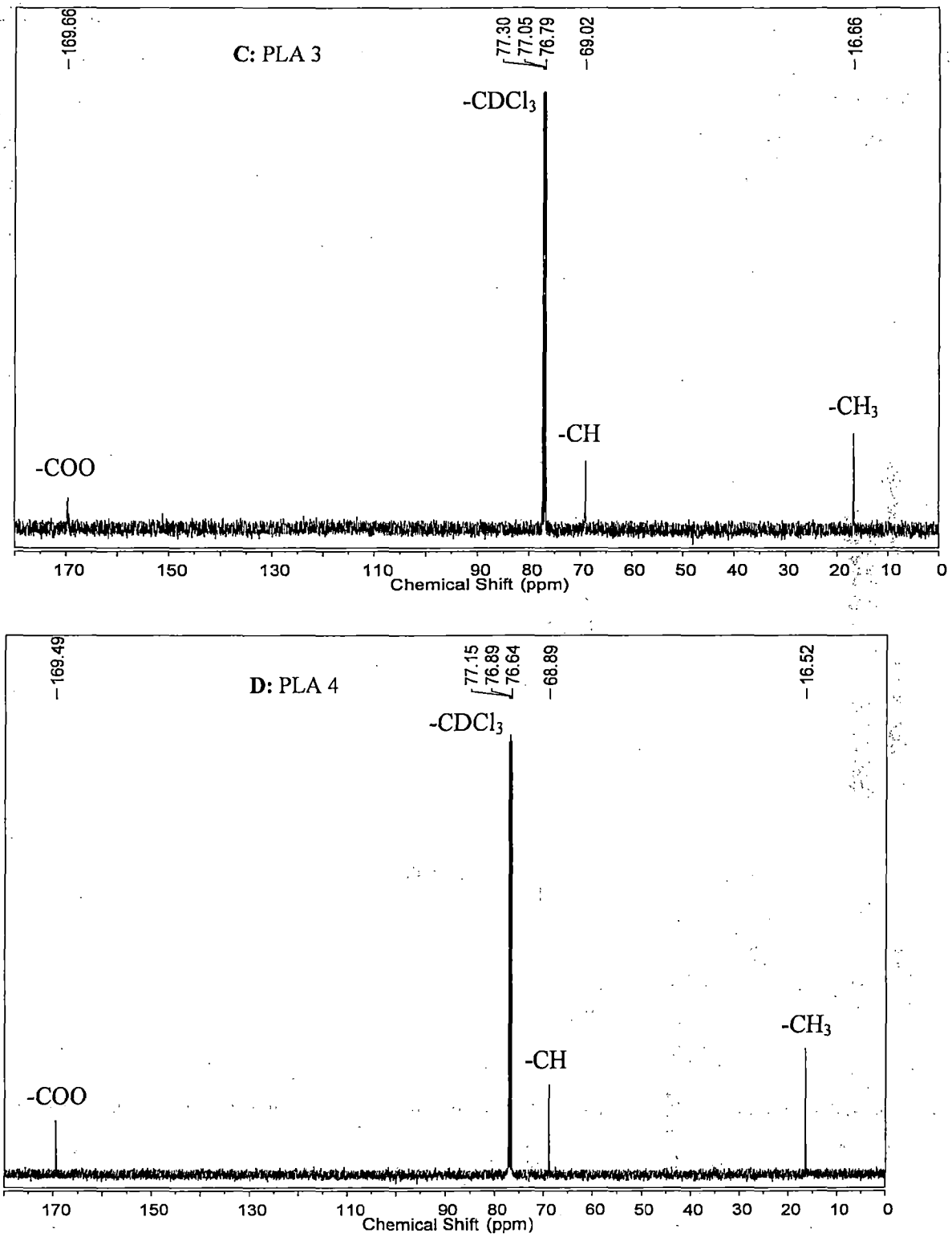

Fig. 4.21 ^{13}C NMR spectra of PLA

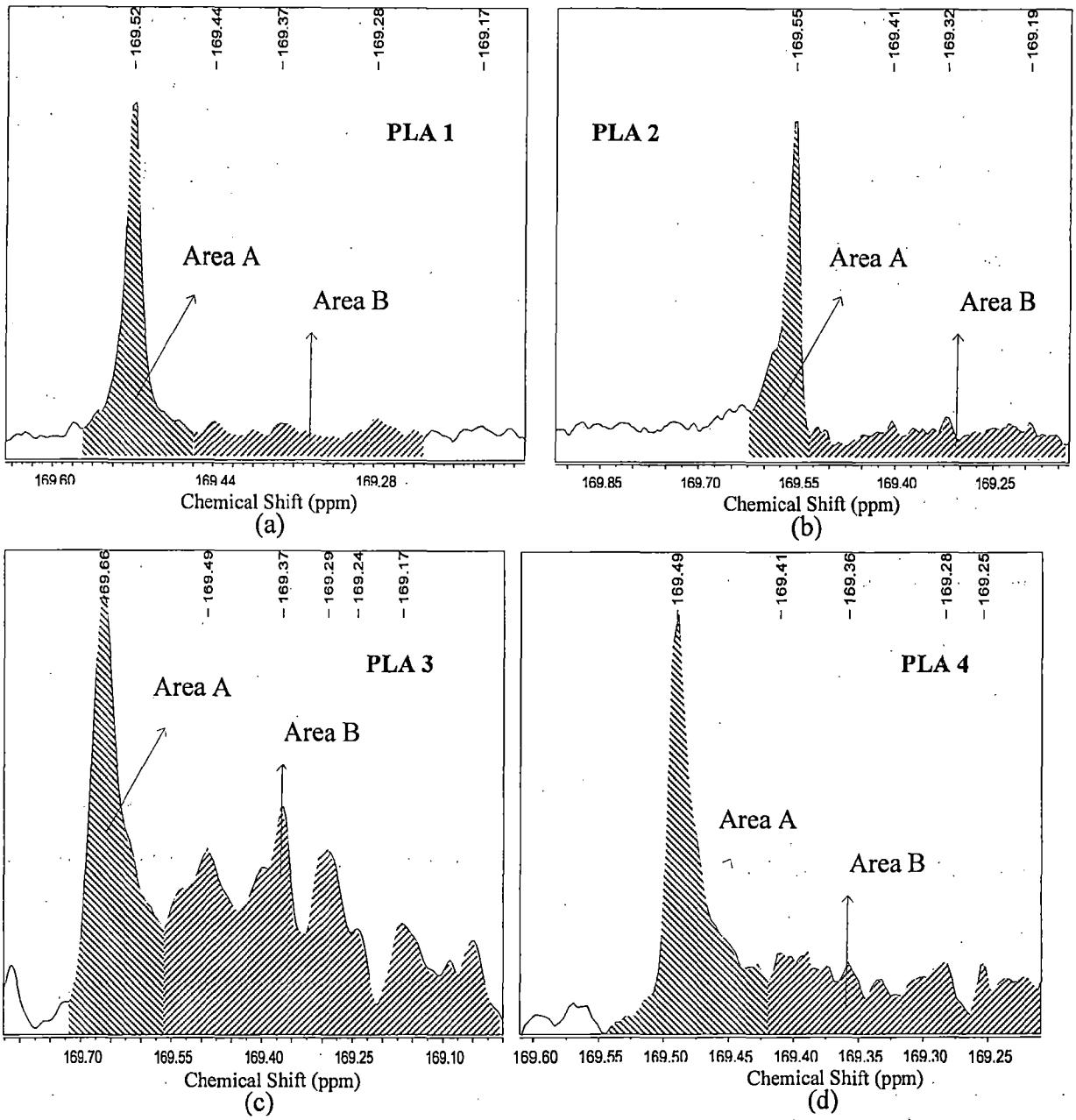

Fig. 4.22 Resolution enhanced ester peak of PLA in ^{13}C NMR

The identification and quantification of end groups is necessary and is important to ascertain the suitability of the PLA for any post-polymerization process, such as chain extension, solid-state polymerization and coupling reactions. The identification of end groups of PLA, using ^{13}C NMR spectroscopy, prepared by MPC has been reported by very few

investigators (Shyamroy, 2003; Shyamroy *et al.,* 2005). Thus, an attempt was made in the present investigation to determine the end groups of PLA by ^{13}C NMR spectroscopy.

In the ^{13}C NMR spectra of PLA 1 sample, a small peak around 179 ppm is observed due to the carboxylic acid end functional group. However, no carboxylic acid end group could be observed for the PLA 2, PLA 2 and PLA 3 samples. This may be due to high noise in ^{13}C NMR spectrum. This may also be due to the fact that the number of end groups in PLA is very small for high molecular weight polymers (Shyamroy, 2003; Shyamroy *et al.,* 2005, Thakur *et al.,* 1997) and is below detectable limit.

Thus, from the above discussion, it can be now safely concluded that the structure of PLA is confirmed from both the FTIR and NMR analysis. The acid end-group present in PLA is confirmed from the ^{13}C NMR spectra.

4.2.3.3 Racemization analysis

The extent of racemization is generally examined using ^{13}C NMR. The high resolution ester peak shown in Fig. 4.22 (a-d) produced a number of small peaks in addition to one large peak. Presence of these small peaks is due to presence of D-isomeric units which originate because of racemization occurring during polymerization reaction (Thakur *et al.,* 1997). According to the theoretical stereosequence distribution, the downfield signal around 169.5 ppm (isotactic (i,mm) in ^{13}C NMR is assigned to the sequence of carbonyl carbon atom containing successive LLA units. The peaks in the upfield region at around 169.3 ppm are assigned to the heterotactic (h, rm) units. And the peaks around 169.2 ppm is assigned to the syndiotactic (s, rr) units present in PLA (Shyamroy, 2003; Chabot *et al.,* 1983; Thakur *et al.,* 1997). From the ratio of area of these peaks, extent of DLA units in the PLA backbone is determined by using Eq. 4.20 A. The %age of D-isomer are found to be 6.52%, 19.05%, 58.76% and 24.45%, for PLA 1, PLA 2, PLA 3 and PLA 4, respectively, and are also given in Table 4.36. However, ^{13}C NMR spectra of PLA samples showed significantly higher level of noise which made the proper quantification somewhat difficult.

% D-isomer = $[I_D/(I_D+I_L)] * 100$ OR %D-isomer = [Area B/(Area A+ Area B)]*100 ... (4.20 A)

Where, I_D & I_L are integral of peaks for D-isomer (Area B) and L-isomer (Area A), respectively.

Further, the stereo crystallization ratio (Sc ratio) can be determined from XRD pattern described in Section 4.2.3.5, by using the Eq. 4.20 B and are given in Table 4.36.

Sc ratio (%) = $(\sum I_{sc} / \sum I_{sc} + I_{HM})*100$ ... (4.20 B)

Where, $I_{sc(i=1 \text{ to } 3)} = I_{sc1} + I_{sc2} + I_{sc3}$, I_{sc} is the integral of peaks around 2θ of 12°, 20.7° and 24° and I_{HM} is the integral of peak derived from a homocrystal which appeared around 2θ =16.50°.

The racemization reactions are most likely due to a dynamic equilibrium of ester interchange reactions occurring between the polymer chains. In the case of the MPC reaction, the D-lactic acid units seemed to be incorporated into the backbone in a purely random manner. Randomization of the stereosequences is observed because of the intensive transesterification (Kim and Woo, 2002; Shyamroy, 2003). During the ester interchange reactions, there are two ways in which the ester linkages between successive lactic acid units can cleave and reform. One is acyl–oxygen cleavage, which does not involve the chiral carbon of lactic acid repeat unit. The other is alkyl–oxygen cleavage, in which the covalent bond between oxygen and the chiral carbon breaks and subsequently reforms. This results in an inversion of the configuration and hence leads to racemization.

4.2.3.4 Thermal characterization

TGA, DTG and DSC thermograms of PLA samples are represented in the Figs. 4.23, 4.24 and 4.25, respectively and the original figures are given in Figs. J.25 –J.28 of Appendix J. Four important thermal characteristics of PLAs, namely, glass transition temperature (T_g), crystallization temperature (T_c), melting temperature (T_m), and degradation temperature (T_d) have been measured from TGA, DTG and DSC thermograms and are discussed in this section. The results of the thermal characterization are summarized in Table 4.36.

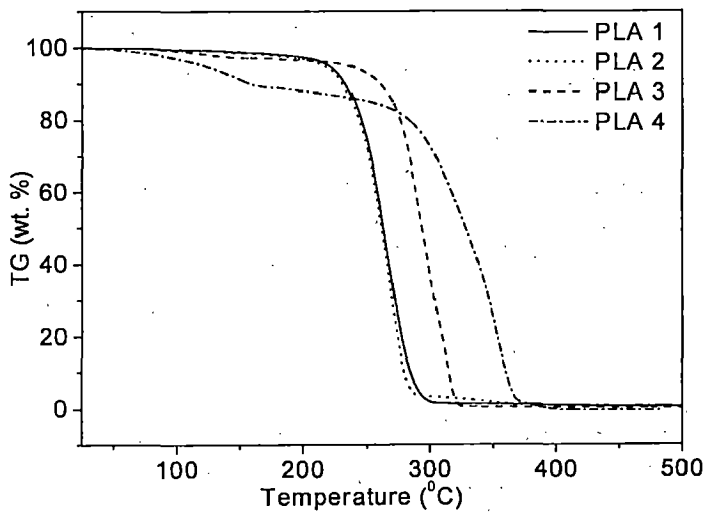

Fig. 4.23 TG thermograms for PLA

Thermal degradation of the polymers was investigated by thermogravimetric analysis (TGA). Thus, from Fig. 4.23, it can be concluded that the PLA 1, PLA 2 and PLA 3 samples are thermally stable up to a temperature of 200°C, whereas; PLA 4 is found to be stable up to 250°C. This may be attributed to the high molecular weight of PLA 4.

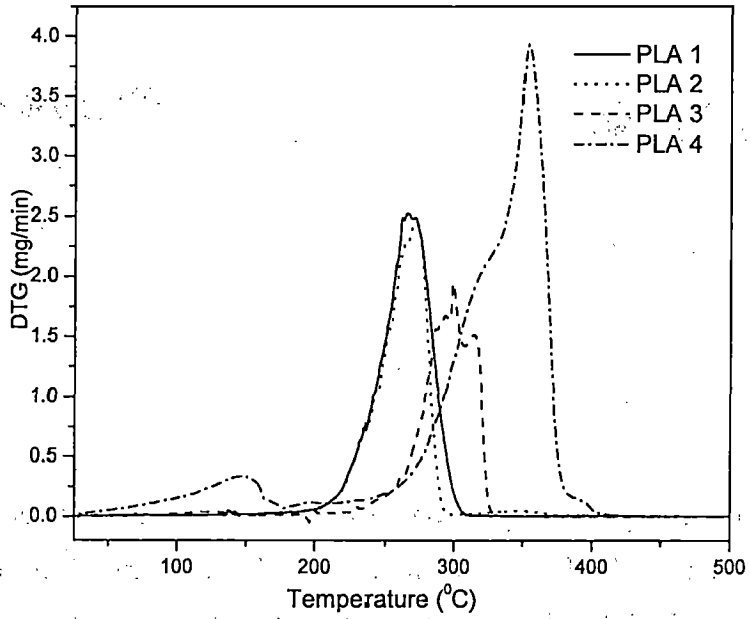

Fig. 4.24 DTG thermograms for PLA

The values of decomposition temperature, T_d, is determined from the DTG thermograms shown in Fig. 4.24 and are given in Table 4.36. It is also seen from the DTG thermograms that T_d increases with the increase in molecular weight of PLA from PLA 1 to PLA 4. The T_g, T_c and T_m are determined from the DSC thermograms shown in Fig. 4.25 and are summarized in Table 4.36. T_g for PLA 3 and PLA 4 could not be well identified. T_g of PLA was found to increase with the increase in molecular weight (Jamshidi *et al.,* 1988) as can be clear from the Table 4.36. The T_m of the PLAs was also found to increase with increase in molecular weight.

The degrees of crystallinity (X_c) are calculated from DSC thermograms and are depicted in Table 4.36. The percentage of crystallinity was calculated by using the Eq. 4.21 and considering a melting enthalpy (ΔH_f^0) of 93 J g^{-1} for 100% crystalline PLA.

$$\% \text{ crystallinity} = (\Delta H_f / \Delta H_f^0) * 100 \quad \ldots (4.21)$$

Typically, X_c was calculated to vary between 15 and 45 %. The low % X_c could be due to presence of higher amount of D-unit and residual lactide. This is due to racemization of L-LA to

D-LA and copolymerization of D- and L-lactic acid units. This observation can be attributed to the racemization of L-lactic acid to D-lactic acid and its incorporation into the polymer chain. The presence of D-lactic acid unit is also confirmed from NMR spectra and X-ray diffractograms.

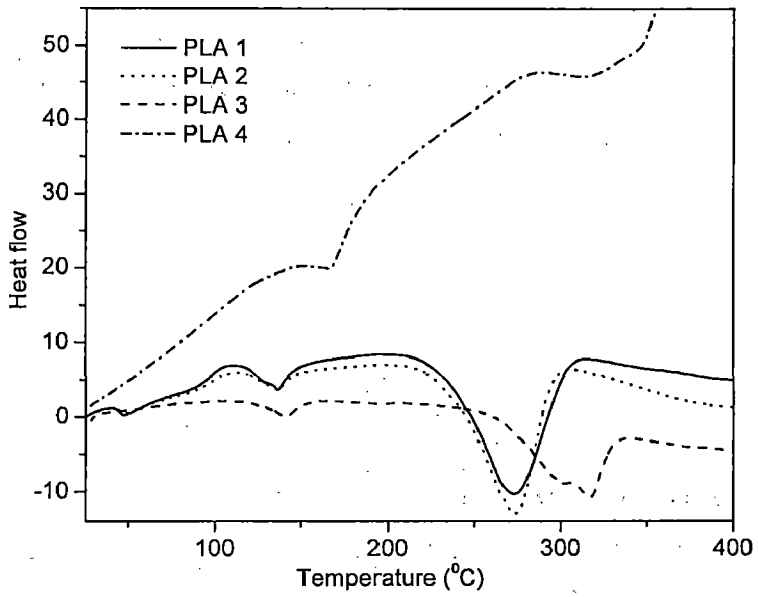

Fig. 4.25 DSC thermograms for PLA

Table 4.36 Thermal characterization and crystallinity values of PLA synthesized by MPC

Polymer	T_g [a] (°C)	T_c [a] (°C)	T_m [a] (°C)	X_c [a] (%)	X_c [b] (%)	T_d [c] (°C)	ΔH_c [a] (mJ/mg)	ΔH_m [a] (mJ/mg)	D-isomer [d] (%)	Sc ratio [b] (%)
PLA-1	47	111	136	14.73	18.8	266	-28.4	13.7	6.52%	14.77
PLA-2	50	112	136	12.58	16.29	272	-24.5	11.7	19.05%	8.95
PLA-3	-	-	140	29.57	21.37	299	-	27.5	58.76%	14.24
PLA-4	-	-	167	43.12	40.29	352	-	40.1	24.45%	10.18

[a] By DSC study; [b] By XRD analysis; [c] By DTG analysis; [d] By ^{13}C NMR.

4.2.3.5 XRD analysis

The powder wide angle X-ray diffraction (XRD) pattern of PLA samples are shown in Fig. 4.26. The original XRD plots are given in Appendix J. All the diffractograms have almost identical pattern and their most intense peak is observed at 2θ values around 16.5° and the peak intensity is assigned a value of 100 (Brizzolara *et al.*, 1996). This peak is due to reflection from 200 and 110 planes. It can be observed from the XRD pattern that PLA exhibits characteristic

peaks at 2 theta values around 15°, 16°, 18.5° and 22.5° due to the presence of L-isomer and peaks at 12°, 21° and 24° due to the presence of D-isomer (Sarasua *et al.,* 1998; Ikada *et al.,* 1987). Thus, it can be concluded that PLA contains both D and L-isomer and the amount of L-lactic acid unit is much higher in comparison to the D-isomer, as the intensity of the peaks corresponding to the L-isomer is very high in comparison to peaks corresponding to D-isomer.

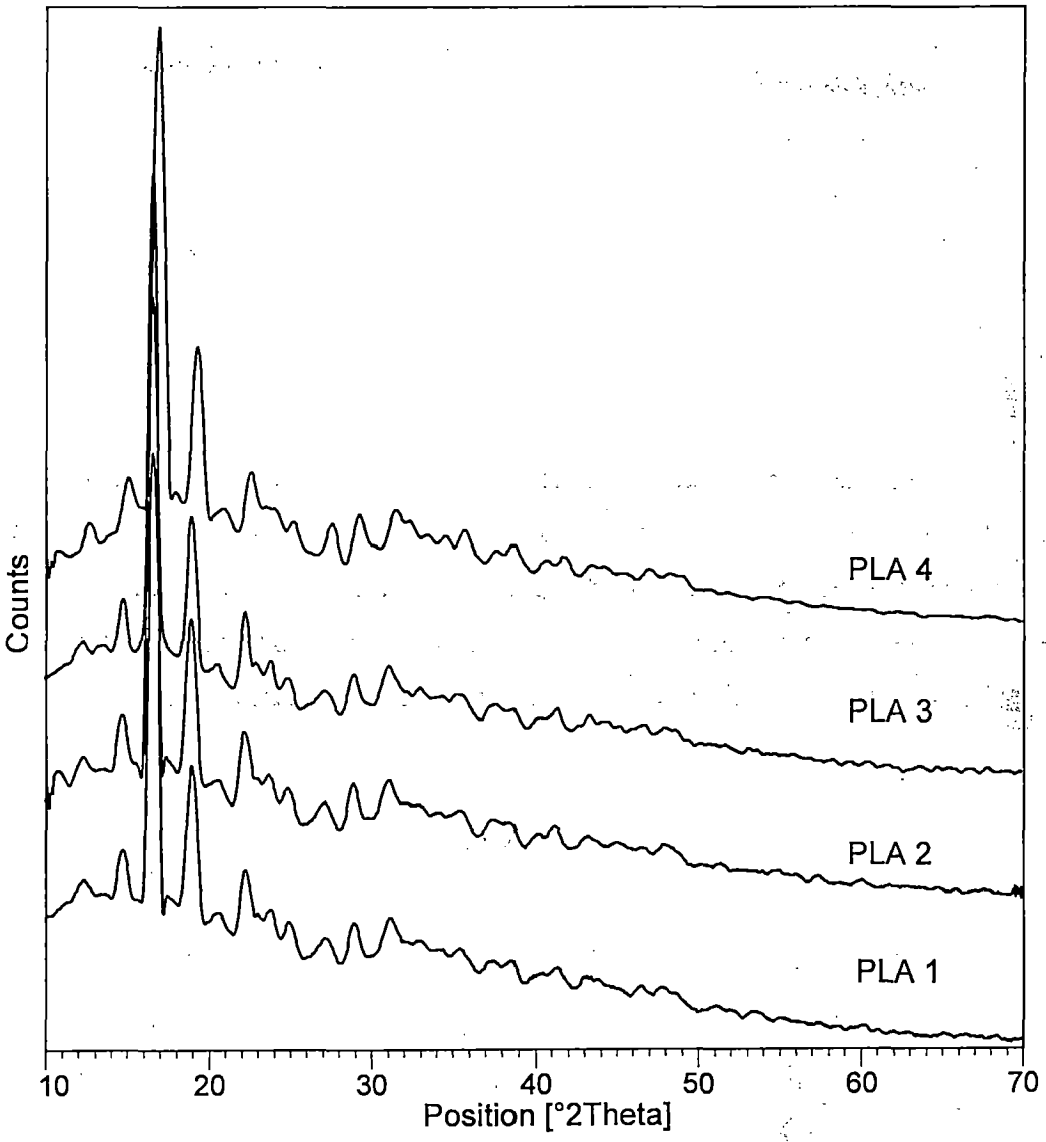

Fig. 4.26 Powder X-ray Diffractogram of PLA synthesized by MPC

The X-ray diffractograms were analyzed by EVA 2 (version 13.0.0.3) supplied by Bruker AXS, Germany. It was found that the peaks matched well with the patterns obtained for

alpha-poly(D(+)lactide) bearing SS-VVV-PPPP number 00-054-1917 (Brizzolara *et al.*, 1996). The matching of XRD of PLA with the standard is shown in Appendix J. The details of the standard are also given in Appendix J. Thus, the PLA crystal was confirmed to have pseudo-orthorhombic space group and exist in alpha form of 10_3 -helix. The % crystallinity is also calculated from powder X-ray diffractograms (Zhang and Wang, 2008) using Eq. 4.22 and are also depicted in Table 4.36.

$$\text{Percent crystallinity} = [I_{crystalline} / (I_{crystalline} + I_{amorphous})]*100 \quad \ldots(4.22)$$

Where, $I_{crystalline}$ =Intensity of crystalline peak and $I_{amorphous}$ = Intensity of amorphous peak

The percentage of crystallinity, as determined by DSC and XRD are in agreement with each other. The difference in % crystallinity of PLA polymers examined by a DSC and WAXD method may be because of the fact that the percentage crystallinity and microscopic morphology of PLA vary with its thermal history and stereosequence distribution (Shyamroy *et al.*, 2005; Thakur *et al.*, 1996). By using the Debye-Scherrer formula, given by Eq. B.1 in Appendix B, the crystallite size are found to be ca. 2.37 Å for PLA 1-3 and 4.07 Å for PLA 4.

4.2.3.6 FESEM analysis

The FESEM image of PLA 1, PLA 2, PLA 3 and PLA 4 are given in Figs. 4.27 A-D. The morphology of PLA is shown to have a porous polymer type surface structure (Gupta *et al.*, 2006). The entangled polymer chains give rise to the porous structure of polymer (Cam *et al.*, 1995). Thus, traces of lactide will tend to be trapped within the polymer matrix. From FESEM, it is also observed that polymer consisted of a series of interconnected channels between fused particles (Ando *et al.*, 2005).

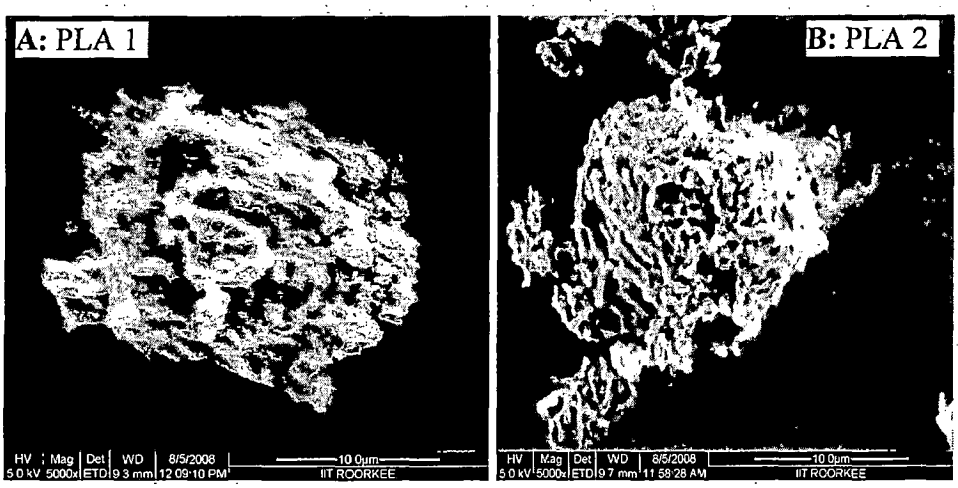

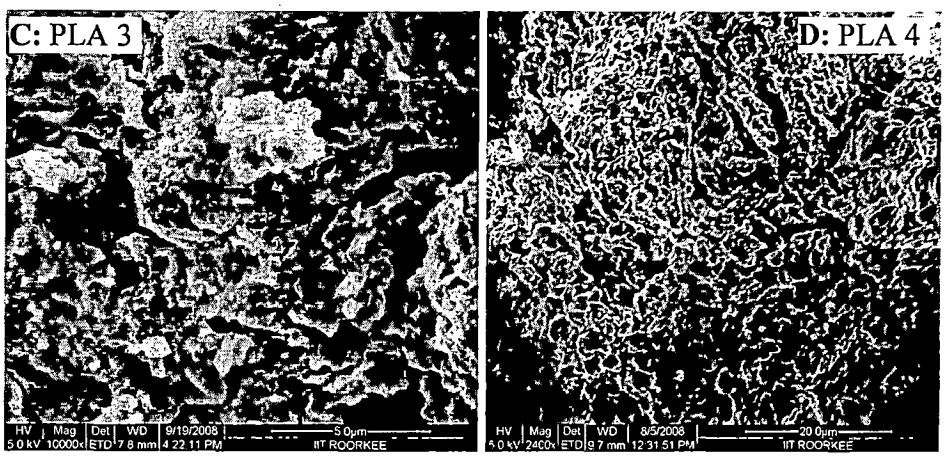

Fig. 4.27 FESEM micrographs of PLA samples

4.2.4 Mechanism of Melt Polycondensation

The polycondensation mechanism of PLA is shown in Fig. 4.28. Polycondensation of lactic acid is basically esterification reaction and forming water as byproduct. The water present in lactic acid and that produced during esterification is removed at high reaction temperature and under vacuum. And subsequently, PLA of high molecular weight is formed as the main product and lactide and water is formed as the byproduct. The lactide and water gets removed under controlled vacuum. But the lactide could not be removed completely and remains in the PLA. The residual lactide and oligomers then gets washed away upon precipitation and thus leading to pure PLA. The formation of lactide and oligomers during polycondensation is confirmed from FTIR and NMR of the white solid condensate deposited at the mouth of the condenser and the liquid collected in the condenser trap. NMR of an unpurified sample did not show any peak for PTSA. This confirms that PTSA molecules did not condense with PLA; rather it only activates the tin chloride catalyst (Moon *et al.*, 2000). The thermal degradation of PLA during polycondensation at high temperature leads to formation of lactide and oligomers by cyclization and chain scission. However, formation of vinyl end group by random chain scission did not occur as can be concluded from FTIR analysis in Section 4.2.3.1.

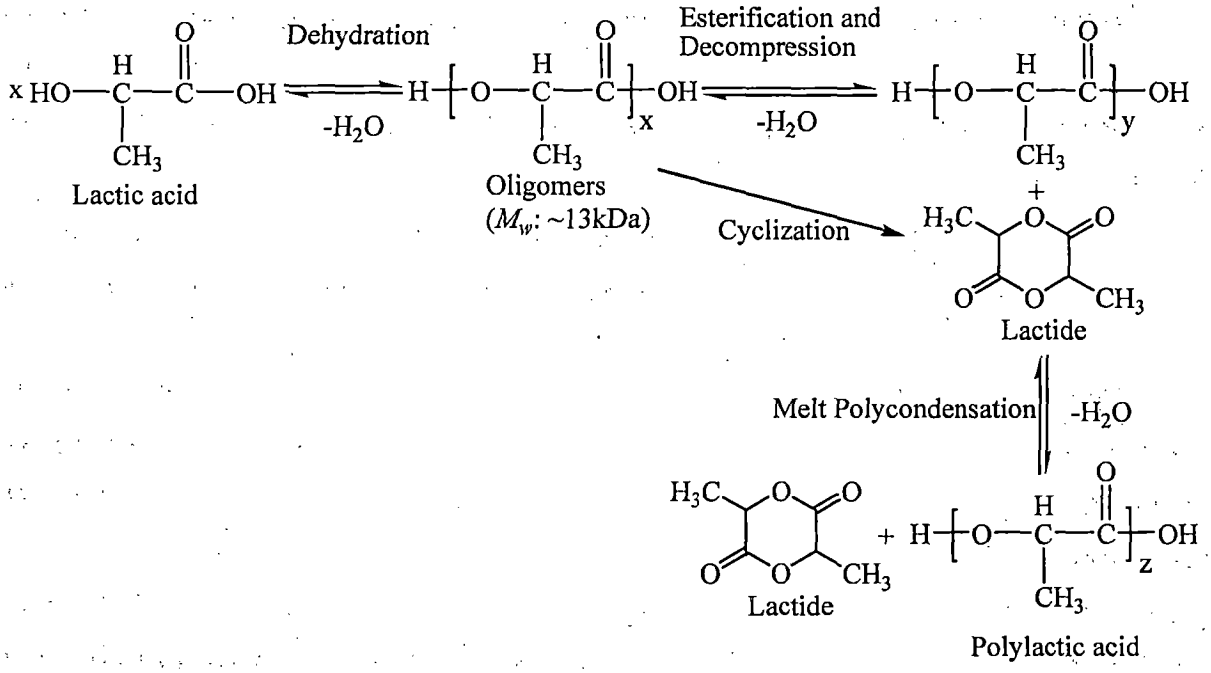

Fig. 4.28 Reaction mechanism of MPC of lactic acid

The polycondensation of PLA involves two equilibrium reactions: (i) dehydration equilibrium for esterification and (ii) ring-chain equilibrium involving the depolymerization of PLA into L-lactide. For the dehydration equilibrium, the condensed water must be removed effectively in order to further enhance the chain extension. And the formation of lactide should be deactivated to promote polycondensation. The rate-determining step during MPC is the mass transfer of water. In order to enhance mass transfer, the MPC reaction is preferably conducted under very intensive mixing in order to homogenize the reaction mixture. Carrying out the reaction under vacuum conditions in an inert atmosphere can further enhance the removal of water from the viscous PLA mass. Therefore, the operating parameters, under which reaction takes place, should be optimized to promote the removal of water byproduct.

The racemization reactions are most likely due to a dynamic equilibrium of ester interchange reactions occurring between the polymer chains which are also called transesterification reaction. It can also be proposed that the terminal groups of PLA are coordinated within the catalyst center. The dehydration is driven among the carboxylate and hydroxyl ligands with the formation of Sn—OH. The proton acid added to the catalyst can work as a ligand of the catalyst site. Furthermore, because the proton acid is not involved in the

esterification, it can fill the open coordination sites of the catalyst to hinder the side reaction (Zhang and Wang, 2008; Moon *et al.,* 2001). Thus, the tin chloride/co-catalyst systems were surely effective catalysts to enhance the molecular weight and to prevent the discoloration of PLA (Moon *et al.,* 2000, 2001).

4.3 SYNTHESIS OF POLY(LACTIC ACID) BY SOLID-STATE POLYCONDENSATION AND ITS SUBSEQUENT CHARACTERIZATIONS

In the present work, PLA has been synthesized by solid-state polycondensation, as discussed in Section 3.2 of Chapter 3. Synthesis of PLA in SSP process is influenced by ten operating parameters as discussed in Table 3.4 of Section 3.2. Out of these, five pertinent parameters are chosen for conducting experiments, as concluded in Section 3.2. These parameters are termed as input parameters. The most significant output parameters for PLA synthesis are yield (wt. %) and wt. average molecular weight (M_w), as these regulate the value addition and physical & mechanical properties of the polymer, respectively. The input parameters and their ranges of variation for PLA synthesis are given in Tables 3.4 and 3.5. For brevity, a part of this table is reproduced below in Table 4.37.

Table 4.37 Input and output parameters involved in SSP of PLA synthesis

Input Parameters		Low level $X_{i,\,min} = -1$	Mid level $X_{i,\,mid} = 0$	High level $X_{i,\,max} = +1$	Output Parameters	
Name(s)	Unit				Name(s)	Unit
X_1: Amount of PLA	g	3	4	5	Yield	wt. %
X_2: HT temperature	°C	100	110	120	M_w	kDa
X_3: HT time	h	1	3	5		
X_4: SSP time	h	10	20	30		
X_5: SSP temperature	°C	130	145	160		

To develop statistically reliable correlations between input and output parameters with almost minimum number of experiments, the technique of design of experiment (DOE) has been used as discussed below:

4.3.1 Design and Analysis of Experiments

Small face centered central composite design (SFCCCD) of RSM consisting of 26 experiments, containing eleven factorial, ten axial and five center points, are developed as given

in Table 3.6, for conduct of experiments. The Table 4.38 contains the different combinations of the five input parameters and two output parameters, namely yield (wt. %) and M_w. The data available in the Table 4.38 are analyzed using statistical software DE7. The analysis indicated that the *degrees of freedom* for *lack of fit* is 1 and that for the *pure error* is 4, whereas; for valid results, the *degrees of freedom* for the *lack of fit* should be ≥ 3 and that for the *pure error* should be ≥ 4. To achieve the minimum value of *lack of fit* as well as *pure error*, the design was augmented by adding 2 model points, which in turn added two vertex points to the design space. Thus, two additional experiments were conducted at above mentioned vertex points (Run No.27-28) and the yield (wt. %) and M_w are recorded in Table 4.38. Table E.2 of Appendix E.2 shows the coded input parameters, whereas; it is shown in terms of actual values in Table 4.38. After augmentation of the SFCCCD design, the design gets converted to D-optimal design which provides the most accurate estimates of the model coefficients. Again, the analysis has been repeated using DE7, for yield (wt. %) as well as M_w. The *lack of fit* and *pure error* for the augmented design has been found to be 3 and 4, respectively, which is satisfactory and is an indication of a better fit to the proposed model.

When experiments were conducted based on different sets of operating conditions as given in Table 4.38, a broad range of molecular weights, M_w, starting from ~60 to 300 kDa are obtained. The values of M_w obtained at five central points (replicate points) of the experimental design ranged between 270 and 300 kDa.

Based on the experimental results presented in Table 4.38, input-output relationships, called regression models, for yield (wt. %) as well as M_w are developed. The different proposed models which are investigated for the above relationships are listed in Table 4.3 of Section 4.2. The generic forms of different regression models (Montgomery, 2004) are also discussed in Section 4.2. The listed models are regressed using statistical software DE7; and based on the results of regression, a particular model is selected which reproduces the experimental results best, with maximum correlation and minimum error. The output parameters for Eq. 4.1-4.3 of Section 4.2 can be either yield (wt. %) or M_w, whereas; the input parameters are fixed and are amount of PLA (X_1), HT temperature (X_2), HT time (X_3), SSP time (X_4) and SSP temperature (X_5).

Table 4.38 M_w and yield (wt. %) obtained at different experimental conditions proposed by DOE for SSP

Run No.	Point Type	X_1: Amount of PLA (g)	X_2: HT temperature (°C)	X_3: HT time (h)	X_4: SSP time (h)	X_5: SSP temperature (°C)	M_w (kDa)	Yield (wt.%)
1	Factorial	5	120	1	30	130	84.691	72.9
2	Factorial	5	100	5	30	130	65.098	83.0
3	Factorial	3	120	5	10	160	70.985	71.1
4	Factorial	5	120	5	10	130	80.553	81.9
5	Factorial	5	120	1	10	160	89.942	76.8
6	Factorial	5	100	1	30	160	78.839	70.9
7	Factorial	3	100	5	30	160	61.276	62.4
8	Factorial	3	120	1	30	160	71.9	71.5
9	Factorial	5	100	5	10	160	75.67	75.1
10	Factorial	3	120	5	30	130	69.984	80.3
11	Factorial	3	100	1	10	130	68.763	82.3
12	Center	4	110	3	20	145	281.54	81.0
13	Center	4	110	3	20	145	280.095	80.1
14	Center	4	110	3	20	145	270.568	82.4
15	Center	4	110	3	20	145	300.195	79.8
16	Center	4	110	3	20	145	275.16	81.6
17	Axial	3	110	3	20	145	259.876	85.9
18	Axial	5	110	3	20	145	278.437	76.3
19	Axial	4	100	3	20	145	130.763	88.9
20	Axial	4	120	3	20	145	165.362	71.2
21	Axial	4	110	1	20	145	224.947	87.0
22	Axial	4	110	5	20	145	271.549	73.5
23	Axial	4	110	3	10	145	248.904	92.6
24	Axial	4	110	3	30	145	188.801	70.8
25	Axial	4	110	3	20	130	184.936	85.2
26	Axial	4	110	3	20	160	239.953	73.3
27	Vertex	5	100	1	10	130	97.601	80.1
28	Vertex	3	120	1	10	130	88.793	79.3

As all input parameters used for the development of correlations should be independent of each other, therefore, before proceeding for the regression analysis, it is felt necessary to know about the correlations between the input parameters. The correlation coefficients obtained through the analysis provided an indication of the extent of relation between one parameter to other. The correlation coefficients between different parameters are represented in Table 4.39. The value of correlation coefficients ranges from –1 (a perfect inverse relationship) to +1 (a perfect direct relationship). A value of 0 indicates no linear relationship.

Table 4.39 Correlation analysis of the input parameters

	X_1: Amount of PLA	X_2: HT temperature	X_3: HT time	X_4: SSP time	X_5: SSP temperature
X_1	1	–0.203	–0.064	–0.064	–0.064
X_2	–0.203	1	–0.064	–0.064	–0.064
X_3	–0.064	–0.064	1	–0.064	–0.064
X_4	–0.064	–0.064	0.064	1	–0.064
X_5	–0.064	–0.064	0.064	0.064	1

From the values of the correlation coefficients given in Table 4.39, it is clear that no correlation exists between the input parameters, as the values are almost close to zero. Thus, it can be safely concluded that no correlationship exists between the input parameters. And, thus, the regression analysis can be carried out to get the desired relationship between the input and output parameters.

4.3.1.1 Regression analysis to develop correlation for the prediction of yield (wt. %)

Experimental results obtained for yield (wt. %) as reported in Table 4.38, are analyzed to figureout the best correlation between yield (wt. %) and input parameters, out of the input-output correlations proposed in Table 4.3.

Case I : Development of linear model

First of all, the linear model was fitted considering all the five main input parameters. The regressed linear model is given by Eq. 4.23. ANOVA results for the linear model for yield (wt. %) are shown in Table 4.40. The regression coefficients of regression analysis are given in Table 4.41.

$$YIELD = 147 - 0.458.X_1 - 0.169.X_2 - 0.333.X_3 - 0.310.X_4 - 0.284.X_5 \quad \text{... (4.23)}$$

Now, from Table 4.40, it is observed that X_5 is the only significant parameter whereas; X_1, X_2, X_3 and X_4 are insignificant. The correlation coefficients "R-square", "adjusted R–square" and "predicted R-square" values for Eq. 4.23 are 0.387, 0.247 and –0.064, respectively. Eq. 4.23 offers negative "predicted R-square" and very small "R-square" values. A negative "Predicted R-Square" implies that the overall mean is a better predictor of response than the current model. "Adequate precision" of 6.752 indicates an adequate signal. For the present model, the *lack of fit* is significant which should be insignificant for a model to be better. Thus,

Table 4.42 ANOVA for RSM variables fitted to 2FI model

Source	Sum of Squares	df	Mean Square	F Value	p-value	Significance
Model	1032.176	15	68.812	4.880	0.004	Significant
X_1: Amount of PLA	265.6107	1	265.6107	18.83779	0.0010	Significant
X_2: HT temperature	365.5065	1	365.5065	25.92265	0.0003	Significant
X_3: HT time	82.60649	1	82.60649	5.858662	0.0323	Significant
X_4: SSP time	241.234	1	241.234	17.10893	0.0014	Significant
X_5: SSP temperature	60.67378	1	60.67378	4.303139	0.0602	Insignificant
X_1X_2	1.648263	1	1.648263	0.116899	0.7383	Insignificant
X_1X_3	0.013307	1	0.013307	0.000944	0.9760	Insignificant
X_1X_4	1.227355	1	1.227355	0.087047	0.7730	Insignificant
X_1X_5	58.98354	1	58.98354	4.183263	0.0634	Insignificant
X_2X_3	1.660698	1	1.660698	0.117781	0.7374	Insignificant
X_2X_4	2.623394	1	2.623394	0.186058	0.6739	Insignificant
X_2X_5	59.01192	1	59.01192	4.185276	0.0633	Insignificant
X_3X_4	2.905384	1	2.905384	0.206057	0.6580	Insignificant
X_3X_5	215.7786	1	215.7786	15.30357	0.0021	Significant
X_4X_5	104.3414	1	104.3414	7.400158	0.0186	Significant
Residual	169.199	12	14.100			
Lack of Fit	164.7446	8	20.59307	18.4935	0.0066	Significant
Pure Error	4.45412	4	1.11353			
Cor Total	1201.375	27				

Table 4.43 Regression analysis for 2-FI model, Eq. 4.24

Predictor	Coefficients	
	Actual	Coded
(Constant)	–741.135	78.64758
X_1: Amount of PLA	37.507	–7.11649
X_2: HT temperature	3.947	–8.34815
X_3: HT time	53.780	–5.84018
X_4: SSP time	4.707	–9.98018
X_5: SSP temperature	6.878	–5.00518
X_1X_2	0.038	0.383434
X_1X_3	–0.039	–0.07804
X_1X_4	0.075	0.749463
X_1X_5	–0.346	–5.19554
X_2X_3	–0.044	–0.87179
X_2X_4	0.011	1.095713
X_2X_5	–0.035	–5.19679
X_3X_4	–0.061	–1.21326
X_3X_5	–0.349	–10.4558
X_4X_5	–0.048	–7.27076

taking all the facts for goodness of fit of a model, discussed in Section 4.2, it can be concluded that the linear model is not a good model. To maintain hierarchy, the terms corresponding to the individual parameters cannot be removed from a model and thus were kept in the model according to the hierarchy principle (Montgomery, 2004).

Table 4.40 ANOVA for RSM variables fitted to linear model

Source	Sum of Squares	df	Mean Square	F-value	p-value	Significance
Model	464.393	5	92.879	2.773	0.043	Significant
X_1: Amount of PLA	2.960	1	2.960372	0.088371	0.769	Insignificant
X_2: HT temperature	40.279	1	40.27935	1.202398	0.285	Insignificant
X_3: HT time	6.520	1	6.519591	0.194619	0.663	Insignificant
X_4: SSP time	141.2155	1	141.2155	4.215491	0.052	Insignificant
X_5: SSP temperature	267.0896	1	267.0896	7.973019	0.010	Significant
Residual	736.982	22	33.499			
Lack of Fit	732.5279	18	40.696	36.54683	0.0016	Significant
Pure Error	4.45412	4	1.11353			
Cor Total	1201.375	27				

Table 4.41 Regression analysis for linear model, Eq. 4.23

Predictor	Coefficients	
	Actual	Coded
(Constant)	147.033	78.25095
X_1: Amount of PLA	–0.458	–0.4581
X_2: HT temperature	–0.169	–1.68976
X_3: HT time	–0.333	–0.66541
X_4: SSP time	–0.310	–3.09684
X_5: SSP temperature	–0.284	–4.25898

Case II: Development of 2-factor interaction model

The 2-factor interaction (2FI) model was developed using the experimental yield (wt. %) values reported in Table 4.38. The regressed 2FI model is given by the Eq. 4.24. ANOVA results for 2FI model for yield (wt. %) are shown in Table 4.42. The regression coefficients of regression analysis are given in Table 4.43.

$$YIELD = -741+37.5.X_1+3.95.X_2+53.8.X_3+4.71.X_4+6.88.X_5+0.038.X_1X_2-0.04.X_1X_3 +0.075.X_1X_4-0.346.X_1X_5-0.044.X_2X_3+0.011.X_2X_4-0.0346.X_2X_5-0.061.X_3X_4 -0.349.X_3X_5-0.0485.X_4X_5 \quad \ldots. (4.24)$$

From Table 4.42, it is evident that the individual parameters and second order interaction terms such as X_1, X_2, X_3, X_4, X_3X_5 and X_4X_5 are only significant, whereas; all the other terms are insignificant. The correlation coefficients "R-square", "adjusted R–square" and "predicted R-square" values for Eq. 4.24 are 0.859, 0.683 and –15.2692, respectively. As the Eq. 4.24 offers negative "predicted R-square", the model can be improved by removing the insignificant model terms. However, for the present case, the removal of insignificant terms did not produce higher "R-square" or "predicted R-square". Observed adequate precision of 8.596 indicates an adequate signal. For the present model, the *lack of fit* is significant. Thus, taking all the facts related to goodness of fit of a model, discussed in Section 4.2, into consideration, it can be concluded that the 2FI model is not an acceptable model.

Case III: Development of quadratic model

The quadratic model was developed using the experimental yield (wt. %) values reported in Table 4.38. The regressed quadratic model is given by the Eq. 4.25. ANOVA results for above quadratic model for yield (wt. %) are shown in Table 4.44. The regression coefficients of regression analysis are given in Table 4.45.

$$\begin{aligned}YIELD = {} & -1246+56.9.X_1+8.07.X_2+56.6.X_3+4.85.X_4+10.1.X_5-0.0599.X_1X_2-0.214.X_1X_3 \\ & +0.040.X_1X_4-0.370.X_1X_5-0.0611.X_2X_3+0.0074.X_2X_4-0.037.X_2X_5-0.0466.X_3X_4 \\ & -0.339.X_3X_5-0.0466.X_4X_5-0.46.X_1^2-0.0147.X_2^2-0.335.X_3^2+0.0011.X_4^2 \\ & -0.0103.X_5^2 \qquad \ldots (4.25)\end{aligned}$$

Now, from Table 4.44, it is apparent that the individual parameters and second order interaction terms such as X_1, X_2, X_3, X_4, X_5, X_1X_5, X_2X_5, X_3X_5 and X_4X_5 are significant. The correlation coefficients "R-square", "adjusted R–square" and "predicted R-square" values for Eq. 4.25 are 0.984, 0.938 and –3.10347, respectively. Observed "adequate precision" value of 20.68 indicates an adequate signal. For the present model, the *lack of fit* is insignificant. In this case, the "R-square" value is higher but the model contains a number of insignificant terms, leading to an inefficient model. Thus, taking all the facts for goodness of fit of a model, discussed in Section 4.2, into consideration, it can be concluded that the quadratic model is not an acceptable model.

Table 4.44 ANOVA for RSM variables fitted to quadratic model

Source	Sum of Squares	df	Mean Square	F-value	p-value	Significance
Model	1182.115	20	59.10576	21.48261	0.0002	Significant
X_1: Amount of PLA	244.362	1	244.362	88.81594	< 0.0001	Significant
X_2: HT temperature	340.3533	1	340.3533	123.705	< 0.0001	Significant
X_3: HT time	90.6175	1	90.6175	32.93588	0.0007	Significant
X_4: SSP time	254.6551	1	254.6551	92.5571	< 0.0001	Significant
X_5: SSP temperature	67.58018	1	67.58018	24.56273	0.0016	Significant
X_1X_2	3.740175	1	3.740175	1.359406	0.2818	Insignificant
X_1X_3	0.401271	1	0.401271	0.145846	0.7139	Insignificant
X_1X_4	0.346456	1	0.346456	0.125923	0.7331	Insignificant
X_1X_5	67.0935	1	67.0935	24.38584	0.0017	Significant
X_2X_3	3.260486	1	3.260486	1.185058	0.3124	Insignificant
X_2X_4	1.209896	1	1.209896	0.439749	0.5285	Insignificant
X_2X_5	67.12374	1	67.12374	24.39683	0.0017	Significant
X_3X_4	1.714582	1	1.714582	0.623183	0.4558	Insignificant
X_3X_5	204.1252	1	204.1252	74.19146	< 0.0001	Significant
X_4X_5	96.33491	1	96.33491	35.01394	0.0006	Significant
X_1^2	0.509035	1	0.509035	0.185014	0.6800	Insignificant
X_2^2	5.297728	1	5.297728	1.925515	0.2078	Insignificant
X_3^2	4.402708	1	4.402708	1.600211	0.2464	Insignificant
X_4^2	0.029108	1	0.029108	0.01058	0.9210	Insignificant
X_5^2	13.2462	1	13.2462	4.814472	0.0643	Insignificant
Residual	19.25931	7	2.75133			
Lack of Fit	14.80519	3	4.935064	4.431909	0.0922	Insignificant
Pure Error	4.45412	4	1.11353			
Cor Total	1201.375	27				

Thus, the removal of insignificant model terms one by one in a stepwise fashion was carried out to improve the model which subsequently produced higher "predicted R-square" value. The regressed "reduced quadratic model" is given by the Eq. 4.26. ANOVA results for "reduced quadratic model" for yield (wt. %) are shown in Table 4.46. The regression coefficients of regression analysis are given in Table 4.47.

$$YIELD = -1414+50.4.X_1+9.61.X_2+43.4.X_3+6.59.X_4+11.5.X_5-0.394.X_1X_5-0.0395.X_2X_5 - 0.323.X_3X_5-0.0522.X_4X_5-0.0213.X_2^2-0.0133.X_5^2 \quad \ldots (4.26)$$

Table 4.45 Regression analysis for quadratic model, Eq. 4.25

Predictor	Coefficients	
	Actual	Coded
(Constant)	–1246.377	81.32521
X_1: Amount of PLA	56.864	–6.83577
X_2: HT temperature	8.066	–8.06743
X_3: HT time	56.646	–6.1209
X_4: SSP time	4.848	–10.2609
X_5: SSP temperature	10.142	–5.2859
X_1X_2	–0.060	–0.59908
X_1X_3	–0.214	–0.42894
X_1X_4	0.040	0.398564
X_1X_5	–0.370	–5.54644
X_2X_3	–0.061	–1.22269
X_2X_4	0.007	0.744814
X_2X_5	–0.037	–5.54769
X_3X_4	–0.047	–0.93254
X_3X_5	–0.339	–10.175
X_4X_5	–0.047	–6.99004
X_1^2	–0.456	–0.45596
X_2^2	–0.015	–1.47096
X_3^2	–0.335	–1.34096
X_4^2	0.001	0.109035
X_5^2	–0.010	–2.32596

Table 4.46 ANOVA for RSM variables fitted to reduced quadratic model

Source	Sum of Squares	df	Mean Square	F Value	p-value	Significance
Model	1158.546	11	105.3224	39.34666	< 0.0001	Significant
X_1: Amount of PLA	267.8382	1	267.8382	100.0598	< 0.0001	Significant
X_2: HT temperature	374.5037	1	374.5037	139.9083	< 0.0001	Significant
X_3: HT time	253.9962	1	253.9962	94.88869	< 0.0001	Significant
X_4: SSP time	523.8087	1	523.8087	195.6861	< 0.0001	Significant
X_5: SSP temperature	326.1623	1	326.1623	121.8488	< 0.0001	Significant
X_1X_5	164.7127	1	164.7127	61.5339	< 0.0001	Significant
X_2X_5	164.7823	1	164.7823	61.5599	< 0.0001	Significant
X_3X_5	450.8123	1	450.8123	168.4159	< 0.0001	Significant
X_4X_5	294.2792	1	294.2792	109.9378	< 0.0001	Significant
X_2^2	15.46154	1	15.46154	5.77617	0.0287	Significant
X_5^2	30.37909	1	30.37909	11.34912	0.0039	Significant
Residual	42.82848	16	2.67678			
Lack of Fit	38.37436	12	3.197864	2.871825	0.1597	Insignificant
Pure Error	4.45412	4	1.11353			
Cor Total	1201.375	27				

Table 4.47 Regression analysis for reduced quadratic model, Eq. 4.26

Predictor	Coefficients	
	Actual	Coded
(Constant)	–1414.495	81.16667
X_1: Amount of PLA	50.448	–6.7498
X_2: HT temperature	9.605	–7.98147
X_3: HT time	43.438	–6.79529
X_4: SSP time	6.592	–9.75845
X_5: SSP temperature	11.458	–4.77044
X_1X_5	–0.394	–5.91702
X_2X_5	–0.039	–5.91827
X_3X_5	–0.323	–9.69022
X_4X_5	–0.052	–7.82917
X_2^2	–0.021	–2.12835
X_5^2	–0.013	–2.98335

Now, from Table 4.46, it is noticeable that the individual parameters and second order interaction terms such as X_1, X_2, X_3, X_4, X_5, X_1X_5, X_2X_5, X_3X_5, X_4X_5, X_2^2 and X_5^2 are significant. The correlation coefficients "R-square", "adjusted R–square" and "predicted R-square" values for Eq. 4.26 are 0.964, 0.940 and 0.841, respectively. Thus, it can be said that Eq. 4.26 offers good "Predicted R-square" value. The "Predicted R-Square" value of 0.841 is in reasonably in agreement with the "Adjusted R-Square" value of 0.940. Eq. 4.26 offers 84.1% [predicted R-Square] of the variability in predicting new obsevations in comparision to approximately 96.4% [R-square] variability in the original data. Observed, adequate precision of 25.35 indicates presence of adequate signal. The *lack of fit* is insignificant. Insignificant *lack of fit* is good for data fitness in the model. Thus, taking all the above facts which qualified goodness of fit of a model (discussed in Section 4.2) into consideration, it can be concluded that the reduced quadratic model is the best model out of the above three developed models to predict yield (wt. %).

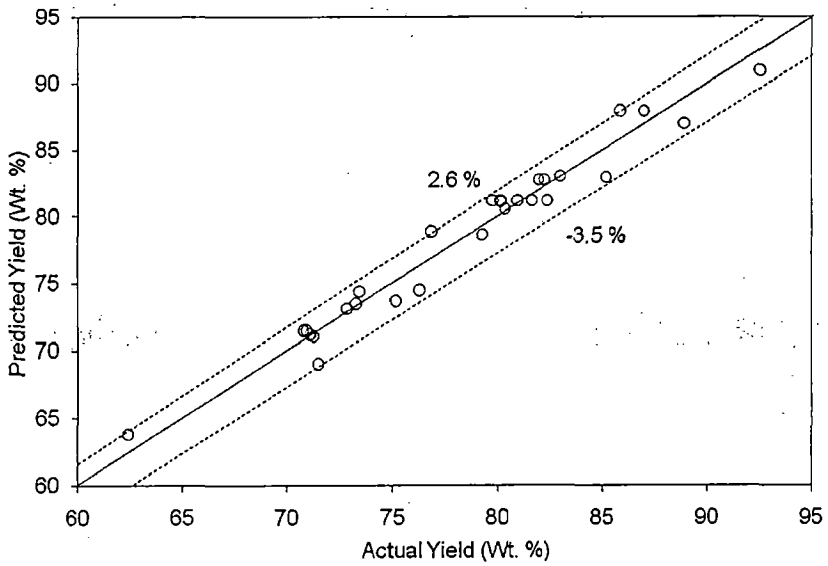

Fig. 4.29 Parity plot for the reduced quadratic model, Eq. 4.26, developed for prediction of yield (wt. %)

The parity plot for the reduced quadratic model given by Eq. 4.26, for the prediction of yield (wt. %), is shown in Fig. 4.29. The error band extends from –3.5 % to +2.6 %, and all data points fall within this error band. Thus, it can be safely concluded that the yield (wt. %) values, predicted by Eq. 4.26, lie within –3.5 % to +2.6 % of experimental values.

Based on the above discussed criteria for individual models, it can be concluded that the reduced quadratic model described by Eq. 4.26 for yield (wt. %) fits the experimental data best. This is because of the fact that the "R-square", "adjusted R-Square" and "predicted R-Square" values are close to each other and also the error band for this model is very small and the band contains all the data points.

4.3.1.2 Regression analysis to develop correlation for prediction of M_w

To determine the best correlation between M_w and input parameters out of the input-output correlations proposed in Table 4.3, Experimental results obtained for M_w, as reported in Table 4.38, are analyzed

Case I: Development of linear model

First of all, the linear model was fitted for M_w, considering all the five main input parameters. The regressed linear model is given by Eq. 4.27. ANOVA results for linear model

for M_w are embodied in Table 4.48. The regression coefficients of regression analysis are given in Table 4.49.

$$M_w = 104 - 0.038.X_1 - 0.087.X_2 + 1.64.X_3 - 0.317.X_4 + 0.497.X_5 \quad \text{... (4.27)}$$

Table 4.48 ANOVA for RSM variables fitted to linear model

Source	Sum of Squares	df	Mean Square	F-value	p-value	Significance
Model	1149.982	5	229.9965	0.022964	0.9997	Insignificant
X_1: Amount of PLA	0.020318	1	0.020318	2.03E-06	0.999	Insignificant
X_2: HT temperature	10.7829	1	10.7829	0.001077	0.974	Insignificant
X_3: HT time	158.4637	1	158.4637	0.015822	0.901	Insignificant
X_4: SSP time	147.6592	1	147.6592	0.014743	0.904	Insignificant
X_5: SSP temperature	819.3614	1	819.3614	0.081809	0.778	Insignificant
Residual	220341.3	22	10015.51			
Lack of Fit	219830.1	18	12212.78	95.56501	0.0002	Significant
Pure Error	511.1822	4	127.7956			
Cor Total	221491.3	27				

Table 4.49 Regression analysis for linear model, Eq. 4.27

Predictor	Coefficients	
	Actual	Coded
(Constant)	103.846	164.7738
X_1: Amount of PLA	–0.038	–0.03795
X_2: HT temperature	–0.087	–0.87428
X_3: HT time	1.640	3.280513
X_4: SSP time	–0.317	–3.1667
X_5: SSP temperature	0.497	7.459584

Now, from Table 4.48, it is found that none of the model terms are significant. The correlation coefficients "R-square", "adjusted R–square" and "predicted R-square" values for Eq. 4.27 are 0.005, –0.221 and –0.770, respectively. Thus, it can be said that Eq. 4.27 offers negative "predicted R-square" and very small "R-square" values. The "Adequate precision" value of 0.64 indicates a non-adequate signal. For the present model, the *lack of fit* is also significant. Thus, taking all the facts for goodness of fit of a model, discussed in Section 4.2, into consideration, it can be concluded that the linear model is not a good model. The insignificant terms corresponding to the individual parameters cannot be removed from a model and thus were kept in the model according to the hierarchy principle (Montgomery, 2004).

Case II: Development of 2-factor interaction model

The 2-factor interaction (2FI) model was developed using the experimental M_w values reported in Table 4.38. The regressed 2FI model is given by Eq. 4.28. ANOVA results for 2FI model for M_w are shown in Table 4.50. The regression coefficients of regression analysis are given in Table 4.51.

Table 4.50 ANOVA for RSM variables fitted to 2FI model

Source	Sum of Squares	df	Mean Square	F Value	p-value	Significance
Model	21992.56	15	1466.171	0.088191	1.0000	Insignificant
X_1: Amount of PLA	226.5849	1	226.5849	0.013629	0.9090	Insignificant
X_2: HT temperature	172.5923	1	172.5923	0.010382	0.9205	Insignificant
X_3: HT time	2243.592	1	2243.592	0.134954	0.7197	Insignificant
X_4: SSP time	1271.888	1	1271.888	0.076505	0.7868	Insignificant
X_5: SSP temperature	2906.775	1	2906.775	0.174845	0.6832	Insignificant
X_1X_2	10843.68	1	10843.68	0.652255	0.4350	Insignificant
X_1X_3	42.3576	1	42.3576	0.002548	0.9606	Insignificant
X_1X_4	5633.708	1	5633.708	0.338872	0.5713	Insignificant
X_1X_5	17.47321	1	17.47321	0.001051	0.9747	Insignificant
X_2X_3	12.68405	1	12.68405	0.000763	0.9784	Insignificant
X_2X_4	5955.497	1	5955.497	0.358228	0.5606	Insignificant
X_2X_5	31.39629	1	31.39629	0.001889	0.9661	Insignificant
X_3X_4	612.4564	1	612.4564	0.03684	0.8510	Insignificant
X_3X_5	2709.623	1	2709.623	0.162986	0.6935	Insignificant
X_4X_5	592.2344	1	592.2344	0.035623	0.8534	Insignificant
Residual	199498.7	12	16624.89			
Lack of Fit	198987.5	8	24873.44	194.6346	< 0.0001	Significant
Pure Error	511.1822	4	127.7956			
Cor Total	221491.3	27				

$$M_w = 1943 - 403.X_1 - 18.3.X_2 + 199.X_3 - 99.X_4 + 7.2.X_5 + 3.11.X_1X_2 - 2.2.X_1X_3 + 5.08.X_1X_4 - 0.19.X_1X_5 - 0.12.X_2X_3 + 0.522.X_2X_4 - 0.025.X_2X_5 + 0.88.X_3X_4 - 1.24.X_3X_5 + 0.115.X_4X_5 \quad \ldots (4.28)$$

Now, from Table 4.50, it is apparent that none of the model terms are significant. The correlation coefficients "R-square", "adjusted R–square" and "predicted R-square" values for Eq. 4.28 are 0.099, –1.027 and –100.395, respectively. Eq. 4.28 offers negative "predicted R-square" and very small "R-square" values. An "Adequate precision" value of 1.46 indicates a non-adequate signal. For the current model, the *lack of fit* is significant. Thus, taking all the facts for goodness of fit of a model, discussed in Section 4.2, into consideration, it can be presumed that the 2FI model is not a good model.

Table 4.51 Regression analysis for 2-FI model, Eq. 4.28

Predictor	Coefficients	
	Actual	Coded
(Constant)	1943.121	172.143
X_1: Amount of PLA	–403.144	6.572921
X_2: HT temperature	–18.282	5.736587
X_3: HT time	198.742	30.43625
X_4: SSP time	–99.416	–22.9163
X_5: SSP temperature	7.239	34.64375
X_1X_2	3.110	31.10036
X_1X_3	–2.201	–4.40282
X_1X_4	5.078	50.77643
X_1X_5	–0.189	–2.82782
X_2X_3	–0.120	–2.40932
X_2X_4	0.522	52.20643
X_2X_5	–0.025	–3.79057
X_3X_4	0.881	17.61525
X_3X_5	–1.235	–37.0515
X_4X_5	0.115	17.322

Case III: Development of quadratic model

The quadratic model was built up using the experimental M_w values reported in Table 4.38. The regressed quadratic model is given by the Eq. 4.29. ANOVA results for quadratic model for M_w are provided in Table 4.52. The regression coefficients of regression analysis are given in Table 4.53.

$$M_w = -19242 + 68.X_1 + 256.X_2 + 244.X_3 - 77.1.X_4 + 75.8.X_5 - 0.379.X_1X_2 - 8.43.X_1X_3 + 3.83.X_1X_4 - 1.02.X_1X_5 - 0.744.X_2X_3 + 0.397.X_2X_4 - 0.108.X_2X_5 + 1.38.X_3X_4 - 0.903.X_3X_5 + 0.182.X_4X_5 + 10.8.X_1^2 - 1.10.X_2^2 - 2.52.X_3^2 - 0.395.X_4^2 - 0.204.X_5^2 \quad \ldots (4.29)$$

Now, from Table 4.52, it is perceptible that the individual parameters and second order interaction terms such as X_4, X_1X_4, X_2X_4, X_2^2, X_4^2 and X_5^2 are significant, whereas; all the other model terms are insignificant. The correlation coefficients "R-square", "adjusted R–square" and "predicted R-square" values for Eq. 4.29 are 0.989, 0.956 and –0.15275, respectively. The "Adequate precision" value of 14.15 indicates an adequate signal. For the present model, the *lack of fit* is insignificant. Thus, taking all the facts for goodness of fit of a model, discussed in Section 4.2, into consideration, it can be deduced that the quadratic model is not a good model.

Table 4.52 ANOVA for RSM variables fitted to quadratic model

Source	Sum of Squares	df	Mean Square	F Value	p-value	Significance
Model	218963.6	20	10948.18	30.31908	< 0.0001	Significant
X_1: Amount of PLA	1430.994	1	1430.994	3.962889	0.0868	Insignificant
X_2: HT temperature	1289.955	1	1289.955	3.572307	0.1007	Insignificant
X_3: HT time	1013.199	1	1013.199	2.805879	0.1378	Insignificant
X_4: SSP time	2615.697	1	2615.697	7.243719	0.0310	Significant
X_5: SSP temperature	1472.592	1	1472.592	4.078087	0.0832	Insignificant
X_1X_2	149.8172	1	149.8172	0.414893	0.5400	Insignificant
X_1X_3	620.2768	1	620.2768	1.717749	0.2313	Insignificant
X_1X_4	3201.772	1	3201.772	8.866752	0.0206	Significant
X_1X_5	509.828	1	509.828	1.41188	0.2735	Insignificant
X_2X_3	482.2998	1	482.2998	1.335645	0.2857	Insignificant
X_2X_4	3445.227	1	3445.227	9.540956	0.0176	Significant
X_2X_5	576.0564	1	576.0564	1.595288	0.2470	Insignificant
X_3X_4	1500.207	1	1500.207	4.154562	0.0809	Insignificant
X_3X_5	1446.098	1	1446.098	4.004717	0.0855	Insignificant
X_4X_5	1468.479	1	1468.479	4.066697	0.0835	Insignificant
X_1^2	288.0956	1	288.0956	0.797831	0.4014	Insignificant
X_2^2	29758.81	1	29758.81	82.41186	< 0.0001	Significant
X_3^2	247.8426	1	247.8426	0.686357	0.4347	Insignificant
X_4^2	3811.751	1	3811.751	10.55598	0.0141	Significant
X_5^2	5150.393	1	5150.393	14.26312	0.0069	Significant
Residual	2527.691	7	361.0987			
Lack of Fit	2016.509	3	672.1695	5.259725	0.0713	Insignificant
Pure Error	511.1822	4	127.7956			
Cor Total	221491.3	27				

In this case, the "R-square" value is higher but the model contains a number of insignificant terms and thus leading to a poor model and negative "predicted R-square" value. Thus, the removal of insignificant terms in a stepwise fashion was carried out to improve the model which produced higher "predicted R-square" value. The regressed reduced quadratic model is given by the Eq. 4.30. ANOVA results for reduced quadratic model for M_w are presented in Table 4.54. The regression coefficients of regression analysis are given in Table 4.55.

$$M_w = -19896 + 155.X_1 + 257.X_2 + 64.4.X_3 - 57.0.X_4 + 81.9.X_5 + 3.27.X_1X_4 - 1.39.X_1X_5 + 0.341.X_2X_4 - 0.146.X_2X_5 + 1.76.X_3X_4 - 0.651.X_3X_5 + 0.0966.X_4X_5 - 1.09.X_2^2 - 0.387.X_4^2 - 0.20.X_5^2 \quad \ldots (4.30)$$

Table 4.53 Regression analysis for quadratic model, Eq. 4.29

Predictor	Coefficients	
	Actual	Coded
(Constant)	–19241.781	267.2331
X_1: Amount of PLA	67.933	16.54205
X_2: HT temperature	255.622	15.70572
X_3: HT time	244.156	20.46711
X_4: SSP time	–77.071	–32.8854
X_5: SSP temperature	75.824	24.67461
X_1X_2	–0.379	–3.7916
X_1X_3	–8.432	–16.8642
X_1X_4	3.832	38.31502
X_1X_5	–1.019	–15.2892
X_2X_3	–0.744	–14.8707
X_2X_4	0.397	39.74502
X_2X_5	–0.108	–16.252
X_3X_4	1.379	27.58439
X_3X_5	–0.903	–27.0824
X_4X_5	0.182	27.29114
X_1^2	10.847	10.8474
X_2^2	–1.102	–110.247
X_3^2	–2.515	–10.0611
X_4^2	–0.395	–39.4566
X_5^2	–0.204	–45.8646

Now, from Table 4.54, it is ascertained that the individual parameters and second order interaction terms such as X_1, X_2, X_4, X_5, X_1X_4, X_2X_4, X_3X_4, X_2^2, X_4^2 and X_5^2 are significant. The correlation coefficients "R-square", "adjusted R–square" and "predicted R-square" values for Eq. 4.30 are 0.983, 0.962 and 0.919, respectively. Thus, it can be said that Eq. 4.30 offers good "predicted R-square" value and it is in reasonable in agreement with the "adjusted R-Square" of 0.962. Further, it can be accomplished that Eq. 4.30 offers 91.9% [predicted R-Square] of the variability in predicting new obsevations in comparision to approximately 98.3% [R-square] variability in the original data. An "Adequate precision" value of 16.75 indicates an adequate signal. The *lack of fit* is insignificant. Insignificant *lack of fit* is good for the fitness of data in the model. Thus, taking all the facts for goodness of fit of a model, discussed in Section 4.2, into consideration, it can be concluded that the "reduced quadratic model" is the best model.

Table 4.54 ANOVA for RSM variables fitted to reduced quadratic model

Source	Sum of Squares	df	Mean Square	F Value	p-value	Significance
Model	217784.5	15	14518.97	47.00277	< 0.0001	Significant
X_1: Amount of PLA	1724.747	1	1724.747	5.583585	0.0359	Significant
X_2: HT temperature	1567.061	1	1567.061	5.073103	0.0438	Significant
X_3: HT time	496.2895	1	496.2895	1.606656	0.2290	Insignificant
X_4: SSP time	2006.774	1	2006.774	6.496603	0.0255	Significant
X_5: SSP temperature	3325.089	1	3325.089	10.76443	0.0066	Significant
X_1X_4	2737.047	1	2737.047	8.860741	0.0116	Significant
X_1X_5	1118.28	1	1118.28	3.620248	0.0813	Insignificant
X_2X_4	2981.656	1	2981.656	9.652624	0.0091	Significant
X_2X_5	1223.665	1	1223.665	3.961415	0.0698	Insignificant
X_3X_4	3133.359	1	3133.359	10.14373	0.0078	Significant
X_3X_5	969.4297	1	969.4297	3.13837	0.1018	Insignificant
X_4X_5	917.2021	1	917.2021	2.969291	0.1105	Insignificant
X_2^2	33836.58	1	33836.58	109.5404	< 0.0001	Significant
X_4^2	4220.767	1	4220.767	13.66404	0.0031	Significant
X_5^2	5736.189	1	5736.189	18.56997	0.0010	Significant
Residual	3706.751	12	308.896			
Lack of Fit	3195.569	8	399.4462	3.125666	0.1430	Insignificant
Pure Error	511.1822	4	127.7956			
Cor Total	221491.3	27				

Table 4.55 Regression analysis for reduced quadratic model, Eq. 4.30

Predictor	Coefficients	
	Actual	Coded
(Constant)	–19896.455	267.1072
X_1: Amount of PLA	154.524	17.86721
X_2: HT temperature	256.790	17.03088
X_3: HT time	64.360	10.09734
X_4: SSP time	–56.951	–25.1659
X_5: SSP temperature	81.871	32.39406
X_1X_4	3.270	32.70155
X_1X_5	–1.394	–20.9027
X_2X_4	0.341	34.13155
X_2X_5	–0.146	–21.8655
X_3X_4	1.756	35.12772
X_3X_5	–0.651	–19.539
X_4X_5	0.097	14.48409
X_2^2	–1.094	–109.444
X_4^2	–0.387	–38.654
X_5^2	–0.200	–45.062

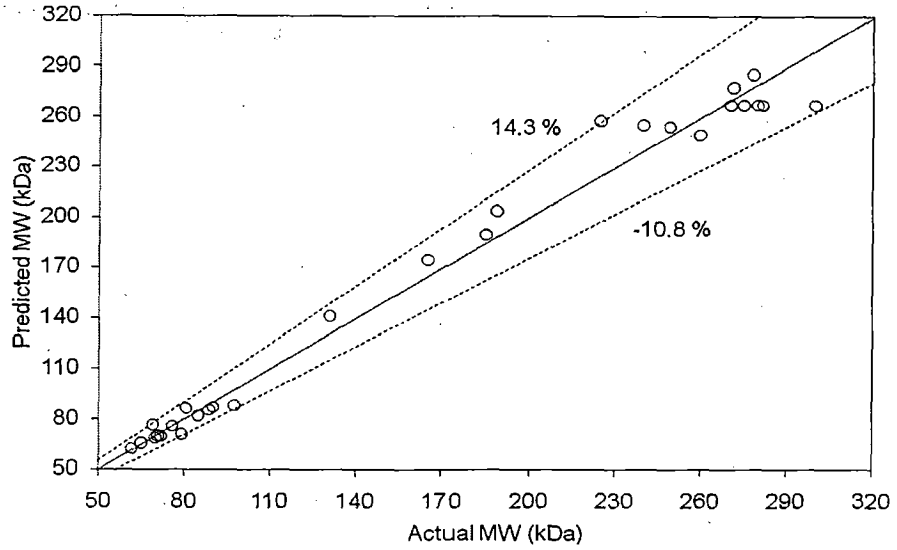

Fig. 4.30 Parity plot for the reduced quadratic model, Eq. 4.30, developed for prediction of M_w

The parity plot for the reduced quadratic model given by Eq. 4.30 for the prediction of M_w is presented in Fig. 4.30. The error band extends from –10.8 % to +14.3 %, and all data points fall within this error band. Thus, the M_w predicted by Eq. 4.30 lie within –10.8 % to +14.3 % of experimental values.

Based on the above discussed criteria for individual models, it can be concluded that the "reduced quadratic model" described by Eq. 4.30 for M_w best fits the experimental values. This is because of the fact that the error band for this model is small and the "R-square", "adjusted R-Square" and "predicted R-Square" values are close to each other and also all the data points fall within the error band specified above.

4.3.1.3 Numerical optimization

Numerical optimization, within the experimental domain of input parameters studied above, was conducted for the simultaneous maximization of both molecular weight and yield (wt. %), as both the responses are of importance to the concerned process. Numerical optimization was carried out using DE7. As the yield (wt. %) cannot exceed 100%, the targeted value for the yield (wt. %) was fixed at 100. The multivariable models (Eq. 4.26 for yield (wt. %) and 4.30 for molecular weight), obtained in the Sections 4.3.1.1 and 4.3.1.2, respectively, were used for predicting the optimal conditions that should allow the synthesis of PLA of high

molecular weight as well as high yield (wt. %), within a short time period. It is suggested that under the conditions listed in Table 4.56, the predicted - M_w is 292.514 kDa and -yield (wt. %) is 99.9 %, with a desirability of 0.895. The predictions were calculated with a 95 % confidence interval.

Table 4.56 Operating conditions for simultaneous maximization of yield (wt. %) and M_w

Parameter	Values
X_1: Amount of PLA (g)	3.769
X_2: HT temperature (°C)	109.9
X_3: HT time (h)	1
X_4: SSP time (h)	13.7
X_5: SSP temperature (°C)	151

To confirm the predicted values of M_w and yield (wt. %), two experiments were conducted for the production of PLA under identical experimental operating conditions given in Table 4.56. The M_w obtained were 288.362 and 285.659 kDa and the yield (wt.%) were 88.9 and 92.7. The mean value for M_w for the above two experiments, is 287.0105 kDa which is 1.88 % less than the predicted value. And the mean value for yield (wt.%) is 90.8 %, which is less than the predicted value with an error of 9.11 %. The lower yield (wt.%) and the lower M_w than the predicted value may be attributed to the fact that during the SSP reaction, lactides and lactic acid oligomers are also formed which get swept with the air in vacuum.

4.3.2 Effect of Various Parameters on Yield (wt. %) and M_w

To visualise how yield (wt. %) and M_w vary with input parameters, such as amount of PLA (X_1), HT temperature (X_2), HT time (X_3), SSP time (X_4) and SSP temperature (X_5), Figs. 4.31 - 4.40 have been plotted. These figures portray the complete picture of the variations in the whole range of the experimental domain studied, when the input parameters are varied from minimum to maximum of the range given in Table 4.38. These one factor main effect plots have been obtained by varying one of the factors and keeping all other factors at the central level as has been defined in the Table 4.57 as "Base Case". The full quadratic equations, Eq. 4.25 and Eq. 4.29, are used to generate the variation of yield (wt. %) and M_w with input parameters,

respectively, as depicted through Figs. 4.31 - 4.40. LSD bars display Fisher's Least Significant Difference bars (95%) at the endpoints of the line on the graph.

Table 4.57 "Base Case" for determining the effects of parameters in SSP

Name of Input Parameters	Base case	Range	
		Lower	Upper
X_1: Amount of PLA (g)	4	3	5
X_2: HT temperature (°C)	110	100	120
X_3: HT time (h)	3	1	5
X_4: SSP time (h)	20	10	30
X_5: SSP temperature (°C)	145	130	160

4.3.2.1 Effect of amount of PLA on yield (wt. %) and M_w

The effects of amount of PLA pre-polymer taken for SSP on yield (wt. %) and M_w are depicted in Figs. 4.31 and 4.32, respectively.

From the above figures, following salient facts emerged out:

1. With the increase in the initial feed (pre-polymer) amount of PLA, the yield (wt. %) of high molecular weight PLA obtained after SSP is found to decrease significantly.
2. The M_w of PLA obtained after SSP is found to increase gradually with the increase in amount of initial feed (pre-polymer) amount of PLA.

The above facts can be explained as:

The decrease in yield (wt. %) with the increase in amount of PLA may be due to the increase of the reaction mixture viscosity as well as the reaction mixture amount. The two factors do not allow the reaction byproduct, water, to get out of the reaction mixture, by increasing the resistance to escape, which is a necessary requirement for shifting the polymerization reaction in a forward direction. This, in turn, activates the reverse polymerization reaction leading to decrease in yield (wt. %) (Proikakis *et al.*, 2002). The decreased yield (wt. %) may also be partially due to the formation of lactide vapor which gets swept away along with the byproduct water vapor from reaction mixture. The effect of initial feed amount of PLA on yield (wt. %) is found to be significant which is also confirmed from the Section 4.3.1.1.

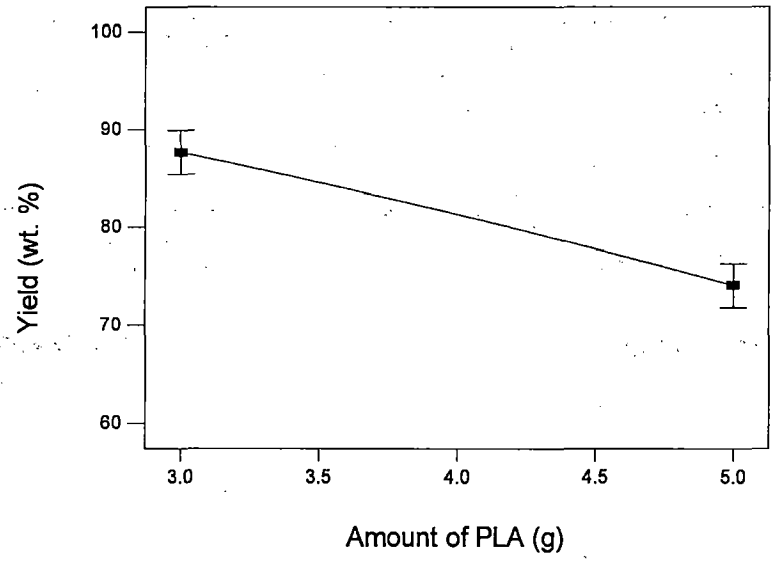

Fig. 4.31 Effect of amount of PLA on yield (wt. %) of PLA

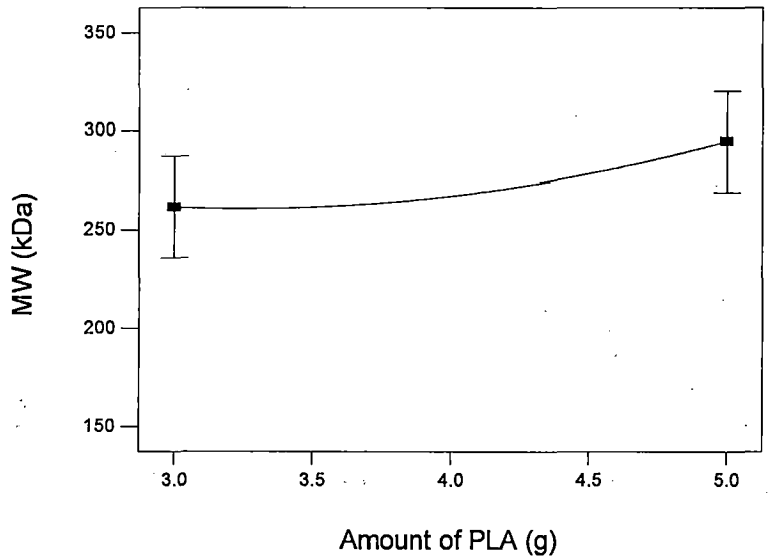

Fig. 4.32 Effect of amount of PLA on M_w of PLA

An increase in the feed amount of PLA prepolymer facilitates the formation of long chain polymers by bringing together the smaller chain molecules and thus, helps in the increase of the M_w of PLA. Further, the number of reactive chain ends increase with the increase in amount of PLA which leads to faster diffusion of reactive chain ends during remelting process during SSP and thus, leading to higher molecular weight (Vouyiouka *et al.*, 2005). The significant effect of initial feed amount of PLA prepolymer on M_w of the PLA, obtained after SSP, is also confirmed from the Section 4.3.1.2.

4.3.2.2 Effect of HT temperature on yield (wt. %) and M_w

The effects of HT temperature on yield (wt. %) and M_w are shown in Figs. 4.33 and 4.34, respectively.

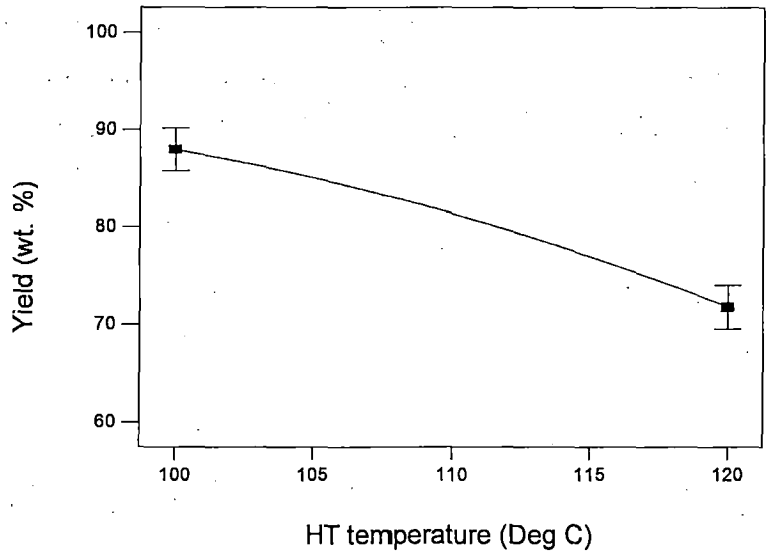

Fig. 4.33 Effect of HT temperature on yield (wt. %) of PLA

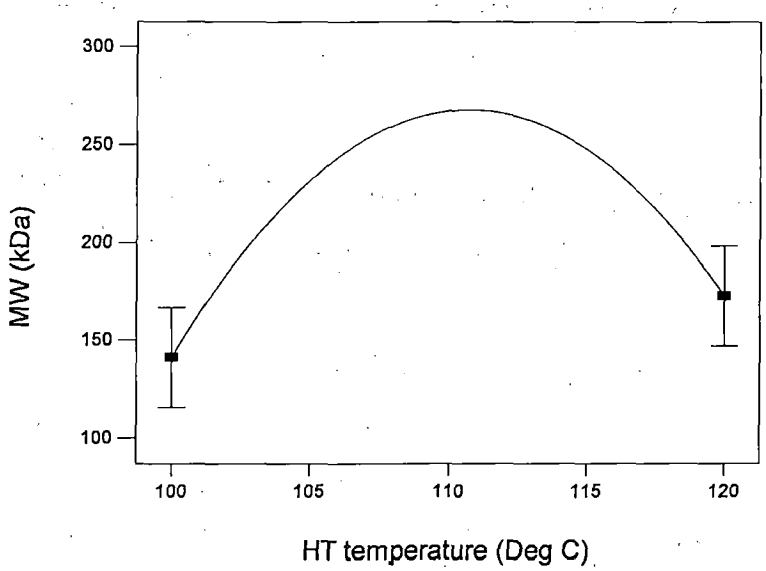

Fig. 4.34 Effect of HT temperature on M_w of PLA

From the above figures, following relevant facts become apparent:

1. With the increase in the heat treatment temperature, the yield (wt. %) decreases significantly.

2. The M_w of PLA increases significantly with the increase in HT temperature from 100 to 110°C. However, a further increase in HT temperature leads to significant decrease in M_w of PLA.

The above facts can be interpreted as:

During the heat treatment, the PLA prepolymer is heated around its crystallization temperature (T_c) to undergo crystallization, which makes it resistive to fusion even when heated at higher temperature. Below the T_c, two phases of PLA coexists: crystalline phase and amorphous phase, whereas; only one phase - i.e. the liquid phase is detected above the T_c. The T_c of PLA prepolymer used for the SSP is around 111°C as discussed in Section 4.2.3.4. In fact, during heat treatment, all the reactive end groups (hydroxy and carboxylic acid groups) and residual lactide that are concentrated in the amorphous region of the polymer help to enhance the rate of polycondensation (Fukushima and Kimura, 2008; Fukushima *et al.,* 2005) which in turn helps in the formation of high molecular weight crystalline product. Thus, heat treatment is carried out before solid state polycondensation which takes place at a higher temperature around 140-150°C.

Further, when the HT temperature increases from 100 to 120°C, the kinetic energy of molecules increases which favors the ease of removal of polycondensation byproducts like water, lactide vapors etc. Increase in HT temperature also facilitates evaporation of byproduct water (as its vapour pressure increases), lactide, residual monomer and some oligomeric compounds which then get swept away with vacuum and thus leads to a decreased yield (wt. %). The significant effect of the HT temperature on yield (wt. %) is also confirmed from Section 4.3.1.1.

When the temperature is increased up to T_c, the active sites of the PLA prepolymer chain ends, and the residual monomer present in the prepolymer gets activated. This happens due to the fact that with increase in temperature, the kinetic energy of molecules increases and they come closer to each other through effective diffusion and offer ample opportunity for polymerization reaction to increase chain length and subsequently M_w increases (Shinno *et al.,* 1997). Thus, M_w of PLA increases with the increase in HT temperature from 100 to 110°C. Further, around T_c of PLA prepolymer, the lactide formation and other side reactions are effectively suppressed as the reaction equilibrium is shifted to the direction of polymer

formation (Moon *et al.*, 2001). However, with further increase in HT temperature beyond T_c, the PLA prepolymer attains a glassy phase and depolymerization reactions sets in, thereby leading to formation of low M_w PLA (Moon *et al.*, 2001). Further, the number of active chain ends decreases gradually (as they undergo polymerization in amorphous zone of PLA). In addition to it, heat treatment increases the dimensions of the crystal and when it becomes large enough after a particular time period, the rate of diffusion of chain end-groups decreases. Both the above phenomena prohibit further growth of polymer chain with the increase in HT temperature above T_c (Xu *et al.*, 2006). Therefore, the M_w of PLA decreases beyond T_c. The significant effect of the HT temperature on M_w is also confirmed from Section 4.3.1.2.

4.3.2.3 Effect of HT time on yield (wt. %) and M_w

The effects of HT time on yield (wt. %) and M_w are depicted in Figs. 4.35 and 4.36, respectively.

From the figures, following salient facts come into view:

1. With the increase in the time period of heat treatment, the yield (wt. %) decreases considerably.
2. With the increase in the time period of heat treatment, M_w of PLA increases to a small extent up to 3 h and further increase in time period have almost no effect on the M_w of PLA.

The above facts can be explained as:

An increase in HT time period, facilitates evaporation of byproduct water and lactide or residual monomer which are swept away under vacuum and thus leads to a decrease in yield (wt. %). The above significant effect of the time period of heat treatment on yield (wt. %) is also confirmed from Section 4.3.1.1.

With the initial increase in HT time period, the prepolymer undergoes crystallization and due to the diffusion of reactive end-groups present in the amorphous region, PLA prepolymer undergoes chain coupling and thereby M_w of PLA increases. However, with further increase in HT time period, the concentration of end-groups decrease to such an extent that no further chain coupling could possibly take place to elongate the chain length. Thus, the M_w remains almost constant after 3 h HT time period (Shinno *et al.*, 1997).

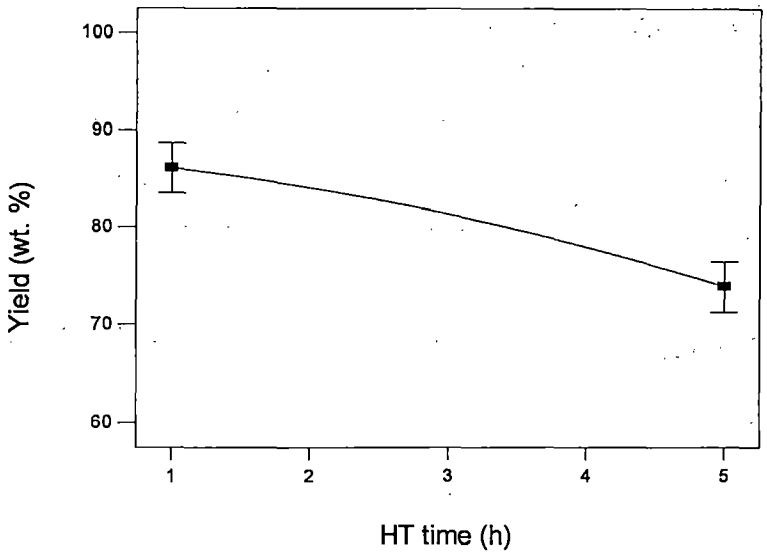

Fig. 4.35 Effect of HT time on yield (wt. %) of PLA

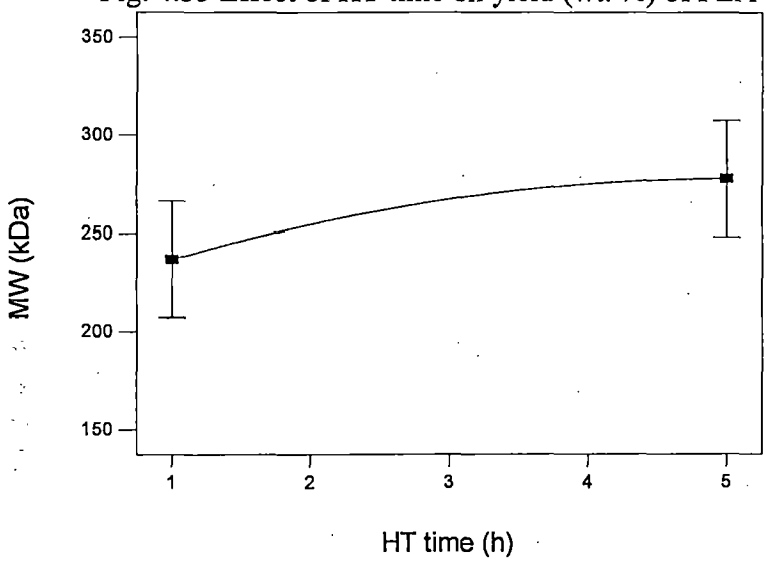

Fig. 4.36 Effect of HT time on M_w of PLA

4.3.2.4 Effect of SSP time on yield (wt. %) and M_w

The effects of SSP time on yield (wt. %) and M_w are represented in Figs. 4.37 and 4.38, respectively.

From the above said figures, following salient facts become obvious:

1. With the increase in the time period of SSP, the yield (wt.%) decreases to great extent.
2. The M_w of PLA increases marginally with the increase in SSP time period from 10 to 15 hour and further increase in the time period leads to considerable decrease in the M_w of PLA.

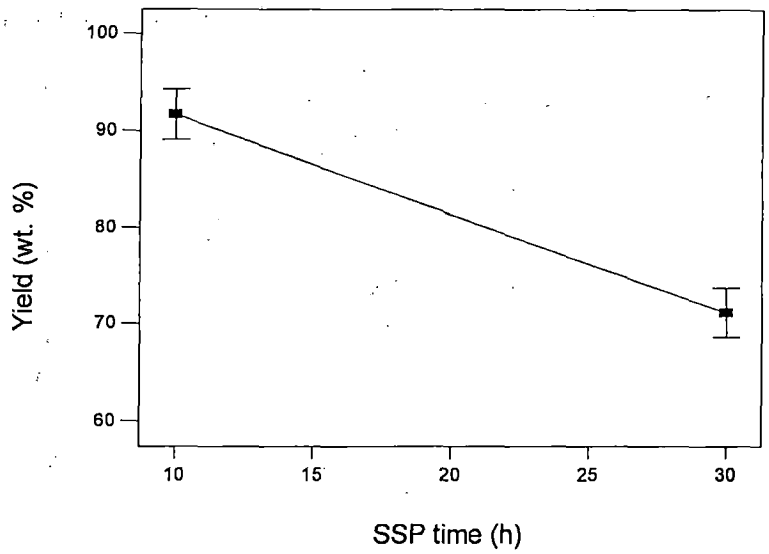

Fig. 4.37 Effect of SSP time on yield (wt. %) of PLA

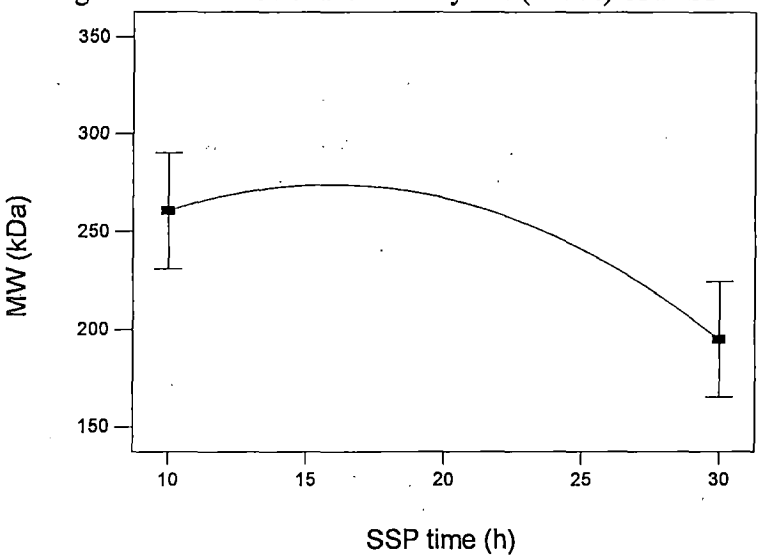

Fig. 4.38 Effect of SSP time on M_w of PLA

The above facts can be explained as:

During the SSP process, the crystallized PLA is allowed to undergo to a glassy state by heating the polymer to a temperature above T_c and below T_m to prevent its decomposition. It has been explained under Section 4.3.2.2, that during HT the crystal grows to a certain extent by consuming un-reacted lactide and reactive chain ends present in amorphous region of reaction mixture. This diminishes the diffusion of active chain end groups present in the crystal formed. Thus, to utilize the reactive end groups present in the crystal for further improvement of M_w of

PLA, it is necessary that mobility of chain end-groups be improved so that they undergo chain coupling to increase the M_w.

Heating of PLA for long duration of time induces the formation of lactide as well as significant polymer decomposition (depolymerization) leading to a decrease in yield (wt. %) as well as molecular weight (Moon *et al.*, 2001; Zhang *et al.*, 2008). The above effect of the time period of SSP on yield (wt. %) is also reported in Section 4.3.1.1. This significant effect of the time period of SSP on M_w is also evident in Section 4.3.1.2.

4.3.2.5 Effect of SSP temperature on yield (wt. %) and M_w

The effects of SSP temperature on yield (wt. %) and M_w are shown in Figs. 4.39 and 4.40, respectively.

From the figures, following important facts emerged out:

1. With the increase in the SSP temperature from 130°C to 160°C, the yield (wt. %) decreases significantly.
2. The M_w of PLA increases significantly with the increase in SSP temperature from 130 to 145°C and further increase in temperature leads to a slight decrease in the M_w of PLA.

The above observations can be clarified as:

During SSP the condensate vapours consisting of water vapour and lactide vapours get swept away under vacuum. At higher temperature, rate of vapour formation increases along with degradation of the macromolecular chain and thus, a decrease in yield (wt. %) is observed with the increase in the SSP temperature (Moon *et al.*, 2001). The significant effect of the SSP temperature on yield (wt. %) has also been observed in Section 4.3.1.1.

During SSP, the prepolymer is heated to a temperature well above T_g but below T_m. When the SSP temperature is below T_m, the PLA chain end groups undergo rapid diffusion leading to an increase in M_w. Thus, the M_w is found to increase up to 145°C which is nearer to the melting point (T_m) of the heat treated prepolymer, which is around 165°C. However, when the SSP temperature increases further, the degradation of the polymer chains as well as the formation of lactide get facilitated and thereby leads to a decrease in the M_w of PLA (Moon *et al.*, 2001;

Zhang *et al.*, 2008). This significant effect of the SSP temperature on M_w is also confirmed from Section 4.3.1.2.

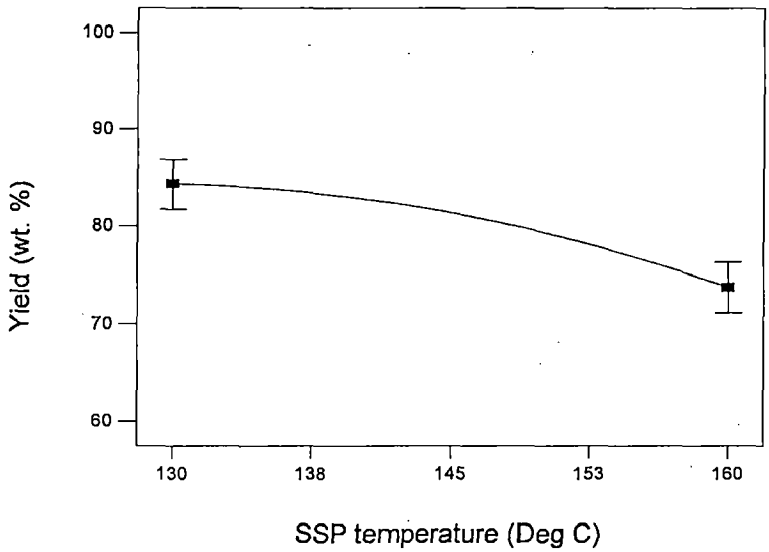

Fig. 4.39 Effect of SSP temperature on yield (wt. %) of PLA

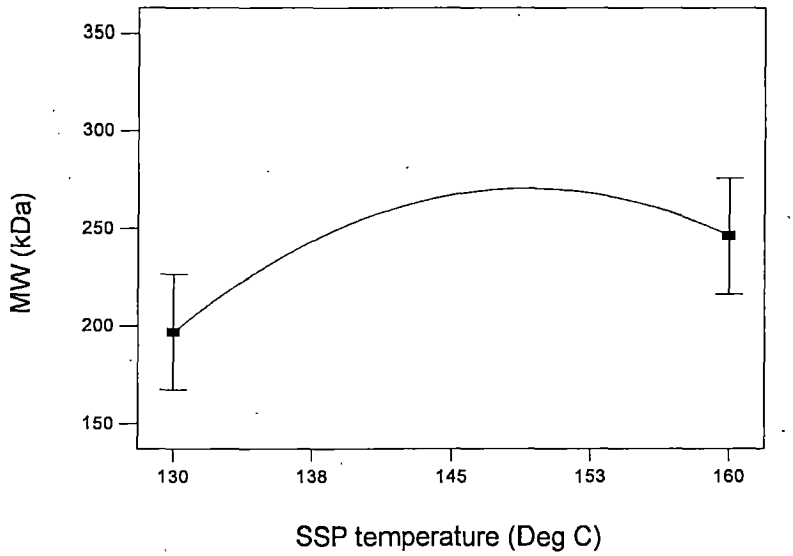

Fig. 4.40 Effect of SSP temperature on M_w of PLA

4.3.2.6 Effect of 2-parameter interactions on yield (wt. %)

Fig. 4.41 reports the 2-parameter interaction plots for yield (wt. %) of PLA, obtained from the analysis carried out using Minitab software, for the different input parameters as given in Table 4.58.

Table 4.58 Two parameter interactions on yield (wt. %) and M_w of PLA

Box No.	2-parameter Interactions	Box No.	2-parameter Interactions
1	Amount of PLA and HT temperature	6	HT temperature and SSP time
2	Amount of PLA and HT time	7	HT temperature and SSP temperature
3	Amount of PLA and SSP time	8	HT time and SSP time
4	Amount of PLA and SSP temperature	9	HT time and SSP temperature
5	HT temperature and HT time	10	SSP time and SSP temperature

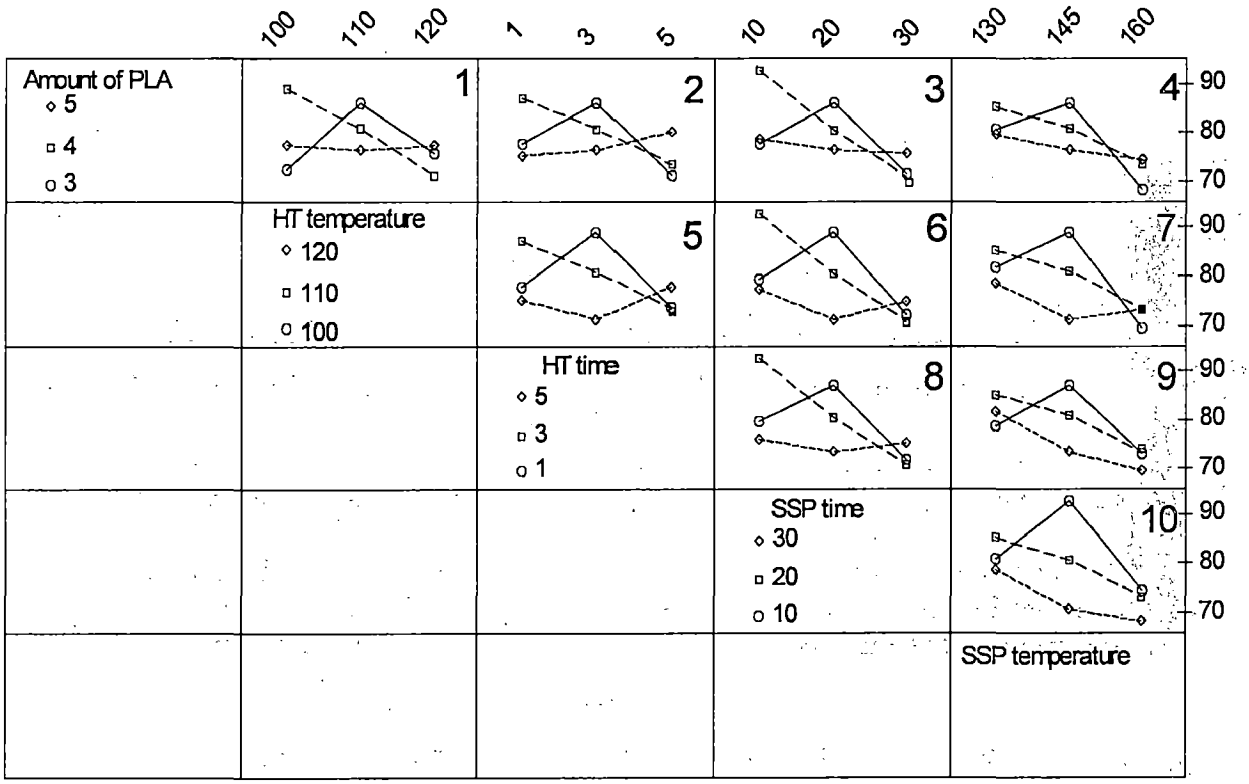

Fig. 4.41 Two-parameter interaction plot for yield (wt. %) of PLA

Interaction is said to occur, when, the effect of a particular input parameter on the output parameter, behaves differently in the presence of another input parameter. The 2-parameter interactions are shown inside the rectangular boxes numbered 1-10 in Fig. 4.41 and has been explained in Table 4.59. For example, the Box No. 1, 2, 3 and 4 contains the effect of HT temperature, HT time, SSP time and SSP temperature, respectively, on yield (wt. %) at different

levels of "Amount of PLA". These rectangular boxes will be addressed through "Box No" in the discussion ahead.

Table 4.59 Order of magnitude of Severity of 2-parameter interaction for yield (wt. %) of PLA

2-parameter Interactions	Coefficient Actual	Coefficient Coded	p-value	F value	Order of severity
Amount of PLA and HT temperature	–0.060	–0.59908	0.2818	1.359406	0.017
Amount of PLA and HT time	–0.214	–0.42894	0.7139	0.145846	0.00027
Amount of PLA and SSP time	0.040	0.398564	0.7331	0.125923	0.00
Amount of PLA and SSP temperature	–0.370	–5.54644	0.0017	24.38584	0.327
HT temperature and HT time	–0.061	–1.22269	0.3124	1.185058	0.014
HT temperature and SSP time	0.007	0.744814	0.5285	0.439749	0.0042
HT temperature and SSP temperature	–0.037	–5.54769	0.0017	24.39683	0.328
HT time and SSP time	–0.047	–0.93254	0.4558	0.623183	0.0067
HT time and SSP temperature	–0.339	–10.175	< 0.0001	74.19146	1.00
SSP time and SSP temperature	–0.047	–6.99004	0.0006	35.01394	0.471

From the above figure, the following fact emerged out:

1. Within the range of parameters studied in the present investigation, all the input parameters were found to be involved in interactions, though the extents of severity of these interactions change considerably.

The above fact can be explained as:

For the present case, an interaction is said to exist between two parameters when one parameter affects the yield (wt. %) differently at different levels of the other parameter. This fact is obvious from the Fig. 4.41 as no two lines, in any of the Box. Nos., are parallel for two different levels of a parameter. For example, if Box No. 10 is examined, it can be observed that, depending on the level of SSP time, the change in yield (wt. %) is different when SSP temperature varies from 130 to 160 °C. The greater the lines depart from being parallel, the greater is the degree of interaction. From the discussions in Section 4.3.1.1, it is also evident that interaction exists between input parameters SSP time as well as SSP temperature. This interaction effect is further reinforced by the fact that in Eq. No. 4.25, the coefficient of

interaction term "X_4X_5" acquires a value of -0.0466 and is found to be significant vide ANOVA analysis of data. Further, it can be observed that significant interactions exist between input parameter "SSP temperature" and other input parameters such as "amount of PLA", HT time, HT temperature and SSP time. The significant interactions can also be observed for box Nos. 4, 7, 9 & 10 of Fig. 4.41. The order of magnitude of severity of 2-parameter interaction, calculated by using Eq. 4.17 of Section 4.2.2.6, in ascending order, is given in Table 4.59.

4.3.2.7 Effect of 2-parameter interactions on M_w

Fig. 4.42 presents the 2-parameter interaction plots, obtained from the analysis carried out using Minitab software, for the different input parameters controlling M_w. The 2-parameter interactions are displayed inside the rectangular boxes numbered as 1-10 in Fig. 4.42 and are same as has been explained in Table 4.58. For example, the Box Nos. 1, 2, 3 and 4 contains the effect of HT temperature, HT time, SSP time and SSP temperature, respectively, on M_w at different levels of "Amount of PLA". These rectangular boxes will be referred through "Box No" in the discussion ahead.

From the Fig. 4.42, the following fact becomes apparent:

1. Within the range of parameters studied in the present investigation, all the input parameters were found to be involved in interactions, though the extent of severity of these interactions changes considerably.

The above fact can be explained as:

For the present case, an interaction is said to exist between two parameters when one parameter affects the M_w differently at different levels of the other parameter. This fact is obvious from the Fig. 4.42 as no two lines, in any of the Box. Nos., are parallel for two different levels of a parameter. For example, if Box No. 6 is examined, it can be observed that, depending on the level of HT temperature, the recorded change in M_w is different, when SSP time varies from 10 to 30 h. The greater the lines depart from being parallel, the greater is the degree of interaction. From the discussions in Section 4.3.1.2, it is also evident that interaction exists between input parameters HT temperature and SSP time. This interaction effect is further reinforced by the fact that in Eq. No. 4.29 the coefficient of interaction term "X_2X_4" acquires a value of +0.397 and is found to be significant vide ANOVA analysis of data. Further, it can be

observed that significant interactions exist between input parameter "Amount of PLA and SSP time" and "HT temperature and SSP time". The significant interactions can be observed in box Nos. 3 & 6 of Fig.4.42.

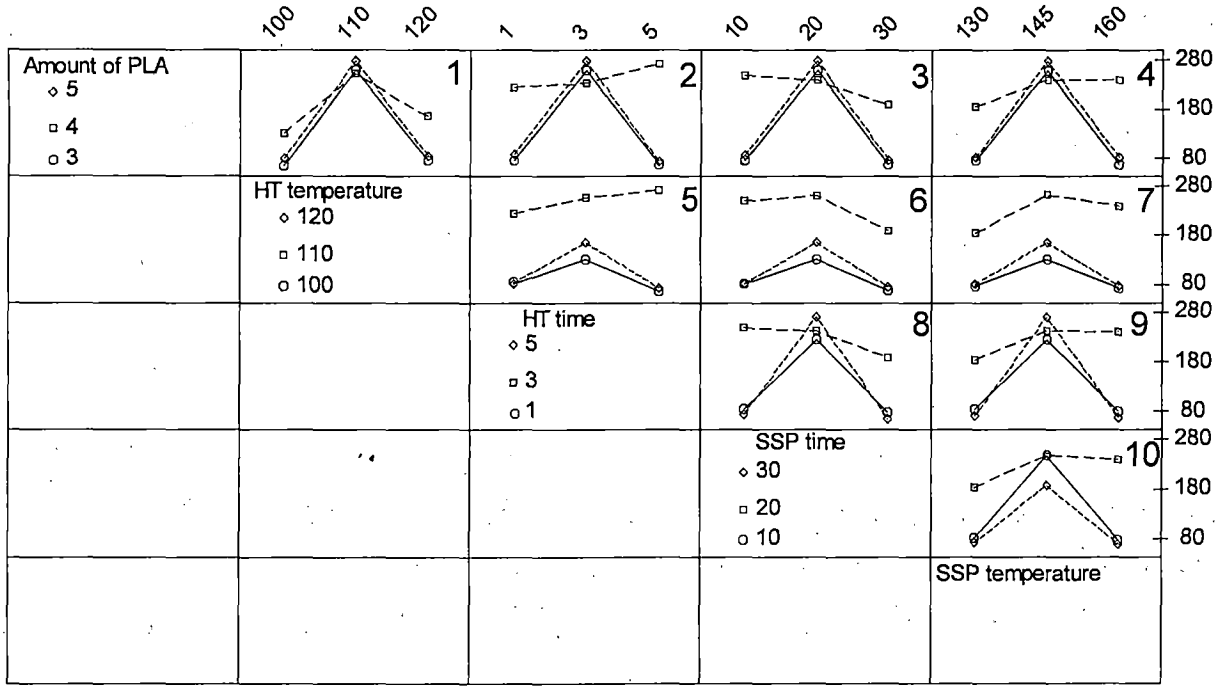

Fig. 4.42 Two-Parameter Interaction plot for M_w of PLA

Table 4.60 Order of magnitude of Severity of 2-parameter interaction for M_w of PLA

2-parameter Interactions	Coefficient Actual	Coefficient Coded	p-value	F value	Order of severity
Amount of PLA and HT temperature	–0.379	–3.7916	0.5400	0.414893	0.00
Amount of PLA and HT time	–8.432	–16.8642	0.2313	1.717749	0.143
Amount of PLA and SSP time	3.832	38.31502	0.0206	8.866752	0.926
Amount of PLA and SSP temperature	–1.019	–15.2892	0.2735	1.41188	0.109
HT temperature and HT time	–0.744	–14.8707	0.2857	1.335645	0.101
HT temperature and SSP time	0.397	39.74502	0.0176	9.540956	1.00
HT temperature and SSP temperature	–0.108	–16.252	0.2470	1.595288	0.129
HT time and SSP time	1.379	27.58439	0.0809	4.154562	0.410
HT time and SSP temperature	–0.903	–27.0824	0.0855	4.004717	0.393
SSP time and SSP temperature	0.182	27.29114	0.0835	4.066697	0.400

The order of magnitude of severity of 2-parameter interaction, calculated by using Eq. 4.17 of Section 4.2.2.6, in ascending order, is given in Table 4.60. Thus, all the five parameters,

as given in Table 4.37, should be considered for SSP reaction to study the proper regulation of various parameters on the yield (wt. %) as well as M_w.

4.3.3 Characterization Studies of PLA synthesized by SSP

In this section, the characterizations of PLA samples, synthesized via SSP, by different analytical techniques such as GPC, FTIR, NMR, thermal analysis, XRD and FESEM are discussed. In this Section detailed characterizations of two PLA samples, PLA S1 and PLA S2, (Table 4.61) one of moderate M_w and the other of high M_w, has been discussed in detail for comparison of their various properties.

4.3.3.1 Molecular weight analysis

The weight average molecular weight (M_w), number average molecular weight (M_n) and molecular weight distribution (MWD) of PLA samples are determined from GPC analysis. The GPC chromatograms of the two PLA samples, one of moderate M_w and the other of high M_w, to be discussed in the present work, are given in Figs. K.24 & K.4 of Appendix K. For the PLA S1 sample, the GPC chromatogram was unimodal, whereas; for the PLA S2 sample, the chromatogram is bimodal. It was also found that most of the high M_w samples produced bimodal GPC chromatograms as can be seen from Appendix-K. The bimodal chromatogram is due to the presence of low molecular weight PLA in association with high molecular weight PLA (Chen *et al.*, 2006). This bimodality arises in PLA samples due to the heterogeneous nature of SSP reaction. The polycondensation of smaller chains occur in a heterogeneous manner and hence most of the high M_w PLAs produced bimodal GPC chromatogram. The detail computational procedure for determination of molecular weight is described in Section 4.2.3.1. The molecular weight and PDI data of above two PLA samples are also available in Table 4.61.

Table 4.61 Molecular weight analysis of PLA using GPC

Polymer	Run No.	M_w kDa	M_n kDa	M_w/M_n PDI
PLA S1	27	97.601	52.965	1.84
PLA S2	15	300.195	178.857	1.68

The PDI value of PLA varies from 1.4 to 2 as expected for a polymer synthesized via polycondensation route (Collins *et al.,* 1973). The M_w, M_n and PDI of all other samples are given in Appendix K.

In case of bimodal GPC chromatograms, the area under the peak corresponding to the low molecular weight fragment is around 10 %, and thus, the weighted average molecular weight of the peak corresponding to the higher M_w is only considered while proceeding for the analysis of experiments. Polymers having a bimodal molecular weight distribution have useful properties. The high molecular weight species imparts higher melt strength properties to the polymer whereas the lower molecular weight species imparts improved processing and melt flow properties to the polymer (White, Donald A. (Keasbey, NJ); US Patent 5578682; 1996).

4.3.3.2 Structure and end-group analysis

The structure of PLA has been determined using FTIR and NMR. And for end group analysis, ^{13}C and ^{1}H NMR are used. In the present study, the presence of end group and residual lactide has been determined using FTIR, whereas; quantification of end group and lactide is carried out using NMR technique.

FTIR analysis

Fig. 4.43 shows the FTIR spectra of PLA samples, PLA S1 and PLA S2. The FTIR spectrum of PLA exhibits characteristic ester absorption peaks at ~1760 cm^{-1} for the stretching vibration of the –COO- group and at ~1090, ~1131, and ~1185 cm^{-1} for the stretching vibration of the C-O-C group. The other characteristic absorption peaks of PLA correspond to the C-H, CH_3 and the O-H groups at ~2997, ~1145, and ~3440 cm^{-1}, respectively (Teng *et al.,* 2004; Achmad *et al.,* 2009). The FTIR spectral interpretation for PLA is reported in Table 4.34 of Section 4.2.3.2.

The FTIR of PLA will exhibit a peak at 1550 cm^{-1} if vinyl end group is present in the sample which is created due to thermal degradation which occurs during polycondensation process. However, in the present samples the above peak (1550 cm^{-1}) is not observed indicating the absence of vinyl end group which also negates the possibility of thermal degradation of the samples. Further, it can be seen that the small absorption peak at 935 cm^{-1} are present in the FTIR spectra due to the presence of the lactide monomer in the sample. The peak at 935 cm^{-1} is

due to the COO ring breathing mode (Braun *et al.*, 2006). Thus, it can be concluded that the PLA samples of present investigation also contained very small amount of residual lactide.

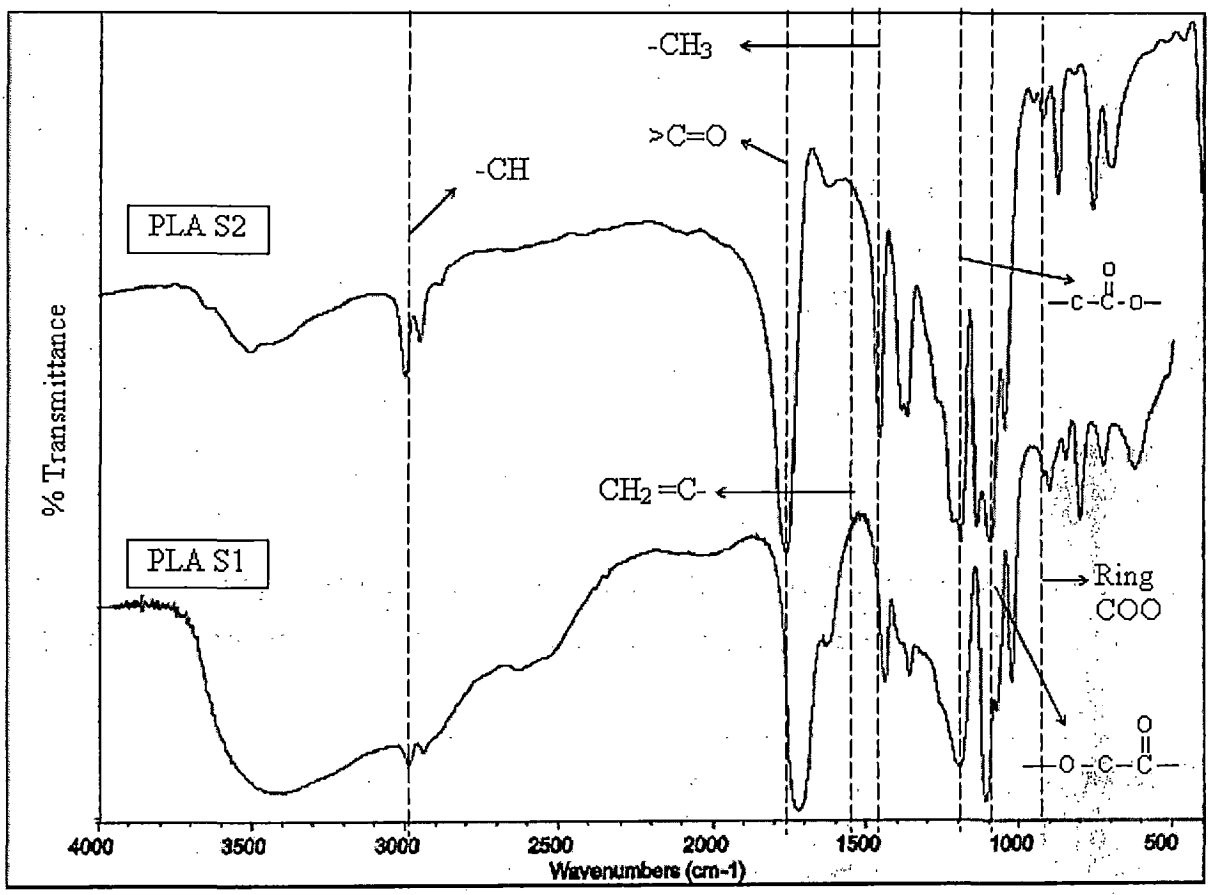

Fig. 4.43 FTIR spectrum of PLA S1 and PLA S2

^{1}H NMR analysis

The ^{1}H NMR spectra of PLA S1 and PLA S2 samples are presented in Fig. 4.44 A and B, respectively. From these figures, it can be observed that both the PLAs produced almost same kind of spectra consisting of mainly three peaks corresponding to the presence of three different kinds of hydrogen atoms in the PLA solution. The details of the origin of these peaks and their chemical shifts are described in Section 4.2.3.2.

The above three peaks are observed around chemical shift, δ (ppm, $CDCl_3$) at 7.25 (s-singlet), 5.15-4.95 (q-quartet, 1H) and 1.60-1.45 (d-doublet, 3H), in the ^{1}H NMR spectra of PLA. The peak at around 7.25 ppm is due to the solvent ($CDCl_3$) in which PLA was dissolved

(Appendix F). The other two peaks around 5.1 ppm and 1.5 ppm are due to the methine (–CH) and methyl ($–CH_3$) groups of PLA, respectively (Ahmed *et al.,* 2009). The peaks corresponding to the acid end group (–COOH: 11.0 ppm) and hydroxyl hydrogen end group (–OH: 2.0 ppm) of PLA are not observed. This is due to the fact that the hydrogen atoms present in above end groups produce very weak signals and are even not observed in the NMR spectrum of lactic acid also (Appendix A), which beyond doubt contains acid (-COOH) and hydroxyl (-OH) end groups. The low intensity peaks for hydrogen present in methyl and methine group of lactic acid is also observed in Figs. 4.44 A & B near the corresponding peaks of PLA present at 1.5 & 5.1 ppm, respectively. These small low intensity peaks near 1.5 and 5.1 ppm are due to presence of very small amount of lactic acid in PLA (Chisolm *et al.,* 2008). The low intensity peaks for hydrogen present in methyl and methine groups of lactide are also observed in Figs. 4.44 A & B around 1.2 & 4.35 ppm, respectively. In NMR, sometimes, satellite peaks are also observed due to the presence of impurity in solvent and the sample, which should not be confused with the peaks originated from the main compound.

The resultant peaks obtained after applying resolution enhancement technique, to the methyl and methine peaks of PLA S1 and PLA S2, are presented in Figs. 4.45 A & B and Figs. 4.46 A & B, respectively. A number of very low intensity peaks to the left and right of the main doublet (Fig. 4.45) and quartet peaks (Fig. 4.46) are observed in the ^1H NMR spectra. These peaks are due to stereodefect present in the PLA polymer chain. The large peaks are due to pure isotactic unit containing L-isomer and the small peaks are due to presence of D-units incorporated randomly in between the L-units and thereby creating stereodefects (Thakur *et al.,* 1997). Thus, it can be manifested that the PLA obtained is predominantly isotactic (Chabot *et al.,* 1983; Thakur *et al.,* 1997).

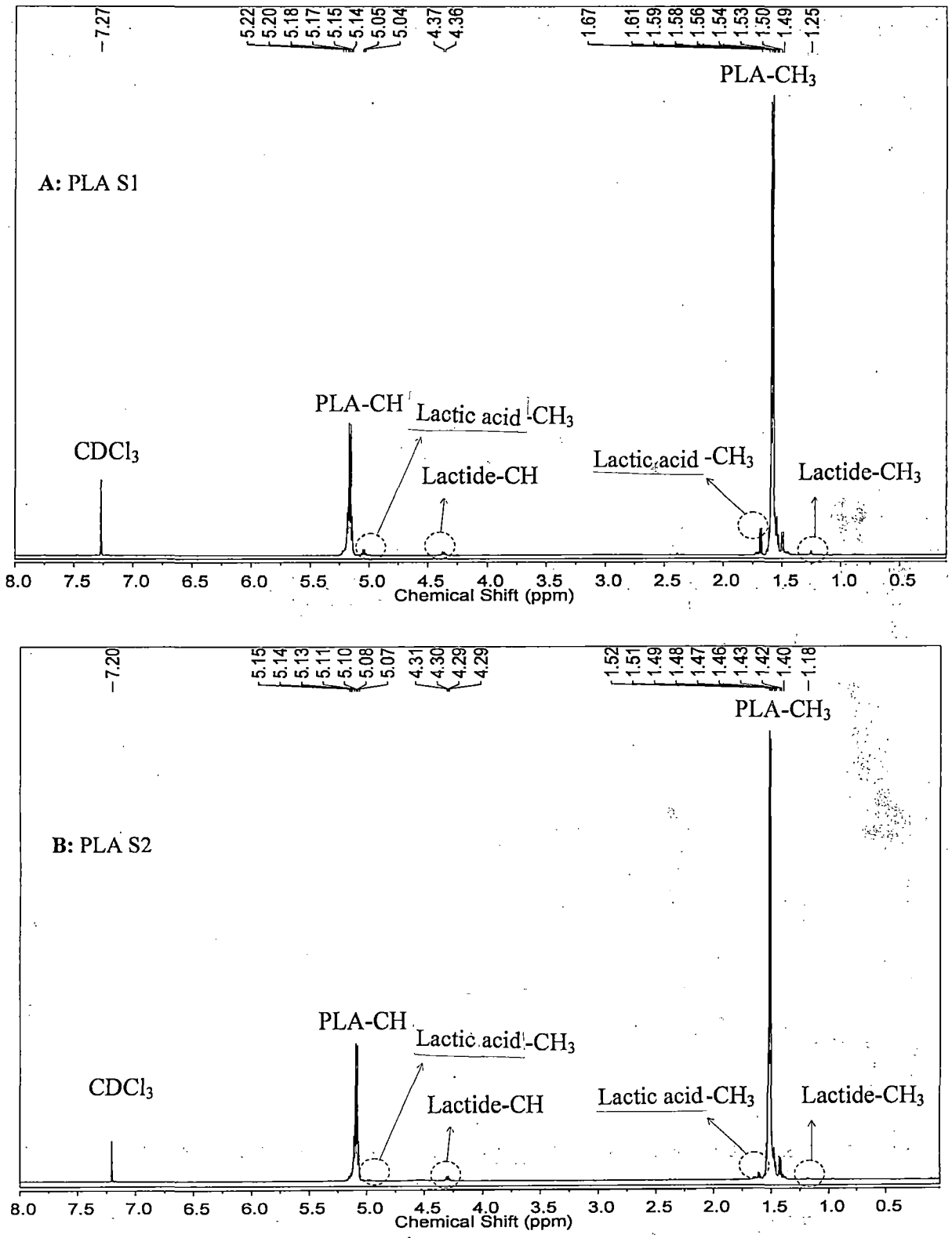

Fig. 4.44 ^{1}H NMR spectra of PLA

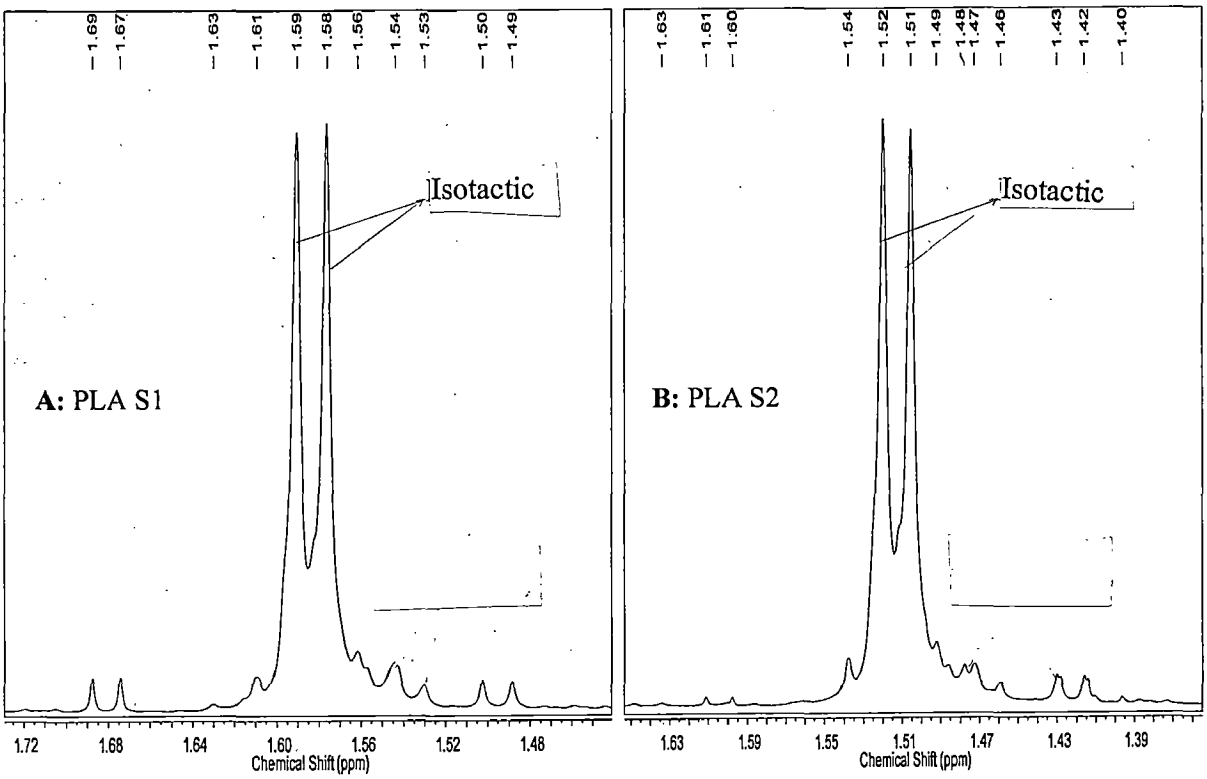

Fig. 4.45 Splitting pattern of methyl peak in.^{1}H NMR spectra of PLA

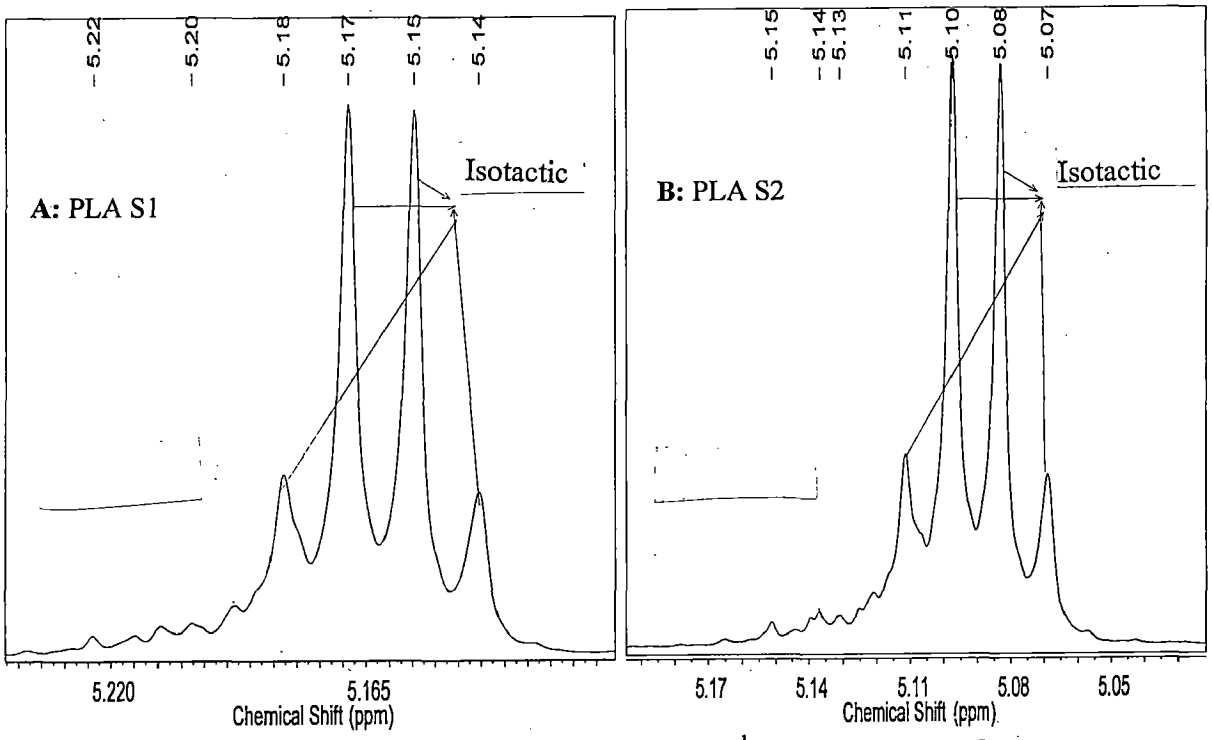

Fig. 4.46 Splitting pattern of methine peak in ^{1}H NMR spectra of PLA

Resolution enhancement technique is also applied to the small peak observed around 4.3-4.4 ppm and is shown in Figs. 4.47 A and B. This peak corresponds to the –CH proton of residual lactide as a doublet of quartet is observed. This is due to the coupling of one –CH proton first with adjacent $-CH_3$ and thus resulting in a quartet which in turn couples with the other –CH proton of the same lactide unit and thus creating a doublet of quartet. Thus, from these figures, the presence of residual lactide in PLA is confirmed. The amount of residual lactide present in PLA is determined from the ratio of area under this peak and the area under the methine peak for lactyl repeat unit of PLA. The percentages of residual lactide are calculated, to be 2.79 % and 4.07 % for PLA S1 and PLA S2, respectively, using the Eq. 4.19 of Section 4.2.3.2.

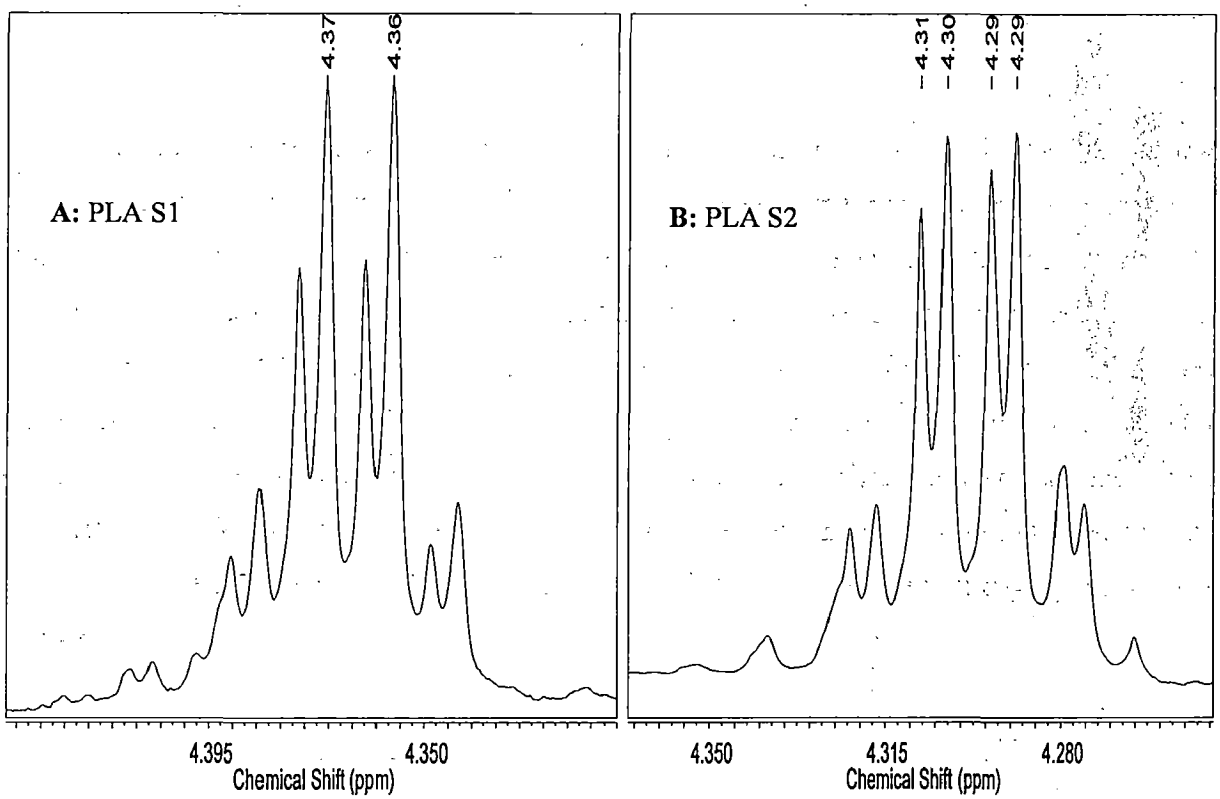

Fig. 4.47 Splitting pattern of end group methine in ^{1}H NMR spectra of PLA

^{13}C NMR analysis

The ^{13}C NMR spectra of PLA S1 and PLA S2 are displayed in Figs. 4.48 A and B, respectively. From these figures, it can be observed that both the PLAs produced almost same

kind of spectral pattern consisting of mainly four peaks corresponding to the presence of four different kinds of carbon atoms in the PLA solution. The four peaks around chemical shift, δ (ppm, $CDCl_3$) 169, 76, 69 and 16 ppm are observed due to the ester, solvent, -CH and $-CH_3$ groups, respectively. These values match well with the reported values by many investigators (Moon *et al.,* 2000, 2001; Chen *et al.,* 2006). However, it can be seen from Figs. 4.48 A and B that, in these PLA samples no peaks are observed around 66 and 20 ppm due to the methine and methyl group of residual lactide or lactic acid present in PLA. This may be due to the fact that all the amount of residual lactide and monomer is very less.

The attempt to detect the fine structure arising from the stereosensitivity in the methyl and methine peaks could not be observed in ^{13}C NMR, as application of resolution enhancement technique to these peaks could not be well resolved because of high noise. However, application of resolution enhancement technique to the ester group, resolves the fine structure of the PLA as represented in Figs. 4.49 A and B. The pattern of ester region is composed of several peaks whose respective intensities depended on the enantiomeric composition of the PLA. A number of very low intensity peaks to the upfield region of the main peak are observed. These peaks are due to stereodefect present in PLA polymer chain. The unique largest peak in downfield region is due to the presence of isotactic unit (Thakur *et al.,* 1997). The small peaks in the up field region are due to the presence of D-units incorporated randomly in between the L-units and thereby creating stereodefects. Thus, it can be manifested that the PLA obtained is predominantly isotactic (Chabot *et al.,* 1983, Thakur *et al.,* 1997).

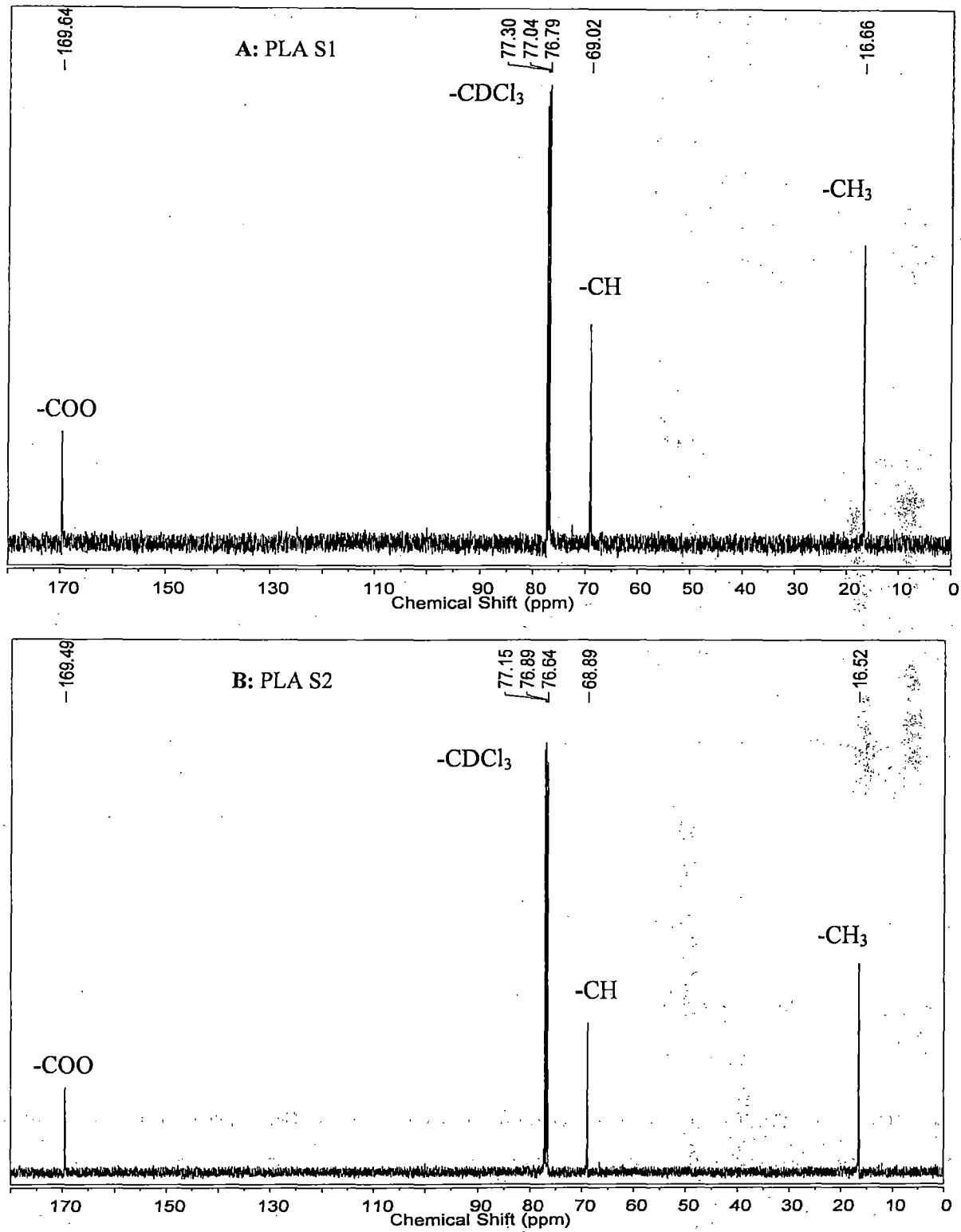

Fig. 4.48 ^{13}C NMR spectra of PLA

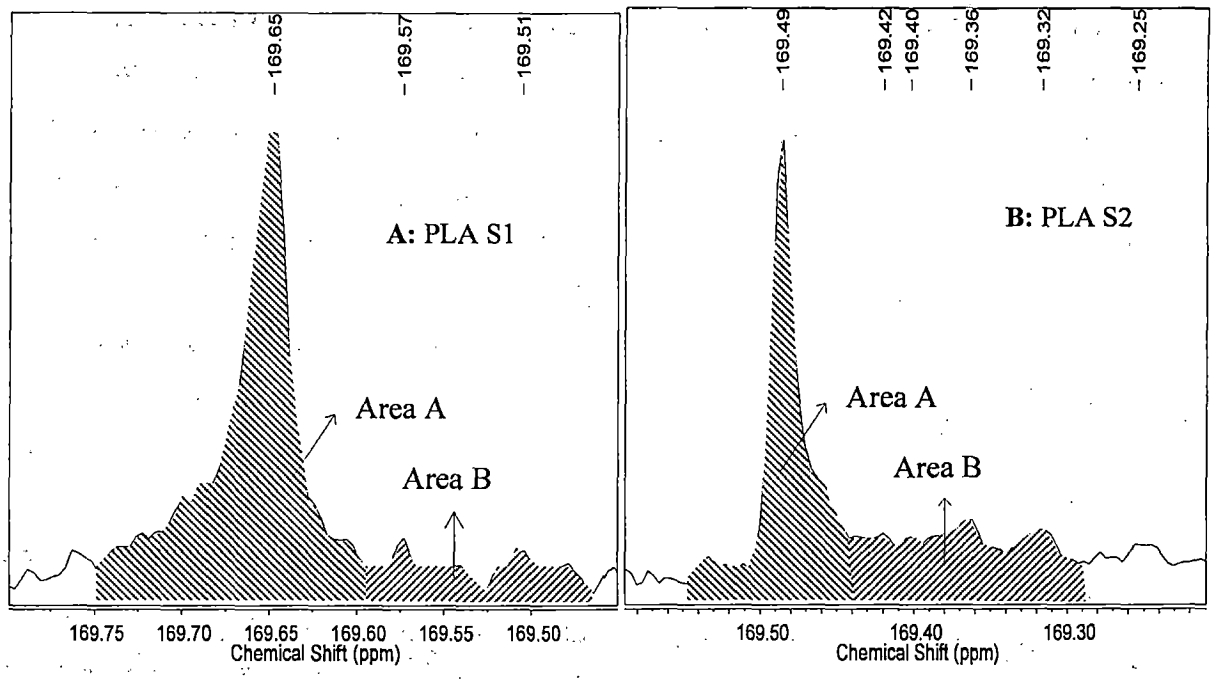

Fig. 4.49 Resolution enhanced ester peak of PLA

From the ^{13}C NMR spectra of PLA samples shown in Figs. 4.48 A and B, it can be seen that no peak is observed for carboxylic acid end functional group at downfield region to ester group. This may be due to the fact that the number of end groups present in PLA is very small for high molecular weight polymers (Shyamroy, 2003; Shyamroy *et al.*, 2005) and is below the detectable limit. Thus, from the above discussion, it can be now safely concluded that the structure of PLA is confirmed from both the FTIR and NMR analysis. The acid end-group present in PLA could not be determined from the ^{13}C NMR spectra.

4.3.3.3 Racemization analysis

The extent of racemization is generally examined using ^{13}C NMR. The high resolution spectrum shown in Figs. 4.49 A and B shows a number of small peaks in addition to one large peak. Presence of these small peaks are due to the presence of D-isomeric units which originate because of racemization occurring during polymerization reaction (Thakur *et al.*, 1997). According to the theoretical stereosequence distribution, the downfield signal around 169.5 ppm (isotactic (i,mm)) is assigned to the sequence of carbonyl carbon atom of successive L-lactic acid units. The peaks in the upfield region at around 169.3 ppm are assigned to the heterotactic

(h, rm) units. And the peaks around 169.2 ppm are assigned to the syndiotactic (s, rr) units present in PLA (Shyamroy, 2003; Chabot *et al.,* 1983; Thakur *et al.,* 1997). From the ratio of area of these peaks as visualized in Fig. 4.49 A and B, the extent of D-lactic acid units in the PLA backbone is determined by using the Eq. 4.20 A of Section 4.2.3.3. Thus, using the Eq. 4.20 A, the extent of D-lactic acid units in the PLA backbone is determined to be 7.80% and 43.86%, for PLA S1 and PLA S2, respectively and is given in Table 4.62. However, ^{13}C NMR spectra of PLA samples showed significantly higher level of noise which made the proper quantification somewhat difficult. Further, the stereo crystallization ratio (Sc ratio) can be determined from XRD pattern by using the Eq. 4.20 B given under Section 4.2.3.3 and are given in Table 4.62.

The racemization reactions are most likely due to a dynamic equilibrium of ester interchange reactions occurring between the polymer chains. During polycondensation reaction, the D-lactic acid units seemed to be incorporated into the backbone in a purely random manner. Randomization of the stereosequences is observed because of the intensive transesterification (Kim and Woo, 2002; Shyamroy, 2003). During the ester interchange reactions, there are two ways in which the ester linkages between successive lactic acid units can cleave and reform. One is acyl–oxygen cleavage, which does not involve the chiral carbon of lactic acid repeat unit. The other is alkyl–oxygen cleavage, in which the covalent bond between oxygen and the chiral carbon breaks and subsequently reforms. This results in an inversion of the configuration.

4.3.3.4 Thermal analysis

TGA, DTG and DSC thermograms of PLA samples are represented in the Figs. 4.50, 4.51 and 4.52, respectively and the original figures are given in Figs. K.22 –K.23 of Appendix K. Four important thermal characteristics of PLAs, namely, glass transition temperature (T_g), crystallization temperature (T_c), melting temperature (T_m), and degradation temperature (T_d) have been measured from TGA, DTG and DSC thermograms and are discussed in this section. The results of the thermal characterization are summarized in Table 4.62.

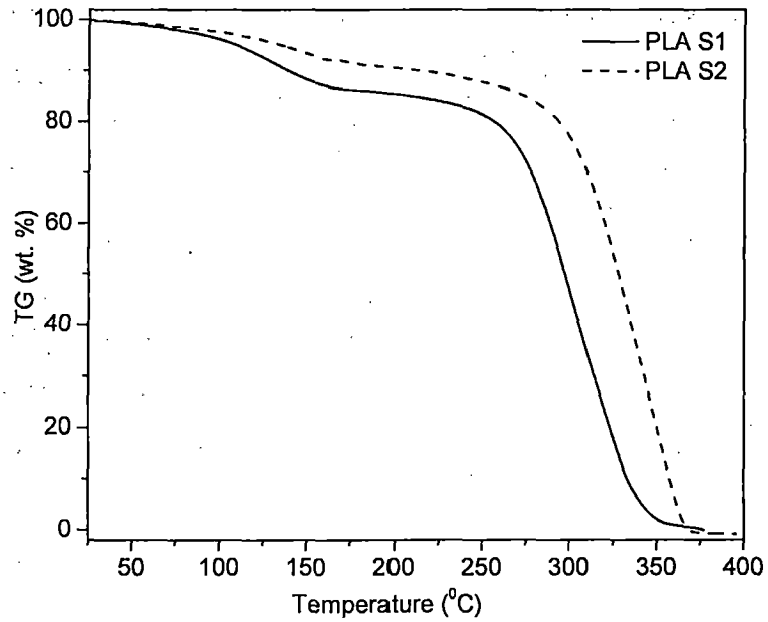

Fig. 4.50 TG thermograms for PLA S1 and PLA S2

Thermal degradation of the polymers was investigated by thermogravimetric analysis (TGA). Thus, from Fig. 4.50, it can be concluded that the PLA S1 is thermally stable up to a temperature of 200°C, whereas; PLA S2 is found to be stable up to 250°C. This may be attributed to the high molecular weight of PLA S2.

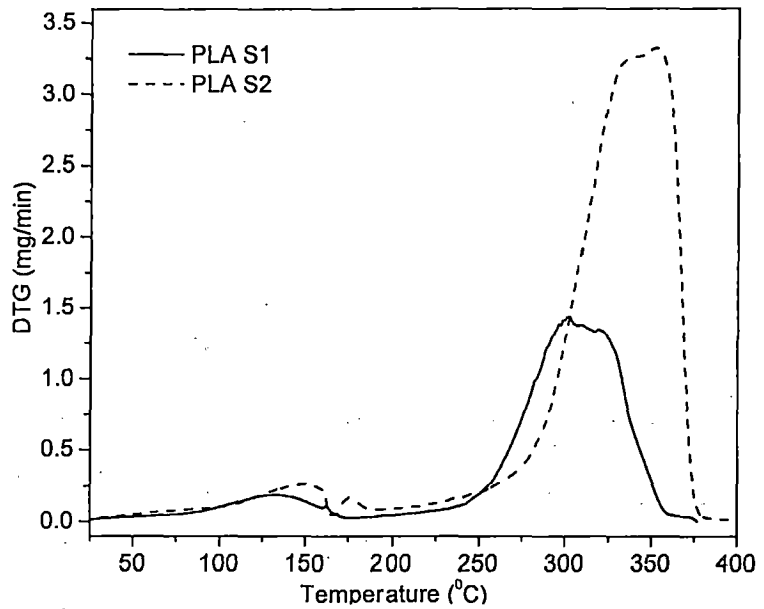

Fig. 4.51 DTG thermograms for PLA S1 and PLA S2

The values of decomposition temperature, T_d, is determined from the DTG thermograms shown in Fig. 4.51 and are given in Table 4.62. It is also seen from the DTG thermograms that T_d increases with the increase in molecular weight of PLA from PLA S1 to PLA S2. The T_g, T_c and T_m are determined from the DSC thermograms shown in Fig. 4.52 and are summarized in Table 4.62. However, T_g and T_c for PLA could not be identified confirming 100 % crystallization has occurred during SSP. During SSP, heat treatment occurs which leads to crystallization of PLA. Thus, T_c could not be identified for the PLA samples obtained from SSP (Moon *et al.*, 2001). The T_m of the PLAs was found to increase with increase in molecular weight as can be evidenced from the Table 4.62. The increase of T_m with prolongation of the SSP time indicates changes of the crystal size and/or perfection along with increase of molecular weight, but the crystal structure (unit cell) probably stays the same as can be comprehensible from the XRD analysis given in Section 4.3.3.5.

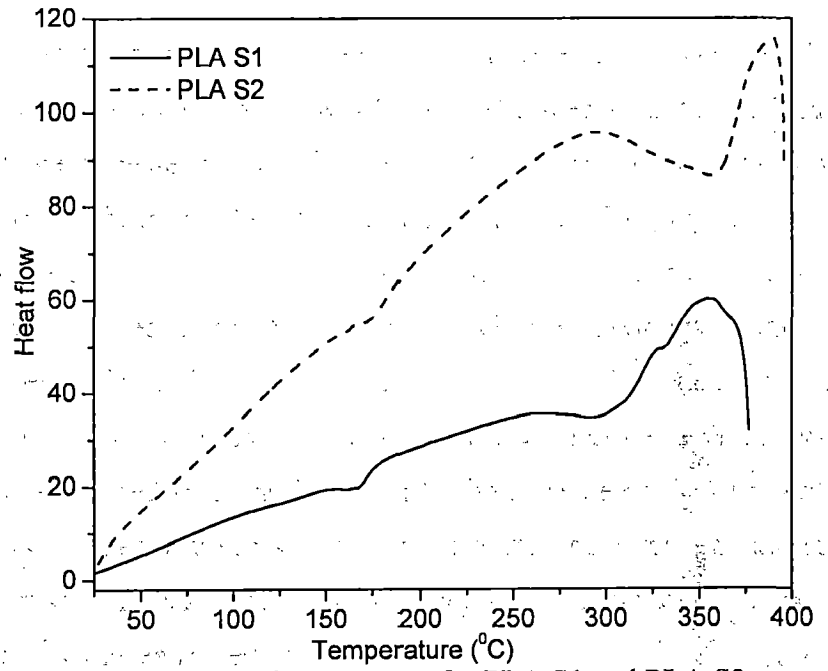

Fig. 4.52 DSC thermograms for PLA S1 and PLA S2

The degrees of crystallinity (X_c) is calculated from DSC thermograms using Eq. 4.21 and are depicted in Table 4.62. The low % X_c could be due to presence of higher amount of D-unit. This is due to racemization of L-LA to D-LA and copolymerization of D- and L-lactic acid units. This observation can be attributed to the racemization of L-lactic acid to D-lactic acid and

its incorporation into the polymer chain. The presence of D-lactic acid unit is also confirmed from NMR spectra and X-ray diffractograms. The higher amount of D-lactic acid units leads to lower % X_c which is substantiated from XRD.

Table 4.62 Thermal characterization and crystallinity values of PLA synthesized by SSP

Polymer	T_g [a] (°C)	T_c [a] (°C)	T_m [a] (°C)	X_c [a] (%)	X_c [b] (%)	T_d [c] (°C)	ΔH_c [a] (mJ/mg)	ΔH_m [a] (mJ/mg)	D-isomer [d] (%)	Sc ratio [b] (%)
PLA-S1	-	-	168	32.21	31.31	303	-	30.5	7.80	11.88
PLA-S2	-	-	176	22.04	21.58	354	-	20.5	43.86	8.45

[a] By DSC instrument; [b] By XRD analysis; [c] By DTG analysis; [d] By ^{13}C NMR

4.3.3.5 XRD analysis

The powder wide angle X-ray diffraction (XRD) pattern of PLA S1 and PLA S2 are shown in Fig. 4.53. The original XRD plots are given in Appendix K. All the diffractograms have almost identical pattern and the most intense peak at 2θ values around 16.5° and the peak intensity is assigned a value of 100 (Brizzolara *et al.,* 1996). This peak is due to reflection from 200 and 110 planes. It can be observed from the XRD pattern that PLA exhibits characteristic peaks at 2 theta values around 15°, 16°, 18.5° and 22.5° due to the presence of L-isomer and peaks at 12°, 21° and 24° due to the presence of D-isomer (Sarasua *et al.,* 1998; Ikada *et al.,* 1987). Thus, it can be concluded that PLA contains both D and L-isomer and the amount of L-lactic acid unit is much higher in comparison to the D-isomer, as the intensity of the peaks corresponding to the L-isomer is very high in comparison to peaks corresponding to D-isomer.

The X-ray diffractograms were analyzed by EVA 2 (version 13.0.0.3) supplied by Bruker AXS, Germany. It was found that the peaks matched well with the patterns obtained for alpha-poly(D(+)lactide) bearing SS-VVV-PPPP number 00-054-1917 (Brizzolara *et al.,* 1996). The matching of XRD of PLA with the standard is shown in Appendix K. The details of the standard are also given in Appendix K. Thus, the PLA crystal was confirmed to have pseudo-orthorhombic space group and it exist in alpha form of 10_3 -helix. The % crystallinity is also calculated from powder X-ray diffractograms (Zhang and Wang, 2008) using Eq. 4.22 and are also depicted in Table 4.62.

The percentage of crystallinity, as determined by DSC and XRD are in agreement with each other. The difference in % crystallinity of PLA polymers examined by a DSC and WAXD method may be because of the fact that the percentage crystallinity and microscopic morphology of PLA vary with its thermal history and stereosequence distribution (Shyamroy *et al.,* 2005; Thakur *et al.,* 1996). By using the Debye-Scherrer formula, given by Eq. B.1 in Appendix B, the crystallite size is found to be ca. 4.07 Å for both PLA S1 and PLA S2.

When a polymer is in the amorphous state, the macromolecular end groups are distributed randomly in the whole polymer matrix while in a semicrystal polymer, the macromolecular end groups are mostly distributed in the amorphous phase and mesophase. Therefore, when PLA prepolymer was crystallized during SSP, the macromolecular end groups are redistributed and result in a rather high concentration of macromolecular end groups in the amorphous phase and mesophase and thereby increases % crystallinity (Xu *et al.,* 2006). This effect of end group's concentration also enhances the apparent rate of SSP of PLA.

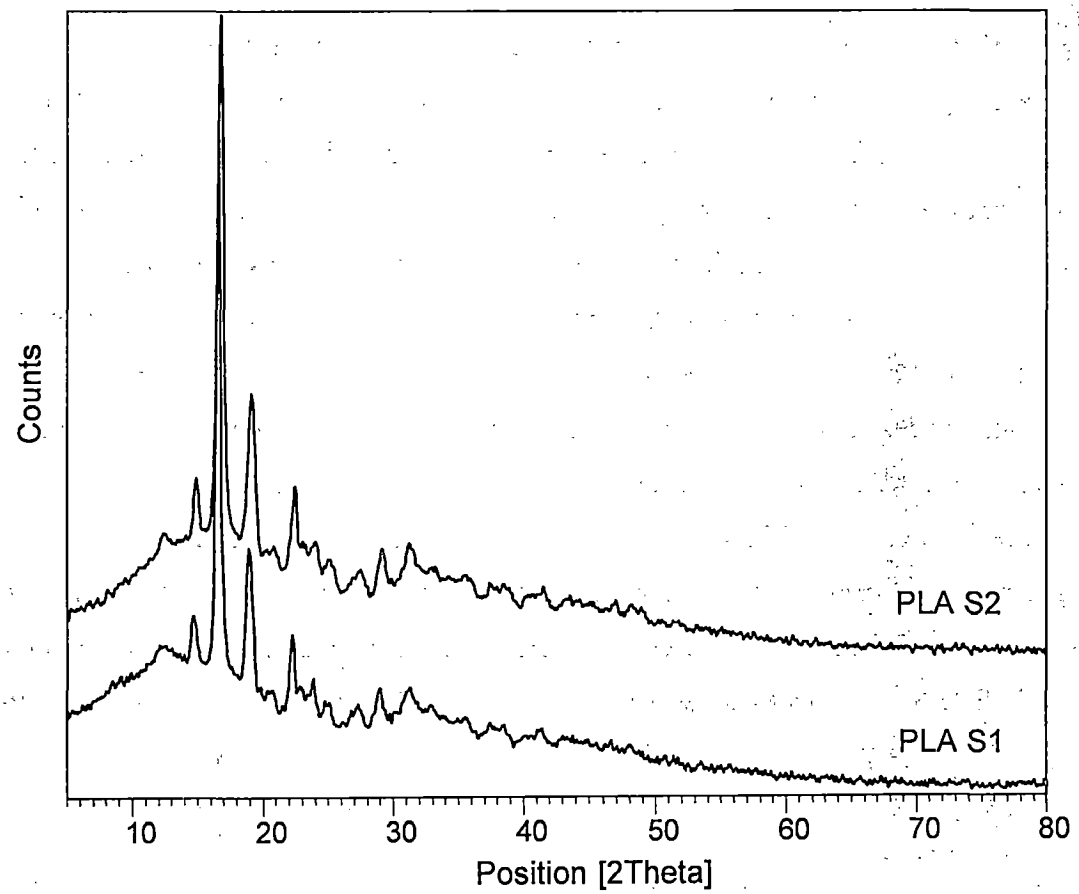

Fig. 4.53 Powder X-Ray diffraction pattern of PLA S1 and PLA S2

4.3.3.6 FESEM analysis

The FESEM image of PLA S1 and PLA S2 are given in Figs. 4.54 A & B. The morphology of PLA is shown to have a porous polymer type surface structure (Gupta *et al.*, 2006). The entangled polymer chains give rise to the porous structure of polymer (Cam *et al.*, 1995). Thus, traces of lactide will tend to be trapped within the polymer matrix. From FESEM, it is also observed that polymer consisted of a series of interconnected channels between fused particles (Ando *et al.*, 2005).

The summary of the different types of instruments used and the type of result obtained from them is given in Table 4.63.

Table 4.63 Instruments used for characterization of PLA

Properties	GPC	FTIR	^{1}H NMR	^{13}C NMR	TGA	DTG	*DSC*	XRD	FESEM
M_w	√								
M_n	√								
PDI	√								
Structure		√	√	√					
End group		√	√	√					
Thermal stability					√				
T_g							√		
T_c							√		
T_m							√		
T_d						√			
ΔH_c							√		
ΔH_m							√		
Racemization		√	√	√				√	
L-isomer presence		√	√	√				√	
D-isomer presence		√	√	√				√	
Lactic acid presence		√	√	√					
Lactide presence		√	√	√				√	
Space group								√	
Crystallite size								√	
% crystallinity							√	√	
Morphology									√

√: Identified by Instrument

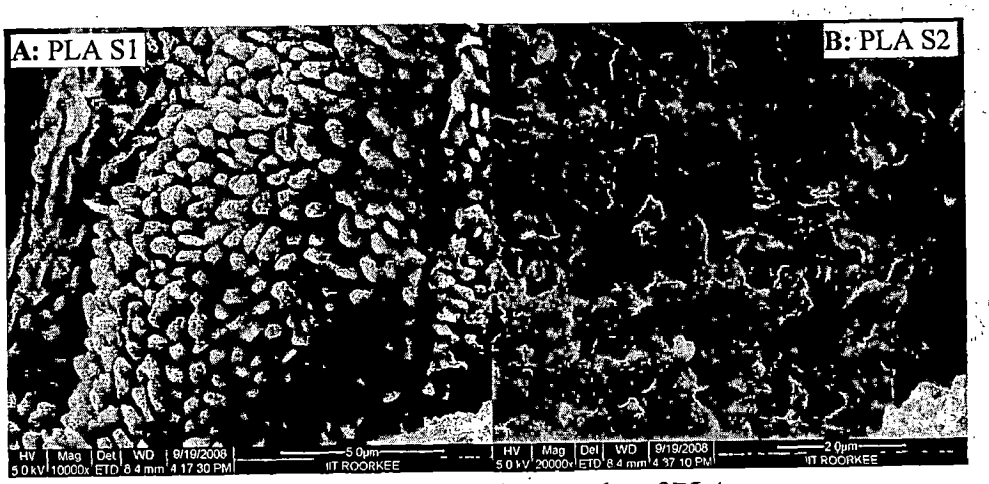

Fig. 4.54 FESEM micrographs of PLA

4.3.4 Mechanism of Solid-State Polycondensation

In the present investigation, solid-state polycondensation is an autocatalytic reaction as no additional catalyst is added during the process. Based on the structural and thermal analyses, a plausible mechanism of SSP of PLA was deduced as shown in Fig. 4.55. The rate of SSP depends on both chemical and physical processes, and the possible rate-determining steps are:

(a) Chemical reaction control: reversible polycondensation and ROP;

(b) Interior diffusion control: diffusion of the volatile reaction products such as lactide and water in the solid PLA;

(c) Surface diffusion control: diffusion of the volatile reaction product from the surface of PLA to the surrounding gaseous atmosphere.

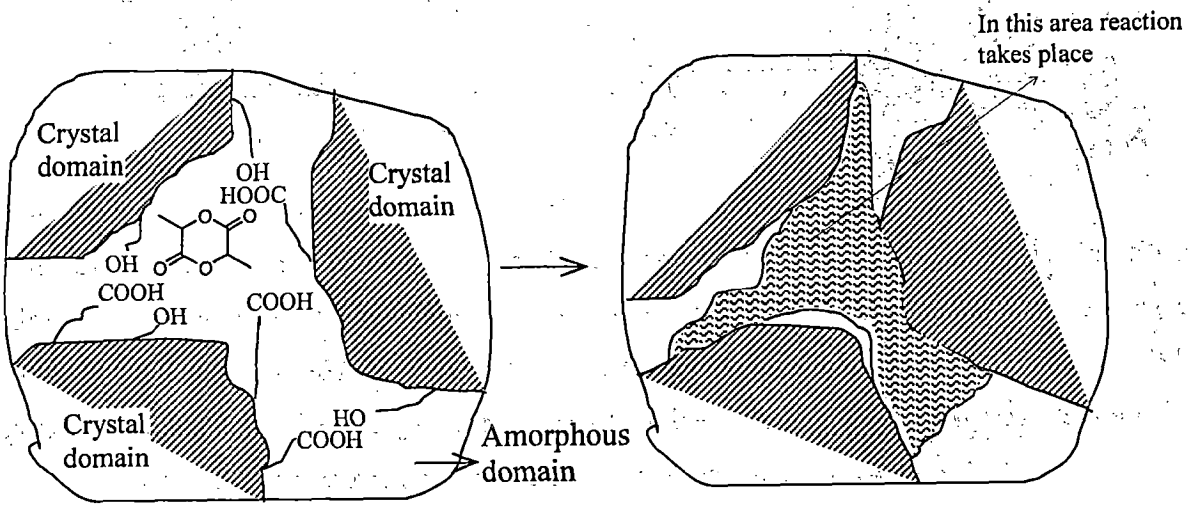

Fig. 4.55 Reaction mechanism of solid-state polycondensation of poly(lactic acid)

The reversible reaction is shown in Fig. 4.28 of Section 4.2. The rate of the polycondensation reaction and diffusion of volatile byproducts in SSP are related to the crystal structure (Xu *et al.*, 2006). During SSP, the polymer is subjected to crystallization.

During crystallization, the polycondensation reaction proceeds in the amorphous phase as the reactive end groups (hydroxy and carboxylic acid groups) are concentrated in the amorphous phase (Shinno *et al.*, 1997; Fukushima *et al.*, 2005; Fukushima and Kimura, 2008) as symbolically depicted in Fig.4.56. Large number of end groups present in amorphous phase enhance the rate of polycondensation. Thus, the concentration of PLA macromolecular end groups in the amorphous region is one of the most important factors that control the rate of SSP. The rate determining step in SSP is mass transport by molecular diffusion (Moon *et al.*, 2001). The mechanism of crystal growth in SSP is conceptualized in Fig. 4.56.

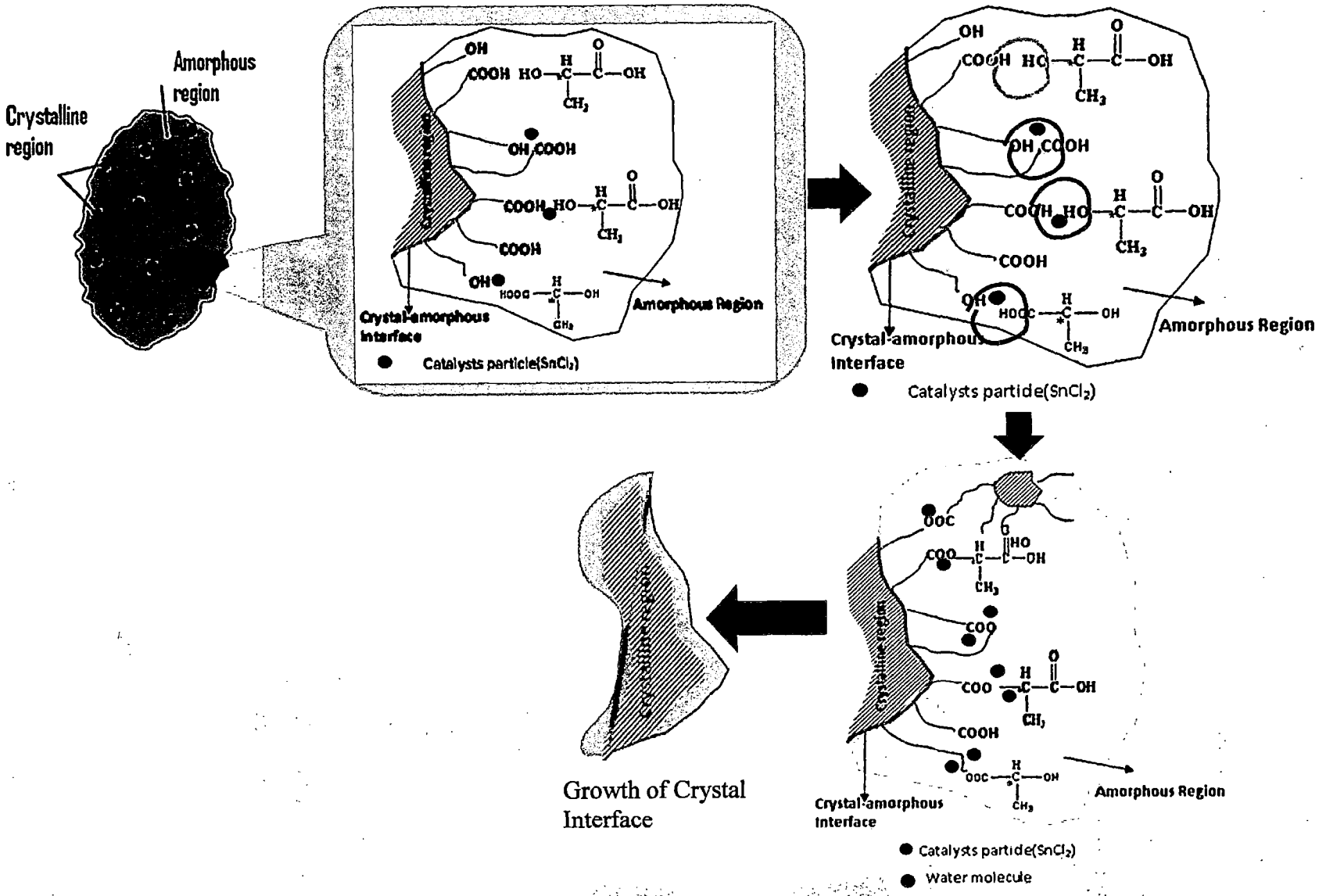

Fig. 4.56 Mechanism of crystal growth during SSP

4.4 PREPARATION OF POLY(LACTIC ACID) NANOPARTICLES BY NANO-PRECIPITATION AND ITS SUBSEQUENT CHARACTERIZATIONS

In the present investigation, PLA nanoparticles (NPs) of a given size range, suitable for the drug delivery system, have been prepared by nanoprecipitation technique - a proven, versatile and flexible technique. Although the preparation of PLA NPs is influenced by eight operating input parameters, four pertinent parameters are selected based on discussion put forward in Section 3.3. The most significant output parameters for PLA NP preparation are yield (wt. %) and size of NPs as these decide value addition and physical and chemical properties of the NPs, respectively. The range and levels of parameters were decided after analyzing the published data in the literature (Legrand *et al.*, 2007, Bilati *et al.*, 2005 and Sussman *et al.*, 2007) and is described in Section 3.3. The range and levels of variation of input parameters, for PLA NP preparation, are given in Tables 3.7 and 3.8. For brevity, a part of this table is reproduced below in Table 4.64. The details of the design of experiment for the present case are described in Section 3.3.

Table 4.64 Input and output parameters involved in PLA NPs preparation

Input Parameters			Level 1	Level 2	Level 3	Level 4	Output Parameters	
Name(s)	Type	Unit					Name(s)	Unit
X_1: Polymer concentration	Numeric	mg/ml	5	10	15	20	Yield	wt. %
X_2: S/NS volume ratio	Numeric	-	0.05	0.20	0.35	0.60	Size of nanoparticles	nm
X_3: Polymer molecular weight	Categoric	kDa	PLAL	PLAH	-	-		
X_4: Solvent (S) type	Categoric	-	Acetone	DMSO	-	-		

PLAL: PLA of M_w 98 kDa; PLAH: PLA of M_w 178 kDa

In the present investigation, the technique of design of experiment (DOE) has been used to develop statistically reliable correlations between input and output parameters with almost minimum number of experiments and is discussed below:

4.4.1 Taguchi Method of Experimental Design (TMED) and its Analysis

The potential of biodegradable polymer-based NPs as drug delivery systems has been extensively investigated in recent years because of their biocompatible nature. For these

applications, the NPs should not only be biodegradable and biocompatible, but also be of controlled diameter and size distribution (Legrand *et al.,* 2007). Thus, in the present investigation, an attempt was made to prepare PLA NPs of controlled diameter by applying statistical design of experiments, so that reliable correlation could be developed for proper regulation of effects of various parameters to get the desired output parameters. Well planned and designed experiments are powerful over the traditional approach, of varying one-factor-at-a-time (OFAT), to experimentation. OFAT is unreliable, not cost-effective and may lead to false optimal conditions. In the present case, the case study was carried out by adopting the ten steps of Taguchi's parameter design methodology, as described in the literature review (Chapter 2) under Section 2.7. The present case study illustrates the application of Taguchi Method of Experimental Design (TMED) for the development of PLA NPs. TMED seems to be the natural selection, since it is quite easy to understand. TMED produces a special set of orthogonal arrays and hence can also be called Taguchi orthogonal array design (TOAD). Taguchi orthogonal arrays (OAs) are practical, simple and have been widely published (Chen *et al.*, 2004; Jahanshahi *et al.,* 2008). It is also important to achieve the objective of the experiment using minimum budget and resources. TOAD allows analyzing many factors with few runs. Thus, in the present study, TOAD was applied to optimize the operating conditions for yield (wt. %) and size of PLA nanoparticles. The ten step methodology of TMED is given in a step-by-step manner as follows:

Step 1: The problem for the present case is recognized and formulated. The objective of the present work is to prepare PLA nanoparticles of smaller size with higher yield (wt. %). Thus, it is of utmost importance to sort out which design parameters affect the size and yield (wt. %) of PLA NPs and also what is the optimal condition to achieve the desired particle size and yield (wt. %).

Step 2: The quality characteristics, the response, also called output parameters, are selected. For the present case, the quality characteristics are size of nanoparticles and yield (wt. %).

Step 3: Four design parameters, can also be called operating parameter or input parameter, are identified as already described in Section 3.3.

Step 4: The design parameters are classified into control, noise and/or signal parameters. However, in the present case, all the four design parameters are classified as control parameters. No noise or signal parameters could be identified.

Step 5: The levels and ranges of the design parameters for the experimentation are determined, which are given in Table 4.64.

Step 6: Interactions between input parameters should be identified. Interaction occurs when the effect of one input parameter, on the output parameter, is different at different levels of the other input parameter. However, interactions between input parameters could not be identified from the published literature.

Step 7: The selection of an orthogonal array (OA) depends on the objectives of the experiment and of course cost and time constraints. Further, depending on the levels and number of input parameters, a 16-trial experiment [L_{16} (4**2, 2**2) OA] was considered, as it seems to be the most suitable design, by the use of Minitab software (version 13.0). Amongst the four input parameters, two input parameters namely, PLA concentration and S/NS volume ratio are varied at four levels and the other two input parameters namely "molecular weight of PLA' and "solvent type" are varied at two levels thus, producing a combination of sixteen runs of experiments.

Step 8: Experiments are conducted based on the chosen experimental layout, as given in Table 3.9. The results of the experiments, the yield (wt. %) and nanoparticle (NP) size, corresponding to each experimental trial condition, are presented in Table 4.65.

Step 9: Statistical analysis was carried out using Minitab software, using data provided in Table 4.65. An ANOVA was performed to establish the relative significance of the individual parameters. The statistical analysis for yield (wt. %) and size of NPs are discussed in Section 4.4.1.1 to 4.4.1.4. The "*main effect*" (effect of an input parameter on the output parameter) and "*interaction effect*" (effect of an input parameter on the output parameter in presence of another input parameter) are discussed in detail in Section 4.4.3. The optimal condition for getting smaller sized NPs with higher yield (wt. %) was also obtained which will be discussed in Section 4.4.2.

Step 10: Finally, two confirmatory experiments have been carried out to verify the optimal settings of input parameters.

Table 4.65 Size and yield (wt. %) of NPs obtained for the complete set of 16 experimental runs

Run. No.	PLA conc. (mg/ml)	S/NS volume ratio	M_w of PLA	Solvent	Yield (wt. %)	NP size (nm)	SNR(db) Yield	SNR(db) NP size
1	5	0.05	PLAL	Acetone	86.3	134	38.7222	-42.5421
2	5	0.20	PLAL	Acetone	89.9	111	39.0742	-40.9065
3	5	0.35	PLAH	DMSO	52.4	220	34.3916	-46.8485
4	5	0.60	PLAH	DMSO	46.6	228	33.3752	-47.1587
5	10	0.05	PLAL	DMSO	75.9	113	37.6071	-41.0616
6	10	0.20	PLAL	DMSO	78.5	109	37.8919	-40.7485
7	10	0.35	PLAH	Acetone	66.7	125	36.4786	-41.9382
8	10	0.60	PLAH	Acetone	52.9	342	34.4642	-50.6805
9	15	0.05	PLAH	Acetone	34.6	221	30.7941	-46.8878
10	15	0.20	PLAH	Acetone	39.5	160	31.9407	-44.0824
11	15	0.35	PLAL	DMSO	37.8	140	31.5452	-42.9226
12	15	0.60	PLAL	DMSO	33.7	270	30.5655	-48.6273
13	20	0.05	PLAH	DMSO	27.6	221	28.8150	-46.8878
14	20	0.20	PLAH	DMSO	33.6	353	30.5345	-50.9555
15	20	0.35	PLAL	Acetone	28.6	302	29.1152	-49.6001
16	20	0.60	PLAL	Acetone	26.0	335	28.2928	-50.5009

4.4.1.1 TMED analysis for yield (wt. %)

TMED suggests the use of signal to noise ratio (SNR) to carry out the complete analysis of experiments including interaction effects. The selection of SNR can be done based on discussion given in Chapter 2 under Section 2.7. The objective of the present investigation is to produce PLA NPs with higher yield (wt. %). Thus, "larger the better" signal to noise ratio (SNR) is the best approach for analysis of yield (wt. %) data given in Table 4.65. Based on the preceding concept, the values of SNR for each experimental run is computed using Eq. 2.4 of Section 2.7 and these are given in Table 4.65.

A "*main effect*" is said to be present, when different levels of an input parameter affect the output parameter differently; and is most useful when effect of several input parameters are to be studied. The "*main effect*" plot for the SNR for yield (wt. %) is shown in Fig. 4.57. Horizontal line (parallel to the *x*-axis) of a particular input parameter in the "*main effect*" plot represents the absence of "*main effect*" for that input parameter and vice versa. It can be seen from Fig. 4.57 that for the input parameters with two levels, such as molecular weight of PLA and solvent type, SNR of one level increases from the mean compared to the other level. This difference attributes to the "*main effect*". And in case of the input parameters with more than

two levels (denoted by dots on the plot or can be seen from Table 4.64), such as concentration of PLA and S/NS volume ratio, the difference between the maximum and minimum SNR shows the presence of the "*main effect*".

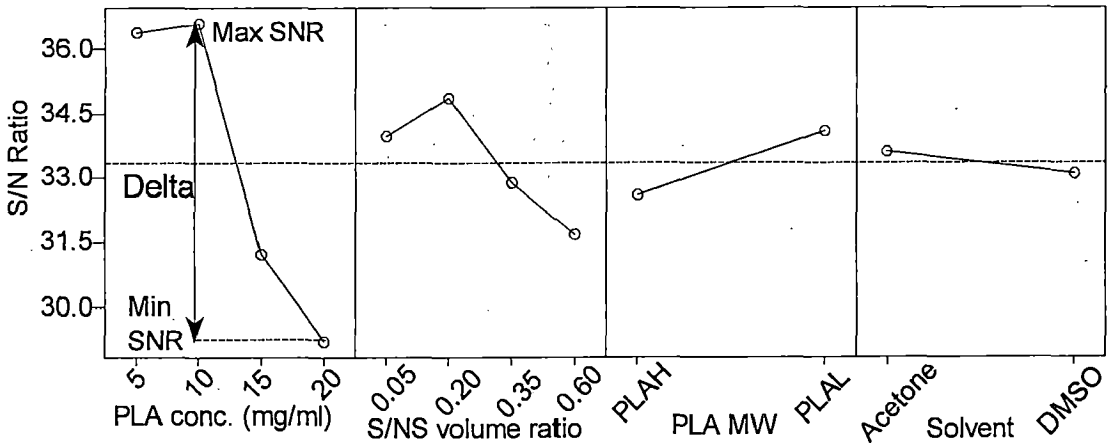

Fig. 4.57 "*Main effect*" plots of SNR for yield (wt. %)

In short, if the difference in the vertical positions of the lowest and highest plotted points, is greater, then the magnitude of the "*main effect*" is greater. In the present case, it can be observed from Fig. 4.57 that with the increase in concentration of PLA and S/NS volume ratio, the SNR is first increasing and then decreasing. However, when molecular weight of PLA (PLA MW) decreases, SNR increases. It is observed that solvent acetone produces larger SNR in comparison to DMSO. Thus, from Fig. 4.57, it can be observed that all the four input parameters have some impact (increasing or decreasing) on the SNR.

Further, it can also be seen from Fig. 4.57, that the plot denoting the effect of PLA concentration has largest delta value (difference between maximum and minimum SNR values that is achieved when the input parameters varies from it's lowest to highest level) indicating that it is the most influential input parameter amongst all input parameters (Montgomery, 2004). The delta value for a particular input parameter is calculated using the Eq. 4.31.

$$D=Delta=SNR_{max}-SNR_{min} \quad ...(4.31)$$

The extent of influence of a particular input parameter on yield (wt. %) is reported in terms of its rank in Table 4.66, which is computed based on delta values. For the present case, the rank of parameters can be given as: PLA concentration (Rank 1) > S/NS volume ratio > PLA MW > Solvent (Rank 4). From the SNR response graph (Fig. 4.57) for yield (wt. %), the

optimum levels of input parameters are estimated as: polymer concentration (10 mg/ml), S/NS volume ratio (0.2), PLAL and acetone. At these optimum levels the corresponding values of SNR value is maximum.

Table 4.66 Response table for SNR values for yield (wt. %)

Level	SNR values for			
	PLA concentration	S/NS volume ratio	PLA MW	Solvent
1	36.3908	33.9846	32.5992	33.6102
2	36.6104	34.8603	34.1018	33.0908
3	31.2114	32.8827		
4	29.1894	31.6744		
Delta	7.4211	3.1859	1.5025	0.5195
Rank	1	2	3	4

4.4.1.2 TMED analysis for size of nanoparticles

The objective of the present work is to prepare smaller PLA nanoparticles (NPs) with higher yield (wt. %). Thus, "smaller the better SNR" is the best approach for the analysis of nanoparticle size data, given in Table 4.65. Based on the preceding concept, the values of SNR for each experimental run is computed using Eq. 2.5 of Section 2.7 and these are given in Table 4.65. The "*main effect*" plot for the SNR for size of PLA NPs is shown in Fig. 4.58. It can be observed from Fig. 4.58 that with the increase in concentration of PLA and S/NS volume ratio, the absolute value of SNR is first decreasing and then increasing. However, when molecular weight (MW) of PLA decreases, absolute value of SNR decreases. It is also observed from Fig. 4.58 that absolute value of SNR is larger for the solvent acetone in comparison to DMSO.

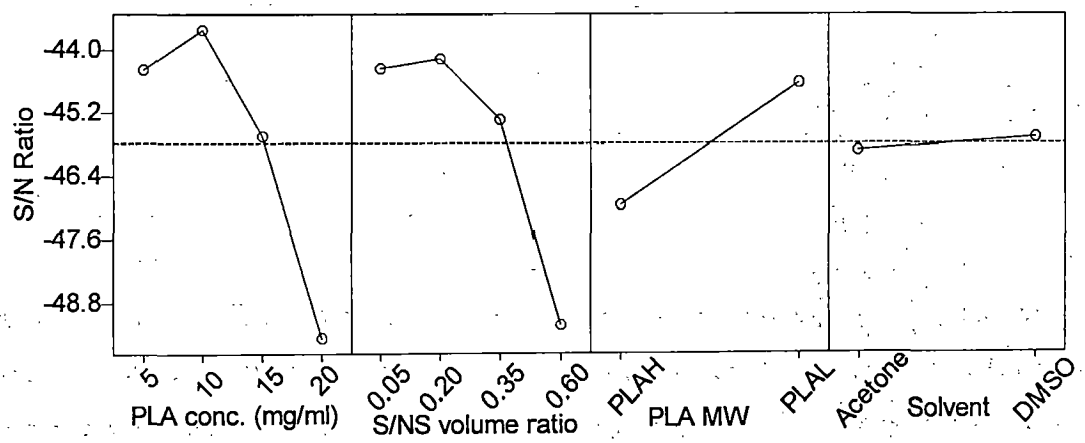

Fig. 4.58 "*Main effect*" plots of SNR for size of nanoparticles

As none of the plots representing "*main effect*" are parallel to the x-axis, it confirms the presence of "*main effect*" for all input parameters. Further, it can also be seen from Fig. 4.58, that the plot denoting the effect of PLA concentration has largest delta value indicating that it is the most influential input parameter amongst all input parameters (Montgomery, 2004). The extent of influence of a particular input parameter on size of NPs is reported in terms of its rank given in Table 4.67, which is computed based on delta values calculated using Eq. 4.31. For the present case, the rank of input parameters can be given as: PLA concentration (Rank 1) > S/NS volume ratio > PLA MW > Solvent (Rank 4). From the SNR response graph (Fig. 4.58) for size of NPs, the optimum levels of input parameters are estimated as: polymer concentration (10 mg/ml), S/NS volume ratio (0.2), PLAL and DMSO. At these optimum levels the corresponding absolute values of SNR is minimum.

Table 4.67 Response Table for SNR values for size of nanoparticles

Level	SNR values for			
	PLA conc.	S/NS volume ratio	PLA MW	Solvent
1	-44.3639	-44.3448	-46.9299	-45.8923
2	-43.6072	-44.1732	-44.6137	-45.6513
3	-45.6300	-45.3273		
4	-49.4861	-49.2418		
Delta	5.8789	5.0686	2.3162	0.2410
Rank	1	2	3	4

4.4.1.3 Regression analysis and ANOVA for yield (wt. %)

In the present investigation, for the preparation of PLA NPs, two continuous parameters namely PLA concentration and S/NS volume ratio; and two categorical parameters namely molecular weight of PLA and type of solvent are involved. Thus, simple regression analysis cannot be applied to this process. Therefore, it is necessary to create special variables to represent the class of the categorical parameters. The simplest and most common method of treating categorical input parameters is by inducting *dummy variables. Dummy variables* are also called *binary variables* as these are coded as one or zero. If an observation is classified as a member of a particular category, then the respective *dummy variable* is coded as *one* otherwise it is coded as *zero*. Further, for a categorical parameter with *n* levels, *n dummy variables* are created however; the regression equation which is formed contains n-1 independent *dummy variables*. This is, because of the fact, that if both the *dummy variables* of the particular category

are considered during regression, then it is not possible to obtain unique estimates of the various input parameters as both the *dummy variables* are perfectly collinear (Gujarati D, 1999), i.e., one of them has a relationship with the other. In the present case, the two categories of the categorical parameter PLA MW and solvent are represented by 0 and 1 as given in Table 4.68. In the present case, D_1 and D_3 are taken in the data matrix table during regression (Taguchi *et al.*, 2005). The category that is assigned the value of *zero* is referred to as the *base/bench mark/control/comparison/omitted category*. In the present study, this category will be referred to as *base category* throughout the text. Thus, in the present case, the comparisons of the models will be made w.r.t. the *base category* PLAL for "PLA MW" and DMSO for "solvent".

Table 4.68 Representation of *Dummy variables*

Category (PLA MW)	D_1	D_2	Category (Solvent)	D_3	D_4
PLAH	1	0	Acetone	1	0
PLAL	0	1	DMSO	0	1

Further, it is a pre-requisite that as all the input parameters used for the development of correlations should be independent of each other, therefore, before proceeding for the regression analysis, it is felt necessary to know about the correlations between the input parameters. The correlation coefficients obtained through the analysis provided an indication of the extent of relation between one input parameter to other. The correlation coefficients between different input parameters are represented in Table 4.69. The value of correlation coefficients ranges from –1 (perfectly inverse relationship) to +1 (perfectly direct relationship). A value of 0 indicates no linear relationship. From the Table 4.69, it can be observed that no correlationship exists between the input parameters as the corresponding entries are zero. Thus, the regression analysis can be applied to get the desired relationship between the input and output parameters.

Table 4.69 Correlation analysis of the input parameters

	X_1	X_2	X_3	X_4
X_1: Polymer concentration	1			
X_2: S/NS volume ratio	0	1		
X_3: Polymer molecular weight	0	0	1	
X_4: Solvent (S) type	0	0	0	1

Generally, additive models are being used in Taguchi method for the regression analysis. The additive model refers to the sum of individual effects of input parameters along with their interaction parameters. Thus, after converting the categorical input parameters into *dummy variables*, regression analysis was applied to the yield (wt. %) data presented in Table 4.65. The regression equation thus obtained, by using all input parameter terms and their interaction terms, is given in Eq. 4.32. The ANOVA of regression analysis is given in Table 4.70. The correlation coefficients "R-square", "adjusted R-square" and "predicted R-square" are 95.6%, 86.8% and 61.87%, respectively. The model p-value is 0.008, which shows the model is significant.

$$Y_i = 140 - 26.4*X_1 - 11.0*X_2 - 55.0*D_1 - 25.0*D_3 + 1.46*X_1*X_2 + 13.3*X_1*D_1 + 0.86*X_1*D_3 + 3.32*X_2*D_1 + 9.05*X_2*D_3 + 7.15*D_1*D_3 \quad \ldots (4.32)$$

However, using Eq. 4.32, four different kinds of correlations can be obtained based on the four different possible combinations of *dummy variables*, which are given through Eqs. 4.33 - 4.36.

Yield (wt %) when PLAL and DMSO used:

$$Y_i (D_1=0, D_3=0, Xi) = 140 - 26.4*X_1 - 11.0*X_2 + 1.46*X_1*X_2 \quad \ldots (4.33)$$

Yield (wt %) when PLAH and DMSO used:

$$Y_i (D_1=1, D_3=0, Xi) = 85 - 13.1*X_1 - 7.68*X_2 + 1.46*X_1*X_2 \quad \ldots (4.34)$$

Yield (wt %) when PLAL and Acetone used:

$$Y_i (D_1=0, D_3=1, Xi) = 115 - 25.54*X_1 - 1.95*X_2 + 1.46*X_1*X_2 \quad \ldots (4.35)$$

Yield (wt %) when PLAH and Acetone used:

$$Y_i (D_1=1, D_3=1, Xi) = 67.15 - 12.24*X_1 + 1.37*X_2 + 1.46*X_1*X_2 \quad \ldots (4.36)$$

Where,

Y_i =Yield (wt %)

X_1=PLA concentration,

X_2 = S/NS volume ratio,

D_1= PLA MW, and

D_3= Solvent.

These conventions will also be followed now onwards in the text. Further, it can be observed from Eq. 4.33-4.36 that the intercept changes remarkably from the correspodning Eq. 4.33 for

the *base category*. Further, the coefficients of X_1 and X_2 also found to change, depending on the category chosen and thus, confirms the presence of interaction between input parameters (Gujarati D, 1999; Taguchi *et al.*, 2005).

Table 4.70 ANOVA of regression analysis for Eq. 4.32

Predictor	Coef	SE Coef	T	P	Significance
Constant	140.02	28.55	4.90	0.004	Significant
PLA concentration	-26.38	13.86	-1.90	0.115	Insignificant
S/NS volume ratio	-10.98	10.24	-1.07	0.333	Insignificant
PLA MW	-55.05	36.78	-1.50	0.195	Insignificant
Solvent	-25.03	24.26	-1.03	0.350	Insignificant
PLA concentration*S/NS volume ratio	1.458	3.578	0.41	0.700	Insignificant
PLA concentration* PLA MW	13.30	12.22	1.09	0.326	Insignificant
PLA concentration* Solvent	0.859	8.000	0.11	0.919	Insignificant
S/NS volume ratio* PLA MW	3.323	7.332	0.45	0.669	Insignificant
S/NS volume ratio* Solvent	9.054	4.800	1.89	0.118	Insignificant
PLA MW* Solvent	7.148	8.000	0.89	0.413	Insignificant

It can be observed from Table 4.70 that all the model terms are insignificant, although the "R-square", "adjusted R–square" and "predicted R-square" values are much higher, although the model p-value is significant. Thus, the insignificant terms are removed one-by-one in a step-wise manner, to produce a better regression equation. After removing the insignificant terms, the regression equation obtained is given by Eq. 4.37. The ANOVA of regression analysis is given in Table 4.71.

$$Y_i = 129 - 23.3*X_1 - 6.59*X_2 - 43.2*D_1 - 21.0*D_3 + 12.2*X_1*D_1 + 10.3*X_2* D_3 \quad \ldots (4.37)$$

However, using Eq. 4.36, four different kinds of correlations can be obtained based on the four different possible combinations of *dummy variables*, which are given in Eqs. 4.38 - 4.41.

Yield (wt %) when PLAL and DMSO used:

$$Y_i (D_1=0, D_3=0, Xi) = 129 - 23.3*X_1 - 6.59*X_2 \quad \ldots (4.38)$$

Yield (wt %) when PLAH and DMSO used:

$Y_i (D_1=1; D_3=0, Xi) = 85.8 - 11.1*X_1 - 6.59*X_2$ ... (4.39)

Yield (wt %) when PLAL and Acetone used:

$Y_i (D_1=0, D_3=1, Xi) = 108 - 23.3*X_1 + 3.71*X_2$ ... (4.40)

Yield (wt %) when PLAH and Acetone used:

$Y_i (D_1=1, D_3=1, Xi) = 64.8 - 11.1*X_1 + 3.71*X_2$ ... (4.41)

Further, it can be concluded from Eqs. 4.38-4.41 that the intercept changes remarkably from the corresponding Eq. 4.38 for the *base category*. Further, the coefficients of X_1 and X_2 also found to change, depending on the category chosen and thus, confirms the presence of interaction between input parameters (Gujarati D, 1999; Taguchi *et al.,* 2005). The correlation coefficients "R-square", "adjusted R-square" and "predicted R-square" are 94.5%, 90.9% and 85.93%, respectively. The model p-value is 0.000, which shows the model is significant.

Table 4.71 ANOVA of regression analysis for Eq. 4.37

Predictor	Coef	SE Coef	T	P	Significance
Constant	129.445	8.324	15.55	0.000	Significant
PLA concentration	-23.310	2.953	-7.89	0.000	Significant
S/NS volume ratio	-6.592	2.953	-2.23	0.052	Significant
PLA MW	-43.22	12.79	-3.38	0.008	Significant
Solvent	-21.013	8.740	-2.40	0.040	Significant
PLA concentration* PLA MW	12.155	4.942	2.46	0.036	Significant
S/NS volume ratio* Solvent	10.320	3.235	3.19	0.011	Significant

It can be observed from Table 4.71 that PLA concentration, S/NS volume ratio, molecular weight of PLA and type of solvent are significant input parameters and also the interaction terms such as, "PLA concentration*PLA MW" and "S/NS volume ratio*Solvent" are significant. The "R-squared", "adjusted R-squared" and "predicted R-squared" values are much higher and are in reasonable agreement with each other. The model p-value is also significant. Thus, the regression model given by Eq. 4.37 is considered to be the best model for prediction of yield (wt. %). Further, it can also be concluded that Eq. 4.37 offers 85.93 % [predicted R-

Square] of the variability in predicting new obsevations in comparision to approximately 94.5 % [R-square] variability in the original data.

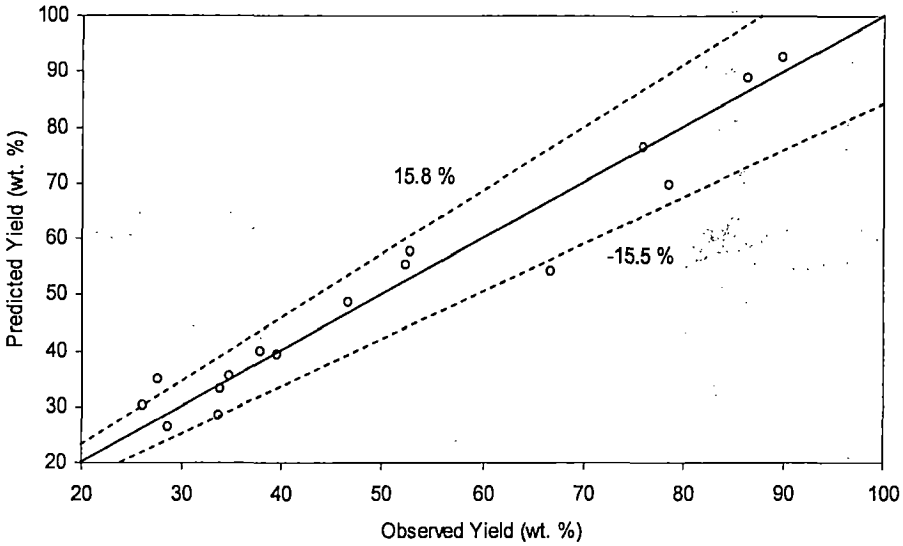

Fig. 4.59 Parity plot for the regression model, Eq. 4.37, developed for prediction of yield (wt. %)

The parity plot for the regression model given by Eq. 4.37 for the prediction of yield (wt. %) is shown in Fig. 4.59. The error band extends from –15.5 % to +15.8 %, and 87.5 % data points fall within this error band. Thus, the yield (wt. %) predicted by Eq. 4.37 lie within –15.5 % to +15.8 % of experimental values.

4.4.1.4 Regression analysis and ANOVA for size of nanoparticles

After converting the categorical input parameters into *dummy variables* and applying regression analysis, as detailed in Section 4.4.1.3, to the data obtained for size of nanoparticles given in Table 4.65, the regression equation obtained is given by Eq. 4.42. The ANOVA of regression analysis is given in Table 4.72.

$$Y_i = 120 - 27*X_1 - 11.8*X_2 - 111*D_1 + 12*D_3 + 19.8*X_1*X_2 + 53*X_1*D_1 + 25.7*X_1*D_3 + 45.8*X_2*D_1 - 13.3*X_2*D_3 - 106*D_1*D_3 \quad \ldots (4.42)$$

In this case, Y_i=NP size and all other conventions as discussed in Section 4.4.1.3 remain same. However, using Eq. 4.42, four different kinds of correlations can be obtained based on the four different possible combinations of *dummy variables*, which are given through Eqs. 4.43 - 4.46.

NP size when PLAL and DMSO used:

$Y_i (D_1=0, D_3=0, Xi) = 120–27*X_1–11.8*X_2 +19.8*X_1*X_2$ ... (4.43)

NP size when PLAH and DMSO used:

$Y_i (D_1=1, D_3=0, Xi) = 9+26*X_1 + 34*X_2 +19.8*X_1*X_2$ ... (4.43)

NP size when PLAL and Acetone used:

$Y_i (D_1=0, D_3=1, Xi) =132 – 1.3*X_1 –25.1*X_2 +19.8*X_1*X_2$ ... (4.45)

NP size when PLAH and Acetone used:

$Y_i (D_1=1, D_3=1, Xi) = –85 +51.7*X_1 +20.7*X_2 +19.8*X_1*X_2$ ... (4.46)

Further, it can be concluded from Eqs. 4.43 - 4.46 that the intercept changes remarkably from the *base category*, Eq. 4.43. Further, the coefficients of X_1 and X_2 also found to change, depending on the category chosen and thus, confirms the presence of interaction between input parameters (Gujarati D, 1999; Taguchi *et al.*, 2005). The correlation coefficients "R-square", "adjusted R-square" and "predicted R-square" are 76.1%, 28.2% and 0.00%, respectively. The model p-value is 0.318, which shows the model is insignificant.

Table 4.72 ANOVA of regression analysis for Eq. 4.42

Predictor	Coef	SE Coef	T	P	Significance
Constant	120.3	266.0	0.45	0.670	Insignificant
PLA concentration	-26.6	129.1	-0.21	0.845	Insignificant
S/NS volume ratio	-11.76	95.46	-0.12	0.907	Insignificant
PLA MW	-110.8	342.7	-0.32	0.759	Insignificant
Solvent	11.8	226.1	0.05	0.960	Insignificant
PLA concentration*S/NS volume ratio	19.80	33.33	0.59	0.578	Insignificant
PLA concentration* PLA MW	53.3	113.9	0.47	0.659	Insignificant
PLA concentration* Solvent	25.67	74.54	0.34	0.745	Insignificant
S/NS volume ratio* PLA MW	45.84	68.32	0.67	0.532	Insignificant
S/NS volume ratio* Solvent	-13.32	44.72	-0.30	0.778	Insignificant
PLA MW* Solvent	-106.00	74.54	-1.42	0.214	Insignificant

It can be observed from Table 4.72 that all the model terms are insignificant. The "R-square", "adjusted R-square" and "predicted R-square" values are not much higher and also the model p-value is insignificant. Thus, the insignificant terms are removed one-by-one in a step-wise manner, to produce a better regression equation. After removing the insignificant terms, the regression equation obtained is given by Eq. 4.47. ANOVA of regression analysis is given in Table 4.73.

$$Y_i = -40.0+41.4* X_1 +37.8* X_2 +97.5* D_1 + 21.0* D_3 - 106* D_1* D_3 \quad \ldots (4.47)$$

However, using Eq. 4.47, four different kinds of correlations can be obtained based on the four different possible combinations of *dummy variables*, which are given in Eqs. 4.48 - 4.51.

NP size when PLAL and DMSO used:

$$Y_i (D_1=0, D_3=0, Xi) = -40.0+41.4* X_1 +37.8* X_2 \quad \ldots (4.48)$$

NP size when PLAH and DMSO used:

$$Y_i (D_1=1, D_3=0, Xi) = 57.5 +41.4* X_1 +37.8* X_2 \quad \ldots (4.49)$$

NP size when PLAL and Acetone used:

$$Y_i (D_1=0, D_3=1, Xi) = -19+41.4* X_1 +37.8* X_2 \quad \ldots (4.50)$$

NP size when PLAH and Acetone used:

$$Y_i (D_1=1, D_3=1, Xi) = -27.5+41.4* X_1 +37.8* X_2 \quad \ldots (4.51)$$

Table 4.73 ANOVA of regression analysis for Eq. 4.47

Predictor	Coef	SE Coef	T	P	Significance
Constant	-40.00	54.25	-0.74	0.478	Insignificant
PLA concentration	41.40	12.97	3.19	0.010	Significant
S/NS volume ratio	37.80	12.97	2.92	0.015	Significant
PLA MW	97.50	41.01	2.38	0.039	Significant
Solvent	62.50	41.01	1.52	0.158	Insignificant
PLA MW* Solvent	-106.00	57.99	-1.83	0.098	Insignificant

It can be observed from Table 4.73 that PLA concentration, S/NS volume ratio and molecular weight of PLA are significant input parameters, whereas; solvent is insignificant input parameter. The interaction term "PLA MW*Solvent" is also found to be insignificant but more significant than the solvent. The "R-square", "adjusted R-square" and "predicted R–

square" values of 71.0%, 56.5 % and 30.58 %, respectively, are not in good agreement with each other. But, the model p-value of 0.016 implies the model is significant. It appears that the low value of R-square is due to presence of less number of model terms, as some model terms are removed during regression due to existence of multicolinearity between the model terms. The low value of "adjusted R–square" and "predicted R–square" are due to less number of experimental runs which leads to low degrees of freedom. For example, if the number of model terms will increase, the degrees of freedom for each model term will become large in comparison to the total degrees of freedom. Thus, the regression model given by Eq. 4.47 can be considered to for the prediction of optimum result. However, as the "predicted R-square" value is low, thus, the prediction will not be appropriate.

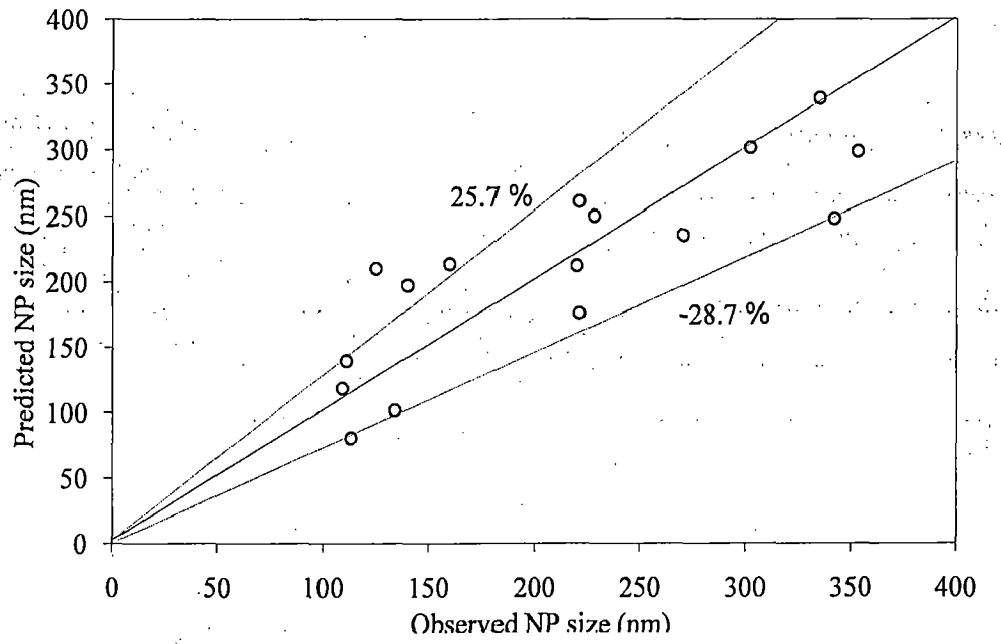

Fig. 4.60 Parity plot for the rgression model, Eq. 4.47, developed for prediction of PLA NP size

The parity plot for the regression model given by Eq. 4.47 for the prediction of size of PLA NP is shown in Fig. 4.60. The error band extends from –28.7 % to +25.7 %, and 81.25 % data points fall within this error band. Thus, the size of PLA NP predicted by Eq. 4.47 lie within –28.7 % to +25.7 % of experimental values.

4.4.2 Optimal Input Condition for Maximum Yield (wt. %) and Minimum NP Size

Search for an optimal condition should be made at which one can get minimum NP size and maximum yield (wt. %). In case of TMED, the optimum condition is defined by studying the main effects of each of the input parameters. Two statistical analysis methods, namely, the "Analysis of Mean (ANOM)" and the "Analysis of Variance (ANOVA)" are utilized to establish the optimum design conditions. In order to obtain the combination of input parameters providing the optimum output, the effects of input parameters are analyzed using ANOM to identify the input parameters which are primarily responsible for inducing variation in the SNR. Thus, from the SNR response graph for yield (wt. %) given in Fig. 4.57, the optimum levels of input parameters are found to be at as given in Table 74. And from the SNR response graph for size of nanoparticles (Fig. 4.58), the optimum levels of input parameters are found to be at as given in Table 4.74, which coincidentally matched with Run No. 6.

Table 4.74 Optimum conditions for maximum yield (wt. %) and minimum NP size

	Optimum condition for maximum Yield (wt. %)	Optimum condition for minimum size of NPs
PLA concentration	10 mg/ml	10 mg/ml
S/NS volume ratio	0.2	0.2
PLA MW	PLAL	PLAL
Solvent	acetone	DMSO

The choice of these optimal conditions is based on the appropriate SNR. Thus, it can be concluded from the above statement that the best settings of input parameters for the optimum are similar for both yield (wt. %) and size of NPs, except for the fact that the solvent is acetone in case of yield (wt. %) and DMSO in case of size of NPs. Further, from the regression analysis discussed under Section 4.4.1.3 and 4.4.1.4, it is obvious that solvent is not a significant parameter in the present case. Thus both the conditions noted above are optimum conditions.

Finally, as per the Step 10, of Section 2.7, two confirmatory experiments were carried out to verify the optimal settings of input parameters. The confirmatory experiments were quite satisfactory as both of the above optimum conditions produced almost the same result. The yield (wt. %) and NP size, based on the optimal settings of the above input parameters, were found to

be 79.3 % and 115 nm, respectively, when acetone was taken as solvent; and 79.8 % and 111 nm, respectively, when DMSO was taken as solvent. The values are almost close to those obtained from the initial experiment, Run No. 6, as can be observed from Table 4.65. These optimum conditions for yield (wt. %) and size of NPs are acceptable as the main objective is to produce smaller size NPs with higher yield (wt. %). However, it was found that the PDI of NPs obtained from Run No. 6 is 0.261, whereas; the PDI for the two confirmatory optimal conditions are 0.089 and 0.229 for the NPs obtained when acetone and DMSO are taken as solvent, respectively. Thus, the optimal condition for the preparation of smaller sized nanoparticles with higher yield (wt. %) should be at polymer concentration (10 mg/ml), S/NS volume ratio (0.2), PLAL and acetone, as lower PDI is much better, which provides uniform distribution, although a PDI in the range of 0-0.3 is acceptable for drug delivery systems (Legrand *et al.*, 2007).

4.4.3 Effect of Various Parameters on the Yield (wt. %) and Size of Nanoparticles

The *"main effect"* plots in terms of SNR for the yield (wt. %) and size of PLA NPs are shown in Figs. 4.57 and 4.58, respectively. The "*main effects*" indicate the general trend of the influence of the factors. In TMED, the "*main effect*" is the difference between the two average effects, of the input parameter, at the two levels. For example, the "*main effect*" of a particular input parameter is the difference between the average values of output parameters at levels 1 and 2 of that particular input parameter. Thus, it indicates the relative influence of the effect of the input parameter. The larger the difference in the output parameter, the stronger is the influence of that particular input parameter.

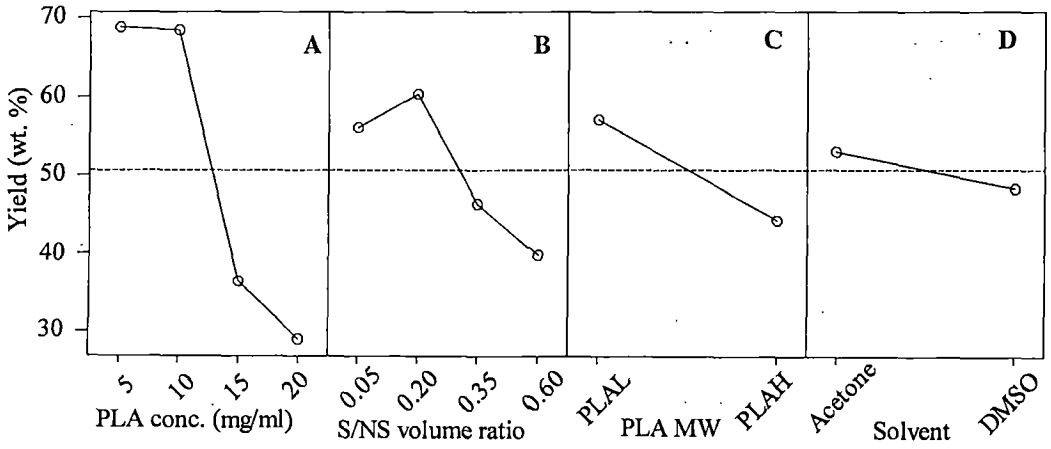

Fig. 4.61 Main effect plots for yield (wt. %)

The "*main effect*" plots for the yield (wt. %) and size of PLA nanoparticles are shown in Figs. 4.61 and 4.62, respectively, which are well described under this Section. Further, it can be observed here that the trend of the "*main effect*" plots obtained from the SNR analysis given in Figs. 4.57 and 4.58, are similar to those obtained from ANOVA analysis given in Figs. 4.61 and 4.62, respectively.

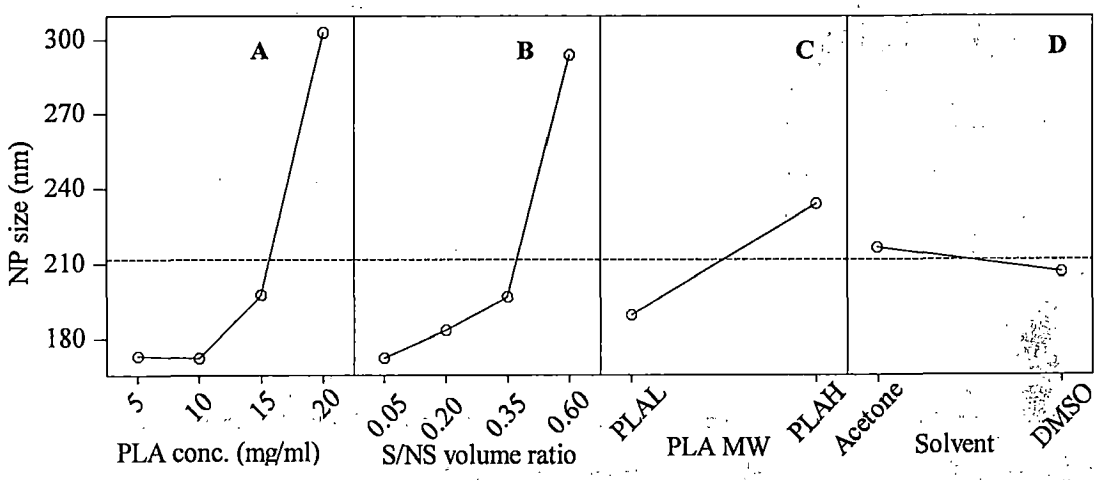

Fig. 4.62 Main effect plots for size of PLA nanoparticles

However, as the main effect plots obtained from TMED provides the average effect, to know about the actual effects, the experimental results are analyzed in a modified way and are discussed below:

4.4.3.1 Effect of PLA concentration on yield (wt. %) of PLA NPs

Figs. 4.63 and 4.64 show the effect of concentration of PLA on yield (wt. %), where solvent used for nanoprecipitation are DMSO and acetone, respectively. These figures also exhibit the effect of high M_w PLA (PLAH) and low M_w PLA (PLAL) used for the preparation of PLA NPs. In this section, the concentration of PLA is computed considering the combined volume of solvent and non-solvent.

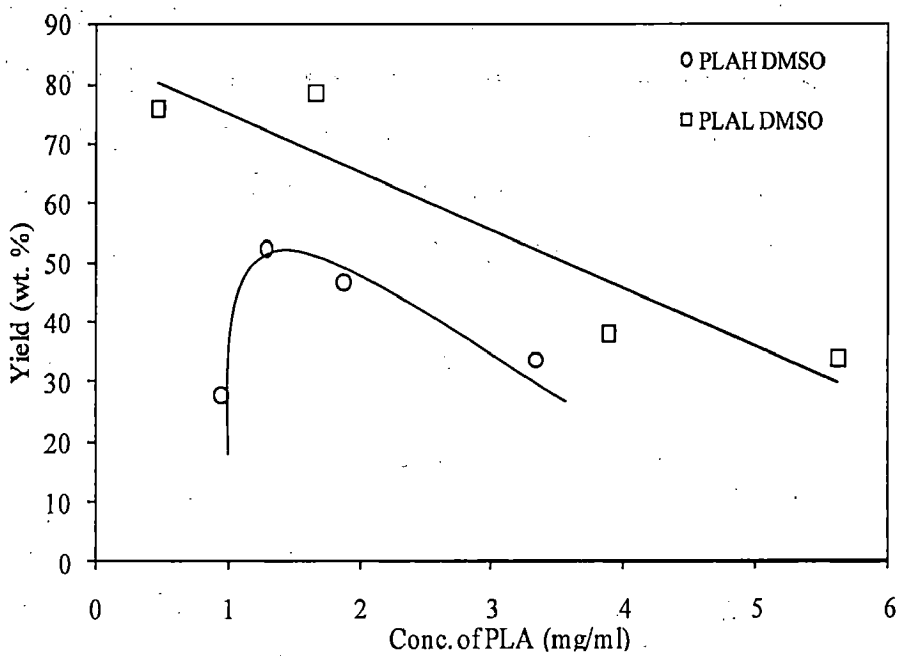

Fig. 4.63 Variation of Yield (wt.%) w.r.t. Concentration of PLA (mg/ml) using DMSO as solvent

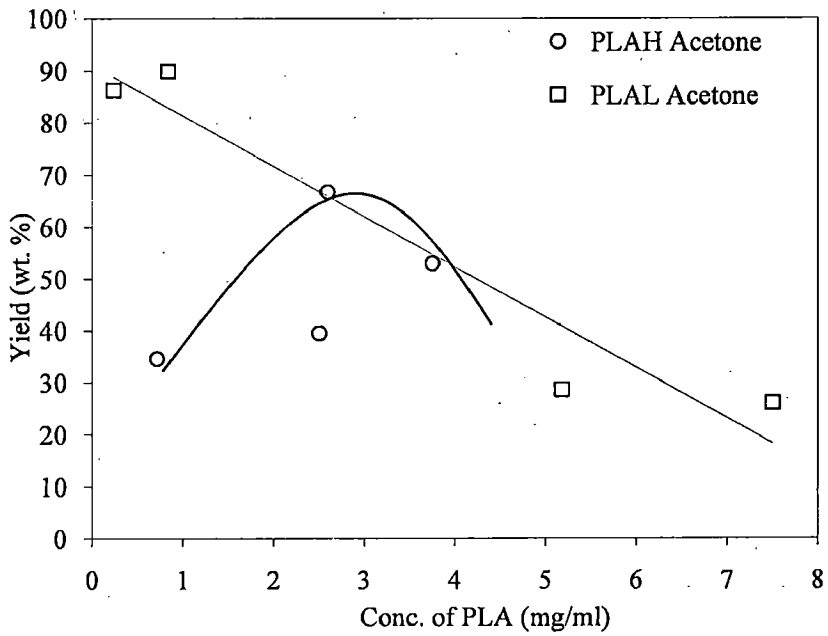

Fig. 4.64 Variation of Yield (wt.%) w.r.t. Concentration of PLA (mg/ml) using acetone solvent

From the above figures, following facts are evident:

1. For low M_w PLA, the yield (wt. %) always decreases when concentration of PLA in solution increases. This fact is true for both the solvents acetone as well as DMSO.

2. However, for high M_w PLA, the relationship between yield (wt. %) and concentration of PLA appears to be different. Up to a certain concentration of PLA, which is about 1 mg/ml for DMSO and 2.6 mg/ml for acetone, the yield (wt. %) increases with the increase in concentration of PLA and after that it decreases.

The above facts can be explained with the help of Figs. 4.65 and 4.66. When the PLA solution, prepared using solvent acetone or DMSO, is injected into the non-solvent methanol under sonication, the PLA NPs are formed. However, during this process, some NPs also come in contact with each other and form agglomerates and aggregates. These agglomerates, being of higher density, settle at the bottom of the mixing vessel. The NPs which remain in the suspension are collected and purified through centrifugation process. Thus, the PLA which settles down does not contribute towards the amount of NPs and thus decreases the yield (wt. %). Thus, more is the weight of aggregate formed, less is the yield (wt. %).

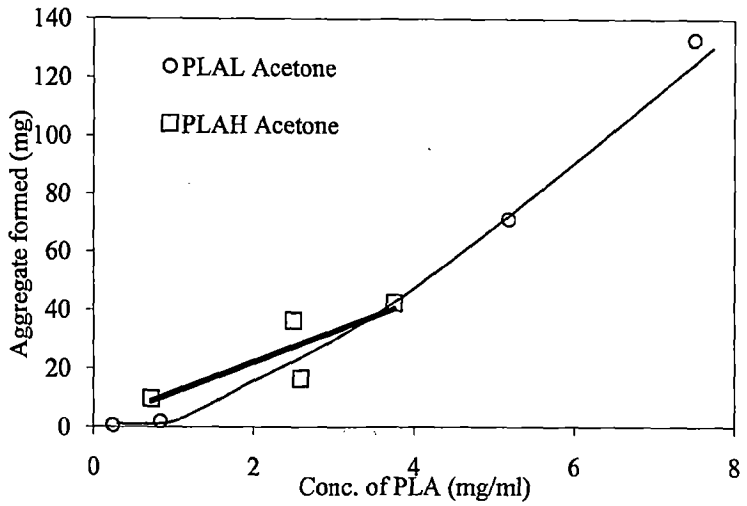

Fig. 4.65 Variation of Aggregate formed (mg) w.r.t. Concentration of PLA (mg/ml) using acetone as solvent

Figs. 4.65 and 4.66 clearly show how the weight of these aggregates increase with increase in the concentration of PLA for both the solvent types, i.e. DMSO and acetone. These figures also show the effect of PLA MW on aggregate formation. From the above figures it is observed that with the rise in the concentration of PLA, irrespective of high/low M_w PLA, the amount of aggregates formed increases. One possible reason for the above fact is that at high concentration of PLAH & PLAL, the NPs come closer to each other and thus get ample

opportunity to form aggregates which then settles at the bottom. More is the concentration of PLA this opportunity is more and thus the yield (wt. %) decreases with increase in PLA concentration.

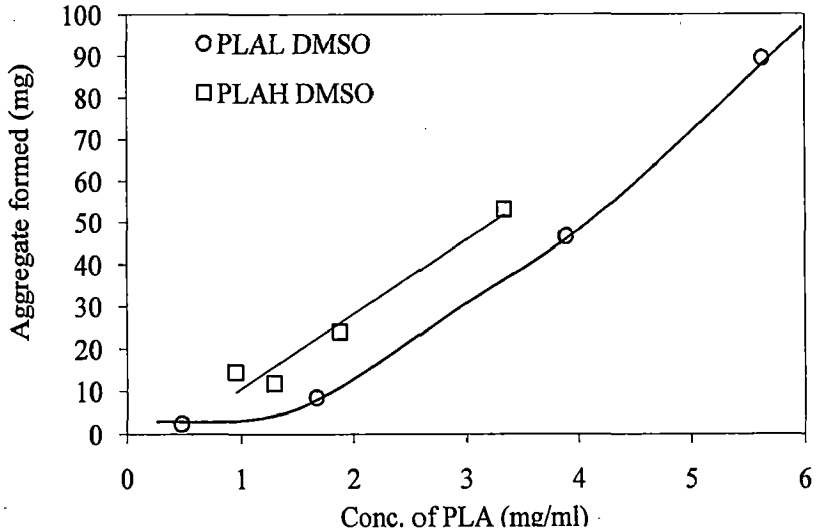

Fig. 4.66 Variation of Aggregate formed (mg) w.r.t. Concentration of PLA (mg/ml) using DMSO as solvent

Further, it can be observed that when the solvent DMSO is used, for a given concentration of PLA, the weight of aggregates formed is more for PLAH than PLAL. However, this is not true in case of acetone. In this case, the wt. of aggregate formed is almost same for both PLAH as well as PLAL. Higher weight of aggregates formed for PLAH is attributed to the gelation effect described under Section 4.4.3.6, through which PLAH form high density aggregates.

Mechanism of formation of aggregates:

When the PLA solution is injected into the non-solvent (methanol) under sonication, small liquid droplets of the PLA in solvent are formed. From these droplets the solvent diffuses to non-solvent and the PLA NPs are formed. Further, sonication process, which creates vigorous mixing, the small droplets may undergo coalescence as well as breaking. The formation of droplet size depends on many factors such as concentration, viscosity, density and surface tension of PLA solution. Once the small droplets of PLA-solvent are formed, their coalescence depends upon the adhering properties of these droplets, distance between the droplets, charge

present on the droplets and Vander Waals forces acting on these droplets. Thus, as a whole, the droplets are under the influence of two forces, viz.

1. The electrostatic repulsive force which do not allow these to come closer for agglomeration.
2. The surface tension that strives to hold the droplet within a spherical shape and the convective forces which brings one droplet closure to other and provide opportunity for agglomeration

At equilibrium, the two forces completely balance each other. When the electrostatic repulsive forces overcome the surface tension of the liquid, the larger droplets disintegrates into smaller droplets and vice versa. Further, more is the concentration of PLA solution, higher is the viscosity of PLA-solvent droplets and the rate of their coalescence will be higher.

Higher concentration of high molecular weight polymer in the droplet also hinders diffusion of the solvent towards the non-solvent (Bilati *et al.,* 2005) and thus delays the precipitation process of PLAH and helps it to remain in droplet form. This in turn enhances agglomeration process. Thus, at higher PLAH concentration, more aggregates were found to form in comparison to PLAL of same concentration. Further, formation of aggregates is mainly dependent on intrinsic viscosity and interaction constants (Thioune *et al.,* 1995, 1997; Stainmesse *et al.,* 1995; Bilati *et al.,* 2005). At higher concentration of PLA, the intrinsic viscosity is high and thus interaction between PLA and solvent increases leading to formation of aggregates. Thus, with the increase in PLA concentration, yield (wt. %) of PLA NPs decreases (Legrand *et al.,* 2007).

4.4.3.2 Effect of PLA concentration on size of PLA nanoparticles

The effect of concentration of PLA on the formation of different sizes of PLA NPs for solvent acetone and DMSO are shown in Figs. 4.67 and 4.68, respectively. Both the figures also contain the effect high M_w PLA (PLAH) and low M_w PLA (PLAL), used for the preparation of PLA NPs, on size of NP formation. In this section, the concentration of PLA is computed considering the combined volume of solvent and non-solvent.

From the Fig. 4.67, following facts are clearly evident:

1. When low M_w PLA is used for preparation of NPs, the size of NPs increase with increase in concentration of PLA.
2. However, this fact is not true for high M_w PLAs. In this case with the increase in PLA concentration up to about 2.5(mg/ml) the size of NPs decreases and then it increase.

From the Fig. 4.68, which is plotted for solvent DMSO, the behavior is somewhat different than the behavior for acetone as given below:

1. For a given concentration of PLA solution, high M_w PLA always produces larger size NPs than low M_w PLA.
2. The particle size remains almost constant up to certain concentration of PLA for both PLAL and PLAH and then the particle size increases with increase in concentration of PLA solution.
3. The above said concentration at which the behavior changes, is about 2 for PLAH and about 2.5 for PLAL.

The facts reported in Fig. 4.67 can be explained as follows:

When concentration of PLA increases, the NPs comes closer to each other and thus, get chance to get enlarged through the process of agglomeration/aggregate formation as discussed in Section 4.4.3.1 above. Thus, it can also be expected that the size of PLA NPs increases with increase in the concentration of PLA. However, the behavior w.r.t. high M_w PLA is difficult to explain. From Fig. 4.68, it is clear that the size of NPs remains almost constant up to a certain concentration of PLA which can be explained as follows:

For the process of agglomeration, the NPs have to approach each other and come to a certain critical distance which will help in the formation of agglomerates. The concentration of PLA in solution basically indicates the average distance between PLA NPs. Thus, up to a certain critical concentration, in which the average gap between two NPs is more than the critical distance, the agglomeration process will not start (Legrand *et al.,* 2007). Once this critical concentration is reached or exceeded, the NPs come closer to each other and the distance between them is less than the critical distance required for the process of agglomeration. This enhances the process of agglomeration.

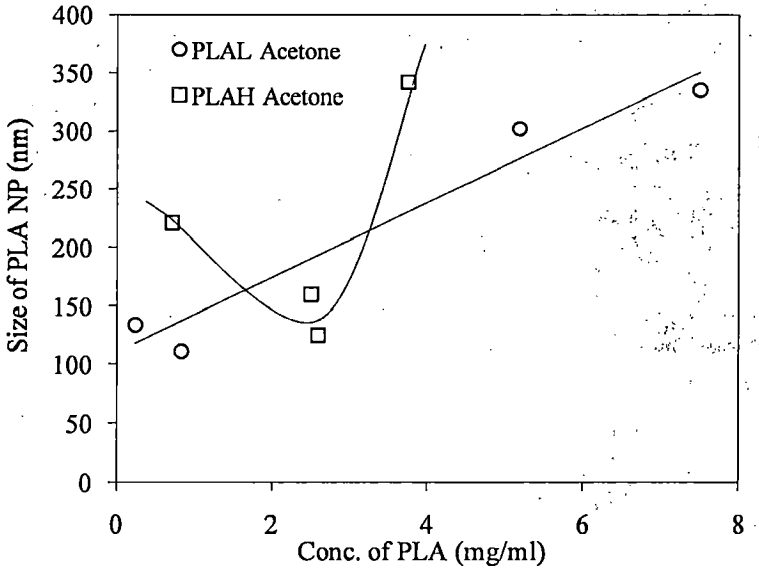

Fig. 4.67 Variation of Size of PLA NPs w.r.t. Concentration of PLA (mg/ml) using acetone solvent

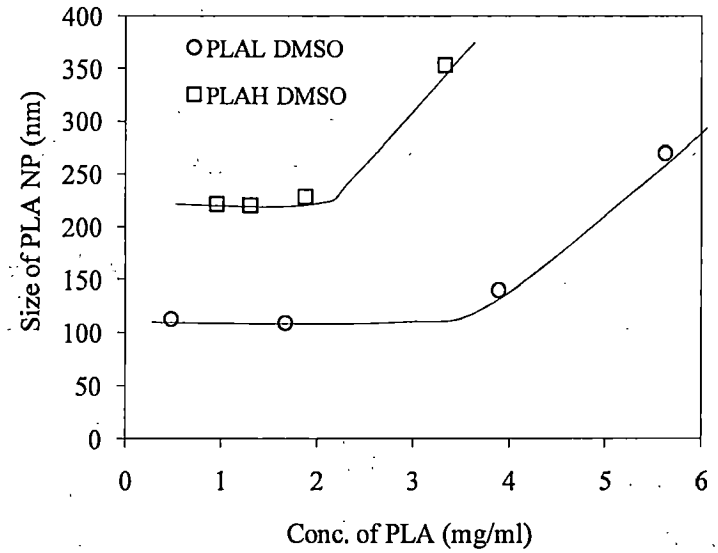

Fig. 4.68 Variation of size of PLA NPs w.r.t. Concentration of PLA (mg/ml) using DMSO as solvent

4.4.3.3 Effect of S/NS volume ratio on yield (wt. %) of PLA nanoparticles

Fig. 4.69 is drawn between S/NS volume ratio and concentration of PLA in terms of total volume of solvent and non-solvent, for all the input parameters such as M_w of PLA and solvent used.

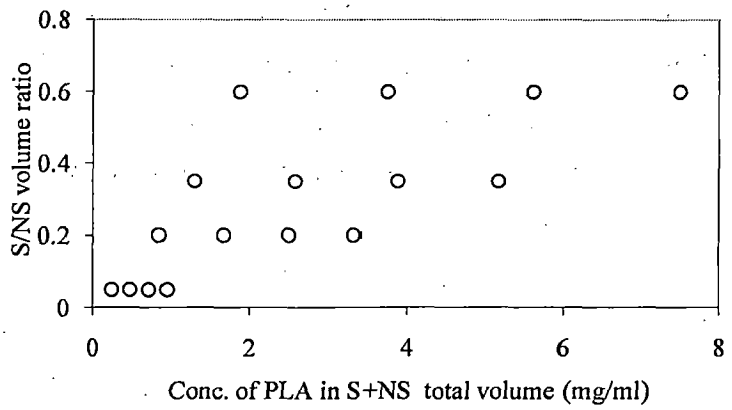

Fig. 4.69 Variation of concentration of PLA in total volume of solvent and non-solvent w.r.t. S/NS volume ratio

The above figure is plotted to show the multiplicity of S/NS volume ratio with concentration of PLA. It is observed from the above figure that for a certain value of S/NS volume ratio, several concentration of PLA exists. In other words, a single value of S/NS volume ratio represents four values of concentration of PLA. Further, it has been seen under Section 4.4.3.1 that the yield (wt. %) is a function of concentration of PLA. This means that for each value of PLA concentration there exists a value of yield (wt %). Thus, when S/NS volume ratio w.r.t. yield (wt %) is plotted, to observe the relationship, the problem of multiplicity of yield (wt %) w.r.t. a certain value of S/NS volume ratio is observed. This means for a certain value of S/NS ratio, four values of yield (wt %) will be available to choose from. This dilemma is created due to the existence of multiplicity discussed above. To solve this kind of multiplicity problem, one logical way is to take the average of the PLA concentration values (or corresponding yield (wt. %) available for that particular value of S/NS volume ratio (Fig. 4.61). However, this will show the approximate variation of yield (wt. %) which may not be accurate. Thus, in the present study, an attempt to study the effect of S/NS volume ratio directly on yield (wt. %) was not attempted.

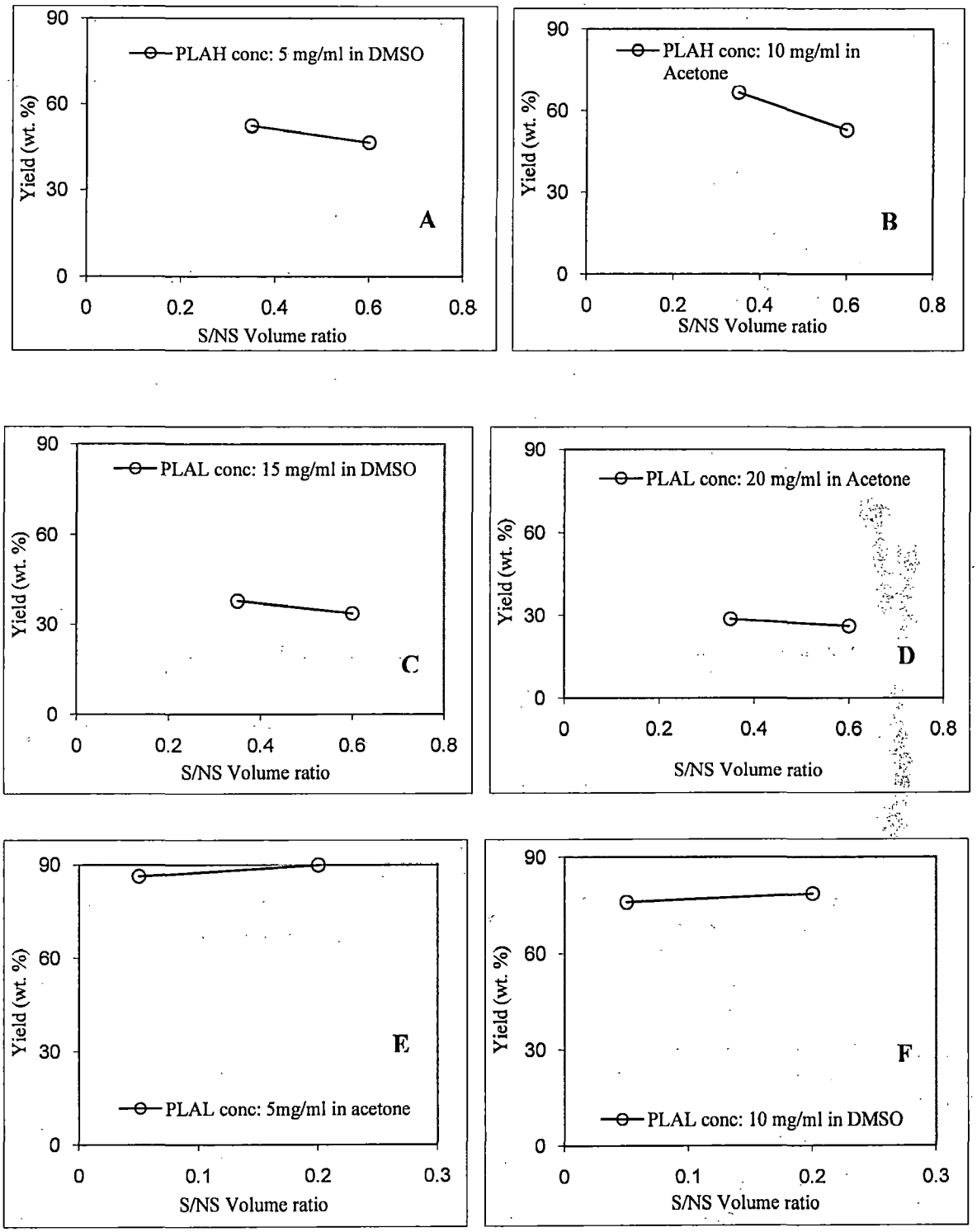

Fig. 4.70 Effect of S/NS volume ratio on yield (wt. %)

However, from the main effect plot obtained from Minitab and shown in Fig. 4.61 B and Fig. 4.70 A-D, some useful characteristics regarding the variation of yield (wt. %) w.r.t. S/NS volume ratio can be extracted as described below:

1. In majority of the cases the yield (wt. %) either decreases or remains almost constant with increase in S/NS volume ratio.

The above facts can be explained as follows:

With increase in S/NS volume ratio, the decrease in yield (wt. %) may be attributed to the increase in concentration of PLA as well as viscosity of PLA solution in solvent (Bilati *et al.*, 2005). In Section 4.4.3.1, it has been explained how the high concentration of PLA favors the formation of agglomeration and thus more aggregates are formed leading to lower yield (wt %). The same explanation is also true in this case. Further, high viscosity obstructs the diffusion of the solvent towards the non-solvent and thus helps in the formation of larger particles probably through the formation of liquid bridge. Thus, when the viscosity of the solution increases, large number of aggregates are formed and thereby leading to decrease in yield (wt. %) of PLA NPs (Thioune *et al.*, 1997; Bilati *et al.*, 2005).

In some cases it has also been seen that the yield (wt %) remains almost constant for some lower values of S/NS volume ratios. This fact has been explained under Section 4.4.3.1, based on the dependency of distance of droplets on concentration. However, in some rare cases, as can be seen from Fig. 4.70 E-F, the reverse trend is also observed, which appears to be baffling and needs some more investigation to accept or reject the hypothesis.

4.4.3.4 Effect of S/NS volume ratio on size of PLA nanoparticles

In this case also, due to the existence of multiplicity of PLA concentration of a given value of S/NS volume ratio (as discussed under Section 4.4.3.3), it is difficult to establish the effect of S/NS volume ratio on the size of PLA NPs and thus it is not attempted. However, from the main effect plot obtained from Minitab, as shown in Fig. 4.62 B, and Figs. 4.71 A-F, some useful relationship can be derived as discussed below:

1. With the increase in the S/NS volume ratio, the size of PLA NPs increases or remains almost constant.

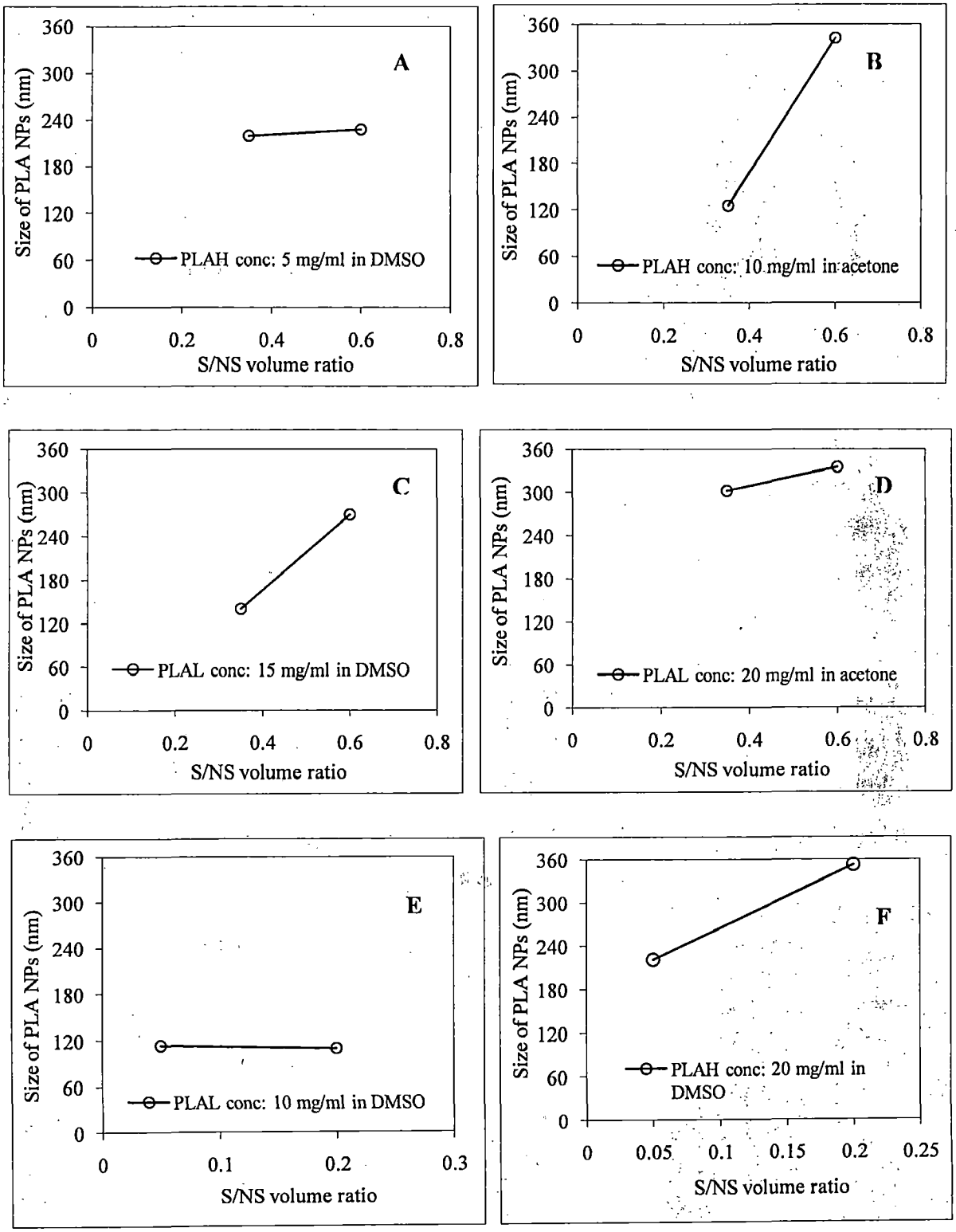

Fig. 4.71 Effect of S/NS volume ratio on size of PLA NPs

The above fact can be explained on the basis of discussion put forth under Section 4.4.3.2, in which it has been discussed that with the increase in concentration of PLA, the size of PLA NPs remains almost constant up to a certain value and with further increase in concentration of PLA, it increases.

However, in some rare cases, as shown in Fig. 4.72, the reverse trend is also observed, which is baffling and needs further investigation for a valid explanation or rejection.

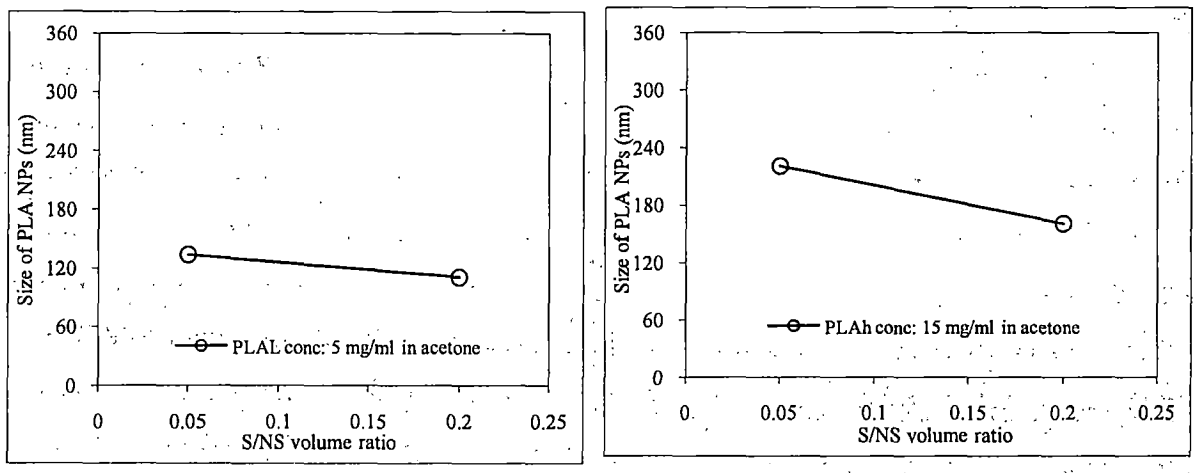

Fig. 4.72 Effect of S/NS volume ratio on size of PLA NPs

4.4.3.5 Effect of M_w of PLA on yield (wt. %) and size of PLA nanoparticles

Attempts were undertaken to obtain the effect of M_w of PLA directly on the yield (wt. %) and size of PLA NPs, while keeping the other input parameters at constant values. However, from the experimental result given in Table 4.65, it is difficult to obtain data points to study such variation. Thus, a direct effect of M_w of PLA on yield (wt. %) or size of PLA NPs could not be obtained. To overcome this, Taguchi uses average value of the response; for e.g. yield (wt. %) or size of PLA NPs in this case, for a particular value of an input parameter; to study the main effect. The main effect plot for M_w of PLA obtained using Minitab are given in Figs. 4.61 (C) and 4.62 (C), for the yield (wt. %) and size of PLA NPs, respectively. From the above mentioned figures, following relevant facts become evident:

1. From Fig. 4.61 (C), it can be seen that low M_w PLA, i.e. PLAL, produces PLA NPs with higher yield (wt. %), whereas; the high M_w PLA, i.e. PLAH produces lower yield (wt. %) of PLA NPs.

2. From Fig. 4.62 (C), it can be observed that low M_w PLA, PLAL, generates smaller sized NPs in comparison to the high M_w PLA which produced larger NPs.

The above facts may be explained as follows:

The formation of higher amounts of aggregates occurs with the high M_w PLA (Legrand *et al.*, 2007). In case of high M_w PLA, the viscosity of the PLA solution is higher than the low M_w PLA. Higher viscosity supports the formation of aggregates and thereby leading to larger PLA NPs with lower yield (wt. %).

The smaller size of PLA NPs produced from low M_w PLA than high M_w PLA. This may be due to the fact that low M_w PLA might have certain surface active properties which enhanced the formation of smaller NPs during nanoprecipitation (Legrand *et al.*, 2007). This hypothesis is supported by the fact that the hydrophilicity of PLA (contributed by –OH and –COOH end groups) has been reported to be affected by the type of catalyst used during its synthesis. However, in the present investigation, the catalyst used for the synthesis of PLA used for the NP formation, is tin chloride dihydrate, which leads to the production of PLA with polar chain ends bearing free carboxylic and hydroxyl end groups as discussed in Section 4.2.3. These polar groups present in the hydrophobic backbone (contributed by $-CH(CH_3)$ groups present in PLA chain) of PLA confer an amphiphilic character to PLA chains which is then closely linked to the chain length. Lower the M_w, the higher their hydrophilic/hydrophobic balance and hence surface active properties (Legrand *et al.*, 2007) and vice versa. In case of low M_w PLA, the charge (contributed by polar hydrophilic end groups) to volume ratio is higher than high M_w PLA.

Further, the process of gelation which is discussed in detail in Section 4.4.3.6 below also contributes towards the difference. Due to gelation the masking of charged chain ends will be more in case of PLAH than PLAL. This means that NPs formed from PLAL will have more charges with them which subsequently will help these not to form aggregates (Sussman *et al.*, 2007). Thus, in case of low M_w PLA, the repulsion between the charged particles prevents aggregation, whereas; aggregation occurs in case of high M_w PLA due to absence of electrostatic and presence of Vander Waals attraction existing between particles. In addition to the above discussions, the effect of M_w of PLA on yield (wt. %) and size of PLA NPs are also discussed under Section 4.4.3.1 and 4.4.3.2, respectively, which also shows same trend as discussed above.

4.4.3.6 Effect of type of solvent on yield (wt. %) and size of PLA nanoparticles

Similarly, attempts were also undertaken to obtain the effect of solvent type used, on the yield (wt. %) and size of PLA NPs, while keeping the other input parameters at constant values. However, from the experimental result given in Table 4.65, it is difficult to obtain data points to study such variation. Thus, a direct effect of solvent type on yield (wt. %) or size of PLA NPs could not be obtained. To overcome this difficulty, the main effect plot obtained from Minitab are used which are given in Fig. 4.61 (D) and 4.62 (D), for yield (wt. %) or size of PLA NPs, respectively.

From the above figures, the following facts become apparent:

1. Higher yield (wt. %) of PLA NPs is produced when acetone was used as solvent, whereas; when DMSO was used as solvent lower yield (wt. %) is obtained.
2. Larger size PLA NPs are found to be formed when acetone was used as solvent than when DMSO was used as solvent.

The above facts can be explained based on the combined effect of dielectric constant, polarity of solvent and non-solvent, Hildebrand solubility parameter (δ), rate of diffusion of the solvent into the non-solvent and interaction parameter. The individual effects of above parameters are discussed below:

Dielectric Constant

The dielectric constant of DMSO is more than double the dielectric constant value of acetone, and can be seen from Table 3.10. Bilati *et al.,* (2005), indicated that lower the dielectric constant of the solvent, larger is the size of NPs it produces. When the dielectric constant of the solvent increases, smaller particles present inside the PLA-solvent droplet, remain far apart from each other and thus preventing aggregation. As the dielectric constant of acetone is lower than DMSO larger NPs are formed with acetone than DMSO.

Polarity

Computation of interaction parameter includes the contribution of polarity. Thus, the effect of this parameter is not discussed separately. Its effect is taken care of in the discussion of interaction parameter.

Hildebrand solubility parameter (δ)

Computation of interaction parameter includes the contribution of Hildebrand solubility parameter. Thus, the effect of this parameter is not discussed separately.

Rate of diffusion

Higher is the rate of diffusion of the solvent into the non-solvent, the smaller is the nanoparticles obtained (Stainmesse *et al.*, 1992). This is because of the fact that high rate of diffusion prevents formation of aggregates.

Interaction parameter

Both the interaction parameters i.e. between "PLA & solvent" and "solvent & non-solvent" should also be taken into consideration (Bilati *et al.*, 2005) while explaining the formation of PLA NPs.

The PLA-solvent interaction parameter (χ_{PS}) is calculated using the Eq. 4.52.

$$\chi_{PS} = (V_S / RT) [(\delta_{dS} - \delta_{dP})^2 + (\delta_{pS} - \delta_{pP})^2] \quad \ldots (4.52)$$

where; V_S = molar volume of the solvent (73.3 for acetone and 71.0 for DMSO)

δ_{dS} and δ_{dP} = solubility parameter (δ_d) of solvent and polymer, respectively

δ_{pS} and δ_{pP} = solubility parameter (δ_p) of solvent and polymer, respectively

R (universal gas constant) =8.314 J/mol.K,

T = temperature in K=298 K

The interaction parameter $\chi_{PLA\text{-}acetone}$ and $\chi_{PLA\text{-}DMSO}$ are calculated by using Eq. 4.52 and are given in Table 4.75.

The solvent & non-solvent interaction parameters (χ) are calculated by using the Eq. 4.53 and are also given in Table 4.75. The V and δ values are taken from Table 3.10 of Chapter 3.

$$\chi = (V_{NS} / RT) (\delta_S - \delta_{NS})^2 \quad \ldots (4.53)$$

where, V_{NS} = molar volume of the non-solvent (here 40.7 cm^3/mol for methanol),

δ_S = solubility parameter (δ_t) of solvent

δ_{NS} = solubility parameter (δ_t) of non-solvent.

Table 4.75 Interaction parameters χ of "S/NS binary mixtures" and "PLA/solvent"

Type of Interaction Parameter (χ)	Value of Interaction Parameter (χ)
Acetone/Methanol (S/NS)	1.45
DMSO/Methanol (S/NS)	0.43
PLA-Acetone	0.105
PLA-DMSO	2.228

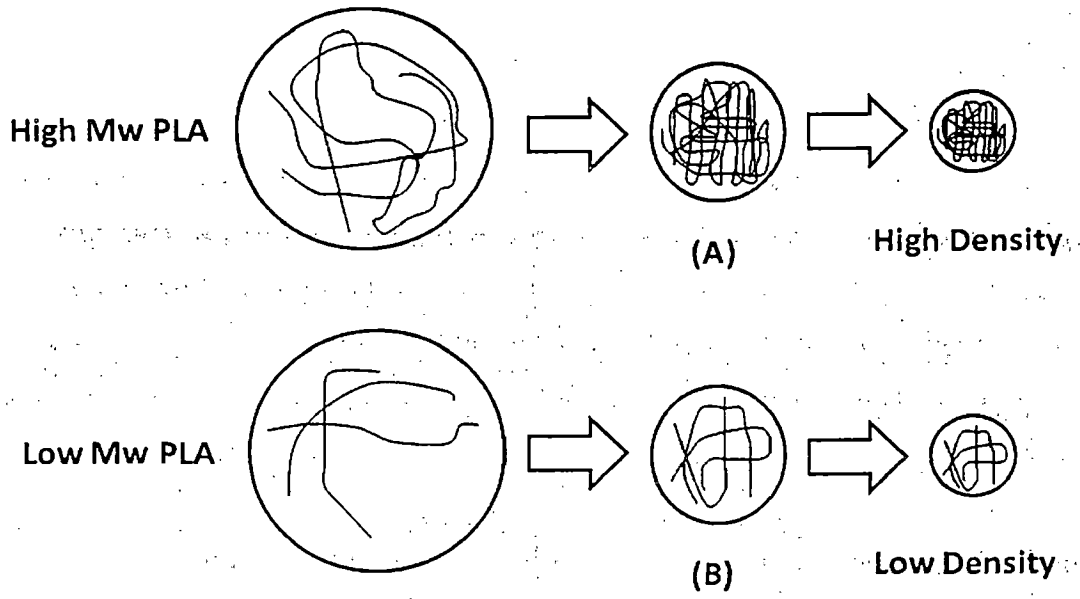

Fig. 4.73 Process of gelation (extended-coil to collapsed-coil transition)

Interaction parameter, $\chi_{PLA\text{-}DMSO}$, is higher than the interaction parameter $\chi_{PLA\text{-}acetone}$. High interaction parameter between PLA & solvent leads to greater affinity between them. Thus, more solvent remain in the supersaturated polymer region and solvent motion towards the non-solvent is hindered. Further, it can be observed from Table 4.75 that the interaction parameter $\chi_{DMSO\text{-}methanol}$ is much lower than $\chi_{acetone\text{-}methanol}$. This signifies that the affinity of DMSO for methanol is less and hence, nanoprecipitation becomes slow (Bilati *et al.,* 2005). Further, the difference between interaction parameter for PLA-DMSO and DMSO-methanol is higher than that between PLA-acetone and acetone-methanol. Higher is the value of interaction parameter, greater is their miscibility. Increased miscibility in case of PLA-DMSO-methanol system

promote more rapid polymer-phase gelation (extended-coil to collapsed-coil transition), whereas; decreased miscibility in case of PLA-acetone-methanol slows down the kinetics of this gelation process (Sussman *et al.,* 2007). When the kinetics of gelation increases, smaller NPs are formed and the solvent diffuses towards the non-solvent and smaller NPs get precipitated. This will facilitate formation of near spherical particles of smaller size and higher density incase of DMSO solvent. As the density increases, few particles will get settled down and adds to the aggregate and leads to lower yield (wt %). The process of gelation is shown conceptually in Fig. 4.73.

4.4.3.7 Effect of 2-parameter interactions on yield (wt. %)

Fig. 4.74 reports the 2-parameter interaction plots for yield (wt. %) of PLA NPs, obtained from the analysis carried out using Minitab software, for the different input parameters, as given in Table 4.76. The 2-parameter interactions are shown inside the rectangular boxes numbered 1-6 in Fig. 4.74 and are mentioned in Table 4.76. For example, the Box No. 1, 2 and 3 contains the effect of S/NS volume ratio, PLA MW and solvent, respectively, on yield (wt. %), at different levels of "PLA concentration". These rectangular boxes will be addressed through "Box No" in the discussion ahead.

Table 4.76 Two-parameter interactions on yield (wt. %) and size of PLA NPs

Box No.	2-parameter Interactions	Box No.	2-parameter Interactions
1	PLA concentration and S/NS volume ratio	4	S/NS volume ratio and PLA MW
2	PLA concentration and PLA MW	5	S/NS volume ratio and Solvent
3	PLA concentration and Solvent	6	PLA MW and Solvent

From the above figure, the following fact emerged out:

1. Within the range of parameters studied in the present investigation, all the input parameters were found to be involved in interactions, though the extents of interactions change considerably.

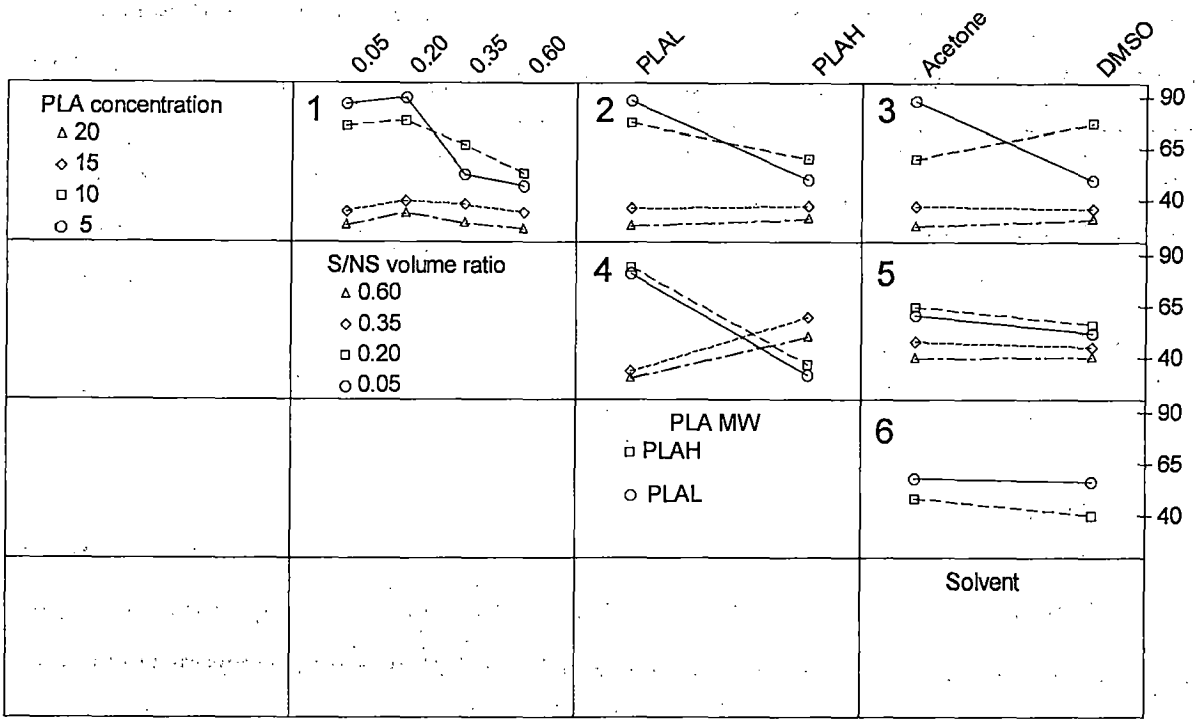

Fig. 4.74 Two-parameter interaction plot for yield (wt. %) of PLA NPs

The above fact can be explained as:

For the present case, an interaction is said to exist between two input parameters when one input parameter affects the yield (wt. %) differently at different levels of the other input parameter. This fact is obvious from the Fig. 4.74 as no two lines, in any of the Boxes are parallel for two different levels of an input parameter. For example, if Box No. 2 is examined, it can be observed that, depending on the level of concentration of PLA, the change in yield (wt. %) is different when MW of PLA varies from low to high. The greater the lines depart from being parallel, the greater is the degree of interaction.

From the discussions in Section 4.4.1.3, it is also evident that significant interaction exists between input parameters "PLA concentration" & "PLA MW" and "S/NS volume ratio" & "solvent". These interaction effects are further reinforced by the fact that in Eq. 4.37, the coefficient of interaction terms acquires a value of 12.155 and 10.320 and are found to be significant vide ANOVA analysis of data. The significant interactions can be observed in box Nos. 2 & 5 of Fig. 4.74. The order of magnitude of severity of 2-parameter interaction, calculated by using Eq. 4.17 of Section 4.2.2.6, in ascending order, is given in Table 4.77.

Table 4.77 Order of magnitude of severity of 2-parameter interaction for yield (wt. %)

2-parameter Interactions	T-value	P- value	Order of severity
PLA concentration and S/NS volume ratio	0.41	0.700	0.169
PLA concentration and PLA MW	1.09	0.326	0.551
PLA concentration and Solvent	0.11	0.919	0.00
S/NS volume ratio and PLA MW	0.45	0.669	0.191
S/NS volume ratio and Solvent	1.89	0.118	1.00
PLA MW and Solvent	0.89	0.413	0.438

4.4.3.8 Effect of 2-parameter interactions on size of PLA nanoparticles

Fig. 4.75 reports the 2-parameter interaction plots for size of PLA NPs, obtained from the analysis carried out using Minitab software, for the different input parameters and as given in Table 4.76. The 2-parameter interactions are shown inside the rectangular boxes numbered 1-6 in Fig. 4.75 and are as given in Table 4.76. For example, the Box No. 1, 2 and 3 contains the effect of S/NS volume ratio, PLA MW and solvent, respectively, on yield (wt. %) at different levels of "PLA concentration". These rectangular boxes will be addressed through "Box No" in the discussion ahead.

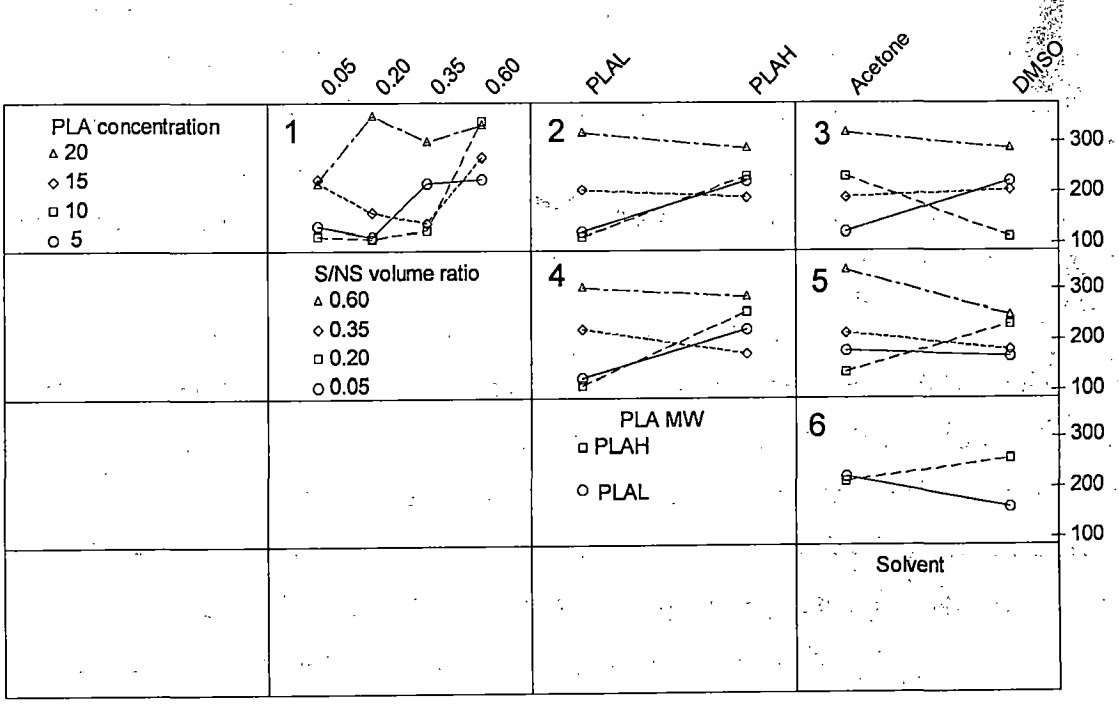

Fig. 4.75 Two-parameter interaction plot for NP size

From the above figure, the following fact emerged out:

1. Within the range of parameters studied in the present investigation, all the input parameters were found to be involved in interactions, though the extents of their interactions change considerably.

The above fact can be explained as:

For the present case, an interaction is said to exist between two input parameters when one input parameter affects the size of PLA NPs differently, at different levels of the other input parameter. This fact is obvious from the Fig. 4.75 as no two lines, in any of the Boxes are parallel for two different levels of an input parameter. For example, if Box No. 6 is examined, it can be observed that, depending on the category of PLA MW, the change in size of PLA NPs is different when solvent is varied from acetone to DMSO. The greater the lines depart from being parallel, the greater is the degree of interaction. From the discussions in Section 4.4.1.4, it is also evident that significant interaction exists between input parameters "PLA MW" & "solvent". This interaction effect is further reinforced by the fact that in Eq. 4.47, the coefficient of this interaction term acquires a value of -106 and is found to be moderately significant vide ANOVA analysis of data. This significant interaction can be observed from Box No. 6 of Fig. 4.75. The order of magnitude of severity of 2-parameter interaction, calculated by using Eq. 4.17 of Section 4.2.2.6, in ascending order, is given in Table 4.78.

Table 4.78 Order of magnitude of Severity of 2-parameter interaction for size of PLA NPs

2-parameter Interactions	T-value	P value	Order of severity
PLA concentration and S/NS volume ratio	0.59	0.578	0.259
PLA concentration and PLA MW	0.47	0.659	0.152
PLA concentration and Solvent	0.34	0.745	0.036
S/NS volume ratio and PLA MW	0.67	0.532	0.330
S/NS volume ratio and Solvent	0.30	0.778	0.00
PLA MW and Solvent	1.42	0.214	1.00

4.4.4 Characterization Studies of PLA Nanoparticles

In the present investigation, wet synthesis method is applied for the synthesis of PLA nanoparticles. These NPs are characterized by modern instrumental techniques like dynamic light scattering (DLS), TEM, and FESEM. Mean NP size is determined by TEM and DLS instrument. The size and size distributions are important to determine the interaction of NPs with the cell membrane and their penetration across the physiological drug barriers. The polydispersity index quantitatively measures the uniformity of the NPs. A monomodal size distribution should be pursued. A mixture of NPs of different sizes can be used to incorporate the desired release kinetics in the design of chemotherapy to meet the needs of the individual patients (Legrand *et al.,* 2007). The surface and bulk morphology are also important in determining the drug release kinetics of the NPs. The morphology is studied by TEM and FESEM. Further, surface charge is important in determining whether the NPs would cluster in blood flow and how they would adhere to and interact with cells whose membranes are negatively charged. The zeta potential has been employed to measure the cell surface charge density, which is also measured by DLS using a special kind of dip cell.

4.4.4.1 DLS analysis

Dynamic light scattering (DLS) instrument measures the hydrodynamic radius. In DLS, the measurements were made at 25°C and with a detection angle of 90°. The mean diameters of the nanoparticles are measured by DLS and are listed in Table 4.65. This mean value was used to analyze the experimental data. The particle size distribution plots obtained from DLS of 8 samples are illustrated in Fig. 4.76, among which four are from PLAL samples and the other four are from PLAH samples. The size distributions of the PLA nanoparticles are presented as intensity distributions as can be seen from the histograms in Figs. 4.76 A-H. Polydispersity index (PDI) is a parameter to define the particle size distribution of NPs which is also obtained from DLS analysis. It is a dimensionless number extrapolated from the autocorrelation function. The PDI of the NPs were found to vary between 0 and 0.3 except for Run No. 8 as evidenced from Table L-1 of Appendix L. Therefore, these preparations could be assumed to be monodisperse. The exceptional case for Run No. 8 may be due to the high molecular weight and high concentration of PLA.

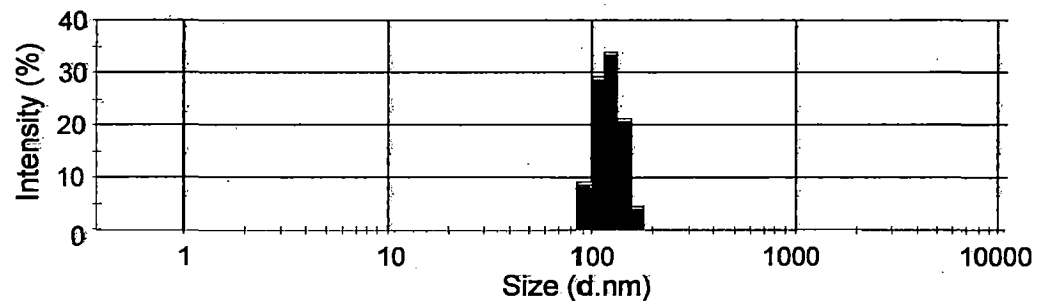

Fig. 4.76 A Mean size: 134 nm; PDI=0.035 (Run No. 1)

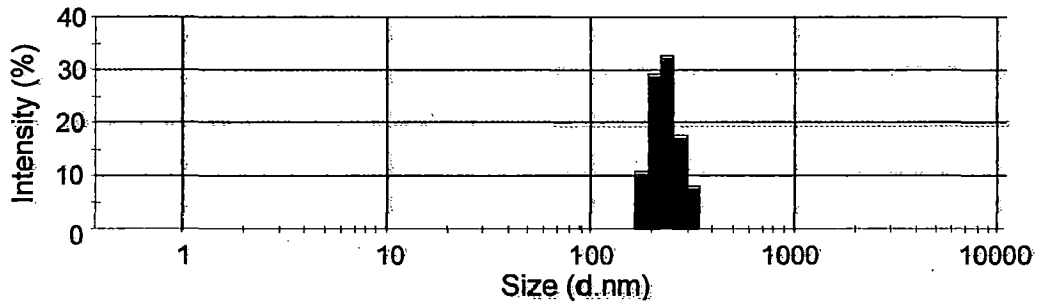

Fig. 4.76 B Mean size: 220 nm; PDI=0.217 (Run No. 3)

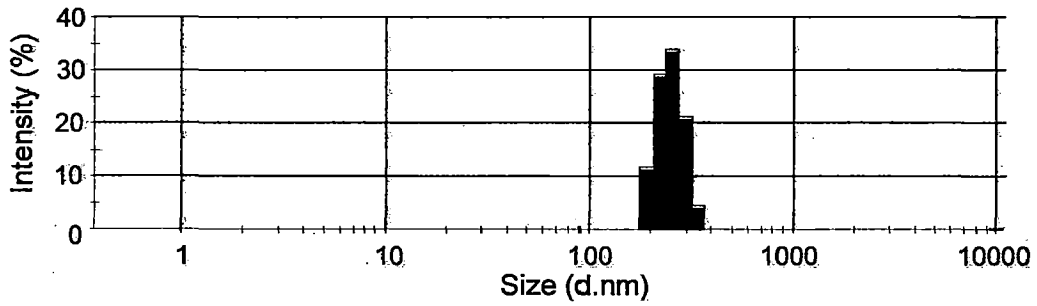

Fig. 4.76 C Mean size: 228 nm; PDI=0.098 (Run No. 4)

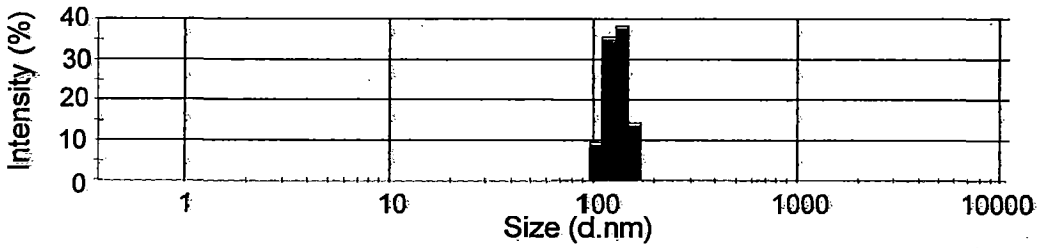

Fig. 4.76 D Mean size: 125 nm; PDI=0.228 (Run No. 7)

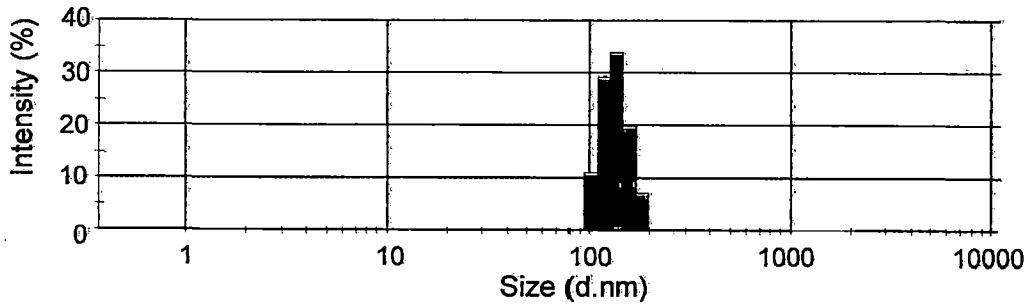

Fig. 4.76 E Mean size: 140 nm; PDI=0.109 (Run No. 11)

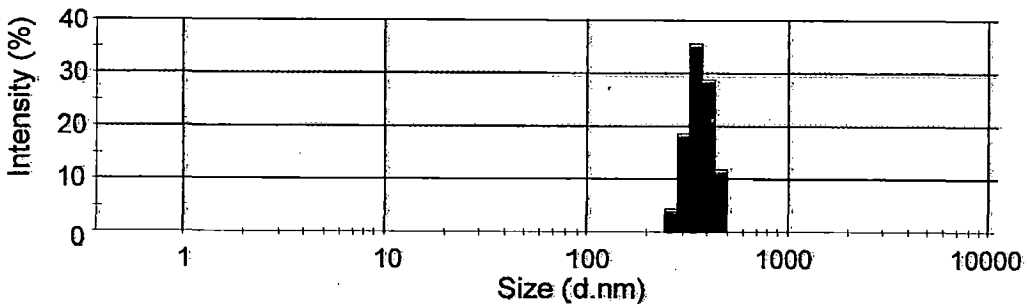

Fig. 4.76 F Mean size: 353 nm; PDI=0.13 (Run No. 14)

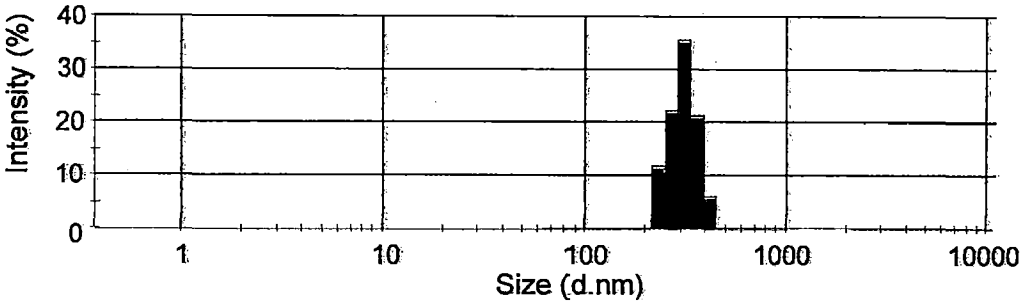

Fig. 4.76 G Mean size: 302 nm; PDI=0.172 (Run No. 15)

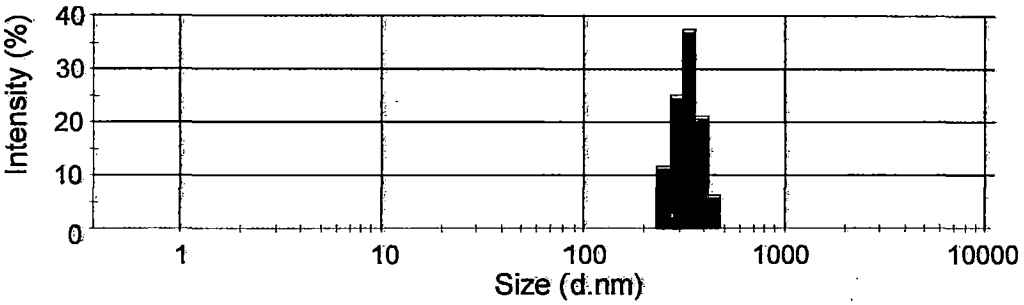

Fig. 4.76 H Mean size: 335 nm; PDI=0.185 (Run No. 16)

Fig. 4.76 DLS measurement of PLA NPs

From the figures, the following facts emerged out:

1. The sizes of the PLA nanoparticles are found to vary from around 70 to 500 nm and the size distribution is monomodal in nature.

The above piece of information can be explained as:

Average particle size calculated by DLS measurement was also confirmed by TEM analysis as given in Section 4.4.4.2. PDI < 0.3 is attributed to monodisperse samples, whereas; PDI >0.3 is obtained from the polydisperse samples (Legrand *et al.,* 2007). The low values of PDI showed that the samples had very well dispersity of the particles and are uniform.

4.4.4.2 TEM analysis

TEM micrographs of PLA NPs are given in Fig. 4.77. From the 16 nanoparticle samples, TEM of 8 samples are presented here, among which four micrographs are from PLAL samples and the other four are from PLAH samples. The TEM images were analyzed using Java based ImageJ (version 1.41o) image analysis software, developed by National Institutes of Health USA, to obtain the particle size diameter data. The diameters of the particles are measured and are averaged out to get the mean diameter of the nanoparticles.

From the afore-mentioned figures, the following facts emerged out:

1. The sizes of PLA NPs are almost same as those obtained from DLS measurement.
2. PLA nanoparticles are smooth, spherical and non-crystalline in nature.
3. The diameters of the individual nanoparticles are found to vary from 75-560 nm.
4. TEM images also show that the sizes of the nanoparticles are not uniformly distributed.

The above facts can be explained as:

The mean size derived from a DLS measurement is the intensity weighted average hydrodynamic size of the collection of particles being measured. As implied by the definition, the mean size is influenced by hydration or solvation effects. The TEM size, on the other hand, is a number weighted average size of a dehydrated hard sphere. Thus, one would expect the mean diameter, obtained from DLS, to be always slightly larger than the TEM measured diameter. This expectation is confirmed when comparing the size of NPs obtained from TEM and DLS. It was observed that the difference is, about 0.5 nm for NPs of size around 100 nm and, about 3 nm for NPs of size around 350 nm. (www.malvern.com/FAQ).

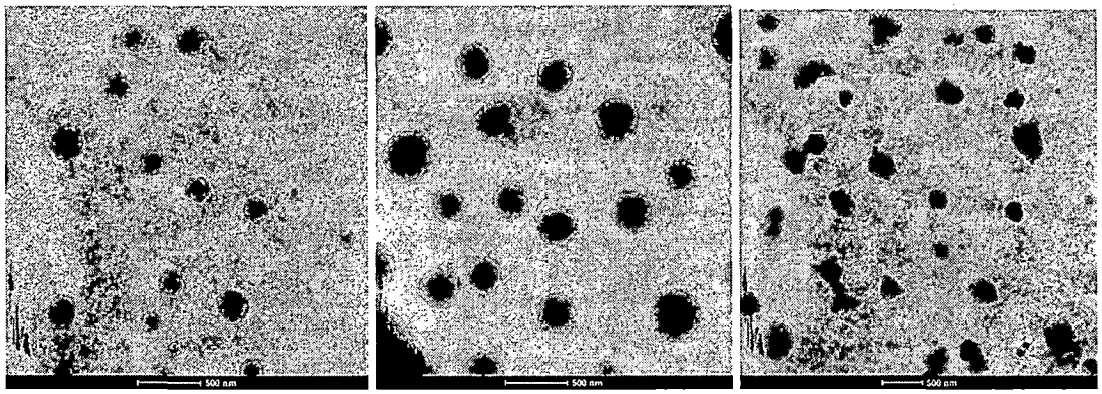

Run No. 1; MD: 133.6 nm Run No. 3; MD: 219.6 nm Run No. 4; MD: 227.2 nm

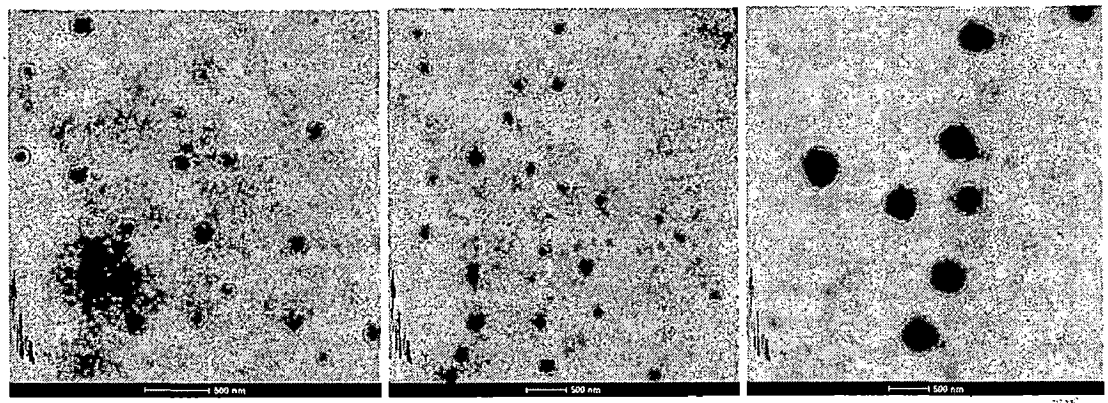

Run No. 7; MD: 124.7 nm Run No. 11; MD: 139.4 nm Run No. 14; MD: 350.5 nm

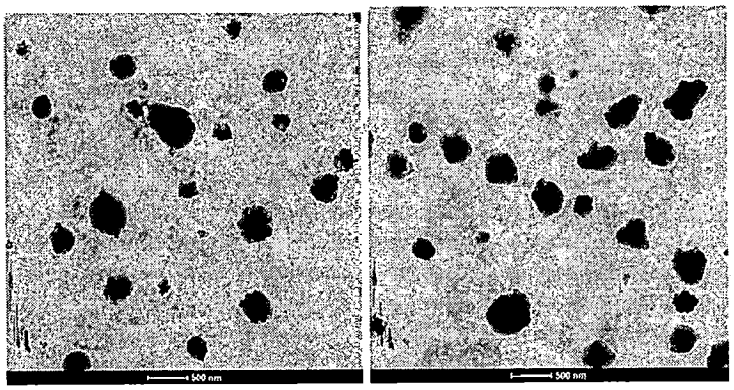

Run No. 15; MD: 300.5 nm Run No. 16; MD: 332.6 nm

Fig. 4.77 TEM micrographs of PLA nanoparticles

4.4.4.3 FESEM analysis

The surface morphology (roundness, smoothness, and formation of aggregates) and the size of nanoparticle formulations were studied by FESEM. Stability and aggregation behavior of PLA nanoparticles in different environments were characterized by FESEM visualizations. FESEM micrographs of PLA NPs obtained from Run No. 1 and 14 are shown in Fig. 4.78 A and B, respectively, one of which is obtained from PLAL and the other from PLAH. FESEM images are analyzed using "ImageJ image analysis" software to obtain the particle size diameter data. From the FESEM micrographs, the following facts emerged out:

1. The NPs are smooth and spherical with a diameter varying from 100–500 nm.
2. It can be seen that nanoparticles are bound together by interparticular bridges.
3. The micrographs clearly indicates that no hairline cracks or heterogeneity appear on the surface of NPs. This obviously presents morphological evidence for solid and smooth NPs.
4. From the micrographs, the non-uniform NPs can also be seen.
5. Cluster formation as a sign of aggregation was observed in FESEM images, when the PLA concentration and molecular weight were increased.

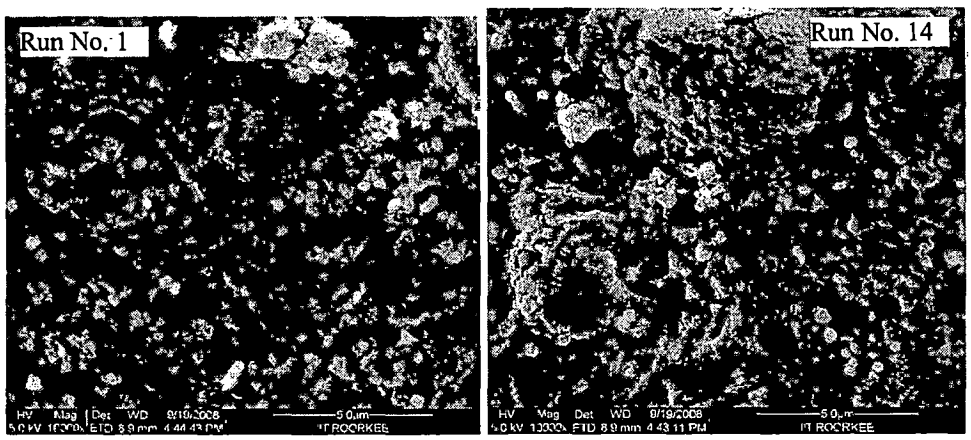

Fig. 4.78 FESEM micrographs of PLA nanoparticles

The above facts may be explained as:

The interparticular bridges were observed most of the time because of the progressive replacement of the non-solvent by water. The nanoparticle aggregation occurred by diffusion and resulted in percolate particle networks. This observation is also supported by visible flocculation that took place during experimentation, when water was added to the PLA solution containing NPs. The fine nanoparticle suspension became turbid upon addition of water, used

for washing, which may impart to the formation of interparticular bridges (Bilati *et al.,* 2005). Interparticular bridges may also have formed during drying, and created due to liquid bridging.

4.4.4.4 Determination of zeta potential

The zeta (ζ) potential measurements provide information about the particle surface charge and, were performed to evaluate the magnitude of the electrostatic stabilization at different conditions. ζ-potential of PLA NPs was determined in aqueous medium, at different pH. The values of ζ-potential of PLA NPs are given in Table 4.79. Surface of PLA NPs has a negative ζ-potential, and thus, it is most likely to favor the electrostatic adsorption of polycations (Sussman *et al.,* 2007). The positively charged drug particles can be adsorbed on the PLA NP surface and thus, can interact with the negatively charged body cells. The negative surface charge of PLA NPs originates from free carboxylic acid groups at the chain ends of PLA.

The normal blood pH is tightly regulated between 7.35 and 7.45. The normal pH of blood running through arteries (large elastic-walled blood vessels that carry blood from the heart to other parts of the body) is 7.4; the pH of blood in the veins (vessels that transports blood to the heart) is about 7.35. Normal urine pH averages about 6.0. Saliva has a pH between 6.0 and 7.4. The pH of stomach is 3. ["The Human Body - What Is The Normal pH of Blood, Urine, And Saliva?." Science Fact Finder. Ed. Phillips Engelbert. UXL-Gale, 1998. eNotes.com. 2006. 28 Aug, 2009 <http://www.enotes.com/science-fact-finder/human-body/what-normal-ph-blood-urine-saliva>]. Thus, in the present case the zeta potential was determined in the pH range of 3.7 to 7.4.

Table 4.79 Zeta potential of PLA NPs at different pH

pH	Zeta potential (mV)
3.7	-11.4
4.0	-11.7
6.0	-14.0
7.4	-33.9

PLA nanoparticles are found to be stable at higher pH. Nanoparticles with a magnitude of zeta potential above 30 mV have been shown to be stable in suspension, as the surface charge

prevents aggregation of the particles and hence favors the drug release from the drug loaded PLA NPs (Hirsjärvi *et al.,* 2008). The stability of PLA NPs can be explained by the fact that when the surface charge is higher, the zeta potential is higher. And when the surface charge is higher, the nanoparticles are stabilized by electrostatic repulsion. In the present investigation, the zeta potential value of -33.9 mV, suggested a stable system at pH 7.4, which is the normal pH of blood. ζ -potential as a function of pH is presented in Fig. 4.79.

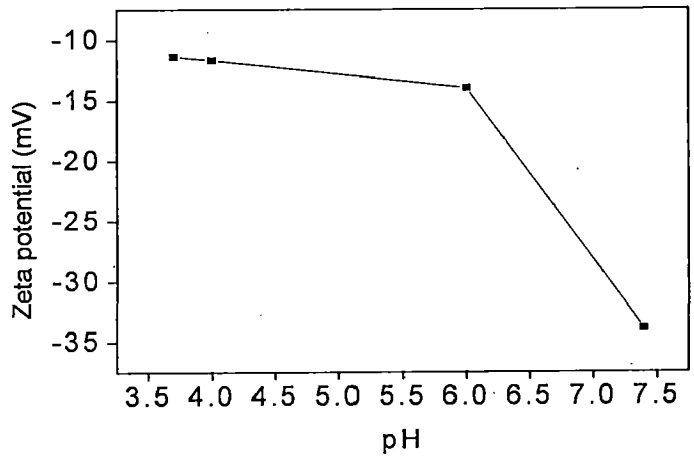

Fig. 4.79 Variation of zeta potential with pH

From the above figure, it can be observed that:

1. As the pH was decreased, the magnitude of ζ-potential values decreased.

The above fact can be explained as follows:

Due to the protonation of the carboxylic acid chains at the surface of PLA particles at low pH values, the ζ-potential was found to decrease with the increase in pH (Hirsjärvi *et al.,* 2008). This is attributed to the fact that protonation reduces the negative surface charge of the PLA NPs. Again, at lower pH, PLA NPs are unstable and hence forming aggregates and thereby lowering the "surface charge/unit area" and thus, leading to lower potential. The PLA NPs are stabilized by electrostatic repulsion because of their surface charge. At neutral pH, the PLA NPs reached their maximum ζ-potential (absolute) value as the electric double layer around the particles extended to a larger distance (Hirsjärvi *et al.,* 2006). When the pH was decreased to around 4 by HCl addition, the dissociated H+ and Cl− ions acts as electrolytes, and thus surpasses the surface charge decreasing effect. Carboxylic acid groups at the surface of PLA NPs are well ionized at basic pH which increases the magnitude of zeta potential. Thus, for

molecules and particles that are small enough, a high zeta potential will confer stability, i.e. the solution or dispersion will resist aggregation. When the potential is low, attraction exceeds repulsion and the dispersion will break and leads to flocculation. So, colloids with high zeta potential (negative or positive) are electrically stabilized while colloids with low zeta potentials tend to coagulate or flocculate.

Stability of nanoparticle dispersion in different environments is one key issue in determining the performance and safety of the drug delivery system in question. All biochemical reactions and electrical (life) energy are under pH control. Alkaline pH on the other hand, biochemically speaking, is slow and cool. In the present case, at alkaline pH the zeta potential is higher. Thus, it can be concluded that, drugs encapsulated into the PLA NPs can help slow release of drugs into the body as the pH of extracellular fluid is 7.4.

The summary of the different types of instruments used and the type of result obtained from them is given in Table 4.80.

Table 4.80 Instruments used for characterization of PLA nanoparticles

Properties	DLS	TEM	FESEM
Particle size	√	√	√
PDI	√		
Zeta potential	√		
Stability	√		
Surface charge	√		
Morphology		√	√

4.4.5 Mechanism of Nanoprecipitation

At low and dilute concentrations, droplets are formed. The droplet is under the influence of two forces, viz.:

1. Disintegrative electrostatic repulsive force.
2. Surface tension that strives to hold the droplet within a spherical shape.

At equilibrium, the two forces completely balance each other. When the electrostatic repulsive forces overcome the surface tension of the liquid, the larger droplets disintegrates into smaller droplets and vice versa. Nanoprecipitation employs rapid mixing of solvent and non-solvent to create high supersaturation to initialize precipitation; rapid mixing uncouples the mixing process from the particle aggregation process and therefore a narrow size range of nanoparticles is attained. The pictorial view of mechanism of nanoprecipitation method is given in Fig. 4.80.

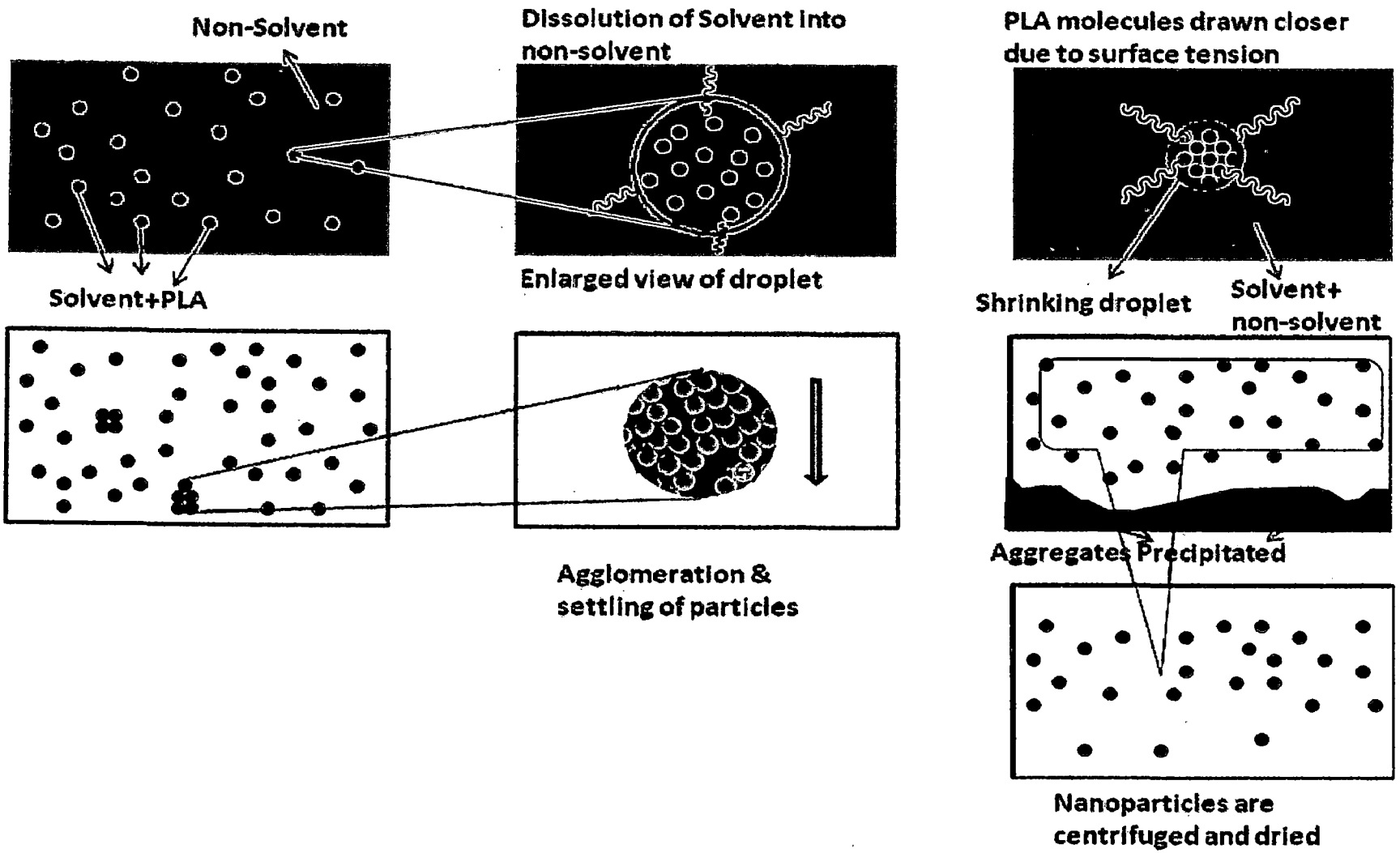

Fig. 4.80 Mechanism of Nanoprecipitation

CONCLUSIONS AND RECOMMENDATIONS

This Chapter summarizes salient conclusions drawn from the present investigations along with recommendations for future work.

5.1 Conclusions

Based on the results and discussions presented in Chapter 4, several significant conclusions can be drawn. The salient conclusions are listed below point wise for the three different types of investigations that had been carried out in the present work.

Melt polycondensation of lactic acid

1. MPC temperature is observed as the most critical parameter followed by MPC time for MPC of lactic acid as far as yield (wt %) is concerned. Regression analysis of the yield (wt. %) data with input parameters of MPC process shows that out of the models tried the quadratic model is the best.
2. MPC temperature is observed as the most critical parameter followed by MPC time for MPC of lactic acid also as far as M_w is concerned. Regression analysis of the M_w data with input parameters of MPC process shows that out of the models tested the quadratic model is the best after square root transformation of M_w data.
3. M_w around 179 kDa could be obtained by MPC after 2h of ES time, 10 h of MPC time and at 180°C MPC temperature. However, with the increase in MPC temperature and MPC time further, the yield (wt. %) and M_w were found to decrease. Further, the effect of ES time was found to be insignificant.
4. The order of significance of input parameters for prediction of yield (wt. %) is: MPC temperature > MPC time > catalyst (wt. %) > ES time > amount of LLA, whereas; that for prediction of M_w is: MPC temperature > MPC time > ES time > amount of LLA > catalyst (wt.%).
5. From statistical analysis, it is evident that interaction between all the five input parameters exists and the most severe interaction exists between MPC temperature and MPC time for the yield (wt. %) whereas; that for M_w is amount of LLA and MPC time.

6. GPC chromatograms of some PLA samples are found to be bimodal in nature indicating that the polymer produced have high as well as low molecular species.
7. From FTIR, NMR and XRD pattern for PLA samples produced, it is confirmed that D-lactic and L-lactic acid units are present in the polymer and racemization has also taken place during the melt polycondensation reaction.
8. The TGA/DTA/DSC analysis of four PLA samples with different M_w shows that T_d and T_m increases with the increase in M_w of PLA. Further, it has been found that the sample having M_w of 179 kDa, is thermally stable up to a temperature of 250°C and the corresponding T_d and T_m are found to be 352°C and 167°C, respectively. The corresponding % crystallinity is found to be 43%.

Solid state polycondensation of PLA

1. All the five parameters such as amount of PLA, HT temperature, HT time, SSP time and SSP temperature are observed to be significant for SSP of PLA as far as yield (wt. %) is concerned. However, SSP time is found to be the most critical parameter followed by HT temperature. Regression analysis of the yield (wt. %) data with input parameters for SSP process shows that out of the models tested in the present work the quadratic model is the best.
2. All the five parameters mentioned above except HT time are significant for SSP process as far as M_w is concerned. Furthermore, SSP temperature is observed to be the most critical parameter followed by SSP time. Regression analysis of the M_w data with input parameters for SSP process shows that out of the models tested the quadratic model is found to be best for expressing the values of M_w with input parameters.
3. A value of M_w around 300 kDa could be obtained by SSP at 110°C HT temperature, 145°C SSP temperature and after 13 h of SSP time. With the increase in HT temperature and SSP temperature, M_w passes through an optimum, at 110°C and 145°C, respectively. However, with the increase in SSP time, M_w decreases. Further, most of the GPC chromatograms of PLA samples are found to be bimodal in nature.
4. The order of significance of input parameters for prediction of yield (wt. %) is: SSP time > HT temperature > SSP temperature > amount of PLA > HT time, whereas; that for

prediction of M_w is: SSP temperature > SSP time > amount of PLA > HT temperature > HT time.

5. From statistical analysis, it is evident that interaction between all the five input parameters exists and the most severe interaction exists between HT time and SSP temperature for the yield (wt. %) whereas; that for M_w is HT temperature and SSP time.
6. The presence of D-lactic acid unit along with the L-lactic acid units are confirmed from studies of FTIR, NMR and XRD pattern for PLA. It is also revealed that racemization has taken place during the solid-state polycondensation process.
7. From the TGA/DTA/DSC analysis of PLA samples, it has been found that the sample having M_w of 300 kDa is thermally stable up to a temperature of 250°C and the corresponding T_d and T_m are found to be 354°C and 176°C, respectively. Further, the corresponding % crystallinity is found to be 22%.

PLA nanoparticle preparation

1. PLA concentration is found to be the most influential input parameter which control the yield (wt. %) as well as the size of PLA NPs. Based on the gradient of maximum to minimum SNR, the relative effects of each input parameter on both the yield (wt. %) and size of PLA NPs in descending order are: PLA concentration > S/NS volume ratio > M_w of PLA > solvent.
2. The optimal condition for the preparation of smaller sized PLA NPs along with higher yield (wt. %) is found to be at polymer concentration (10 mg/ml), S/NS volume ratio (0.2), low M_w PLA (PLAL) and acetone.
3. For low M_w PLA, the yield (wt. %) is always found to decrease with increase in concentration of PLA in solution. However, for high M_w PLA, up to a certain concentration of PLA, which is about 1 mg/ml for DMSO and 2.6 mg/ml for acetone, the yield (wt. %) increases with the increase in concentration of PLA and thereafter it decreases.
4. When acetone is used as solvent, the size of NPs produced from low M_w PLA is found to increase with increase in the concentration of PLA. However, for high M_w PLA, the NP size decreases with the increase in PLA concentration up to about 2.5(mg/ml) and thereafter it increases.

5. For DMSO as solvent and for a given concentration of PLA solution, high M_w PLA always produces larger size NPs than low M_w PLA. The particle size remains almost constant up to certain concentration of PLA (both high and low molecular weight of polymer) and then the particle size increases with increase in concentration of PLA solution. The above said concentration at which the behavior changes is about 2 for high M_w PLA and about 2.5 for low M_w PLA.
6. The yield (wt. %) mostly decreases or remains almost constant in a few cases with increase in S/NS volume ratio. However, with the increase in the S/NS volume ratio, the size of PLA NPs mostly increases but in few cases it also remains constant.
7. Low M_w PLA produces higher yield (wt. %) whereas; the high M_w PLA produces lower yield (wt. %) of PLA NPs. However, low M_w PLA generates smaller sized NPs in comparison to the high M_w PLA which produced larger NPs.
8. PLA NPs of higher yield (wt. %) is produced when acetone is used as solvent, whereas; lower yield (wt. %) is obtained when DMSO is used as solvent. However, large sized PLA NPs are formed when acetone is used than when DMSO is used as solvent.
9. Under the range of input parameters such as concentration of PLA, S/NS volume ratio, M_w of PLA and two different solvents DMSO & Acetone investigated, the sizes of the PLA NPs are found to vary from around 70 to 500 nm. The size distribution, for most of the samples, is found to be monomodal in nature having variation of PDI from 0-0.3. The sizes of PLA NPs observed from TEM are almost same as those obtained from DLS measurement and are found to be smooth, spherical and non-crystalline in nature.
10. The zeta potential of PLA NPs is found to be negative and varied from -11.4 to -33.9 mV, in the pH range 3.7 to 7.4, respectively. Further, at alkaline pH (7.4), the zeta potential of PLA NPs is higher than acidic pH (3.7 - 6.0) and thus, stable NPs are formed which can facilitate the encapsulation of polycationic drugs.

5.2 Recommendations

For the advancement of knowledge in the area of synthesis of PLA and its nanoparticles, following recommendations for future work are made:

1. During MPC and SSP, the reaction mixture becomes highly viscous and thus it becomes difficult to remove water molecules -a byproduct of the reaction which is the rate determining step of this process. Thus, in order to enhance both mass and heat transfer, MPC and SSP should be conducted in an apparatus which will facilitate efficient and speedy renewal of reaction mixture surface to facilitate water removal and to provide intensive mixing. The apparatus could be a rotating disc type reactor for both MPC and SSP which will create a thin layer of reaction mixture for efficient removal of water.
2. A special kind of experimental setup should be designed, in which ultrasonication could be used to enhance the mobility of end-groups and thereby increase the molecular weight.
3. A detailed investigation is needed for confirmation of mechanistic features of MPC, SSP reactions and nanoprecipitation and process of agglomeration of nanoparticles.
4. Metal catalysts can be replaced by ionic liquids, which are stable in presence of water at high temperatures.
5. Enzymatic polymerization of L-lactic acid should be tested as the enzymatic reaction takes place at lower temperature than those attempted in this study. This will prohibit de-colorization and degradation of product.
6. Elevated temperature resistant, highly reactive, stereoselective and non-toxic organocatalysts should be developed for the MPC of lactic acid.
7. As concentration of PLA and S/NS volume ratio are found to be the governing input parameters for the synthesis of PLA NPs, for further studies and DOE, these parameters should only be considered to reduce experimentation time and effort.
8. As the incorporation of water during NP purification, may destabilize the suspension, NPs should be freeze dried after centrifugation without repeated washing with water.

ANALYSIS OF L-LACTIC ACID

A.1 FTIR OF L-LACTIC ACID

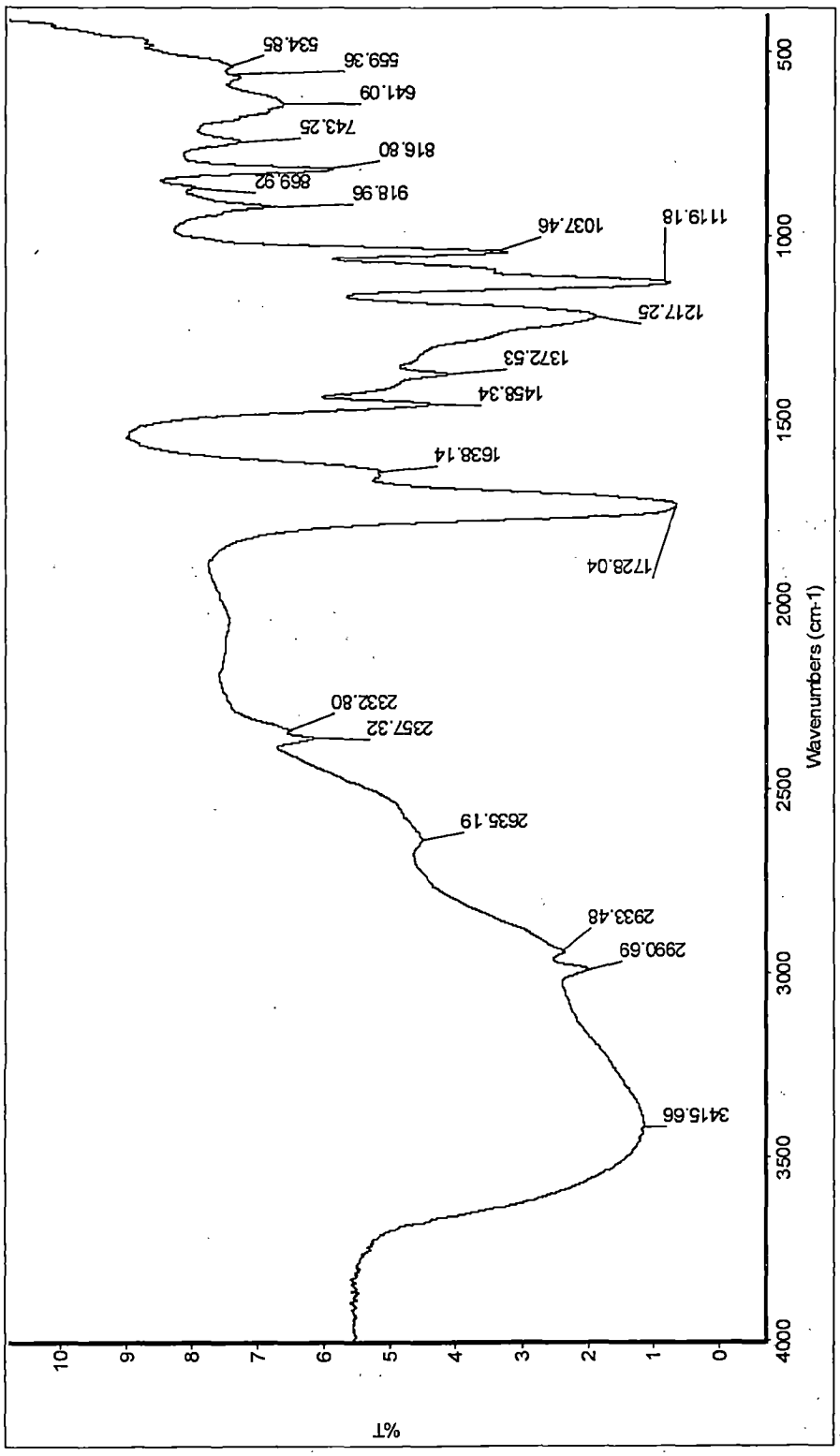

Fig. A.1 FTIR spectrum of L-lactic acid

Table A.1 FTIR spectral interpretation for L-lactic acid

Characteristic peaks	Wavenumber (cm^{-1})
Primary Aliphatic Alcohols	
-OH stretching	3415.66
-C-O stretching	1037.46
Aliphatic Carboxylic Acid group	
OH stretching	3100 - 2200
C=O stretching	1728.04
C-O stretching (1)	1458.34
C-O stretching (2)	1217.25
Acid OH deformation	918.96
Aliphatic hydrocarbons	
C-H stretching bands of CH_3	~3000
-CH deformation	1372.53
CH_3 asymmetric deformation	1470-1440
asymmetric CH_3 stretching	743.25
symmetric CH_3 vibration	1390-1370

A.2 NMR of LLA

Lactic acid was dissolved in D_2O for proceeding for the NMR analysis. The ^1H NMR and the ^{13}C NMR are given in Figure A.2 and A.4, respectively. The ^1H NMR with the peak integrals are given in Fig. A.3. In ^1H NMR spectrum, the –OH and –COOH peaks are very week and thus are not visible. The ^1H NMR in Fig. A.2, spectrum shows a doublet centered at 1.135ppm and a quartet at 4.125ppm corresponding to methyl (CH_3) and methane (CH) protons of lactic acid, respectively. It is also noted that commercial lactic acid also contains oligomers as depicted by a quartet at 4.8 ppm corresponding to $CH^{b'}$ of the main chain and quartet at 4.2ppm representing $CH^{b''}$ of the ultimate unit of the oligomers. In the ^{13}C NMR, given in Fig. A.4, the peaks around 16, 69 and 171 are due to the –CH3, –CH and –COOH groups, respectively.

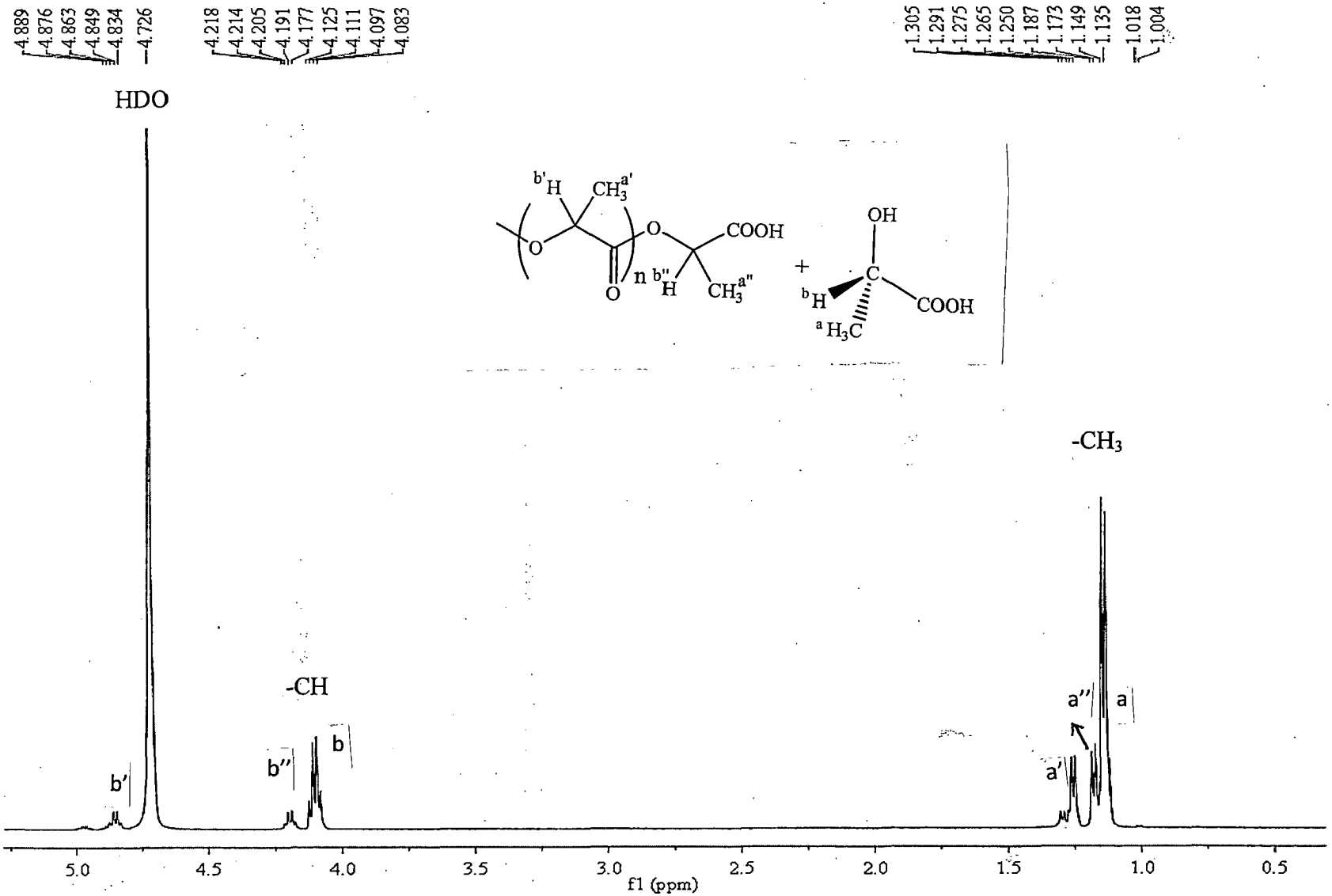

Fig. A.2 ^{1}H NMR spectrum of L-lactic acid

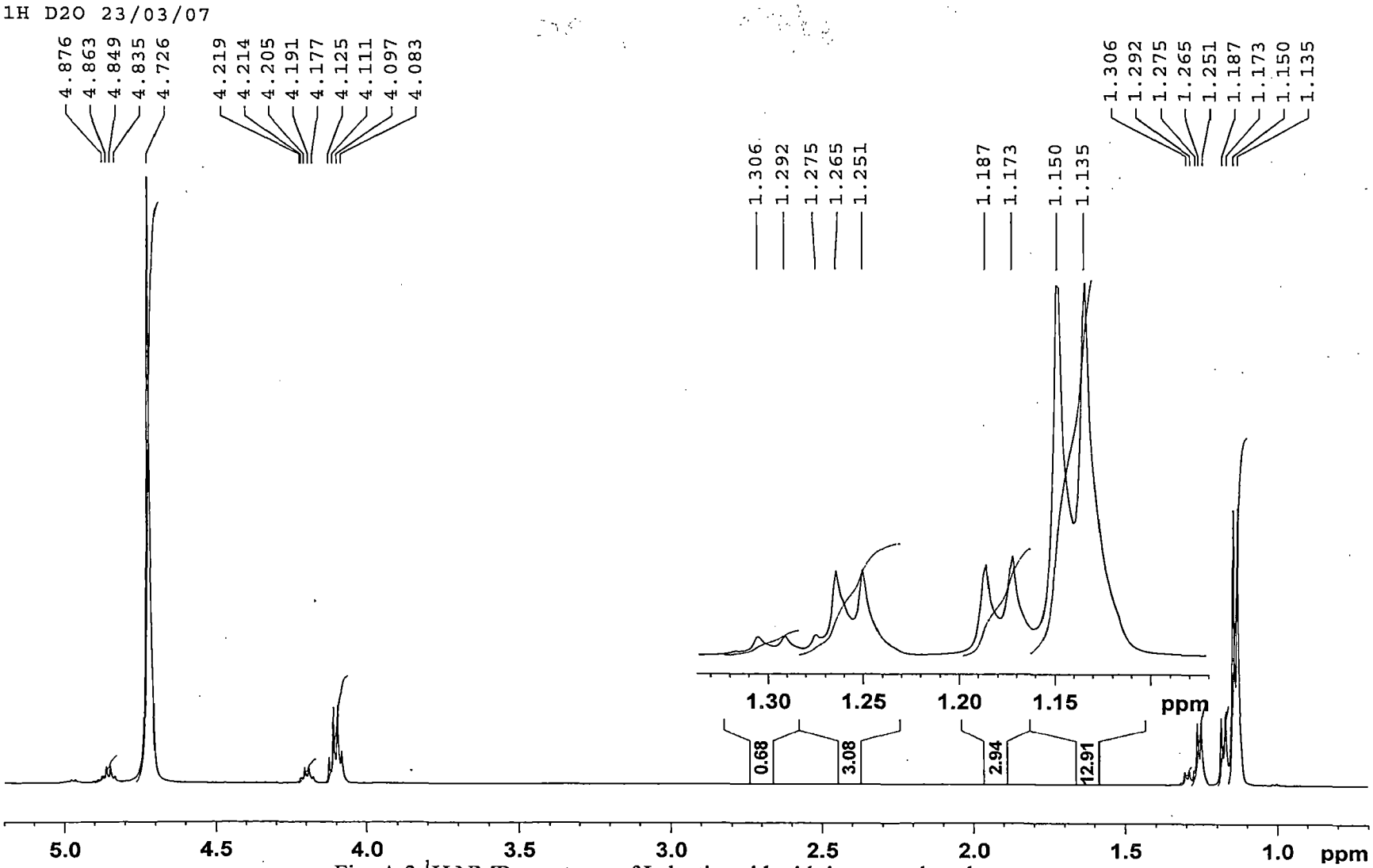

Fig. A.3 ^{1}H NMR spectrum of L-lactic acid with integrated peaks

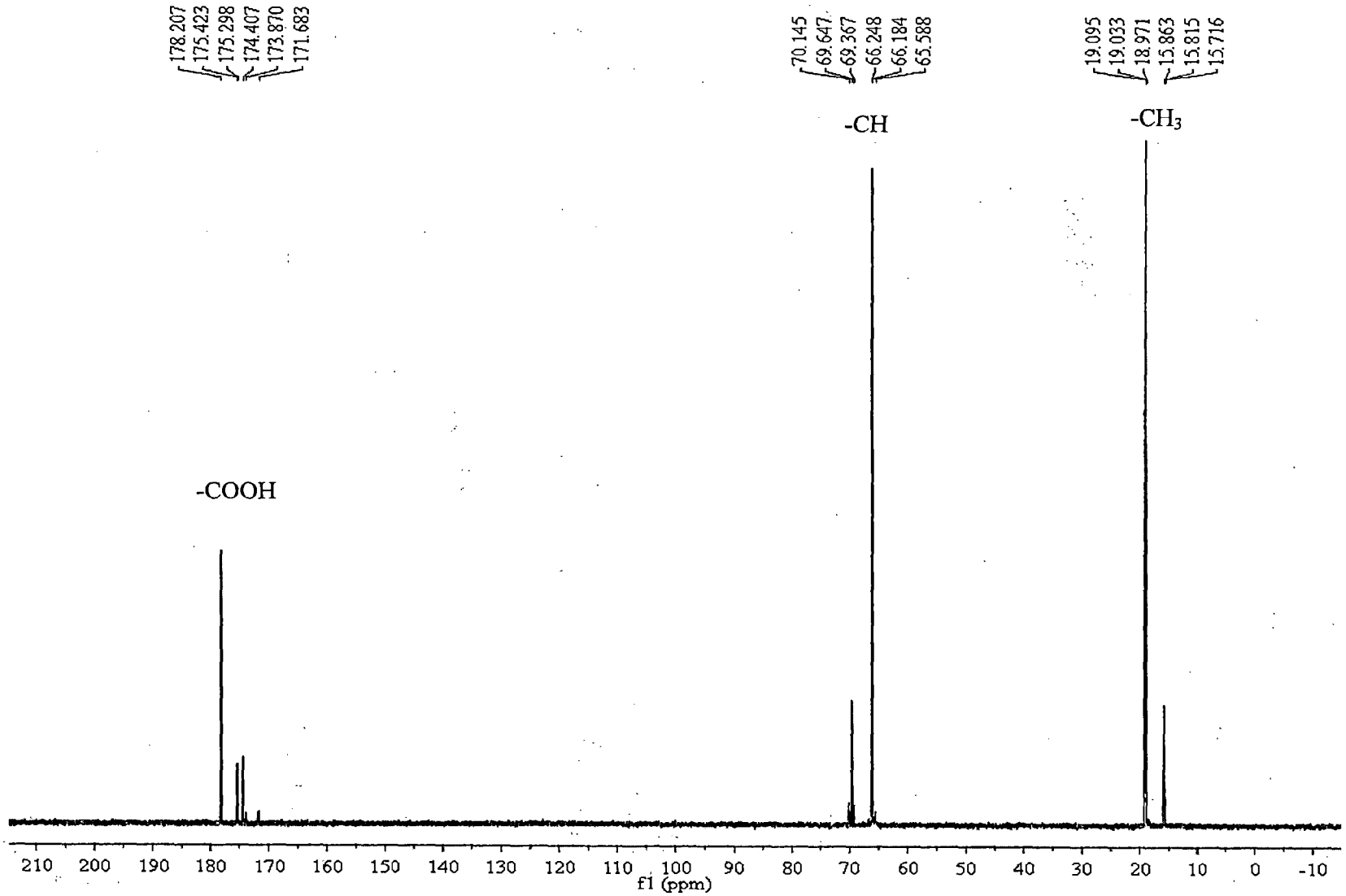

Fig. A.4 ^{13}C NMR spectrum of L-lactic acid

A.3 Optical rotation of LLA

Stereochemical purity = $(\alpha_{obs} / \alpha_{pure})*100$ ... Eq. A.1

Where, α_{obs} and α_{pure} are the specific rotation denoted by $[\alpha]_D^{25}$ of the sample and the 100 % pure L-Lactic acid, respectively. The specific rotation $[\alpha]_D^{25}$ for the 100% pure L-lactic acid is reported to be -2.6 [Merck Index 1977]. The specific rotation for the sample provided by Lactochem was found to be 2.48. Thus, the stereochemical purity is calculated to be 95.38 % which is in agreement with the NMR analysis.

A.4 Refractive index of LLA

The refractive index of the L-lactic acid is observed to be 1.4253 at 25°C when a sodium D-line light is used.

ANALYSIS OF TIN CHLORIDE DIHYDRATE

B.1 Melting Point Determination

The melting point of stannous chloride dihydrate was determined using the melting point apparatus supplied by DBK Instruments Mumbai, India. The melting point is found to be 38°C.

B.2 FESEM-EDAX Analysis

The elemental analysis is done by using the FESEM-EDAX analysis. The FESEM is shown in Fig. B1 and the elements present at the point indicated by a plus (+) symbol inside the crystal is given in Fig. B2. And the elemental analysis data is given in Table B1. Similarly, the elements present in the area indicated by a rectangle, inside the crystal shown in Fig. B3, are given in Fig. B4. And the elemental analysis data is given in Table B2.

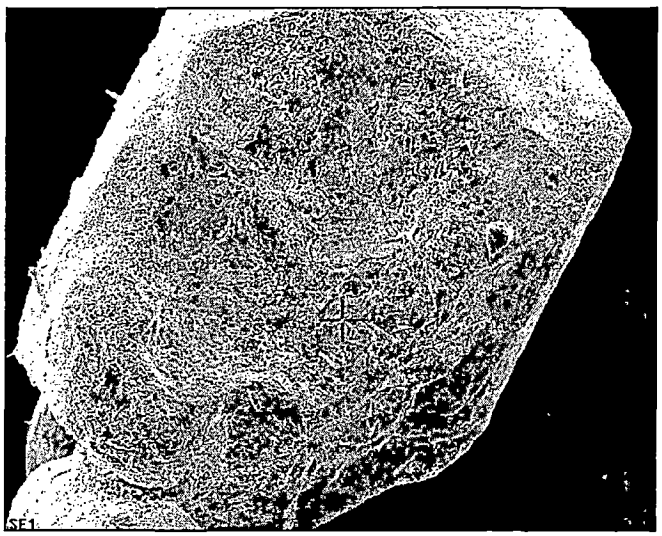

Fig. B.1 FESEM micrograph of $SnCl_2.2H_2O$ crystal showing a point

Table B.1 Elemental analysis using FESEM-EDAX at the point

Element	*Wt%*	*At%*
FeL	05.36	06.31
RbL	01.27	00.97
WM	00.98	00.35
ClK	31.70	58.76
PdL	00.00	00.00
SnL	60.69	33.60
Matrix	Correction	ZAF

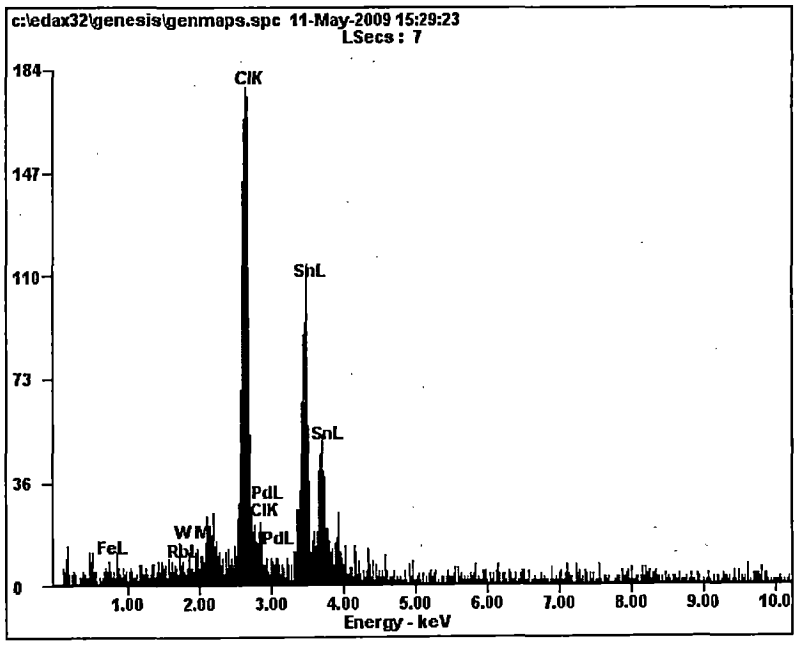

Fig. B.2 EDAX analysis of $SnCl_2.2H_2O$ at the point

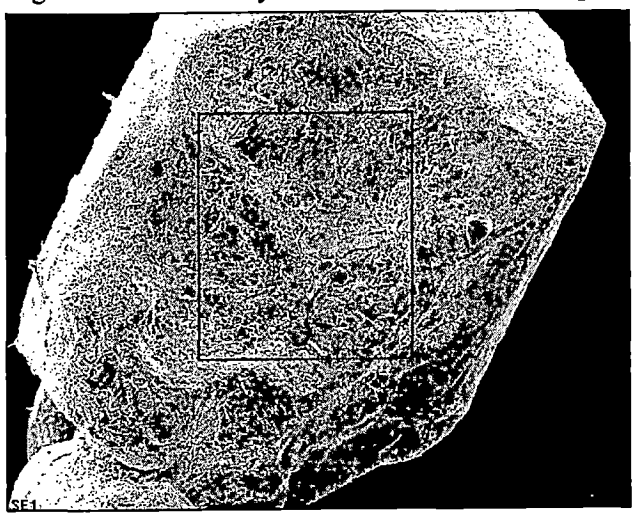

Fig. B.3 FESEM micrograph of $SnCl_2.2H_2O$ crystal showing an area

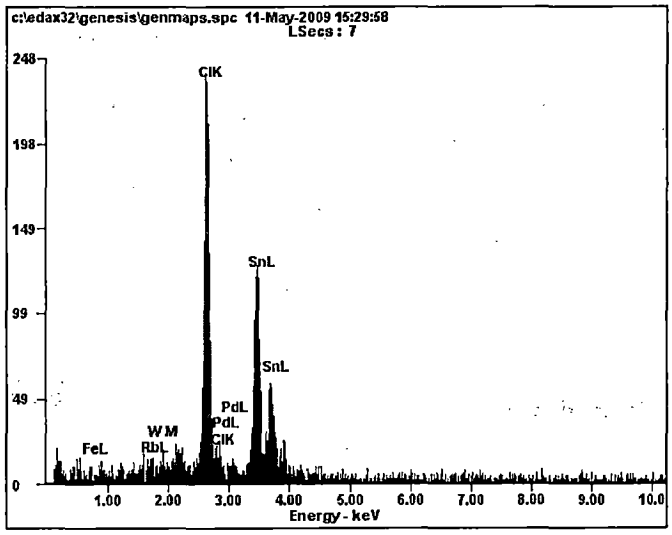

Fig. B.4 EDAX analysis of mentioned area of $SnCl_2.2H_2O$ crystal

Table B.2 Elemental analysis of the area using FESEM-EDAX

Element	*Wt%*	*At%*
FeL	08.72	10.60
RbL	02.46	01.95
WM	02.18	00.81
ClK	27.56	52.76
PdL	01.28	00.82
SnL	57.80	33.06
Matrix	Correction	ZAF

B.3 XRD Analysis

The XRD pattern of Tin chloride dihydrate is given in Fig. B5. The XRD lines were identified by comparing the measured patterns to the JCPDS data cards. All the diffraction peaks are indexed to tin chloride hydrate (JCPDS #01-0521), and no impurity peaks are detected. The crystallite size of tin chloride hydrate is determined using the Scherrer formula (Eq. B.1) and is estimated to be 23.81 Å.

$$D = \frac{k\lambda}{\beta \cos\theta} \qquad \ldots(B.1)$$

Where, D is the average crystallite size, k is the shape factor or Scherrer constant, λ is the X-ray wavelength (1.5406 Å for Copper target), β (in radians) is the line width at half the maximum intensity (FWHM) corrected for instrumental and strain broadening and θ is the Bragg's angle in radians. The value of k, is taken to be 0.89 which is dimensionless.

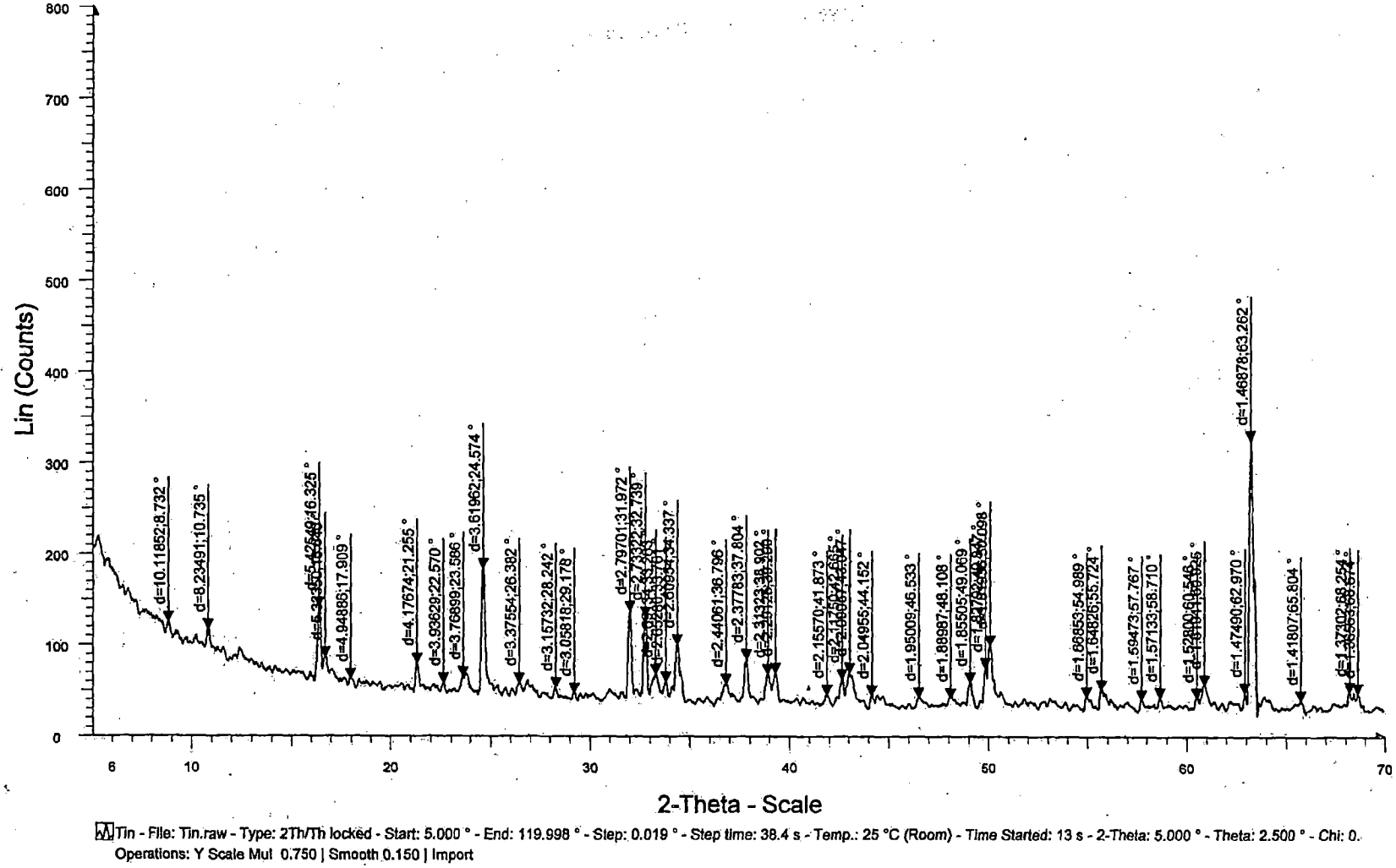

Fig. B.5 XRD pattern of $SnCl_2.2H_2O$

ANALYSIS OF *p*-TOLUENE SULFONIC ACID (PTSA)

C.1 FTIR Analysis

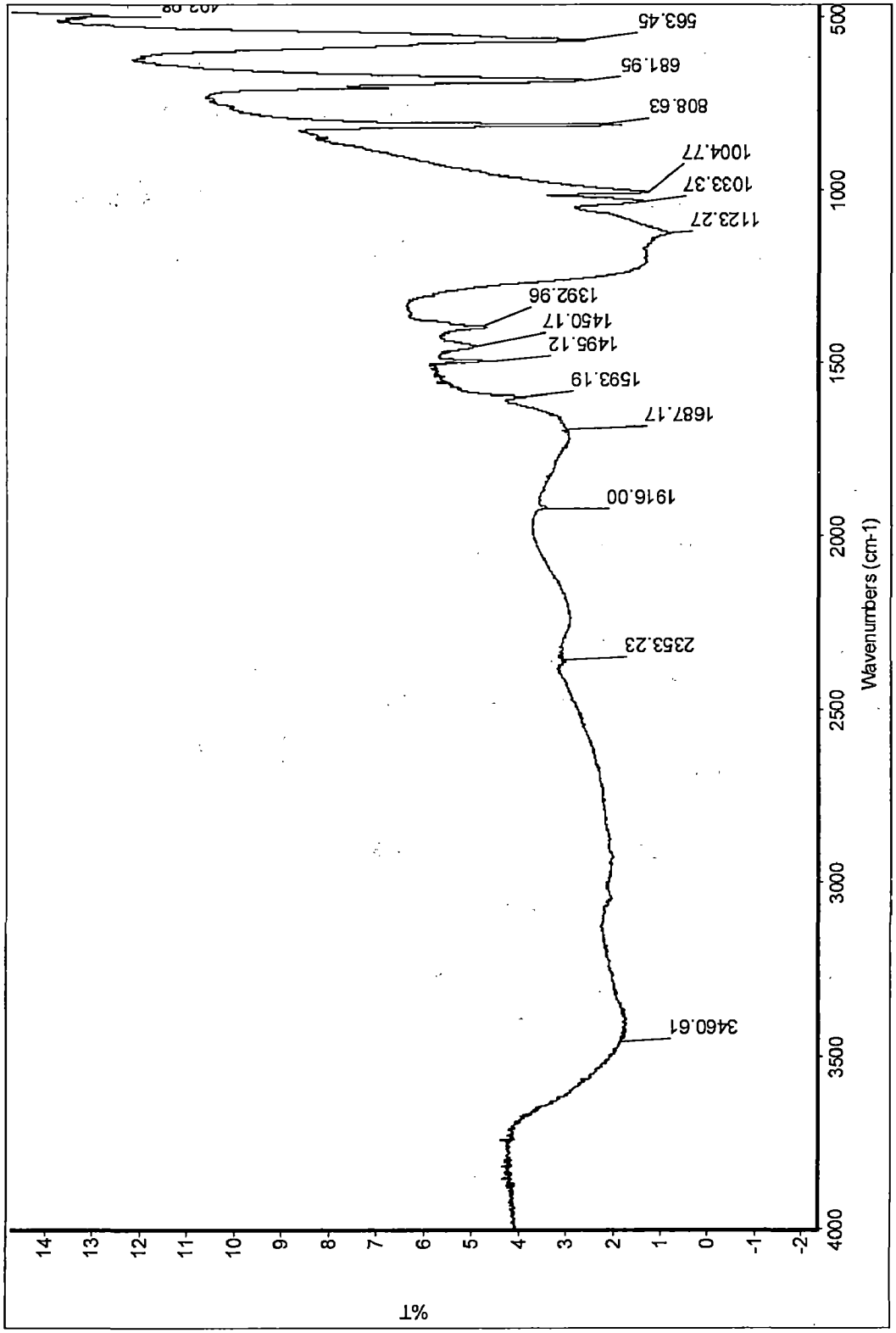

Fig. C.1 FTIR spectrum of PTSA

Table C.1 FTIR spectral interpretation for PTSA

Characteristic peaks	Wavenumber (cm^{-1})
Aromatic sulfonic acid	
$-SO_3$-C Assymetric stretching	1392.96; 1123.27
Para substituted aromatic hydrocarbons	
CH of benzene ring	~3000
Benzenoid ring (1)	1593.19
Benzenoid ring (2)	1495.12
CH in-plane	1033.37
CH out of plane	681.95
p-substitute aromatic ring	808.63

C.2 NMR ANALYSIS

The NMR analysis of PTSA was carried out using D_2O as the solvent. As per the ^{13}C NMR and ^{1}H NMR spectra of PTSA presented in Fig. C.2 and Fig. C.3, respectively, the structure was confirmed. The corresponding peaks are annotated in the corresponding figures.

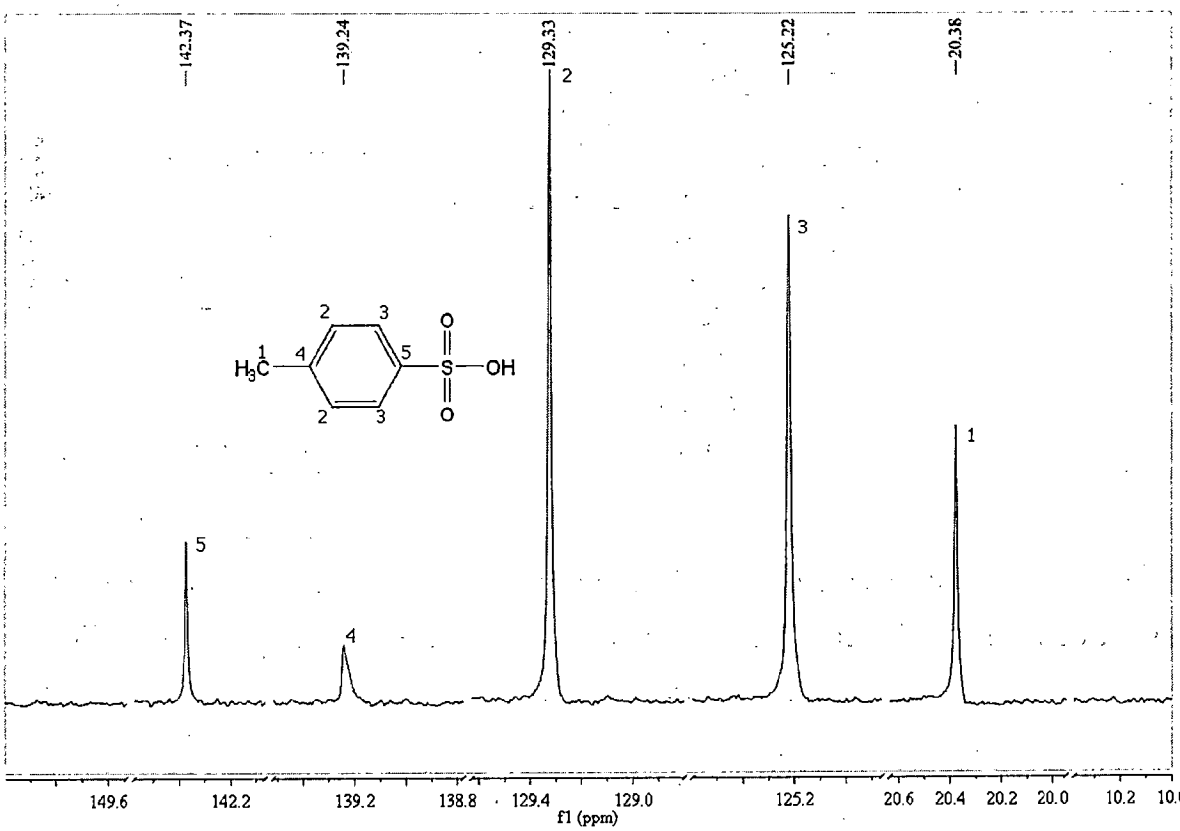

Fig. C.2 ^{13}C NMR spectrum of PTSA

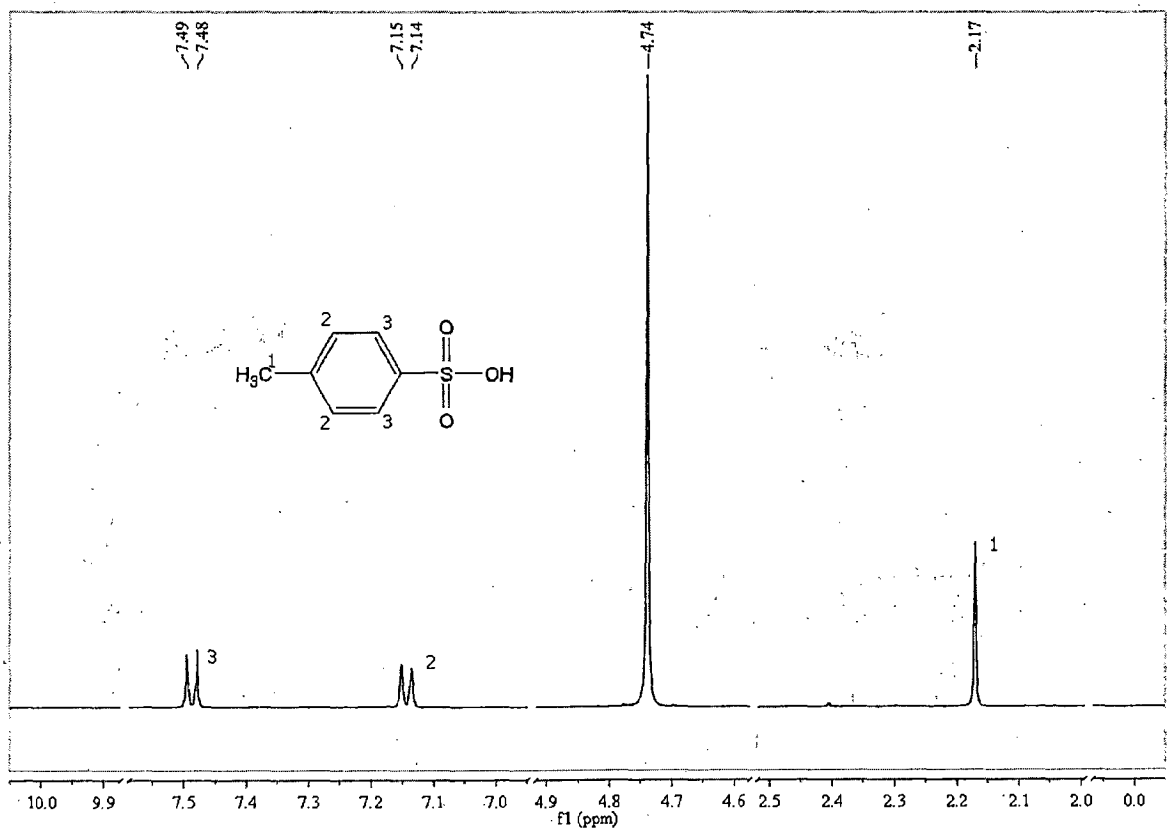

Fig. C.3 ^{1}H NMR spectrum of PTSA

C.3 Refractive index analysis of PTSA

The PTSA solution was directly put onto the refractometer and the refractive index was noted down to be 1.3821 at 25°C which is in well agreement with the reported value (1.3825) http://www.chemicalbook.com/ChemicalProductProperty_EN_CB3173385.htm .

C.4 CHNSO analysis of PTSA

From the CHNS analysis of PTSA, it was observed that the %age of CHNS are 45.01, 6.23, 0.001 and 17.32, respectively, which is very close to the calculated value of 44.20, 5.30, 0 and 16.86, respectively.

INDIVIDUAL PARTS OF EXPERIMENTAL SETUP

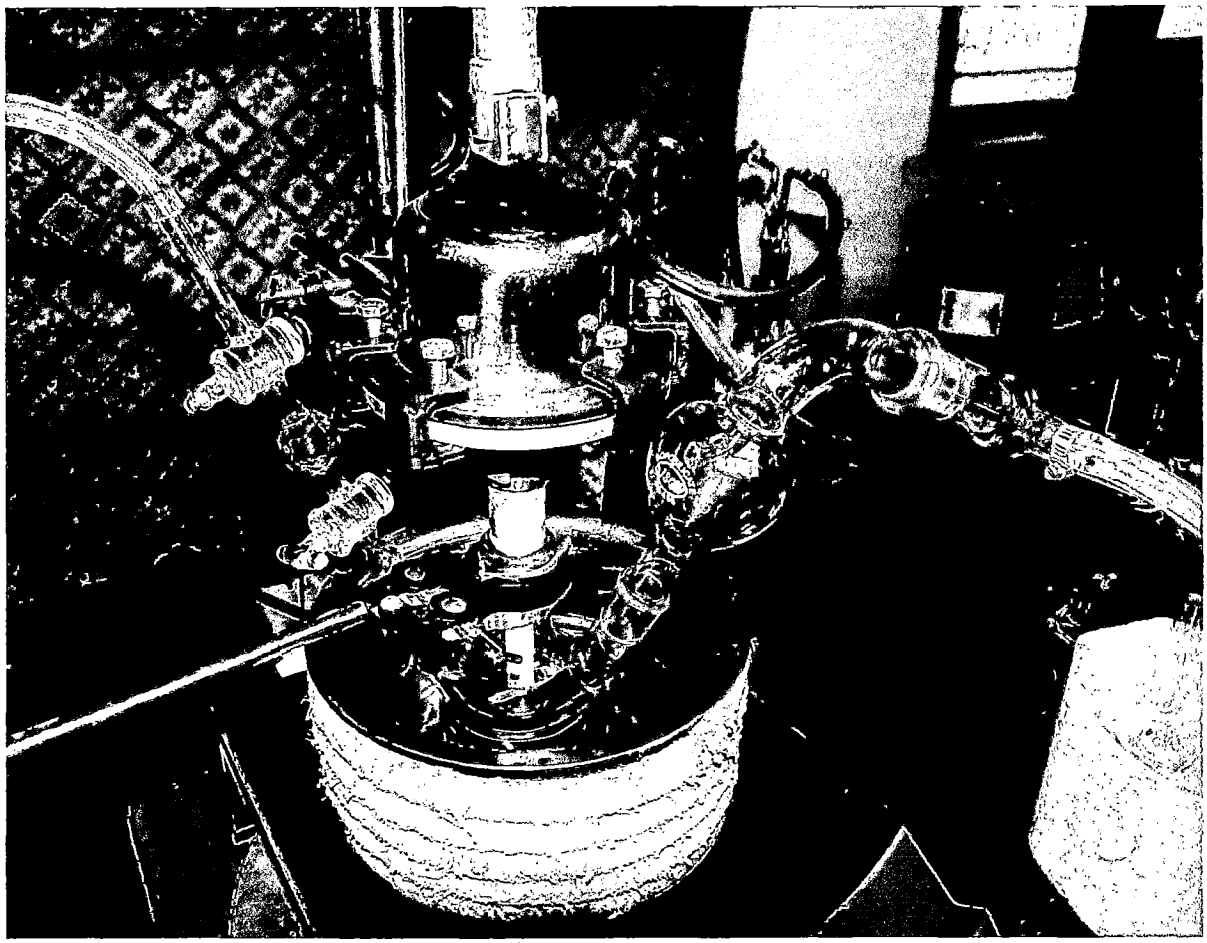

Fig. D.1 Reactor for melt polycondensation reaction

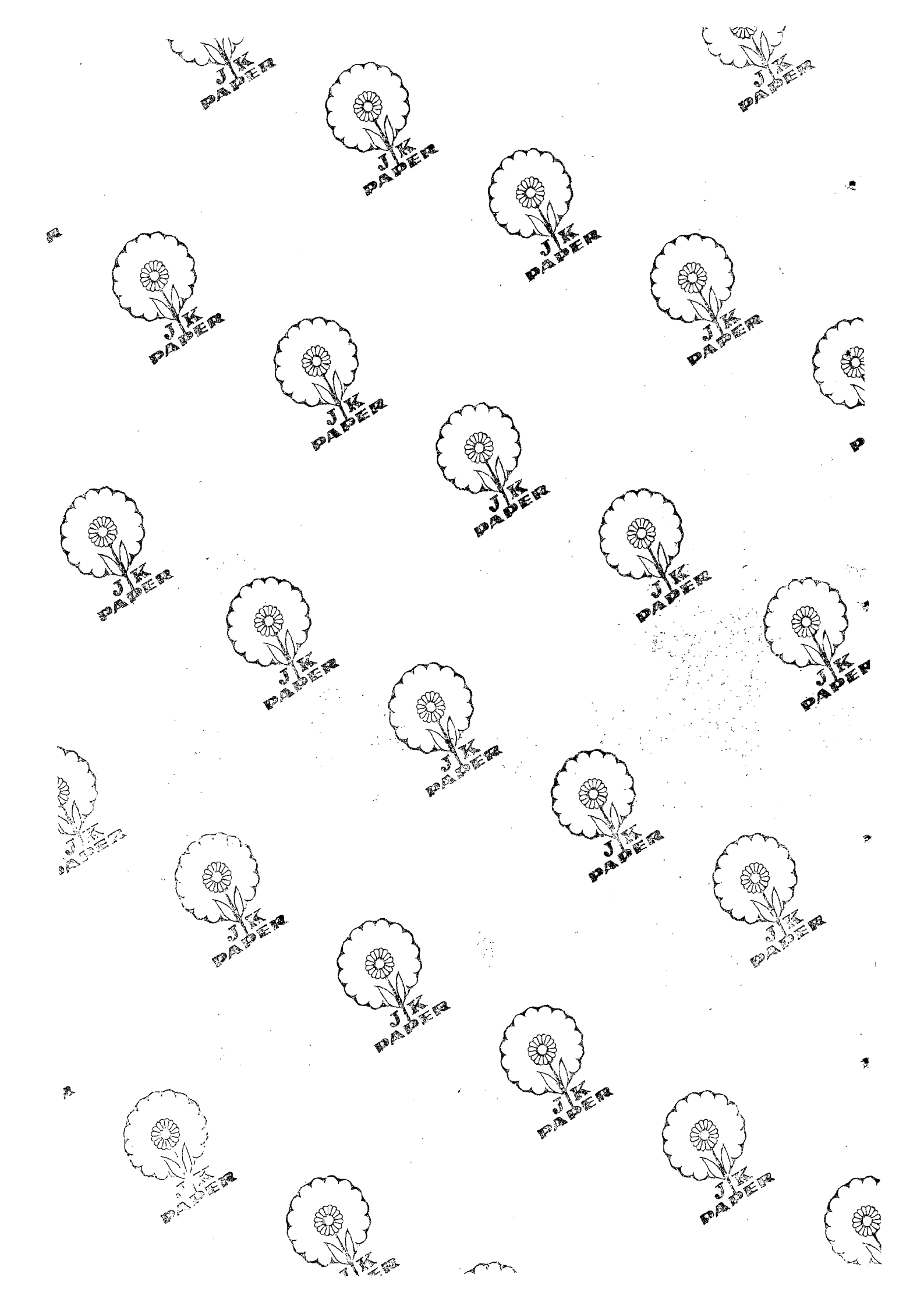
J K
PAPER

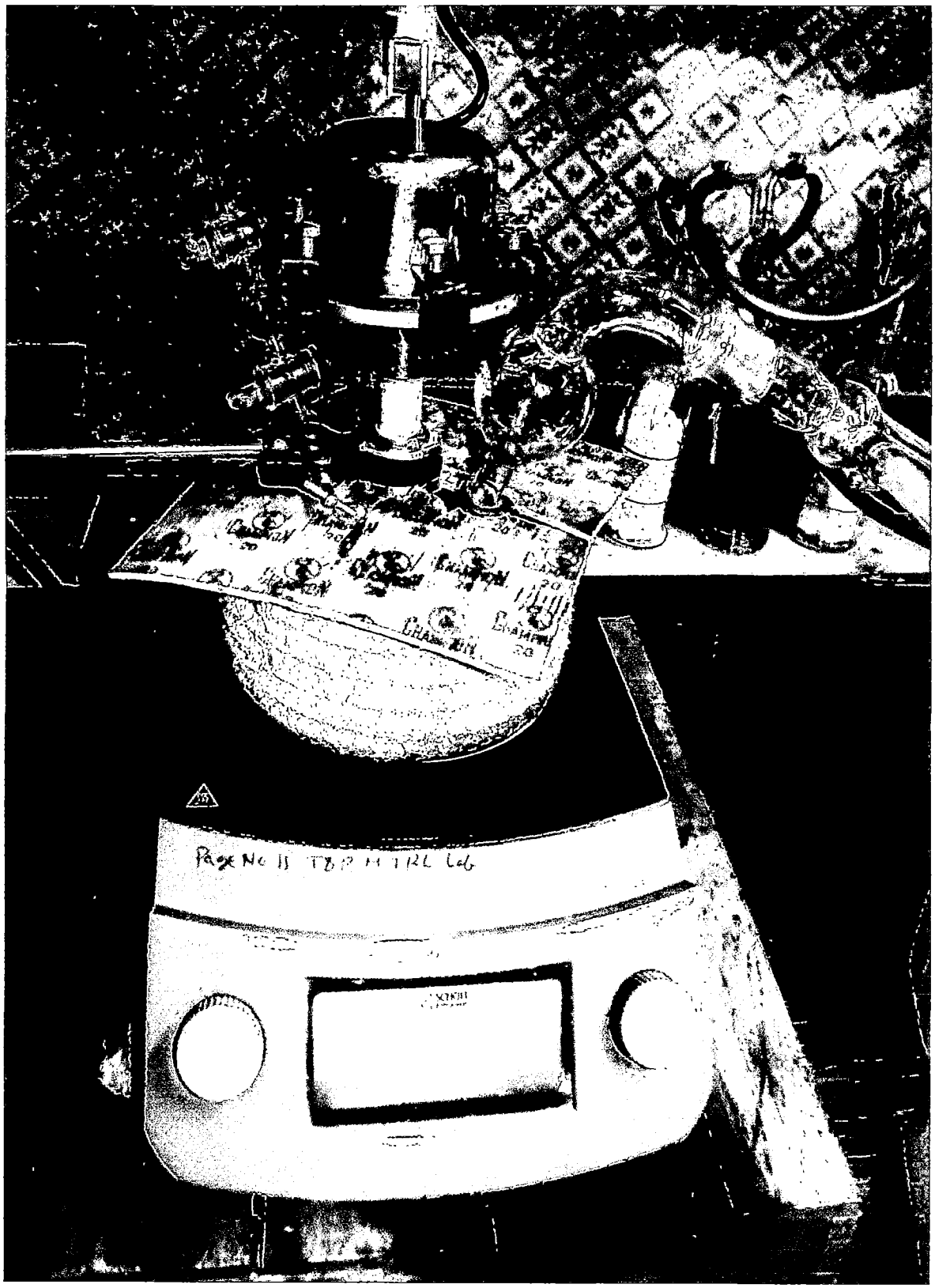

Fig. D.2 Reactor during polycondensation to prevent heat loss

J.K
PARIS

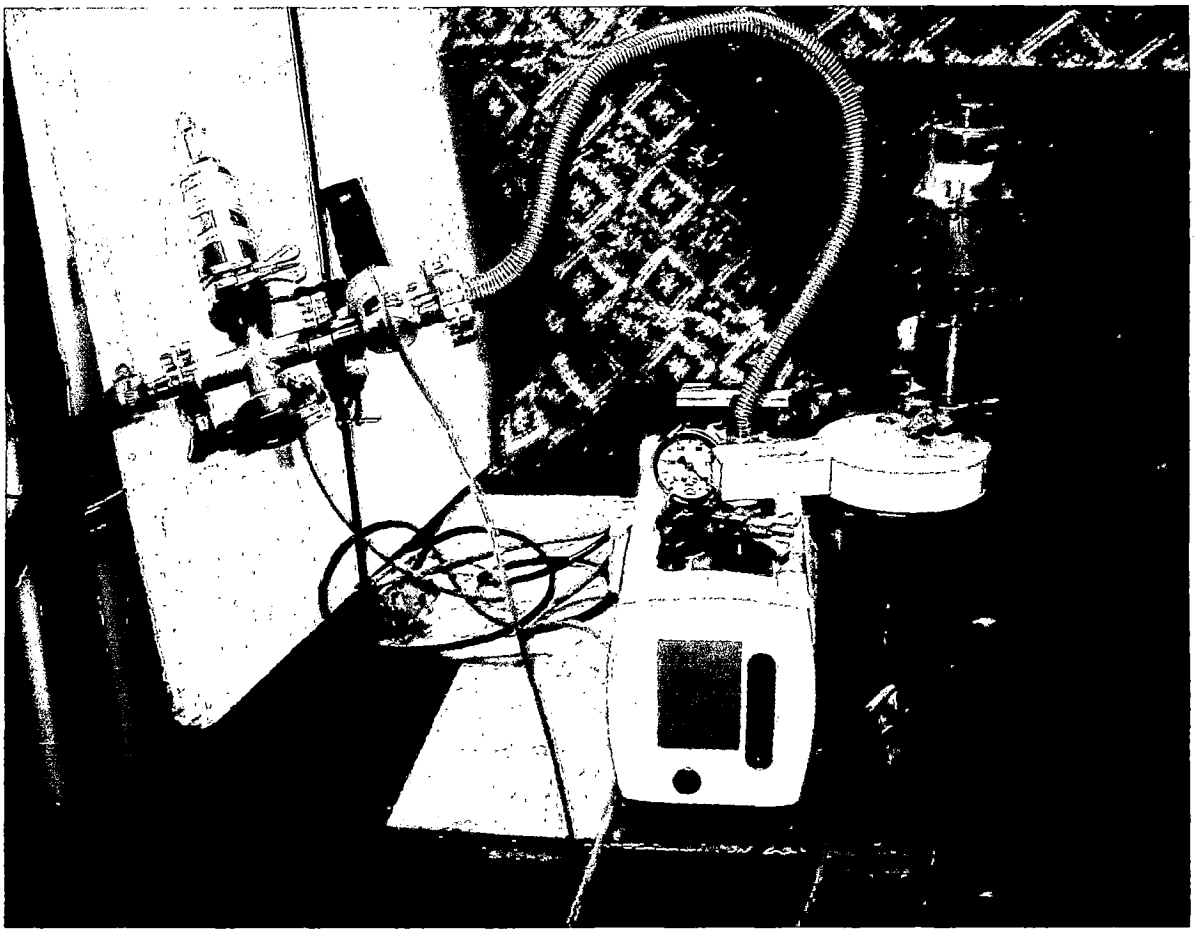

Fig. D.3 Vacuum pump

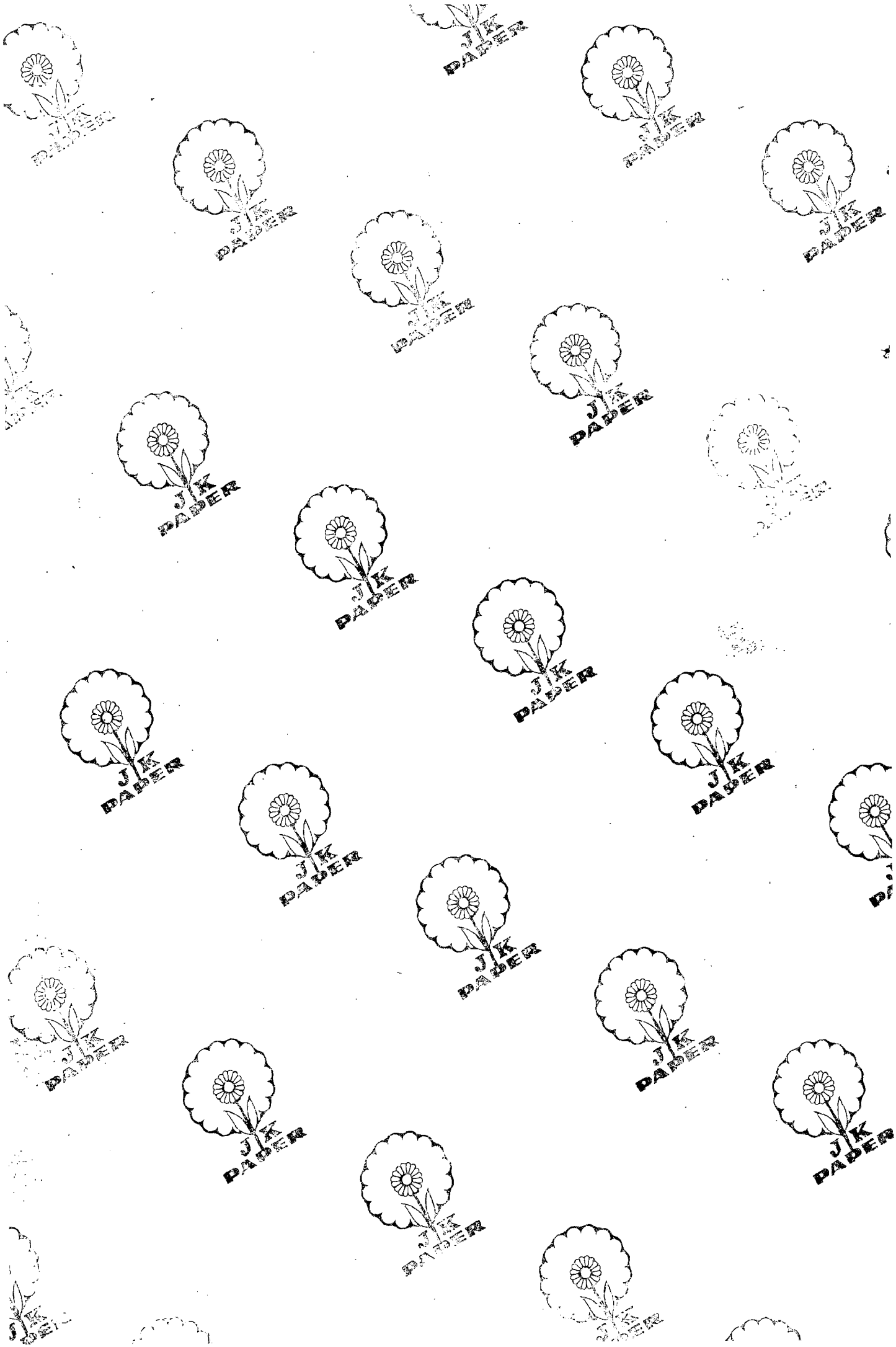
J K
PAPER

EXPERIMENTAL DESIGN

E.1 SYNTHESIS OF POLY(LACTIC ACID) BY MELT POLYCONDENSATION

The coded small face centered CCD of RSM is presented in Table E.1.

Table E.1 Experimental design points obtained by CCD of RSM in terms of coded values

		Factor 1	Factor 2	Factor 3	Factor 4	Factor 5	Response 1	Response 2
Run No.	Point Type	X_1: Amount of LLA(g)	X_2: Catalyst (wt.%)	X_3: ES time (h)	X_4: MPC temperature (°C)	X_5: MPC time(h)	M_w (kDa)	Yield (wt.%)
1	Factorial	1	1	-1	1	-1	2.943	35.6
2	Factorial	1	-1	1	1	-1	0.951	39.2
3	Factorial	-1	1	1	-1	1	8.514	45.3
4	Factorial	1	1	1	-1	-1	98.470	68.9
5	Factorial	1	1	-1	-1	1	55.634	65.2
6	Factorial	1	-1	-1	1	1	1.572	30.3
7	Factorial	-1	-1	1	1	1	0.447	29.0
8	Factorial	-1	1	-1	1	1	2.266	40.3
9	Factorial	1	-1	1	-1	1	89.675	65.3
10	Factorial	-1	1	1	1	-1	4.072	37.6
11	Factorial	-1	-1	-1	-1	-1	178.857	85.3
12	Center	0	0	0	0	0	45.871	55.6
13	Center	0	0	0	0	0	46.645	56.4
14	Center	0	0	0	0	0	44.352	52.6
15	Center	0	0	0	0	0	40.974	46.0
16	Center	0	0	0	0	0	39.046	46.3
17	Axial	-1	0	0	0	0	35.874	53.3
18	Axial	1	0	0	0	0	48.579	46.2
19	Axial	0	-1	0	0	0	34.265	49.7
20	Axial	0	1	0	0	0	23.465	57.4
21	Axial	0	0	-1	0	0	32.606	45.2
22	Axial	0	0	1	0	0	45.301	52.4
23	Axial	0	0	0	-1	0	75.929	66.2
24	Axial	0	0	0	1	0	6.923	21.3
25	Axial	0	0	0	0	-1	68.896	59.4
26	Axial	0	0	0	0	1	40.123	46.6
27	Vertex	1	-1	-1	-1	-1	97.408	79.0
28	Vertex	-1	1	-1	-1	-1	98.486	69.9
29	Vertex	-1	-1	-1	-1	1	9.103	59.6
30	Vertex	-1	-1	-1	1	-1	2.079	30.7

E.2 SYNTHESIS OF POLY(LACTIC ACID) BY SOLID-STATE POLYCONDENSATION

The coded small face centered CCD of RSM is presented in Table E.2.

Table E.2 Experimental design points obtained by CCD of RSM in terms of coded values

		Factor 1	Factor 2	Factor 3	Factor 4	Factor 5	Response 1	Response 2
Run No.	Point Type	X_1: Amount of PLLA(g)	X_2: HT temperature (°C)	X_3: HT time (h)	X_4: SSP time (h)	X_5: SSP temperature (°C)	M_w (kDa)	Yield (wt.%)
1	Factorial	1	1	-1	1	-1	84.691	72.9
2	Factorial	1	-1	1	1	-1	65.098	83.0
3	Factorial	-1	1	1	-1	1	70.985	71.1
4	Factorial	1	1	1	-1	-1	80.553	81.9
5	Factorial	1	1	-1	-1	1	89.942	76.8
6	Factorial	1	-1	-1	1	1	78.839	70.9
7	Factorial	-1	-1	1	1	1	61.276	62.4
8	Factorial	-1	1	-1	1	1	71.9	71.5
9	Factorial	1	-1	1	-1	1	75.67	75.1
10	Factorial	-1	1	1	1	-1	69.984	80.3
11	Factorial	-1	-1	-1	-1	-1	68.763	82.3
12	Center	0	0	0	0	0	281.54	81.0
13	Center	0	0	0	0	0	280.095	80.1
14	Center	0	0	0	0	0	270.568	82.4
15	Center	0	0	0	0	0	300.195	79.8
16	Center	0	0	0	0	0	275.16	81.6
17	Axial	-1	0	0	0	0	259.876	85.9
18	Axial	1	0	0	0	0	278.437	76.3
19	Axial	0	-1	0	0	0	130.763	88.9
20	Axial	0	1	0	0	0	165.362	71.2
21	Axial	0	0	-1	0	0	224.947	87.0
22	Axial	0	0	1	0	0	271.549	73.5
23	Axial	0	0	0	-1	0	248.904	92.6
24	Axial	0	0	0	1	0	188.801	70.8
25	Axial	0	0	0	0	-1	184.936	85.2
26	Axial	0	0	0	0	1	239.953	73.3
27	Vertex	1	-1	-1	-1	-1	97.601	80.1
28	Vertex	-1	1	-1	-1	-1	88.793	79.3

DETAILS OF NMR SOLVENTS

All the deuterated solvents were supplied by Sigma Aldrich and are hygroscopic in nature.

Table F.1 Chemical shift, multiplicity and coupling constant (J) of NMR solvents

Solvent	Experiment	Peak type	*Chemical Shift (ppm)	*Temperature	*Multiplicity	*J (Hz)
Chloroform-d ($CDCl_3$) 99.8 Atom % D 0.03% v/v TMS	^{1}H	TMS	0.000	25°C	1	-
		solvent	7.261	-do-	1	-
	^{13}C	TMS	-0.029	-do-	1	-
		solvent	76.950	-do-	3	32.0
	^{2}D	solvent	7.289	-do-	-	-
(Methyl Sulfoxide)-d6 DMSO (C_2D_6OS) 99.9 Atom % D 0.03% v/v TMS	^{1}H	TMS	0.075	-do-	1	-
		solvent	2.577	-do-	5	1.9
	^{13}C	TMS	0.036	-do-	1	-
		solvent	39.115	-do-	7	21.0
	^{2}D	solvent	2.633	-do-	-	-
Heavy water D_2O- Deuterium Oxide 99.9 Atom % D	^{1}H	TMS	-0.092	-do-	-	-
		DSS	-0.074	-do-	-	-
		TSP	-0.083	-do-	-	-
		HOD	4.717	-do-	-	-
	^{2}D	D_2O	4.789	-do-	-	-

*The values were taken from the NMR solvent software.

CALCULATION OF ZEROTH-ORDER AND FIRST-ORDER CONNECTIVITY INDICES FOR THE PLA REPEAT UNIT

The graph theoretical treatment of molecular species, for the evaluation of connectivity indices is established by the construction of the hydrogen-suppressed graph of PLA repeat unit, which is shown in Fig. G.1. Hydrogen suppressed graph for PLA (Fig. G.1(B)) was built by omitting the hydrogen atoms from the valence bond (Lewis) structure of the repeat unit of PLA given in Fig. G.1(A). For polymers, this procedure utilizes the repeat unit. It takes chain continuation into account without considering truncation errors (Kier and Hall, 1976, 1986).

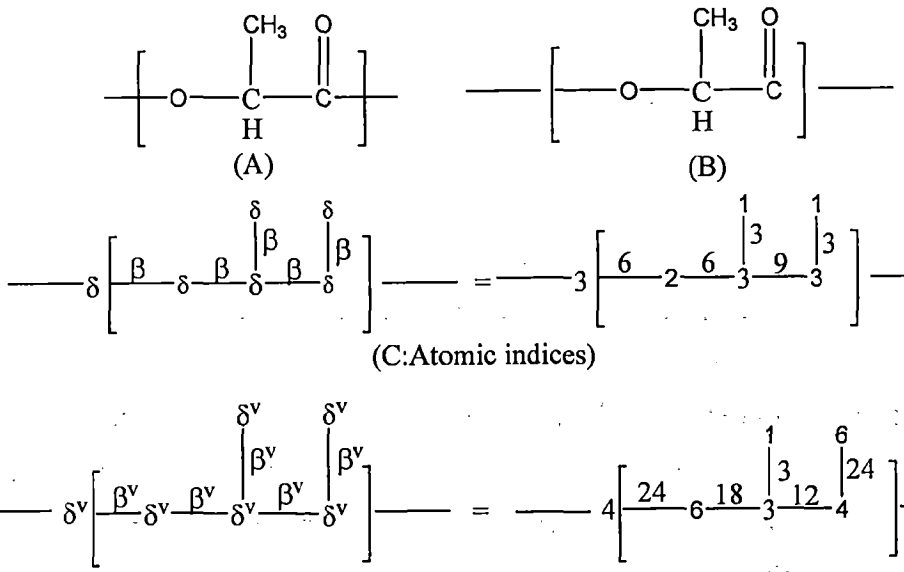

Fig. G.1 Connectivity indices for PLA

The value of two indices, δ and δ^v, given in Fig. G.1, which describe the electronic environment and the bonding configuration of each non-hydrogen atom in the molecule, respectively, are assigned, and listed at the vertices of the hydrogen suppressed graph. The first atomic index *(δ)*, i.e. the simple connectivity index, equals the number of non-hydrogen atoms to which a given non-hydrogen atom is bonded. For example, in case of PLA, C of CH is connected to C of CH_3, C of CO and one O. Thus, δ=3 for C of CH, 1 for C of CH_3 and 3 for C of CO, 1 for O of CO and 2 for O. The second atomic index is the valence connectivity index, δ^v, incorporating information on details of the electronic configuration of each non-hydrogen atom. Equivalently, the δ of any vertex (δ^v) in the hydrogen-suppressed graph is the number of

edges or bonds emanating from it. Its value for the lowest oxidation states of the element will be generally assigned by Eq. G.1, where Z^V is the number of valence electrons of an atom, N_H is the number of hydrogen atoms bonded to it, and Z is its atomic number (i.e. Z equals Z^V plus the number of inner shell electrons).

$$\delta^v \equiv \frac{Z^V - N_H}{Z - Z^V - 1} \qquad \text{(G.1)}$$

Bond indices β and β^v can be defined for each bond not involving a hydrogen, as products of the atomic indices (δ and δ^v) at the two vertices (i and j) which define a given edge or bond. Bond indices are calculated by using Eq. G.2a. Zeroth-order (atomic) connectivity indices ${}^0\chi$ (simple index) and ${}^0\chi^V$ (valence index) for the repeat unit are defined in terms of summation over vertices of the hydrogen suppressed graph and are determined using Eq. G.2b. First-order (bond) connectivity indices ${}^1\chi$ (simple index) and ${}^1\chi^V$ (valence index) for the repeat unit are defined in terms of summations over the edges of the hydrogen suppressed graph (Kier and Hall, 1976, 1986) and are determined using Eq. G.2c.

$$\beta_{ij} \equiv \delta_i \delta_j \; ; \qquad \beta_{ij}^v \equiv \delta_i^v \delta_j^v \qquad \text{(G.2a)}$$

$${}^0\chi \equiv \sum_{[\text{vertices}]} (1/\sqrt{\delta}); \qquad {}^0\chi^V \equiv \sum_{[vertices]} (1/\sqrt{\delta^v}) \qquad \text{(G.2b)}$$

$${}^1\chi \equiv \sum_{[\text{edges}]} (1/\sqrt{\beta}); \quad {}^1\chi^V \equiv \sum_{[\text{edges}]} (1/\sqrt{\beta^V}) \qquad \text{(G.2c)}$$

Calculation of the zeroth-order and first-order connectivity indices for PLA using Eq. G.2b and G.2c is shown as follows:

$${}^0\chi = \frac{1}{\sqrt{2}} + \frac{1}{\sqrt{3}} + \frac{1}{\sqrt{1}} + \frac{1}{\sqrt{1}} + \frac{1}{\sqrt{3}} = 3.8618$$

$${}^1\chi = \frac{1}{\sqrt{6}} + \frac{1}{\sqrt{6}} + \frac{1}{\sqrt{3}} + \frac{1}{\sqrt{9}} + \frac{1}{\sqrt{3}} = 2.3045$$

$${}^0\chi^v = \frac{1}{\sqrt{6}} + \frac{1}{\sqrt{3}} + \frac{1}{\sqrt{1}} + \frac{1}{\sqrt{4}} + \frac{1}{\sqrt{6}} = 2.8938$$

$${}^1\chi^v = \frac{1}{\sqrt{24}} + \frac{1}{\sqrt{18}} + \frac{1}{\sqrt{3}} + \frac{1}{\sqrt{12}} + \frac{1}{\sqrt{24}} = 1.50998$$

These values are used for calculation of molar volume of PLA as can be seen in Appendix H.

CALCULATION OF MOLAR VOLUME (V) OF PLA

H.1 CALCULATION OF MOLAR VOLUME (V) OF PLA

The molar volume (V) is calculated using the Eq. H.1.

$$V(cc/mol) = 3.642770({}^{0}\chi) + 9.798697({}^{0}\chi^{V}) - 8.542819({}^{1}\chi) + 21.693912({}^{1}\chi^{V}) + 0.978655(N_{MV}) \quad \text{...(H.1)}$$

Where, ${}^{0}\chi$, ${}^{0}\chi^{v}$, ${}^{1}\chi$ and ${}^{1}\chi^{v}$ are the connectivity indices defined in Appendix G and N_{MV} is the dimensionless constant defined by Eq. H.2

$$N_{MV} = 24N_{Si} - 18N_{(-S-)} - 5N_{sulfone} - 7N_{Cl} - 16N_{Br} + 2N_{(backbone\ ester)} + 3N_{ether} + 5N_{carbonate} + 5N_{(C=C)} - 11N_{cyc} - 7N_{(fused\text{-}1)} \quad \text{...(H.2)}$$

$$= 0-0-0-0-0+2*1+0+0+0-0-0=2$$

Last term to be used only when $N_{fused} \geq 2$, where N_{fused} is any ring structure containing at least one aromatic ring which shares at least one edge with another ring and all of the other rings with which it shares an edge. By putting the value of N_{MV} and connectivity indices, obtained from Appendix G, in Eq. H.1, the value of V is calculated to be 57.45 cc/mol.

The values of the connectivity indices (see Appendix G for calculations), molar volume, and the dimensionless constants, are summarized in Table H.1.

Table H.1 Connectivity indices, cohesive energy and molar volume of PLA

Connectivity indices and constants for calculating δ		PLA
Zeroth-order and first-order connectivity indices	${}^{0}\chi$	3.8618
	${}^{0}\chi^{v}$	2.8938
	${}^{1}\chi$	2.3045
	${}^{1}\chi^{v}$	1.50998
Molar Volume (V) from van Krevelen correlation	N_{MV}	2
	V (cc/mol)	57.45

DETERMINATION OF HANSEN SOLUBILITY PARAMETERS (HSP) FOR PLA

The values of Hansen solubility parameters (HSP) for PLA have been obtained using the group contributions by van Krevelen and Hoftyzer (1976). They have reported the group contributions, F_d (dispersion component of molar attraction constant), F_p (polar component of molar attraction constant) and E_h (hydrogen bonding component of total cohesive energy). The values of F_d, F_p, E_h for different structural groups of PLA, acetone and DMSO are given in Table I.1.

Table I.1 Group contributions (van Krevelen and Hoftyzer, 1976), towards F_d, F_p, E_h of each constituent structural group of PLA, acetone, DMSO and methanol

Name of the structural group	F_{di} ($J^{1/2}.cc^{1/2}.mol^{-1}$)	F_{pi} ($J^{1/2}.cc^{1/2}.mol^{-1}$)	E_{hi} (J/mol)
$-CH_3$	420	0	0
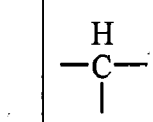	80	0	0
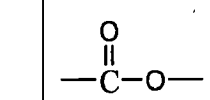	390	490	7000
-CO-	290	770	2000
-OH	210	500	20000
-S-	440	-	-
-O-	100	400	3000

Expressions for HSPs in terms of F_{di}, F_{pi}, E_{hi} are given in Eq. I.1, where i stands for the individual group. Molar volume (V) of PLA is 57.45 cc/mol, as reported in Appendix H. The values of ΣF_{di}, ΣF_{pi}^2, ΣE_{hi} for PLA are calculated to be 890, 240100 and 7000, respectively, by using the values reported in Table I.1.

$$\delta_d = \frac{\sum F_{di}}{V};\ \delta_p = \frac{\sqrt{\sum F_{pi}^2}}{V};\ \delta_h = \sqrt{\frac{\sum E_{hi}}{V}} \qquad \ldots \text{I.1}$$

Using Eq. I.1, values of δ_d, δ_p and δ_h obtained are 15.49, 8.53 and 11.04 $(J/cc)^{1/2}$, respectively.

Table J.1 Raw experimental data for synthesis of PLA by melt polycondensation

				Dehydration step			Esterification step			Decompression step			Melt PC step							
Run No.	Amt of LLA	Amt of cat	Amt of co-cat	DH time	DH temp	DHP	ES time	ES temp	ESP	DC time	DC temp	DCP	MPC time	MPC Temp	MPCP	wt. of PLA	Yield	M_w	M_n	PDI
	(ml)	(g)	(ml)	(h)	(°C)	(mm Hg)	(h)	(°C)	(mm Hg)	(h)	(°C)	(mm Hg)	(h)	(°C)	(mm Hg)	(g)	(wt.%)	(kDa)	(kDa)	
1	33	0.4	0.3	2,2,4	100,150,150	760,100,30	2	180	30	1	180	30-10	10	240	10	14.2442	35.6	2.943	1.264	2.33
2	33	0.16	0.1	2,2,4	100,150,150	760,100,30	8	180	30	1	180	30-10	10	240	10	15.6921	39.2	0.951	0.447	2.13
3	16.5	0.2	0.1	2,2,4	100,150,150	760,100,30	8	180	30	1	180	30-10	30	180	10	9.0564	45.3	8.514	5.109	1.67
4	33	0.4	0.3	2,2,4	100,150,150	760,100,30	8	180	30	1	180	30-10	10	180	10	27.5763	68.9	98.470	82.295	1.20
5	33	0.4	0.3	2,2,4	100,150,150	760,100,30	2	180	30	1	180	30-10	30	180	10	26.0959	65.2	55.634	26.759	2.08
6	33	0.16	0.1	2,2,4	100,150,150	760,100,30	2	180	30	1	180	30-10	30	240	10	12.1041	30.3	1.572	1.078	1.46
7	16.5	0.08	0.1	2,2,4	100,150,150	760,100,30	8	180	30	1	180	30-10	30	240	10	5.7961	29.0	0.447	0.429	1.04
8	16.5	0.2	0.1	2,2,4	100,150,150	760,100,30	2	180	30	1	180	30-10	30	240	10	8.0582	40.3	2.266	1.230	1.84
9	33	0.16	0.1	2,2,4	100,150,150	760,100,30	8	180	30	1	180	30-10	30	180	10	26.1124	65.3	89.675	65.712	1.36
10	16.5	0.2	0.1	2,2,4	100,150,150	760,100,30	8	180	30	1	180	30-10	10	240	10	7.5124	37.6	4.072	1.679	2.43
11	16.5	0.08	0.1	2,2,4	100,150,150	760,100,30	2	180	30	1	180	30-10	10	180	10	17.0643	85.3	178.857	90.531	1.98
12	24.8	0.21	0.1	2,2,4	100,150,150	760,100,30	5	180	30	1	180	30-10	20	210	10	16.6863	55.6	45.871	22.695	2.02
13	24.8	0.21	0.1	2,2,4	100,150,150	760,100,30	5	180	30	1	180	30-10	20	210	10	16.9171	56.4	46.645	23.246	2.01
14	24.8	0.21	0.1	2,2,4	100,150,150	760,100,30	5	180	30	1	180	30-10	20	210	10	15.7654	52.6	44.352	22.298	1.99
15	24.8	0.21	0.1	2,2,4	100,150,150	760,100,30	5	180	30	1	180	30-10	20	210	10	13.7942	46.0	40.974	20.437	2.00
16	24.8	0.21	0.1	2,2,4	100,150,150	760,100,30	5	180	30	1	180	30-10	20	210	10	13.8962	46.3	39.046	20.558	1.90
17	16.5	0.14	0.1	2,2,4	100,150,150	760,100,30	5	180	30	1	180	30-10	20	210	10	10.6523	53.3	35.874	19.731	1.82
18	33	0.28	0.2	2,2,4	100,150,150	760,100,30	5	180	30	1	180	30-10	20	210	10	18.4957	46.2	48.579	24.271	2.00
19	24.8	0.12	0.1	2,2,4	100,150,150	760,100,30	5	180	30	1	180	30-10	20	210	10	14.9011	49.7	34.265	19.422	1.76
20	24.8	0.3	0.2	2,2,4	100,150,150	760,100,30	5	180	30	1	180	30-10	20	210	10	17.2258	57.4	23.465	15.684	1.50
21	24.8	0.21	0.1	2,2,4	100,150,150	760,100,30	2	180	30	1	180	30-10	20	210	10	13.5634	45.2	32.606	18.053	1.81
22	24.8	0.21	0.1	2,2,4	100,150,150	760,100,30	8	180	30	1	180	30-10	20	210	10	15.7083	52.4	45.301	22.638	2.00
23	24.8	0.21	0.1	2,2,4	100,150,150	760,100,30	5	180	30	1	180	30-10	20	180	10	19.8691	66.2	75.929	50.096	1.52
24	24.8	0.21	0.1	2,2,4	100,150,150	760,100,30	5	180	30	1	180	30-10	20	240	10	6.3813	21.3	6.923	4.509	1.54
25	24.8	0.21	0.1	2,2,4	100,150,150	760,100,30	5	180	30	1	180	30-10	10	210	10	17.8084	59.4	68.896	34.319	2.01
26	24.8	0.21	0.1	2,2,4	100,150,150	760,100,30	5	180	30	1	180	30-10	30	210	10	13.9889	46.6	40.123	20.092	1.99
27	33.0	0.16	0.1	2,2,4	100,150,150	760,100,30	2	180	30	1	180	30-10	10	180	10	31.5922	79.0	97.408	80.721	1.21
28	16.5	0.2	0.1	2,2,4	100,150,150	760,100,30	2	180	30	1	180	30-10	10	180	10	13.9741	69.9	98.486	81.632	1.21
29	16.5	0.08	0.1	2,2,4	100,150,150	760,100,30	2	180	30	1	180	30-10	30	180	10	11.9119	59.6	9.103	7.379	1.23
30	16.5	0.08	0.1	2,2,4	100,150,150	760,100,30	2	180	30	1	180	30-10	10	240	10	6.1332	30.7	2.079	1.117	1.86

Amt: Amount; LLA: L-lactic acid; DH: Dehydration; DHP: Dehydration pressure; ES: Esterification; ESP: Esterification pressure; DC: Decompression; DCP: Decompression pressure; MPC: Melt polycondensation; MPCP: MPC pressure

J.2 ANALYSIS RESULTS

The output printouts of GPC and XRD of few samples have been given in this Appendix.

iit delhi polymer science
Project Name: May2008
Reported by User: System

Breeze

SAMPLE INFORMATION			
Sample Name:	Roorkee_PLA-O	Acquired By:	System
Sample Type:	Broad Unknown	Date Acquired:	5/16/2008 2:48:48 PM
Vial:	1	Acq. Method:	std_curve
Injection #:	5	Date Processed:	5/16/2008 4:34:16 PM
Injection Volume:	20.00 ul	Channel Name:	SATIN-2
Run Time:	30.00 Minutes	Sample Set Name:	

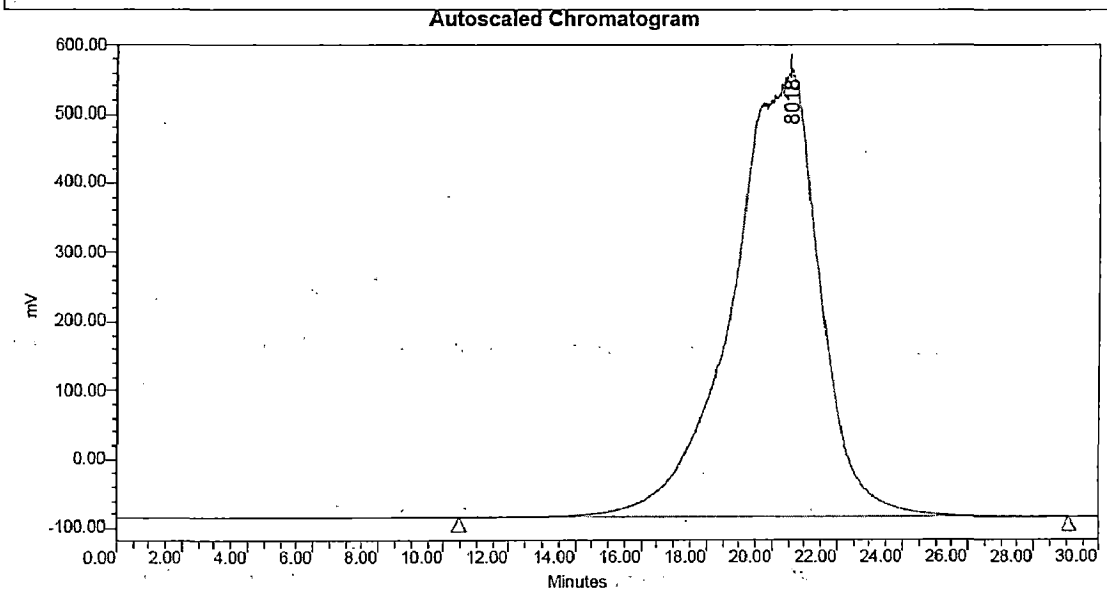

GPC Results

	Dist Name	Elution Volume (ml)	Retention Time (min)	Adjusted RT (min)	Mn	Mw	MP	Mz	Mz+1	Mz/Mw
1		20.611	20.611	20.611	8729	13632	8018	28403	98078	2.083539

GPC Results

	Mz+1/Mw	Area (V*sec)	% Area	Height (V)	% Height	Integration Type	Peak Codes	Points Across Peak	Start Time (min)
1	7.194566	120416324	100.00	652489	100.00	BB		22321	10.480

GPC Results

	End Time (min)	Baseline Start (min)	Baseline End (min)	Slope (V/sec)	Offset (V)
1	29.081	10.480	29.081	9.139376e-004	-8.410858e+001

Report Method: Untitled Printed 12:58:01 PM7/17/2008 Page: 1 of 5

Fig. J.1 GPC chromatogram of PLA oligomer

iit delhi polymer science
Project Name: May2008
Reported by User: System

Breeze

SAMPLE INFORMATION

Sample Name:	roorkee PLA 5	Acquired By:	System
Sample Type:	Broad Unknown	Date Acquired:	5/9/2008 3:43:25 PM
Vial:	1	Acq. Method:	std_curve
Injection #:	2	Date Processed:	5/19/2008 2:45:08 PM
Injection Volume:	20.00 ul	Channel Name:	SATIN-2
Run Time:	25.00 Minutes	Sample Set Name:	

Autoscaled Chromatogram

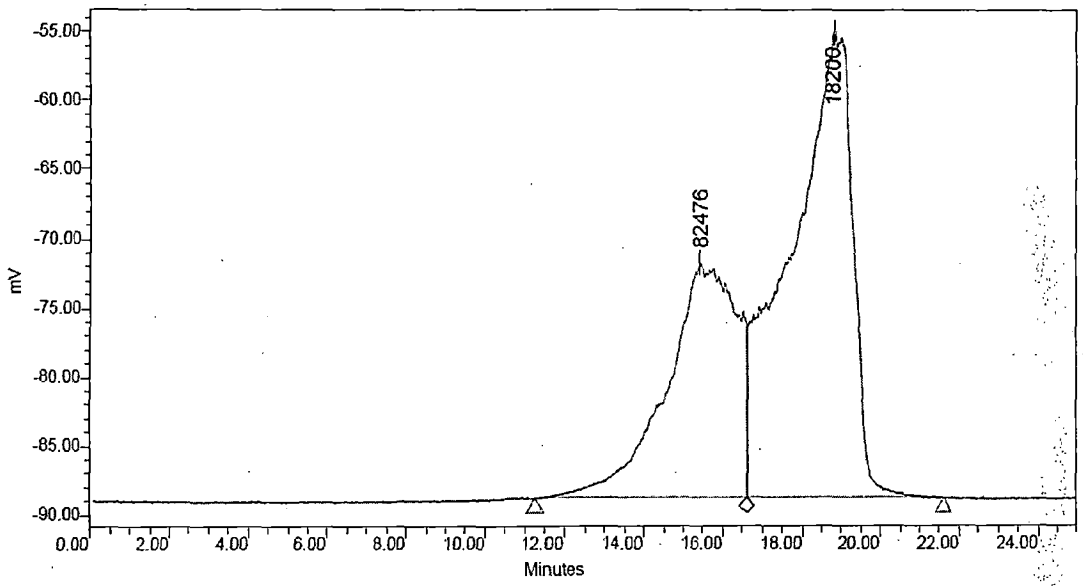

GPC Results

	Dist Name	Elution Volume (ml)	Retention Time (min)	Adjusted RT (min)	Mn	Mw	MP	Mz	Mz+1	Mz/Mw
1		15.450	15.450	15.450	82295	98470	82476	127785	176706	1.297702
2		18.796	18.796	18.796			18200			

GPC Results

	Mz+1/Mw	Area (V*sec)	% Area	Height (V)	% Height	Integration Type	Peak Codes	Points Across Peak	Start Time (min)
1	1.794510	2147352	36.57	17056	33.57	BV		6403	11.293
2		3724083	63.43	33754	66.43	VB		5998	16.629

Report Method: Untitled Printed 1:01:02 PM 7/17/2008 Page: 1 of 6

Fig. J.2 GPC chromatogram of PLA (Run No. 4)

GPC_REPORT

SAMPLE INFORMATION			
Sample Name:	PLA-TM-1	Acquired By:	System
Sample Type:	Broad Unknown	Acquired Method:	Std_curve
Vial:	1	Reported Method:	GPC_Report
Injection:	1	Date Acquired:	12/06/2008 01:05:11 PM
Injection Volume:	20ul		
Run Time:	30.0 Minutes		

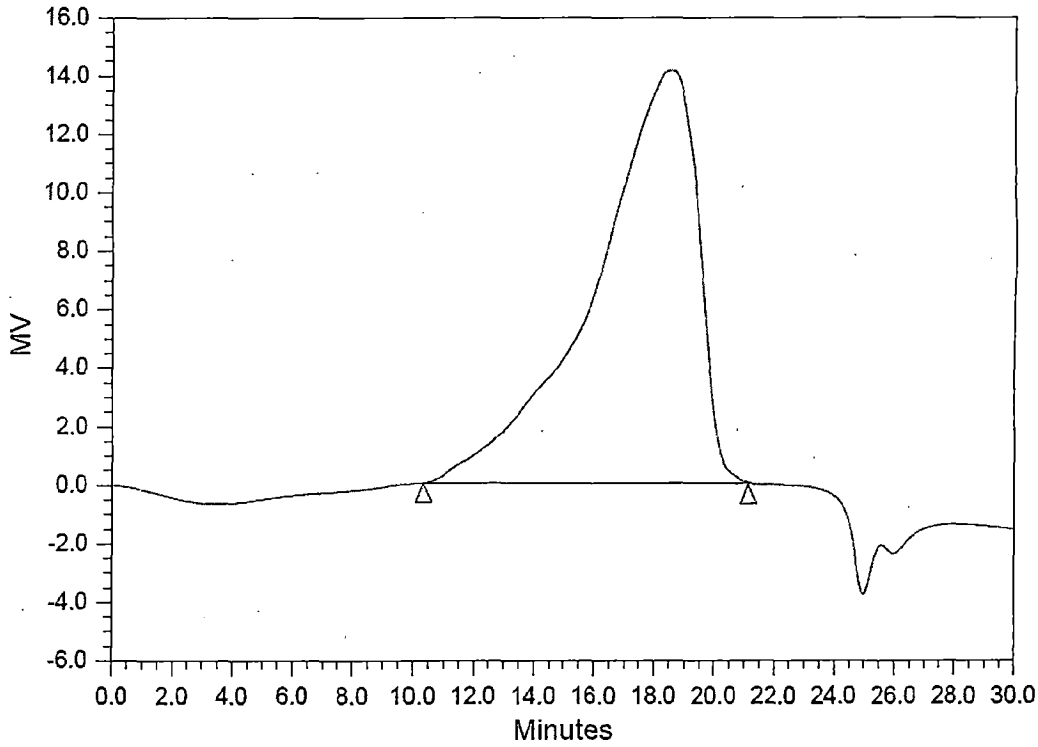

	RT	Mn	Mw	Polydispersity
1	18.55	26759	55634	2.079

Fig. J.3 GPC chromatogram of PLA (Run No. 5)

GPC_REPORT

SAMPLE INFORMATION			
Sample Name:	PLA-TM-24	Acquired By:	System
Sample Type:	Broad Unknown	Acquired Method:	Std_curve
Vial:	1	Reported Method:	GPC_Report
Injection:	5	Date Acquired:	12/16/2008 11:54:06 PM
Injection Volume:	20ul		
Run Time:	30.0 Minutes		

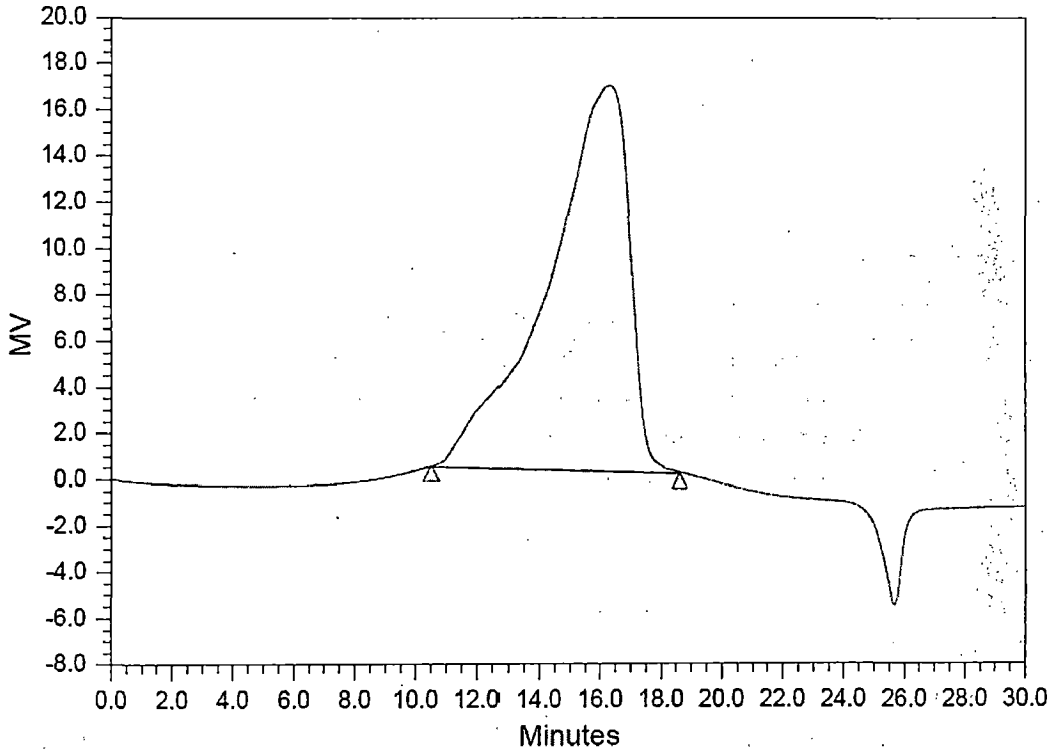

	RT	Mn	Mw	Polydispersity
1	16.34	65712	89675	1.365

Fig. J.4 GPC chromatogram of PLA (Run No. 9)

GPC_REPORT

SAMPLE INFORMATION			
Sample Name:	PLA-TM-7	Acquired By:	System
Sample Type:	Broad Unknown	Acquired Method:	Std_curve
Vial:	1	Reported Method:	GPC_Report
Injection:	2	Date Acquired:	12/07/2008 05:13:43 PM
Injection Volume:	20ul		
Run Time:	30.0 Minutes		

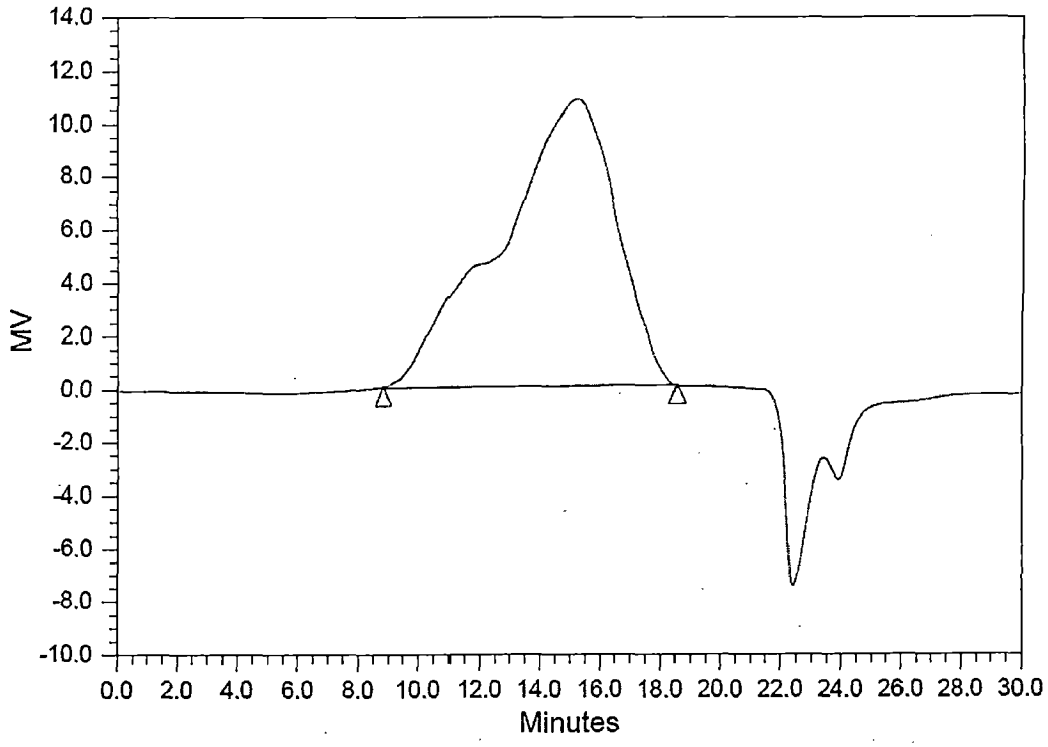

	RT	Mn	Mw	Polydispersity
1	15.31	90531	178857	1.976

Fig. J.5 GPC chromatogram of PLA (Run No. 11)

GPC_REPORT

SAMPLE INFORMATION			
Sample Name:	PLA-TM-5	Acquired By:	System
Sample Type:	Broad Unknown	Acquired Method:	Std_curve
Vial:	1	Reported Method:	GPC_Report
Injection:	5	Date Acquired:	12/06/2008 05:30:39 PM
Injection Volume:	20ul		
Run Time:	30.0 Minutes		

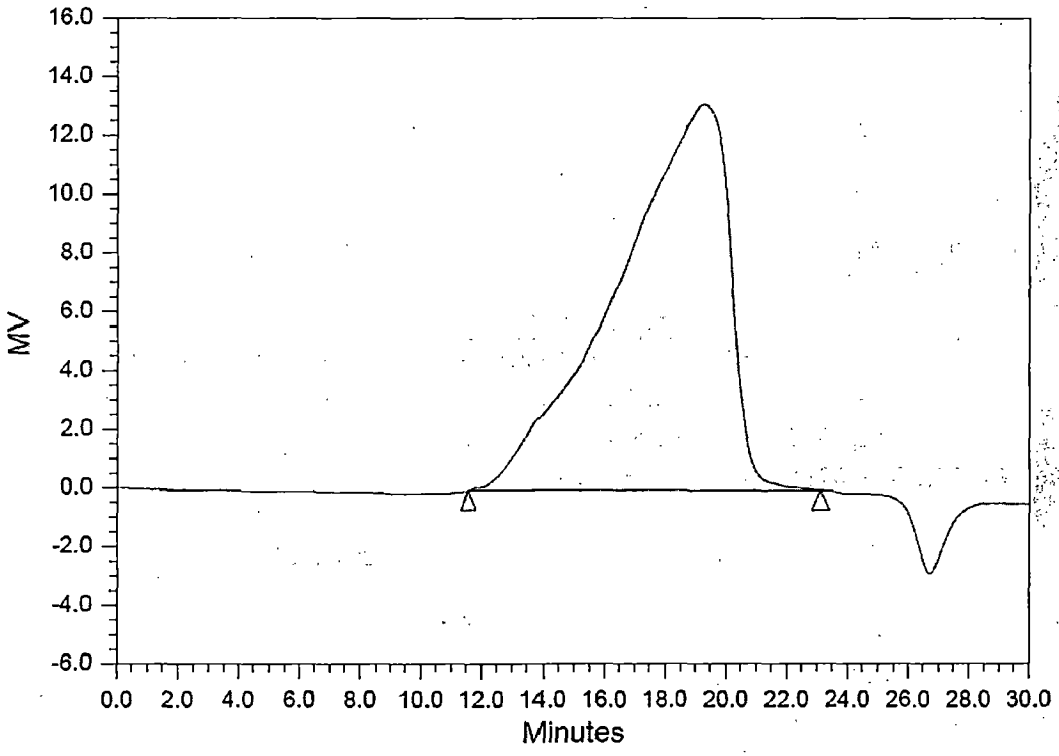

	RT	Mn	Mw	Polydispersity
1	19.31	20558	39046	1.899

Fig. J.6 GPC chromatogram of PLA (Run No. 16)

GPC_REPORT

SAMPLE INFORMATION			
Sample Name:	PLA-TM-20	Acquired By:	System
Sample Type:	Broad Unknown	Acquired Method:	Std_curve
Vial:	1	Reported Method:	GPC_Report
Injection:	5	Date Acquired:	12/16/2008 07:12:53 PM
Injection Volume:	20ul		
Run Time:	30.0 Minutes		

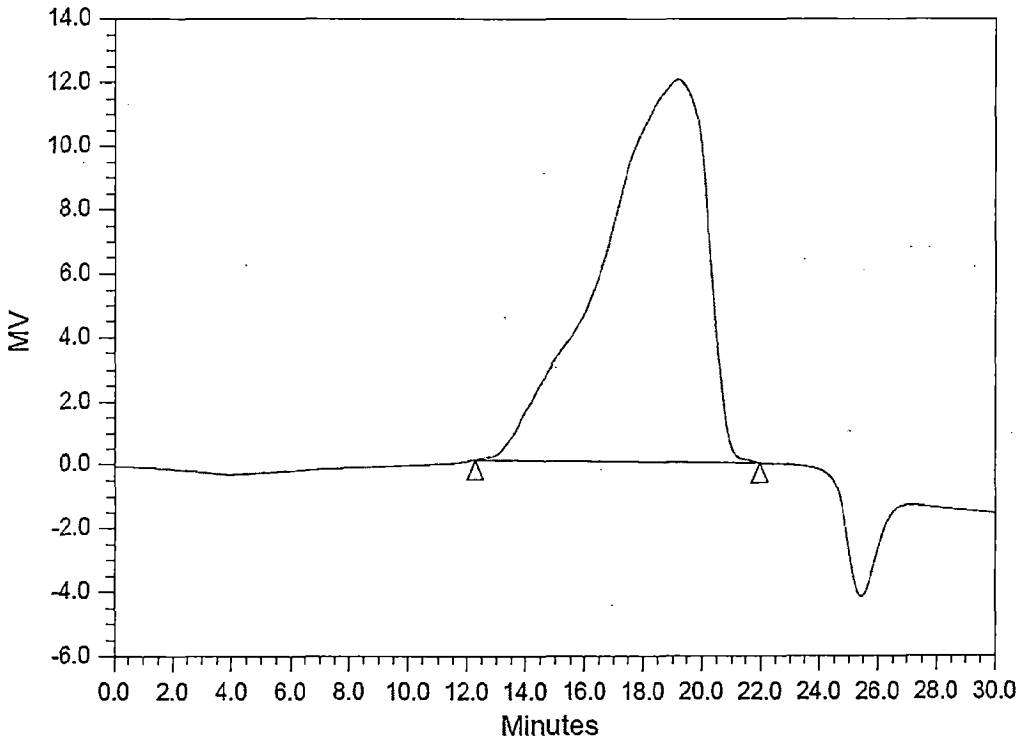

	RT	Mn	Mw	Polydispersity
1	19.26	19422	34265	1.764

Fig. J.7 GPC chromatogram of PLA (Run No. 19)

iit delhi polymer science
Project Name: May2008
Reported by User: System

Breeze

SAMPLE INFORMATION

Sample Name:	roorkee_PLA 1	Acquired By:	System
Sample Type:	Broad Unknown	Date Acquired:	5/16/2008 12:43:47 PM
Vial:	1	Acq. Method:	std_curve
Injection #:	2	Date Processed:	5/16/2008 2:20:42 PM
Injection Volume:	20.00 ul	Channel Name:	SATIN-2
Run Time:	30.00 Minutes	Sample Set Name:	

Autoscaled Chromatogram

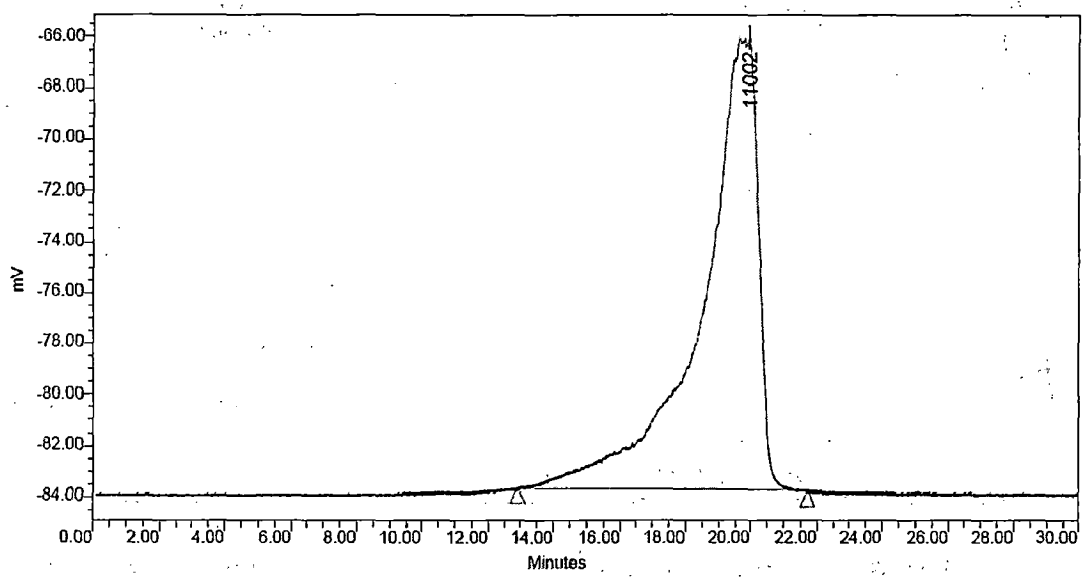

GPC Results

	Dist Name	Elution Volume (ml)	Retention Time (min)	Adjusted RT (min)	Mn	Mw	MP	Mz	Mz+1	Mz/Mw
1		19.911	19.911	19.911	15684	23465	11002	48716	95592	2.076084

GPC Results

	Mz+1/Mw	Area (V*sec)	% Area	Height (V)	% Height	Integration Type	Peak Codes	Points Across Peak	Start Time (min)
1	4.073790	2134340	100.00	17731	100.00	BB		10583	12.919

GPC Results

	End Time (min)	Baseline Start (min)	Baseline End (min)	Slope (V/sec)	Offset (V)
1	21.739	12.919	21.739	-1.349206e-002	-8.349870e+001

Report Method: Untitled Printed 12:59:11 PM7/17/2008 Page: 1 of 5

Fig. J.8 GPC chromatogram of PLA (Run No. 20)

GPC_REPORT

SAMPLE INFORMATION			
Sample Name:	PLA-TM-21	Acquired By:	System
Sample Type:	Broad Unknown	Acquired Method:	Std_curve
Vial:	1	Reported Method:	GPC_Report
Injection:	1	Date Acquired:	12/16/2008 08:01:59 PM
Injection Volume:	20ul		
Run Time:	30.0 Minutes		

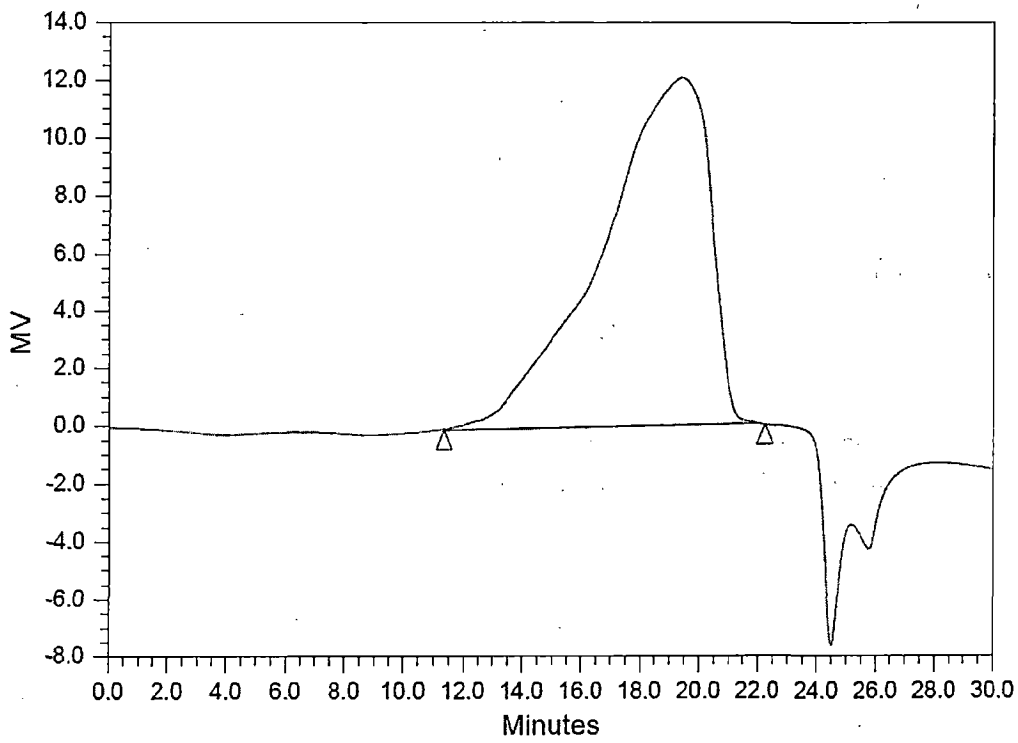

	RT	Mn	Mw	Polydispersity
1	19.57	18053	32606	1.806

Fig. J.9 GPC chromatogram of PLA (Run No. 21)

iit delhi polymer science
Project Name: May2008
Reported by User: System

Breeze

SAMPLE INFORMATION

Sample Name:	Roorkee_PLA 3	Acquired By:	System
Sample Type:	Broad Unknown	Date Acquired:	5/2/2008 4:07:05 PM
Vial:	1	Acq. Method:	std_curve
Injection #:	5	Date Processed:	5/19/2008 2:39:53 PM
Injection Volume:	20.00 ul	Channel Name:	SATIN-2
Run Time:	20.00 Minutes	Sample Set Name:	

Autoscaled Chromatogram

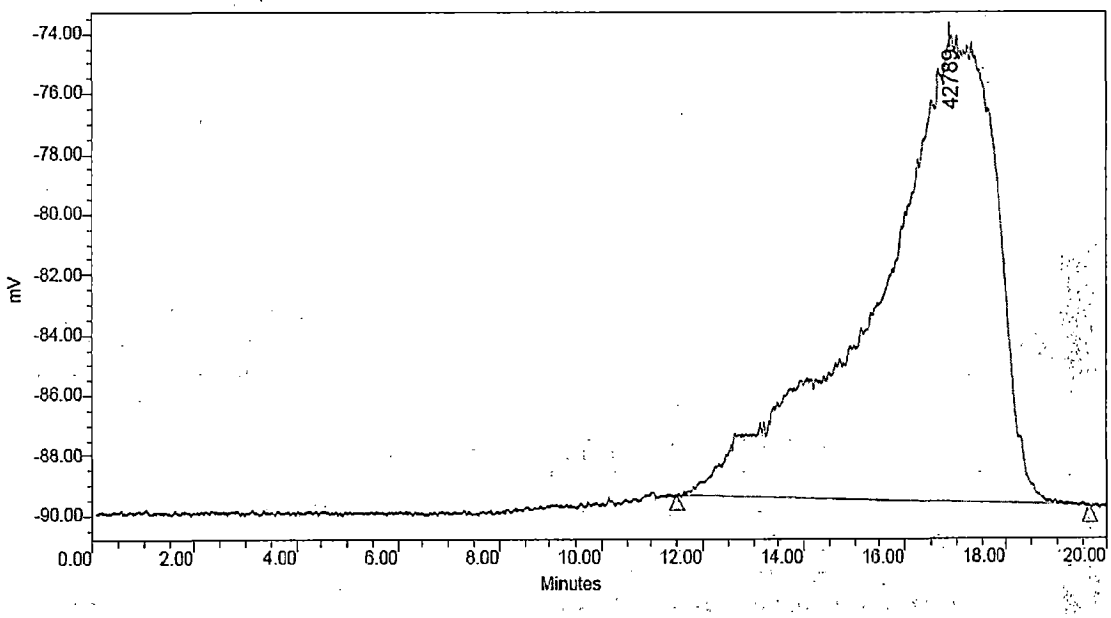

GPC Results

	Dist Name	Elution Volume (ml)	Retention Time (min)	Adjusted RT (min)	Mn	Mw	MP	Mz	Mz+1	Mz/Mw
1		16.903	16.903	16.903	50096	75929	42789	130560	200593	1.719510

GPC Results

	Mz+1/Mw	Area (V*sec)	% Area	Height (V)	% Height	Integration Type	Peak Codes	Points Across Peak	Start Time (min)
1	2.641867	2587053	100.00	15527	100.00	bB		9786	11.500

GPC Results

	End Time (min)	Baseline Start (min)	Baseline End (min)	Slope (V/sec)	Offset (V)
1	19.655	11.500	19.655	-5.088903e-002	-8.874578e+001

Report Method: Untitled Printed 1:00:23 PM 7/17/2008 Page: 1 of 5

Fig. J.10 GPC chromatogram of PLA (Run No. 23)

GPC_REPORT

SAMPLE INFORMATION			
Sample Name:	PLA-TM-6	Acquired By:	System
Sample Type:	Broad Unknown	Acquired Method:	Std_curve
Vial:	1	Reported Method:	GPC_Report
Injection:	1	Date Acquired:	12/07/2008 02:30:53 PM
Injection Volume:	20ul		
Run Time:	30.0 Minutes		

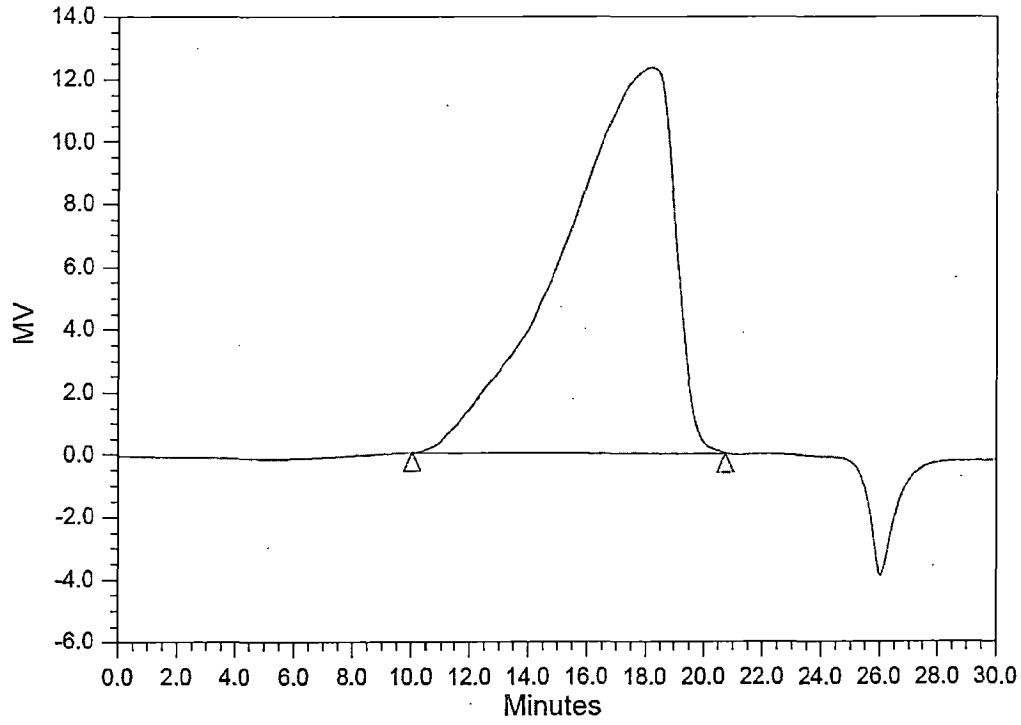

	RT	Mn	Mw	Polydispersity
1	18.26	34319	68896	2.008

Fig. J.11 GPC chromatogram of PLA (Run No. 25)

GPC_REPORT

SAMPLE INFORMATION			
Sample Name:	PLA-TM-11	Acquired By:	System
Sample Type:	Broad Unknown	Acquired Method:	Std_curve
Vial:	1	Reported Method:	GPC_Report
Injection:	4	Date Acquired:	12/14/2008 01:04:39 PM
Injection Volume:	20ul		
Run Time:	30.0 Minutes		

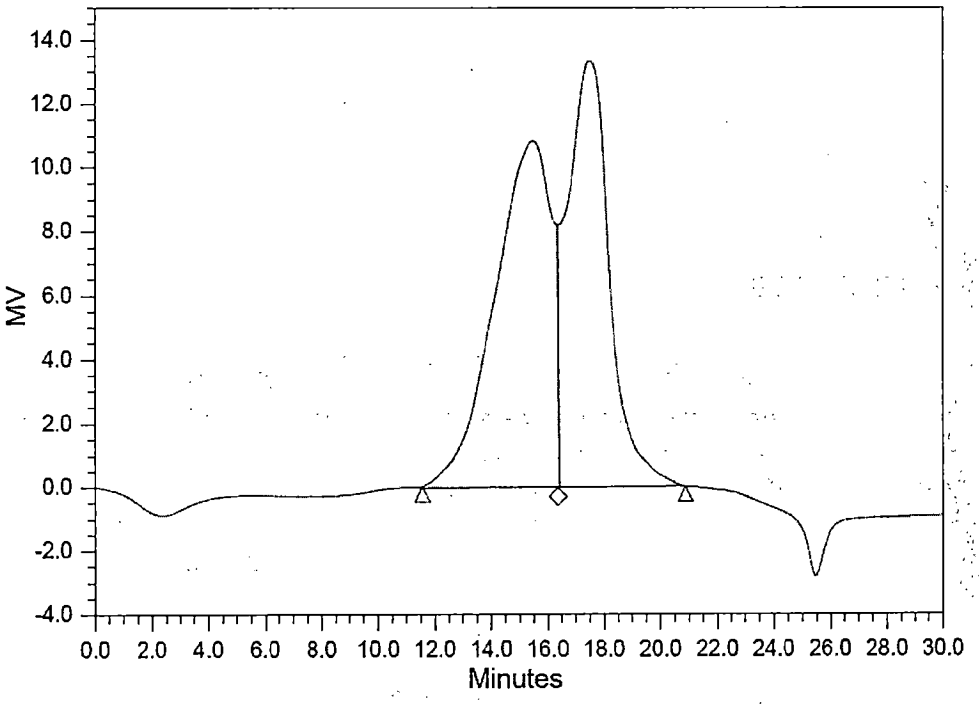

	RT	Mn	Mw	Polydispersity
1	15.49	80721	97408	1.207
2	17.52			

Fig. J.12 GPC chromatogram of PLA (Run No. 27)

GPC_REPORT

SAMPLE INFORMATION			
Sample Name:	PLA-TM-10	Acquired By:	System
Sample Type:	Broad Unknown	Acquired Method:	Std_curve
Vial:	1	Reported Method:	GPC_Report
Injection:	3	Date Acquired:	12/13/2008 11:10:13 PM
Injection Volume:	20ul		
Run Time:	30.0 Minutes		

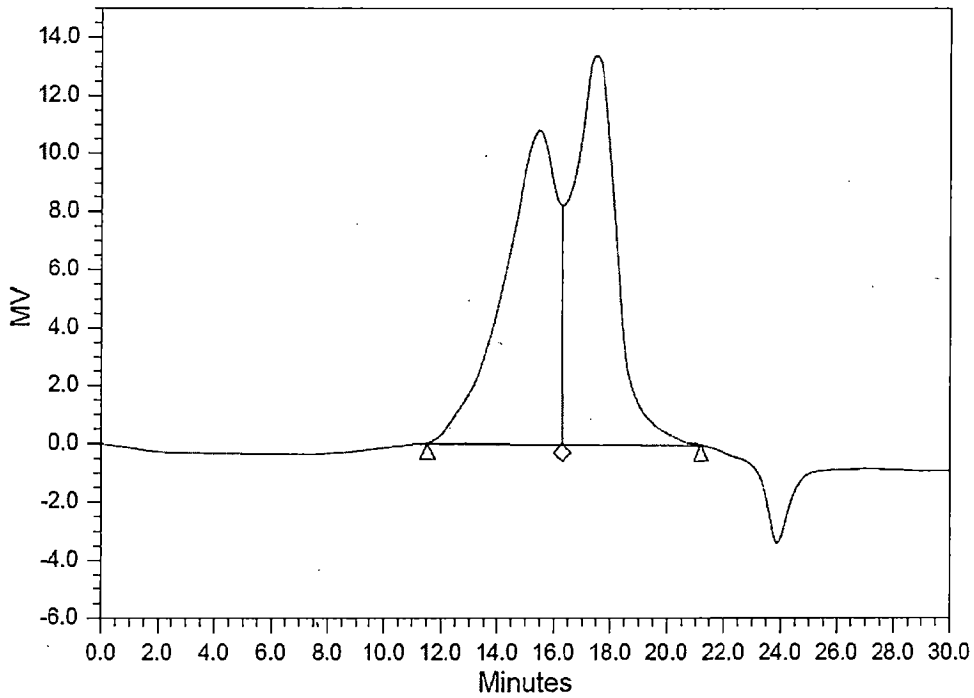

	RT	Mn	Mw	Polydispersity
1	15.48	81632	98486	1.206
2	17.47			

Fig. J.13 GPC chromatogram of PLA (Run No. 28)

iit delhi polymer science

Project Name: May2008

Reported by User: System

Breeze

SAMPLE INFORMATION

Sample Name:	Roorkee_PLA-7	Acquired By:	System
Sample Type:	Broad Unknown	Date Acquired:	5/16/2008 3:20:46 PM
Vial:	1	Acq. Method:	std_curve
Injection #:	6	Date Processed:	5/19/2008 2:49:10 PM
Injection Volume:	20.00 ul	Channel Name:	SATIN-2
Run Time:	35.00 Minutes	Sample Set Name:	

Autoscaled Chromatogram

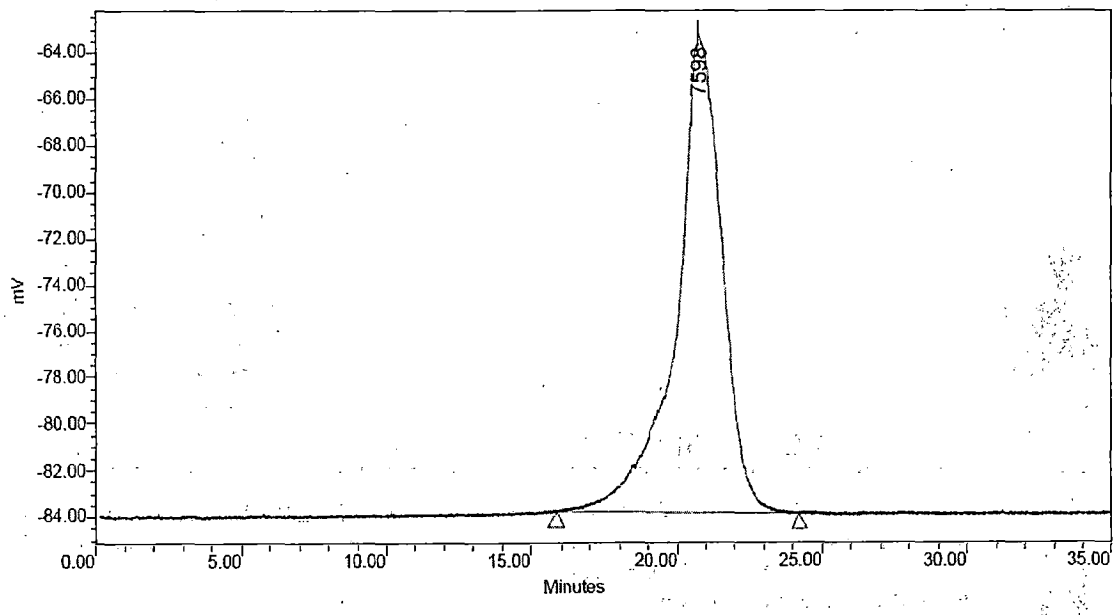

GPC Results

	Dist Name	Elution Volume (ml)	Retention Time (min)	Adjusted RT (min)	Mn	Mw	MP	Mz	Mz+1	Mz/Mw
1		20.731	20.731	20.731	7379	9103	7598	12611	19602	1.385413

GPC Results

	Mz+1/Mw	Area (V*sec)	% Area	Height (V)	% Height	Integration Type	Peak Codes	Points Across Peak	Start Time (min)
1	2.153423	2261009	100.00	20604	100.00	BB		10022	15.868

GPC Results

	End Time (min)	Baseline Start (min)	Baseline End (min)	Slope (V/sec)	Offset (V)
1	24.219	15.868	24.219	-1.221313e-002	-8.356121e+001

Report Method: Untitled Printed 12:58:26 PM7/17/2008 Page: 1 of 5

Fig. J.14 GPC chromatogram of PLA (Run No. 29)

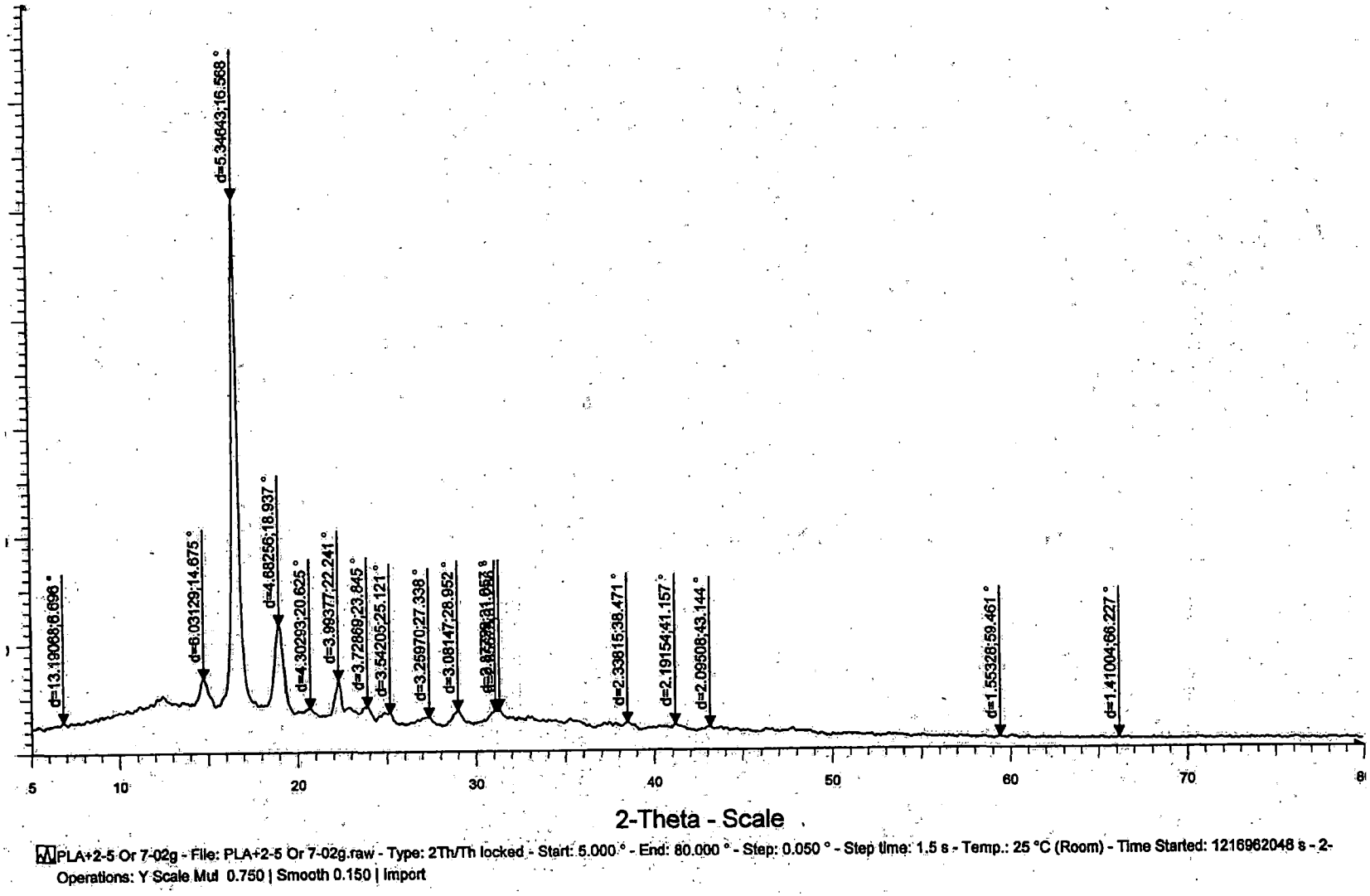

Fig. J.15 XRD pattern of PLA 1

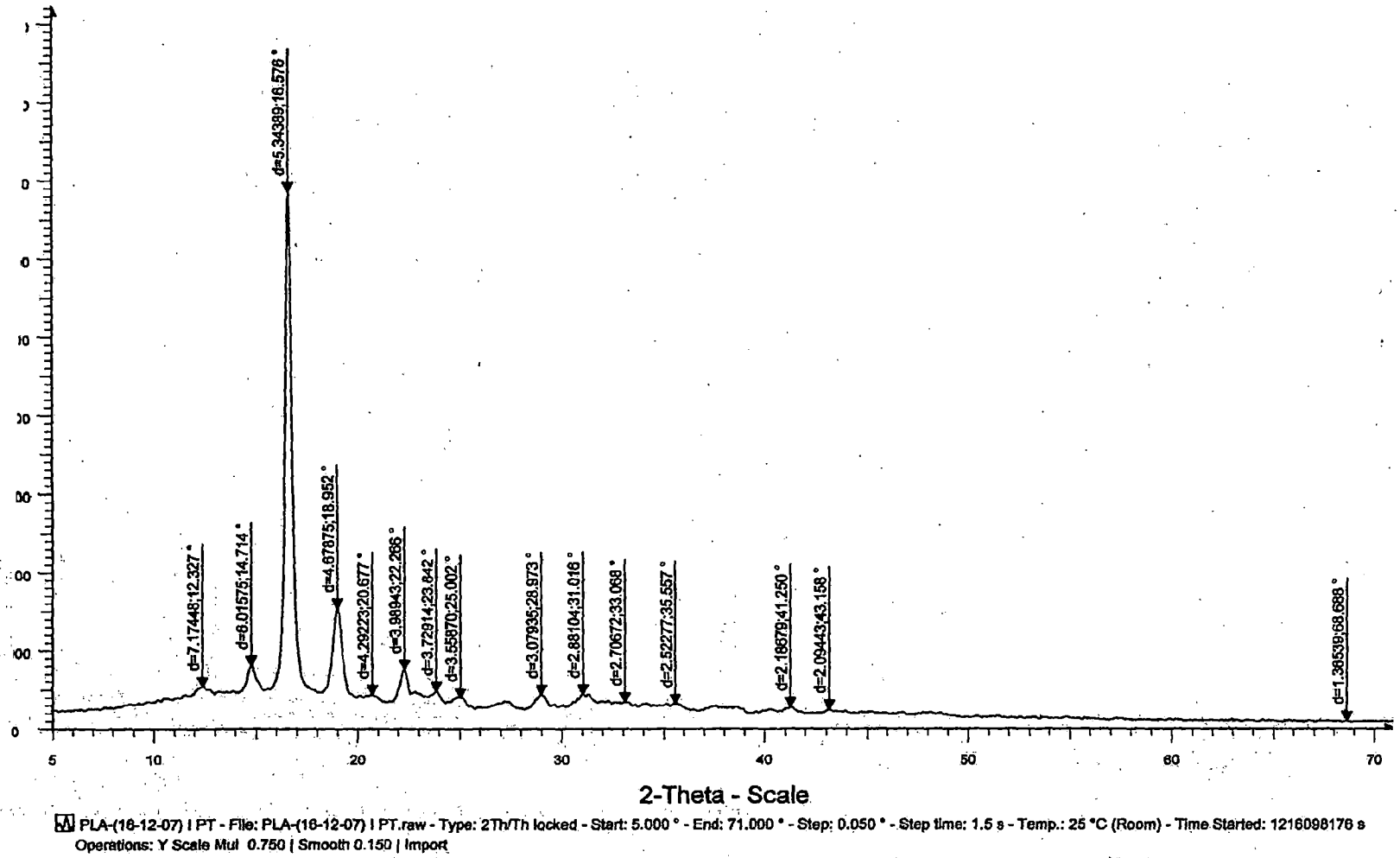

Fig. J.16 XRD pattern of PLA 2

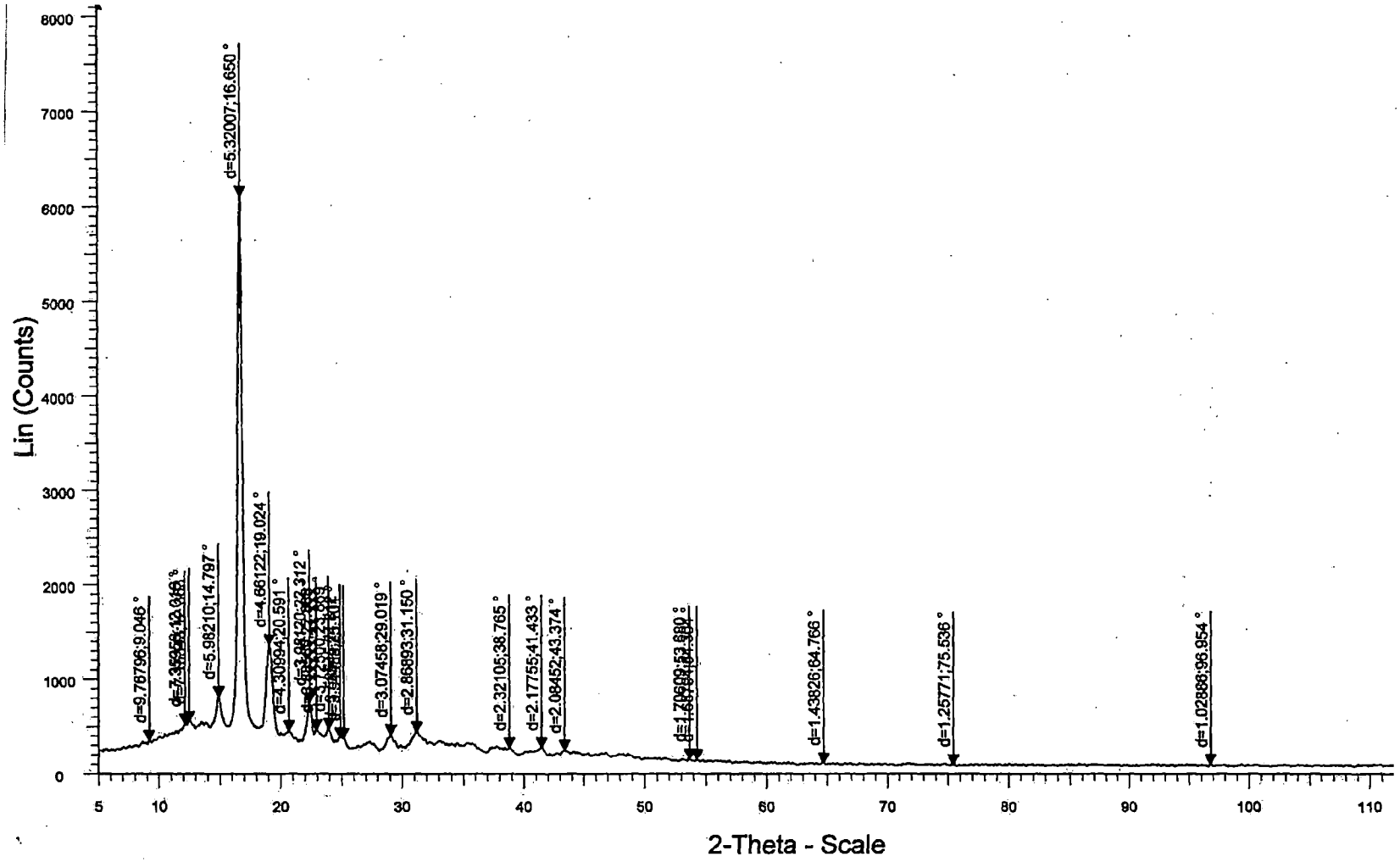

Fig. J.17 XRD pattern of PLA 3

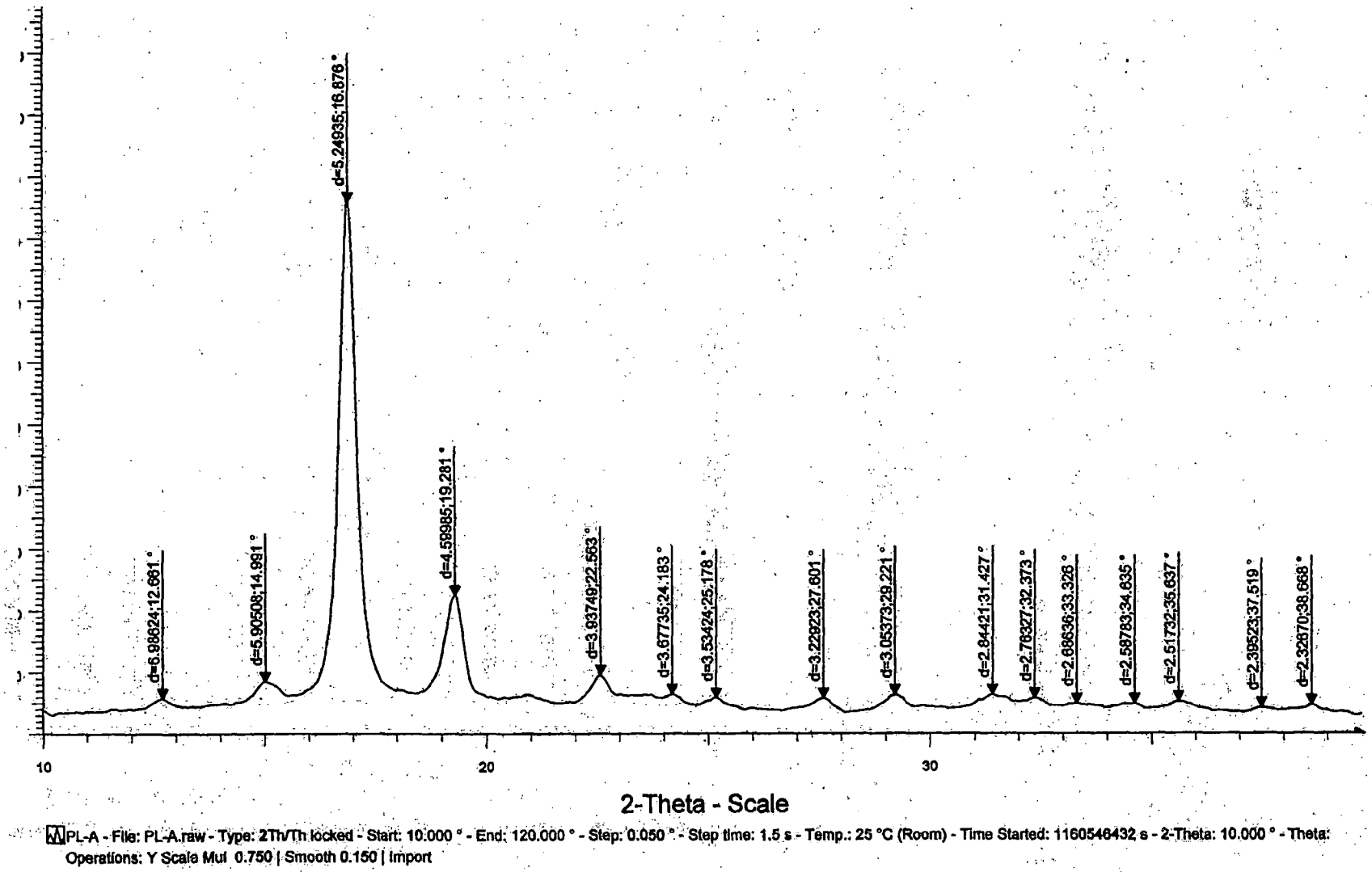

Fig. J.18 XRD pattern of PLA 4

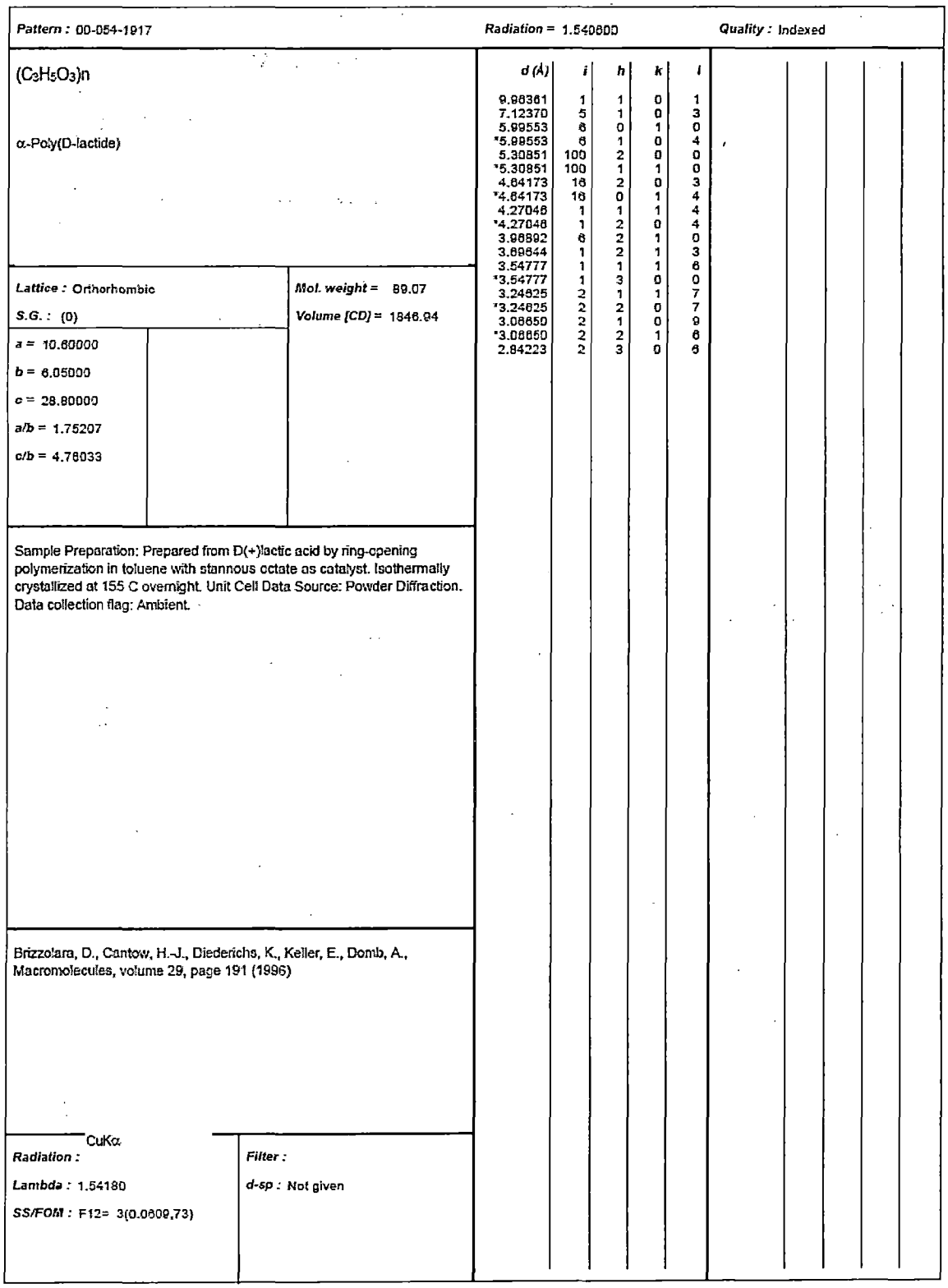

Pattern : 00-054-1917 Radiation = 1.540600 Quality : Indexed

$(C_3H_5O_3)n$

α-Poly(D-lactide)

Lattice : Orthorhombic
S.G. : (0)
Mol. weight = 89.07
Volume [CD] = 1846.94

a = 10.60000
b = 6.05000
c = 28.80000
a/b = 1.75207
c/b = 4.76033

Sample Preparation: Prepared from D(+)lactic acid by ring-opening polymerization in toluene with stannous octate as catalyst. Isothermally crystallized at 155 C overnight. Unit Cell Data Source: Powder Diffraction. Data collection flag: Ambient.

Brizzolara, D., Cantow, H.-J., Diederichs, K., Keller, E., Domb, A., Macromolecules, volume 29, page 191 (1996)

Radiation : CuKα
Lambda : 1.54180
SS/FOM : F12= 3(0.0609,73)

Filter :
d-sp : Not given

d (Å)	i	h	k	l
9.98361	1	1	0	1
7.12370	5	1	0	3
5.99553	6	0	1	0
*5.99553	6	1	0	4
5.30851	100	2	0	0
*5.30851	100	1	1	0
4.64173	18	2	0	3
*4.64173	18	0	1	4
4.27048	1	1	1	4
*4.27048	1	2	0	4
3.99892	6	2	1	0
3.69844	1	2	1	3
3.54777	1	1	1	6
*3.54777	1	3	0	0
3.24825	2	1	1	7
*3.24825	2	2	0	7
3.08650	2	1	0	9
*3.08650	2	2	1	6
2.84223	2	3	0	6

Fig. J.19 Details of the standard alpha-poly(D(+)-lactide)

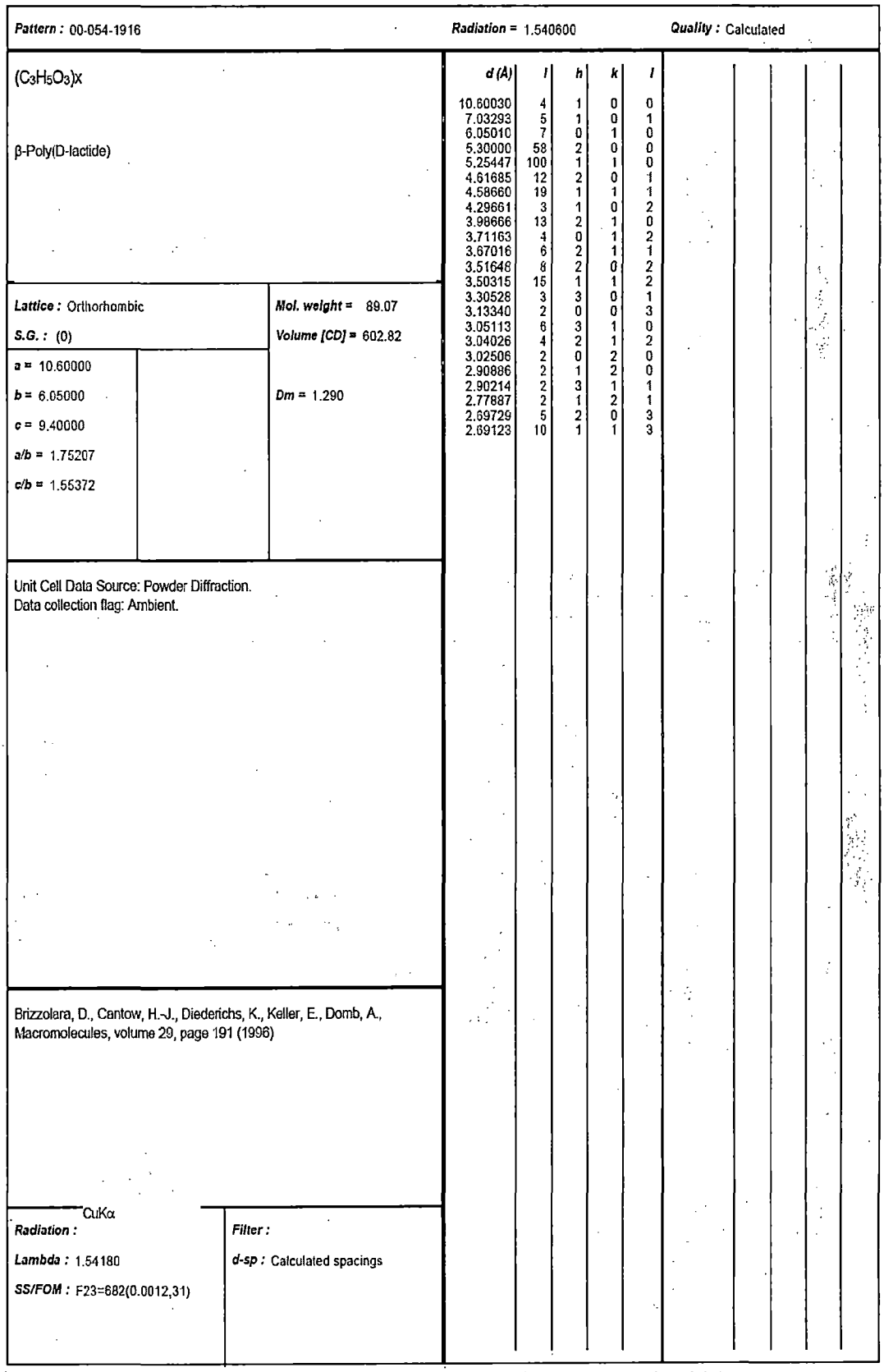

Pattern : 00-054-1916 Radiation = 1.540600 Quality : Calculated

$(C_3H_5O_3)x$

β-Poly(D-lactide)

Lattice : Orthorhombic
S.G. : (0)

a = 10.60000
b = 6.05000
c = 9.40000
a/b = 1.75207
c/b = 1.55372

Mol. weight = 89.07
Volume [CD] = 602.82

Dm = 1.290

Unit Cell Data Source: Powder Diffraction.
Data collection flag: Ambient.

Brizzolara, D., Cantow, H.-J., Diederichs, K., Keller, E., Domb, A., Macromolecules, volume 29, page 191 (1996)

Radiation : CuKα
Lambda : 1.54180
SS/FOM : F23=682(0.0012,31)

Filter :
d-sp : Calculated spacings

d (Å)	I	h	k	l
10.60030	4	1	0	0
7.03293	5	1	0	1
6.05010	7	0	1	0
5.30000	58	2	0	0
5.25447	100	1	1	0
4.61685	12	2	0	1
4.58660	19	1	1	1
4.29661	3	1	0	2
3.98666	13	2	1	0
3.71163	4	0	1	2
3.67016	6	2	1	1
3.51648	8	2	0	2
3.50315	15	1	1	2
3.30528	3	3	0	1
3.13340	2	0	0	3
3.05113	6	3	1	0
3.04026	4	2	1	2
3.02506	2	0	2	0
2.90886	2	1	2	0
2.90214	2	3	1	1
2.77887	2	1	2	1
2.69729	5	2	0	3
2.69123	10	1	1	3

Fig. J.20 Details of the standard beta-poly(D(+)-lactide)

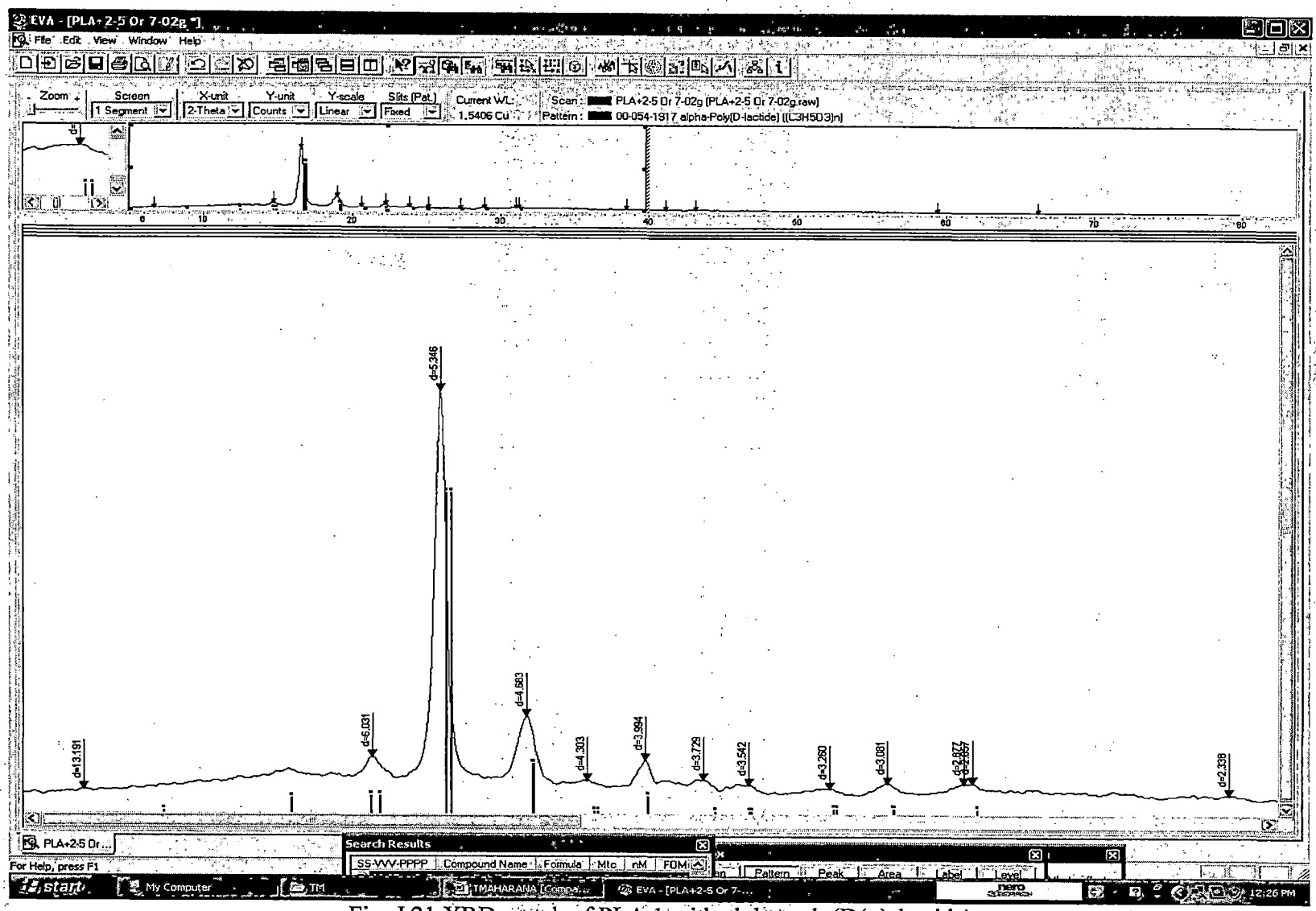

Fig. J.21 XRD match of PLA 1 with alpha-poly(D(+)-lactide)

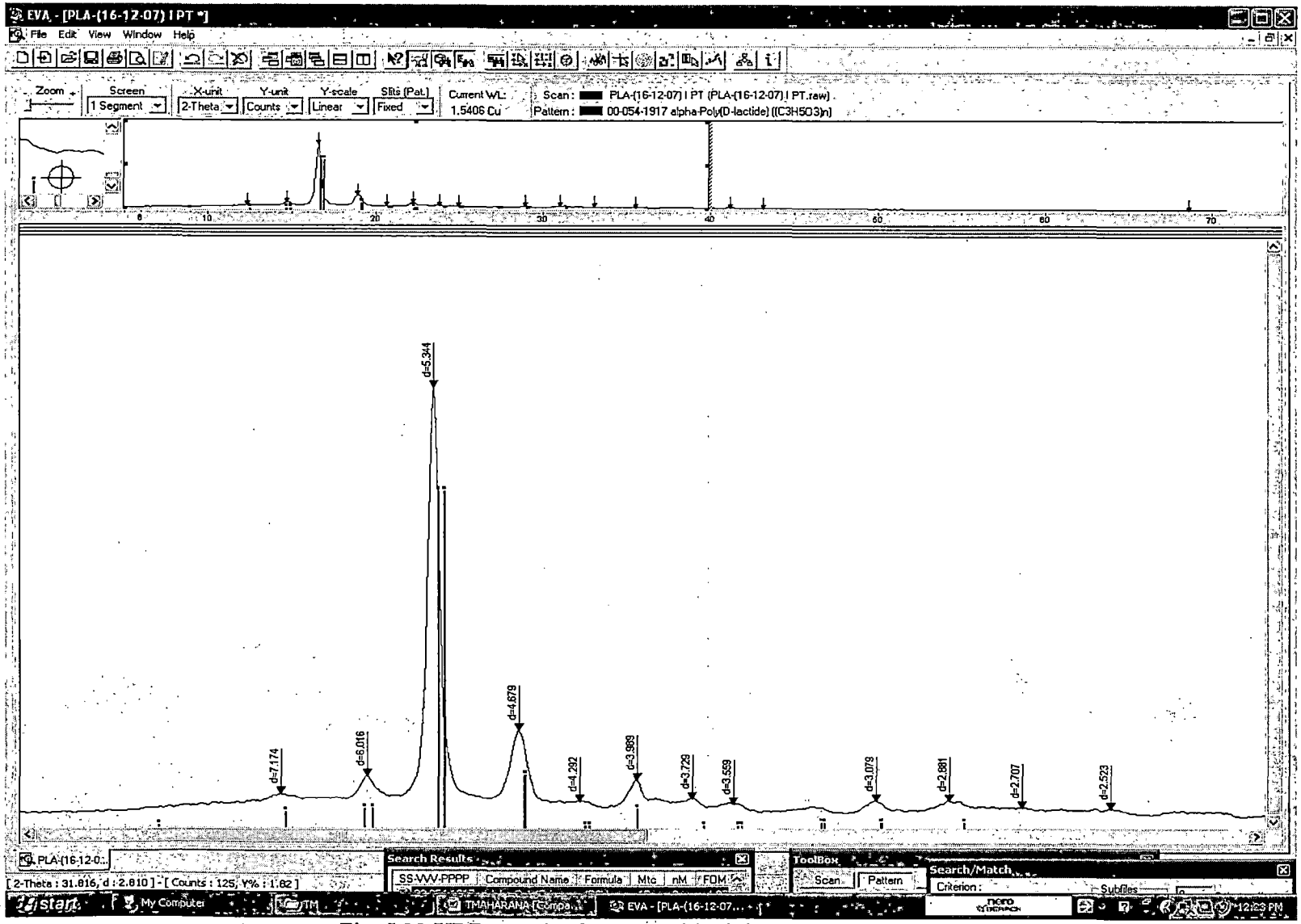

Fig. J.22 XRD match of PLA 2 with alpha-poly(D(+)-lactide)

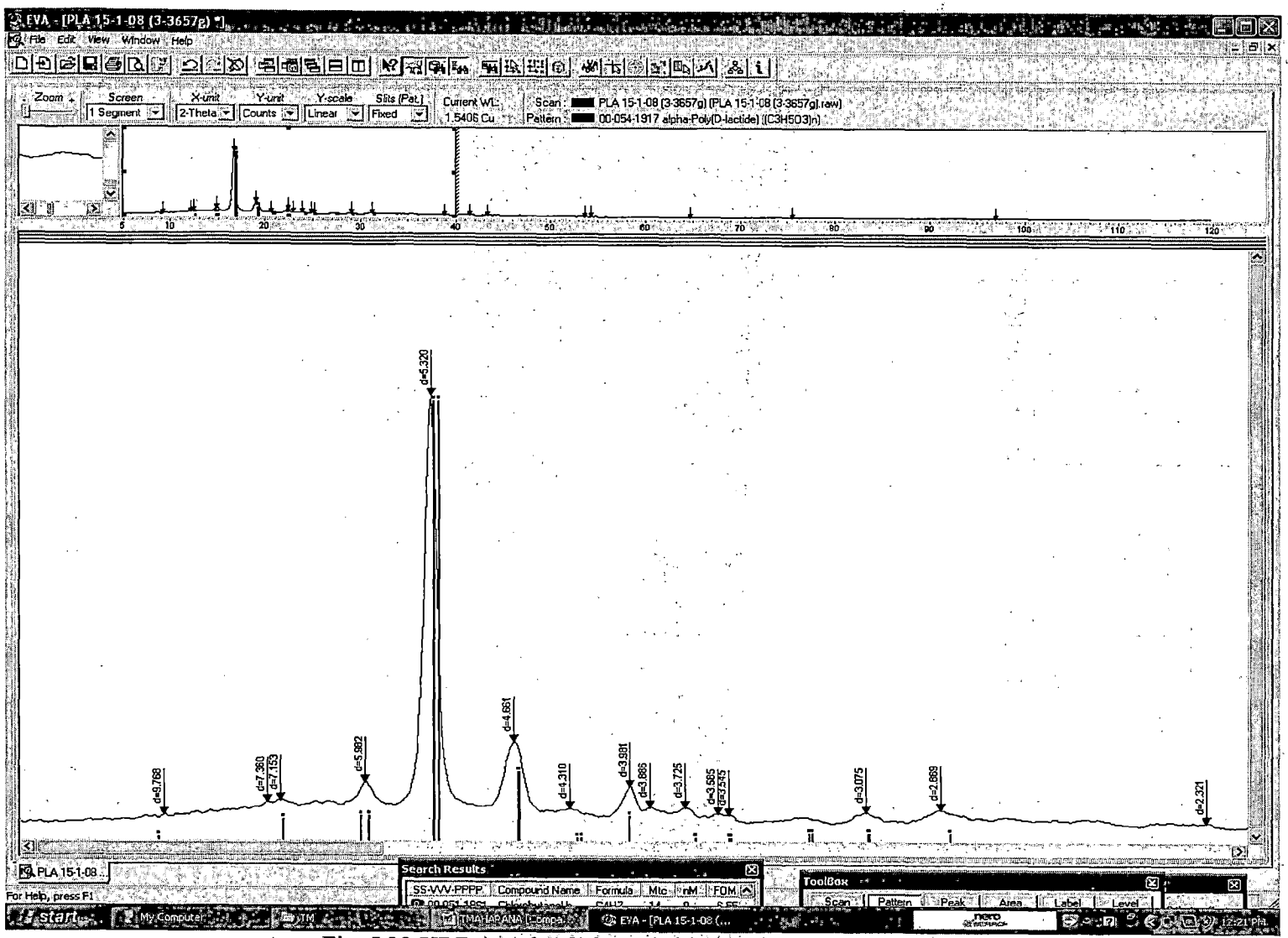

Fig. J.23 XRD match of PLA 3 with alpha-poly(D(+)-lactide)

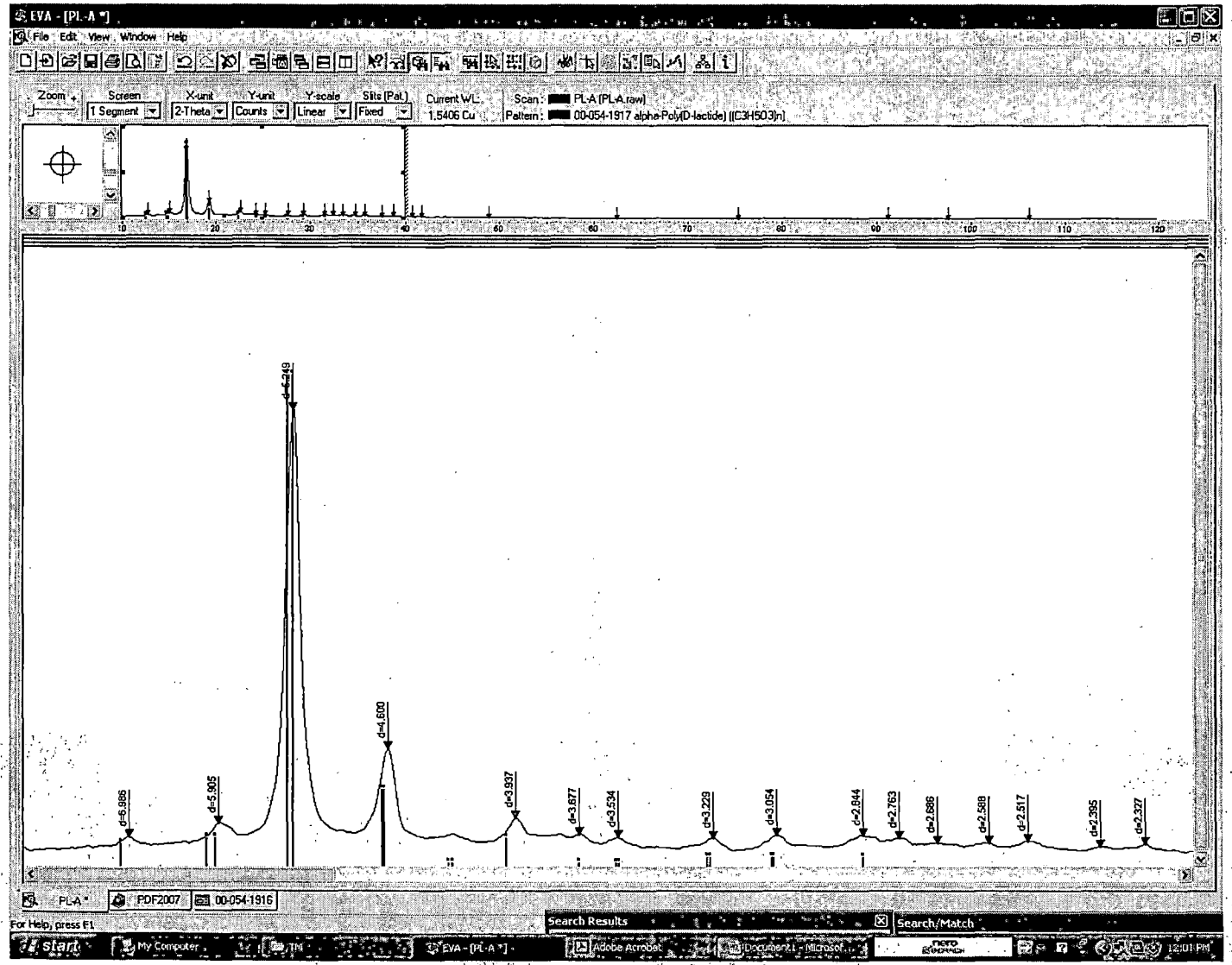

Fig. J.24 XRD match of PLA 4 with alpha-poly(D(+)-lactide)

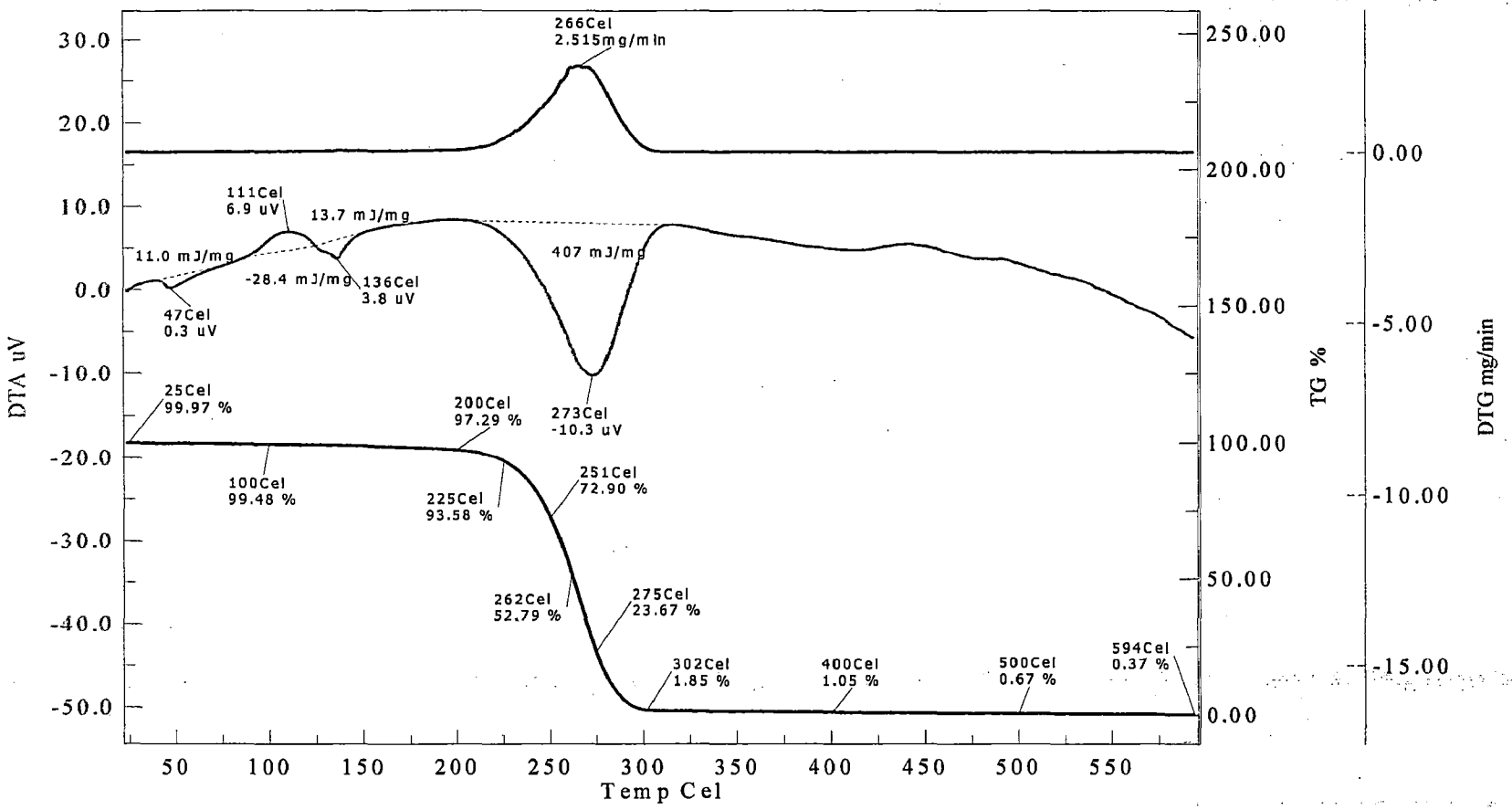

Fig. J.25 Thermal analysis of PLA 1

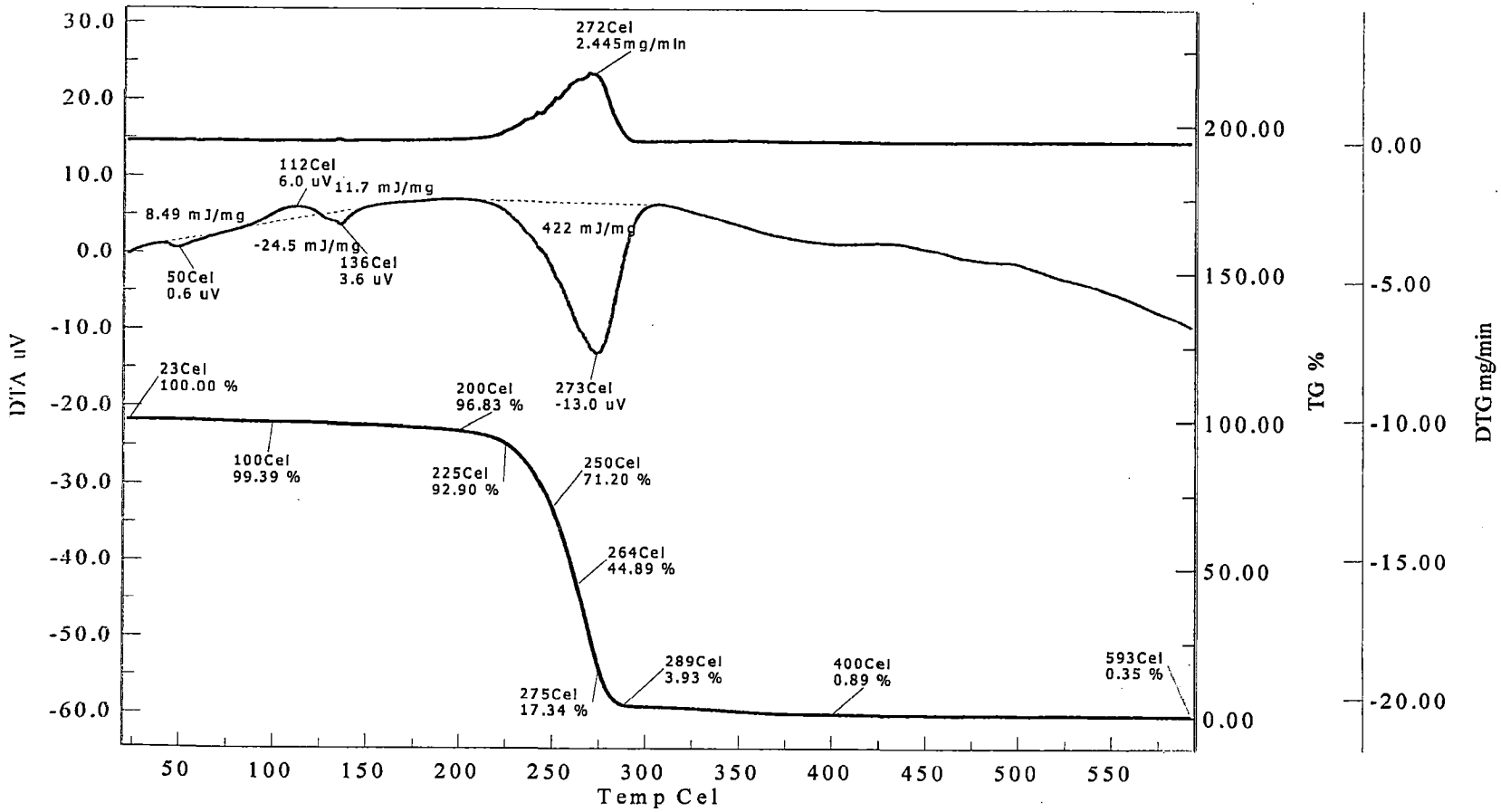

Fig. J.26 Thermal analysis of PLA 2

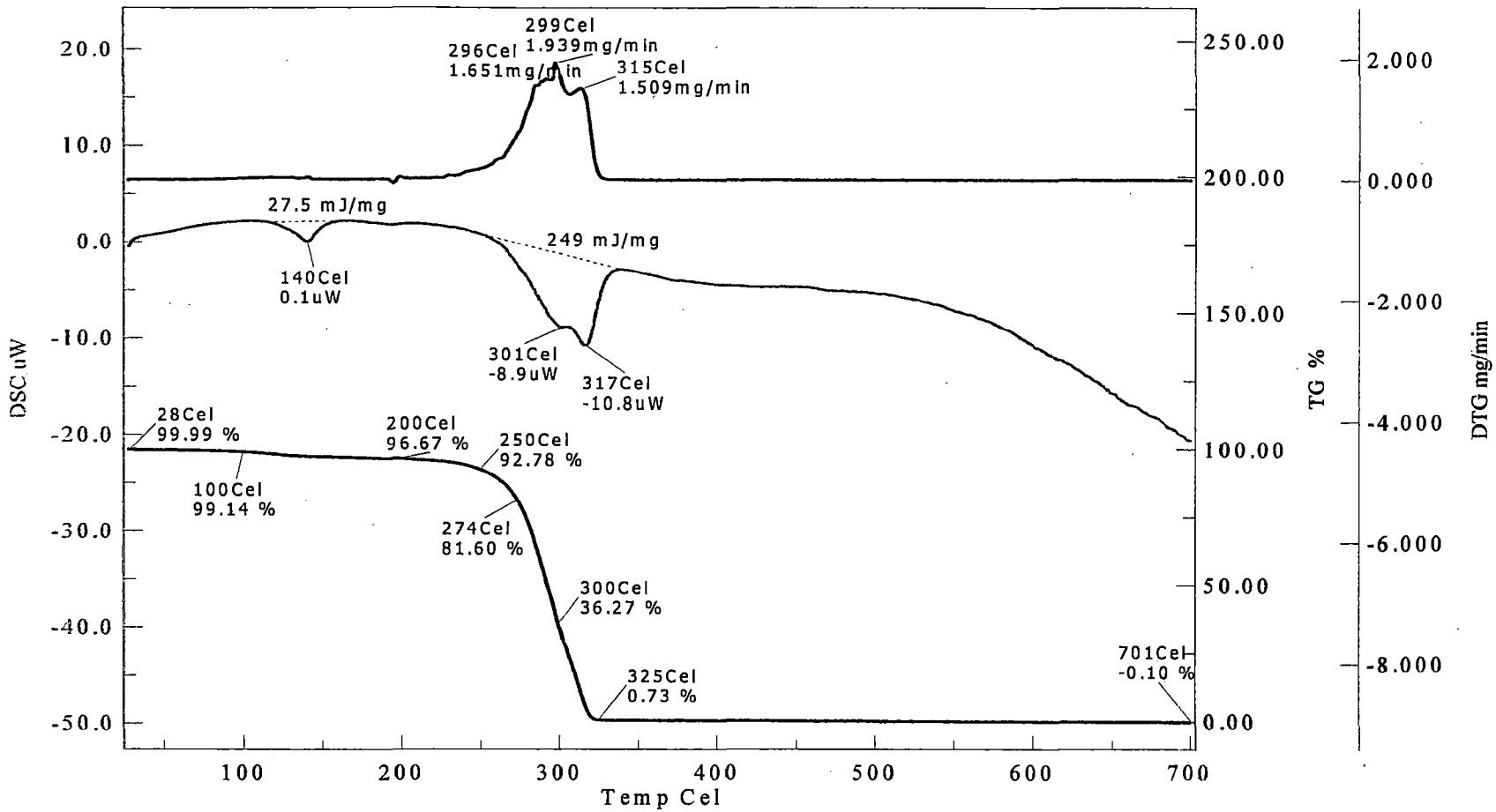

Fig. J.27 Thermal analysis of PLA 3

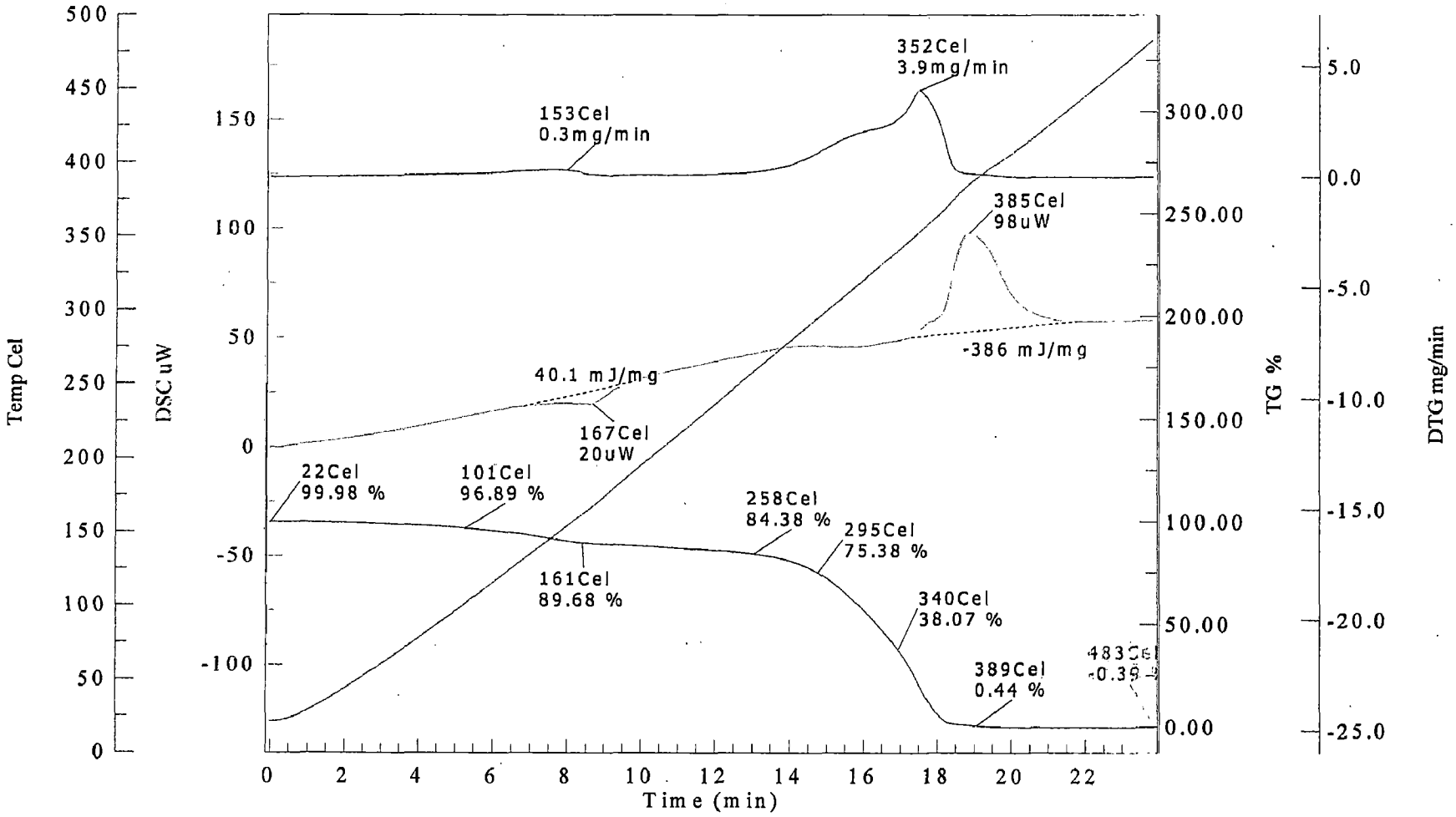

Fig. J.28 Thermal analysis of PLA 4

K.1 RAW EXPERIMENTAL DATA

Table K.1 Raw experimental data for synthesis of PLA by solid state polycondensation

			Heat treatment		Solid-state polycondensation						
Run No.	Point Type	X_1: Amount of PLLA	X_2: HT temperature	X_3: HT time	X_4: SSP time	X_5: SSP temperature	Wt. of PLA obtained	Yield	M_w	M_n	PDI
		(g)	(°C)	(h)	(h)	(°C)	(g)	(wt.%)	(kDa)	(kDa)	
1	Fact	5	120	1	30	130	3.6435	72.9	84.691	42.568	1.990
2	Fact	5	100	5	30	130	4.1485	83.0	65.098	43.401	1.500
3	Fact	3	120	5	10	160	2.1327	71.1	70.985	35.792	1.983
4	Fact	5	120	5	10	130	4.0965	81.9	80.553	44.758	1.80
5	Fact	5	120	1	10	160	3.8415	76.8	89.942	45.269	1.987
6	Fact	5	100	1	30	160	3.547	70.9	78.839	39.519	1.995
7	Fact	3	100	5	30	160	1.8711	62.4	61.276	30.839	1.987
8	Fact	3	120	1	30	160	2.1438	71.5	71.9	35.801	2.008
9	Fact	5	100	5	10	160	3.7565	75.1	75.67	38.092	1.987
10	Fact	3	120	5	30	130	2.4096	80.3	69.984	35.217	1.987
11	Fact	3	100	1	10	130	2.4675	82.3	68.763	34.455	1.996
12	Center	4	110	3	20	145	3.2388	81.0	281.54	168.995	1.666
13	Center	4	110	3	20	145	3.2056	80.1	280.095	178.281	1.571
14	Center	4	110	3	20	145	3.294	82.4	270.568	172.183	1.571
15	Center	4	110	3	20	145	3.1904	79.8	300.195	178.857	1.68
16	Center	4	110	3	20	145	3.264	81.6	275.16	175.122	1.571
17	Axial	3	110	3	20	145	2.5764	85.9	259.876	155.447	1.672
18	Axial	5	110	3	20	145	3.8155	76.3	278.437	176.618	1.576
19	Axial	4	100	3	20	145	3.5568	88.9	130.763	74.524	1.755
20	Axial	4	120	3	20	145	2.8496	71.2	165.362	96.039	1.722
21	Axial	4	110	1	20	145	3.4788	87.0	224.947	150.399	1.496
22	Axial	4	110	5	20	145	2.938	73.5	271.549	177.672	1.528
23	Axial	4	110	3	10	145	3.7024	92.6	248.904	162.984	1.527
24	Axial	4	110	3	30	145	2.8304	70.8	188.801	132.684	1.423
25	Axial	4	110	3	20	130	3.406	85.2	184.936	131.411	1.407
26	Axial	4	110	3	20	160	2.932	73.3	239.953	159.497	1.504
27	Vertex	5	100	1	10	130	4.006	80.1	97.601	52.965	1.84
28	Vertex	3	120	1	10	130	2.3778	79.3	88.793	43.786	2.028

K.2 ANALYSIS RESULTS

The output printouts of GPC, XRD and thermal analysis of few samples have been given in this Appendix.

GPC_REPORT

SAMPLE INFORMATION			
Sample Name:	PLA-S-10	Acquired By:	System
Sample Type:	Broad Unknown	Acquired Method:	Std_curve
Vial:	1	Reported Method:	GPC_Report
Injection:	6	Date Acquired:	12/20/2008 05:52:47 PM
Injection Volume:	20ul		
Run Time:	30.0 Minutes		

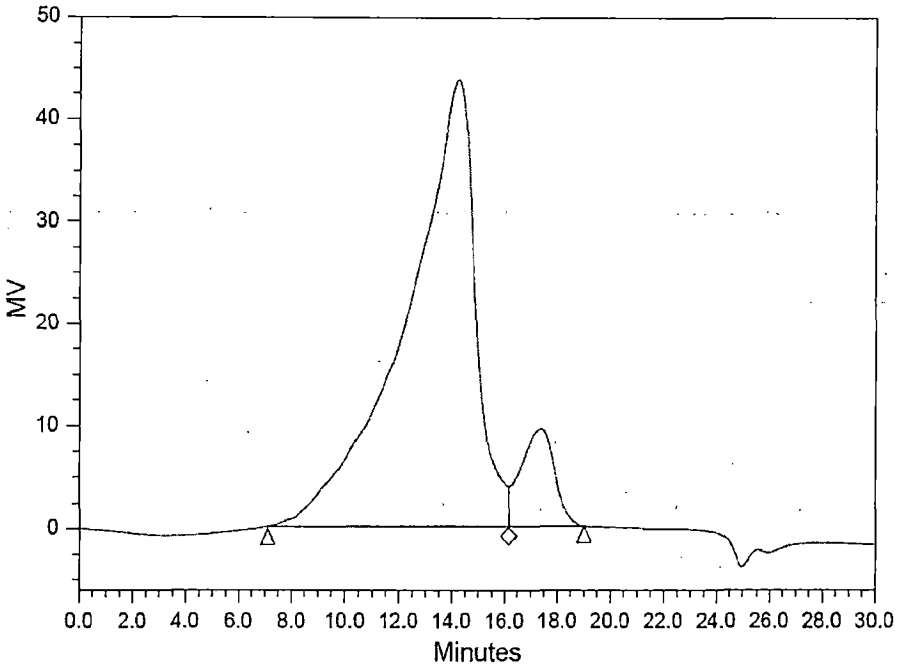

	RT	Mn	Mw	Polydispersity
1	14.24	168995	281540	1.666
2	17.42			

Fig. K.1 GPC chromatogram of PLA (Run No. 12)

GPC_REPORT

SAMPLE INFORMATION			
Sample Name:	PLA-S-12	Acquired By:	System
Sample Type:	Broad Unknown	Acquired Method:	Std_curve
Vial:	1	Reported Method:	GPC_Report
Injection:	2	Date Acquired:	12/21/2008 10:46:15 AM
Injection Volume:	20ul		
Run Time:	30.0 Minutes		

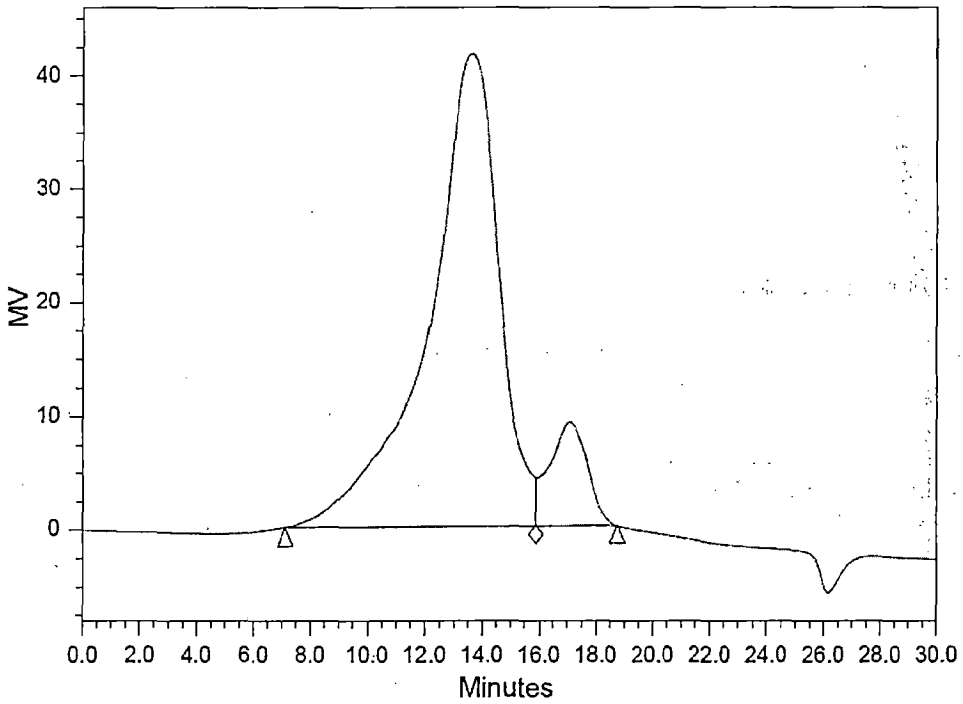

	RT	Mn	Mw	Polydispersity
1	13.61	178281	280095	1.571
2	17.13			

Fig. K.2 GPC chromatogram of PLA (Run No. 13)

GPC_REPORT

SAMPLE INFORMATION			
Sample Name:	PLA-S-13	Acquired By:	System
Sample Type:	Broad Unknown	Acquired Method:	Std_curve
Vial:	1	Reported Method:	GPC_Report
Injection:	3	Date Acquired:	12/21/2008 11:21:56 AM
Injection Volume:	20ul		
Run Time:	30.0 Minutes		

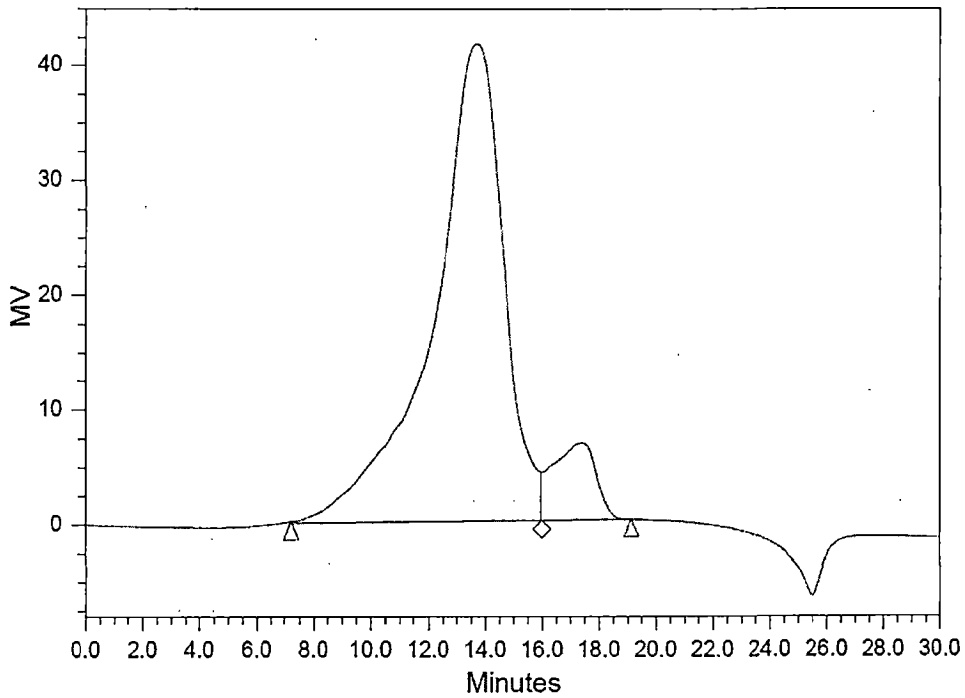

	RT	Mn	Mw	Polydispersity
1	13.72	172183	270568	1.571
2	17.41			

Fig. K.3 GPC chromatogram of PLA (Run No. 14)

iit delhi polymer science
Project Name: May2008
Reported by User: System

Breeze

SAMPLE INFORMATION

Sample Name:	roorkee PLA-6	Acquired By:	System
Sample Type:	Broad Unknown	Date Acquired:	5/14/2008 1:28:01 PM
Vial:	1	Acq. Method:	std_curve
Injection #:	1	Date Processed:	5/16/2008 4:41:43 PM
Injection Volume:	20.00 ul	Channel Name:	SATIN-2
Run Time:	25.00 Minutes	Sample Set Name:	

Autoscaled Chromatogram

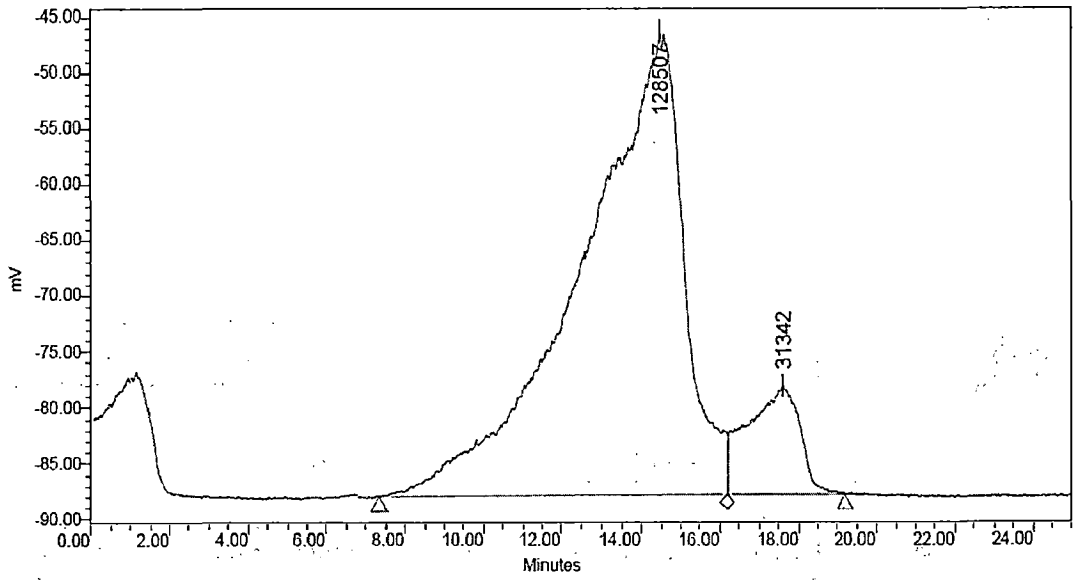

GPC Results

	Dist Name	Elution Volume (ml)	Retention Time (min)	Adjusted RT (min)	Mn	Mw	MP	Mz	Mz+1
1		14.468	14.468	14.468	178857	300195	128507	619917	1126126
2		17.593	17.593	17.593			31342		

GPC Results

	Mz/Mw	Mz+1/Mw	Area (V*sec)	% Area	Height (V)	% Height	Integration Type	Peak Codes	Points Across Peak
1	2.065050	3.751316	7475189	89.18	41460	80.97	BV		10600
2			906755	10.82	9743	19.03	VB	108	3624

Fig. K.4 GPC chromatogram of PLA (Run No. 15)

GPC_REPORT

SAMPLE INFORMATION			
Sample Name:	PLA-S-14	Acquired By:	System
Sample Type:	Broad Unknown	Acquired Method:	Std_curve
Vial:	1	Reported Method:	GPC_Report
Injection:	4	Date Acquired:	12/21/2008 12:08:27 PM
Injection Volume:	20ul		
Run Time:	30.0 Minutes		

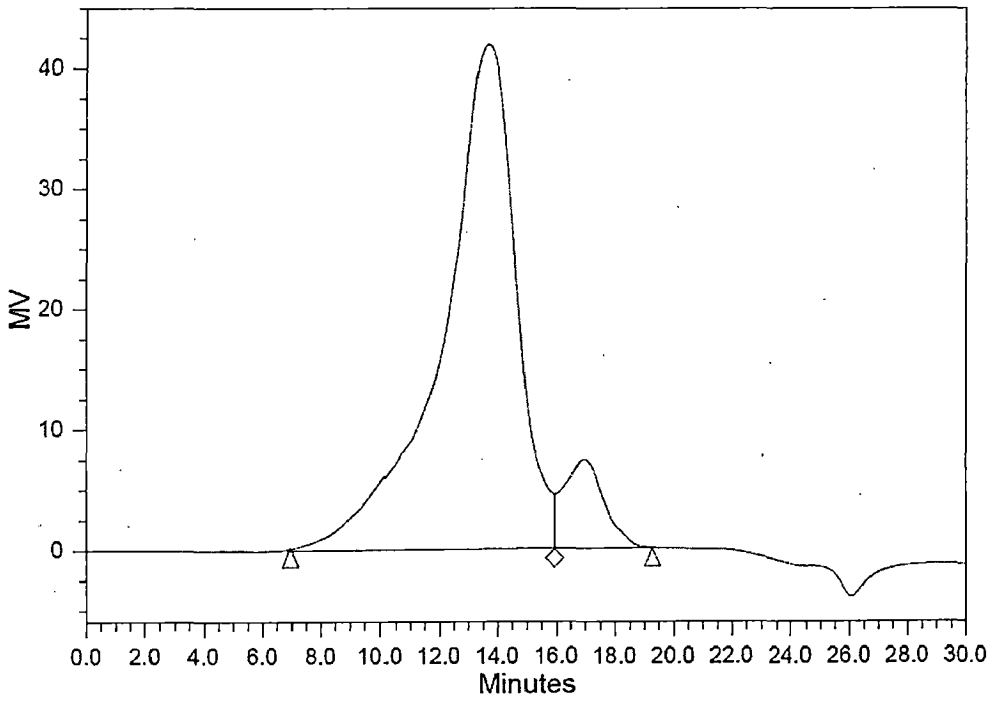

	RT	Mn	Mw	Polydispersity
1	13.66	175122	275160	1.571
2	17.01			

Fig. K.5 GPC chromatogram of PLA (Run No. 16)

GPC_REPORT

SAMPLE INFORMATION			
Sample Name:	PLA-S-15	Acquired By:	System
Sample Type:	Broad Unknown	Acquired Method:	Std_curve
Vial:	1	Reported Method:	GPC_Report
Injection:	1	Date Acquired:	12/21/2008 04:13:16 PM
Injection Volume:	20ul		
Run Time:	30.0 Minutes		

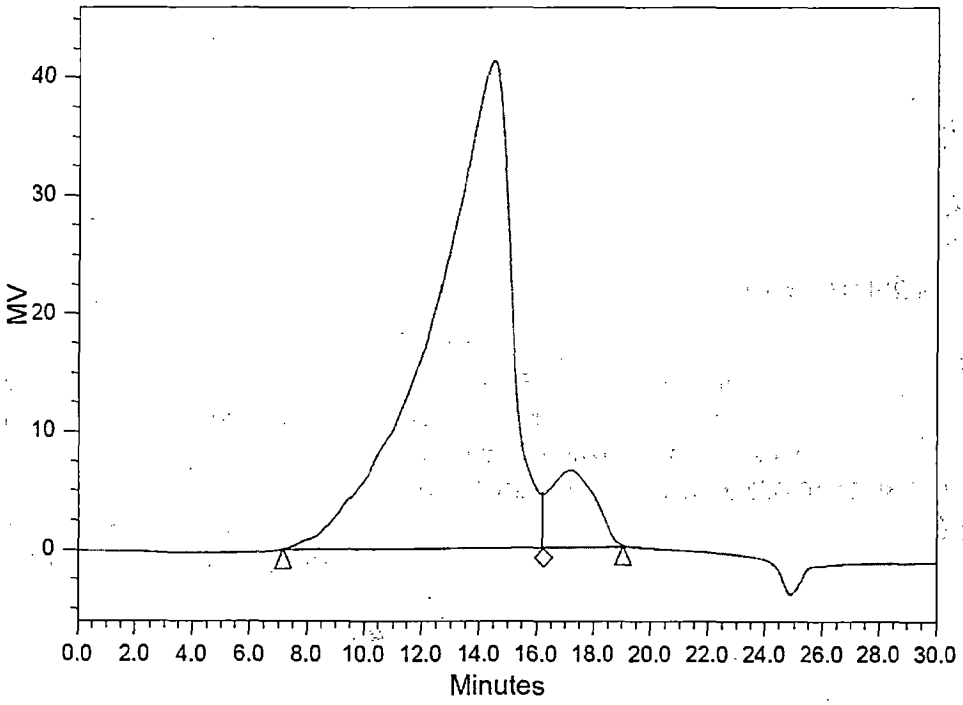

	RT	Mn	Mw	Polydispersity
1	14.46	155447	259876	1.672
2	17.24			

Fig. K.6 GPC chromatogram of PLA (Run No. 17)

GPC_REPORT

SAMPLE INFORMATION			
Sample Name:	PLA-S-16	Acquired By:	System
Sample Type:	Broad Unknown	Acquired Method:	Std_curve
Vial:	1	Reported Method:	GPC_Report
Injection:	2	Date Acquired:	12/21/2008 04:59:21 PM
Injection Volume:	20ul		
Run Time:	30.0 Minutes		

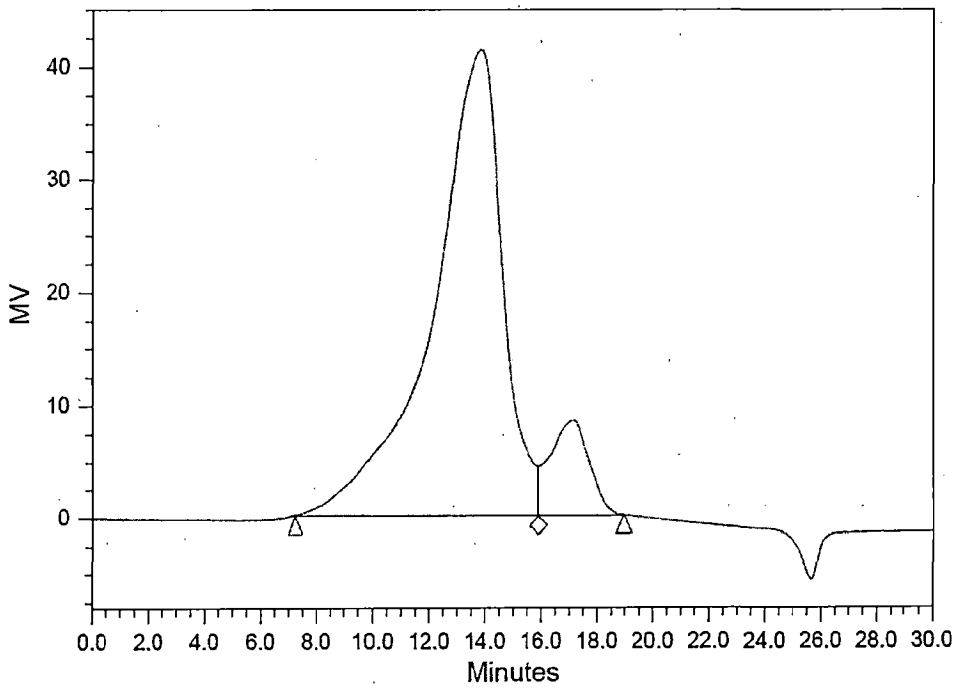

	RT	Mn	Mw	Polydispersity
1	13.86	176618	278437	1.576
2	17.17			

Fig. K.7 GPC chromatogram of PLA (Run No. 18)

GPC_REPORT

SAMPLE INFORMATION			
Sample Name:	PLA-TM-9	Acquired By:	System
Sample Type:	Broad Unknown	Acquired Method:	Std_curve
Vial:	1	Reported Method:	GPC_Report
Injection:	2	Date Acquired:	12/13/2008 10:10:43 PM
Injection Volume:	20ul		
Run Time:	30.0 Minutes		

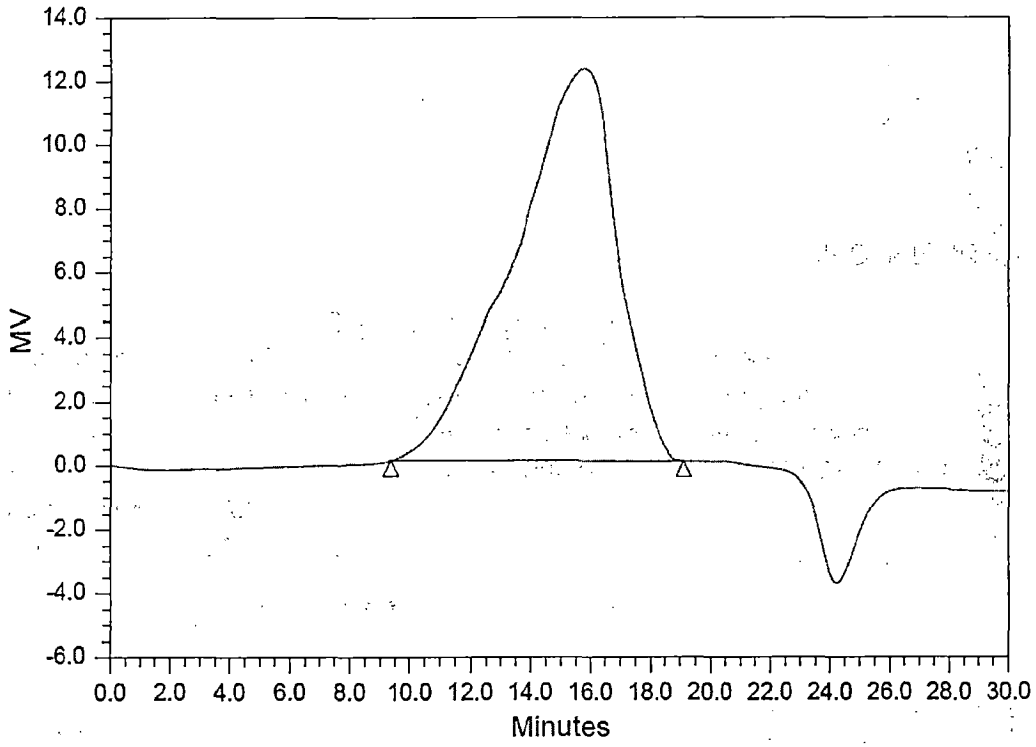

	RT	Mn	Mw	Polydispersity
1	15.82	74524	130763	1.755

Fig. K.8 GPC chromatogram of PLA (Run No. 19)

GPC_REPORT

SAMPLE INFORMATION			
Sample Name:	PLA-S-17	Acquired By:	System
Sample Type:	Broad Unknown	Acquired Method:	Std_curve
Vial:	1	Reported Method:	GPC_Report
Injection:	3	Date Acquired:	12/21/2008 10:09:03 PM
Injection Volume:	20ul		
Run Time:	30.0 Minutes		

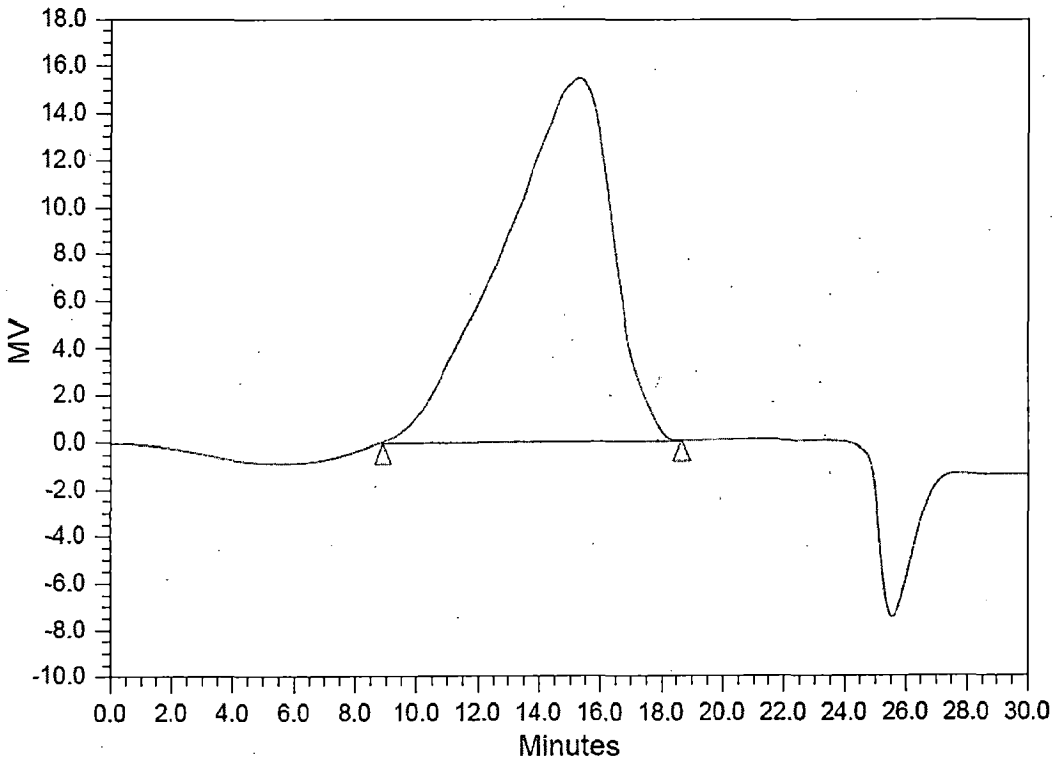

	RT	Mn	Mw	Polydispersity
1	15.36	96039	165362	1.722

Fig. K.9 GPC chromatogram of PLA (Run No. 20)

GPC_REPORT

SAMPLE INFORMATION			
Sample Name:	PLA-S-18	Acquired By:	System
Sample Type:	Broad Unknown	Acquired Method:	Std_curve
Vial:	1	Reported Method:	GPC_Report
Injection:	4	Date Acquired:	12/21/2008 10:48:03 PM
Injection Volume:	20ul		
Run Time:	30.0 Minutes		

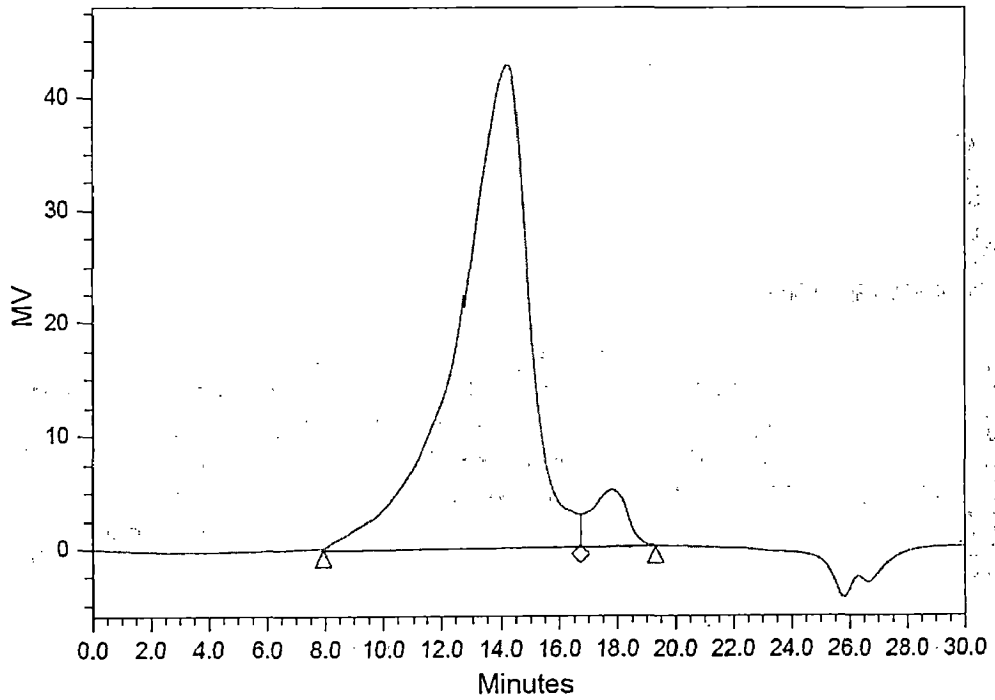

	RT	Mn	Mw	Polydispersity
1	14.22	150399	224947	1.496
2	17.86			

Fig. K.10 GPC chromatogram of PLA (Run No. 21)

GPC_REPORT

SAMPLE INFORMATION			
Sample Name:	PLA-S-20	Acquired By:	System
Sample Type:	Broad Unknown	Acquired Method:	Std_curve
Vial:	1	Reported Method:	GPC_Report
Injection:	2	Date Acquired:	12/24/2008 10:05:56 PM
Injection Volume:	20ul		
Run Time:	30.0 Minutes		

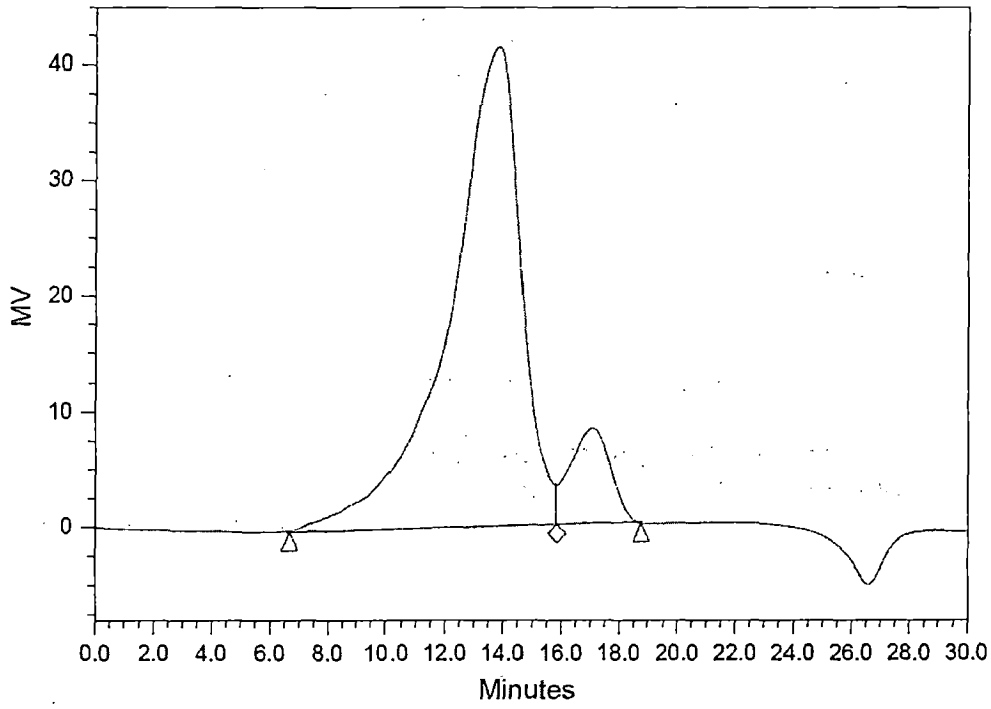

	RT	Mn	Mw	Polydispersity
1	13.83	177672	271549	1.528
2	17.06			

Fig. K.11 GPC chromatogram of PLA (Run No. 22)

GPC_REPORT

SAMPLE INFORMATION			
Sample Name:	PLA-S-21	Acquired By:	System
Sample Type:	Broad Unknown	Acquired Method:	Std_curve
Vial:	1	Reported Method:	GPC_Report
Injection:	1	Date Acquired:	12/25/2008 09:56:10 AM
Injection Volume:	20ul		
Run Time:	30.0 Minutes		

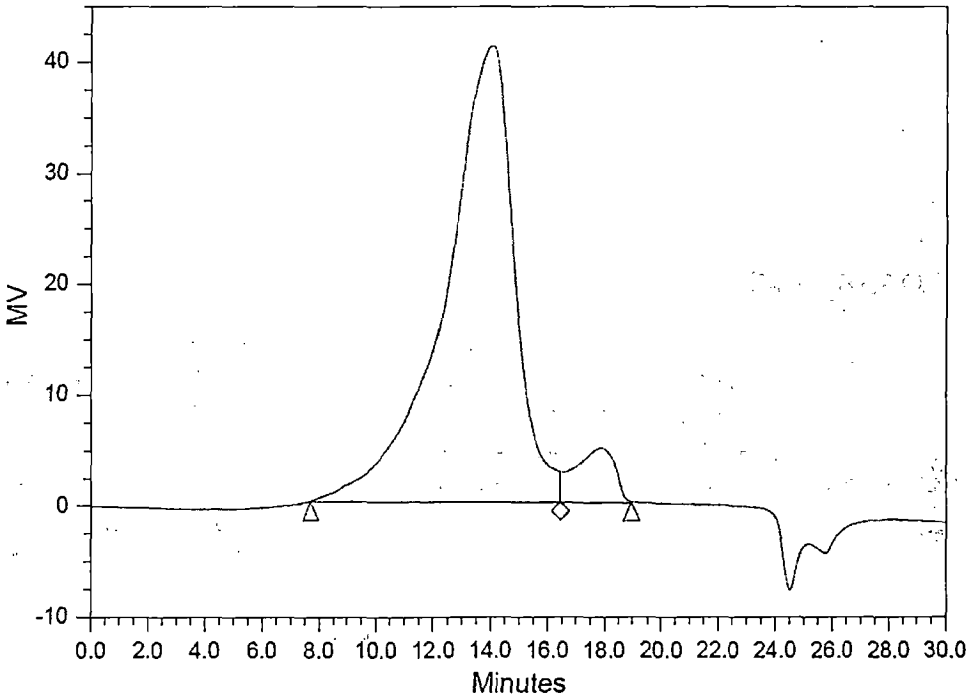

	RT	Mn	Mw	Polydispersity
1	14.05	162984	248904	1.527
2	17.85			

Fig. K.12 GPC chromatogram of PLA (Run No. 23)

GPC_REPORT

SAMPLE INFORMATION			
Sample Name:	PLA-S-19	Acquired By:	System
Sample Type:	Broad Unknown	Acquired Method:	Std_curve
Vial:	1	Reported Method:	GPC_Report
Injection:	1	Date Acquired:	12/24/2008 09:20:13 PM
Injection Volume:	20ul		
Run Time:	30.0 Minutes		

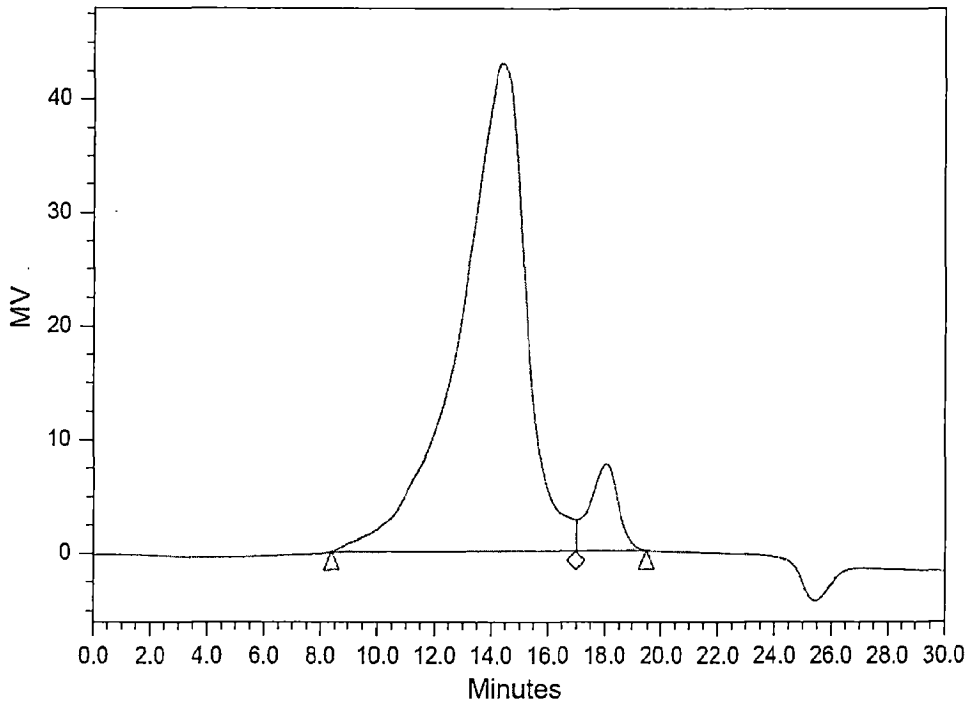

	RT	Mn	Mw	Polydispersity
1	14.40	132684	188801	1.423
2	18.04			

Fig. K.13 GPC chromatogram of PLA (Run No. 24)

GPC_REPORT

SAMPLE INFORMATION			
Sample Name:	PLA-S-22	Acquired By:	System
Sample Type:	Broad Unknown	Acquired Method:	Std_curve
Vial:	1	Reported Method:	GPC_Report
Injection:	2	Date Acquired:	12/25/2008 10:41:19 AM
Injection Volume:	20ul		
Run Time:	30.0 Minutes		

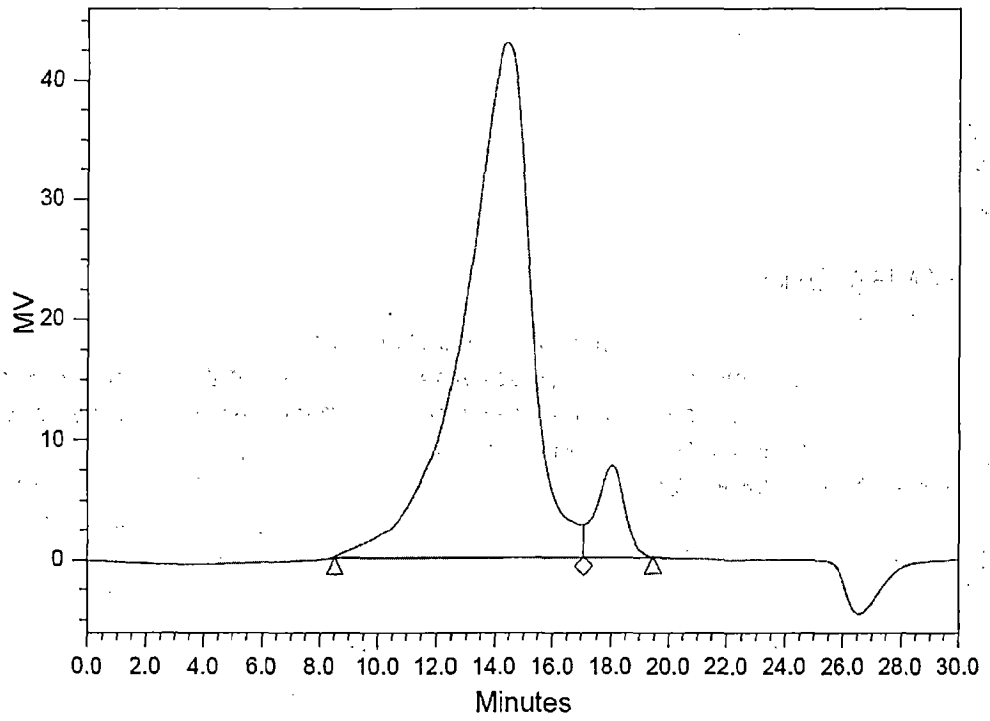

	RT	Mn	Mw	Polydispersity
1	14.39	131411	184936	1.407
2	18.03			

Fig. K.14 GPC chromatogram of PLA (Run No. 25)

GPC_REPORT

SAMPLE INFORMATION			
Sample Name:	PLA-S-24	Acquired By:	System
Sample Type:	Broad Unknown	Acquired Method:	Std_curve
Vial:	1	Reported Method:	GPC_Report
Injection:	4	Date Acquired:	12/25/2008 05:06:22 PM
Injection Volume:	20ul		
Run Time:	30.0 Minutes		

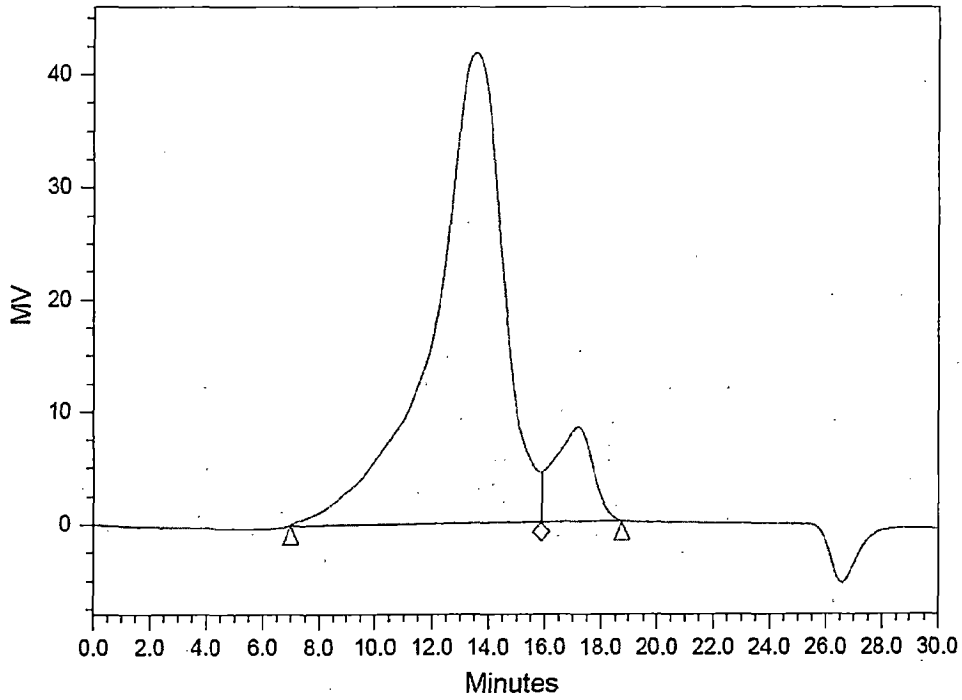

	RT	Mn	Mw	Polydispersity
1	13.55	183696	288362	1.570
2	17.23			

Fig. K.15 GPC chromatogram of PLA (Optimum condition-1)

GPC_REPORT

SAMPLE INFORMATION			
Sample Name:	PLA-S-25	Acquired By:	System
Sample Type:	Broad Unknown	Acquired Method:	Std_curve
Vial:	1	Reported Method:	GPC_Report
Injection:	5	Date Acquired:	12/25/2008 05:51:14 PM
Injection Volume:	20ul		
Run Time:	30.0 Minutes		

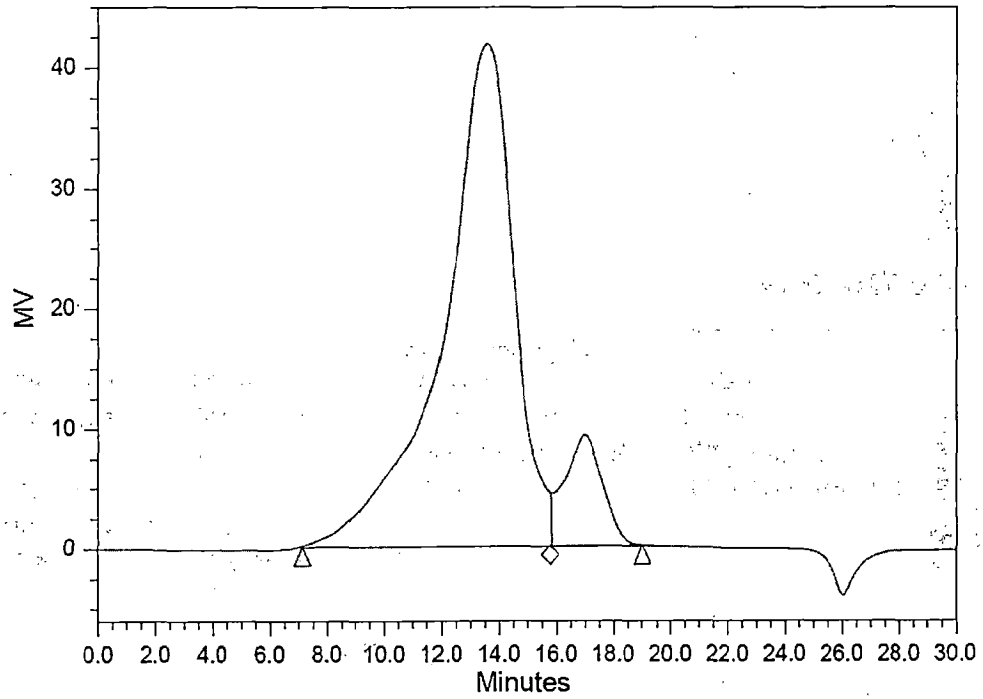

	RT	Mn	Mw	Polydispersity
1	13.60	181807	285659	1.571
2	17.00			

Fig. K.16 GPC chromatogram of PLA (Optimum condition-2)

GPC_REPORT

SAMPLE INFORMATION			
Sample Name:	PLA-S-23	Acquired By:	System
Sample Type:	Broad Unknown	Acquired Method:	Std_curve
Vial:	1	Reported Method:	GPC_Report
Injection:	3	Date Acquired:	12/25/2008 11:31:12 AM
Injection Volume:	20ul		
Run Time:	30.0 Minutes		

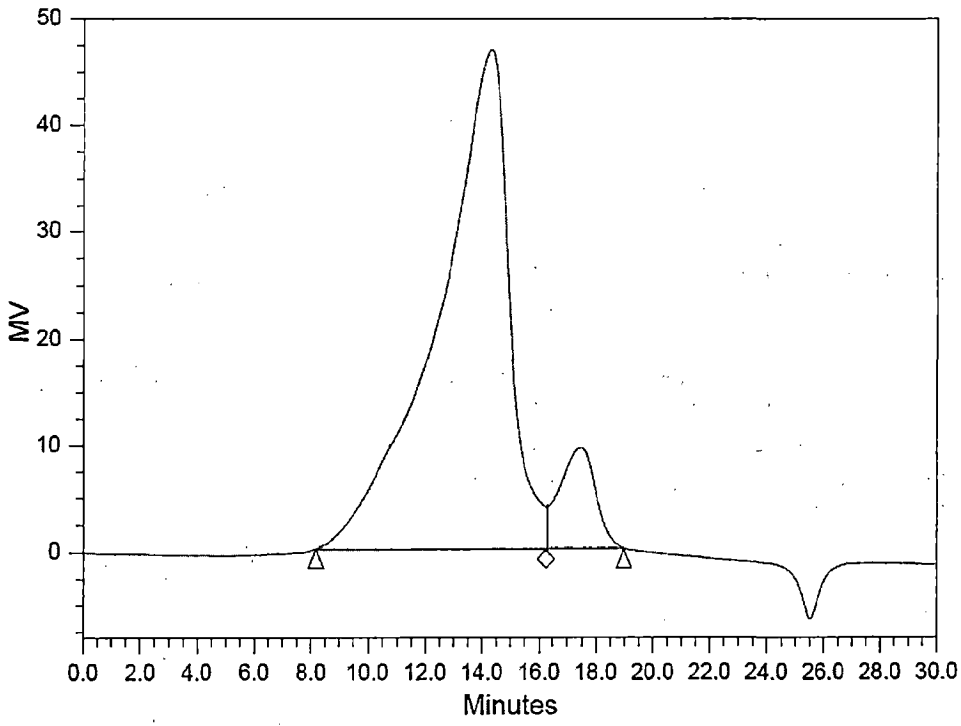

	RT	Mn	Mw	Polydispersity
1	14.28	159497	239953	1.504
2	17.46			

Fig. K.17 GPC chromatogram of PLA (Run No. 26)

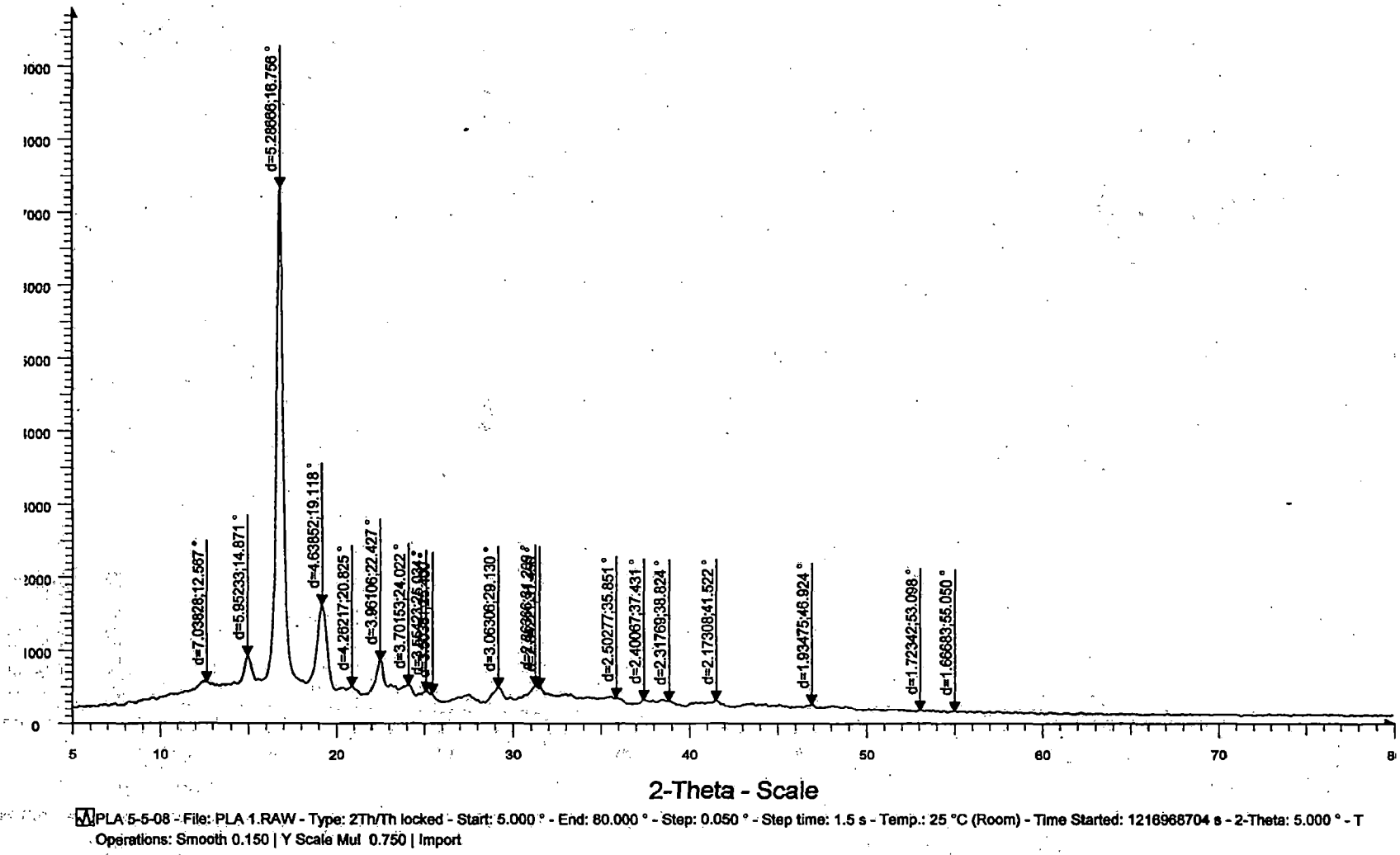

Fig. K.18 XRD of PLA S1

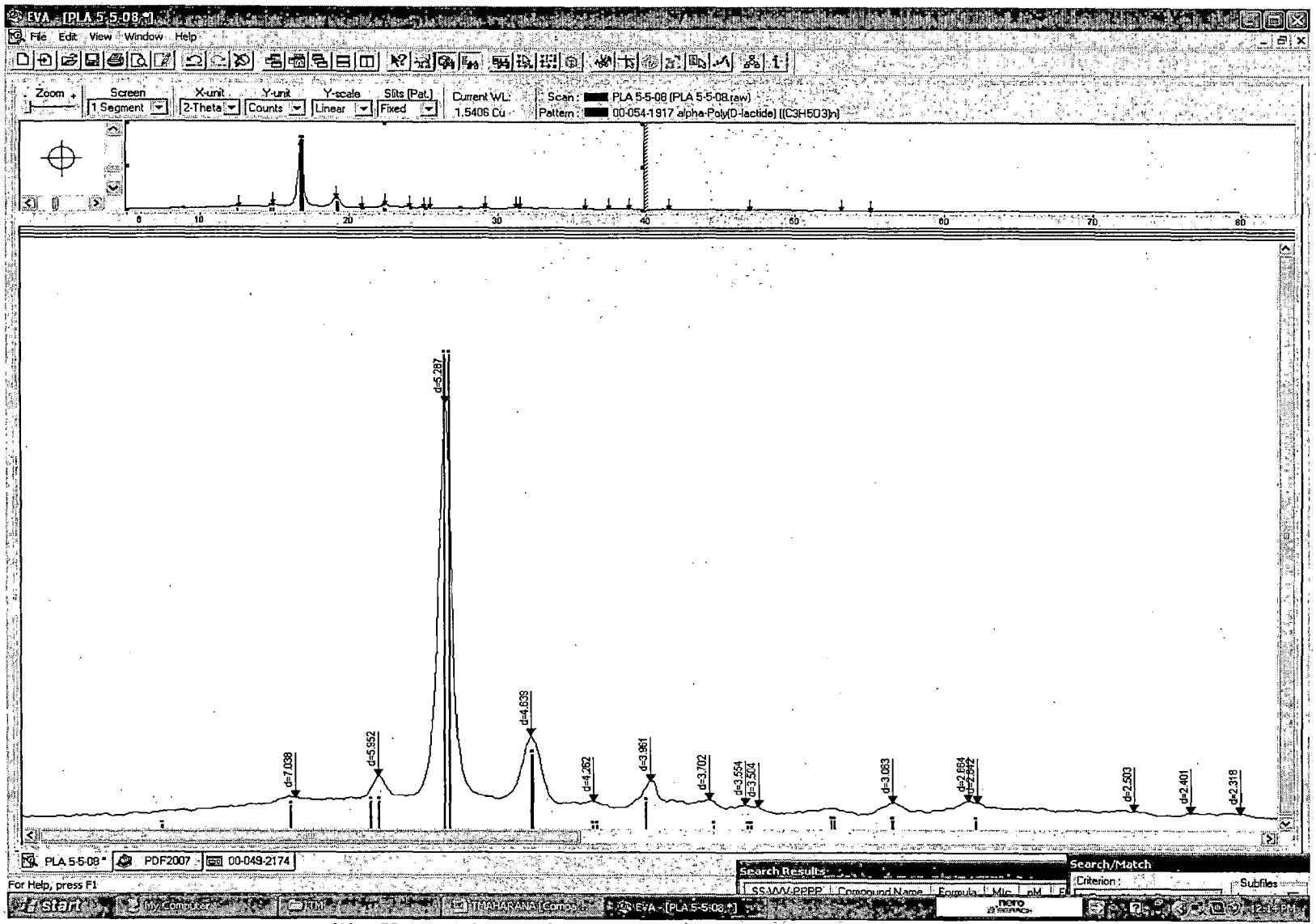

Fig. K.19 XRD match of PLA S1 with alpha-poly(D(+)-lactide)

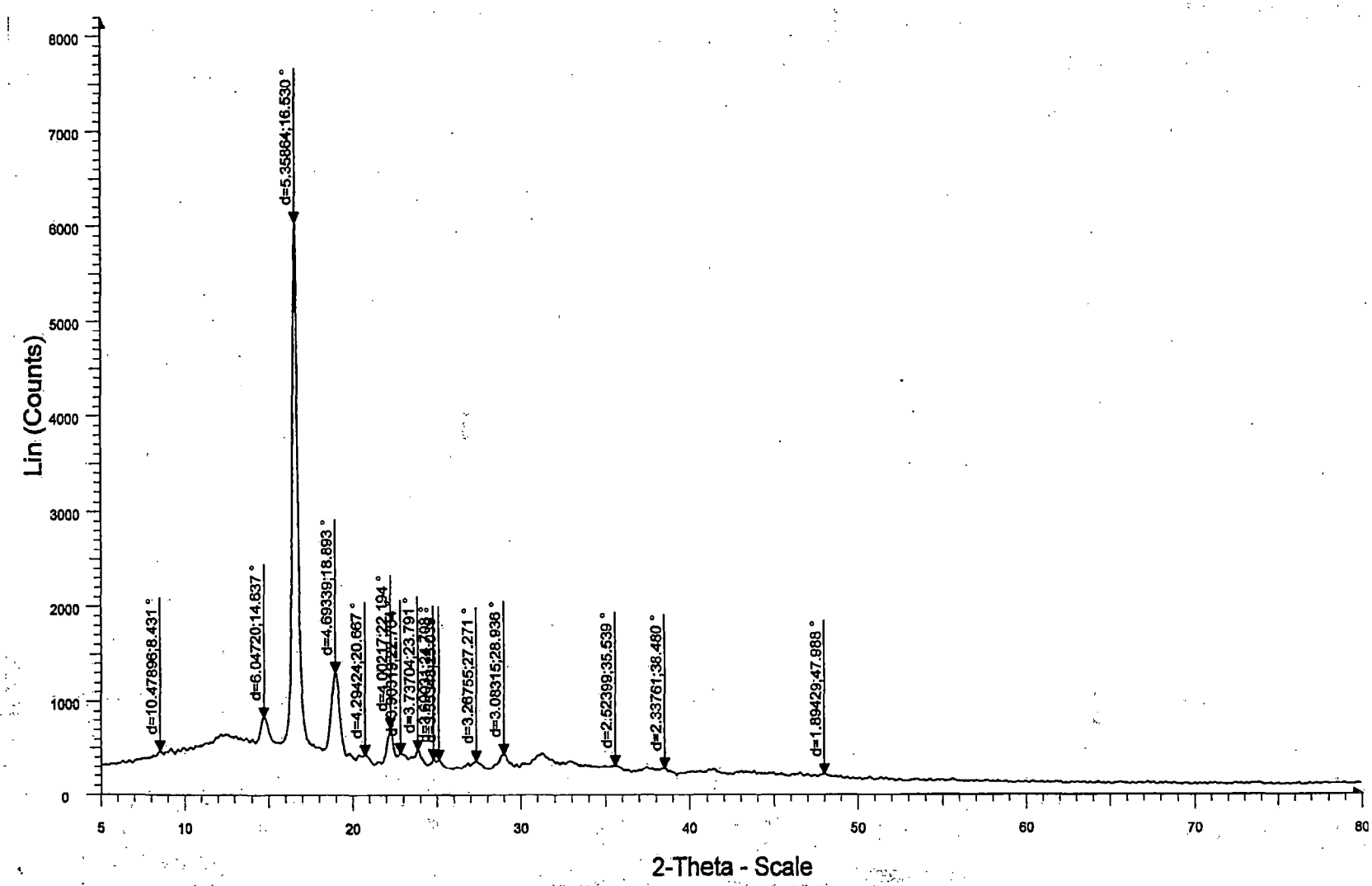

Fig. K.20 XRD of LA S2

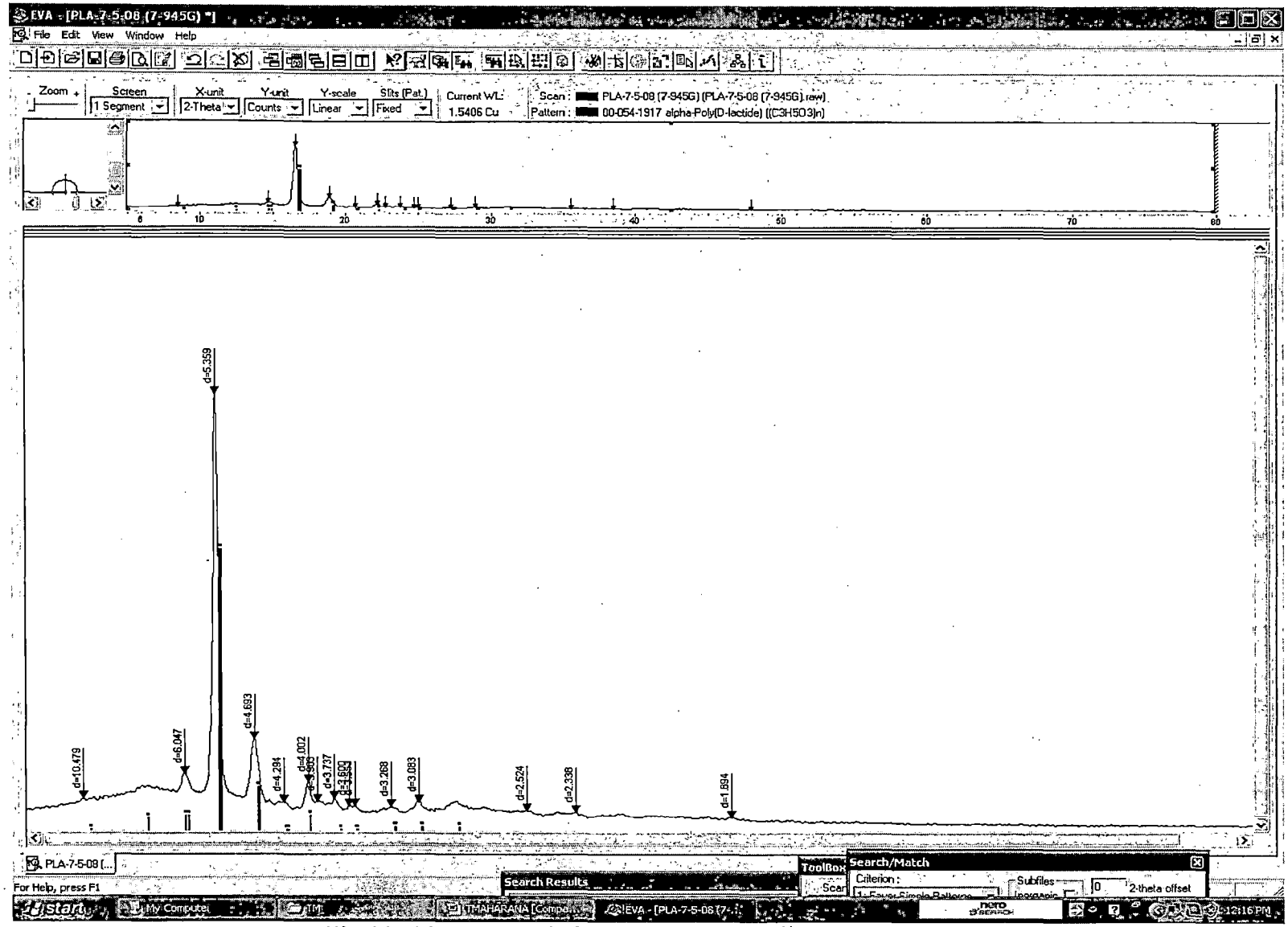

Fig. K.21 XRD match of PLA S2 with alpha-poly(D(+)-lactide)

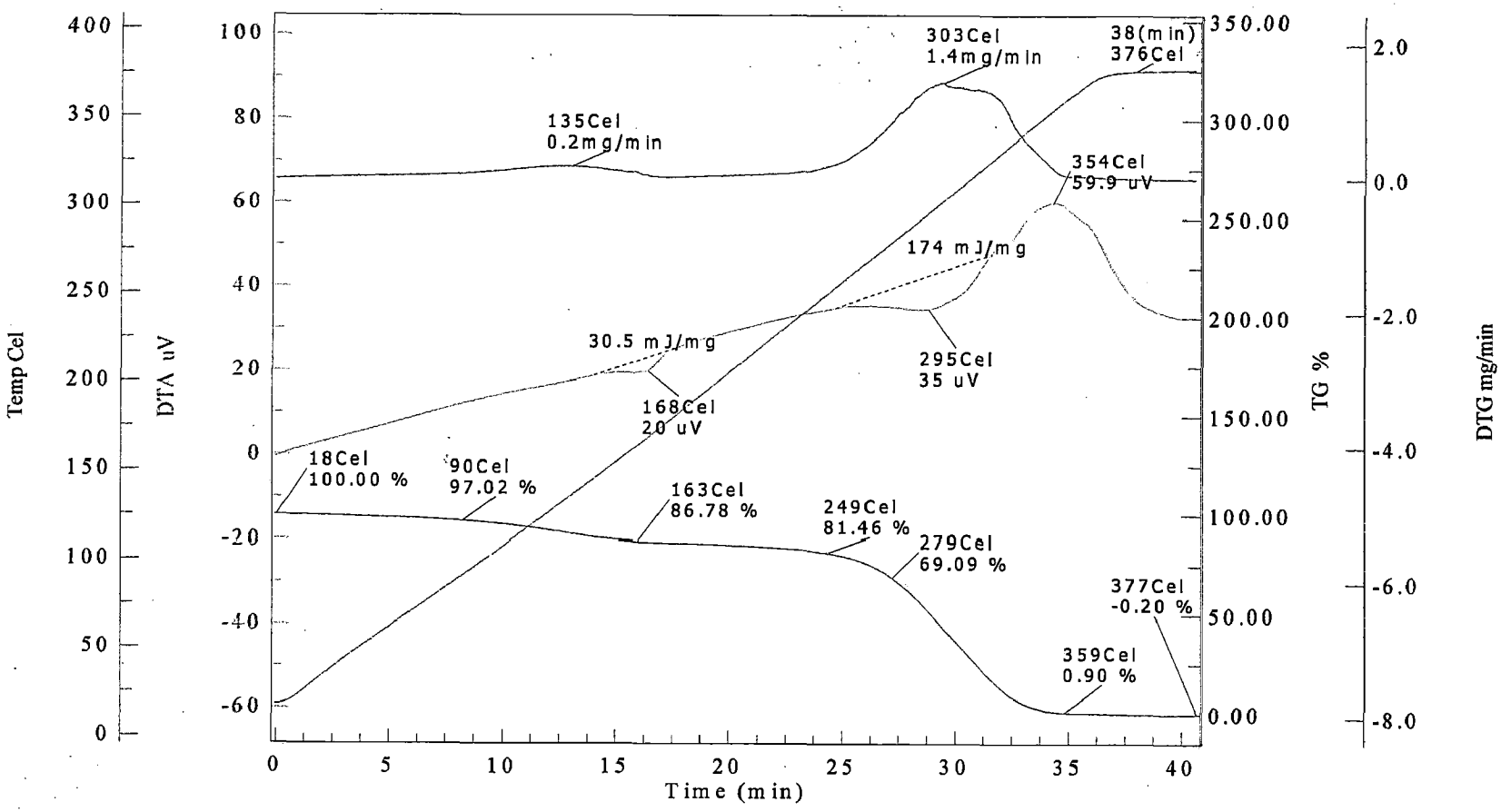

Fig. K. 22 Thermal analysis of PLA S1

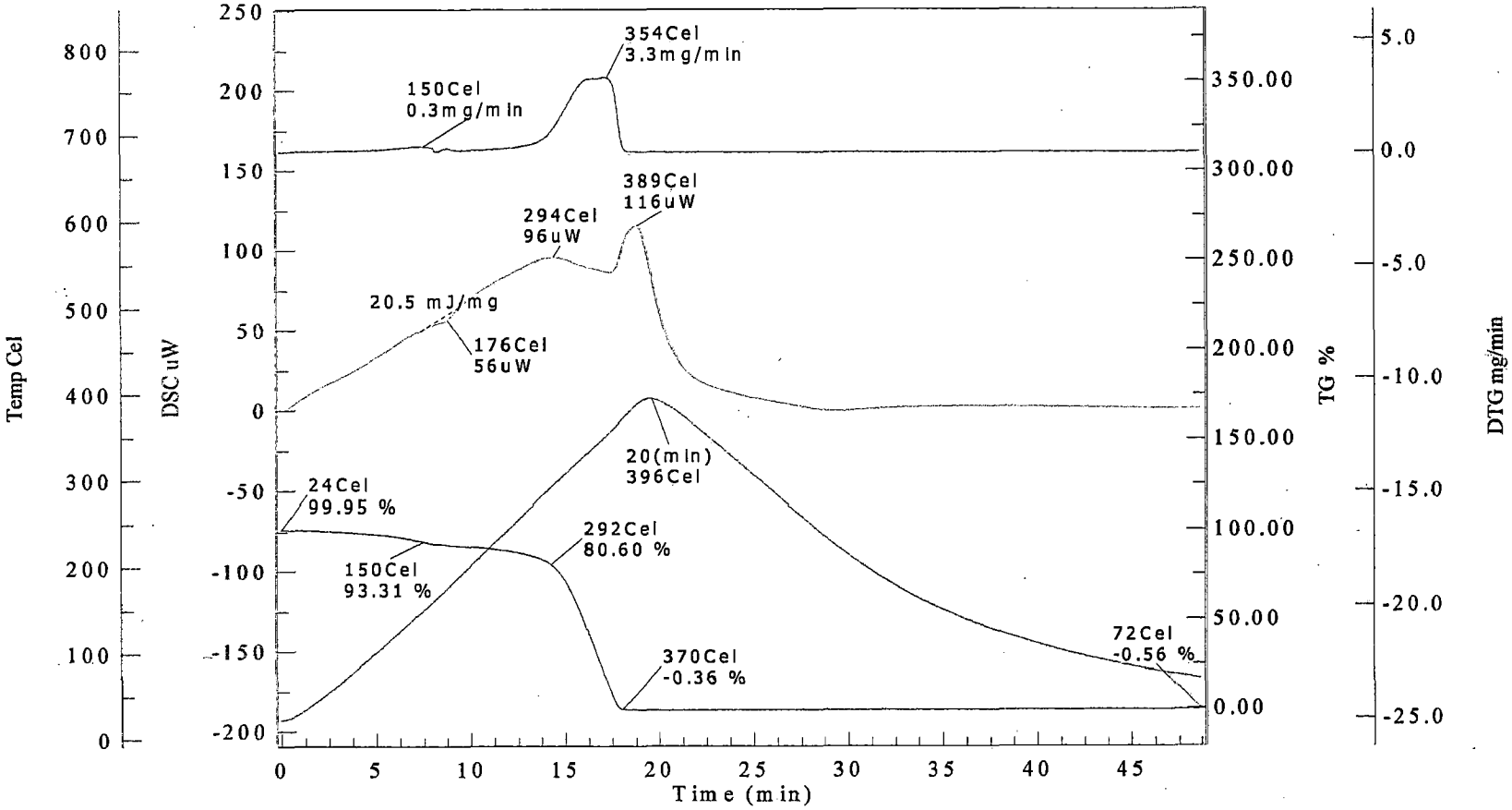

Fig. K. 23 Thermal analysis of PLA S2

iit delhi polymer science
Project Name: May2008
Reported by User: System

Breeze

SAMPLE INFORMATION

Sample Name:	Roorkee_PLA 4	Acquired By:	System
Sample Type:	Broad Unknown	Date Acquired:	5/2/2008 1:30:09 PM
Vial:	1	Acq. Method:	std_curve
Injection #:	2	Date Processed:	5/19/2008 2:34:15 PM
Injection Volume:	20.00 ul	Channel Name:	SATIN-2
Run Time:	30.00 Minutes	Sample Set Name:	

Autoscaled Chromatogram

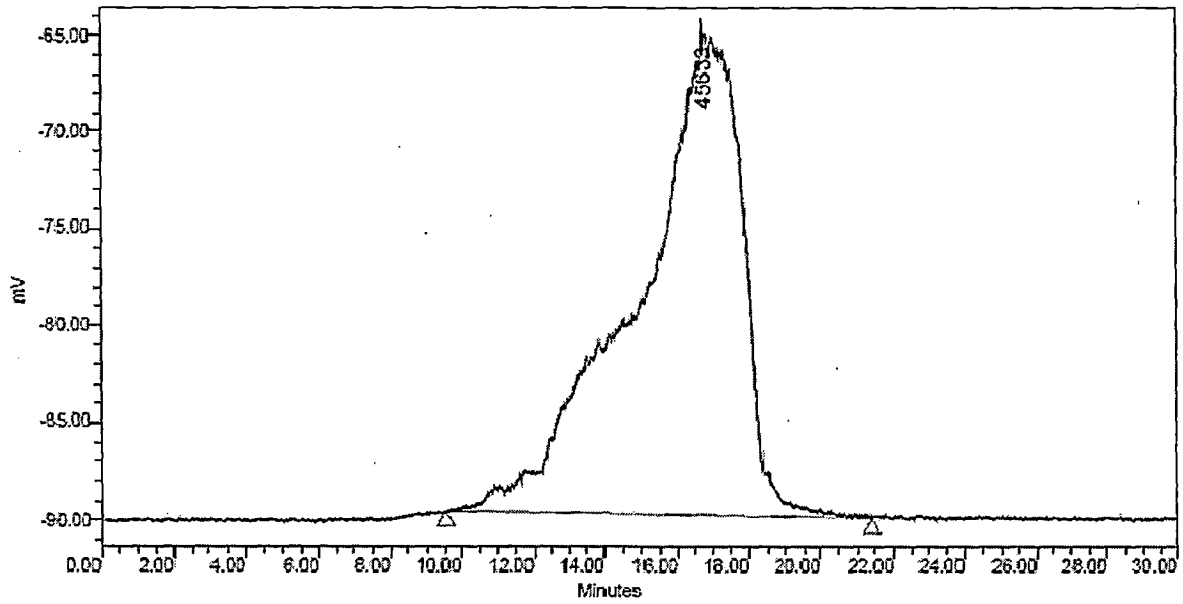

GPC Results

	Dist Name	Elution Volume (ml)	Retention Time (min)	Adjusted RT (min)	Mn	Mw	MP	Mz	Mz+1	Mz/Mw
1		16.761	16.761	16.761	52965	97601	45633	217633	407557	2.229831

GPC Results

	Mz+1/Mw	Area (V*sec)	% Area	Height (V)	% Height	Integration Type	Peak Codes	Points Across Peak	Start Time (min)
1	4.175755	5040005	100.00	24872	100.00	BB		14259	9.548

GPC Results

	End Time (min)	Baseline Start (min)	Baseline End (min)	Slope (V/sec)	Offset (V)
1	21.430	9.548	21.430	-2.499474e-002	-6.928537e+001

Fig. K.24 GPC chromatogram of PLA (Run No. 27)

RAW EXPERIMENTAL DATA OF PLA NANOPARTICLE PREPARATION

L.1 RAW EXPERIMENTAL DATA

Table L.1 Raw experimental data for preparation of PLA nanoparticles

Run No.	M_w of PLA	Name of Solvent	Amount of PLA	Solvent	PLA conc.	Non-solvent	S/NS volume ratio	Wt. of PLA NP	Yield	NP size	PDI
	kDa		(mg)	(ml)	(mg/ml)	(ml)		(mg)	(wt. %)	(nm)	
1	PLAL	Acetone	5	1.0	5	20.0	0.05	4.3152	86.3	134	0.035
2	PLAL	Acetone	20	4.0	5	20.0	0.20	17.9811	89.9	111	0.072
3	PLAH	DMSO	25	5.0	5	14.3	0.35	13.1030	52.4	220	0.217
4	PLAH	DMSO	45	9.0	5	15.0	0.60	20.9714	46.6	228	0.098
5	PLAL	DMSO	10	1.0	10	20.0	0.05	7.5931	75.9	113	0.128
6	PLAL	DMSO	40	4.0	10	20.0	0.20	31.4301	78.5	109	0.261
7	PLAH	Acetone	50	5.0	10	14.3	0.35	33.3353	66.7	125	0.228
8	PLAH	Acetone	90	9.0	10	15.0	0.60	47.5924	52.9	342	0.342
9	PLAH	Acetone	15	1.0	15	20.0	0.05	5.1885	34.6	221	0.118
10	PLAH	Acetone	60	4.0	15	20.0	0.20	23.6882	39.5	160	0.125
11	PLAL	DMSO	75	5.0	15	14.3	0.35	28.3354	37.8	140	0.109
12	PLAL	DMSO	135	9.0	15	15.0	0.60	45.4815	33.7	270	0.097
13	PLAH	DMSO	20	1.0	20	20.0	0.05	5.5156	27.6	221	0.086
14	PLAH	DMSO	80	4.0	20	20.0	0.20	26.8643	33.6	353	0.13
15	PLAL	Acetone	100	5.0	20	14.3	0.35	28.5951	28.6	302	0.172
16	PLAL	Acetone	180	9.0	20	15.0	0.60	46.7642	26.0	335	0.185

PLAL: PLA of M_w 98 kDa; PLAH: PLA of M_w 178 kDa; Non-solvent (NS): Methanol

L.2 ANALYSIS RESULTS

The DLS plots of the other experimental runs are given below:

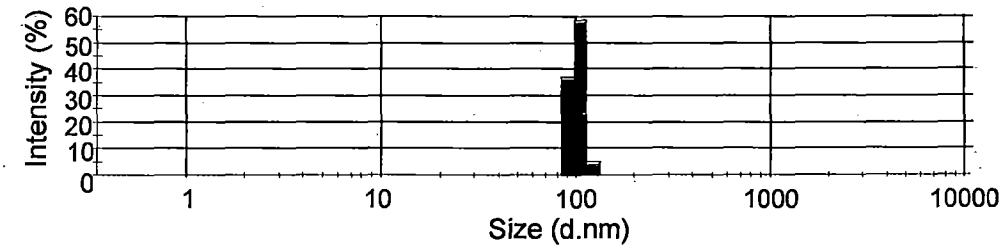

Run No. 2; Peak 1: 111 nm; PDI: 0. 072

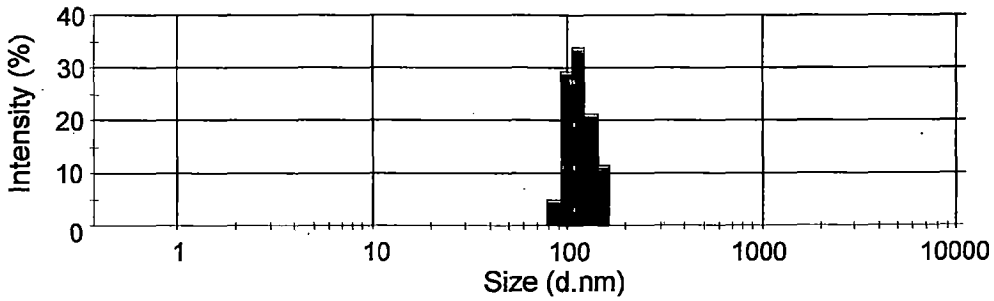

Run No. 5; Peak 1: 113 nm; PDI: 0.128

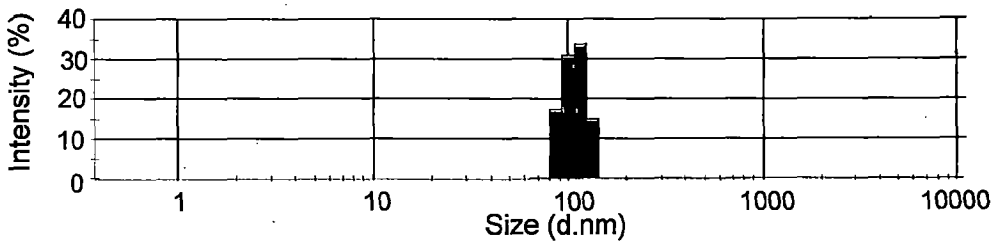

Run No. 6; Peak 1: 109 nm; PDI: 0.261

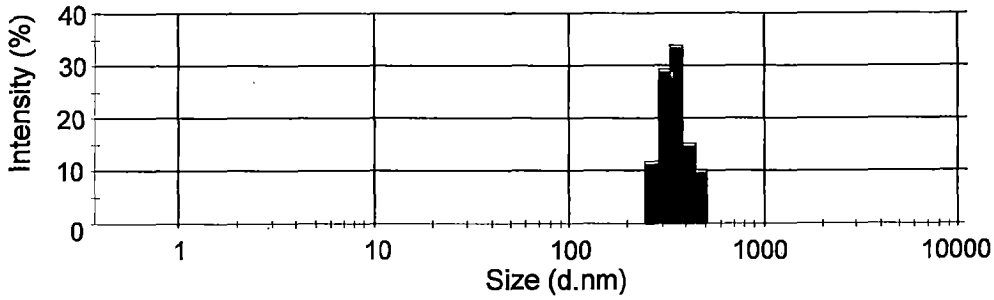

Run No. 8; Peak 1: 342 nm; PDI: 0.342

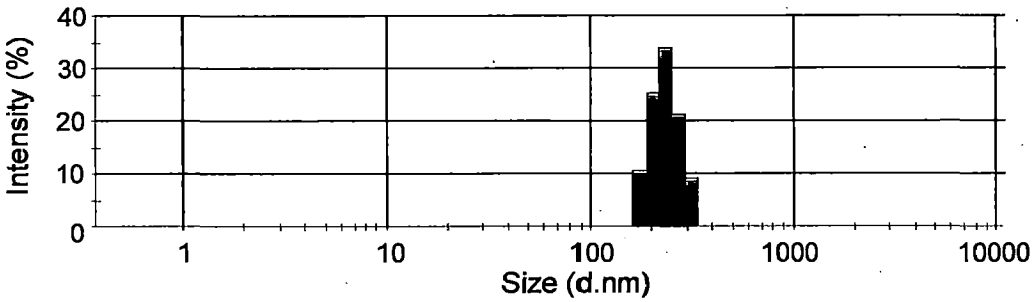

Run No. 9; Peak 1: 221 nm; PDI: 0.118

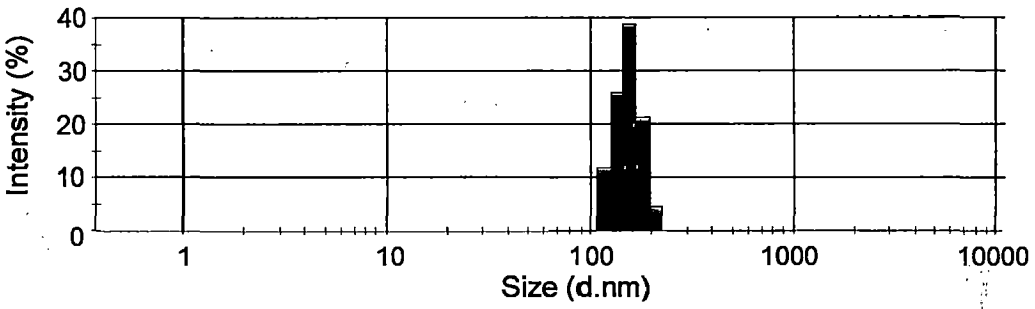

Run No. 10; Peak 1: 160 nm; PDI: 0.125

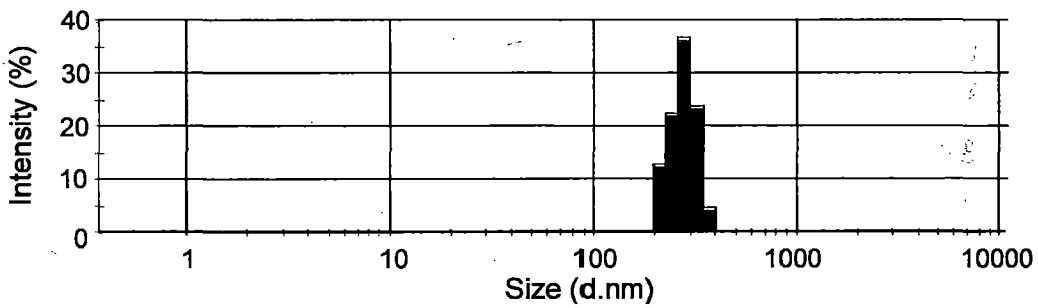

Run No. 12; Peak 1: 270 nm; PDI: 0.097

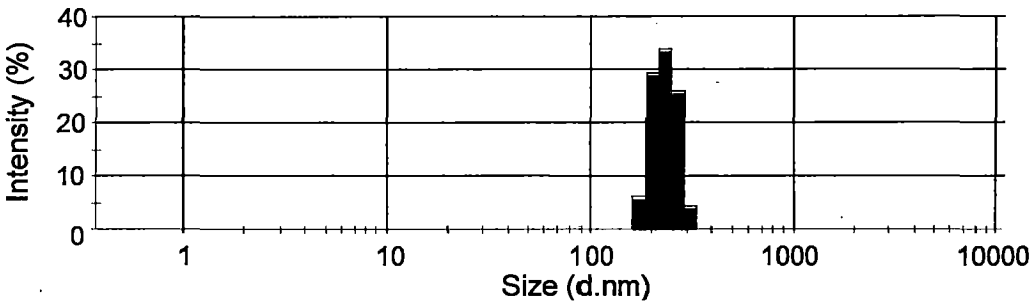

Run No. 13; Peak 1: 221 nm; PDI: 0.086

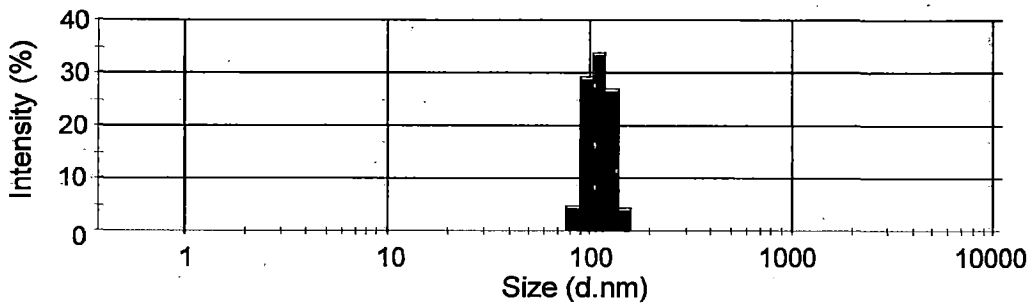

Run No. 17 (Optimization Run with acetone); Peak 1: 115 nm; PDI: 0.089

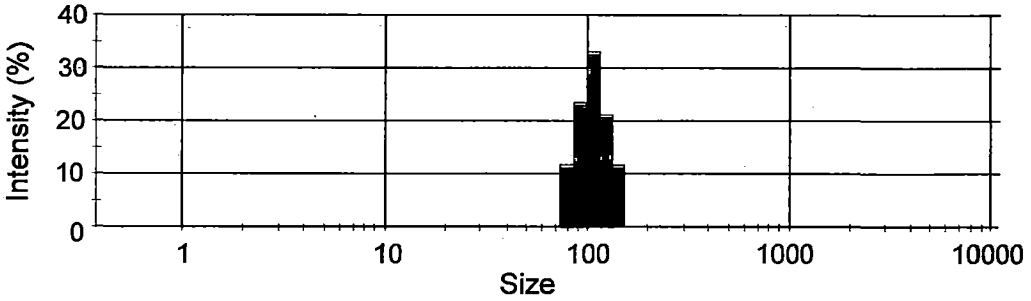

Run No. 18 (Optimization Run with DMSO); Peak 1: 111 nm; PDI: 0.229

Fig. L.1 DLS measurements of PLA NPs

Table L.2 Correlation analysis of the input parameters

	X_1	X_2	X_3	X_4	X_1*X_2	X_1*X_3	X_1*X_4	X_2*X_3	X_2*X_4	X_3*X_4	X_1^2	X_2^2	X_3^2	X_4^2
X_1	1													
X_2	0	1												
X_3	0	0	1											
X_4	0	0	0	1										
X_1*X_2	0.6742	0.6742	-0.24121	0.1206	1									
X_1*X_3	0.3780	-0.30237	0.845154	0	-0.15289	1								
X_1*X_4	0.3780	0.151186	0	0.8451	0.458682	0.028571	1							
X_2*X_3	-0.3024	0.377964	0.845154	0	-0.15289	0.485714	-0.0571	1						
X_2*X_4	0.1512	0.377964	0	0.8451	0.458682	-0.05714	0.8286	0.142857	1					
X_3*X_4	0	0	0.57735	0.5773	-0.06963	0.48795	0.4879	0.48795	0.48795	1				
X_1^2	**0.9844**	0	0	0	0.663665	0.372058	0.3721	-0.29765	0.148823	-0.1017	1			
X_2^2	0	0.984374	0	0	0.663665	-0.29765	0.1488	0.372058	0.372058	0	0	1		
X_3^2	0	0	**1**	0	-0.24121	0.845154	0	0.845154	0	0.5773	0	0	1	
X_4^2	0	0	0	**1**	0.120605	0	0.8452	0	0.845154	0.5773	0	0	0	1

Highly correlated terms are represented in bold letters.

X_1-PLA concentration

X_2-S/NS volume ratio

X_3-PLA MW

X_4-Solvent

ERROR ANALYSIS FOR YIELD

In this Appendix, the experimental error in the computed value of yield, as a result of the errors in the measurement of weight of PLA, has been determined. The instrument used to measure the weight of PLA is a weighing balance of accuracy up to four decimal. The derivation of required relationship for the determination of experimental error is shown below:

If Y is a function of $X_1, X_2 \ldots\ldots X_n$, as given by Eq. M.1, then the error in Y (E_Y) is given by Eq. M.2, where, E_{Xi} = Error in X_i.

$$Y = f(X_1, X_2 \ldots X_n) \qquad \ldots (M.1)$$

$$E_Y = \sqrt{\sum_{i=1}^{n} (E_{X_i} \frac{dY}{dX_i})^2} \qquad \ldots (M.2)$$

The yield of PLA is calculated by using Eq. M.3.

$$\text{Yield}\,(Y) = \frac{\text{wt. of PLA obtained } (X_1)}{\text{wt. of LA taken initially} (X_2)} x100 \qquad \ldots (M.3)$$

$$\text{Yield}\,(Y) = \frac{\text{wt. of PLA obtained } (X_1)}{\text{Volume of LA taken initially} (X_2) x \rho} x100 \qquad \ldots (M.4)$$

Where, ρ is the density of LA and is equal to 1.21 g/cc.

Now employing the definition of error given by Eq. M.2, into Eq. M.4, the expression for error in yield, E_Y, is as follows:

$$E_Y = \sqrt{(E_{X_1} \frac{dY}{dX_1})^2 + (E_{X_2} \frac{dY}{dX_2})^2} \qquad \ldots (M.5)$$

$$E_Y = \sqrt{(E_{X_1} \frac{1}{\rho X_2})^2 + (E_{X_2} \frac{-X_1}{\rho X_2^2})^2} \qquad \ldots (M.6)$$

Where, E_{X_1} =0.0001 g and E_{X_2} =0.1 ml as the least count of the weighing balance is 0.0001 g and least count of pipette equal to 0.1 ml, respectively.

To demonstrate the calculation of error in the value of yield, Run No. 11 of Table J.1 of Appendix J has been selected and is reproduced below:

For the Run No. 11,

Volume of LA (X_2) = 16.5 ml; Wt. of PLA (X_1) = 17.0643 g and Yield= 0.853

Substituting the values of the above quantities in Eq. M.6, the value of error in yield (E_Y) is calculated to be 0.00607.

The % error in the measurement of average yield is

% E_Y = (Error/Experimental yield)x100 =(0.00607/0.853)*100

=0.711%

LIST OF PAPERS PUBLISHED AND COMMUNICATED

1. **Maharana T.**, Mohanty B., Negi Y.S.; Melt-Solid Polycondensation of Lactic Acid and Its Biodegradability; Progress in Polymer Science (2009), 34(1), 99-124.

2. **Maharana T.**, Negi Y. S., Mohanty B.; Review Article: Recycling of Polystyrene; Polymer-Plastics Technology and Engineering (2007), 46(7), 729-736.

3. **Maharana T.**, Mohanty B., Negi Y.S.; Response Surface Methodology and Modeling for Synthesis of Polylactic Acid by Melt Polycondensation; Polymer- Plastics Technology and Engineering (Submitted 2009).

4. **Maharana T.**, Mohanty B., Negi Y.S.; Preparation of polylactic acid nanoparticles and optimization of particle size; Polymer Bulletin (Submitted 2010).

5. **Maharana T.**, Mohanty B., Negi Y.S.; Application of statistical experimental methods to optimize production of Poly(Lactic Acid) by Solid State Polycondensation; Industrial Engineering & Chemistry Research (Submitted 2010).

International Conferences:

1. **Maharana T.**, Mohanty B., Ray A.K. Negi Y.S.; Physico-Thermal and Temperature Dependent Computational Thermal Kinetic Studies of Poly(Lactic Acid); ICAPP 2007 – The 2nd International Conference on Advances in Petrochemicals and Polymers June 25th – 28th, 2007, Bangkok, Thailand.

2. **Maharana T.**, Mohanty B., Negi Y.S.; Synthesis of poly(lactic acid) by melt polycondensation and their characterizations; "Asian Polymer Association International Conference POLY-08" January 28th – 31st, 2008, IIT Delhi, India.

3. **Maharana T.**, Mohanty B., Negi Y.S.; Application of Response Surface Methodology to Optimize Production of Polylactic Acid by Melt Polycondensation; "Polymer Science & Technology: Vision & Scenario (APA-2009)" at New Delhi, India on December 17-20, 2009.

4. **Maharana T.**, Mohanty B., Negi Y.S.; Preparation of Polylactic acid nanoparticles by nanoprecipitation method; "Polymer Science & Technology: Vision & Scenario (APA-2009)" at New Delhi, India on December 17-20, 2009.

5. **Maharana T.**, Mohanty B., Negi Y.S.; A novel method for the synthesis of high molecular weight polylactic acid by melt-solid polycondensation under vacuum; International Conference on "Advancements in Polymeric Materials; APM-2010, Trends & Technology" at CIPET Bhubaneswar on February 20-22, 2010.

REFERENCES

1. Achmad F, Yamane K, Quan S, Kokugan T. Synthesis of polylactic acid by direct polycondensation under vacuum without catalysts, solvents and initiators. Chem Eng J 2009;151:342–350.

2. Ahmed J, Zhang JX, Song Z, Varshney SK. Thermal properties of polylactides- effect of molecular mass and nature of lactide isomer. J Therm Anal Calorim 2009;95:957–964.

3. Ajioka M, Enomoto K, Suzuki K, Yamaguchi A. The basic properties of poly(lactic acid) produced by the direct condensation polymerization of lactic acid. J Environ Polym Degrad 1995;3:225-234.

4. Ajioka M, Enomoto K, Suzuki K, Yamaguchi A. Basic properties of polylactic acid produced by the direct condensation of lactic acid. Bull Chem Soc Jpn 1995;68:2125-2131.

5. Akutsu F, Inoki M, Uei H, Sueyoshi M, Kasahima Y, Naruchi K, Yamaguchi Y, Sunahara M. Synthesis of poly(lactic acid) by direct polycondensation of lactic acid using 1,1'-carbonyldiimidazole, N,N,N',N'-tetramethylchloroformamidinium chloride, and N,N'-dicyclohexylcarbodiimide as condensing agents. Polym J (Tokyo) 1998;30:421-423.

6. Alariqi SAS, Kumar AP, Rao BSM, Singh RP. Effect of γ-dose rate on crystallinity and morphological changes of γ-sterilized biomedical polypropylene. Polym Degrad Stab 2009; 94:272–277.

7. Albertsson AC, Varma IK. Recent developments in ring opening polymerization of lactones for biomedical applications. Biomacromolecules 2003;4:1466-1486.

8. Anderson MJ, Whitcomb PJ. Optimize your process-optimization efforts. Chem Eng Prog 1996;92:51-60.

9. Ando A, Kimura K, Onda Y, Yamashita Y. New attempt at the stereoselective polymerization of lactide by using crystallization during polymerization. Macromol Rapid Commun 2005;26:98-102.

10. Angellier H, Choisnard L, Molina-Boisseau S, Ozil P, Dufresne A. Optimization of the preparation of aqueous suspensions of waxy maize starch nanocrystals using a response surface methodology. Biomacromolecules 2004;5:1545-1551.

11. Antony J, Perry D, Wang C, Kumar M. An application of Taguchi method of experimental design for new product design and development process. Assembly Autom 2006;26:18-24.

12. Bajaj IB, Lele SS, Singhal RS. A statistical approach to optimization of fermentative production of poly(γ-glutamic acid) from Bacillus licheniformis NCIM 2324. Bioresource Technol 2009;100:826–832.

13. Barantian S, Hall ES, Lin JS, Xu R, Runt J. Crystallization and solid-state structure of random polylactide copolymers: poly(L-lactide-co-D-lactide)s. Macromolecules 2001;34:4857-64.

14. Barichello JM, Morishita M, Takayama K, Nagai T. Encapsulation of hydrophilic and lipophilic drugs in PLGA nanoparticles by the nanoprecipitation method. Drug Dev Ind Pharm 1999;25:471-476.

15. Bendix D. Chemical synthesis of polylactide and its copolymers for medical applications. Polym Degrad Stab 1998;59:129-135.

16. Bergsma JE, Rozema FR, Bos RRM, de Bruijn WC, Boering G. Poly(L-lactic acid) implants in repair of defects of the orbital floor: A five-year animal study. Cells Mater 1994;4:31-36.

17. Berkland C, Kim KK, Pack DW. Fabrication of PLG microspheres with precisely controlled and monodisperse size distributions. J Control Release 2001;73:59-74.

18. Bero M, Kasperezyk J, Jedlinski ZJ. Coordination polymerization of lactides, 1. Structure determination of obtained polymers. Makromol Chem 1990;191:2287-2296.

19. Bilati U, Allémann E, Doelker E. Development of a nanoprecipitation method intended for the entrapment of hydrophilic drugs into nanoparticles. Eur J Pharm Sci 2005;24: 67-75.

20. Birkinshaw C, Buggy M, Henn GG, Jones E. Irradiation of poly-D,L-lactide. Polym Degrad Stab 1992;38:249-53.

21. Bishara A, Domb A J. PLA stereocomplexes for controlled release of somatostatin analogue. J Control Release 2005;107:474-483.

22. Boaler VJ. Electron beam processing. In: Clegg DW, Collyer AA, Editors, Irradiation effects on polymers, London: Elsevier. 1991. Chapter 7.

23. Bodmeier R, Oh KH, Chen H. The effect of the addition of low molecular weight poly(D,L-lactide) on drug release from biodegradable poly(D,L-lactide) drug delivery systems. Int J Pharm 1989;51:1-8.

24. Braun B, Dorgan JR, Dec SF. Infrared spectroscopic determination of lactide concentration in polylactide: an improved methodology. Macromolecules 2006;39:9302-9310.

25. Brizzolara D, Cantow HJ, Diederichs K, Keller E, Domb AJ. Mechanism of the stereocomplex formation between enantiomeric Poly(lactide)s. Macromolecules 1996;29:191-197.

26. Buchholz B. Analysis and characterization of resorbable DL-lactide-trimethylene carbonate copolyesters. J Mater Sci: Mater Med 1993;4:381-8.

27. Buchholz B. Preparation of polyesters from hydroxyalkanoic acids. DE 4005415 A1 19910822;1991.

28. Cam D, Hyon SH, Ikada Y. Degradation of high molecular weight poly(L-lactide) in alkaline medium. Biomaterials 1995;16:833-843.

29. Carothers W, Dorough G, Van Natta F. Studies on polymerisation and ring formation. X. The reversible polymerisation of six-membered cyclic esters. J Am Chem Soc 1932;54:761-772.

30. Cattelan AM, Bauer U, Trevenzoli M, Sasset L, Campostrini S, Facchin C, Pagiaro E, Gerzeli S, Cadrobbi P, Chiarelli A. Use of polylactic acid implants to correct facial lipoatrophy in human immunodeficiency virus 1–positive individuals receiving combination antiretroviral therapy. Arch Dermatol 2006;142:329–334.

31. Celli A, Scandolat M. Thermal properties and physical ageing of poly(L-lactic acid). Polymer 1992;33:2699-2703.

32. Chabot F, Vert M, Chapelle S, Granger P. Configurational structures of lactic acid stereocopolymers as determined by 13C-{1H}NMR. Polymer 1983;24:53-59.

33. Chamberlain BM, Jazdzewski BA, Pink M, Hillmeyer MA, Tolman WB. Controlled polymerization of DL-lactide and ε-caprolactone by structurally well-defined alkoxo-bridged di- and triyttrium(III) complexes. Macromolecules 2000;33:3970-3977.

34. Chen FC, Griskey RG, Beyer GH. Thermally induced solid state polycondensation of nylon 66, nylon 6-10 and polyethylene terephthalate. AIChE J 1969;15:680-685.

35. Chen GX, Kim HS, Kim ES, Yoon JS. Synthesis of high-molecular-weight poly(L-lactic acid) through the direct condensation polymerization of L-lactic acid in bulk state. Eur Polym J 2006;42:468-472.

36. Chen HY, Huang BH, Lin CC. A highly efficient initiator for the ring-opening polymerization of lactides and ε-caprolactone: a kinetic study. Macromolecules 2005; 38:5400-5405.

37. Chen X, Zhang Y, Pickrell G, Antony J. Experimental design in fiber optic sensor development. Int J Prod Perform Meas 2004;53:713-725.

38. Cheng J, Teply BA, Sherifi I, Sung J, Luther G, Gu FX, Levy-Nissenbaum E, Radovic-Moreno AF, Langer R, Farokhzad OC. Formulation of functionalized PLGA-PEG nanoparticles for in vivo targeted drug delivery. Biomaterials 2007;28:869-876.

39. Chisholm MH, Gallucci JC, Quisenberry KT, Zhou Z. Complexities in the ring-opening polymerization of lactide by chiral salen aluminum initiators. Inorg Chem 2008; 48:2613-2624.

40. Choi SW, Kwon HY, Kim WS, Kim JH. Thermodynamic parameters on poly(d,l-lactide-co-glycolide) particle size in emulsification–diffusion process. Colloids Surf 2002; A 201:283-289.

41. Chorny M, Fishbein I, Danenberg HD, Golomb G. Study of the drug release mechanism from tyrphostin AG-1295-loaded nanospheres by in situ and external sink methods. J Control Release 2002;83:389-400.

42. Chu CC. Degradation phenomena of two linear aliphatic polyester fibers used in medicine and surgery. Polymer 1985;26:591-594.

43. Cochran WG, Cox GM. Experimental designs, 2nd ed. Wiley-Interscience, 1992 (chapter 8 A).

44. Cohn D, Younes H, Marom G. Amorphous and crystalline morphologies in glycolic acid and lactic acid polymers. Polymer 1987;28:2018-2022.

45. Collins EA, Bares J, Billmeyer EW. Experiments in polymer science. Wiley Interscience, Chichester. 1973.

46. Contado C, Dalpiaz A, Leo E, Zborowski M, Williams P S. Complementary use of flow and sedimentation field-flow fractionation techniques for size characterizing biodegradable poly(lactic acid) nanospheres. J Chromatogr A 2007;1157:321-335.

47. Cooper A I. Polymer synthesis and processing using supercritical carbon dioxide. J Mater Chem 2000;10:207-234.

48. D'Alelio GF, Haberli R, Pezdirtz GF. Effect of ionizing radiation on a series of saturated polyesters. J Macromol Sci Chem 1968;2:501-588.

49. de Jong SJ, van Dijk-Wolthuis WNE, Kettenes-van den Bosch JJ, Schuyl PJW, Hennink WE. Monodisperse enantiomeric lactic acid oligomers preparation, characterization and stereocomplex formation. Macromolecules 1998;31:6397-6402.

50. Drumright RE, Gruber PR, Henton DE. Polylactic acid technology. Adv Mater 2000;12:1841-1846.

51. Dubois P, Jacobs C, Jerome R, Teyssie P. Macromolecular engineering of polylactones and polylactides. 4. Mechanism and kinetics of lactide homopolymerization by aluminum isopropoxide. Macromolecules 1991;24:2266-2270.

52. Duclairoir C, Nakache E, Marchais H, Orecchioni AM. Formation of gliadin nanoparticles: influence of the solubility parameter of the protein solvent. Colloid Polym Sci 1998;276:321-327.

53. Duh B. Effect of antimony catalyst on solid-state polycondensation of poly(ethylene terephthalate). Polymer 2002;43:3147-3154.

54. Dutkiewicz S, Lapienis DG, Tomaszewski W. Synthesis of poly(L(+) lactic acid) by polycondensation method in solution. Fibres Text East Eur 2003;11:66-70.

55. Eguiburu JL, Berridi MJF, Roman JS. Functionalization of poly(L-lactide) macromonomers by ring-opening polymerization of L-lactide initiated with hydroxyethyl methacrylate-aluminium alkoxides. Polymer 1995;36:173-179.

56. Engelberg I, Kohn J. Physico-mechanical properties of degradable polymers used in medical applications: a comparative study. Biomaterials 1991;12:292-304.

57. Enomoto K, Ajioka M, Yamaguchi A. Polyhydroxycarboxylic acid and preparation process thereof. US5310865, 1994.

58. Fambri L, Pegoretti A, Fenner R, Incardona SD, Migliaresi C. Biodegradable fibers of poly(L-lactic acid) produced by melt spinning. Polymer 1997;38:79-85.

59. Fessi H, Puisieux F, Devissaguet JP, Ammoury N, Benita S. Nanocapsule formation by interfacial polymer deposition following solvent displacement. Int J Pharm 1989;55:R1-R4.

60. Fessi HC, Devissaguet JP, Puisieux F, Thies C. Process for the preparation of dispersible colloidal systems of a substance in the form of nanoparticles. US005118528A, 1992.

61. Fortunato B, Pilati F, Manaresi P. Solid state polycondensation of poly(butylene terephthalate). Polymer 1981;22:655-657.

62. Freitas S, Merkle H P, Gander B. Microencapsulation by solvent extraction/evaporation: reviewing the state of the art of microsphere preparation process technology. J Control Release 2005;102:313-332.

63. Fukushima K, Furuhashi Y, Sogo K, Miura S, Kimura Y. Stereoblock poly(lactic acid): synthesis via solid-state polycondensation of a stereocomplexed mixture of poly(L-lactic acid) and poly(D-lactic acid). Macromol Biosci 2005;5:21-29.

64. Fukushima K, Kimura Y. An efficient solid-state polycondensation method for synthesizing stereocomplexed poly(lactic acid)s with high molecular weight. J Polym Sci Part A: Polym Chem 2008;46:3714-3722.

65. Fukushima T, Sumihiro Y, Koyanagi K, Hashimoto N, Kimura Y. Manufacture of high molecular-weight poly(lactic acid) using the diphenyl ether solid solution. JP 2000212425 A2, 2000.

66. Galindo-Rodriguez SA, Puel F, Briancon S, Allémann E, Doelker E, Fessi H. Comparative scale-up of three methods for producing ibuprofen-loaded nanoparticles. Eur J Pharm Sci 2005;25:357-367.

67. Garlotta D. A literature review of poly(lactic acid). J Polym Environ 2001;9:63-84.

68. Gilding DK, Reed AM. Biodegradable polymers for use in surgery-polyglycolic/poly(lactic acid) homo- and copolymers: 1. Polymer 1979;20:1459-64.

69. Gorner T, Gref R, Michenot D, Sommer F, Tran MN, Dellacherie E. Lidocaine-loaded biodegradable nanospheres. I. Optimization of the drug incorporation into the polymer matrix. J Control Release 1999;57:259–268.

70. Govender T, Stolnik S, Garnett MC, Illum L, Davis SS. PLGA nanoparticles prepared by nanoprecipitation: drug loading and release studies of a water soluble drug. J Control Release 1999;57:171-185.

71. Gregson CKA, Blackmore IJ, Gibson VC, Long NJ, Marshall EL, White AJP. Titanium-salen complexes as initiators for the ring opening polymerisation of rac-lactide. Dalton Trans 2006:3134-3140.

72. Grijpma DW, Joziasse CAP, Pennings AJ. Star-shaped polylactide-containing block copolymers. Makromol Chem Rapid Commun 1993;14:155-161.

73. Grijpma DW, Pennings AJ. Copolymers of L-lactide.2. Mechanical properties. Macromol Chem Phys 1994;195:1649-1663.

74. Grijpma DW, Zondervan GJ, Pennings AJ. High molecular weight copolymers of L-lactide and ε-caprolactone as biodegradable elastomeric implant materials. Polym Bull 1991;25:327-333.

75. Grizzi I, Garreau H, Li S, Vert M. Hydrolytic degradation of devices based on poly(DL-lactic acid) size-dependence. Biomaterials 1995;16:305-311.

76. Gujarati D. Essentials of econometrics. 2nd Ed. 1999, McGraw-Hill International Editions.

77. Gupta B, Revagade N, Hilborn J. Poly(lactic acid) fiber: an overview. Prog Polym Sci 2007;32:455-482.

78. Gupta B, Revagade N, Anjum N, Atthoff B, Hilborn J. Preparation of Poly(lactic acid) fiber by dry-jet-wet spinning. II. Effect of process parameters on fiber properties. J Appl Polym Sci 2006;101:3774-3780.

79. Gupta MC, Deshmukh VG. Radiation effects on poly(lactic acid). Polymer 1983;24:827-830.

80. Hakkarainen M, Albertsson AC, Karlsson S. Weight losses and molecular weight changes correlated with the evolution of hydroxyl acids in simulated in vivo degradation of homo and copolymers of PLA and PGA. Polym Degrad Stab 1996;52:283-291.

81. Hans ML, Lowman AM. Biodegradable nanoparticles for drug delivery and targeting. Curr Opin Solid St Mater Sci 2002;6:319-327.

82. Hatada K, Ute K, Kashiyama M, Imanari M. Direct determination of molecular weight and its distribution by the absolute calibration method using the on-line GPC/NMR. Polym J 1990;22:218-222.

83. Hiltunen K, Seppala JV, Harkonen M. Lactic acid based poly(ester-urethanes): use of hydroxyl terminated prepolymer in urethane synthesis. J Appl Polym Sci 1997;63:1091-1100.

84. Hiltunen K, Seppala JV, Harkonen M. Effect of catalyst and polymerization conditions on the preparation of low molecular weight lactic acid polymers. Macromolecules 1997;30:373-379.

85. Hirsjärvi S, Peltonen L, Hirvonen J. Surface pressure measurements in particle interaction and stability studies of poly(lactic acid) nanoparticles. Int J Pharm 2008;348:153-160.

86. Horacek I, Kudlacek L. Influence of molecular weight on the resistance of polylactide fibres by radiation stabilization. J Appl Polym Sci 1993;50:1-5.

87. Huang J, Lisowski MS, Runt J, Hall ES, Kean RT, Buehler N, Lin JS. Crystallization and microstructure of poly(L-lactide-co-meso-lactide) copolymers. Macromolecules 1998;31:2593-2599.

88. Hung WC, Huang Y, Lin CC. Efficient initiators for the ring-opening polymerization of l-lactide: synthesis and characterization of NNO-tridentate schiff-base zinc complexes. J Polym Sci: Part A: Polym Chem 2008;46:6466-6476.

89. Hyon SH, Jamshidi K, Ikada Y. Synthesis of polylactides with different molecular weights. Biomaterials 1997;18:1503-1508.

90. Ikada Y, Jamshidi K, Tsuji H, Hyon SH. Stereocomplex formation between enantiomeric poly(lactides). Macromolecules 1987;20:904-906.

91. Ikada Y, Tsuji H. Biodegradable polyesters for medical and ecological applications. Macromol Rapid Commun 2000;21:117-132.

92. Ikura Y, Kudo T. Isolation of a microorganism capable of degrading poly-(L-lactide). J Gen Appl Microbiol 1999;45:247-251.

93. Jacobsen S, Fritz HG, Degee P, Dubois P, Jerome R. Single-step reactive extrusion of PLLA in a corotating twin-screw extruder promoted by 2-ethylhexanoic acid tin(II) salt and triphenylphosphine. Polymer 2000;41:3395-3403.

94. Jacobsen S, Degée P, Fritz HG, Dubois P, Jérome R. Polylactide (PLA)- A new way of production. Polym Eng Sci 1999;39:1311-1319.

95. Jahanshahi M, Sanati MH, Hajizadeh S, Babaei Z. Gelatin nanoparticle fabrication and optimization of the particle size. Phys Status Solidi A 2008;205:2898-2902.

96. Jain RA. The manufacturing techniques of various drug loaded biodegradable poly(lactide-co-glycolide) (PLGA) devices. Biomaterials 2000;21:2475-2490.

97. Jamshidi K, Hyon SH, Ikada Y. Thermal characterization of polylactides. Polymer 1988;29:2229-2234.

98. Jeon HJ, Jeong YI, Jang MK, Park YH, Nah JW. Effect of solvent on the preparation of surfactant-free poly(dl-lactide-co-glycolide) nanoparticles and norfloxacin release characteristics. Int J Pharm 2000;207:99-108.

99. Jie R, Zhang N, Wang Q. Method for preparing high molecular weight polylactic acid via solid-phase polymerization. CN1718607 A, 2006.

100. Joziasse CAP, Grablowitz H, Pennings AJ. Star-shaped poly[(trimethyllene carbonate)-co-(ε-caprolactone)] and its copolymers with lactide/glycolide; synthesis, characterization and properties. Macromol Chem Phys 2000;201:107-112.

101. Joziasse CAP, Topp MDC, Veenstra H, Grijpma DW, Pennings AJ. Super tough poly(lactide)s. Polym Bull 1994;33:599-605.

102. Joziasse CAP, Veenstra H, Topp MDC, Grijpma DW, Pennings AJ. Rubber toughened linear and star-shaped poly(D,L-lactide-co-glycolide); synthesis, properties and in vitro degradation. Polymer 1998;39:467-473.

103. Karlsson A, Albertsson AC. New selective method for quantification of organosilanol groups in silicone pre-elastomers. Biomacromolecules 2002;3:850-856.

104. Keki S, Bodnar I, Borda J, Deak G, Zsuga M. Melt polycondensation of D,L-lactic acid: MALDI-TOF MS investigation of the ring-chain equilibrium. J Phys Chem B 2001;105:2833-2836.

105. Kier LB, Hall LH. Molecular connectivity in chemistry and drug research. New York: Academic Press; 1976.

106. Kier LB, Hall LH. Molecular connectivity in structure–activity analysis. New York: Wiley; 1986.

107. Kim KW, Woo SI. Synthesis of high-molecular-weight poly(L-lactic acid) by direct polycondensation. Macromol Chem Phys 2002;203:2245-2250.

108. Kim SH, Kim YH. Direct condensation polymerization of lactic acid. Macromol Symp 1999;144:277-287.

109. Kimura Y, Fukushima K, Miura S, Kara O, Sogo K, Toyohara K. A method of producing polylactic acid block copolymer having high molecular weight and melting point. JP 2006028336 A2, 2006.

110. Knott PD, Newman J, Keller GS, Apfelberg DB. A novel bio-absorbable device for facial suspension and rejuvenation. Arch Facial Plast Surg 2009;11:129-135.

111. Kolstad JJ. Crystallization kinetics of poly(L-lactide-co-meso-lactide). J Appl Polym Sci 1996;62:1079-1091.

112. Kowalski A, Duda A, Penczek S. Kinetics and mechanism of cyclic esters polymerization initiated with tin(II) octoate. 3. polymerization of L,L-dilactide. Macromolecules 2000;33:7359-7370.

113. Kricheldorf HR, Lee SR. Polylactones: 32. High-molecular-weight polylactides by ring-opening polymerization with dibutylmagnesium or butylmagnesium chloride. Polymer 1995;36:2995-3003.

114. Kricheldorf HR, Serra A. Polylactones 6. Influence of various metal salts on the optical purity of poly(L-lactide). Polym Bull 1985;14:497-502.

115. Kricheldorf HR, Kreiser-Saunders I, Boettcher C. Polylactones 31. Sn(II)octoate-initiated polymerisation of lactide: a mechanistic study. Polymer 1995;36:1253-1259.

116. Kricheldorf HR, Kreiser-Saunders I, Stricker A. Polylactones 48. $SnOct_2$-initiated polymerisations of lactide: A mechanistic study. Macromolecules 2000;33:702-709.

117. Labrecque LV, Kumar RA, Dave V, Gross RA, McCarthy SP. Citrate esters as plasticizers for poly(lactic acid). J Appl Polym Sci 1997;66:1507-1513.

118. Lamprecht A, Ubrich N, Yamamoto H, Schäfer U, Takeuchi H, Lehr CM, Maincent P, Kawashima Y. Design of rolipram-loaded nanoparticles: comparison of two preparation methods. J Control Release 2001;71:297-306.

119. Lassalle V, Ferreira M L. PLA nano- and microparticles for drug delivery: an overview of the methods of preparation. Macromol Biosci 2007;7:767-783.

120. Lee MW, Tan HT, Chandrasekaran M, Ooi CP. Synthesis and characterization of PLLA by melt polycondensation using binary catalyst system. SIMTech Technical Reports 2005;6(3):40-44.

121. Legrand P, Lesieur S, Bochot A, Gref R, Raatjes W, Barratt G, Vauthier C. Influence of polymer behaviour in organic solution on the production of polylactide nanoparticles by nanoprecipitation. Int J Pharm 2007;344:33-43.

122. Leo E, Brina B, Forni F, Vandelli MA. In vitro evaluation of PLA nanoparticles containing a lipophilic drug in water-soluble or insoluble form. Int J Pharm 2004;278:133-141.

123. Li SM, Garreau H, Vert M. Structure-property relationships in the case of the degradation of massive aliphatic poly-(α-hydroxy acids) in aqueous media, Part 1, Poly(D,L-lactic acid). J Mater Sci: Mater Med 1990;1:123-130.

124. Li LF, Huang NX, Tang ZL, Hagen, R. Reaction kinetics and simulation for the solid-state polycondensation of nylon 6. Macromol Theory Simul 2001;10:507-517.

125. Luciano RM, Zavaglia CAC, Duek EAR, Alberto-Rincon MC. Synthesis and characterization of poly(L-lactic acid) membranes: Studies in vivo and in vitro. J Mater Sci: Mater Med 2003;14:87-94.

126. Luft G, Henning W, Dorn M. High-pressure polymerization of ethylene using methyl isobutyl ketone peroxide as initiator. Angew Makromol Chem 1986;141:207-218.

127. Lunt J. Large-scale production, properties and commercial applications of polylactic acid polymers. Polym Degrad Stab 1998;59:145-152.

128. Maharana T, Mohanty B, Negi YS. Melt-solid polycondensation of lactic acid and its biodegradability. Prog Polym Sci 2009;34:99-124.

129. Martin O, Averous L. Poly(lactic acid): plasticization and properties of biodegradable multiphase systems. Polymer 2001;42:6209-6219.

130. McCleverty JA and Meyer TJ. Comprehensive coordination Chemistry II: From Biology to nanotechnology. Vol 9; 2005.

131. Mehta R, Kumar V, Bhunia H, Upadhyay SN. Synthesis of poly(lactic acid): a review. J Macromol Sci Part C: Polym Rev 2005; 45:325-349.

132. Mehta RC, Thanoo BC, Deluca PP. Peptide containing microspheres from low molecular weight and hydrophilic poly(D,L-lactide-co-glycolide). J Control Release 1996;41:249-257.

133. Migliaresi C, Cohn D, De Lollis A, Fambri L. Dynamic mechanical and calorimetric analysis of compression-molded PLLA of different molecular weights; effect of thermal treatments. J Appl Polym Sci 1991;43:83-95.

134. Migliaresi C, De Lollis A, Fambri L, Cohn D. The effect of thermal history on the crystallinity of different molecular weight PLLA biodegradable polymers. Clin Mater 1991;8:111-118.

135. Miyata T, Masuko T. Crystallization behavior of poly(L-lactide). Polymer 1998;39: 5515-5521.

136. Miyoshi R, Hashimoto N, Koyanagi K, Sumihiro Y, Sakai T. Biodegradable poly(lactic acid) with high molecular weight: preparation by continuous melt polycondensation process combined with reactive processing technology. Int Polym Process 1996;11:320-328.

137. Mochizuki M, Hirami M. Structural effects on the biodegradation of aliphatic polyesters. Polym Adv Technol 1997;8:203-209.

138. Mohanty AK, Misra M, Hinrichsen G. Biofibers, biodegradable polymers and biocomposites—an overview. Macromol Mater Eng 2000;276/277:1-24.

139. Molceperes J, Guzman M, Arberturas MR, Chacon M, Berges L. Application of central composite designs to the preparation of polycaprolactone nanoparticles by solvent displacement. J Pharm Sci 1996;85:206-213.

140. Montgomery DC. Design and Analysis of experiments, 5th ed. Wiley-Interscience, 2004 (Chapter 11).

141. Moon SI, Lee CW, Miyamoto M, Kimura Y. Melt polycondensation of l-lactic acid with sn(ii) catalysts activated by various proton acids: a direct manufacturing route to high molecular weight poly(l-lactic acid). J Polym Sci: Part A: Polym Chem 2000;38:1673-1679.

142. Moon SI, Lee C W, Taniguchi I, Miyamoto M, Kimura Y. Melt/solid polycondensation of L-lactic acid: an alternative route to poly(L-lactic acid) with high molecular weight. Polymer 2001;42:5059-5062.

143. Moon SI, Taniguchi I, Miyamoto M, Kimura Y, Lee CW. Synthesis and properties of high molecular weight poly(L-lactic acid) by melt/solid polycondensation under different reaction conditions. High Perform Polym 2001;13:189-196.

144. Moon SI, Kimura Y; Melt polycondensation of L-lactic acid to poly(L-lactic acid) with Sn(II) catalysts combined with various metal alkoxides. Polym Int 2003;52:299-303.

145. Munguia O, Delgado A, Farina J, Evora C, Llabres M. Optimization of dl-PLA molecular weight via the response surface method. Int J Pharm 1992;86:107-111.

146. Murakami H, Kobayashi M, Takeuchi H, Kawashima Y. Further application of a modified spontaneous emulsification solvent diffusion method to various types of PLGA and PLA polymers for preparation of nanoparticles. Powder Technol 2000;107:137-143.

147. Nagasawa N, Kaneda A, Kanazawa S, Yagi T, Mitomo H, Yoshii F, Tamada M. Application of poly(lactic acid) modified by radiation crosslinking. Nucl Instrum Methods Phys Res Sect B 2005;236:611-616.

148. Nakagawa T, Nakiri T, Hosoya R, Tajitsu Y. Electrical properties of biodegradable polylactic acid film. IEEE Trans Ind Appl 2004;40:1020-1024.

149. Nijenhuis AJ, Grijpma DW, Pennings AJ. Crosslinked poly(L-lactide) and poly(ε-caprolactone). Polymer 1996;37:2783-2791.

150. Nijenhuis AJ, Grijpma DW, Pennings AJ. Lewis acid catalyzed polymerization of L-lactide, kinetics and mechanism of the bulk polymerization. Macromolecules 1992;25:6419-6424.

151. Niwa T, Takeuchi T, Hino T, Kunou N, Kawashima Y. Preparations of biodegradable nanospheres of water-soluble and insoluble drugs with d,l-lactide/glycolide copolymer by a novel spontaneous emulsification solvent diffusion method, and the drug release behavior. J Control Release 1993;25:89-98.

152. Nugroho P, Mitomo H, Yoshii F, Kume T. Degradation of poly(L-lactic acid) by γ-irradiation. Polym Degrad Stab 2001;72:337-343.

153. O'Keefe BJ, Hillmyer MA, Tolman WB. Polymerization of lactide and related cyclic esters by discrete metal complexes. J Chem Soc Dalton Trans 2001:2215-2224.

154. Obara H, Sawa S, Ito M. Solid-state polymerization in manufacture of high-molecular-weight poly(lactic acid). JP 08151436 A2, 1996.

155. Okada K, Iijima M, Shimamatsu M, Sato N, Nagata T. Manufacture of colorless transparent biodegradable aliphatic polyesters. JP 2000273165 A2, 2000.

156. Otera J, Kawada K, Yano T. Direct condensation polymerization of L-lactic acid catalyzed by distannoxane. Chem Lett 1996;25:225-226.

157. Pan X, Chi Z, Cheng D, Jin M, Bu H. Solid-state polymerization of a liquid crystalline copolyester derived from 2,6-naphthalene dicarboxylic acid, terephthalic acid, 4-acetoxybenzoic acid and hydroquinone diacetate. J Macromol Sci, Part B: Phys 2005;44:249-259.

158. Panyam J, Labhasetwar V. Biodegradable nanoparticles for drug and gene delivery to cells and tissue. Adv Drug Deliv Rev 2003;55:329-347.

159. Peltonen L, Aitta J, Hyvönen S, Karjalainen M, Hirvonen J. Improved entrapment efficiency of hydrophilic drug substance during nanoprecipitation of poly(L)lactide nanoparticles. AAPS Pharm Sci Tech 5: article 16(2004).

160. Peltonen L, Koistinen P, Hirvonen J. Preparation of nanoparticles by nanoprecipitation of low molecular weight poly(l)lactide. STP Pharma Sci 2003;5:299-304.

161. Peng W, Jing S, Liuyi T. Preparation of polylactic acid by melt polycondensation with microwave radiation. CN1594394 A, 2005.

162. Perego G, Cella GD, Bastioli C. Effect of molecular weight and crystallinity on poly(lactic acid) mechanical properties. J Appl Polym Sci 1996;59:37-43.

163. Perego G, Albizzati E. Process for the synthesis of lactic acid polymers in the solid state and products thus obtained; US005359027 A, 1994.

164. Pranamuda H, Tokiwa Y. Degradation of poly(L-lactide) by strains belonging to genus Amycolatopsis. Biotech Lett 1999;21:901-905.

165. Proikakis CS, Mamouzelos NJ, Tarantili PA, Andreopoulos AG. Swelling and hydrolytic degradation of poly(D,L-lactic acid) in aqueous solutions. Polym Degrad Stab 2006;91:614-619.

166. Proikakis CS, Tarantili PA, Andreopoulos AG. Synthesis and characterization of low molecular weight polylactic acid. J Elastomers Plastics 2002;34:49-63.

167. Qian G, Zhou X-G, Zhu L-B, Yuan W-K. Increasing the molecular weight of poly(L-lactic acid) by solid state polycondensation in a closed system. J Polym Eng 2003;23: 413-422.

168. Qu X, Wirsen A, Albertsson AC. Structural change and swelling mechanism of pH-sensitive hydrogels based on chitosan and D,L-lactic acid. J Appl Polym Sci 1999;74:3186-192.

169. Quintanar-Guerrero D, Allémann E, Fessi H, Doelker E. Preparation techniques and mechanisms of formation of biodegradable nanoparticles from preformed polymers. Drug Dev Ind Pharm 1998;24:1113-1128.

170. Radano CP, Baker GL, Smith MR. Stereoselective polymerization of a racemic monomer with a racemic catalyst: direct preparation of the polylactic acid stereocomplex from racemic lactide. J Am Chem Soc 2000;122:1552-1553.

171. Reich L, Stivala SS. Elements of Polymer Degradation. McGraw Hill: New York. 1971.

171'. Ren J, Zhang N, Wang Q. Method for preparing high molecular weight polylactic acid via solid-phase polymerization. CN1718607 A, 2006.

172. Reverchon E, Antonacci A. Polymer microparticles production by supercritical assisted atomization. J Supercrit Fluids 2007;39:444-452.

173. Roy R, Hinduja S, Teti R. Recent advances in engineering design optimisation: Challenges and future trends. CIRP Ann 2008;57:697-715.

174. Saha SK, Tsuji H. Effects of molecular weight and small amounts of D-lactide units on hydrolytic degradation of poly(L-lactic acid)s. Polym Degrad Stab 2006;91:1665-1673.

175. Sailynoja E, Koskinen M, Salonen J, Holmlund P, Sodergard A, Koskinen M. Immobilization of a biologically active coating on a hydrophobic L-lactide-ε-caprolactone copolymer. J Mater Sci: Mat Med 1999;10:703-705.

176. Sarasua JR, Prud'homme RE, Wisniewski M, Le Borgne A, Spassky N. Crystallization and melting behaviour of polylactides. Macromolecules 1998;31:3895-3905.

177. Seo KS, Cloyd JD. Kinetics of hydrolysis and thermal degradation of polyester melts. J Appl Polym Sci 1991;42:845-850.

178. Shih IL, Van YT, Chang YN. Application of statistical experimental methods to optimize production of poly(γ-glutamic acid) by Bacillus licheniformis CCRC 12826. Enzyme Microb Technol 2002;31:213-220.

179. Shinno K, Miyamoto M, Kimura Y, Hirai Y, Yoshitome H. Solid-state postpolymerization of L-lactide promoted by crystallization of product polymer: an effective method for reduction of remaining monomer. Macromolecules 1997;30:6438-6444.

180. Shyamroy S, Garnaik B, Sivaram S. Structure of poly(l-lactic acid)s prepared by the dehydropolycondensation of l-lactic acid with organotin catalysts. J Polym Sci, Part A: Polym Chem 2005;43:2164-2177.

181. Shyamroy S. Synthesis of biodegradable poly(lactic acid) polymers. Ph.D. Thesis. NCL Pune, India. 2003.

182. Siemann U. The solubility parameter of poly(DL-lactic acid). Eur Polym J 1992;28:293-297.

183. Singh RP, Pandey JK, Rutot D, Degée Ph., Dubois Ph. Biodegradation of poly(ε-caprolactone)/starch blends and composites in composting and culture environments:

the effect of compatibilization on the inherent biodegradability of the host polymer. Carbohyd Res 2003; 338:1759-1769.

184. Sodergard A, Nasman JH. Materials and interfaces; melt stability study of various types of poly(L-lactide). Ind Eng Chem Res 1996;35:732-735.

185. Sodergard A, Nasman JH. Stabilization of poly(L-lactide) in the melt. Polym Degrad Stab; 1994;46:25-30.

186. Sodergard A, Niemi M, Selin JF, Nasman JH. Changes in peroxide melt-modified poly(L-lactide). Ind Eng Chem Res 1995;34:1203-1207.

187. Sodergard A, Selin JF, Nasman JH. Hydrolytic degradation of peroxide modified poly(L-lactide). Polym Degrad Stab 1996;51:351-359.

188. Sodergard A, Stolt M. Properties of lactic acid based polymers and their correlation with composition. Prog Polym Sci 2002;27:1123-1163.

189. Sodergard A, Stolt M. Novel process for the preparation of polylactic acid. US 200910036600 A1; 2009.

190. Sodergard A. Modification of polylactide. Recent Res Dev Polym Sci 1998;2:263-275.

191. Sodergard A. Properties of peroxide melt-modified poly(L-lactide). Ph.D. Thesis. Abo Academi University: Finland. 1996.

192. Soppimath KS, Aminabhavi TM, Kulkarni AR, Rudzinski WE. Biodegradable polymeric nanoparticles as drug delivery devices. J Control Release 2001;70:1-20.

193. Spassky N. Ring-opening polymerization. Rapra Rev Rep 1995;8:1-29.

194. Stainmesse, S., Fessi, H., Devissaguet, J.P., Puisieux, F., Thies C.; Process for the preparation of dispersible colloidal systems of a substance in the form of nanoparticles. US005133908A, Jul. 28, 1992.

195. Stainmesse S, Orecchioni AM, Nakache E, Puisieux F, Fessi H. Formation and stabilization of a biodegradable polymeric colloidal suspension of nanoparticles. Colloid Polym Sci 1995;273:505-511.

196. Stolt M, Sodergard A. Use of monocarboxylic iron derivatives in the ring-opening polymerization of L-lactide. Macromolecules 1999;32:6412-6417.

197. Sumihiro K, Koyanagi K, Fukushima T, Hashimoto N. Manufacture of high molecular-weight poly(lactic acid) by direct polycondensation of lactic acid and its manufacturing apparatus. JP 11106499 A2, 1999.

198. Sussman EM, Clarke MB Jr, Shastri VP. Single-step process to produce surface-functionalized polymeric nanoparticles. Langmuir 2007;23:12275-12279.

199. Taguchi G, Chowdhury S, Wu Y. Taguchi's Quality Engineering Handbook. 2005, John Wiley & Sons , NJ.

200. Takahashi K, Taniguchi I, Miyamoto M, Kimura Y. Melt/solid polycondensation of glycolic acid to obtain high-molecular-weight poly(glycolic acid). Polymer 2000;41:8725-8728.

201. Tang HY, Chen HY, Huang JH, Lin CC. Synthesis and structural characterization of magnesium ketiminate complexes: efficient initiators for the ring-opening polymerization of l-lactide. Macromolecules 2007;40:8855-8860.

202. Teng C, Yang K, Ji P, Yu M. Synthesis and characterization of poly(l-lactic acid)–poly(ε-caprolactone) multiblock copolymers by melt polycondensation. J Polym Sci: Part A: Polym Chem 2004;42:5045-5053.

203. Terado Y, Mizutsu H, Takagi M, Ajioka M, Hiraoka S, Sakai K, Suzuki H, Shinagawa A, Ogawa S, Kotaki Y. Preparation of aliphatic polyesters with excellent rigidity by crystallization and solid-phase polymerization. JP 2001192443 A2, 2001.

204. Terado Y, Suizu H, Takagi M, Ajioka M, Hiraoka S, Sakai M, Suzuki H, Shinagawa R, Ogawa S, Kotaki Y. Process for preparing aliphatic hydroxy carboxylic acid polyesters. EP 953589 A2, 1999.

205. Thakur KAM, Kean RT, Hall ES, Kolstad JJ, Lindgren TA, Doscotch MA, Siepmann JI, Munson EJ. High resolution ^{13}C and ^{1}H NMR study of poly(lactide). Macromolecules 1997;30:2422-2428.

206. Thakur KAM, Kean RT, Zupfer JM, Buehler NU, Doscotch MA, Munson EJ. Solid State ^{13}C CP-MAS NMR studies of the crystallinity and morphology of poly(l-lactide). Macromolecules 1996;29:8844-8851.

207. Thioune O, Fessi H, Devissaguet JP, Puisieux F. Preparation of pseudolatex by nanoprecipitation: Influence of the solvent nature on intrinsic viscosity and interaction constant. Int J Pharm 1997;146:233-238.

208. Tokiwa Y, Konno M, Nishida H. Isolation of silk degrading microorganisms and its poly(L-lactide) degradability. Chem Lett 1999;28:355-356.

209. Tormala P. Biodegradable self-reinforced composite materials; manufacturing structure and mechanical properties. Clin Mater 1992;10:29-34.

210. Torres A, Li SM, Roussos S, Vert M. Screening of microorganisms for biodegradation of poly(lactic acid) and lactic acid-containing polymers. Appl Environ Microbiol 1996;62:2393-2397.

211. Trotta M, Debernardi F, Caputo O. Preparation of solid lipid nanoparticles by a solvent emulsification-diffusion technique. Int J Pharm 2003;257:153-160.

212. Tsuji H, Ikada Y. Crystallization from the melt of poly(lactide)s with different optical purities and their blends. Macromol Chem Phys 1996;197:3483-3499.

213. Tsuji H, Ikada Y. Stereocomplex formation between enantiomeric poly(lactic acid)s. XI. Mechanical properties and morphology of solution-cast films. Polymer 1999;40:6699-6708.

214. Tsuji H, Ikarashi K, Fukuda N. Poly(L-lactide): Part XII. Formation, growth, and morphology of crystalline residues as extended-chain crystallites through hydrolysis of poly(L-lactide) films in phosphate-buffered solution. Polym Degrad Stab 2004;84:515-523.

215. Tu LS, Dehghani F, Foster NR. Micronisation and microencapsulation of pharmaceuticals using a carbon dioxide antisolvent. Powder Technol 2002;126:134-149.

216. Ueda N, Ishiyama J, Iwama M. Manufacture of aliphatic polyesters with high molecular weight. JP 2005336238 A2, 2005.

217. Van Krevelen DW, Hoftyzer PJ. Properties of polymers: their estimation and correlation with chemical structure; 2nd Edition, 1976; Elsevier Scientific Publishing Company.

218. Vasanthakumari R, Pennings AJ. Crystallization kinetics of poly(lactic acid). Polymer 1983;24:175-178.

219. Vasir JK, Tambwekar K, Garg S. Bioadhesive microspheres as a controlled drug delivery system; Int J Pharm 2003;255:13-32.

220. Vega E, Egea MA, Valls O, Espina M, García ML. Flurbiprofen loaded biodegradable nanoparticles for ophthalmic administration. J Pharm Sci 2006;95:2393-2405.

221. Vouyiouka SN, Karakatsani EK, Papaspyrides CD. Solid state polymerization. Prog Polym Sci 2005;30:10-37.

222. Wang Q, Sun X, Ma R. Direct preparation of polylactic acid from lactate by melt/solid phase polycondensation. CN 1557853 A, 2004.

223. Wei Q, Wei W, Lai B, Wang LY, Wang YX, Su ZG, Ma GH. Uniform-sized PLA nanoparticles: Preparation by premix membrane emulsification. Int J Pharm 2008;359: 294-297.

224. White, Donald A. (Keasbey, NJ); Bimodalization of polymer molecular weight distribution; United States Patent 5578682; 11/26/1996.

225. Wichert B, Rohdewald P. A new method for the preparation of drug containing polylactic acid microparticles without using organic solvents. J Control Release 1990; 14:269-283.

226. Wu J, Yu TL, Chen CT, Lin CC. Recent developments in main group metal complexes catalyzed/initiated polymerization of lactides and related cyclic esters. Coord Chem Rev 2006;250:602-626.

227. Wua JC, Huanga BH, Hsueha ML, Laib SL, Lin CC. Ring-opening polymerization of lactide initiated by magnesium and zinc alkoxides. Polymer 2005;46:9784-9792.

228. Xing Y, Yuan M. Method for preparing high molecular weight polylactic acid by melt and solid phase polycondensation. CN 1616515 A, 2005.

229. Xu H, Luo M, Yu M, Teng C, Xie S. The effect of crystallization on the solid state polycondensation of poly(l-lactic acid). J Macromol Sci Part B Phys 2006;45:681-687.

230. Yeo SD, Kiran E. Formation of polymer particles with supercritical fluids: A review. J Supercrit Fluids 2005;34:287-308.

231. You Y, Min BM, Lee SJ, Lee TS, Park WH. In vitro degradation behavior of electrospun polyglycolide, polylactide, and poly(lactide-co-glycolide). J Appl Polym Sci 2005;95:193-200.

232. Younes H, Cohn D. Phase separation in poly(ethylene glycol)/poly(lactic acid) blends. Eur Polym J 1988;24:765-773.

233. Zhang N, Wang Q, Ren J. Method for preparing solid-polycondensed poly(lactic acid) with improved viscosity. CN 101054438 A, 2007.

234. Zhang WX, Wang YZ. Synthesis and properties of high molecular weight poly(lactic acid) and its resultant fibers. Chin J Polym Sci 2008;26:425-432.

235. Zhou Z, Xu W. Method for preparing high molecular weight poly(L-lactic acid) by melt polycondensation-solid phase polymerization. CN 1594393 A, 2005.

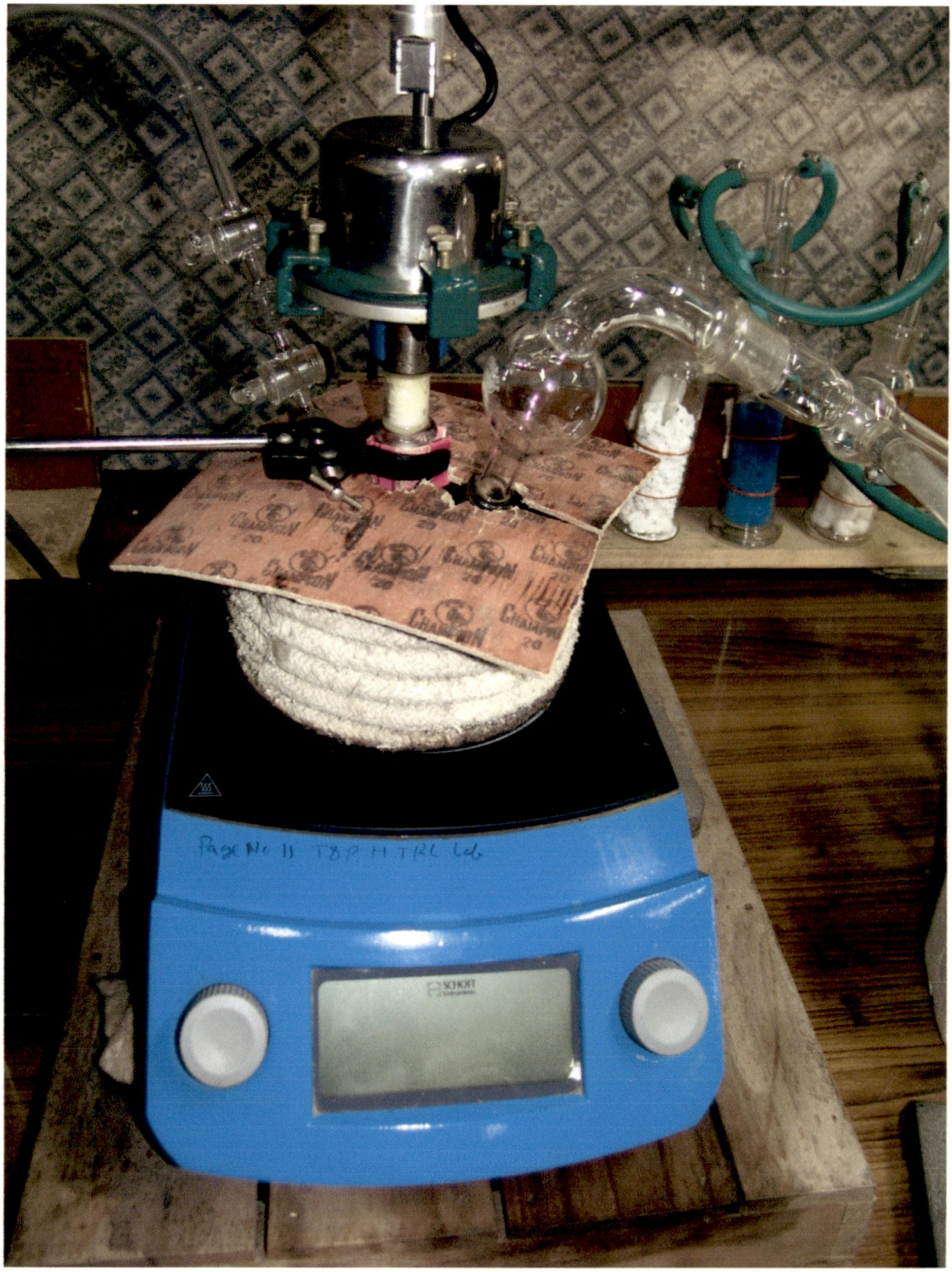

Fig. D.2 Reactor during polycondensation to prevent heat loss

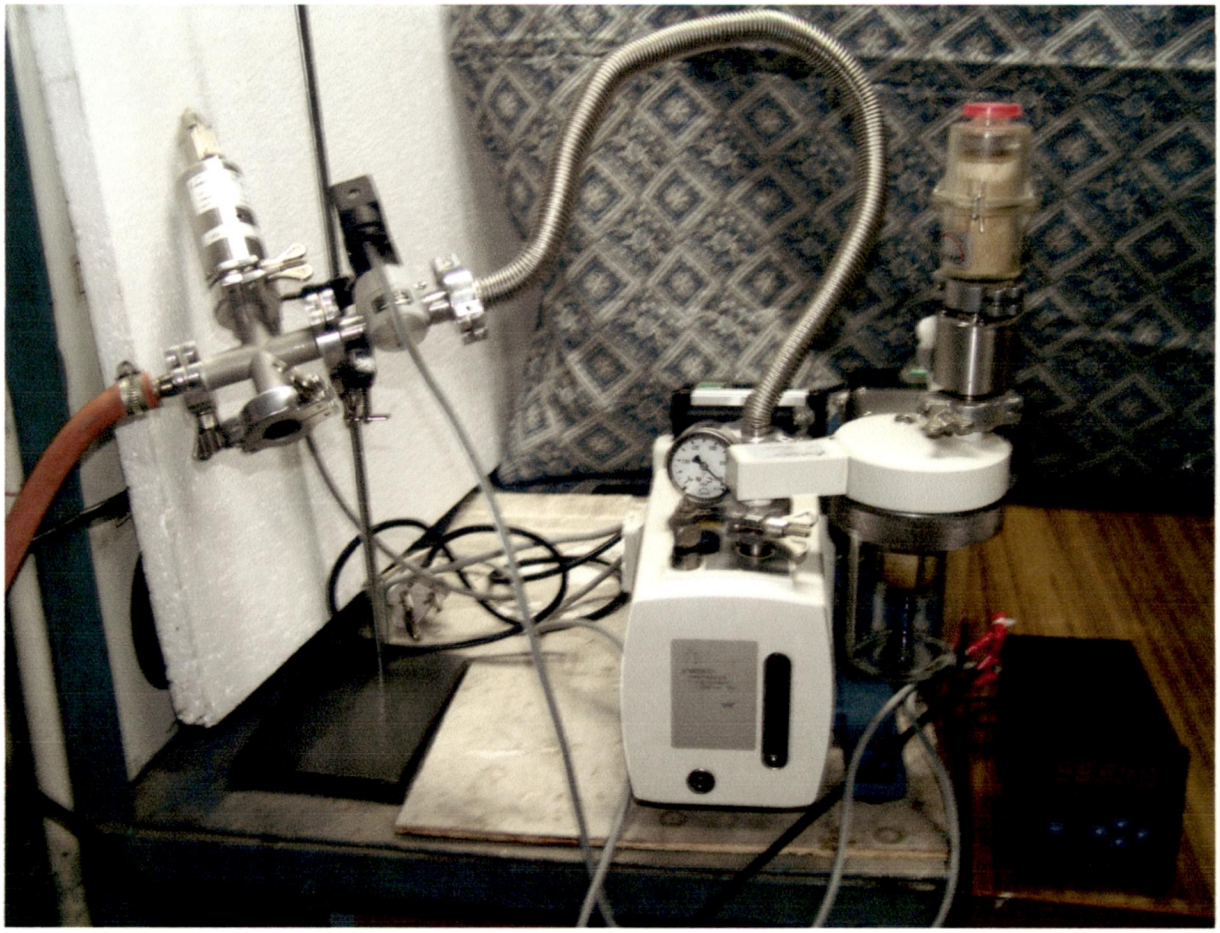

Fig. D.3 Vacuum pump